UNIVERSITY OF MICHIGAN
AUG 23 1954
PHYSICS LIBRARY

THE JOURNAL OF CHEMICAL PHYSICS

VOLUME 22 NUMBER 8

AUGUST, 1954

Published by the

AMERICAN INSTITUTE OF PHYSICS

Incorporated

LANCASTER, PA., AND NEW YORK, N. Y.

THE JOURNAL OF CHEMICAL PHYSICS

BOARD OF EDITORS

CLYDE A. HUTCHISON, JR., *Editor*

Associate Editors

Term ending December 31, 1954

THEODORE H. BERLIN
B. F. DAILEY
HARALD H. NIELSEN
HARRISON SHULL
CHARLES P. SMYTH
FRANK H. WESTHEIMER

Term ending December 31, 1955

RICHARD M. BADGER
DAVID M. DENNISON
JOHN G. KIRKWOOD
G. B. KISTIAKOWSKY
A. W. LAWSON
S. S. PENNER
ROBERT L. SCOTT

Term ending December 31, 1956

BRYCE L. CRAWFORD, JR.
H. S. GUTOWSKY
WILLIAM N. LIPSCOMB
ELLIOTT W. MONTROLL
GEORGE SCATCHARD
J. W. STOUT
GREGORY H. WANNIER

THE JOURNAL OF CHEMICAL PHYSICS is published monthly by the American Institute of Physics. Its purpose is to bridge a gap between journals of physics and journals of chemistry. The artificial boundary between physics and chemistry has now been in actual fact completely eliminated, and a large and active group is engaged in research which is as much the one as the other. It is to this group that the Journal is rendering its principal service and makes its greatest appeal, both as a prompt and efficient medium for publication of research and as a convenient and carefully edited assemblage of pertinent information.

Information for Contributors

Send manuscripts to Clyde A. Hutchison, Jr., Editor, *The Journal of Chemical Physics*, Institute for Nuclear Studies, University of Chicago, Chicago 37, Illinois. Unless otherwise stated submission of a manuscript is a representation that it has been neither copyrighted, published, nor submitted for publication elsewhere. Textual material (abstract, body of the paper, tabular material, references, and figure captions) must be in English, typewritten (except mathematical expressions) double spaced with wide margins on a durable, white paper, preferably letter size. The original copy, not the carbon, should be submitted. For general style, spellings, abbreviations, and form, consult recent issues of this journal. The authors' institutions are requested to pay a publication charge of $15.00 per page which, if honored, entitles them to 100 free reprints. Instructions will be sent with galley proofs.

An abstract must accompany each article. It should be adequate as an index and as a summary.

All but the simplest mathematical expressions should be carefully printed in by hand. Be sure to distinguish between capital and small letters. Indicate clearly superscripts and subscripts by inverted carets and carets, respectively. Avoid complicated superscripts and subscripts. Avoid repetition of a complicated expression by representing it by a symbol. Identify in the margin Greek letters and unusual symbols. Use fractional exponents instead of root signs. Use the solidus (/) for fractions wherever its use will save vertical space.

References should appear as footnotes, numbered consecutively. Literature citations of technical journals should be in the form indicated in the Style Manual of the American Institute of Physics and Chemical Abstracts (Chem. Abstracts 45, I-CCLV (1951)).

Tables may be typewritten on sheets separate from the running text. Each table must have a caption which will make the data in the table intelligible without reference to the text. Avoid complicated column headings.

Wherever possible figures should be planned for the width of a column (3 in.). A convenient reduction ratio is about 2:1 or 3:1. Lettering should be large enough on the original that when reduced it shall not be less than about $\frac{1}{16}$ in. (~1.5 mm). Line drawings must be in *india ink* on white paper or tracing cloth. Coordinate paper is not desirable but if used must be blue lined and the coordinate lines which are to show must be inked over. Photographs should have maximum black and white contrast. Identify each original drawing or photograph on the back with the author's name and the figure number. Figures should be numbered consecutively. Captions should be typed on a separate sheet of paper.

A limited number of alterations in proof are unavoidable, but the cost of making extensive alterations after the article has been set in type will be charged to the author.

Proof and all correspondence concerning papers in the process of publication should be addressed to the Publication Manager, American Institute of Physics, 57 East 55 Street, New York 22, New York.

Subscription Price

	U. S. and Canada	Elsewhere
To members of the American Institute of Physics and Affiliated Societies	$12.00	$13.00
To all others	15.00	16.00

Back Number Prices

Yearly rate when complete year is available: $17.00.
Single copies: $1.50 each.

Subscriptions, renewals, and orders for single copies should be addressed to the American Institute of Physics, 57 East 55 Street, New York 22, New York.

Changes of address should be sent to the American Institute of Physics.

The Journal of Chemical Physics is published monthly at Prince and Lemon Streets, Lancaster, Pennsylvania.

Entered as second-class matter December 30, 1932, at the Post Office at Lancaster, Pa., under the Act of August 24, 1912. Acceptance for mailing at special rate of postage, provided for in paragraph (d-2), section 34.40, P. L. & R. of 1948, authorized February 3, 1933.

THE JOURNAL
OF
CHEMICAL PHYSICS

VOLUME 22, NUMBER 8 AUGUST, 1954

Ultrasonic Propagation and Its Relation to Molecular Structure in the Diols*†

T. A. LITOVITZ, R. HIGGS, AND R. MEISTER
Physics Department, Catholic University of America, Washington 17, D. C.
(Received August 6, 1953)

Measurements of viscosity, ultrasonic absorption, and velocity were made in a group of associated organic liquids, known as the diols. Included in the measurements were ethanediol, two isomers of propanediol, and three isomers of butanediol. In these liquids the values of absorption ranged from 1.66 to 2.20 times that value calculated from Stokes formula. The effect of the structural differences indicated the following, when the addition of CH_2 groups was considered, (1) an increase in shear viscosity, (2) an increase in adiabatic compressibility, (βad), and (3) an increase in the ratio of $\alpha_{obs}/\alpha_{calc}$. Effects caused by isomeric changes were (1) an increase in βad and (2) an increase in $\alpha_{obs}/\alpha_{calc}$ as the (OH) groups were brought closer together. It was concluded that a relationship existed between the ratio of $\alpha_{obs}/\alpha_{calc}$ and βad.

Measurement of absorption *vs* temperature in ethanediol over a viscosity range of 24:1 indicated that the difference in activation energy of shear and compressional viscosity could be no greater than 0.1 percent.

I. INTRODUCTION

ULTRASONIC propagation in liquids has been characterized in general by measured values of absorption which are in excess of those values based on consideration of the effects of shear viscosity alone. In one group, the associated liquids, this excess absorption has been attributed to the existence of a structural type of compressional viscosity. In these liquids this excess loss is related to the structural changes caused in the liquid lattice when the molecules flow into different packing arrangements when under the influence of sonic stress. This compressional viscosity of liquids cannot be measured directly as for example the shear viscosity can. A theoretical calculation has been done by Hall[1] who has calculated the value of compressional viscosity for water, but in general not enough data is available to do this for most liquids. In order to obtain a further understanding of this process it is of interest to relate the magnitude of the compressional viscosity to the molecular structure and also to the shear viscosity.

Ethanediol, two isomers of propanediol, and three isomers of butanediol are investigated. (See Table II for formulas.) This group of liquids offers the possibility of considering the effect of the addition of CH_2 groups and also the effect of isomeric changes on the compressional viscosity exhibited by associated liquids. Within an isomeric group the structural differences in these diols are due to changes in the position of the (OH) radicals which are attached to different carbon atoms in each isomer.

II. EXPERIMENTAL METHOD

Ultrasonic absorption in these liquids was measured using a pulse technique at frequency of 22.5 Mc (except ethanediol where 30.0 Mc was used). These measurements are reproducible to ±5 percent. The electronic equipment, interferometer, and thermal bath used are described elsewhere.[2] To increase the accuracy, the ultrasonic velocities were measured at one megacycle using a continuous wave technique and an acoustic interferometer described elsewhere.[3,4] Since no evidence of dispersion exists in the temperature ranges over which the absorption measurements were made it is assumed the 1-Mc velocities are the same as those at the higher frequencies. All of the measurements of absorption are

* Parts of this paper are taken from Master's dissertations submitted by R. Meister and R. Higgs to the faculty of the Graduate School of Arts and Sciences in partial fulfilment of the requirements for the degree Master of Science.

† This research aided by U. S. Office of Ordnance Research contract DA-36-034-ORD 1221 RD and by U. S. Office of Naval Research.

[1] L. Hall, Phys. Rev. **73**, 775 (1948).

[2] T. A. Litovitz, J. Acoust. Soc. Am. **23**, 75 (1951).

[3] J. A. Hunter, J. Acoust. Soc. Am. **13**, 36 (1941).

[4] F. E. Fox, Phys. Rev. **52**, 973 (1937).

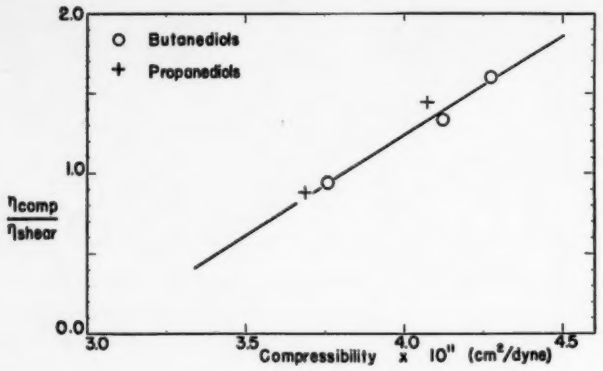

FIG. 1. Plot of the ratio of the compressional to shear viscosity as a function of the adiabatic compressibility in various diols.

at frequencies which are far below any relaxation frequency. The velocity data are reproducible to ±0.2 percent. All measurements were made in a thermal bath in which the temperature was controlled to 0.1°C.

Viscosity measurements were made with a Cannon-Fenske viscometer and are accurate to better than one-half percent.

III. PROPAGATION IN DIOLS

The measured values of ultrasonic velocity, absorption and shear viscosity at 20°C appear in Table I. The calculated values of absorption were obtained using the expression, due to Stokes

$$\alpha_{\text{calc}}=\frac{8\pi^2 f^2 \eta_s}{3\rho v^3}, \tag{1}$$

where f is the frequency, η_s the shear viscosity, ρ the density, and v the velocity. It can be seen that in all cases the measured values of absorption exceeds the calculated values. The values of $\alpha_{\text{obs}}/\alpha_{\text{calc}}$ lie in the range normally found for associated liquids and indicate the existence of a compressional viscosity.

The solution of the wave equation[5] taking this into account yields the following:

$$\alpha=\frac{2\pi^2 f^2}{3\rho v^3}(\eta_c+4/3\eta_s), \tag{2}$$

TABLE I. Ultrasonic propagation in ethanediol.

T°C	v m/sec	η_s poise	α_{obs} cm^{-1}	$\alpha_{\text{obs}}/\alpha_{\text{calc}}$
43	1623	0.088	0.74	1.68
31.5	1650	0.132	1.07	1.70
24.0	1668	0.178	1.38	1.69
15.8	1687	0.254	1.92	1.71
5.9	1710	0.405	2.98	1.74
−5.2	1737	0.758	5.44	1.79
−13.1	1756	1.32	9.06	1.78
−19.4	1771	2.14	14.0	1.75

where η_c is the compressional viscosity coefficient. This should represent the observed absorption. Combining Eqs. (1) and (2), one obtains

$$\eta_c/\eta_s=4/3(\alpha_{\text{obs}}/\alpha_{\text{calc}}-1), \tag{3}$$

showing that the ratio of compressional to shear viscosity varies directly as the ratio $\alpha_{\text{obs}}/\alpha_{\text{calc}}$.

IV. ABSORPTION *vs* TEMPERATURE IN ETHANEDIOL

The ultrasonic velocity and absorption in ethanediol was measured over a temperature range from 43°C to −19.4°C. The purpose of this was to detect if possible differences in the temperature behavior of the shear and compressional viscosity. The results tabulated in Table I show that the absorption in this temperature range has increased by a factor of 19:1, the shear viscosity increasing by a factor of 24:1. The absorption values have been taken from a smooth curve. The ratio of $\alpha_{\text{obs}}/\alpha_{\text{calc}}$ has an average value of 1.73, rising from 1.68 to a maximum of 1.79 and then decreasing. The significance of this maximum is doubtful when considering the experimental accuracy.

Pinkerton has measured the absorption over large temperature ranges in both water and ethyl alcohol. The variation in α_{obs} for water was 8:1 and for ethyl alcohol 3:1. In both of these instances a minimum in the value of $\alpha_{\text{obs}}/\alpha_{\text{calc}}$ was observed as opposed to the maximum found here for ethanediol.

From the results obtained in ethanediol, it does not seem possible to conclude that a difference in the activation energies for shear and compressive viscous flow exists.

TABLE II. Ultrasonic propagation in diols at 20°C.

		v m/sec	β_{ad} cm²/dyne ×10¹¹	η_s stokes	α_{obs}[a] cm^{-1}	$\alpha_{\text{obs}}/\alpha_{\text{calc}}$	η_c/η_s
Butanediol 2,3	$CH_3CH(OH)CH(OH)CH_3$	1496	4.27	1.075	9.38	2.20	1.60
Butanediol 1,3	$CH_2(OH)CH_2CH(OH)CH_3$	1539	4.13	1.303	9.56	2.00	1.33
Butanediol 1,4	$CH_2(OH)CH_2CH_2CH_2(OH)$	1616	3.76	0.835	4.52	1.71	0.94
Propanediol 1,2	$CH_2(OH)CH(OH)CH_3$	1523	4.15	0.598	4.52	2.08	1.44
Propanediol 1,3	$CH_2(OH)CH_2CH_2(OH)$	1608	3.69	0.466	2.51	1.66	0.88
Ethanediol	$CH_2(OH)CH_2(OH)$	1677	3.19	0.188	1.59	1.68	0.91

[a] All measurements of absorption are at 22.5 Mc except for ethanediol, 30 Mc.

[5] L. Tisza, Phys. Rev. **61**, 531 (1942).

TABLE III. Ultrasonic propagation in alcohols.

	T°C	βad cm³/dyne $\times 10^{11}$	$\alpha_{obs}/\alpha_{calc}$	η_c/η_s	η_s 20°C cp	Reference
Methanol	19.3	9.89	2.64	2.19	0.597	[a]
Ethanol	20.0	8.73	2.08	1.44	1.20	[b]
Propanol	27.5	8.19	1.95	1.26	2.26	[a]
Butanol	2.0	7.15	1.64	0.86	2.95	[a]

[a] Pellam and Galt, J. Chem. Phys. **14**, 608 (1946).
[b] J. M. Pinkerton, Proc. Phys. Soc. (London) **B**, 62 (1949).

However, assuming that the variation from 1.68 at 43°C to 1.79 at −5.2°C is real and is due only to a difference in activation energies, then a difference of less than 0.1 percent could account for the results. These conclusions are in agreement with other works.[1,6]

V. EFFECT OF ISOMERIC CHANGES

In the isomeric group of butanediols the positions of the (OH) radicals have affected the adiabatic compressibility, βad, the shear viscosity, and the ratio of compressional to shear viscosity, η_c/η_s. The variations in shear viscosity are not related in any simple manner with the variation in η_c/η_s. For example the butanediol 1, 3 has the highest value of shear viscosity but exhibits an intermediate value of η_c/η_s. The adiabatic compressibility and η_c/η_s both increase together. In Fig. 1 the ratio η_c/η_s for the butanediols is plotted as a function of the compressibility and it can be seen that within the accuracy of the measurement this ratio increases roughly linearly with the compressibility. This increase in compressibility and the ratio η_c/η_s occurs as the (OH) radicals are brought closer together; e.g., the butanediol 2, 3 where the OH radicals are on adjacent carbon atoms exhibits the largest values of βad and η_c/η_s.

Considering the isomers of propanediol, one again finds that when the (OH) radicals are on adjacent carbon atoms the values of βad and η_c/η_s are larger. In Fig. 1 we see that the ratio η_c/η_s for the propanediols also increases with increasing compressibility and has about the same slope as the curve for the butanediols. Actually the data for the propanediols appears to lie on the same line as that for butanediols, but the value of η_c/η_s for ethanediol does not lie on this curve at all.

[6] T. A. Litovitz and D. Sette, J. Chem. Phys. **21**, 17 (1953).

VI. EFFECT OF ADDITION OF CH_2 GROUPS

When considering the effect of adding CH_2 groups the following trends appear to exist as seen in Table II. The shear viscosity increases, with the butanediols being most viscous followed by the propane- and ethanediols, respectively. The measured values of absorption increase with increasing shear viscosity. The ratio of compressional to shear viscosity also increases, the value rising from 0.91, in ethanediol, to 1.60 in butanediol 2, 3. This increase is not evident when considering butanediol 1, 4 and propanediol 1, 3. In both of these liquids however the value is the same as in ethanediol within the uncertainty of the measurement. The addition of CH_2 groups increases the adiabatic compressibility of the liquids.

It is of interest to compare these effects in the diols with results obtained by other authors in the primary alcohols. These results are tabulated in Table III. The addition of (CH_2) radicals has caused the adiabatic compressibility of the alcohols to decrease which is opposite to the increase found in the diols. The decrease in βad is accompanied by a corresponding decrease in the ratio of η_c/η_s. This is in agreement with the results found in the diols.

VII. SUMMARY AND CONCLUSIONS

The results observed in the diols indicate that structural changes affect the shear viscosity in a different manner than the compressional viscosity. The isomer studies showed that the changes in η_c/η_s are not related to the changes in shear viscosity caused by isomeric differences. This is further emphasized by the comparison of the addition of CH_2 groups in the diols and primary alcohols. In both series the CH_2 groups caused the shear viscosity to increase but the ratio of η_c/η_s increased in the former and decreased in the latter.

Only when variations in βad are considered does the data fall into any pattern. The results indicate that some relationship exists between βad and η_c/η_s such that those liquids with larger values of βad tend to exhibit larger values of η_c/η_s.

The Effect of Pressure on Thermal Diffusion in *n*-Paraffin Hydrocarbon-CS_2 Mixtures*

W. M. Rutherford and H. G. Drickamer
Department of Chemistry and Chemical Engineering, University of Illinois, Urbana, Illinois

(Received March 8, 1954)

Thermal diffusion measurements have been made to 10 000 atmospheres at 40°C and 78°C pressure for the systems.

n-hexane (20 percent)–CS_2 (80 percent),
n-heptane (20 percent)–CS_2 (80 percent),
n-octane (20 percent)–CS_2 (80 percent),

at 40°C and 78°C. The data are interpreted in terms of a modified regular solution theory presented previously. The results are consistent with the theory and the regularities indicate that a general quantitative theory of thermal diffusion is possible.

THERMAL diffusion measurements have been made on binary mixtures of CS_2 with *n*-hexane, *n*-heptane, and *n*-octane, to 10,000 atmospheres pressure at 40° and 78°C. The experimental methods are discussed in a previous paper.[1] Because of the sampling methods, most of the data were taken on mixtures containing 80 percent CS_2, although one mixture containing 50 percent CS_2 was studied. Isotherms were obtained at 40° and 78°C. The results are analyzed in terms of the theory presented earlier.[1] Denbigh[2] has developed a molecular interpretation of the thermodynamics of irreversible processes for regular solutions which gives for α_D

$$\alpha_D=\frac{(X_1H_1^{\frac{1}{3}}+X_2H_2^{\frac{1}{3}})(H_2^{\frac{1}{3}}-H_1^{\frac{1}{3}})}{2[RT-X_1X_2(H_1^{\frac{1}{3}}-H_2^{\frac{1}{3}})^2}. \tag{1}$$

We have modified the theory to take care of differences in shape and size of the molecules obtaining

$$\alpha=\frac{(X_1H_1^{\frac{1}{3}}+X_2H_2^{\frac{1}{3}})(H_2^{\frac{1}{3}}-H_1^{\frac{1}{3}})+(\psi_1-\psi_2)(X_1H_1^{\frac{1}{3}}+X_2H_2^{\frac{1}{3}})^2}{2\left\{RT\left[1+X_1X_2\left(\frac{\Delta V}{\bar{V}}\right)^2\right]-X_1X_2(H_1^{\frac{1}{3}}-H_2^{\frac{1}{3}})^2\right\}}, \tag{2}$$

where the ψ_1 and ψ_2 are measures of the effect of shape and size, i.e., ψ_1 is the average number of molecules which will enter a hole left by a molecule of type one, with a similar definition for ψ_2.

The hydrocarbons used were Phillips pure grade. The carbon disulfide was Baker's reagent grade.

The results are shown in Tables I to III, and Figs. 1 to 7. Figures 1 to 3 show plots of α and α_D *versus* pressure.

Table I. Measured and calculated coefficients for the system carbon disulfide-normal hexane (80 percent CS_2 and 40°C).

P (atmos)	α	α_D	ψ_1	ψCS_2
300	0.75	−0.54	1.360	0.905
1000	0.48	−0.94	1.315	0.920
1800	0.31	−1.18	1.335	0.915
3000	0.22	−1.50	1.325	0.915
5000	−0.03	−1.62	1.260	0.935
7000	−0.21	−1.86	1.230	0.945
8250	−0.20	−2.14	1.265	0.935
9900	−0.58	−2.28	1.250	0.940
Measured and calculated coefficients for the system carbon disulfide-normal hexane (80 percent CS_2 and 78°C).				
350	0.67	−0.44	1.330	0.920
1000	0.54	−0.81	1.335	0.915
1800	0.42	−1.12	1.345	0.910
3800	0.19	−1.53	1.350	0.910
6650	−0.02	−1.87	1.350	0.910
8250	−0.13	−2.14	1.330	0.920
10 000	−0.37	−2.18	1.350	0.925
Measured and calculated coefficients for the system carbon disulfide-normal hexane (50 percent CS_2 and 40°C).				
1000	0.40	−0.95	1.175	0.825
7000	−0.16	−1.91	1.140	0.860

Positive α indicates CS_2 goes to cold wall.

Table II. Measured and calculated coefficients for the system carbon disulfide-normal heptane (80 percent CS_2 and 40°C).

P (atmos)	α	α_D	ψ_1	ψCS_2
300	0.69	−0.80	1.445	0.890
1000	0.40	−1.14	1.385	0.905
1800	0.24	−1.40	1.370	0.910
3000	0.04	−1.60	1.340	0.915
5000	−0.13	−1.80	1.300	0.925
7000	−0.28	−1.93	1.250	0.935
10 300	−0.40	−2.00	1.240	0.940
Measured and calculated coefficients for the system carbon disulfide-normal heptane (80 percent CS_2 and 78°C).				
200	0.68	−0.64	1.485	0.880
300	0.67	−0.70	1.470	0.885
1000	0.46	−1.02	1.395	0.900
1580	0.34	−1.22	1.380	0.905
2800	0.17	−1.49	1.390	0.905
4700	−0.02	−1.70	1.370	0.910
6650	−0.18	−1.85	1.340	0.915
8100	−0.19	−1.94	1.290	0.930
9500	−0.36	−1.96	1.260	0.935

Positive α indicates CS_2 goes to cold wall.

* This work was supported in part by the U. S. Atomic Energy Commission.

[1] W. M. Rutherford and H. G. Drickamer, J. Chem. Phys. 22, 1157 (1954).

[2] K. G. Denbigh, Trans. Faraday Soc. 48, 1 (1952).

TABLE III. Measured and calculated coefficients for the system carbon disulfide-normal octane (80 percent CS_2 and 40°C).

P (atmos)	α	α_D	ψ_1	ψCS_2
300	0.45	−1.00	1.465	0.880
1000	0.23	−1.34	1.425	0.895
1800	0.15	−1.58	1.420	0.895
4500	−0.27	−1.96	1.365	0.910
6000	−0.42	−2.34	1.375	0.905
8000	−0.73			
Measured and calculated coefficients for the system carbon disulfide-normal octane (80 percent CS_2 and 78°C).				
300	0.59	−0.80	1.505	0.875
950	0.42	−1.14	1.450	0.890
1800	0.22	−1.40	1.420	0.895
2800	0.16	−1.60	1.430	0.890
4200	−0.02	−1.76	1.435	0.890
5700	−0.11	−2.04	1.480	0.880
7600	−0.21			

Positive α indicates CS_2 goes to cold wall.

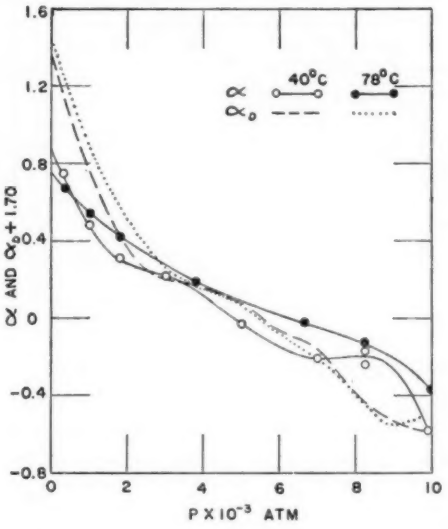

FIG. 1. α and α_D *vs* pressure CS_2–*n*-hexane.

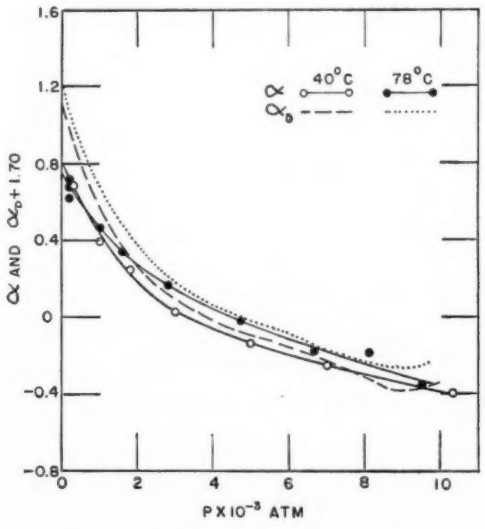

FIG. 2. α and α_D *vs* pressure CS_2–*n*-heptane.

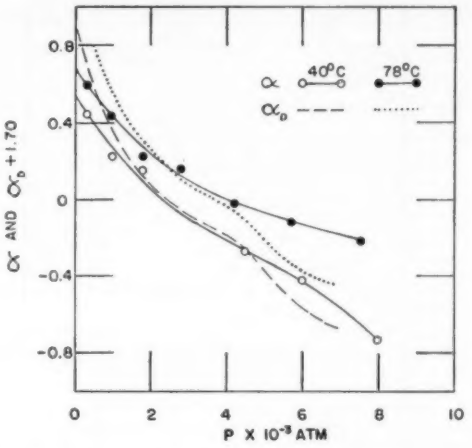

FIG. 3. α and α_D *vs* pressure CS_2–*n*-octane.

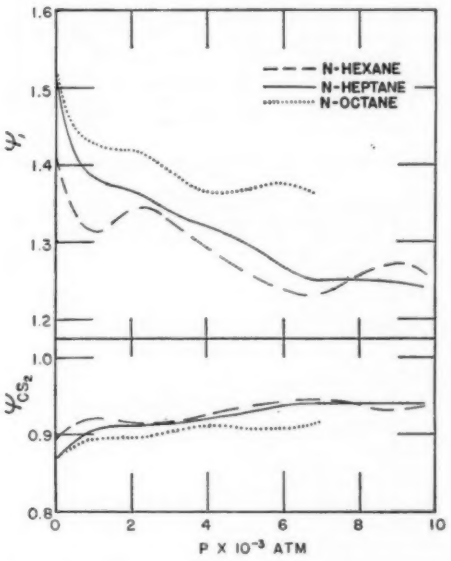

FIG. 4. Steric factors ψ_1 and ψ_{CS_2} *vs* pressure at 40°C.

The PVT data of Bridgman[3] were used in calculating the H_i. The values for H_i are plotted in Fig. 8. It is seen that $\alpha-\alpha_D$ is nearly the same for the three systems, and is virtually independent of pressure above 1000 atmos-

TABLE IV. Hole energies $W_{L_2}=\psi_2 W_L$ for CS_2 (80 percent) in paraffin hydrocarbons (20 percent) 40°C (Kcal/mole).

P (atmos)	NC_6	NC_7	NC_8
950	2.45	2.46	2.54
1950	2.87	2.90	3.02
2900	3.23	3.31	3.43
3900	3.47	3.68	3.74
4900	3.82	3.91	4.12
5800	4.30	4.35	4.65
6800	4.65	4.70	5.10
7750	4.97	4.98	
8700	5.12	5.07	
9700	5.16	5.12	

[3] P. W. Bridgman, Proc. Am. Acad. **49**, 4 (1913); **66**, 185 (1931); **68**, 4 (1933).

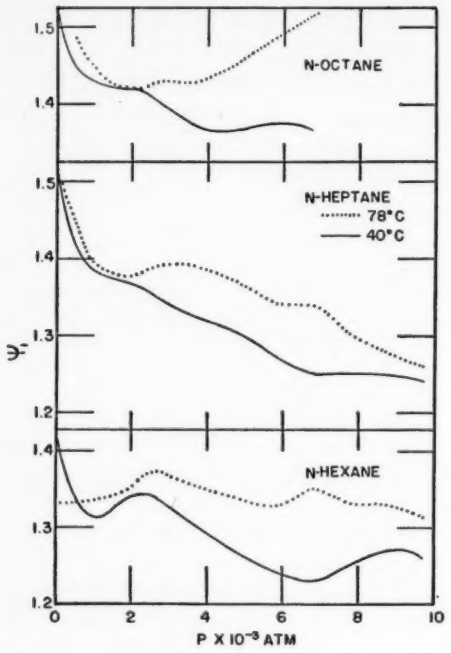

FIG. 5. Steric factors ψ_1 for hydrocarbons at 40° and 78°C.

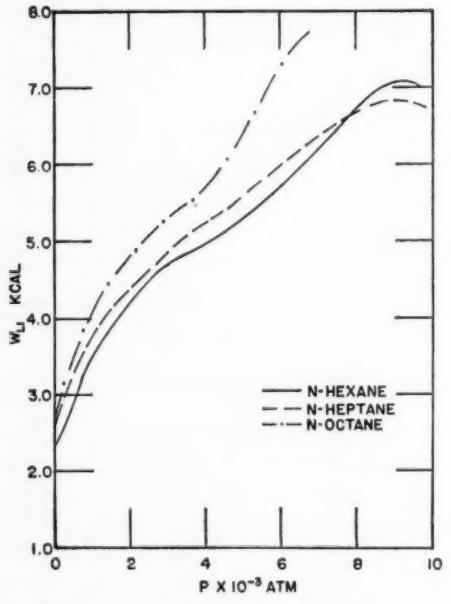

FIG. 6. Hole energies W_{L1} *vs* pressure.

pheres. It is interesting to note that the equations predict the temperature dependence reasonably well. The values of ψ_1 and ψ_2 are shown in Figs. 4 and 5. As might be expected, the longer the chain, the more molecules necessary to fill the hole that is left. It may be noted that the values for the butyl halides published previously[1] were about 1.1, which is consistent with the present results. Figures 6 and 7 show the values of $W_{L1}=\psi_1 W_L$, the energy supplied when the hole left by a hydrocarbon molecule is filled. At low pressures the values of W_{L1} are proportional to chain length, but at high pressure the W_{L1} for heptane apparently crosses that for hexane. This is reasonable, because at high pressure the method of packing is important, and the chains with an odd number of carbon atoms pack less efficiently than the even membered chains. In Fig. 7 the W_{L1} are presented for both isotherms. The scales are translated, as otherwise there is too much overlapping

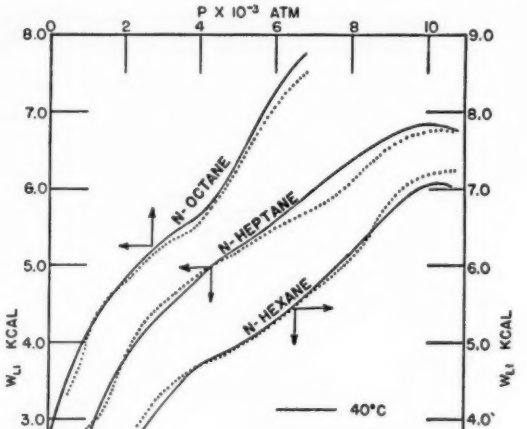

FIG. 7. Effect of temperature on W_{L1}.

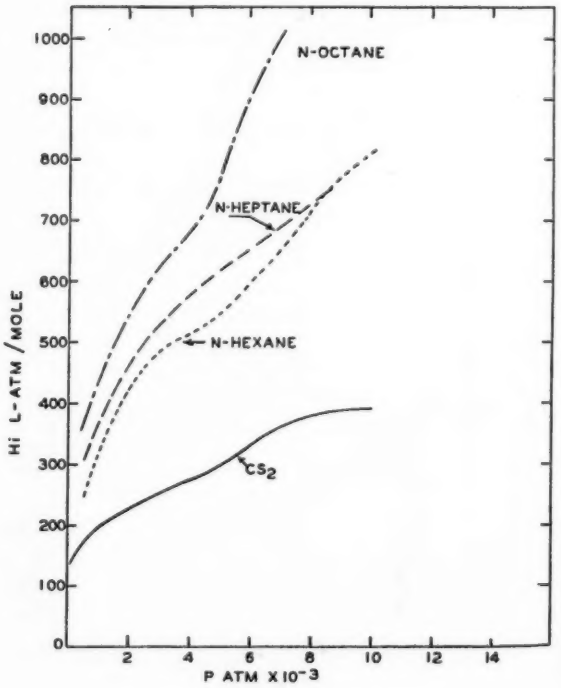

FIG. 8. Cohesive energies *vs* pressure.

of the curves. It is interesting to note that although the ψ (Fig. 5) are temperature dependent, the W_{L1} are essentially independent of temperature. Values of W_{L2} for CS_2 are shown in Table IV. It can be seen that these increase with pressure and are independent of the hydrocarbon with which they are mixed.

It appears possible that, with sufficient further data, a general quantitative theory of the ψ's and of the hole energies may be possible.

W. M. Rutherford would like to acknowledge financial assistance from the Standard Oil Company of Ohio, and from the U. S. Atomic Energy Commission.

THE JOURNAL OF CHEMICAL PHYSICS VOLUME 22, NUMBER 8 AUGUST, 1954

Thermal Diffusion in Mixtures of Tetrachloroethane with Normal Paraffin Hydrocarbons*

R. L. Saxton and H. G. Drickamer
Department of Chemistry and Chemical Engineering, University of Illinois, Urbana, Illinois

(Received March 8, 1954)

Thermal diffusion measurements have been made on a series of binary mixtures of normal paraffin hydrocarbons with tetrachloroethane over a range of temperatures from 5–55°C. The results are analyzed in terms of a previously published theory. The size of hole left by the hydrocarbon seems independent of chain length up to an eight or nine carbon chain. If the moving segment is assumed to be eight carbon atoms long, the size of hole left by the segment is independent of total chain length.

In previous papers[1–3] a theory of thermal diffusion in liquids has been developed and applied to a series of binary mixtures. This paper represents a continuation of the work. Binary mixtures of tetrachloroethane with a series of normal paraffin hydrocarbons (nC_6, nC_7, nC_8, nC_9, nC_{14}, nC_{18}) have been studied over a range of temperatures from 5°C to 55°C at atmospheric pressure. Each mixture contained 50-mole percent tetrachloroethane. Since the theory (1) and the experimental procedure (2) have been previously described, we can proceed directly to a discussion of the results. The values

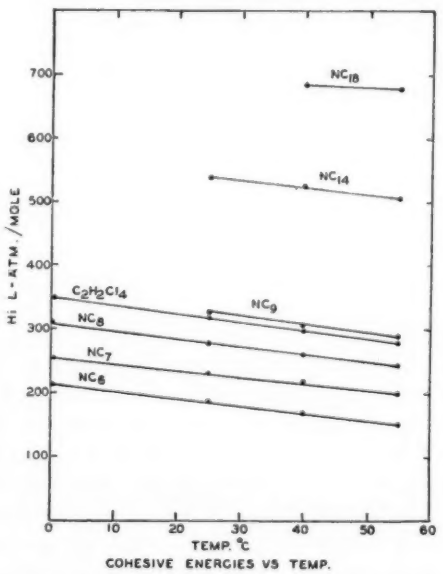

FIG. 1. Cohesive energies *vs* temperature.

TABLE I. Thermal diffusion ratios for mixtures of tetrachloroethane with normal paraffin hydrocarbons.

System[a]	Temp	α	$\alpha-\alpha_D$	ψ_1	ψ_2
(1) (2)					
$C_2H_2Cl_4-nC_6$	10°C	5.1	4.05	0.63	1.37
	25°	4.3	3.1	0.64	1.36
	40°	3.9	2.86	0.63	1.37
	55°	3.8	2.72	0.63	1.37
(1) (2)					
$C_2H_2Cl_4-nC_7$	10°	4.75	4.2	0.66	1.34
	25°	4.28	3.4	0.665	1.335
	40°	3.80	3.05	0.66	1.34
	55°	3.65	2.95	0.65	1.35
(1) (2)					
$C_2H_2Cl_4-nC_8$	10°	4.3	4.02	0.68	1.32
	25°	3.95	3.56	0.69	1.31
	40°	3.75	3.36	0.66	1.34
	55°	3.62	3.25	0.655	1.345
(1) (2)					
$C_2H_2Cl_4-nC_9$	25°	3.65	3.85	0.67	1.33
	40°	3.45	3.6	0.66	1.34
	55°	3.35	3.48	0.64	1.36
(1) (2)					
$C_2H_2Cl_4-nC_{14}$	25°	3.40	4.94	0.57	1.43
	40°	3.0	4.47	0.57	1.43
	55°	2.8	4.21	0.55	1.45
(1) (2)					
$C_2H_2Cl_4-nC_{18}$	40°	2.70	4.80	0.49	1.51
	55°	2.55	4.66	0.46	1.54

[a] No. 1 compound concentrated at cold wall.

* This work was supported in part by the U. S. Atomic Energy Commission.

[1] W. M. Rutherford and H. G. Drickamer, J. Chem. Phys. **22**, 1157 (1954).

[2] Saxton, Dougherty, and Drickamer, J. Chem. Phys. **22**, 1166 (1954).

[3] W. M. Rutherford and H. G. Drickamer, J. Chem. Phys. **22**, 1284 (1954).

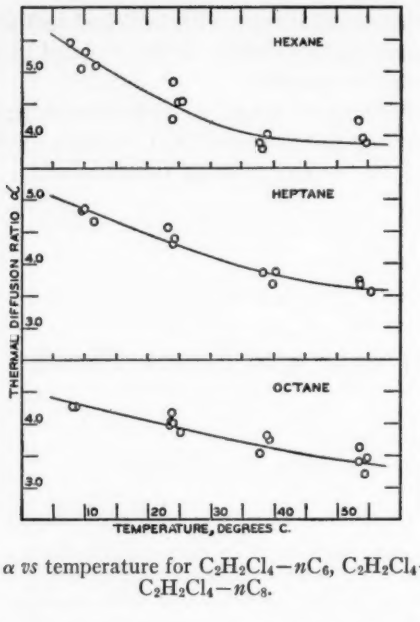

FIG. 2. α *vs* temperature for $C_2H_2Cl_4-nC_6$, $C_2H_2Cl_4-nC_7$, $C_2H_2Cl_4-nC_8$.

of and for the steric factors ψ_1 and ψ_2 are listed in Table I. The cohesive energies for tetrachloroethane and for the hydrocarbons was estimated from vapor pressure data as previously described. They are shown in Fig. 1. Direct measurements[4] of the thermal pressure were available for nC_7, and the H_i for all hydrocarbons were corrected relative to this value.

The values of α are shown in Figs. 2 and 3. Figure 4 gives a comparison between the values for different

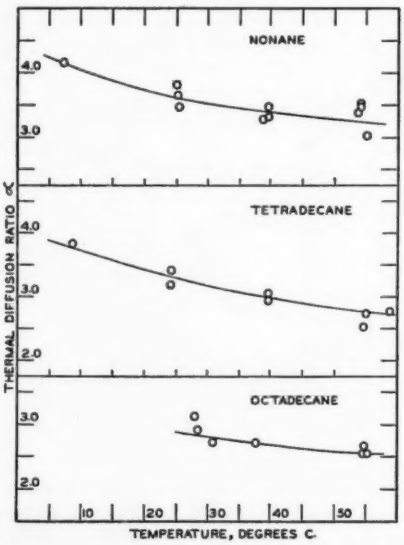

FIG. 3. α *vs* temperature for $C_2H_2Cl_4-nC_9$, $C_2H_2Cl_4-nC_{14}$, $C_2H_2Cl_4-nC_{18}$.

[4] Westwater, Frantz, and Hildebrand, Phys. Rev. **31**, 135 (1928).

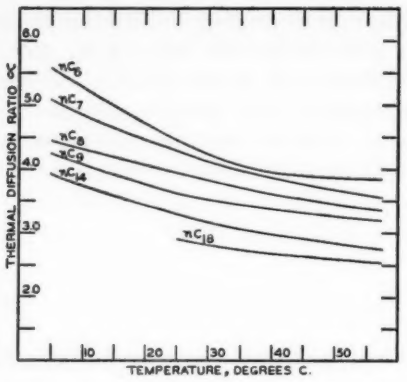

FIG. 4. Comparison of α for a homologous series of normal paraffins *vs* $C_2H_2Cl_4$.

hydrocarbon-tetrachloroethane mixtures. From Table I we see that the steric factors ψ_1 and ψ_2 (i.e., the "number of molecules which fill a hole" left by a type one or type two molecule) follow an interesting pattern. In each case the necessary number of molecules to fill a hole is greater for the hydrocarbon than for tetrachloroethane. This is consistent with the high-pressure data in the preceding paper (3), obtained on hydrocarbon-carbon disulfide mixtures. The values of ψ are relatively independent of chain length up to about C_8 or C_9. Beyond

TABLE II. Values for the steric factors ψ_1 and ψ_2 assuming segmental motion with eight carbon atoms per segment.

System	Temp. °C	ψ_1	ψ_2
(1) (2) $C_2H_2Cl_4-nC_9$	25	0.69	1.31
	40	0.67	1.33
	55	0.66	1.34
(1) (2) $C_2H_2Cl_4-nC_{14}$	25	0.67	1.33
	40	0.68	1.32
	55	0.67	1.33
(1) (2) $C_2H_2Cl_4-nC_{18}$	40	0.69	1.31
	55	0.67	1.33

this point the values increase with chain length, which would be expected. If we now assume segmental motion with the moving segment eight-carbon atoms long we can calculate values of the cohesive energies H_i as a fraction of the total per molecule and thus calculate the values of ψ_1 and ψ_2 for the mixtures. These are listed in Table II. We see that the ψ for an eight-carbon segment is essentially independent of the molecule in which we find it, which makes the segmental type motion seem quite reasonable.

R. L. Saxton would like to acknowledge a fellowship from the E. I. du Pont Company.

Thermal Diffusion in Binary Mixtures of CS_2 and Hexane Isomers*

W. M. Rutherford, E. L. Dougherty, and H. G. Drickamer
Department of Chemistry and Chemical Engineering, University of Illinois, Urbana, Illinois

(Received March 8, 1954)

Thermal diffusion measurements have been made for binary mixtures of CS_2 and the five isomeric hexanes at atmospheric pressure and under pressure to 10 000 atmospheres. The data, measured in two different types of apparatus, are consistent. The results indicate that the further the deviation from spherical symmetry, the larger the value of the steric correction factor ψ. Thus, for mixtures of molecules of the same size and cohesive energy, the more spherically symmetrical will concentrate at the cold wall.

In a series of previous papers,[1–4] we have presented a general theory of thermal diffusion in liquids and applied it to a number of mixtures at atmospheric pressure and over a pressure range to 10 000 atmospheres.

The theory is based on the thermodynamics of irreversible processes and a molecular interpretation of the heats of transport, based on the work of Denbigh.[5] For strictly regular solutions, mixtures of molecules of approximately the same size and shape randomly distributed, one obtains for the thermal diffusion ratio α:

$$\alpha_D=\frac{(X_1H_1^{\frac{1}{3}}+X_2H_2^{\frac{1}{3}})(H_2^{\frac{1}{3}}-H_1^{\frac{1}{3}})}{2[RT-X_1X_2(H_1^{\frac{1}{3}}-H_2^{\frac{1}{3}})^2]}. \tag{1}$$

For mixtures of molecules of different size and shape, we obtain:

$$\alpha=\frac{(X_1H_1^{\frac{1}{3}}+X_2H_2^{\frac{1}{3}})(H_2^{\frac{1}{3}}-H_1^{\frac{1}{3}})+(\psi_1-\psi_2)(X_1H_1^{\frac{1}{3}}+X_2H_2^{\frac{1}{3}})^2}{2\left\{RT\left[1+X_1X_2\left(\frac{V_2-V_1}{\bar{V}}\right)^2\right]-X_1X_2(H_1^{\frac{1}{3}}-H_2^{\frac{1}{3}})^2\right\}}, \tag{2}$$

where the steric factor ψ_i is the "probable number of molecules which will fill a hole" left by a molecule of type i. The ψ_i are related to the size and shape of the molecules.

We have defined the cohesive energies (or enthalpies) H_i by the equation

$$H_i=\left[T\left(\frac{\partial p}{\partial T}\right)_v\left(V-T\frac{\partial V}{\partial T}\right)\right]_i,$$

and have presented some theoretical arguments which make this reasonable.

In this paper we present thermal diffusion measurements on the fine isomers of hexane each in binary solution with carbon disulfide. The isomers of hexane have very nearly the same molar volume, so those data consititute a test of the effect of molecular shape at constant size. The hydrocarbons were Phillips Pure Grade. The CS_2 was reagent grade (Bakers). The atmospheric pressure data were obtained at 20 mole percent

TABLE I. Atmospheric pressure thermal diffusion ratios 8°C.

mol fr CS_2	α	α_D	ψCS_2	ψ_1
n-hexane–CS_2				
0.8	1.02	−0.37	0.9	1.4
0.5	0.98	−0.358	0.76	1.24
2-MP–CS_2				
0.8	0.94	−0.266	0.94	1.344
0.5	0.78	−0.253	0.801	1.199
3-MP–CS_2				
0.8	0.76	−0.304	0.924	1.304
0.5	0.71	−0.291	0.819	1.181
2,3-DMB–CS_2				
0.8	0.41	−0.266	0.95	1.197
0.5	0.42	−0.253	0.875	1.125
2,2-DMB–CS_2				
0.8	0.19	−0.11	0.979	1.084
0.5	0.28	−0.105	0.927	1.073

A positive α indicates that CS_2 goes to the cold wall.

TABLE II. Measured and calculated coefficients for the system carbon disulfide–2-methylpentane (80 percent CS_2 and 40°C).

P (atmos)	α	α_D	ψ_1	ψCS_2
300	0.73	−0.35	1.290	0.930
1000	0.39	−0.88	1.285	0.930
1800	0.15	−1.15	1.275	0.930
3000	−0.01	−1.35	1.250	0.935
5000	−0.36	−1.65	1.210	0.950
7000	−0.67	−1.98	1.190	0.950
8500	−0.46	−1.99	1.205	0.950
9500	−0.63	−2.09	1.210	0.950
Measured and calculated coefficients for the system carbon disulfide–2-methylpentane (50 percent CS_2 and 40°C).				
950	0.38	−0.90	1.165	0.835
7000	−0.37	−1.99	1.125	0.875

A positive value of α denotes that CS_2 goes to the cold wall.

* This work is supported in part by the U. S. Atomic Energy Commission.

[1] W. M. Rutherford and H. G. Drickamer, J. Chem. Phys. **22**, 1157 (1954).
[2] Saxton, Dougherty, and Drickamer, J. Chem. Phys. **22**, 1166 (1954).
[3] W. M. Rutherford and H. G. Drickamer, J. Chem. Phys. **22**, 1284 (1954).
[4] R. L. Saxton and H. G. Drickamer, J. Chem. Phys. **22**, 1287 (1954).
[5] K. G. Denbigh, Trans. Faraday Soc. **48**, 1 (1952).

TABLE III. Measured and calculated coefficients for the system carbon disulfide–3-methylpentane (80 percent CS_2 and 40°C).

P (atmos)	α	α_D	ψ_1	ψCS_2
300	0.50	−0.30	1.215	0.945
1000	0.31	−0.86	1.260	0.935
1800	0.10	−1.14	1.260	0.935
3000	−0.09	−1.36	1.235	0.940
5000	−0.31	−1.56	1.200	0.950
7000	−0.38	−1.76	1.180	0.955
8500	−0.62	−2.04	1.195	0.950
10 500	−0.72			
Measured and calculated coefficients for the system carbon disulfide–3-methylpentane (50 percent CS_2 and 40°C).				
1000	+0.26	−0.95	1.160	0.840

A positive value of α indicates CS_2 goes to cold wall.

and 50 mole percent hydrocarbon. They were run in the apparatus previously described[2] at an average temperature of 6–7°C using a 10° ΔT. The low temperature was necessary to eliminate loss of CS_2 from the atmospheric pressure cell.

TABLE IV. Measured and calculated coefficients for the system carbon disulfide–2,3-dimethylbutane (80 percent CS_2 and 40°C).

P (atmos)	α	α_D	ψ_1	ψCS_2
350	0.28	−0.40	1.185	0.955
1000	0.07	−0.78	1.195	0.955
1800	−0.17	−1.10	1.185	0.955
3000	−0.43	−1.42	1.190	0.955
5000	−0.56	−1.71	1.195	0.955
7000	−0.89	−1.78	1.125	0.970
10 500	−0.99	−2.29	1.205	0.950
Measured and calculated coefficients for the system carbon disulfide–2,3-dimethylbutane (50 percent CS_2 and 40°C).				
7000	−1.03	−1.95	1.160	0.840

A positive value of α indicates CS_2 goes to cold wall.

Measurements were also made to 10 000 atmos pressure at 40°C using the high pressure apparatus described in a previous article.[1,†] These measurements were made, in general, on 20 mole percent hydrocarbon mixtures,

TABLE V. Measured and calculated coefficients for the system carbon disulfide–2,2-dimethylbutane (80 percent CS_2 and 40°C).

P (atmos)	α	α_D	ψ_1	ψCS_2
350	−0.11			
500		−0.56	1.155	0.960
1050	−0.17	−1.01	1.185	0.955
1850	−0.47	−1.22	1.160	0.960
3000	−0.95	−1.43	1.090	0.975
4500	−1.15	−1.64	1.085	0.980
6000	−1.24	−1.80	1.080	0.980
Measured and calculated coefficients for the system carbon disulfide–2,2-dimethylbutane (50 percent CS_2 and 40°C).				
1000	−0.09	−1.02	1.120	0.880

A positive value of α indicates CS_2 goes to cold wall.

† The *n*-hexane data at high pressure were previously reported (3). The results are used for comparison purposes here.

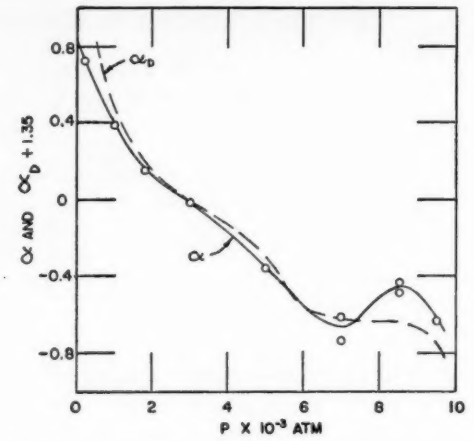

FIG. 1. α and α_D *vs* pressure CS_2–2-methylpentane.

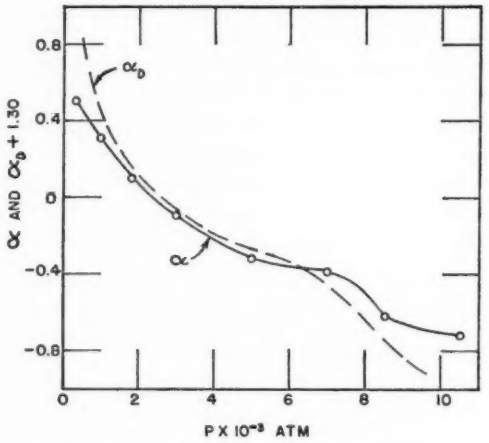

FIG. 2. α and α_D *vs* pressure CS_2–3-methylpentane.

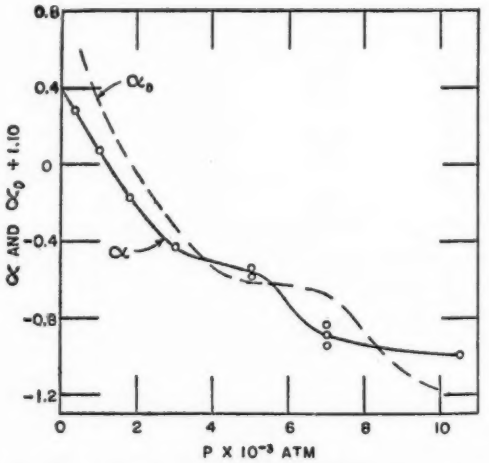

FIG. 3. α and α_D *vs* pressure CS_2–2,3-dimethylbutane.

although points were obtained at 1000 atmos and 7000 atmos on 50 mole percent mixtures.

The atmospheric pressure results are shown in Table I. The high pressure results are in Tables II–V, and Figs. 1–6.

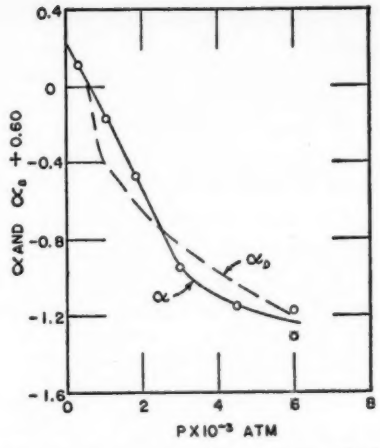

FIG. 4. α and α_D *vs* pressure CS_2–2,2-dimethylbutane.

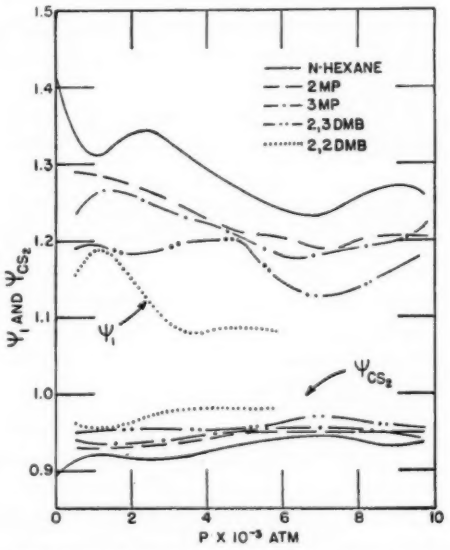

FIG. 5. Steric factors ψ_1 and ψ_{CS_2} *vs* pressure.

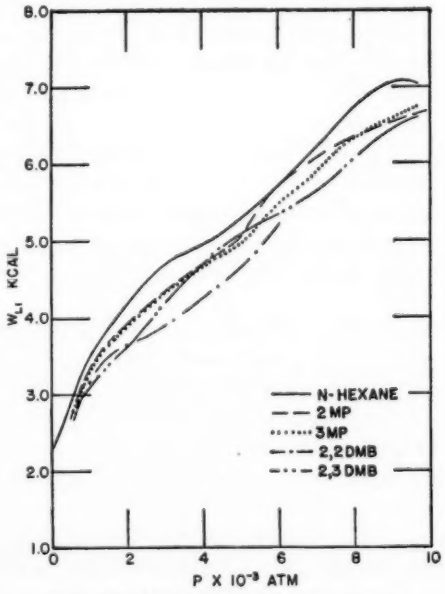

FIG. 6. Hole energies W_{L1} *vs* pressure.

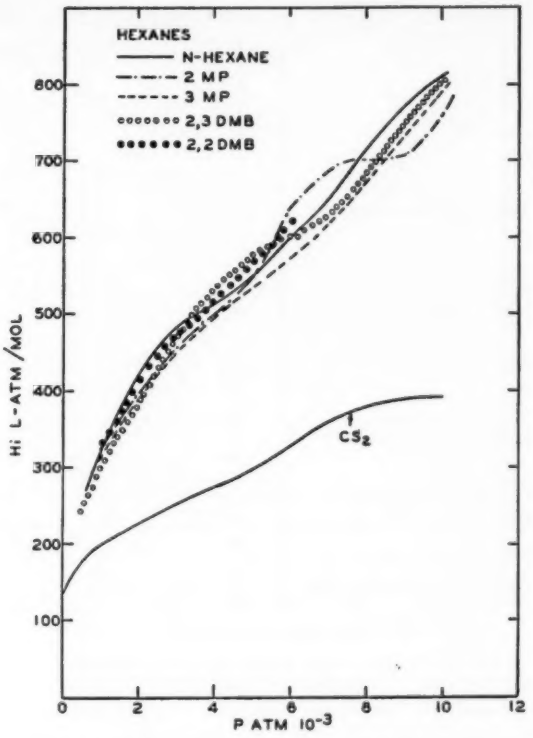

FIG. 7. Cohesive energies *vs* pressure.

The values of H_i for the high pressures were calculated from Bridgman's PVT data[6] and are shown in Fig. 7. For the atmospheric pressure results the H_i were evaluated from vapor pressure and thermal expansion data in API American Petroleum Institute Project 44 Reports. As shown by Hildebrand[7]

$$T\left(\frac{\partial p}{\partial T}\right)_v = \frac{(\Delta E)_{\text{vap}}}{V_{\text{liq}}}. \tag{4}$$

The values of H_i thus calculated are listed in Table VII.

It should be noted that the values of ψ obtained at atmospheric pressure fit very closely on the curves of ψ

TABLE VI. Hole energies $W_{L_2}=\psi_2(X_1H_1^{\frac{1}{2}}+X_2H_2^{\frac{1}{2}})^2$ for CS_2 (80 percent in binary mixture with isomers of hexane (20 percent). Kcal/mol.

P	n-C_6	2-MP	3-MP	2,3-DMB	2,2-DMB
950	2.45	2.42	2.42	2.47	2.54
1950	2.87	2.86	2.90	2.89	3.00
2900	3.23	3.27	3.27	3.30	3.37
3900	3.47	3.57	3.57	3.66	3.78
4850	3.82	3.87	3.82	3.95	4.04
5800	4.30	4.38	4.30	4.40	4.48
6800	4.65	4.77	4.60	4.73	
7750	4.97	5.00	4.93	5.02	
8700	5.12	5.10	5.10	5.22	
9700	5.16	5.17	5.17	5.30	

[6] P. W. Bridgman, Proc. Am. Acad. Arts Sci. **49**, No. 1, 4 (1913); **66**, No. 5, 185 (1931).

[7] J. H. Hildebrand and R. L. Scott, *Solubility of Nonelectrolytes* (Reinhold Publishing Corporation, New York, 1950), third edition.

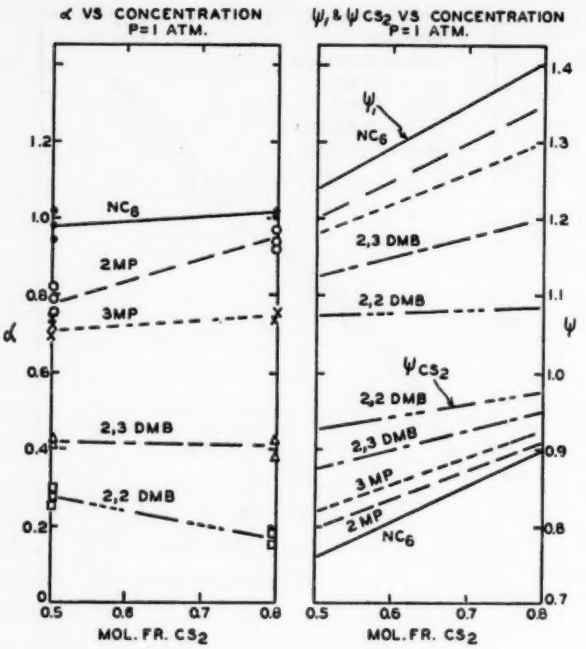

FIG. 8. α and steric factors *vs* concentration at atmospheric pressure.

versus pressure (Fig. 5) extrapolated to atmospheric pressure. This indicates a very close check between the two, somewhat different, experimental methods for measuring α.

The curves of α and α_D *versus* pressure have substantially the same shape, which further confirms our definition of the cohesive energy.

From the results it can be seen that $\alpha-\alpha_D$ is largest for normal hexane, smaller for 2-methylpentane and 3-methylpentane, still smaller for 2,3-dimethylbutane, and smallest for 2,2-dimethylbutane which is most nearly spherically symmetrical. Of course $\psi-1$ varies in a similar manner.

It is evident that, for molecules of the same size, the more nearly spherically symmetrical the molecule the more nearly it forms a strictly regular solution with molecules of simple symmetry. One would thus predict that for isomers having about the same cohesive energy the one which is most nearly spherically symmetrical should concentrate at the cold wall.

From Fig. 6 it can be seen that the values of the "hole" energy W_{L1} for the different hydrocarbons:

$$W_{L1}=(X_1H_1^{\frac{1}{3}}+X_2H_2^{\frac{1}{3}})^2\psi_1 \qquad (5)$$

varies only slightly among the hydrocarbons. From Table VI it is seen that $(W_L)_{CS_2}$ is substantially independent of the hydrocarbon with which it is mixed.

The effect of increasing the concentration of the larger hydrocarbon molecule is always to decrease the values of ψ_1 and ψ_2 as one would expect, and to increase the values of W_{L1} and W_{L2}.

In Fig. 8 are plotted the values of α and of ψ_1 and ψ_1 *versus* composition for the atmospheric pressure data. It can be seen that, while α varies with composition in a different manner for each isomer, the effect of increasing hydrocarbon concentration is always to decrease ψ both for the hydrocarbon and for CS_2. The largest concentration effect on ψ is for mixtures containing the straight chain *n*-hexane, and the smallest concentration effect is for the nearly spherical 2,2-dimethylbutane. This result is to be expected.

TABLE VII. Cohesive energies of hexane isomers at 7°C and one atmosphere (calculated from vapor pressure data).

	H_i (liter-atmos/mole)
n-hexane	184
2-methylpentane	171.5
3-methylpentane	177
2,3-dimethylbutane	171.5
2,2-dimethylbutane	156
CS_2	142.4

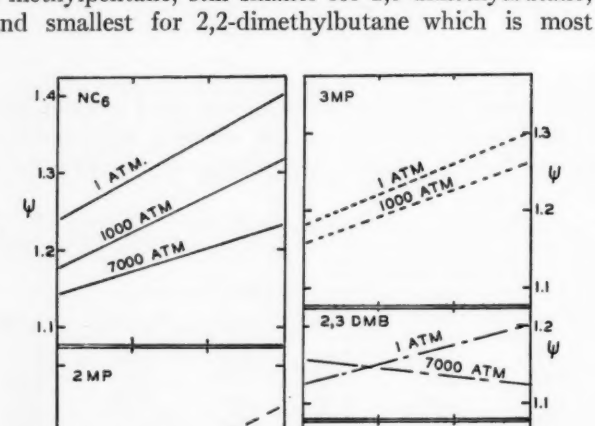

FIG. 9. Effect of pressure and concentration on the steric factor for the hydrocarbons.

Figure 9 shows the effect of pressure on the concentration dependence of ψ. The concentration dependence of ψ is the same at all pressures except for the system CS_2–2,3-dimethylbutane. Relatively small errors in α or in PVT data could have affected the results for this system.

The results are entirely consistent with our previously published data on CS_2–normal paraffin mixtures and CS_2–butyl and ethyl halide mixtures.

Further tests of the shape effect are planned for various other isomeric combinations.

W. M. Rutherford would like to acknowledge a fellowship from the Standard Oil Company (Ohio), and from the U. S. Atomic Energy Commission. E. L. Dougherty would like to acknowledge a fellowship from the Pan American Refining Corporation.

Vibrational Spectra and Calculated Thermodynamic Properties of Ethyl Chloride and 1,1-Dichloroethane*

LESTER W. DAASCH, *Naval Research Laboratory, Washington, D. C.*

AND

C. Y. LIANG† AND J. RUD NIELSEN, *Department of Physics, University of Oklahoma, Norman, Oklahoma*

(Received August 24, 1953)

The infrared absorption spectra of H_3C-CH_2Cl and $H_3C-CHCl_2$ in the gaseous and liquid states have been obtained in the region from 2 to 38μ with the aid of LiF, NaCl, KBr, and KRS-5 prisms. The Raman spectra of the liquids have been photographed with a 3-prism glass spectrograph of linear dispersion 15 A/mm at 4358A. Relative intensities and depolarization ratios have been measured for most of the Raman bands. Complete assignments of fundamental vibrational frequencies have been made, the spectra have been interpreted in detail, and thermodynamic functions have been calculated for the compounds in the gaseous state.

INTRODUCTION

THE infrared spectrum of H_3C-CH_2Cl has been investigated by Cross and Daniels,[1] and the C–H overtone bands have been studied by Mecke *et al.*[2–4] The Raman spectrum of ethyl chloride has been observed by a number of investigators.[5–11] Assignments of fundamentals have been made by some of these authors and by Linnett,[12] Pitzer,[13] and Sheppard.[14]

The infrared spectrum of $H_3C-CHCl_2$ has been studied by Emschwiller and Lecomte,[15] and by Thompson and Torkington;[16] and the Raman spectrum has been investigated by Pestemer,[17] Cleeton and Dufford,[7] Kohlrausch and Köppl,[18] and Bishui.[19] An assignment of most of the fundamentals for $H_3C-CHCl_2$ is given by Landolt-Börnstein.[20]

In the present paper more accurate and complete spectral data are presented, assignments of fundamentals are made, the spectra are interpreted in detail, and thermodynamic properties are calculated.

EXPERIMENTAL

The samples were kindly supplied by the Dow Chemical Company. The ethyl chloride was stated to be 99.9 percent pure. Its infrared spectrum indicated the presence of a trace of unidentified impurities. The sample of 1,1-dichloroethane, stated to be 99.3 percent pure, was found to contain a trace of H_3C-CCl_3. The spectral measurements were made with the instruments and in the manner described previously.[21–24]

RESULTS AND DISCUSSION OF RESULTS

The infrared absorption spectra of gaseous and liquid ethyl chloride are shown in Figs. 1 and 2. The wave numbers of the observed absorption maxima are listed in Table I. The partly-resolved rotational structure of the band at 785 cm^{-1} in the spectrum of the gas is indicated in Table II. The Raman data for liquid ethyl chloride are given in Table III.

In Figs. 3 and 4 are shown the infrared absorption of gaseous and liquid 1,1-dichloroethane. The wave numbers of the observed absorption maxima or shoulders are listed in Table IV. The Raman data for this compound in the liquid state are presented in Table V.

If the lower resolution and narrower spectral region of the previous infrared data are considered, the agreement with the present data is as close as could be expected. The previous and present Raman frequencies for $H_3C-CHCl_2$ agree within the experimental error, except that the Raman shift[5] of 439 cm^{-1} was not verified and the weak band observed by Wagner at 1238 cm^{-1} was observed at 1244 cm^{-1}. In addition, five new

* A part of this work has been supported by the U. S. Atomic Energy Commission under Contract No. AT-(40-1)-1074.

† Present address; Harrison M. Randall Laboratory of Physics, University of Michigan, Ann Arbor, Michigan.

[1] P. C. Cross and Farrington Daniels, J. Chem. Phys. **1**, 48 (1933).
[2] R. Mecke and O. Vierling, Z. Physik **96**, 559 (1935).
[3] B. Timm and R. Mecke, Z. Physik **98**, 363 (1935).
[4] O. Vierling and R. Mecke, Z. Physik **99**, 204 (1936).
[5] A. Dadieu and K. W. F. Kohlrausch, Sitz. ber. Akad. Wiss. Wien, **138**, 635 (1929); **139**, 717 (1930); Monatsh. Chem. **55**, 58 (1930); **57**, 488 (1931).
[6] J. Söderquist, Z. Physik **59**, 446 (1930).
[7] C. D. Cleeton and R. T. Dufford, Phys. Rev. **37**, 362 (1931).
[8] W. West and M. Farnsworth, Trans. Faraday Soc. **27**, 145 (1931).
[9] W. D. Harkins and R. Haun, J. Am. Chem. Soc. **54**, 2920 (1932).
[10] J. Wagner, Z. physik. Chem. **B40**, 439 (1938), **B45**, 69 (1939).
[11] V. Tatevskij, J. Phys. Chem. (U.S.S.R.) **20**, 129 (1946).
[12] J. W. Linnett, Trans. Faraday Soc. **36**, 527 (1940).
[13] See J. Gordon and W. F. Giauque, J. Am. Chem. Soc. **70**, 1506 (1948).
[14] N. Sheppard, J. Chem. Phys. **17**, 79 (1949).
[15] G. Emschwiller and J. Lecomte, J. phys. radium **8**, 130 (1937).
[16] H. W. Thompson and P. Torkington, Proc. Roy. Soc. (London) **A184**, 21 (1945); Trans. Faraday Soc. **42**, 432 (1946).
[17] M. Pestemer, Sitz. ber. Akad. Wiss. Wien, **134**, 667 (1930); Monatsh. Chem. **57**, 469 (1931).
[18] K. W. F. Kohlrausch and F. Köppl, Sitz. ber. Akad. Wiss. Wien **143**, 537 (1934); Monatsh. Chem. **65**, 185 (1935).
[19] B. M. Bishui, Indian J. Phys. **22**, 319 (1948).
[20] Landolt-Börnstein, *Zahlenwerte und Funktionen, I. Atom- und Molekularphysik* (Springer, Berlin-Göttingen-Heidelberg, 1951), sixth edition, part 2, p. 247.
[21] Nielsen, Crawford, and Smith, J. Opt. Soc. Am. **37**, 296 (1947).
[22] Smith, Nielsen, and Claassen, J. Chem. Phys. **18**, 326 (1950).
[23] Smith, Brown, Nielsen, Smith, and Liang, J. Chem. Phys. **20**, 473 (1952).
[24] Nielsen, Liang, and Smith, J. Chem. Phys. **20**, 1090 (1952).

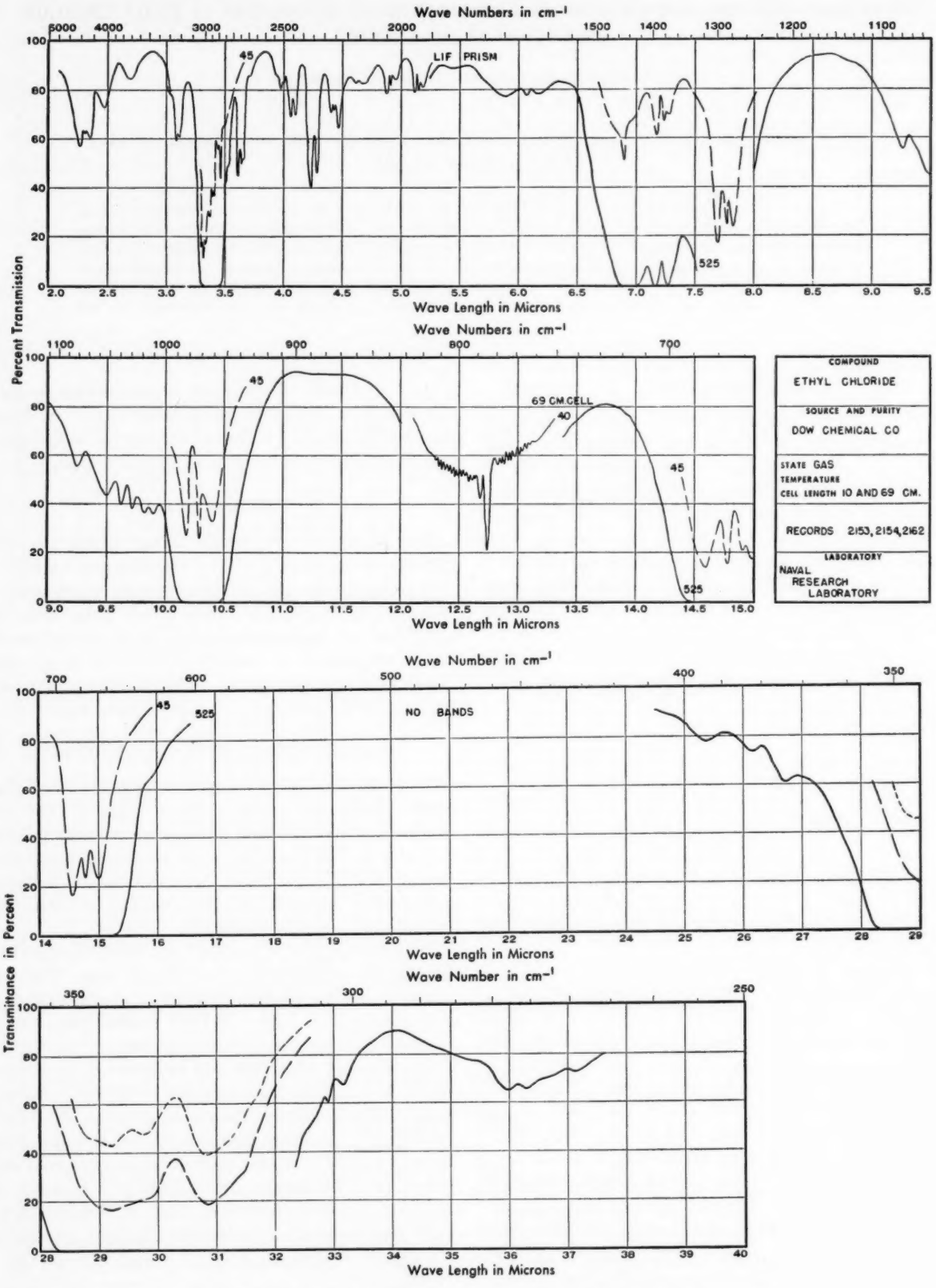

FIG. 1. Infrared absorption spectrum of gaseous H_3C-CH_2Cl.

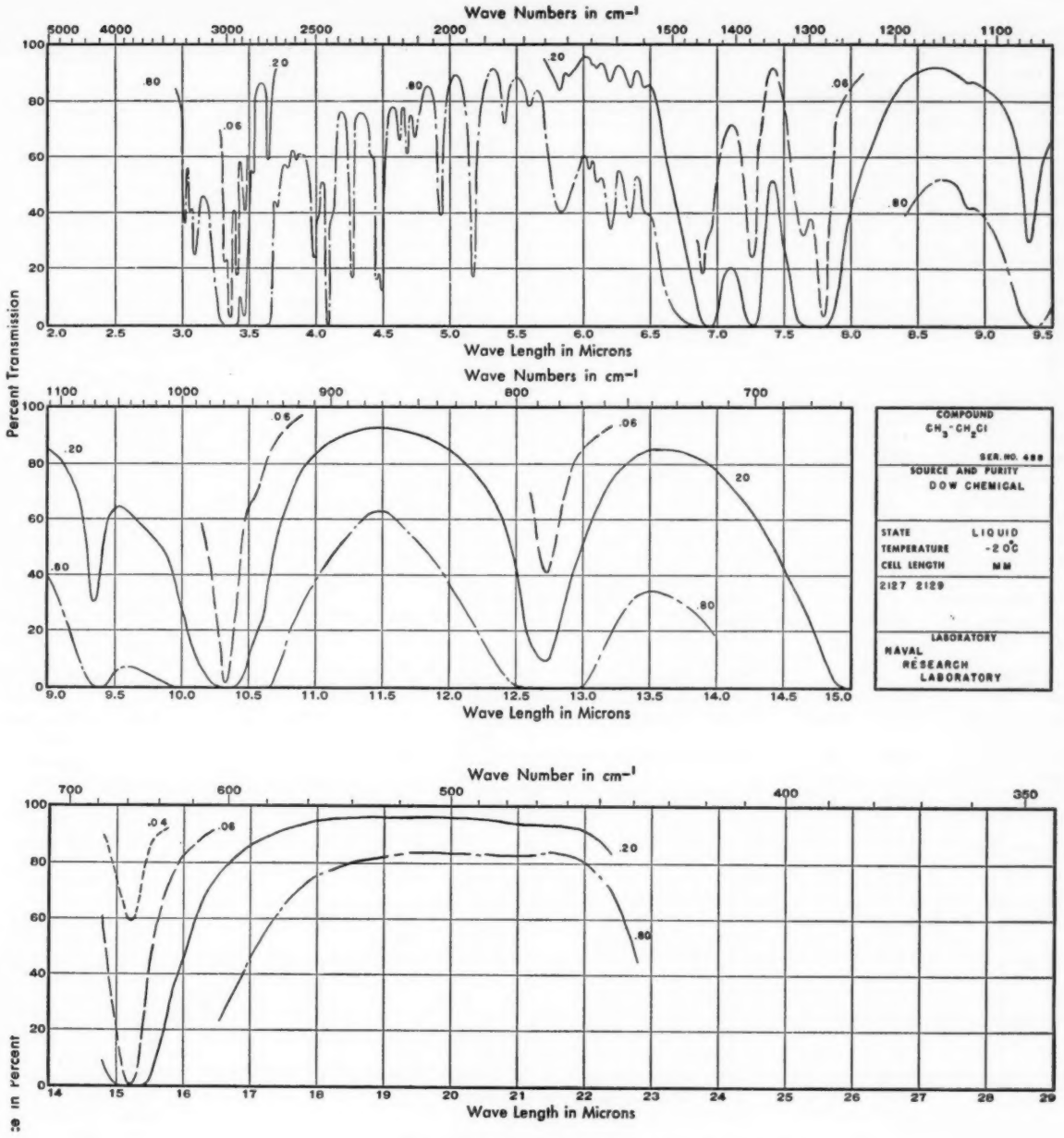

FIG. 2. Infrared absorption spectrum of liquid H_3C-CH_2Cl.

Raman bands were observed for H_3C-CH_2Cl in the present work. For $H_3C-CHCl_2$ more than a dozen new Raman shifts were found. However, the shifts of 168, 905, 1352, and 3072 cm^{-1}, reported by Bishui,[19] were not observed. The present results agree more closely with those of the Austrian workers,[17,18] than with the more recent data of Bishui.[19]

INTERPRETATION

1. H_3C-CH_2Cl

This molecule undoubtedly has the symmetry C_s, and the 18 normal vibrations consist of 11 of species a' and seven of species a''. Assuming the atomic distances C—H 1.09, C—C 1.54, and C—Cl 1.77A, and the value 110° for the C—C—Cl angle and tetrahedral values for the H—C—H and C—C—H angles, we obtain the following moments of inertia: 27.2, 150.1, and 166.7 $\times 10^{-40}$ g cm^2, the axis of smallest moment making an angle of 43° 14′ with the C—C bond. The range of the curves given by Badger and Zumwalt[25] is too narrow to permit a prediction of the contours of the infrared bands. However, since the molecule is approximately a symmetrical top, the theory of Gerhard and Dennison[26]

[25] R. M. Badger and L. R. Zumwalt, J. Chem. Phys. 6, 711 (1938).
[26] S. L. Gerhard and D. M. Dennison, Phys. Rev. 43, 197 (1933).

TABLE I. Infrared spectrum of ethyl chloride.

Gas Wave number	Gas Description	Liquid Wave number	Liquid Description	Interpretation[a]
269				
276	w			a'' fundamental
278				
302				
304	vvw			impurity?
307				
324				
336	vs			a' fundamental
342				$676-336=340\ A'$
375				
382	vw			impurity?
394				
667				
671				
676	vs	659	vs	a' fundamental
685				
785	m	786	s	a'' fundamental
		946	w	$(276+667=943\ A'')$
962				
972	vs	968	vs	$a'+a''$ fundamentals
983				
1012	w			$336+676=1012\ A'$
				$(1287-276=1011\ A'')$
1019	w			impurity
1029	w			impurity
1039	w			$1383-336=1047\ A'$, or impurity
1053	w			$276+785=1061\ A''$
1080	w	1072	m	a' fundamental
1135	vvw	1126	vvw	$336+785=1121\ A'$
1277				
1287	vs	1280	vs	a' fundamental
1299				
		1307	s	$336+972=1318$
1375				
1383	vs	1376	s	a' fundamental
1393				
1440		1435	m	
1452	vs	1456	s	$2a'+a''$ fundamentals
1465				
		1553	w	$276+1287=1563\ A''$
		1572	w	$2\times785=1570\ A'$, $336+1244=1580\ A''$
1620	vw	1613	w	$336+1287=1623\ A'$
1645	vw	1634	vvw	$676+972=1648$, $(667+972=1639)$
1694		1695	vvs	$276+1433=1709\ A'$
		1712	w	$336+1383=1719\ A'$
		1790	vvw	$336+1456=1792$
		1846	vw	$785+1080=1865\ A'$?

Gas Wave number	Gas Description	Liquid Wave number	Liquid Description	Interpretation[a]
1933				
1942	vw	1932	w	$2\times972=1944\ A'$
1952				
2025				
2034	vw	2028	w	$785+1244=2029\ A''$
2047				
		2112	vw	$(667+1456=2123)$
2130		2135	vw	
2160		2162	vw	$785+1383=2168\ A'$
2237	w	2231	w	$785+1456=2241$
2256	vw	2243	w	$972+1287=2259$
2266	vw	2265	vvw	
2337	m			$1080+1244=2324\ A''$
		2343	w	$972+1383=2355$
2360	m			$1080+1287=2367\ A'$
		2418	vw	$972+1456=2428$
2443	w	2442	w	
2462	w			$1080+1383=2463\ A'$
		2491	vvw	$2\times1244=2488\ A'$
2500				
2514	vw	2509	vw	$1080+1433=2513\ A''$
2538				
		2597	vvw	$2\times1287=2574\ A'$
		2642	vvw	$1244+1383=2627\ A''$
				$1287+1383=2670\ A'$
		2695	vvw	$1244+1456=2700$
2740				
2747	w	2736	w	$1287+1456=2743$
2761				
2840	w	2834	m	$1383+1456=2839$
2852	w			$2\times1433=2866\ A'$
2878	m			a'' fundamental
2890	s	2886	s	a' fundamental
2908				
2935	s	2932	s	a' fundamental
3945				
2958				
2983	s	2985	vs	a' fundamental
2998				
3012	s	3010	s	a'' fundamental
3206	w			$276+2935=3211\ A''$, $336+2890=3214\ A'$
3234	w	3231	vw	$336+2890=3226\ A'$
		3262	vvw	$276+2983=3259\ A''$, $336+2935=3271\ A'$
3311	vvw	3311	vw	$336+2983=3319\ A'$
3704	vw			$785+2935=3720\ A'$
4032	vw			$1080+2935=4015\ A'$
4255	w			$1244+3012=4256\ A'$, $1383+2878=4261\ A''$
4348	w			$1456+2890=4346$
4425	w			$1456+2983=4439$

[a] Wave numbers enclosed in parentheses are for the liquid state.

can be applied to estimate the infrared band contours. Parallel bands should have a *PQR* structure with a *PR* separation of 19.5 cm^{-1}, and the intensity of the *Q* branch should be about 13 percent of the total intensity of the band. Perpendicular bands should be considerably broader and should not exhibit three maxima. Fundamentals of species a'' should give rise to perpendicular bands, and fundamentals of species a' should have contours intermediate between those of parallel and perpendicular bands.

The three a' and two a'' fundamentals associated with C−H stretching are readily identified by their spectral positions and high intensities in both spectra. Because of the low resolution in the infrared, the assignment of species must be based entirely on Raman depolarization ratios. The intense Raman bands at 2965, 2932, and 2881 cm^{-1} (in liquid H_3C-CH_2Cl) are definitely polarized and are interpreted as a' fundamentals involving asymmetrical C−H stretching of the methyl group and symmetrical C−H stretching of the methyl and the methylene groups. The very strong depolarized Raman band at 2980 cm^{-1} and the strong diffuse Raman band at 2872 cm^{-1} are identified as a'' fundamentals involving asymmetrical CH_3 and CH_2 stretch-

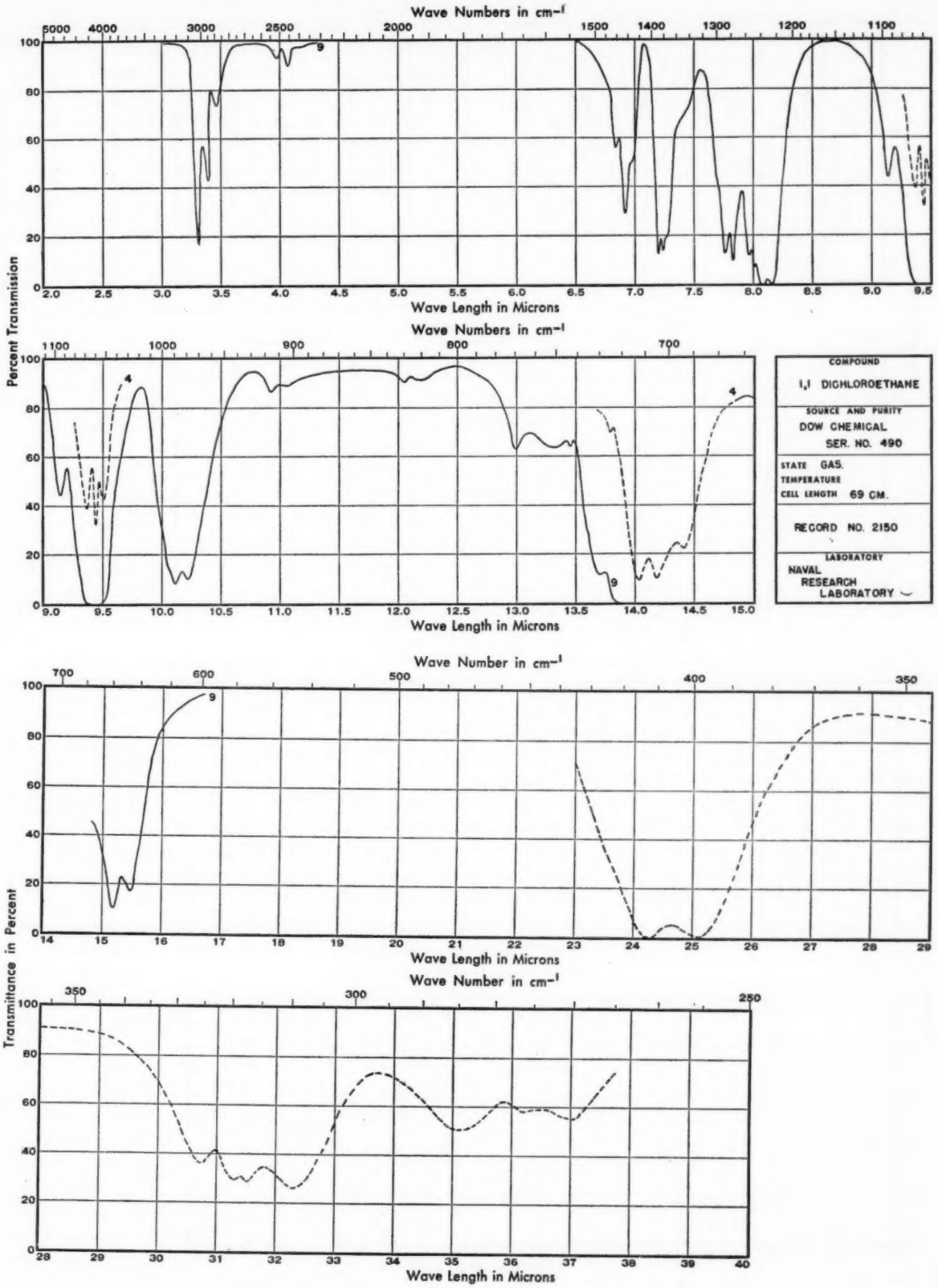

FIG. 3. Infrared absorption spectrum of gaseous $H_3C-CHCl_2$.

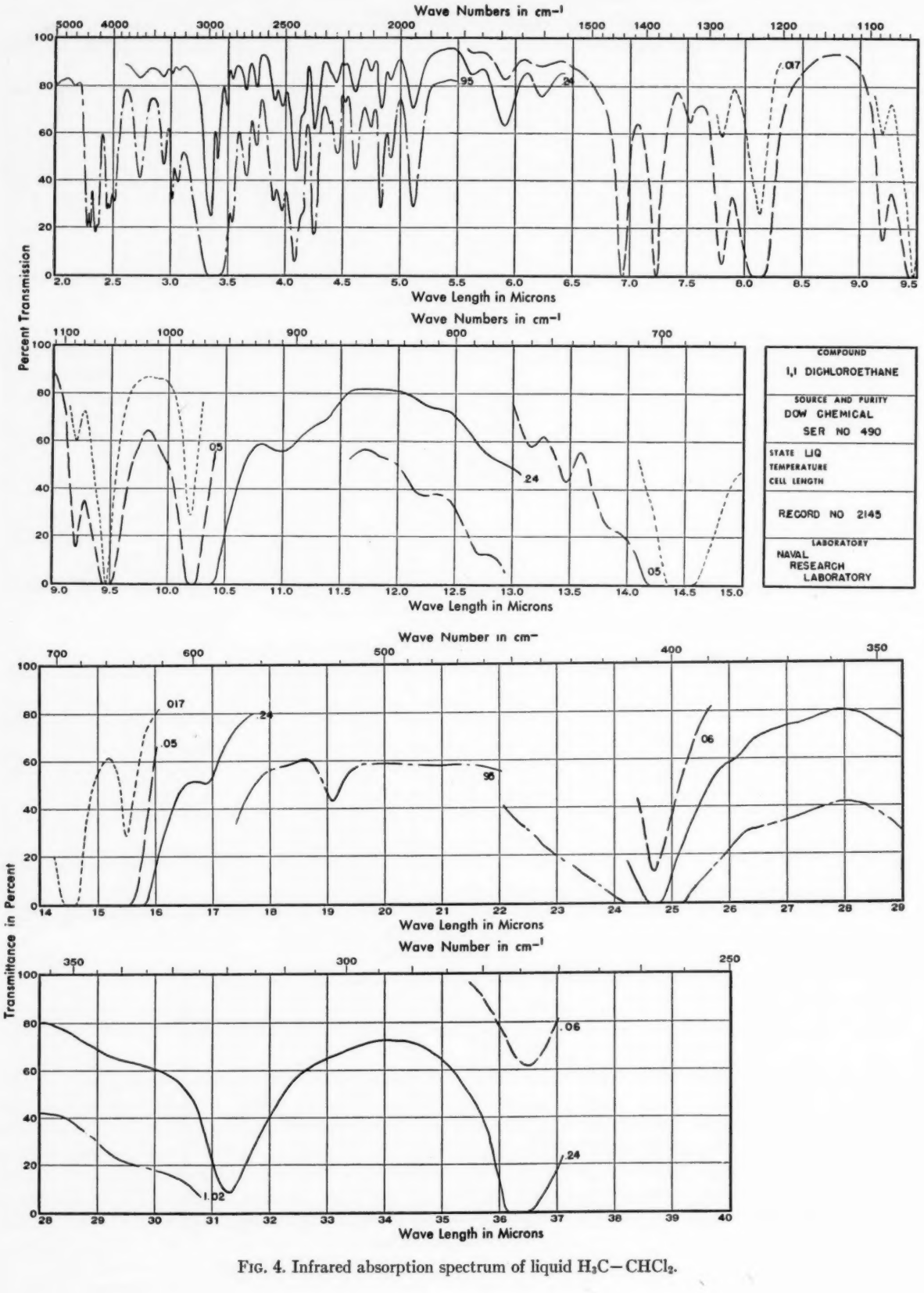

FIG. 4. Infrared absorption spectrum of liquid $H_3C-CHCl_2$.

ing. The a' and a'' fundamentals associated with asymmetrical methyl deformation and the a' fundamental associated with methylene deformation are not separated in either spectrum. In the infrared spectrum of gaseous H_3C-CH_2Cl they appear as a broad band with a single sharp peak at 1452 cm^{-1}. In the Raman spectrum of the liquid they appear as a broad, slightly polarized band which, with 4046A excitation, is barely separated into 2 components with maxima at approximately 1442 and 1450 cm^{-1}. The weak, sharp Raman band and the strong, parallel-type infrared band at 1383 cm^{-1} are interpreted as an a' fundamental involving largely symmetrical methyl deformation.

The very intense parallel-type infrared band at 1287 cm^{-1} in gaseous H_3C-CH_2Cl, and the medium, polarized Raman band at 1280 cm^{-1} in the liquid, are interpreted as an a' fundamental involving largely CH_2 wagging. The depolarized Raman band at 1245 cm^{-1} seems too strong to represent the combination 276+968 =1244 and is, therefore, interpreted as an a'' fundamental. It probably involves mostly CH_2 twisting.

The very strong, polarized Raman band at 1071 cm^{-1}, which has only a weak counterpart in the infrared, undoubtedly represents an a' fundamental. It probably involves largely a rocking of the methyl group in the molecular symmetry plane. The moderately polarized and fairly diffuse Raman band at 968 cm^{-1}, and the very intense parallel-type infrared band observed at 972 cm^{-1} in gaseous H_3C-CH_2Cl are identified with an a' fundamental associated with a skeletal motion involving C—C stretching.

The broad infrared band at 785 cm^{-1}, which has a contour rather similar to that of the band at 810 cm^{-1} in the infrared spectrum of H_3C-CH_2F, is interpreted as an a'' fundamental involving largely CH_2 rocking. This fundamental has not been observed in the Raman spectrum, while it was observed in H_3C-CH_2F, though with very low intensity.[27]

In the region from about 800 to 1100 cm^{-1} there should lie another a'' fundamental associated largely with CH_3 rocking. No conclusive evidence for this fundamental has been found. However, it is tentatively assumed that it coincides approximately with the a' fundamental at 968 cm^{-1}. This assumption explains the appearance and the rather high observed depolarization ratio of the Raman band at this wave number.

The intense, strongly polarized Raman band at 657 cm^{-1} undoubtedly represents an a' fundamental. It must correspond to a motion of the C—C—Cl skeleton involving largely C—Cl stretching. The polarized Raman band at 335 cm^{-1} is interpreted as an a' fundamental involving bending of the C—C—Cl angle.

The last a'' fundamental is tentatively identified with the weak infrared band observed at 276 cm^{-1} with KRS-5 prism. It corresponds largely to a torsional motion of the methyl group.

[27] Smith, Saunders, Nielsen, and Ferguson, J. Chem. Phys. **20**, 847 (1952).

TABLE II. Rotational structure of 785 cm^{-1} infrared band of ethyl chloride.

762.2 cm^{-1}	793.3 cm^{-1}
763.9	795.0
765.6	796.7
767.5	798.7
769.1	800.3
770.8	802.2
772.7	804.0
774.1	805.9
776.0	807.6
777.7	809.1
779.5	811.4
784.9	812.5
789.3	814.0
791.5	816.0

The fundamental vibrational frequencies assigned for methyl chloride are listed in Table VI. On the basis of these assignments it has been possible to interpret all of the observed Raman bands and all but five or six very weak infrared absorption maxima. The interpretations of the spectra are given in the last columns of Tables I and III.

2. $H_3C-CHCl_2$

This molecule undoubtedly also has a symmetry C_s, and hence 11 normal vibrations of species a' and seven of species a''. Assuming the atomic distances C—H 1.09, C—C 1.54 and C—Cl 1.76A, the values 112° for the Cl—C—Cl angle and 110° for the C—C—Cl angle, and tetrahedral values for the H—C—H and C—C—H angles, we obtain 125.7, 261.5, and 364.5×10^{-40} g cm^2 for the principal moments of inertia. The symmetry plane contains the largest and the intermediate axes of inertia, the latter making an angle of 22° 33′ with the C—C bond. According to the theory of Badger and Zumwalt,[25] the PR separation should be 14.1 cm^{-1} for type A bands and 11.3 cm^{-1} for bands of types B and C. Bands of species a'' should have type A contours, while bands of species a' should have contours intermediate between types B and C.

TABLE III. Raman spectrum of $H_3C—CH_2Cl$ (liquid).

Wave number	Description	Depolarization	Exciting Hg lines	Interpretation
335	s, sh	0.30	$\pm e$	a' fundamental
657	vs, sh	0.10	*efgki*	a' fundamental
968	m, d	0.72	*e*	$a'+a''$ fundamentals
1071	s, sh	0.09	*ek*	a' fundamental
1245	w, d	0.85	*e*	a'' fundamental
1280	w, sh	0.30	*e*	a' fundamental
1382	vvw		*e*	a' fundamental
~1442	m, d	0.78	*ek*	$2a'+a''$ fundamentals
~1450	m, d			
2737	w	0.17	*e*	$2\times1382=2764\ A'$
2872	m, d		*ek*	a'' fundamental
2881	s, sh	0.12	*eki*	a' fundamental
2897	w, sh	p	*ek*	$2\times1442=2884\ A'$
2913	w, sh	p	*ek*	$2\times1450=2900\ A'$
2932	vs, sh	0.2	*eki*	a' fundamental
2965	vs, sh	0.3	*eki*	a' fundamental
2980	s, d	dp	*ek*	a'' fundamental

TABLE IV. Infrared spectrum of 1,1-dichloroethane.

Gas Wave number	Gas Description	Liquid Wave number	Liquid Description	Interpretation[a]
270	s			
277	s	274	vs	a' fundamental
285	s			
309	s			
317	s	318	vs	a'' fundamental
320	s			
325	s			
397	s			
412	s	405	vs	a' fundamental (405)
		524	w	(239+275=514 A'') CH_3CCl_3 impurity
		592	m	(317+275=592 A'')
646	s			
656	s	647	s	a' fundamental (652)
694	s			
705	s	691	vvs	a'' fundamental
713	s			
726	m	~720	m	317+405=722 A'' (318+405=723 A'')
730	m			
744	w	742	m	1058−317=741 A'
~752	w			988−239=749 A''
		759	m	
770	w			1094−317=777 A'' (1087−317=770 A')
		~785	m	(1056−275=781 A'')?
~822	vw	817	w	2×405=810 A'?
830	vw			1239−405=834 A''?
		880	vw	(239+645=884 A'')
904	vw			
917	vw	912	w	277+652=929 A' (275+645=920 A')
976	s			
988	s	981	vs	a' fundamental
993	m			
1051	vs			
1058	vs	1054	vs	a'' fundamental
1068	vs			
1094	m	1086	s	a' fundamental
1228	s			
1239	s	1230	vs	a'' fundamental
1247	m			
1255	m			277+988=1265 A'
1277	s	1280	s	a' fundamental
1287	s			
		1328	m	(275+1056=1331 A'') (239+1086=1325 A'')
1372	m			
1380	s	1383	s	a' fundamental
1385	s			
1435	m			
1445	s	1441	s	$a'+a''$ fundamentals
1462	m			405+1058=1463 A''
		1605	w	(317+1280=1597 A'') (239+1381=1620 A'')
		1692	w	(645+1058=1703 A'')
		1779	vw	(690+1087=1777 A'')
		1957	w	(2×980=1960 A')
		2032	w	(980+1055=2035 A''); (645+1382=2027 A')
		2070	w	(690+1382=2072 A''); (980+1087=2067 A')
		2105	vw	(2×1055=2110 A')
		2169	w	(2×1087=2174 A')
		2212	vvw	(980+1229=2209 A'')
		2248	vw	(980+1280=2260 A')
		2278	vw	(1055+1229=2284 A')
		2352	w	(980+1382=2362 A'); (1087+1280=2367 A')
		2410	w	(980+1442=2422)
2460	vw	2445	m	2×1238=2478 A'; (2×1229=2458 A') 1058+1380=2438 A'' (1055+1382=2437 A'')
2506	vw	2512	w	1058+1443=2501 (1229+1287=2516 A'')
		2558	w	(2×1280=2560 A')
		2668	vw	(1229+1442=2671) (1280+1382=2662 A')
		2732	vw	(1280+1442=2722)
		2825	vw	(1382+1442=2824)
2873	w	2865	w	a' fundamental
2941	m	2932	m	a' fundamental
		2986	m	a'' fundamental
3012	s			a' fundamental
		3258	vvw	(275+2989=3264 A'') (318+2936=3254 A'') (239+3008=3247 A'')?
		3312	vvw	(318+3008=3326 A'') (318+2989=3307 A')
		3397	vw	(405+2989=3394 A'')
		3658	vw	(645+3008=3653 A')
		3995	w	(1056+2936=2992 A'') (980+3008=2988 A') (1087+2936=4023 A')
		4049	w	(1056+3008=4064 A'') (1056+2989=4045 A')
		4082	w	(1229+2865=4094 A'') (1087+3008=4095 A') (1087+2989=4076 A'')
		4220	w	(1229+2989=4218 A') (1229+3008=4237 A'') (1280+2936=4216 A')
		4259	w	(1280+2989=4269 A'') (1382+2865=4247 A')
		4339	w	(1382+2936=4318 A') (1442+2865=4307) (1382+2989=4371 A'')
		4386	w	(1382+3008=4390 A') (1442+2936=4378)

[a] Wave numbers for the liquid state are enclosed in parentheses.

The four highest fundamentals, associated with C—H stretching, are readily assigned on the basis of the Raman spectrum alone. The bands at 3008 and 2986 cm^{-1} lie too close together to permit separate measurements of their depolarization ratios. However, it appears that the former belongs to a' and the latter to a''. These bands are not resolved in the infrared. The very intense polarized Raman band at 2935 cm^{-1} is certainly an a' fundamental, as is undoubtedly the weaker band at 2865 cm^{-1}.

The strong, diffuse, and almost depolarized Raman band at 1442 cm^{-1} is interpreted as a superposition of a' and a'' fundamentals associated with asymmetrical deformation of the methyl group. Their overtones, at

TABLE V. Raman spectrum of $H_3C-CHCl_2$ (liquid).

Wave number	Description	Depolarization	Exciting Hg lines	Interpretation
239	vw		$\pm e$	a'' fundamental
275	vs, sh	0.58	$\pm ef$	a' fundamental
318	m	0.86	$\pm e$	a'' fundamental
367	vvw, sh		e	
405	vs, sh	0.25	$\pm efk$	a' fundamental
523	vvw, sh		e	CH_3CCl_3 impurity
643	vvs, sh	0.12	$\pm efgki$	a' fundamental
689	s, d	0.85	$\pm ek$	a'' fundamental
980	m, sh	0.55	ef	a' fundamental
1056	m	0.83	e	a'' fundamental
1088	m, sh	0.35	e	a' fundamental
1227	m, d	0.74	e	a'' fundamental
1279	m, sh	0.45	e	a' fundamental
1382	w, sh	p	e	a' fundamental
1442	s	0.83	e	$a'+a''$ fundamentals
1699	vw, d		e	$643+1056=1699$ A''
1914	vvw		e	$689+1227=1916$ A'
1956	vvw		e	$2\times980=1860$ A'
2358	vvw		e	$1088+1279=2367$ A'
2439	vw, d		e	$1056+1382=2438$ A''
2450	vw		e	$2\times1227=2454$ A'
2740	w, sh		e	$2\times1382=2764$ A'
2865	m, sh	0.2	ek	a' fundamental
2881	vw, sh		e	$2\times1442=2884$
2895	vw, sh		e	
2935	vvs, sh	0.15	eki	a' fundamental
2990	vs	dp	eki	a'' fundamental
3008	s	p	ek	a' fundamental
3253	vvw, d		e	$2990+275=3265$ A''

2881 and 2895 cm^{-1}, are well separated. The polarized band at 1382 cm^{-1}, and the infrared counterpart which appears to have a *PQR* contour with a *PR* separation of 13 cm^{-1}, undoubtedly represent an a' fundamental involving symmetrical methyl deformation. Its overtone shows the usual anharmonicity.[28]

The bands at 1282 and 1239 cm^{-1} are interpreted as an a' and an a'' fundamental, respectively. The former has a doublet contour with separation 10 cm^{-1} in the infrared and is polarized in the Raman effect. The contour of the latter is not well resolved in the infrared because of too strong absorption, but it appears to have a *PQR* structure with a *PR* separation of 19 cm^{-1}. Its rather low observed depolarization ratio is undoubtedly a result of overlapping with the 2991 and 3008 cm^{-1}

[28] See reference 23, p. 484.

TABLE VI. Fundamental vibrational frequencies for H_3C-CH_2Cl.

Symmetry species	Infrared (gas)	Wave number Infrared (liquid)	Raman (liquid)	Approximate character
a''	276 w			Torsion
a'	336 vs		335 s	C—C—Cl bending
a'	676 vs	659 vvs	657 vs	C—Cl stretching
a''	785 m	786 vs		CH_2 rocking
$a'+a''$	972 vs	968 vs	968 m	C—C stretching, CH_3 rocking
a'	1080 w	1072 w	1071 s	CH_3 rocking
a''			1245 w	CH_2 twisting
a'	1287 vs	1280 vvs	1280 w	CH_2 wagging
		1308 s		
a'	1383 vs	1376 vs	1382 vvw	CH_3 symmetrical deformation
		~1455 shoulder	1442	
$2a'+a''$	1452 vs	1456 vs	1450 m	CH_2 and CH_3 deformation
a''	2878 m		2872 m	C—H stretching
		2886 s		
a'	2890 s		2881 s	
a'	2940 s	2932 s	2932 vs	
a'	2983 s	2985 s	2965 vs	
a''	3012 s	3010 s	2980 s	

bands excited by the 4047A mercury line. These fundamentals are associated with C—H bending, probably mostly in the $CHCl_2$ group.

The polarized Raman band at 1088 cm^{-1} and the depolarized band at 1056 cm^{-1} undoubtedly represent an a' and an a'' fundamental, respectively. The infrared contour of the former is not well resolved. The latter has a *PQR* contour with a *PR* separation of 17 cm^{-1}. These fundamentals probably involve largely methyl rocking.

The four polarized Raman bands at 980, 643, 405, and 275 cm^{-1} all correspond to strong infrared bands with doublet or *PQR* contours with separations equal to or only slightly larger than predicted for types *B* and *C* bands. They must be interpreted as a' fundamentals.

TABLE VII. Fundamental vibrational frequencies for $H_3C-CHCl_2$.

Symmetry species	Infrared (gas)	Wave number Infrared (liquid)	Raman (liquid)	Approximate character
a''			239	Torsion
a'	277 s	274 vs	275 vs	CCl_2 rocking
a''	317 s	318 vs	318 m	CCl_2 wagging or twisting
a'	405 s	405 vs	405 vs	CCl_2 deformation
a'	651 s	647 s	643 vvs	CCl stretching
a''	705 s	691 vvs	689 s	CCl stretching
a'	982 s	981 vs	980 m	CC stretching
a''	1058 vs	1054 vs	1056 m	CH_3 rocking
a'	1094 m	1086 s	1088 m	CH_3 rocking
a''	1239 s	1230 vs	1227 m	CH bending
a'	1282 s	1280 s	1279 m	CH bending
a'	1383 s	1383 s	1382 w	CH_3 deformation
$a'+a''$	1445 s	1441 s	1442 s	CH_3 deformation
a'	2873 w	2865 w	2865 m	CH stretching
a'	2941 m	2932 m	2935 vvs	CH_3 stretching
a''		2986 m	2990 vs	CH_3 stretching
a'	3012 s		3008 s	CH_3 stretching

The bands at 689 and 318 cm^{-1}, which are depolarized in the Raman spectrum and have *PQR* contours with *PR* separations of about 19 and 16 cm^{-1}, respectively, in the infrared, undoubtedly represent a'' fundamentals. These six fundamentals are associated with motions of the $C-C-Cl_2$ skeleton. The three highest involve mainly C—C and C—Cl stretching, and the three lowest C—C and C—Cl bending.

The remaining a'' fundamental is tentatively identified with the faint Raman band at 439 cm^{-1}. It involves largely a twisting of the methyl group.

The fundamental frequencies assigned for 1,1-dichloroethane are given in Table VII. On the basis of these frequencies, all but one of the observed Raman bands and all but two or three of the infrared absorption maxima have been satisfactorily interpreted. The interpretations are given in the last columns of Tables IV and V.

DISCUSSION

Eight of the frequencies assigned here as fundamentals for H_3C-CH_2Cl are so assigned by Landolt-Börnstein,[20] two of them, however, with different species. Except for a change in the value of one of the a'' fundamentals from 1030 to 1245 cm^{-1}, and except for the fact that Sheppard did not assign the lowest a'' fundamental, the present assignments for H_3C-CH_2Cl are essentially the same as those given by Sheppard.[14] The 13 fundamental vibrational frequencies for $H_3C-CHCl_2$, and the species assignments for 6 of these, given by Landolt-Börnstein,[21] are verified by the present work.

It may be of interest to point out that for $H_3C-CHCl_2$ the average observed *PR* separation for fundamental infrared bands of species a' is about 10 percent, and the average separation for a'' fundamentals is about 20 percent larger than the predicted value. This indicates that the assumed molecular dimensions and configuration may be somewhat in error.

The assigned fundamental vibrational frequencies for H_3C-CH_2Cl and $H_3C-CHCl_2$ are plotted and correlated with those of ethane[29] and H_3C-CCl_3[30] in Fig. 5. Solid vertical lines denote infrared bands, broken vertical lines denote Raman bands, and dash-dotted lines denote frequencies that are inactive in both spectra. Coinciding infrared and Raman bands are indicated by slightly separated lines. The height of each vertical line roughly indicates the intensity of the band. The slanting correlation lines in Fig. 5 are drawn according to vibrational species, solid lines being used to denote totally symmetric fundamentals. No solid (or broken) lines connecting the fundamentals of a molecule of symmetry C_s with those of the corresponding, more symmetrical molecule may cross. The correlation lines do not in general connect like "group frequencies." The regularity of the correlation diagram supports the assignments made.

THERMODYNAMIC FUNCTIONS

From the fundamental vibrational frequencies listed in Tables VI and VII, and from the molecular dimensions and moments of inertia listed above, the heat capacity, entropy, Gibbs free-energy function, and heat-content function have been calculated for H_3C-CH_2Cl and $H_3C-CHCl_2$ as ideal gases at 1 atmos. pressure and at different temperatures. The contributions from the lowest a'' fundamental or torsional

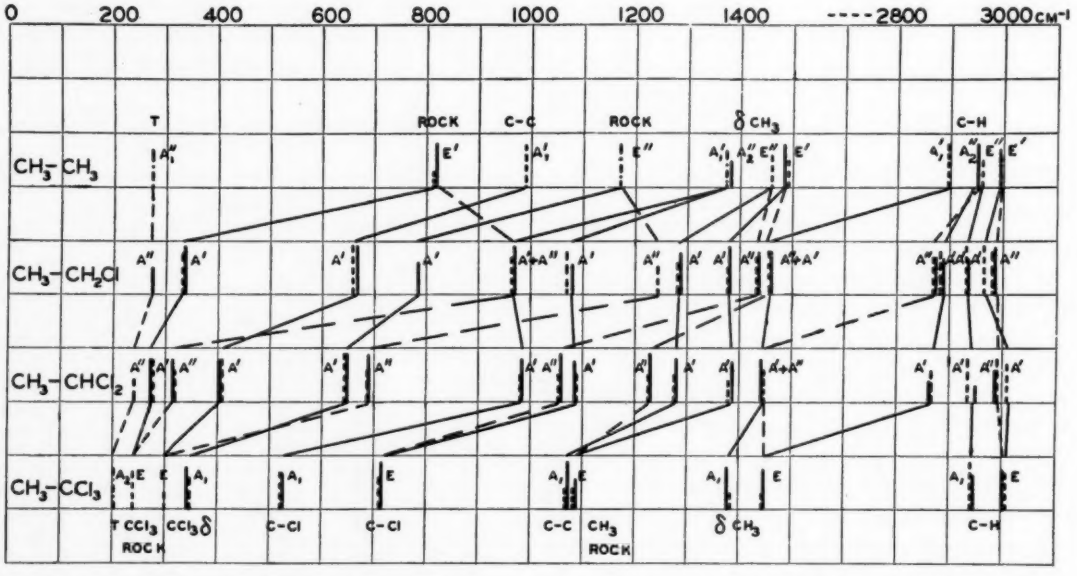

FIG. 5. Fundamental vibrational frequencies of H_3C-CH_3, H_3C-CH_2Cl, $H_3C-CHCl_2$, and H_3C-CCl_3.

[29] L. G. Smith, J. Chem. Phys. **17**, 139 (1949).
[30] See reference 23. See also P. Venkateswarlu, J. Chem. Phys. **19**, 293 (1951), and El-Sabban, Meister, and Cleveland, J. Chem. Phys. **19**, 855 (1951).

TABLE VIII. Calculated thermodynamic functions for H_3C-CH_2Cl at one atmosphere (in cal M^{-1} deg^{-1}).

T°K		$(H^0-H_0^0)/T$	C_p^0	S^0	$-(F^0-H_0^0)/T$
	Tr.+Rot.	7.949	7.949	55.490	47.541
134.46	Vib.	0.218	0.875	0.276	0.058
(mp)	Tor.	0.331	1.057	0.437	0.109
	Total	8.50	9.88	56.20	47.71
	Tr.+Rot.	7.949	7.949	58.639	50.690
200	Vib.	0.628	2.153	0.842	0.214
	Tor.	0.658	1.550	0.956	0.303
	Total	9.24	11.65	60.44	51.21
	Tr.+Rot.	7.949	7.949	61.471	53.522
285.36	Vib.	1.430	4.589	1.993	0.563
(bp)	Tor.	0.979	1.907	1.570	0.592
	Total	10.36	14.44	65.03	54.68
	Tr.+Rot.	7.949	7.949	61.819	53.870
298.16	Vib.	1.575	5.008	2.204	0.629
	Tor.	1.023	1.947	1.648	0.630
	Total	10.55	14.90	65.67	55.13
	Tr.+Rot.	7.949	7.949	64.155	56.206
400	Vib.	2.887	8.454	4.156	1.269
	Tor.	1.283	2.152	2.262	0.975
	Total	12.12	18.56	70.57	58.45
	Tr.+Rot.	7.949	7.949	65.929	57.980
500	Vib.	4.323	11.614	6.389	2.066
	Tor.	1.469	2.216	2.748	1.287
	Total	13.74	21.78	75.07	61.33
	Tr.+Rot.	7.949	7.949	67.378	59.429
600	Vib.	5.772	14.352	8.755	2.983
	Tor.	1.593	2.180	3.152	1.561
	Total	15.31	24.48	79.28	63.97

TABLE IX. Calculated thermodynamic functions for CH_3CHCl_2 at 1 atmos. (in cal M^{-1} deg^{-1}).

T°K		$(H^0-H_0^0)/T$	C_p^0	S^0	$-(F^0-H_0^0)/T$
	Tr.+Rot.	7.949	7.949	61.769	53.820
176.46	Vib.	1.518	4.188	2.164	0.646
(mp)	Tor.	0.675	1.575	0.988	0.317
	Total	10.14	13.71	64.92	54.78
	Tr.+Rot.	7.949	7.949	65.938	57.989
298.16	Vib.	3.214	8.130	4.802	1.588
	Tor.	1.155	2.074	1.952	0.790
	Total	12.32	18.15	72.69	60.37
	Tr.+Rot.	7.949	7.949	66.756	58.808
330.46	Vib.	3.766	9.323	5.715	1.949
(bp)	Tor.	1.250	2.135	2.168	0.960
	Total	12.96	19.41	74.64	61.72
	Tr.+Rot.	7.949	7.949	68.274	60.325
400	Vib.	4.942	11.682	7.760	2.818
	Tor.	1.410	2.204	2.630	1.171
	Total	14.30	21.84	78.66	64.31
	Tr.+Rot.	7.949	7.949	70.084	62.135
500	Vib.	6.597	14.684	10.656	4.059
	Tor.	1.572	2.174	3.087	1.503
	Total	16.12	24.81	83.83	67.70
	Tr.+Rot.	7.949	7.949	71.497	63.548
600	Vib.	8.161	17.195	13.563	5.402
	Tor.	1.663	2.075	3.460	1.806
	Total	17.77	27.22	88.52	70.76
	Tr.+Rot.	7.949	7.949	72.723	64.774
700	Vib.	9.606	19.293	16.376	6.770
	Tor.	1.712	1.945	3.786	2.060
	Total	19.27	29.19	92.88	73.60

oscillation have been calculated in a manner described in a previous paper.[23] The height of the barrier opposing internal rotation was estimated by a previously described method[23] to be 4470 cal M^{-1} for H_3C-CH_2Cl and 3750 cal M^{-1} for $H_3C-CHCl_2$. The calculated thermodynamic data are listed in Tables VIII and IX. The calculated entropy 65.03 cal M^{-1} deg^{-1}, of H_3C-CH_2Cl at 285.36°K agrees fairly well with the value 65.31 obtained calorimetrically by Gordon and Giauque.[31] On the other hand, the calculated values of C_p^0 are considerably lower than those measured by Gordon and Giauque.[31]

ACKNOWLEDGMENT

The assistance of Mr. R. A. Saunders, Naval Research Laboratory, who obtained the infrared spectrum of liquid ethyl chloride, is gratefully acknowledged.

[31] J. Gordon and W. F. Giauque, J. Am. Chem. Soc. **70**, 1506, 4277 (1948).

Calculation of Ionization Potentials

J. L. FRANKLIN
Humble Oil and Refining Company, Baytown, Texas
(Received August 10, 1953)

Based upon a united atom model, it has been shown that the ionization potentials of complex molecules can be calculated from molecular orbitals formed from group or united atom orbitals. With this method ionization potentials have been calculated for a large number of paraffins, olefins, aromatics, alkyl halides, amines, and oxygen compounds. With a few exceptions, the agreement of calculated and measured values is excellent.

THE method of equivalent orbitals has been applied by Hall[1] and by Lennard-Jones and Hall[2] to calculations of the ionization potentials of normal paraffins with gratifying success. This method requires the solution of the secular equation

$$|e_{mn}-E\delta_{mn}|=0, \tag{1}$$

where m and n refer to the various bonds in the molecule. The roots of the secular equation represent the ionization potentials of the molecule, the lowest root being the ionization potential commonly measured.

Where the various equivalent orbitals refer to bonds and lone pairs of electrons, the number of terms in the secular equation becomes great with large molecules, and solution of the equation becomes very laborious. Recently Hall[3] has shown that for planar molecules having an orbital antisymmetric in the plane of the molecule considerable simplification of the equivalent orbital treatment of ionization potentials can be obtained. Such planar molecules can be divided into groups having characteristic orbitals and this, of course, greatly reduces the order of the secular equation that must be solved. Hall[4] has used this technique to calculate the ionization potentials of the methylethylenes with satisfactory results. He also attempted to calculate the ionization potentials of the chloroethylenes, but with considerably less success; the poorer results in this case may well be attributable, at least in part, to experimental inaccuracies, however.

The wave function of a molecule can be assumed to contain components of both separated atom and united atom wave functions. The separate atom wave function is useful in describing phenomena associated with bonds; the united atom wave function appears to be useful in describing interactions between saturated groups.

The methane united atom is neon with an electron configuration $1s^2$, $2s^2$, $2p_x^2 2p_y^2 2p_z^2$. Similarly, ethane is isoelectronic with F_2, propane with FOF, *n*-butane with FOOF, isobutane with NF_3, neopentane with CF_4, etc. These electromers have one or more p orbitals per united atom which can serve as π functions with respect to a particular bond and which can serve as the agent for interaction across the bond.

The united atom model of alkyl groups appears first to have been suggested by Burkhardt and Evans[5] and has been used by Matsen[6] to describe the effect of methyl substitution on benzene. Mulliken, Rieke, and Brown[7] have used a united atom approach in developing the concept of "hyperconjugation." They treat the three hydrogen atoms of a methyl group as an H_3 atom so that the methyl group resembles a —C≡N. The interaction with other groups is then described in terms of π-type orbitals on both the carbon and the united atom, H_3.

We will assume that in saturated hydrocarbons each carbon atom with its associated hydrogens can be treated as a united atom (F, O, N, etc.) and that high energy molecular orbitals can be formed from these united atom orbitals, taking one orbital from each united atom. The usual variational treatment then results in a secular determinant of order equal to the number of united atoms in the molecule. This will be much simpler than the treatment of Lennard-Jones and Hall based upon bond functions.

PARAFFINS AND CYCLOPARAFFINS

The secular equation for a molecule using group orbitals is

$$|e_{ij}-E\delta_{ij}|=0, \tag{2}$$

where the i and j refer to various groups in the molecule. In almost all instances it will be assumed that all interactions except those of adjacent groups are zero. Although the united atom treatment would suggest that different parameters should be used for the different groups (CH_3, CH_2, CH, and quaternary carbon) occurring in paraffin hydrocarbons, it will, nevertheless, be assumed as a first approximation that all e_{ij} in saturated hydrocarbons are equal, as are all interactions between first neighbors. All other interactions are taken as zero. The secular equation for 2-methylbutane is

[1] G. G. Hall, Proc. Roy. Soc. (London) **205A**, 541 (1951).
[2] J. Lennard-Jones and G. G. Hall, Discussions Faraday Soc. **10**, 18 (1951).
[3] G. G. Hall, Proc. Roy. Soc. (London) **213A**, 102 (1952).
[4] G. G. Hall, Trans. Faraday Soc. **49**, 113 (1953).
[5] G. N. Burkhardt and M. G. Evans, Mem. Proc. Manchester Lit. & Phil. Soc. **77**, 37 (1933).
[6] F. A. Matsen, J. Am. Chem. Soc. **72**, 5243 (1950).
[7] Mulliken, Rieke, and Brown, J. Am. Chem. Soc. **63**, 41 (1941).

illustrated as

$$\begin{vmatrix} e-E & & b & & \\ & e-E & b & & \\ b & b & e-E & b & \\ & & b & e-E & b \\ & & & b & e-E \end{vmatrix} = 0. \quad (3)$$

Following Hall's[3,4] treatment e was taken as a first approximation as the ionization potential of methane (13.04 v) as determined by Honig.[8] With this value and the ionization potential of ethane (11.76 v) b was found to be 1.28 volts. The ionization potentials of a number of paraffins were calculated using these constants, and the results are in fair agreement with the measured values. Above the butanes, however, the ionization potentials calculated in this way seem to be about 0.2 to 0.4 v higher than the experimental values.

In his treatment of the substituted ethylenes, Hall[4] included terms for secondary interactions of groups attached to the same carbon atom. These interaction terms were small, but would provide a means of correcting discrepancies in the same order as those found in this study of the paraffins. However, such secondary interaction terms greatly complicate the computation in the case of large molecules and a means of avoiding this was sought. In the case of the paraffins e and b were calculated from the secular equations for ethane and n-butane using the measured ionization potentials of these two compounds. The values of e and b found in this way are 13.31 and 1.55 v, respectively. With these constants, the ionization potentials of the paraffins were recalculated, and it will be observed that calculated and measured values are in good agreement although the calculated values exceed the measured by about 0.15 v at the higher molecular weights. We thus find that over a fairly wide range this simplified treatment gives reasonably good results. It must be admitted, however, that somewhat closer agreement with experiment might be achieved if higher order interactions are taken into account. For most purposes, however, the simpler treatment gives sufficiently good results.

Hall[4] has shown that the group orbital treatment is rigorously applicable only to planar molecules having an orbital antisymmetric in the plane of the molecule. Normal paraffins can be oriented in such a way as to achieve coplanarity of the carbon skeleton. Branched paraffins, however, cannot become planar, and any attempt to apply group orbital calculations to such compounds would necessarily involve a considerable approximation. Nevertheless, it seemed worth while to ascertain to what extent branched paraffins might be treated by the group orbital method, and so the ionization potentials of several branched paraffins are included in Table I. Unfortunately, there are no reliable data with which to compare these calculated values. In general, as would be expected, the branched paraffins have calculated ionization potentials somewhat below the normal paraffins and indeed the reduction in ionization potential for a given molecular weight increases with the degree of branching. In the case of neopentane, for example, the value of 10.21 is calculated for the ionization potential. The ionization potential of neopentane has not been measured, and the mass spectrometer shows no parent ion for this compound. Apparently, the molecule breaks up into a *tert*-butyl ion and a methyl radical immediately upon ionization and the appearance potential of the *tert*-butyl ion has been found to be 10.29 v.[9] Since ionization must occur before fragmentation the ionization potential of neopentane must be approximately 10.29 v. Similar considerations apply in the case of neohexane, 2,2,3-trimethylbutane, and 2,2,3,3-tetramethylbutane. Calculated and measured values agree quite well for these compounds. In spite of this good agreement, it would seem advisable to view group orbital calculations of branched paraffins with caution, at least until sufficient experimental results are available to permit a reliable evaluation of the method.

When the unbranched single-ring cycloparaffins are treated in the aforementioned manner, the lowest roots

TABLE I. Ionization potentials of paraffins and cycloparaffins.

	Calc		Meas	Ref
e	13.04	13.31		
b	1.28	1.55		
Methane	(13.04)	13.31	13.04	a
			13.12	b
			13.20	c
			13.18	d
			13.30	e
Ethane	(11.76)	(11.76)	11.76	a
Propane	11.23	11.12	11.21	a
n-Butane	10.97	(10.80)	10.80	a
n-Pentane	10.82	10.63	10.55	a
n-Hexane	10.72	10.52	10.43	a
n-Heptane	10.67	10.43	10.35	a
n-Octane	10.63	10.39	10.24	a
n-Decane	10.58	10.33	10.19	a
Isobutane	10.82	10.63	...	...
Isopentane	10.67	10.43	...	...
Neopentane	10.48	10.21	10.29[f]	g
2,3-Dimethylbutane	10.48	10.21	...	...
2,2-Dimethylbutane	10.40	10.11	10.19[f]	g
Trimethylbutane	10.26	9.94	10.09[f]	g
Tetramethylbutane	10.09	9.74	9.79[f]	g
Cyclopropane	11.76	11.76	10.23	h
Methylcyclopropane	11.12	10.98	9.88	i
Cyclobutane	10.48	10.21	...	...
Cyclopentane	10.97	10.80	...	...
Cyclohexane	10.48	10.21	10.40	d
			11.0	j

[a] R. E. Honig, J. Chem. Phys. **16**, 105 (1948).
[b] C. A. McDowell and J. W. Warren, Discussions Faraday Soc. **10**, 53 (1951).
[c] L. G. Smith, Phys. Rev. **51**, 663 (1937).
[d] F. H. Field and J. L. Franklin, unpublished data.
[e] J. Geerk and H. Neuert, Z. Naturforsch. **5A**, 502 (1950).
[f] Appearance potential of the *t*-butyl ion.
[g] D. P. Stevenson, Discussions Faraday Soc. **10**, 35 (1951).
[h] F. H. Field, J. Chem. Phys. **20**, 1734 (1952).
[i] F. H. Field, private communication.
[j] Hustrulid, Kusch, and Tate, Phys. Rev. **54**, 1937 (1938).

[8] R. E. Honig, J. Chem. Phys. **16**, 105 (1948).

[9] D. P. Stevenson, Discussions Faraday Soc. **10**, 35 (1951).

of all of the compounds having an even number of carbons are found to be $e-2b$. Those having an odd number of ring carbons have lowest roots that decrease with increasing numbers of ring carbons thus: cyclopropane $E-b$; cyclopentane, $E-1.62b$; cycloheptane $E-1.81b$; cyclononane $E-1.88b$. Unfortunately, few measurements have been made of the ionization potentials of cycloparaffins. Indeed, the only reliable value in the literature is that of Field[10] for cyclopropane, and our calculated value fails by almost 1.5 v to reproduce the measured value. The only other measured ionization potential given in the literature is a value of 11.0 v for cyclohexane.[11] This appears to be too high, and an approximate value of 10.4 v has recently been obtained in this laboratory. This is in fair agreement with the calculated values.

Field[12] has also measured the ionization potential of methyl cyclopropane and found it to be 9.88 v. As would be expected, the calculated value fails to reproduce this. Unfortunately, the ionization potentials of no other alkyl cycloparaffins have been measured, so it is impossible to determine at this time whether the group orbital method can be satisfactorily applied to the higher alkyl cycloparaffins. It is anticipated that closer agreement will be realized with the higher alkyl cycloparaffins than was obtained with methyl cyclopropane. However, none of the substituted cycloparaffins is planar and so the calculated values can be expected to be only approximate. The paucity of data and the interest that attaches to the problem suggest that studies of the ionization potentials of cycloparaffins should be made.

It is apparent, from the data in Table I, that the method of group orbitals gives good results in calculating ionization potentials. Further, the calculations employing the higher value of the potential parameter give much the better agreement with experiment and will be used in calculations involving other compound types. Indeed, the better fit of the experimental data implies that Honig's[8] value for the ionization potential of methane may be too low and that the higher values obtained by Smith,[13] Geerk, and Neuert,[14] etc. may be more accurate.

ALKYL HALIDES

The united atom approach makes it apparent that various derivatives of saturated hydrocarbons can be treated in an analogous manner employing group functions. This will require only that suitable values be used for the potential and interaction parameters in Eq. (2.) Of course, an approximation is involved whenever the molecule is not planar, and this occurs with substitution at any except a terminal carbon. It is obvious that, in the case of the alkyl halides, the halogen can be treated as one group. However, one may also treat the halogen, together with the carbon to which it is bonded and any associated hydrogens, as one group. Thus, in isopropyl chloride, HCCl could be treated as a single group. The two methods are illustrated below for 2-halo butane.

1. Using the halogen as a group

$$\begin{vmatrix} e-E & b & & & & \\ b & e-E & b & & & \\ & b & e-E & c & b & \\ & & c & f-E & & \\ & & b & & e-E & \end{vmatrix} = 0;$$

2. Using HCX as a group

$$\begin{vmatrix} e-E & b & & & \\ b & e-E & c & & \\ & c & f-E & c & \\ & & c & e-E & \end{vmatrix} = 0,$$

where f is the potential parameter of the substituent group and c is its interaction with an adjacent alkyl group. In all cases the ionization potential of the lowest hydride of the substituent has been taken as its potential parameter. Thus, with isopropyl chloride f is the ionization potential of HCl or of methyl chloride depending upon whether —Cl or HC—Cl is treated as the substituent group.

Calculations have been made on both bases and with two exceptions discussed below good agreement with experiment is encountered. Indeed, it is quite gratifying to note that even in the case of the 1-bromobicyclo-(2,2,1) heptane and 1-bromobicyclo-(2,2,2) octane, agreement is within experimental accuracy. It is of interest in the case of the bromides to note that branching again is predicted to cause some reduction in ionization potential for a given molecular weight. This is not borne out by the measured values for the ionization potential, but, unfortunately, the discrepancies are apparently within the accuracy of the measurements and so no conclusions can be drawn.

In the case of both *tert*-butyl bromide and *tert*-butyl chloride few parent ions are found in the mass spectrometer. The calculated value agrees rather closely with measured appearance potential of the *tert*-butyl ion in the case of the *tert*-butyl chloride, as was found with neopentane above. The agreement in the case of *tert*-butyl bromide is poorer and suggests that the appearance potential of the *tert*-butyl ion is somewhat too high or that departure from coplanarity is effective.

The two exceptions noted above to the generally good agreement with experiment are the values for cyclo-

[10] F. H. Field, J. Chem. Phys. **20**, 1734 (1952).
[11] Hustrulid, Kusch, and Tate, Phys. Rev. **54**, 1037 (1938).
[12] F. H. Field, private communication.
[13] L. G. Smith, Phys. Rev. **51**, 663 (1937).
[14] J. Geerk and H. Neuert, Z. Naturforsch. **5A**, 502 (1950).

propyl chloride and that for *tert*-butyl chloride obtained when using —C—Cl as a group. The high calculated values for cyclopropyl chloride are not unexpected in view of the failure of the method to reproduce the measured ionization potentials in the case of cyclopropane and methyl cyclopropane. Indeed, it is somewhat surprising to find good agreement of calculated and measured values in the case of the 1,1-dichlorocyclopropane. The exceptionally high value calculated for *tert*-butyl chloride suggests that the measured ionization potentials of the ethyl and *n*-propyl chlorides may be somewhat too high. A value for ethyl chloride lower by 0.2 v would give better agreement in all cases and would provide a more reasonable sequence of ionization potentials for the alkyl chlorides. Moreover, the calculated values for ethyl and *n*-propyl chlorides using —Cl as a group are 0.2–0.3 v below the measured values, which also suggests that the measured values may be somewhat too high. Results are given in Tables II–IV.

TABLE II. Ionization potentials of aliphatic chlorides.

	—Cl as a group	—C(—Cl) as a group	Meas	Ref
e	13.31	13.31		
b	1.55	1.55		
f	12.78	11.46		
c	1.56	0.77		
CH_3Cl	(11.46)	(11.46)	11.46	a
C_2H_5Cl	10.96	(11.18)	11.18	a
n-C_3H_7Cl	10.71	10.99	10.96	a
t-C_4H_9Cl	10.13	10.75	10.10[b]	c
Cyclo-C_3H_5Cl	10.85	11.14	10.10	d
1,1-Cyclo $C_3H_4Cl_2$	10.30	···	10.30	d

[a] J. D. Morrison and A. J. C. Nicholson, J. Chem. Phys. **20**, 1021 (1952).
[b] Appearance potential of the *tert*-butyl ion.
[c] D. P. Stevenson and J. A. Hipple, J. Am. Chem. Soc. **64**, 2766 (1942).
[d] F. H. Field, private communication.

TABLE III. Ionization potential of alkyl bromides.

	Br as a group	—C(Br) as a group	Meas	Ref
e	13.31	13.31		
b	1.55	1.55		
f	11.69	10.73		
c	1.58	0.82		
CH_3Br	(10.73)	(10.73)	10.73	a
C_2H_5Br	10.47	(10.49)	10.49	a
n-C_3H_7Br	10.35	10.40	10.29	a
n-C_4H_9Br	10.29	10.36	10.12	a
2-C_3H_7Br	10.16	10.30	10.11	a
2-C_4H_9Br	10.08	10.22	10.15	a
iso-C_4H_9Br	10.18	10.27	10.24	a
t-C_4H_9Br	9.87	10.12	10.36[b]	c
$(CH_2)_2Br_2$	10.14	···	10.30	a
$(CH_2)_3Br_2$	10.16	10.18	10.28	a
$(CH_2)_4Br_2$	10.17	10.28	10.28	a
1-bromobicyclo(2,2,1)heptane	···	9.95	9.90	c
1-bromobicyclo(2,2,2)octane	9.46	9.74	9.76	c

[a] J. D. Morrison and A. J. C. Nicholson, J. Chem. Phys. **20**, 1021 (1952).
[b] Appearance potential of the *t*-butyl ion.
[c] J. L. Franklin and F. H. Field, J. Chem. Phys. **21**, 550 (1953).

TABLE IV. Ionization potentials of aliphatic iodides.

	—I as a group	—C(—I) as a group	Meas[a]
e	13.31	13.31	
b	1.55	1.55	
f	10.48	9.67	
c	1.71	0.88	
CH_3I	(9.67)	(9.67)	9.67
C_2H_5I	9.54	(9.47)	9.47
nC_3H_7I	9.51	9.43	9.41
nC_4H_9I	9.50	9.42	9.32

[a] J. D. Morrison and A. J. C. Nicholson, J. Chem. Phys. **20**, 1021 (1952).

TABLE V. Ionization potentials of aliphatic amines.

		Meas	Ref
e	13.31		
b	1.55		
f	10.52		
c	2.08		
CH_3NH_2	(9.41)	9.41 9.8	a b
$C_2H_5NH_2$	9.26	9.32	a
n-$C_3H_7NH_2$	9.24	9.17	a
n-$C_4H_9NH_2$	9.23	9.19	a
iso-$C_4H_9NH_2$	9.20	9.00	a
2-$C_3H_7NH_2$	9.10		
2-$C_4H_9NH_2$	9.08	8.98	a
t-$C_4H_9NH_2$	8.93		
$(CH_3)_2NH$	8.67	9.6	b
$(CH_3)_3N$	8.06	9.4	b

[a] J. D. Morrison and A. J. Nicholson, J. Chem. Phys. **20**, 1021 (1952).
[b] Sugden, Walsh, and Price, Nature **148**, 373 (1941); W. C. Price, Chem. Revs. **41**, 257 (1947).

ALIPHATIC AMINES, ALCOHOLS, AND ETHERS

The united atom for $—NH_2$ and —OH is fluorine, and one would expect, in view of their success in treating saturated hydrocarbons and alkyl halides, that group functions could be successfully employed to calculate the ionization potentials of saturated amines, alcohols, and ethers. Several such calculations have been made and the results are given in Tables V and VI. The ionization potentials of ammonia and water were used as the potential parameters, respectively, for the amines and for the alcohols and ethers. The values measured by Morrison and Nicholson[15] are probably more reliable and certainly more consistent than those of Sugden, Walsh, and Price[16] and have been used as the basis for these calculations. Our calculated results, as would be expected, agree best with the data of Morrison and Nicholson[15] and, indeed, the agreement is excellent. Agreement with the results of Sugden, Walsh, and Price[16] would have been somewhat better had the potential and interaction parameters been taken from their data, but even when this is done agreement is quite poor. This is especially true of the dimethyl and trimethyl amines where the disagreement

[15] J. D. Morrison and A. J. C. Nicholson, J. Chem. Phys. **20**, 1021 (1952).
[16] Sugden, Walsh, and Price, Nature **148**, 373 (1941).

TABLE VI. Ionization potentials of alcohols and ethers.

		Meas	Ref
e	13.31		
b	1.55		
f	12.76		
c	2.06		
Methanol	(10.95)	10.95	a
		10.8	b
Ethanol	10.54	10.60	a
		10.7	b
n-Propanol	10.38	10.46	a
		10.7	b
Dimethyl ether	10.10	10.5	a
Diethyl ether	9.76	9.72	b
		10.2	a
1,4-Dioxane	9.32	9.52	b

[a] J. D. Morrison and A. J. C. Nicholson, J. Chem. Phys. **20**, 1021 (1952).
[b] Sugden, Walsh, and Price, Nature **148**, 373 (1941); W. C. Price, Chem. Revs. **41**, 257 (1947).

is quite large. It is unfortunate that other measurements on these compounds are not available.

OLEFINS AND POLYENES

Hall[4] has calculated the ionization potentials of the methyl-ethylenes using as *e* and *f* the ionization potentials, respectively, of methane and ethylene. In order to obtain best agreement, Hall introduced second-neighbor secondary interactions when two methyls were substituted on the same carbon of the double bond. He reported no results on olefins other than the methyl-ethylenes. We have calculated the ionization potentials of a number of olefins using for *e*, 13.31 v instead of the ionization potential of methane as was used by Hall. Like Hall, we have used the ionization potential of ethylene for *f*. With these values quite satisfactory agreement of calculated and measured values have been obtained without the necessity of employing a second-order interaction constant [Table VII(a)].

TABLE VII(a). Ionization potentials of olefins and polyolefins.

	Calc	Meas	Ref
e	13.31		
b	1.55		
f	10.62		
c	1.65		
g	1.38		
Ethylene	(10.62)	10.62	a
Propylene	(9.84)	9.84	a
Butene-1	9.70	9.76	a
Pentene-1	9.67	9.66	a
Hexene-1	9.65	9.59	a
Butene-2	9.28	9.30	a
Hexene-3	9.11	9.12	a
Cyclohexene	9.16	9.24	b
Isobutene	9.28	9.35	a
2-Methylbutene-2	8.81	8.85	a
		8.80	c
2,3-Dimethylbutene-2	8.40	8.30	c
1,4-Pentadiene	9.28	...	...

[a] R. E. Honig, J. Chem. Phys. **16**, 105 (1948).
[b] J. D. Morrison and A. J. C. Nicholson, J. Chem. Phys. **20**, 1021 (1952).
[c] W. C. Price and W. T. Tutte, Proc. Roy. Soc. (London) **174A**, 207 (1940).

If polyenes having conjugated systems of double bonds are to be treated by this method it is necessary to determine the parameter for the interaction of two adjacent ethylenic groups. One might expect to obtain this value from the ionization potential of butadiene; however, Sugden and Walsh[17] have shown that the *cis* and *trans* isomers of butadiene differ in ionization potential by about 0.3 v, so that the equivalent orbital description of the two isomers will require different interaction parameters. Naturally other polyenes can be expected to exhibit similar isomerism, but unfortunately the ionization potentials of the various structural isomers of other dienes have not been measured. It is interesting, however, to calculate the ionization potentials of several such polyenes and to speculate as to the structure of the compounds measured. Accordingly, the ionization potentials of several polyenes have been calculated using interaction parameters for both *cis* and *trans* isomers as determined from the ionization potentials of butadiene-1,3. Since substantially all of the ionization potentials of polyenes suitable for comparison have been obtained by spectroscopic methods, the spectroscopic ionization potential of ethylene was used as the potential parameter in these calculations. The results are given in Table VII(b). These calculations suggest that the isoprene and 2,3-dimethylbutadiene had the double bonds in the *trans* configuration. The measured ionization potential for hexatriene falls between the two calculated values suggesting that the sample studied was either a mixture of *cis* and *trans* isomers or that it consisted of a single compound having both *cis* and *trans* orientation in the same molecule. If one assumes the latter to be true one calculates an ionization potential of 8.26 v for hexatriene, which agrees exactly with the measured value. Further, if the sample were indeed a mixture of

TABLE VII(b).

	Trans	*Cis*	Meas	Ref
e	13.31	13.31		
b	1.55	1.55		
f	10.50	10.50		
c	1.5	1.5		
g	1.4	1.75		
Butadiene	(9.07)	(8.75)	9.07 *trans* 8.75 *cis*	d,e
Isoprene	8.8	8.5	8.86	e
2,3-Dimethylbutadiene	8.6	8.3	8.67	e
Hexatriene	8.5	8.05	8.26	f
Octatetraene	8.23	7.66	7.8 estm.	f
Cyclopentadiene	9.1	8.75	8.58	g
Cyclohexadiene	8.42	8.12	8.40	g

[d] T. M. Sugden and A. D. Walsh, Trans. Faraday Soc. **41**, 76 (1945).
[e] W. C. Price and A. D. Walsh, Proc. Roy. Soc. (London) **174A**, 220 (1940).
[f] W. C. Price and A. D. Walsh, Proc. Roy. Soc. (London) **185A**, 182 (1945).
[g] W. C. Price and A. D. Walsh, Proc. Roy. Soc. (London) **179A**, 201 (1941).

[17] T. M. Sugden and A. D. Walsh, Trans. Faraday Soc. **41**, 76 (1945).

two compounds, there should have been two ionization potentials, but apparently only one was found. It seems reasonable that the compound studied was a mixed *cis-trans* isomer. The value estimated for octatetraene by Price and Walsh[18] falls between those calculated by the present method for the *cis* and *trans* isomers.

It would seem reasonable in calculating the ionization potentials of cyclic dienes to employ only the interaction coefficient for *cis* configurations. However, for purposes of comparison, calculations were also made employing the coefficient for *trans* isomers. The expected agreement of experimental ionization potential with that calculated using the *cis*-interaction coefficient is found for cyclopentadiene, but the opposite is true for cyclohexadiene, the calculation based upon the *trans* isomer agreeing best with experiment. Since the cyclic dienes can only be considered as involving the *cis* configuration, the observed discrepancy, it appears, must be accepted as an indication of the reliability of the method for conjugated dienes. The uncertainty, while larger than one would like, is no greater than one would expect in view of the approximations involved.

TABLE VIII. Ionization potentials of aromatics.

	Calc	Meas	Ref
e	13.31		
b	1.55		
f	9.52		
c	1.09		
C_6H_6	(9.52)	9.52	a
$C_6H_5CH_3$	(9.23)	9.23	a
$C_6H_4(CH_3)_2$	8.96	8.97	b
$C_6H_3(CH_3)_3$	8.74		
$C_6H_2(CH_3)_4$	8.53		
$C_6H(CH_3)_5$	8.34		
$C_6(CH_3)_6$	8.15		
$C_6H_5C_2H_5$	9.18	9.12	a
$C_6H_4(C_2H_5)_2$	8.91	8.88	b
n-$C_3H_7C_6H_5$	9.18	9.14	a
iso-$C_3H_7C_6H_5$	9.13	9.13	a
n-$C_4H_9C_6H_5$	9.18	9.14	a
2-$C_4H_9C_6H_5$	9.17	9.19	a
t-$C_4H_9C_6H_5$	9.06	9.35	a

[a] J. D. Morrison and A. J. C. Nicholson, J. Chem. Phys. **20**, 1021 (1952).
[b] F. H. Field and J. L. Franklin, unpublished data. The values shown are averages of several determinations on ortho, meta, and paraxylenes.

SUBSTITUTED AROMATICS

In view of the success which attended the calculations for the olefins when treating the C=C as a group it is reasonable to expect that the ionization potentials of alkyl benzenes could be similarly calculated when treating the benzene ring as a group. Several such calculations have been made, using the ionization potential of benzene as *f*. The agreement is excellent for all molecules except *tert*-butyl benzene for which the calculated value is somewhat low. It may be that this discrepancy is attributable to the nonplanar structure of the molecule. Results are given in Table VIII.

[18] W. C. Price and A. D. Walsh, Proc. Roy. Soc. (London) 185A, 182 (1945).

TABLE IX. Ionization potentials of aldehydes and ketones.

		Meas	Ref
e	13.31		
b	1.55		
f	10.88		
c	1.35		
$H_2C=O$	(10.88)	10.88	a
CH_3CHO	(10.28)	10.28	b
C_2H_5CHO	10.11	10.06	b
n-C_3H_7CHO	10.08	10.01	b
$(CH_3)_2CH-CH_2CHO$	9.99	9.92	b
$(CH_3)_2CO$	9.84	9.92	b
$C_2H_5(CH_3)CO$	9.74	9.76	b
n-$C_3H_7(CH_3)CO$	9.72	9.59	b
n-$C_4H_9(CH_3)CO$	9.71	9.58	b

[a] W. C. Price, J. Chem. Phys. **41**, 256 (1947).
[b] J. D. Morrison and A. J. C. Nicholson, J. Chem. Phys. **20**, 1021 (1952).

ALDEHYDES, KETONES, AND CARBOXYLIC ACID AND ESTER

One would expect that $\diagdown C{=}O \diagup$ could be treated as a group in the same manner as $\diagdown C{=}C \diagup$ and that the ionization potentials of aldehydes and ketones could be satisfactorily calculated. Several such calculations were made using the ionization potential of formaldehyde as the potential parameter for $\diagdown C{=}O \diagup$. The results given Table IX are quite satisfactory.

One might expect that carboxylic acids could be similarly treated if suitable allowance is made for the interaction of the —OH and $\diagdown C{=}O \diagup$ groups. However, since the OH or —O—, and $\diagdown C{=}O \diagup$ always occur together in carboxylic acids or esters, it is more convenient to treat $-C(=O)-O-$ as a single group. When this is done,

TABLE X. Ionization potentials of carboxylic acids and esters.

		Meas[a]
e	13.31	
b	1.55	
f	11.51	
c	1.46	
Formic acid	(11.51)	11.51
Acetic acid	(10.70)	10.70
n-Propionic acid	10.46	10.47
n-Butyric acid	10.35	10.22
Ethyl acetate	10.03	9.97

[a] J. D. Morrison and A. J. C. Nicholson, J. Chem. Phys. **20**, 1021 (1952).

TABLE XI. Interaction parameters.

R_1	R_2	c^2	R_1	R_2	c^2
CH_3	CH_3	2.4	$-I$	$-I$	1.2
CH_3	$-CN$	1.4		$-CN$	−1.7
CH_3	$-Cl$	2.4		$-Cl$	0.3
CH_3	$-O-$	4.3		$-O-$	1.8
CH_3	$-Br$	2.5		$-Br$	0.2
CH_3	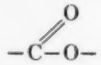	2.1		$-C\equiv C-$	0.8
CH_3	$-C\equiv C-$	2.6			−0.3
CH_3	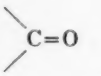	1.8		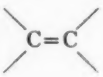	1.2
CH_3	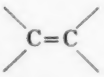	2.7		I	0.6
CH_3	$-NH_2$	4.3			
CH_3	$-I$	2.9			
CH_3	$-S-$	3.0			
CH_3		1.2			
$-CN$	$-CN$	0.1			
$-Cl$	$-Cl$	1.0			
$-Br$	$-Br$	0.6			
$-C\equiv C-$	$-C\equiv C-$	0.4			
$-Cl$	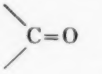	−0.5			
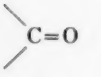	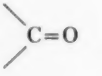	−0.3			
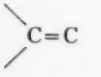	$-CN$	−0.5			
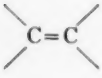	$-Cl$	1.7			
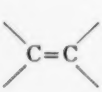	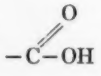	−0.2			
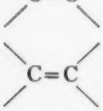	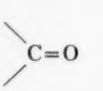	0.1			
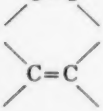	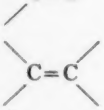	2.0 (*trans*)			
C=C	C=C	3.1 (*cis*)			

using the ionization potential of formic acid as the potential parameter of the 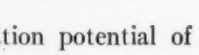 group, good agreement with experiment is obtained as shown in Table X with the small number of acids and esters whose ionization potentials have been reported.

THE REQUIREMENT OF PLANARITY

Hall[4] has shown from theoretical considerations that the group orbital treatment is rigorous for planar molecules having an orbital antisymmetric in the plane of the molecule. However, our calculations have been applied to a large number of compounds which are not planar and the results in almost all cases have been satisfactory. Indeed, we find no examples among the data available where serious disagreement of measured and calculated ionization potentials are unquestionably attributable to nonplanarity. Several examples of such disagreement, e.g., *t*-butyl benzene and *t*-butyl bromide, may well be due to nonplanarity, but in most cases the discrepancy could also be the result of experimental inaccuracies. In any event, the largest discrepancies that may be attributed to nonplanarity are in the order of 0.3–0.5 v and these are rather rare; the great majority of nonplanar molecules show agreement of calculated and measured ionization potentials within the accuracy of the measurements. Where very exact agreement is desired, the requirement of planarity may well prove important, but for most calculations where the result need only be within the accuracy of ordinary electron impact measurements, i.e., 0.1–0.2 v, it does not appear to be significant.

INTERACTION PARAMETERS

The interaction parameter c used in these calculations is a measure of the influence of a neighboring group upon ionization potential. It may be looked upon as the reduction in the ionization potential that would occur if the hydrides of all of the groups in the molecule had the same ionization potential. In addition to the interaction parameters that have been given above, interaction parameters for several additional groups have been calculated from data given by Morrison and Nicholson,[15] and by Price.[19] Table XI lists a number of values for c^2. It will be noted that in a few cases c^2 is negative. This occurs where the ionization potential of a compound falls above that of one of its constituent groups. The significance of these imaginary parameters is not apparent. Most of them can probably be attributed to experimental error, but this seems unlikely for such large imaginary values as that for benzonitrile.

It is especially noteworthy that where systems of π orbitals are involved, c^2 tends to be small. This is particularly true in cases where the parent molecule is capable of some degree of resonance interaction in the ground state. The interaction parameters for the benzene ring with the , $-C\equiv N$ and $-C\equiv C-$

[19] W. C. Price, Chem. Revs. **41**, 257 (1947).

groups are quite small. On the other hand, it is interesting that the aliphatic, amine, sulfur, and —O— groups tend to show large interactions with alkyl groups. It is also interesting that groups such as 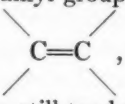 , which give small interaction with each other, still tend to give fairly large interaction coefficients with alkyls.

These results suggest that systems of π electrons, and especially those capable of a strong degree of resonance, are but little affected by substituents, and that ionization tends to be highly localized. The electron ejected from such substances is likely to be a π electron, and the interaction of this system with nearby π-electron systems is small. On the other hand, saturated compounds, such as the paraffins, amines, alcohols, and ethers, upon ionization seem to lose electrons from largely delocalized molecular orbitals. Under such conditions the strength of the bonds in the ions is small, whereas the strength of bonds in ions having a highly localized charge tends to be large.

ACKNOWLEDGMENTS

The author wishes to acknowledge his indebtedness to Dr. F. A. Matsen and Dr. F. H. Field for many helpful discussions and to Humble Oil and Refining Company for permission to publish this paper.

THE JOURNAL OF CHEMICAL PHYSICS VOLUME 22, NUMBER 8 AUGUST, 1954

Szilard-Chalmers Reaction on CH_3I

TOR BRUSTAD AND JOHAN BAARLI
Physical Institute, University of Olso, Norway
(Received March 23, 1954)

Studies on the "hot atom" reactions resulting from slow neutron irradiation of methyl iodide have been carried out. The results show that concentration of free iodine below 0.007 percent in CH_3I during irradiation has a great influence on the distribution of the 25-min I^{128} between CH_3I, CH_2I_2, and I_2.

Comparison of experiments at temperatures below −55°C with carefully purified CH_3I indicates that the yield of the reactions in pure CH_3I is: CH_3I, 44.4 percent; CH_2I_2, 11.2 percent; and I_2, 44.2 percent.

The influence of the temperature on this reaction shows that no change in yield has been found at the shift between liquid and solid state. Co^{60} rays at a rate of 2 roentgen per min at the side of sampling during neutron irradiation, do not change the distribution of the radioactive I^{128} between the compounds.

INTRODUCTION

IN experiments on the relative distribution of the 25 min I^{128} between CH_3I, CH_2I_2, and I_2 after slow neutron irradiation of CH_3I, Gluckauf and Fay[1] report that reproducibility of these experiments was obtained when a small crystal of iodine and a drop of CH_2I_2 was added to the CH_3I before irradiation. The authors used a Ra−Be source in their experiments.

In the experiments reported here we have investigated the influence of the presence of free iodine in CH_3I, during neutron irradiation, on the relative distribution of the I^{128} between the compounds mentioned above. Such experiments indicate that it is necessary to know the concentration of the free iodine in order to obtain reproducibility for concentrations below 0.007 percent free iodine in CH_3I.

The impurities in the compound under irradiation have a great influence on the relative distribution of the I^{128}. By irradiating CH_3I purified more and more carefully and comparing the results obtained at low temperatures, where impurities play a less important role, deduction of the most probable distribution of I^{128} between CH_3I, CH_2I_2, and I_2 has been made for absolutely pure CH_3I.

All our experiments have been carried out using neutrons from a $D-D$ neutron generator, where practically no γ radiation is present. Our results are in very good agreement with those obtained by Gluckauf and Fay.

Fox and Libby[2] have investigated the hot atom reactions in propyl bromide and found a change in yield in the phase shift from liquid to solid state which we do not find in the case of CH_3I.

The absence of γ-ray influence on these reactions is in agreement with what Rowland and Libby[3] have found for *n*-propyl bromide. In our investigations we made use of a Co^{60} source, which gave a dose rate of 2 roentgen per min at the site of the CH_3I under neutron irradiation. No change in yield was found.

EXPERIMENTAL

CH_3I was obtained from L. Light and Company, London. Due to the photodecomposition of this compound, special precautions were taken in order to

[1] H. Gluckauf and J. W. J. Fay, J. Chem. Soc., 390 (1936).

[2] M. S. Fox and W. F. Libby, J. Chem. Phys. **20**, 487 (1952).

[3] F. S. Rowland and W. F. Libby, J. Chem. Phys. **21**, 1945 (1953).

TABLE I. Distribution of I^{128} in different experiments after irradiating CH_3I distilled twice in a Vigreux column.

	I, %	CH_3I, %	CH_2I_2, %	Error, %
	0.7	90.8	8.5	2.0
	0.7	89.4	9.9	1.6
	1.1	90.7	8.2	1.4
	0.9	90.3	8.8	0.8
	1.0	89.5	9.5	0.5
	0.7	89.3	10.0	1.7
	1.0	89.7	9.3	0.9
Mean value	0.9%	90.0%	9.1%	

avoid this. The material was stored in dark bottles in dark rooms. All the handling was done in dimmed light.

Twenty cc CH_3I was irradiated 50 min in the neutron flux from a $D-D$ neutron generator. The irradiation container was a dark soft glass bottle with glass cork surrounded by paraffin as a moderator for the fast neutrons produced by the $D-D$ reactions. Just after irradiation, 4 cc of CH_2I_2 was added, and this mixture was shaken with an aqueous solution of KI and SO_2-saturated water in order to extract the free iodine formed by the neutron irradiation. The composition of the extracting liquid was 1 gr KI: 4 cc SO_2-saturated water: 10 cc distilled H_2O. After separation of the aqueous and organic liquid, the radioactivity of the aqueous solution was measured with cylindrical glass Geiger-Muller tubes (20th Century) with annular jackets for 10 cc of the liquid to be counted.

The organic phase was dried with $CaCl_2$ and the radioactivity of the organic solution was measured. A part of the organic phase was distilled in a 70-cm Vigreux column, and a middle fraction of 5 cc of the CH_3I was then taken out and the radioactivity of this was measured.

The residue was distilled further by raising the temperature up to *ca* 100°C. The radioactivity in the residue was then measured. In order to have the same geometry under the measurement of the radioactivity, the CH_3I and residue were diluted by $C_6H_3-CH_3$.

In order to do quantitative investigations on this problem it was necessary to investigate the content of each of the compounds in each other. The residue very likely has a high concentration of CH_3I in CH_2I_2.

By using a refractometer it was possible to determine the content of CH_3I in CH_2I_2. The content of CH_3I and CH_2I_2 in the aqueous solution was determined by a Beckman spectrophotometer. This concentration was a function of the time used for extraction. The results show that more than 2 min extracting time give approximately the same concentration in the aqueous solution. In our case the concentration of CH_3I was 0.35 vol percent and of CH_2I_2 0.13 vol percent.

Experiments were carried out in order to determine the adequate quantity of extraction liquid, and for all our experiments 50 cc were used.

The "wall effect" was avoided by shaking the container successively with a few cc extracting liquid. The active iodine left in the container after this procedure was quite negligible.

Since the density of the "counted" liquids was different, corrections were made for self-absorption. In all the experiments the following relation has to be fulfilled: Radioactivity in org. component = radioactivity in CH_3I component + radioactivity in CH_2I_2 component. (1)

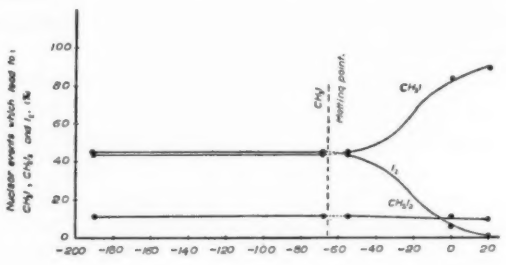

FIG. 1. Distribution of I^{128} between CH_3I, CH_2I_2, and I_2 as functions of temperature.

None of the experiments had a greater deviation than 2 percent from this relationship.

RESULTS

In order to obtain reproducibility for pure CH_3I, it was necessary to purify the substance in a special way. CH_3I distilled twice in a 70-cm Vigreux column, where *ca* 60 percent middle fractions were taken out, gave good reproducibility.

Table I gives the results from 7 different experiments. The error given indicates the deviation from the control relation (1).

In the case where CH_3I had been distilled only once, the variation in the distribution of the radioactivity was very great. However, the percentage for CH_2I_2 was quite constant.

Since impurities have an exceptionally great influence on the hot atom reactions, an attempt was made to purify the CH_3I further. After ozonization, the methyl iodide was shaken with successive quantities of sul-

TABLE II. Distribution of I^{128} after irradiating CH_3I purified in different manners.

	I, %	CH_3I, %	CH_2I_2, %
Twice distilled	0.9	90.0	9.1
Specially purified	2.5	88.3	9.2
Spinning band column	6.1	84.1	9.8

TABLE III. Distribution of I^{128} after irradiating CH_3I at different temperatures.

	20°C	0°C	−55°C	−191°C
I in %	0.9	5.2	44.7	41.1
CH_2I_2 in %	9.1	10.9	11.1	19.8
CH_3I in %	90.0	83.9	44.3	37.9

furic acid, then washed with sodium thiosulfate and distilled water, dried over $CaCl_2$, and then distilled. The results of this procedure are given in Table II, second line. In the third line the results are given where a special distillation equipment was used instead of the Vigreux column. Here we made use of a spinning band column, which is designed for small quantities and has 25 theoretical plates.

Still further investigation on the role of the impurities were made by determining the distribution of the radioactive iodine between these compounds at different temperatures. Especially at low temperatures, where CH_3I is in the solid state, the impurities should be "frozen" out of the methyl-iodide lattice. The results of this investigation are shown in Table III.

Figure 1 shows the result in graphical form. The conclusion from this is that there is no discontinuity in the yield at the phase shift which occurs at $-66.1°C$.

The yield was also investigated using CH_3I containing a known amount of free iodine. All these experiments were carried out at room temperature. Table IV shows the results, which are also presented in Fig. 2. The concentration is given in percent by weight.

TABLE IV. Distribution of I^{128} after irradiating CH_3I with different concentration of free iodine.

Conc.	I%	CH_3I, %	CH_2I_2, %	Error %
0.003	26.9	62.0	11.1	0.3
0.0069	44.6	44.3	11.1	0.9
0.0262	46.2	43.2	10.6	0.7
0.0369	46.4	42.5	11.4	0.9
0.0742	47.4	41.2	11.4	2.0
0.108	48.9	40.1	11.0	0.9
0.161	49.6	40.7	9.6	0.5
0.244	50.2	39.2	10.6	1.0
0.640	53.9	35.0	11.1	0.3
1.639	57.3	31.9	10.8	1.7
2.765	64.1	26.8	9.2	0.1
3.701	69.2	22.5	8.3	0.2

The total organic yield is shown in Fig. 3.

The conclusion from these experiments is that the most probable distribution of the I^{128} following (n,γ) reaction in CH_3I will be for the pure substance:

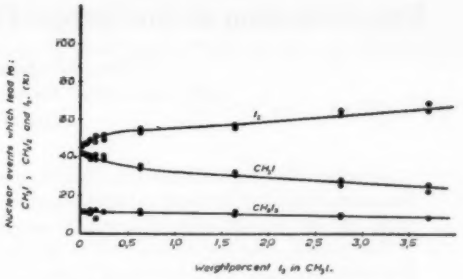

FIG. 2. Distribution of I^{128} between CH_3I, CH_2I_2, and I_2 as functions of the free iodine concentration in CH_3I.

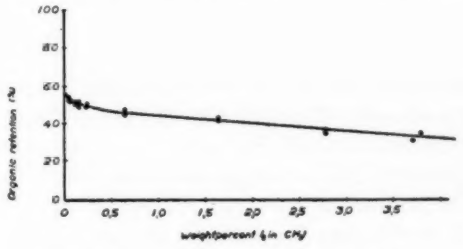

FIG. 3. Organic yield as a function of free dissolved iodine in CH_3I.

I_2	44.4 percent,
CH_2I_2	11.2 percent,
CH_3I	44.4 percent.

An examination of the influence of the γ radiation on this distribution was carried out. The $D-D$ neutron generator gives practically no γ-ray background. A Co^{60} source was then placed so that the CH_3I received a dose rate of 2 roentgens per min during neutron irradiation. The irradiation was carried out in the solid state at $-78°C$ and the total dose given to the liquid was 100 roentgens. No observable effect on the distribution of the I^{128} was found, which is in good agreement with Rowland and Libby's results.[3]

We wish to thank Professor L. Vegard for use of the facilities at the Physical Institute, University of Oslo, and to Norges Teknisk-Naturvitenskapelige Forskningsråd for financial support.

Exact Solution of the Debye-Hückel Equations for a Polarized Electrode

J. Ross Macdonald and Malcolm K. Brachman
Texas Instruments Incorporated, 6000 Lemmon Avenue, Dallas, Texas

(Received September 16, 1953)

A recent solution of the Debye-Hückel equations for a single polarized electrode obtained by Breyer and Gutmann is revised to yield an exact solution of this problem. This solution is compared with an earlier result of H. Müller derived from different initial equations and the solutions are shown to be identical.

The present solution applies only to the diffuse part of the double layer of electrolyte theory and yields the following expression for the mean local potential within the material as a function of the distance x from a polarized anode

$$\psi=(2kT/e)\ln\{\coth[\tfrac{1}{2}(x/L_D+\sinh^{-1}\{\operatorname{csch}(eV_0/2kT)\})]\},$$

where L_D is the Debye length and V_0 the potential applied between electrode and charge-containing material.

A STATIC solution of the Debye-Hückel equations has recently been given by Breyer and Gutmann[1] for a polarized electrode which leads to an expression for charge density that diverges immediately at the electrode. In the present work, we shall show how this nonphysical result may be avoided and shall discuss the derivation of the correct solution of the problem with reference to an earlier correct solution obtained from different initial equations by Müller[2] and summarized by Grahame.[3] This problem is of particular interest because it may be solved exactly in terms of elementary transcendental functions and may be applied quite accurately to other physical situations whose exact solutions are either unobtainable or are considerably more complicated.[4]

Let us consider unit area of a semi-infinite extent of material containing univalent noncombining mobile charge carriers and extending indefinitely in the $+x$ direction from the ideal polarized electrode at $x=0$. In order that the potential and electric field strength within the material be positive quantities decreasing as x increases, we shall choose the polarized electrode to be the anode; the mathematical solution of the space-charge problem is, of course, independent of this choice. If we denote the local concentrations of positive and negative charge carriers by $p(x,t)$ and $n(x,t)$, respectively, the Debye-Hückel equations may be written

$$\frac{\partial n}{\partial t}=\mu_n\frac{\partial}{\partial x}\left[\frac{kT}{e}\frac{\partial n}{\partial x}+n\mathcal{E}\right], \tag{1}$$

$$\frac{\partial p}{\partial t}=\mu_p\frac{\partial}{\partial x}\left[\frac{kT}{e}\frac{\partial p}{\partial x}-p\mathcal{E}\right], \tag{2}$$

where μ_p and μ_n are the carrier mobilities and $\mathcal{E}$ is the local electric field strength within the medium. It is assumed to be composed of a homogeneous Laplacian part E and an inhomogeneous contribution $-d\psi/dx$ arising from possible inhomogeneous charge distribution in the material. Here ψ is the local potential arising from such a distribution, and its level is selected by specifying $\psi=0$ at $x=\infty$. The electric fields satisfy the relations

$$\mathcal{E}=E-d\psi/dx, \tag{3}$$

$$\int_0^\infty \mathcal{E}dx=-V_0, \tag{4}$$

and

$$\frac{d^2\psi}{dx^2}=\frac{4\pi e}{\epsilon}(n-p). \tag{5}$$

Here V_0 is any dc potential applied between the anode at $x=0$ and ground at $x=\infty$. Equation (5) is Poisson's equation; ϵ is the dielectric constant of the material in the absence of free charges.

The following boundary conditions apply to the present problem. Since we shall be concerned with the equilibrium space-charge distribution produced by a dc applied potential, we shall assume that this potential has been applied sufficiently long that equilibrium has been attained. Then, $\partial n/\partial t=\partial p/\partial t=0$. Further, at $x=\infty$ there will be no space-charge and the charge concentrations will have their mutual bulk value c_0. Thus, we also have $\psi=d\psi/dx=d^2\psi/dx^2=0$ at $x=\infty$. At $x=0$, the anode is polarized. Thus, it is blocking for both positive and negative carriers and no mass current can pass from material into electrode or vice versa. For electrolytes, there will be a double layer at this electrode and ions will be prevented from approaching arbitrarily close to the electrode. For the present, we shall neglect this complication but will discuss it later.

It will now be convenient to introduce the following normalized variables: $n^*=n/c_0$; $p^*=p/c_0$; $\psi^*=\psi/(kT/e)$; $V_0^*=V_0/(kT/e)$; $\mathcal{E}^*=\mathcal{E}/(kT/eL_D)$; $E^*=E/(kT/eL_D)$; $z=x/L_D$. In these expressions L_D is the Debye length and is given by

$$L_D=[\epsilon kT/8\pi e^2c_0]^{\frac{1}{2}}. \tag{6}$$

In terms of normalized variables, the equations now

[1] B. Breyer and F. Gutmann, J. Chem. Phys. **21**, 1323 (1953).
[2] H. Müller, Cold Spring Harbor Symposia Quant. Biol. **1**, 1 (1933).
[3] D. C. Grahame, Chem. Revs. **41**, 441 (1947).
[4] See the succeeding paper: J. R. Macdonald, J. Chem. Phys. **22**, 000 (1954).

become

$$\frac{d}{dz}\left[\frac{dn^*}{dz}+n^*\mathcal{E}^*\right]=0, \tag{1a}$$

$$\frac{d}{dz}\left[\frac{dp^*}{dz}-p^*\mathcal{E}^*\right]=0, \tag{2a}$$

$$\mathcal{E}^*=E^*-d\psi^*/dz, \tag{3a}$$

$$\int_0^\infty \mathcal{E}^* dz=-V_0^*, \tag{4a}$$

$$\frac{d^2\psi^*}{dz^2}=\tfrac{1}{2}(n^*-p^*). \tag{5a}$$

Equations (1a) and (2a) may be immediately integrated to give

$$\frac{dn^*}{dz}+n^*\mathcal{E}^*=A, \tag{6}$$

$$\frac{dp^*}{dz}-p^*\mathcal{E}^*=B, \tag{7}$$

where A and B are constants. These constants are directly proportional to j_n/μ_n and j_p/μ_p, respectively, where the j's are carrier convection current densities. Since the electrode is blocking for carriers of both charges, the convection currents are individually zero at $z=0$. Since the above integration indicates that the currents are constant, they must also be zero at $z=\infty$, and A and B are identically zero. The value of $\mathcal{E}^*$ at $z=\infty$ is E^* and dn^*/dz and dp^*/dz are zero there. Thus, Eqs. (6) and (7) indicate that E^* is zero at $z=\infty$, and therefore is zero at all points within the medium.

When final equilibrium is established, no current flows and the externally applied potential is balanced by an equal potential produced by the final space-charge distribution within the material. There is then no Laplacian field E^* within the medium. We have discussed the reasons why E^* must be zero in some detail because, by not taking it zero, Breyer and Gutmann[1] were led to the erroneous conclusion that their solution of the space-charge problem was more general than that of Müller[2] and Grahame[3] (who do not introduce E^*), in spite of the fact that their final solution did not involve E^* at all. It might also be pointed out in this connection that taking $|E^*|>0$ requires the application of an infinite potential V_0, as shown by Eq. (4).

With E^*, A, and B all zero, we are now in a position to solve the differential equations and compare the solution of Breyer and Gutmann with the correct solution. From (6) and (7) we obtain

$$\frac{1}{n^*}\frac{dn^*}{dz}=\frac{d}{dz}(\ln n^*)=-\frac{1}{p^*}\frac{dp^*}{dz}=-\frac{d}{dz}(\ln p^*)=\frac{d\psi^*}{dz}. \tag{8}$$

Thus, $\ln(n^*p^*)=$constant. At $z=\infty$, $n^*p^*=1$ so the constant is zero and $n^*p^*=1$ for all z. We also obtain from (8)

$$n^*=e^{\psi^*}, \tag{9}$$

$$p^*=e^{-\psi^*}, \tag{10}$$

with the help of the limiting values $n^*=p^*=1$ at $z=\infty$. Substituting (9) and (10) in (5a), one finds

$$\frac{d^2\psi^*}{dz^2}\equiv\frac{1}{2}\frac{d}{d\psi^*}\left(\frac{d\psi^*}{dz}\right)^2=\sinh\psi^*. \tag{11}$$

This equation may now be solved for ψ^*; this was the course followed by Müller[2] and Grahame.[3] Müller did not start his analysis with the Debye-Hückel equations, however, as in the present work, but instead used only Poisson's equation and Boltzmann distribution functions for n^* and p^*. The justification for the Boltzmann distribution assumption is discussed by both Müller and Grahame. Since Eqs. (9) and (10) are just such distributions for n^* and p^*, we see that the Debye-Hückel equations are consistent with such choice and should lead to the same solution as that obtained by Müller. For ψ^*, Müller obtains as the solution to (11) (written in the present notation and applying to a polarized anode)

$$\psi^*=4\tanh^{-1}[e^{-(z+\alpha)}], \tag{12}$$

where α is an integration constant.

The fundamental equations may also be solved in a different way. If we differentiate (8) with respect to z and substitute the result in (5a), we obtain, after using $n^*p^*=1$,

$$\frac{d^2n^*}{dz^2}=\frac{1}{n^*}\left(\frac{dn^*}{dz}\right)^2+\frac{n^{*2}}{2}-\frac{1}{2}. \tag{13}$$

This equation may be directly integrated[5] to yield

$$\left(\frac{dn^*}{dz}\right)^2=n^{*3}-2n^{*2}+n^*\equiv n^*(n^*-1)^2, \tag{14}$$

where the constant of integration has been evaluated through the use of the boundary conditions at $z=\infty$. Equation (14) may now be integrated by elementary methods and yields

$$n^*=\coth^2[\tfrac{1}{2}(z+\alpha)], \tag{15}$$

where α is again (the same) integration constant. Equation (9) now gives

$$\psi^*=\ln n^*=2\ln\coth[\tfrac{1}{2}(z+\alpha)]. \tag{16}$$

Breyer and Gutmann obtained a differential equation analogous to (14) but one that involved E. After neglecting all terms in E, they solved the equation in terms of an elliptic function which simplified to give the

[5] E. L. Ince, *Ordinary Differential Equations* (Dover Publications, New York, 1944), p. 335.

result (15) but with the omission of α. As we have seen above, the introduction of elliptic functions is an unnecessary complication. The neglect of α has serious consequences, for if α is zero, both n^* and ψ^* approach infinity at $z=0$. We shall show below how α may be evaluated to avoid this catastrophe. Applying the solution (with α omitted) only up to some minimum value of z $(=z_0)$ greater than zero is still incorrect since the potential at z_0 predicted by this solution will depend only on the value of z_0. However, the actual potential at z_0 is related to that applied across the system. Breyer and Gutmann compared their solution for ψ with that of Grahame[3] (with the omission of the integration constant from Grahame's result) and found that series expansions of both results indicated that they were essentially the same for small z. It was not recognized that since the two solutions were derived from the same initial equations (if E is taken zero) the solutions should be identical. In spite of the apparent difference in the forms of the expressions for ψ^* in (12) and (16), it may be shown that the expressions are in fact mathematically identical for a given α.

Now we may evaluate the constant α in terms of the applied potential V_0. Such evaluation was unnecessary for Grahame's purposes and so was not carried out by him. For mathematical convenience we assume that charge carriers (ions, electrons, ion vacancies, etc.) can approach arbitrarily close to the polarized electrode; physically, this condition cannot, of course, be completely realized. If the carriers can reach the $z=0$ point, then the entire potential V_0 between $z=0$ and $z=\infty$ is effective in establishing the space-charge distribution. Then $V_0=\psi(0)-\psi(\infty)=\psi(0)$. We obtain

$$V_0^*=2\ln\coth(\alpha/2). \tag{17}$$

The solution of this equation for α yields

$$\alpha=\sinh^{-1}[\operatorname{csch}(V_0^*/2)]. \tag{18}$$

On substituting this value of α into Eq. (16) for ψ^*, one obtains the complete, exact, mathematical solution of the original equations. The resulting normalized internal field strength, determined from Eqs. (3a), (16), and (18) is then

$$\mathcal{E}^*=2\operatorname{csch}\{z+\operatorname{csch}^{-1}(\sinh\tfrac{1}{2}V_0^*)\}. \tag{19}$$

It will be noted that ψ^* and $\mathcal{E}^*$ are functions of the two variables (x/L_D) and (eV_0/kT). When (V_0/T) is zero, there is no space-charge region. As (V_0/T) increases from zero, a space-charge layer starts to form at and near the polarized electrode. The dependence of the present solution on applied potential and position in the double layer and its application to physical situations will be further discussed in the succeeding paper.[4]

THE JOURNAL OF CHEMICAL PHYSICS VOLUME 22, NUMBER 8 AUGUST, 1954

Static Space-Charge Effects in the Diffuse Double Layer

J. Ross Macdonald
Texas Instruments Incorporated, 6000 Lemmon Avenue, Dallas 9, Texas
(Received December 2, 1953)

Exact solutions of the static Debye-Hückel space-charge equations for one and for two blocking electrodes are compared analytically and graphically. It is found that the simpler one-electrode solution may be employed to characterize the diffuse double layer with high accuracy in most experimental situations in place of the less tractable two-electrode solution which involves Jacobian elliptic functions. Some consequences of the strong nonlinear voltage dependence of the exact solutions are considered and the application of the solutions to physical situations is discussed.

INTRODUCTION

THE treatment of space-charge formation problems in solids, liquids, and gases involves the solution of systems of nonlinear partial differential equations. These equations have never been solved exactly in complete generality, but a number of exact solutions have been obtained for specific limiting cases. Thus, Jaffé[1] has obtained an exact solution for the one-dimensional, static space-charge distribution in a material containing univalent free positive and negative charges without recombination for the case of two blocking (polarized), plane parallel electrodes separated by a distance L. Unfortunately, this solution involves Jacobian elliptic functions and, because of the inadequacy of published tables of these functions, is difficult to use in practice.

Recently, Prim[2] has solved the same problem anew but with different boundary conditions. Prim considers an intrinsic semiconductor region bounded by n- and by p-type extrinsic regions. The junctions between extrinsic and intrinsic regions are not, therefore, blocking in this case, but the solution is of the same form as Jaffé's.

The solution of the space-charge equations in the time-varying case is immeasurably more difficult than their solution in the static case. Recently, Keilson[3] has given an exact solution for the time variation of injected carriers in semiconductors, but the exact dependence of carrier concentration on position is not obtained. Jaffé and LeMay[4] have given an approximate solution for the time-dependent charging current pertaining to the one-dimensional problem involving two blocking electrodes separated by a distance L to which a dc voltage is suddenly applied. Also, the author[5] has published a linearized theory of space-charge effects for ac applied voltages in the case of two blocking electrodes for any degree of dissociation and for any ratio of the mobilities of positive and negative carriers.

In the preceding paper,[6] the author and M. K. Brachman discussed an exact solution to the static diffuse-double-layer problem where only one plane parallel blocking electrode is present at the boundary of a material of semi-infinite extent containing mobile free charges of both signs. This solution is of particular interest because it involves only the usual well-tabulated elementary transcendental functions. Since both this solution and that of Jaffé for two electrodes are exact, they show clearly the nonlinear dependence of space-charge concentration, space-charge capacitance, etc., on the applied voltage. In this paper, the two solutions are first compared in order to indicate in what physical situations the simpler transcendental solution may be employed in place of the more complicated elliptic solution. Then, some of the implications of the great nonlinearity of the solutions are discussed and application of the solutions to physical situations considered.

EXACT STATIC SOLUTIONS FOR THE DIFFUSE DOUBLE LAYER

Diffuse double-layer formation in the physical situation involving a blocking anode at $x=0$ and an infinite extent of material containing free charges in the positive x direction was considered in the preceding paper.[6] The free charges are assumed univalent and do not recombine. A dc potential V_0 is applied between the anode and the cathode at infinity and the zero of potential is taken at the cathode. The results obtained in II for this situation may be summarized as follows

$$\psi^* \equiv \psi/(kT/e) = \ln\{\coth^2\tfrac{1}{2}[x/L_D + \sinh^{-1}(\operatorname{csch}\tfrac{1}{2}V_0^*)]\} \tag{1}$$

$$n^* \equiv n/c_0 = c_0/p \equiv 1/p^* = \exp(\psi^*) \tag{2}$$

$$\mathcal{E}^* \equiv \mathcal{E}/(kT/eL_D) = 2\operatorname{csch}\{x/L_D + \operatorname{csch}^{-1}(\sinh\tfrac{1}{2}V_0^*)\}. \tag{3}$$

In these equations, ψ is the potential within the material, n is the concentration of negative charge carriers, p the concentration of positive carriers, and $\mathcal{E}$ the electric field strength. The quantity c_0 is the common,

[1] G. Jaffé, Ann. Physik **16**, 217 (1933).
[2] R. C. Prim, Bell System Tech. J. **32**, 665 (1953).
[3] J. Keilson, J. Appl. Phys. **24**, 1198 (1953).
[4] G. Jaffé and C. Z. LeMay, J. Chem. Phys. **21**, 920 (1953).
[5] J. R. Macdonald, Phys. Rev. **92**, 4 (1953).
[6] J. R. Macdonald and M. K. Brachman, J. Chem. Phys. **22**, 1314 (1954). We shall, in the present work, refer to this paper as II and that of reference 5 as I.

homogeneous, equilibrium value of n and p before the application of V_0; V_0^* is $V_0/(kT/e)$; and L_D is given by

$$L_D=[\epsilon kT/8\pi e^2 c_0]^{\frac{1}{2}}, \tag{4}$$

where ϵ is the dielectric constant of the material in the absence of free carriers.

Next, let us consider the case of a blocking anode at $x=0$ and a blocking cathode at $x=L$. Expressed in terms of the variable $y=(x/L_D-L/2L_D)$, Jaffé's exact results for this problem[1] are

$$\psi^*=\ln\{(dny-k_1sny)/(dny+k_1sny)\} \tag{5}$$

$$n^*=1/p^*=\exp(\psi^*) \tag{6}$$

$$\mathcal{E}^*(y)=2k_1/cny. \tag{7}$$

Here,

$$k_1=\{cnM/snM\}\sinh(V_0^*/4), \tag{8}$$

and

$$dnM/cnM=\cosh(V_0^*/4). \tag{9}$$

The quantity M is the dimensionless constant $L/2L_D$. Equation (9) was not given by Jaffé but follows from his work and is useful in simplifying the exact formulas in specific cases. The zero of potential is taken at $x=L/2$. The above exact solution only applies to the case $\mathcal{E}^*(0)\leqslant 2$. This condition is usually well satisfied in cases of practical interest. Jaffé also gives exact solutions for $\mathcal{E}^*(0)=2$ and $\mathcal{E}^*(0)\gtrless 2$, but we need not consider them in this paper.

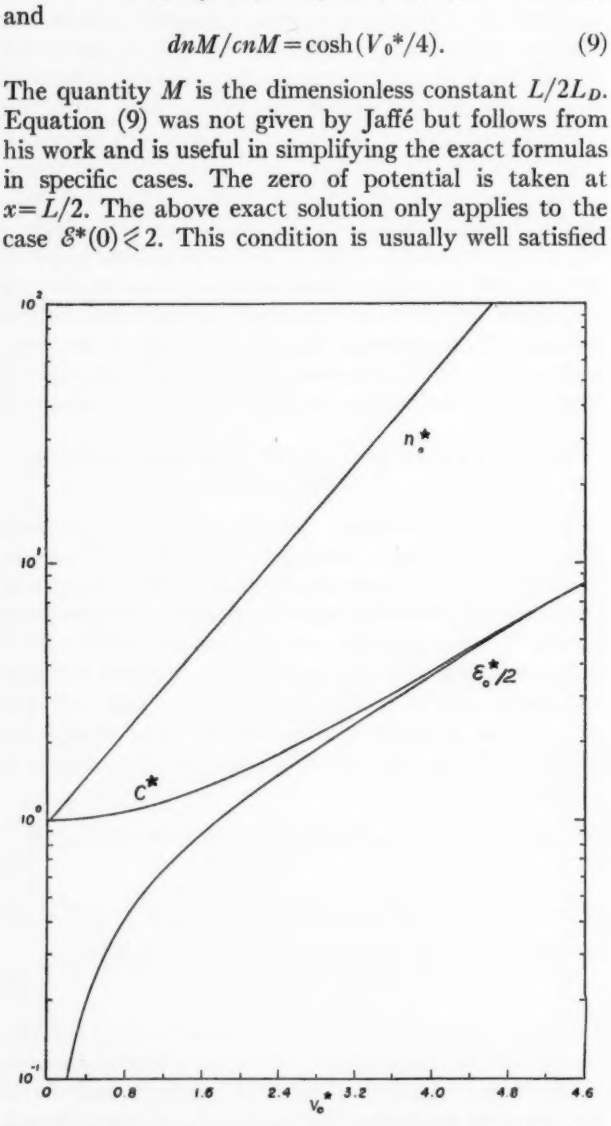

FIG. 1. Dependence on normalized voltage $V_0^*=V_0/(kT/e)$ of normalized carrier concentration n_0^* and electric field strength $\mathcal{E}_0^*$ at the surface of a blocking electrode for single-electrode case. The normalized layer capacitance C^* is also shown.

In most cases of interest, M will be greater than five. When M is this large or larger, k_1 will be much smaller than unity for any value of V_0^*. The Jacobian elliptic functions dn, cn, and sn are functions of both their argument y or M and of k_1. Thus, Eq. (8) is actually a transcendental equation for k_1. For $k_1\ll 1$, no tables of these functions are available. In order to compare the predictions of Eqs. (5), (6), and (7) with those of (1), (2), and (3), it is therefore necessary to use approximate expressions for the elliptic functions which apply in the case $k_1\ll 1$. These expressions are

$$sny=\tanh y+(k_1^2/4)\,\mathrm{sech}^2 y(\sinh y\cosh y-y) \tag{10}$$

and

$$cny=[1-(k_1^2/4)\tanh y(\sinh y\cosh y-y)]\,\mathrm{sech}y. \tag{11}$$

The function dny may be calculated using (10) and (11) from the exact relation

$$dny=[(cny)^2+k_1^2(sny)^2]^{\frac{1}{2}}. \tag{12}$$

When y is greater than about three, the final y terms in (10) and (11) may be neglected with little loss of accuracy.

If expressions of the form (10) and (11) are substituted in Eq. (8) for k_1, a cubic equation in k_1 is obtained. The cubic term is many orders of magnitude smaller than the other terms for $k_1\ll 1$ and may be neglected. The exact solution of the resulting quadratic equation for k_1 is

$$k_1=2\,\mathrm{csch}M\tanh(V_0^*/8). \tag{13}$$

This equation is a good approximation so long as the value of k_1 computed from it is less than about 1/20. This expression for k_1 is considerably different from that given by Jaffé[1] for the same case of large M. Furthermore, it leads to quite different y dependence for ψ^* and $\mathcal{E}^*$ than that obtained by Jaffé. The difference arises from the inclusion in the present work of the $k_1^2/4$ terms in the approximate expressions (10) and (11), in contrast to their neglect by Jaffé. Such neglect is permissible in the expression for sny but is a poor approximation for the cny expression. The inclusion of these terms in the present work thus gives more accurate final approximate expressions for k_1 and for ψ^* and $\mathcal{E}^*$.

Before comparing the two dc space-charge solutions graphically, it is of interest to compute the space-charge capacitance represented by the concentration of charge near the electrode(s). Let a subscript zero denote the value of a quantity at $x=0$. Then the total differential capacitance[7] is

$$C_T{}^d=-\partial\sigma_0/\partial V_0=(\epsilon/4\pi)(\partial\mathcal{E}_0/\partial V_0), \tag{14}$$

[7] All results apply to unit area of the system.

and the less important static capacitance is simply $-\sigma_0/V_0$, where σ_0 is the surface charge density in the material at the electrode. Using expression (3) for $\mathcal{E}^*$, we obtain for the differential capacitance

$$C_T{}^d=(\epsilon/4\pi L_D)\cosh(V_0{}^*/2) \tag{15}$$

in the one-electrode case. In the two-electrode case, it follows from Eqs. (7) and (8) that

$$\mathcal{E}_0{}^*=2(snM)^{-1}\sinh(V_0{}^*/4). \tag{16}$$

Using the approximate expression (11) for snM with neglect of the small $k_1{}^2/4$ term, we obtain

$$\mathcal{E}_0\cong(2kT/eL_D)\coth M\sinh(V_0{}^*/4). \tag{17}$$

Thus, we find for $C_T{}^d$

$$\begin{aligned}C_T{}^d&=(\epsilon/4\pi L_D)\tfrac{1}{2}\coth M\cosh(V_0{}^*/4)\\&=C_g M\coth M\cosh(V_0{}^*/4).\end{aligned} \tag{18}$$

This expression represents the total capacitance of the two space-charge layers in series, in parallel with the geometrical capacitance of the material, $C_g=\epsilon/4\pi L$. In the one-electrode case, there was only one space-charge layer and no geometrical capacitance, since L was infinite in this case. The space-charge capacitance for both layers in series in the present case is given by $C_s{}^d=(C_T{}^d-C_g)$ and may be written

$$C_s{}^d=C_g[M\coth M\cosh(V_0{}^*/4)-1]. \tag{19}$$

For comparison with Eq. (15), the space-charge capacitance of a single layer is $2C_s$. For large M or V^*, the C_g correction is negligible and $2C_s{}^d(\equiv C_{s1}{}^d)$ becomes

$$C_{s1}{}^d\cong(\epsilon/4\pi L_D)\coth M\cosh(V_0{}^*/4). \tag{20}$$

This expression differs from that of (15) by the factor coth M which is essentially unity for $M>3$ and by the appearance of $V_0{}^*/4$ in place of $V_0{}^*/2$.

It is worth noting that the linearized, small-signal theory of ac space-charge effects presented in I yields for positive and negative carriers of nonzero mobility an expression for low-frequency limiting capacitance C in the two-electrode case of exactly the form (19) but with cosh $(V_0{}^*/4)$ replaced by unity. The present solution shows under what conditions the earlier solution for C is valid. Of course in a linear solution there is no difference between the static and differential capacitances.

COMPARISON OF EXACT STATIC SOLUTIONS FOR THE DIFFUSE DOUBLE LAYER

We are now in a position to compare the predictions of the two exact space-charge solutions. Before comparing the solutions graphically, valuable conclusions may be drawn from comparison of the analytical expressions at $x=0$. In the one-electrode case, $\psi^*=V_0{}^*$ at $x=0$; thus $n_0{}^*=\exp(V_0{}^*)$, $\mathcal{E}_0{}^*=2\sinh(V_0{}^*/2)$. For the two-electrode case, on the other hand, $\psi^*=V_0{}^*/2$ at $x=0$, and $n_0{}^*=\exp(V_0{}^*/2)$, $\mathcal{E}_0{}^*=2(snM)^{-1}\sinh(V_0{}^*/4)$. The principal difference in these expressions lies in the substitution of $V_0{}^*/2$ for $V_0{}^*$ when passing from the one to the two-electrode case. This result is physically plausible because in the two-electrode case one would expect that half the applied voltage drop would occur near each of the two space-charge layers. Since there is only one layer in the one-electrode case, the full voltage drop occurs in this layer.

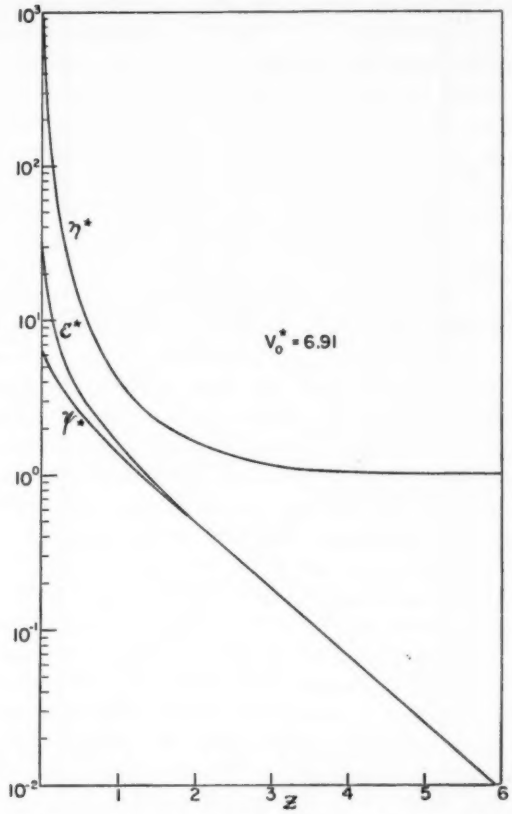

FIG. 2. Dependence for one-electrode case of n^*, $\mathcal{E}^*$, and normalized potential ψ^* on distance from blocking anode in Debye-length units for $V_0{}^*=6.91$.

Figure 1 shows how the quantities $n_0{}^*$, C^*, and $\mathcal{E}_0{}^*$ depend on $V_0{}^*$ for the one-electrode case. Here $C^*=C_T{}^d/(\epsilon/4\pi L_D)$. This graph also closely gives the dependence of $n_0{}^*$ and $\mathcal{E}_0{}^*$ on $V_0{}^*$ in the two-electrode case if the abscissa is taken as $2V_0{}^*$ instead of $V_0{}^*$. The presence of the term $(SnM)^{-1}$ in the two-electrode expression for $\mathcal{E}_0{}^*$ may be neglected because this term is very close to unity. The C^* curve represents $C_{s1}{}^d$ (see Eq. 20) closely since coth M will also be essentially unity for $M\gtrsim 3$.

Figure 2 shows the dependence of n^*, $\mathcal{E}^*$, and ψ^* on position measured from the blocking electrode for the one-electrode case. The value of $V_0{}^*$ is selected to make $n_0{}^*=10^3$. At room temperature, this corresponds to an applied voltage of only about 0.18 volt. Thus, only very small voltages are required to establish very inhomogeneous space-charge distributions. Since this is a semilogarithmic plot, the linear decay of $\mathcal{E}^*$ and ψ^* for $z\equiv x/L_D>1.5$ implies that these quantities depend exponentially on z in this range.

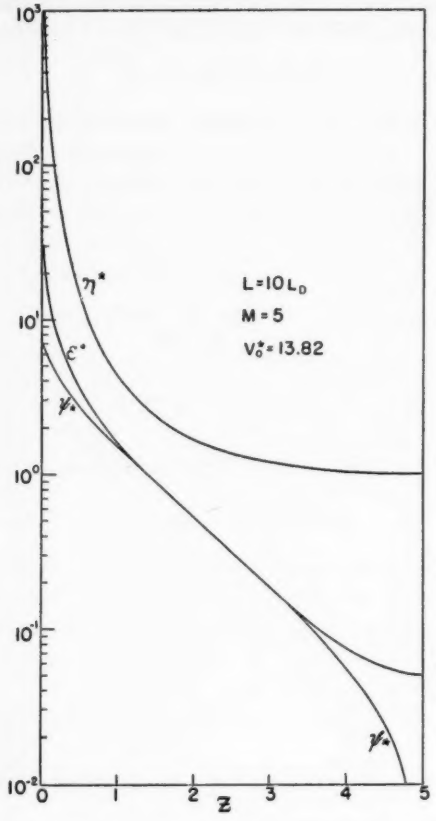

FIG. 3. Dependence for two-electrode case of n^*, $\mathcal{E}^*$, and ψ^* on distance from blocking anode at $x=0$ in Debye-length units for $V_0^*=13.82$ and $M=L/2L_D=5$.

Figure 3 is similar to Fig. 2 except it is for the two-electrode case with $M=5$. The dependence of n^*, $\mathcal{E}^*$, and ψ^* is plotted for only half the separation between electrodes. n^* and ψ^* are odd functions about the center line; $\mathcal{E}^*$ is an even function. It will be noted that the curves of Fig. 3 are plotted for twice the value of V_0^* used in Fig. 2. Half of the voltage drop should take place between $x=0$ and $x=5L_D(z=5)$ and the other half from $5L_D$ to $10L_D(=L)$. Thus, by using twice the value of V_0^* as that used in Fig. 2, we ensure that the space-charge layer near $x=0$ in Fig. 3 for the two-electrode case will have the same voltage applied across it as the single layer in the one-electrode case. We are thus enabled to compare the two cases directly.

Comparison of the curves of Figs. 2 and 3 for $0 \leqslant z \leqslant 5$ shows very close agreement. For z less than about 3.3, the eye is unable to distinguish any difference in the respective curves when they are centered over one another. For $3.3<z \leqslant 5$, the influence of the finite separation of electrodes in the two-electrode case becomes apparent. In this case, n^* must reach unity at $z=5$, whereas unity is not reached in the one-electrode case until $z=\infty$. Nevertheless, the difference in the entire n^* curves in the common region is difficult to detect by eye and is essentially negligible. The distinction shows up more clearly in the $\mathcal{E}^*$ and ψ^* curves in the region $3.3<z \leqslant 5$. For example, at $z=5$, $\mathcal{E}^*$ is 0.05 in the two-electrode case and 0.025 in the one-electrode case. ψ is the quantity most accessible to measurement, however. The distinction between the two ψ curves would be difficult to establish experimentally because in the region where the difference appears, the potential will have fallen to values much smaller than the applied voltage.

The foregoing discussion indicates that for $M \geqslant 5$ the simpler one-electrode solution is sufficiently accurate in the two-electrode case for practically all cases. To use the one-electrode solution for this purpose, one-half of the potential V_0 applied between the two electrodes is used in the one-electrode equations. In most cases of experimental interest there will indeed be two electrodes separated by a distance L, but M will usually be far greater than 5. The larger the value of M, the closer will the two solutions coincide over their common region. In the exceptional cases when $M<5$, Jaffé's exact solutions for $\mathcal{E}_0^* \geqslant 2$ may be used together with the approximate expressions (10) and (11). Note that if one of the two electrodes is not blocking but ohmic, the one-electrode solution will apply very closely with the entire applied voltage drop occurring across the single space-charge layer at the blocking electrode.

DISCUSSION OF VOLTAGE-DEPENDENT NONLINEARITY FOR THE DIFFUSE DOUBLE LAYER

We shall now restrict attention to the consequences of the voltage-dependent nonlinearity of the one-electrode solution as shown graphically in Fig. 1. Table I shows how rapidly some of the pertinent space-charge quantities increase with applied voltage. The last column gives the electric field strength at the blocking electrode for a typical Debye length of 10^{-5} cm. These results indicate clearly that the exact solution must fail for various reasons for some voltage between 0.1 and 3 volts. For example, the solution gives a value of n_0^* which exceeds the number of conduction band levels available at $x=0$ for a voltage of the order of one volt.

Even before these limits are reached, the solution will fail because of dielectric saturation, which decreases the dielectric constant in the high-field region near the electrode, and because of high-field emission from the electrode itself. Such failure will occur between 10^{-1} and 1 volt for $L_D=10^{-5}$ cm as shown by the high values of $\mathcal{E}_0$ in Table I in this voltage range. It should be especially noted that if the electrode is not completely blocking for all charge carriers, the field will not be by any means so large as that specified by the present solution with complete blocking. For example, Von Hippel, Gross, Jelatis, and Geller[8] have given an approximate solution for the field at a rectifying

[8] Von Hippel, Gross, Jelatis, and Geller, Phys. Rev. 91, 568 (1953).

electrode with the neglect of diffusion. These authors treat the case of two rectifying electrodes back-to-back so that charges may leave through the electrodes but may not enter, and find a square root dependence of $\mathcal{E}_0$ on applied voltage rather than the present essentially exponential dependence. The reason for the difference is that in the rectifying case charges will be entirely withdrawn from the material at one electrode until an exhaustion layer forms at the other electrode. The space-charge density in the exhaustion layer is limited by the donor (or acceptor) concentration originally present and hence cannot rise to the astronomical values to which the mathematical solution for n_0^* leads in the blocking, one-electrode case. In practical cases, of course, dielectric saturation and high-field emission will limit the exponential increase to a maximum value in the blocking-electrode case also.

The dependence of the space-charge-layer differential capacitance on $\cosh(V_0^*/2)$ is of considerable interest. The foregoing discussion indicates that the observed capacitance arising from space charge may be expected to increase from a constant small-signal value up to a value ten or more times greater before breakdown limits the increase. Such voltage dependence might be of considerable value for such applications as dielectric amplifiers if it could be attained in practice.

APPLICATION TO PHYSICAL SITUATIONS

Both the Jaffé[1] and the Müller-Macdonald-Brachman[6] solutions apply to the situation where mobile, univalent, noncombining charges of both signs are present. This is the case, for example, in strong electrolytes, which are completely dissociated. In weak electrolytes, dissociation is incomplete and recombination must be taken into account. If bimolecular recombination terms are added to the Debye-Hückel differential equations which govern the space-charge distribution, the equations become even more nonlinear and, apparently, cannot be solved exactly in closed form. The linearized solution of the author[5] with the ac frequency taken zero applies to this case, however, for very small applied voltages ($V_0^* \ll 1$). When V_0^* is no longer small compared to unity, neither the linearized solution nor either of the present nonlinear solutions apply. Of course, in this case, the nonlinear solutions will be better approximations to the exact solution.

TABLE I. Voltage dependence of various space-charge quantities at room temperature.

V_0 (volts)	V_0^*	n_0^*	$\mathcal{E}_0^*$	C^*	$\mathcal{E}_0$ for $L_D=10^{-5}$ cm (volt/cm)
10^{-2}	0.385	1.47	0.388	1.02	1.0×10^{3}
0.0316	1.22	3.39	1.298	1.19	3.4×10^{3}
10^{-1}	3.85	47.0	6.74	3.52	1.8×10^{4}
0.316	12.2	2×10^{5}	446	223	1.2×10^{6}
1	38.5	5×10^{16}	2.2×10^{8}	1.1×10^{8}	6×10^{11}
3.16	122	1×10^{53}	3×10^{26}	1.5×10^{26}	8×10^{29}

Another case of considerable physical interest is that where charges of only one sign are mobile. An insulator containing donors such as the F centers in alkali-halide crystals is an example. Also, a semiconductor containing a fairly high concentration of donors or acceptors may represent this situation provided that the carriers originating from donors or acceptors are present in much higher concentration than are the intrinsic carriers. If the mobile carriers can recombine, no matter how infrequently, with the immobile charges of opposite sign (e.g., donor ions), it is easy to show that the final static space-charge distribution is specified exactly by either the Jaffé or the Müller-Macdonald-Brachman solution as the case may be, provided that the ionized donor concentration predicted by theory never exceeds the total neutral donor concentration originally present at any point. Effectively, charges of both sign are mobile because the release of a mobile charge at one position in the material and its capture by a center of opposite sign at another position represents an actual transfer of an immobile charged center from one position to the other. If recombination is very infrequent, a long time will be required before the space-charge distribution will be close to that represented by the exact solution; nevertheless, the exact solution will eventually apply. If we denote by L_{D1} and L_{D2} the Debye lengths corresponding to univalent mobile carriers of only one sign and to mobile carriers of both signs, respectively, then $\sqrt{2}L_{D1}=2L_{D2}$. When one is dealing with mobile, recombining charges of a single sign, M may be equivalently given as $L/\sqrt{2}L_{D1}$ in all the preceding equations. Note that $\sqrt{2}L_{D1}$ is the rms Debye length for a single carrier.

When charges of only one sign are mobile but there is no recombination (infinite recombination time), there is no way for the immobile charges of opposite sign to move and they will not, therefore, contribute to the space charge. Unfortunately, the Debye-Hückel equations pertaining to this case cannot, apparently, be solved exactly in terms of closed functions for either the one-electrode or the two-electrode case. The linearized solution of I shows that $M=L/2L_{D1}$ here as would be expected. However, the nonlinear voltage dependence required by the nonlinearity of the differential equations does not appear in this solution. It is possible to obtain a series solution to the differential equations by means of the reversion method,[9] first employed by Helmholtz. Unfortunately, in the case of most interest, for which the nonlinearity is appreciable and $V_0^* \gtrsim 1$, the convergence of the series is too slow to make the solution practical. A physical situation where charges of a single sign only are mobile and where there is absolutely no recombination is unlikely. On

[9] G. I. Cohn and B. Saltzberg, J. Appl. Phys. 24, 180 (1953).

the other hand, if the recombination time is very long, an initial space-charge distribution involving the mobile charges only may be established long before recombination can effectively mobilize the immobile charges of opposite sign so that they can contribute to the space-charge distribution. The final static distribution will be the same as if both carriers were mobile, but there may be an initial quasistatic distribution which may persist relatively unchanged for a long time.

In many physical cases, it will be a poor approximation to assume that the charge carriers can approach arbitrarily close to the blocking electrode. Thus, in electrolytes, the center of a charged ion will certainly be unable to approach much closer than the normal ionic radius. If there is negligible ionic chemisorption at the polarized electrode, the double layer may be characterized by an essentially surface charge on the electrode, a region next to the electrode containing no charge, and a diffuse-layer region extending into the solution within which the concentration of ions of one sign decreases toward the bulk value and that of opposite polarity increases toward this value. In some cases, the charge-free layer may consist of a layer of hydration between the electrode and the nearest ions in addition to a layer of thickness determined by the distance of closest approach of the unhydrated ions. The mathematical solutions discussed in this paper apply only to the final diffuse layer in electrolytes. All the above results may be applied for this region, however, provided that it is recognized that the potential across the diffuse layer is not V_0, the total applied potential, but is less than V_0 because of a potential drop in the charge-free layer, and provided that the distance x in the foregoing formulas is measured not from the electrode but from the boundary between the charge-free and the diffuse layers. The present solution is, therefore, not a complete solution for double-layer structure and behavior in electrolytes, but it will be applicable when the charge carriers are electrons. A theory of the complete double layer in unadsorbed electrolytes will be presented in a later paper.

The author is much indebted to Dr. Malcolm K. Brachman for several valuable discussions.

THE JOURNAL OF CHEMICAL PHYSICS VOLUME 22, NUMBER 8 AUGUST, 1954

Infrared Reflection Spectra of Phosphate and Arsenate Crystals*

GEORGE M. MURPHY AND GEORGE WEINER,
Chemistry Laboratories of Washington Square College, New York University, New York, New York
AND
JOHN J. OBERLY,† *Crystal Branch, Metallurgy Division, Naval Research Laboratory, Washington, D. C.*
(Received October 22, 1953)

Crystals of KH_2PO_4, $NH_4H_2PO_4$, KH_2AsO_4, and $NH_4H_2AsO_4$ were examined in the 1–25 micron region. Data were obtained at room temperature for all four crystals, and in addition the spectra of the potassium compounds were examined below their Curie points. In order to avoid the use of thin crystal cuts required for absorption measurements, an optical system was designed which permitted recording of reflection spectra. At the low temperature an increase in the number of bands was observed, and the phosphate and arsenate spectra seemed displaced to higher frequencies. The transition from hydrogen bonding prevailing at room temperature to hydroxyl bonding below the Curie points is considered likely.

I. INTRODUCTION

IN a previous communication to this journal[1] we reported on the infrared reflection spectra of KH_2PO_4, $NH_4H_2PO_4$, KH_2AsO_4, and $NH_4H_2AsO_4$ crystals. These observations have now been extended toward both longer and shorter wavelengths. It is well known that these piezoelectric crystals become ferroelectric below certain temperatures known as the Curie points. These temperatures are 122.0°K, 147.9°K, 95.6°K, and 216.1°K for KH_2PO_4, $NH_4H_2PO_4$, KH_2AsO_4, and $NH_4H_2AsO_4$, respectively.[2] By far the largest polarization is exhibited along the z axis. We conducted experiments at room temperature and at the temperature of liquid nitrogen, 72.6°K, which lies below the Curie points of these compounds.

When cooled below the respective Curie points, these crystals break up into smaller regions.[2] The potassium salts develop some parallel cracks but generally remain optically homogeneous and transparent. In contrast, $NH_4H_2PO_4$ and $NH_4H_2AsO_4$ shatter completely, becoming an inhomogeneous, nontransparent, white mass.[2,3] For this reason we could make low-temperature measurements with only the potassium salts.

* Based on a dissertation presented by George Weiner in partial fulfillment of the requirements for the degree of Doctor of Philosophy at New York University, February, 1953.

† Now at Sprague Electric Company, North Adams, Massachusetts.

[1] J. J. Oberly and G. Weiner, J. Chem. Phys. **20**, 740 (1952).

[2] W. G. Cady, *Piezoelectricity* (McGraw-Hill Book Company, Inc., New York, 1946).

[3] Matthias, Merz, and Scherrer, Helv. Phys. Acta **20**, 273 (1947).

A large amount of information is now available on the electrical properties of these crystals, but relatively little is known either theoretically or experimentally about their atomic behavior. It is the purpose of this paper to investigate the infrared spectrum of the tetragonal class of phosphates and arsenates in the hope of gaining a better understanding of the interesting properties of these compounds.

II. STRUCTURE

Above the Curie points these isomorphic crystals have been assigned by x-ray crystallographers[4,5] to the tetragonal space group V_d^{12} in which the z axis is a preferred axis, the x and y axes being equivalent. The symmetry elements of this group are a fourfold rotation-reflection axis S_4 parallel to the z axis and two twofold rotation axes C_2 parallel to the x and y axes. The phosphorus and arsenic atoms (henceforth to be designated X) as well as the potassium ions lie on points with symmetry S_4; the oxygen atoms lie in "general" positions (i.e., on no symmetry element of the space group) about the X atoms, probably in the tetrahedral arrangement.

The space group below the Curie point has been determined,[6,7] for the potassium salts only, to be the group C_{2v}^{19} of the orthorhombic system. This group differs from V_d^{12} in that the S_4 axis becomes a twofold rotation axis C_2 also parallel to the z axis and in that the twofold rotation axes parallel to the x and y axes are absent. The X atoms remain in symmetry fixed positions analogous to the ones held in V_d^{12}, but the K ions can lie anywhere on the C_2 axes. The O atoms remain in general positions but distribute themselves in two nonequivalent groups.

Slater[8] showed from a statistical argument that for KH_2PO_4 the spontaneous polarization below the Curie point was due to the definite attachment of two H atoms to each PO_4 group. Each hydrogen bond thus caused a dipole due to the displacement of the H atom along the line joining the O atoms of neighboring PO_4 groups. The hydrogen bonds, however, lie essentially in the xy plane, their plane being only slightly inclined towards the z axis. Therefore, it is unlikely that the H displacement alone is responsible for the large polarization along this axis. For this reason De Quervain[6] suggested that the deformation of the hydrogen bond caused in turn a displacement of the P atom along the z axis. Frazer and Pepinsky[9,10] in their recent x-ray investigation of KH_2PO_4 further suggested that as the crystal is cooled the K ions build up a preferred vibration parallel to the z axis. At the critical temperature, however, the K ions "lock in" to a position displaced from their previous centers of oscillation and then exert a polarizing influence on the PO_4 groups and an electrostatic influence on the H's. In this way the P's become displaced within their O_4 tetrahedra and the H's become more ordered.

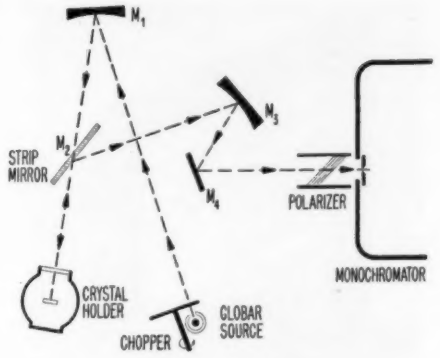

FIG. 1. Optical system.

III. EXPERIMENTAL

The instrument used was a Perkin-Elmer 12C infrared spectrometer equipped with NaCl, KBr, and KRS-5 (TlI, TlBr) prisms. A globar served as a source of infrared radiation. A thermocouple and a Golay cell were used as detectors.

Infrared spectra may be studied by means of absorption or reflection measurements. In order to obtain satisfactory absorption spectra in our region, extremely thin cuts (about 30 microns) would have to be used in order to give measurable transmission in the neighborhood of bands. To circumvent this difficulty we have made reflection measurements.

The longest wavelengths to which measurements could be made was limited by the radiant energy available. This was not the same for all the materials. No low-temperature measurements were made at wave numbers greater than 4000 cm^{-1} because we were not primarily interested in this region.

Figure 1 shows the optical system. Radiation from the Globar source is reflected from the spherical mirror M_1 and passes through the strip mirror M_2 to the sample contained in the crystal holder, an image of the source being formed at the sample. The strip mirror, shown in Fig. 2, consists of several equally spaced aluminized glass strips with air spaces between them. From the sample the light is reflected back to the strip mirror from which it is again reflected to the spherical mirror M_3 and to the plane mirror M_4, and is finally focused on the slit of the Perkin-Elmer spectrometer. A silver chloride polarizer is located between the mirror M_4 and the slit.

In order to take measurements below the Curie points a specially designed cryostat was used. It consisted of outer and inner assemblies shown in Fig. 3. The inner assembly is seen to consist of a cubical brass

[4] S. B. Hendricks, Am. J. Sci. **14**, 269 (1927).
[5] J. West, Z. Krist. **74**, 306 (1930).
[6] M. De Quervain, Helv. Phys. Acta **17**, 509 (1944).
[7] A. R. Ubbelohde and I. Woodward, Nature **155**, 170 (1945); 156, 20 (1945); Proc. Roy. Soc. (London) **A188**, 358 (1947).
[8] J. C. Slater, J. Chem. Phys. **9**, 18 (1941).
[9] B. C. Frazer and R. Pepinsky, Phys. Rev. **85**, 479 (1952).
[10] B. C. Frazer and R. Pepinsky, Acta Cryst. **6**, 273 (1953).

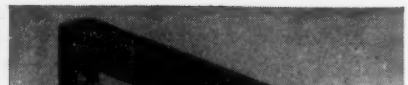

FIG. 2. Strip mirror.

sample holder with four windows which was cooled by liquid nitrogen contained in an adjacent chamber above it. The chamber was supported by three thin-walled Inconel tubes, two of which served as inlet tubes for the liquid nitrogen. A long handle was necessary to turn the inner assembly while the cryostat was evacuated. The vacuum seal consisted of a metal-to-metal contact lubricated by vacuum grease. Both metal surfaces were brass, but that of the inner assembly was chromium plated to reduce friction. One window of the sample chamber was occupied by an aluminized mirror used as a standard reference reflection taken to be 100 percent. The three other windows could be occupied by different crystals which were in direct contact with and nearly surrounded by metal cooled by the liquid nitrogen in the can above. We also checked the temperature by means of a thermocouple.

The outer assembly consisted of a metal container having a KBr window mounted in front of the sample holder. The space between the assemblies was evacuated to prevent condensation on this window.

The whole cryostat was oriented about its vertical axis so that the light beam was incident on the window slightly off normal. This was done in order that the specular reflection from the window surfaces would not fall on the spectrometer slit.

IV. SELECTION RULES

In interpreting our data we have made the assumption that reflection spectra obey the same selection rules as absorption spectra.

The phosphate ion is known, from measurements on solutions, to have tetrahedral symmetry, its molecular group being T_d.[11]

It has four optically active frequencies, A, B, and T_2, the latter class containing two different frequencies. The arsenate ion is believed to be of the same symmetry but only three of the four frequencies have so far been detected.[12,13]

A point which is situated on a symmetry element of the space group and which is left invariant by some of the operations of the space group has been called a "site" by Halford,[14] and the operations forming the group comprise the "site group." It is a subgroup of any occupant's molecular group, meaning that the set of all symmetry operations which carry a site into itself must be contained in the set of all symmetry operations which carry the occupant molecule into itself.

The significance of the site group, as will now be shown, lies in the fact that the occupant of the site is treated just as if it were an independent molecule having the symmetry of the site. The site group will, therefore, to a great extent, determine the selection rules.

Let us, then, investigate the relations between the molecular group and the site group or, speaking mathematically, map the former onto the latter. To do this we follow the familiar method available for the resolution of the symmetry types of a point group into those of a point group of lower symmetry.[15]

X-ray analysis determines the positions of the heavier atoms such as the K, X, and O atoms only; the positions of the H atoms are only inferred and are rather uncertain. When H atoms are introduced into the arrangement of the heavier atoms, they may alter the space symmetry of the entire crystal and lower the site symmetry.

Let us first assume for the purpose of illustration that the H atoms can be ignored and that the site symmetry

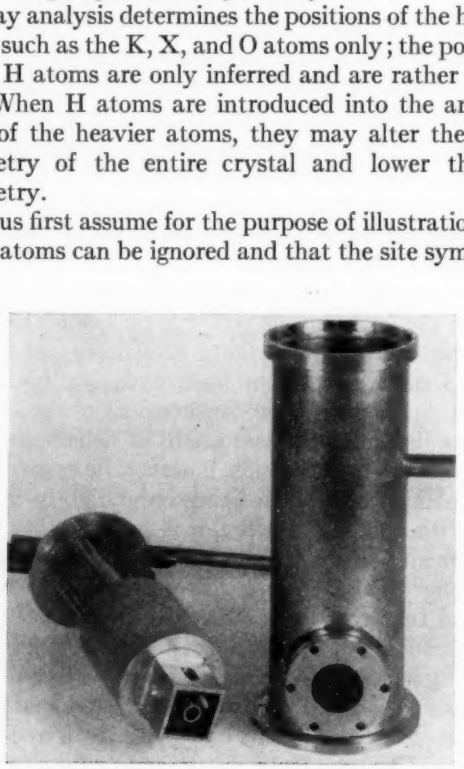

FIG. 3. Outer and inner assembly of the Dewar.

[11] A. Simon and G. Schulze, Z. anorg. u. allgem. Chem. **242**, 329 (1939).

[12] F. Feher and G. Morgenstern, Z. anorg. u. allgem. Chem. **232**, 169 (1937).

[13] J. Gupta and M. P. Guha, Indian J. Phys. **22**, 64 (1948).

[14] R. S. Halford, J. Chem. Phys. **14**, 8 (1946).

[15] G. Herzberg, *Infrared and Raman Spectra of Polyatomic Molecules* (D. Van Nostrand Company, Inc., New York, 1945).

is not lowered. Consider now the X atoms which lie on site S_4. Let us further assume that the XO_4 ions have the same symmetry in the crystal as in solution, namely T_d. This assumption is compatible with the finding of x-ray analysis at room temperature for S_4 is a subgroup of T_d. The corresponding mapping is shown in Fig. 4(a) in which the molecular group T_d is mapped onto the site group S_4.

Should, however, a deformation lower the symmetry of the molecular group to C_{2v}, then S_4 can no longer remain the site, for group C_{2v} contains $\sigma_v(xz)$ and $\sigma_v(yz)$, operations not contained in group S_4. In Fig. 4(b) the group T_d (for we have to start from known frequencies) is mapped onto the group C_{2v}, and this group is mapped onto the assumed site group C_2. In giving polarization characteristics we have not distinguished between the equivalent x and y axes but have labeled all vibrations normal to the z axis with the letter x.

It should be understood that many alternate mappings could be made. We have chosen the above because they seemed the choices most consistent with the findings of x-ray analysis and with our own results. Most other mappings which could be made would yield the same or approximately the same number of lines active in the infrared as either of our two mappings and hence would be physically indistinguishable from them by infrared measurements. We also have not considered selection rules for frequencies arising when molecules lying on various sites couple their vibrations. In that case we would have to map the site group onto the space group, causing a fine structure which has not been observed. We have, therefore, considered sites only.

Furthermore, it must be emphasized that the above selection rules give only a first idea of what to expect. For in the work of Winston and Halford[16] as well as that of Hornig[17] it has been shown that a fundamental frequency forbidden in the infrared by the above selection rules might be activated due to its combination with a long-wave lattice frequency.

V. DATA AND INTERPRETATION

The infrared reflection curves are shown in Figs. 5–8. Our room temperature data for KH_2PO_4 confirm in substance the reflection spectrum recorded by La Lau[18] in the 4 to 14 micron region. Our spectrum shows somewhat improved resolution, possibly because we employed a Golay detector. The reflection maxima obtained by us are summarized in Table I, which is an extension of the table published in our previous communication.[1] Some of the previous data have been corrected. The last column of this table lists the probable assignments for the frequencies observed.

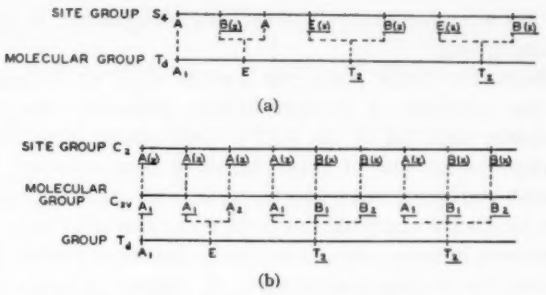

FIG. 4. Possible vibration frequencies of the XO_4 ion in the crystal. Symmetry types active in the infrared are underlined.

We are inclined to interpret the room temperature data on the assumption that the XO_4 ion possesses the tetrahedral symmetry T_d. We consider this symmetry of the ion despite the fact that the totally symmetric vibration $\nu_1(A_1)$ is observed in all our spectra with both polarizations, although this frequency is forbidden to appear in the infrared by the selection rules of Fig. 5(a). Nevertheless, although this may indicate that the true site symmetry is not S_4 but C_{2v} or C_2 instead, still in most other respects we can explain our high-temperature spectra on the basis of the site group S_4 and, as mentioned in Sec. IV, such a band might be activated by combination with a lattice mode. We might have assumed that these bands are due to a splitting of the $\nu_3(T_2)$ degeneracy; but as this splitting would thus amount to 200 cm^{-1}, we thought this very improbable. Also, the wave number of about 890 cm^{-1} corresponds closely to that recorded for a KH_2PO_4 solution.[11] The fact that it occurs considerably below the ν_1 vibration of the PO_4 ion is probably due to the loosening of the PO_4 structure by hydrogen bonds which, however, do not destroy the tetrahedral symmetry. The PO_4 ion thus seems to behave dynamically in most respects as an individual having tetrahedral symmetry perturbed by an environment having perhaps the symmetry S_4 or more probably C_{2v} or C_2. The ν_3 vibrations occur closely to those recorded for the solutions[11] and the difference of about 70 cm^{-1} between the polarizations is probably due to a splitting of the degeneracy. The two intense bands on the short-wave side of the ν_3 vibration (1297 cm^{-1} and 1578 cm^{-1} for KH_2PO_4) appear to be combination bands of the ν_3 frequency with lattice vibrations. The band at 1578 cm^{-1} might be, as La Lau suggests, a P—O—H bending vibration. It is interesting to note that this band appears at the same wave number with both phosphates and arsenates.

At the other end of the spectrum the ν_4 vibration shows a splitting into normal and parallel bands which are close to those recorded for solutions.

As stated in Sec. IV, only three of the four frequencies typical of tetrahedral XO_4 molecules have been reported so far for the arsenate ion. Gupta and Guha[18] attribute this to accidental degeneracy of the ν_1 and ν_3 frequencies. From the spectra of our arsenate crystals, it appears most likely that we have observed

[16] H. Winston and R. S. Halford, J. Chem. Phys. **17**, 607 (1944).
[17] D. F. Hornig, J. Chem. Phys. **16**, 1063 (1948).
[18] C. La Lau, dissertation, University of Amsterdam, Amsterdam, The Netherlands, 1947 (unpublished).

the missing frequency though our assignment is not unambiguous.

Below the Curie point our spectra show an increase in the number of intense bands, probably due to complete removal of the $\nu_3(T_2)$ degeneracy. Contrary to expectation one of these bands is seen to occur at almost the same wavelength with both polarizations. The bands are much narrower than at room temperature and more intense; also, it appears that most bands are shifted to higher frequencies. It seems noteworthy that the arsenate spectrum at low temperature resembles closely that of the phosphate ion.

A possible interpretation of these data should not be overlooked. De Quervain[6] stated that the H atoms might be engaged in a continuous change of position at the high temperature and become frozen into definite positions below the Curie points. Frazer and Pepinsky[10] also assume the H atoms more ordered at the low temperature, as already pointed out in Sec. II. It is thus not unlikely that the increased number of intense bands observed by us is due to a better resolution of the spectrum at the low temperature because of the increased order prevailing.

La Lau[18] reports a broad O—H···O absorption band at 3.58 microns (2793 cm^{-1}) for KH_2PO_4. This we did not observe in our reflection spectrum, but we recorded bands at 2400 cm^{-1} and 2200 cm^{-1} for this crystal and similar bands for the other crystals. Bands in this neighborhood were recently reported by Rundle and

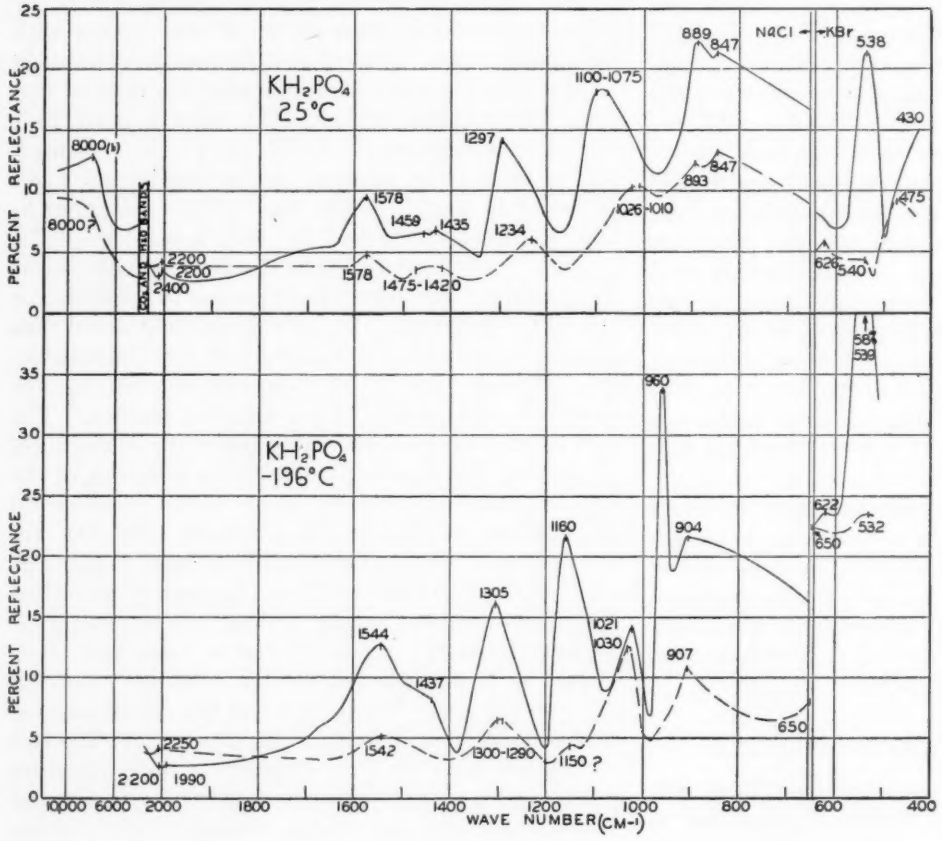

FIG. 5. Infrared spectra of the KH_2PO_4 crystal at 25°C and −196°C. Solid line: polarization normal to z axis. Broken line: polarization parallel to z axis. b = broad.

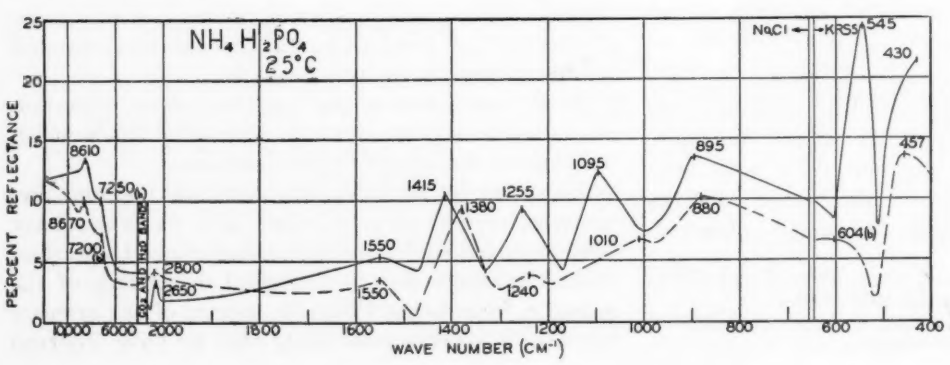

FIG. 6. Infrared spectrum of the $NH_4H_2PO_4$ crystal at 25°C. Solid line: polarization normal to z axis. Broken line: polarization parallel to z axis. b = broad.

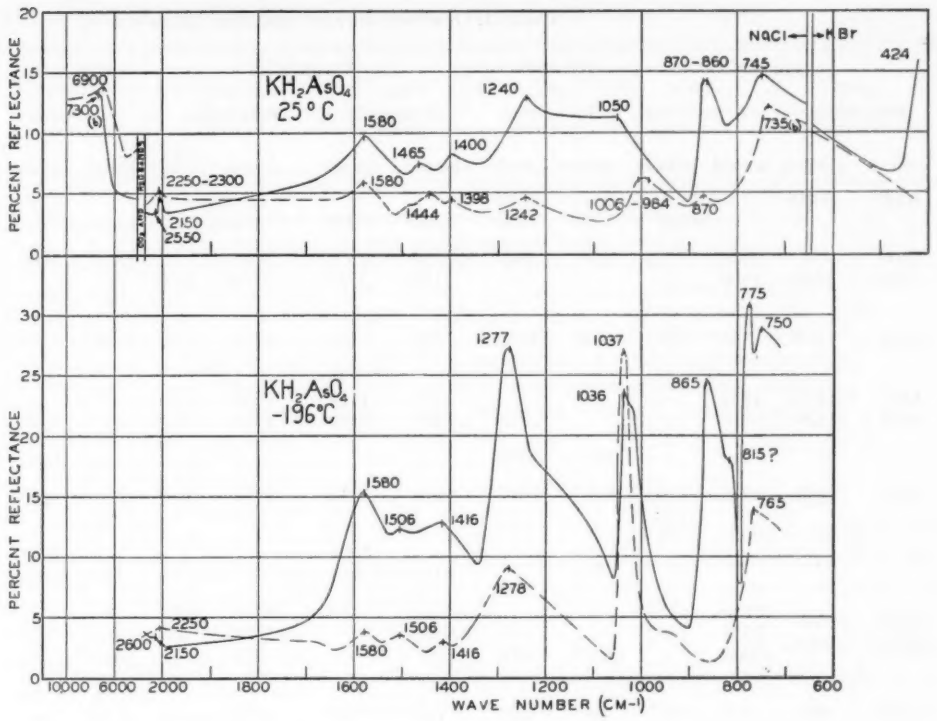

FIG. 7. Infrared spectra of the KH_2AsO_4 crystal at 25°C and −196°C. Solid line: polarization normal to z axis. Broken line: polarization parallel to z axis. b = broad.

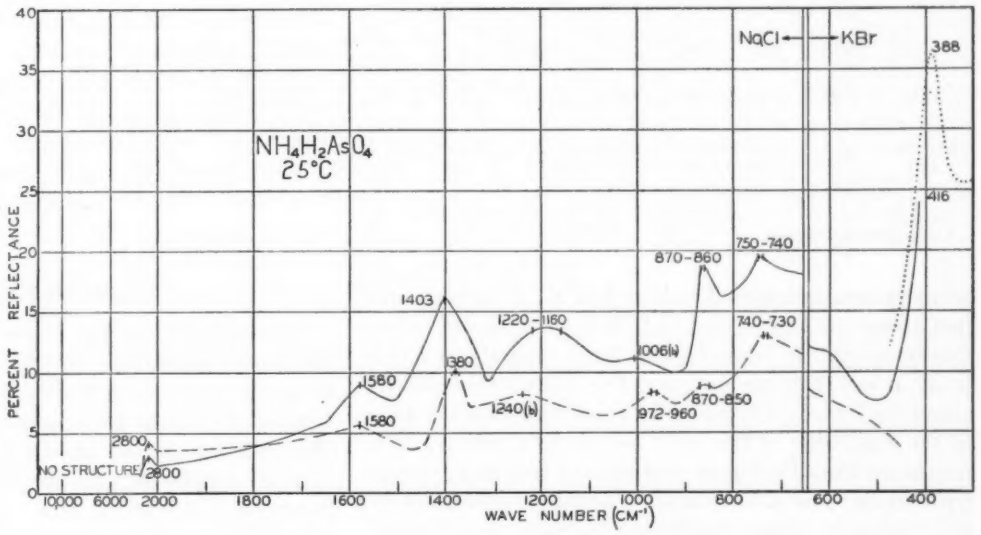

FIG. 8. Infrared spectrum of the $NH_4H_2AsO_4$ crystal at 25°C. Solid line: polarization normal to z axis. Broken line: polarization parallel to z axis. Dotted line: natural light. b = broad.

Parasol[19] and Lord and Merrifield.[20] These bands are weak in intensity and apparently they are less resolved at the low temperature in contrast with the behavior of the other bands. Further experimentation in this spectral region seems desirable.

VI. DISCUSSION

It has been noted in the previous section that the XO_4 spectrum seems displaced to higher frequencies at the low temperature. This might indicate a weakening of the hydrogen bond and a possible transition to a hydroxyl bond as described by Simon and Schulze.[11] In the hydroxyl bond the hydrogen atom rests in the electronic shell of the oxygen atom, and this system attracts another such OH group by homopolar bonding. However, in hydrogen bonding, the hydrogen atom oscillates between the two oxygen atoms. The minimum O—O distance observed in hydroxyl bonding amounts to 2.71A and the maximum O—O distance in hydrogen bonding to 2.55A. Also, there will be transitions between these two types of bonds. Frazer and Pepinsky[9,10] report that when the KH_2PO_4 crystal is cooled, the O—H···O distance, which amounts to 2.53A at room

[19] R. E. Rundle and M. Parasol, J. Chem. Phys. **20**, 1487 (1952).
[20] R. C. Lord and R. E. Merrifield, J. Chem. Phys. **21**, 166 (1953).

TABLE I. Observed infrared reflection bands (cm^{-1}).

KH_2PO_4 25°C Polarization to z axis		KH_2PO_4 −196°C Polarization to z axis		$NH_4H_2PO_4$ 25°C Polarization to z axis		KH_2AsO_4 25°C Polarization to z axis		KH_2AsO_4 −196°C Polarization to z axis		$NH_4H_2AsO_4$ 25°C Polarization to z axis		Probable assignment
normal	parallel	normal	parallel	normal	parallel	normal	parallel	normal	parallel	normal	parallel	
8000[a]	8000?	no data recorded		8610 7250[a]	8670 7200[a]	7300[a]	6900[a]	no data recorded		no structure		?
2400 2200	... 2200	2200 1990	2250 ...	2650 ...	2800 ...	2550 2150	{2300} {2250}	2600 2150	 2250	2800	2800	Hydrogen bond vibrations
1578	1578	1544	1542	1550	1550	1580	1580	1580	1580	1580	1580	Combination band of ν_3 with lattice vibration or X−O−H bending vibration
1459 1435	{1475} {1420}	1437 ...	... ...	... ...	... ...	1465 1400	1444 1398	1506 1416	1506 1416	... ...	... ...	Combination bands of ν_3 with lattice vibration
...	...	...	...	1415	1380	...	...	...	...	1403	1380	$\nu_4(T_2)$ of NH_4 ion
1297	1234	1305	{1300} {1290}	1255	1240	1240	1242	1277	1278	{1220} {1160}	1240[a]	Combination band of $\nu_3(T_2)$ of XO_4 ion with lattice band
...	...	...	...	...	...	1050	{1006} {984}	...	...	1006[a]	{972} {960}	Possibly same assignment as above band
{1100} {1075}	{1026} {1010}	1160 1021 960	1150? 1030 ...	 1095	 1010	{870} {860} 745[a]	870	1036 865, 815? 775	1037	... {870} {860}	... {870} {850}	$\nu_3(T_2)$ of XO_4 ion
889	893	904	907	895	880	745[a]	735[a]	750	765	{750} {740}	{740} {730}	$\nu_1(A_1)$ of XO_4 ion
847	847	...	...	...	...	...	...	no data recorded		...	...	Difference band of $\nu_1(A_1)$ of PO_4 ion and lattice band
...	626	622	650	...	604[a]	...	...			...	...	?
538	540	539	532	545	...	...	...			...	...	Combination band of $\nu_4(T_2)$ of PO_4 ion and lattice band
below 430	475	no data recorded		below 430	457	below 424	...			below 416	388[b] ...	$\nu_4(T_2)$ of XO_4 ion

[a] Broad.
[b] Unpolarized radiation.

temperature, becomes 2.44A at 126°K, a temperature just above the Curie point (122°K); when cooled below this temperature, however, this bond expands to 2.51A which is less than the minimum O−O distance reported above for hydroxyl bonding for room temperature. Due to the expansion of the bond below the Curie point, a transition from hydrogen to hydroxyl bonding appears quite likely. The X−O linkages, no longer disturbed by the hydrogen atoms oscillating between neighboring groups, become stronger, and consequently the frequencies appear at shorter wavelengths. This reasoning is compatible with the Slater model in which two hydrogen atoms attach themselves to each XO_4 group below the Curie point to form the H_2XO_4 ion.

A definite interpretation of these spectra will have to await the finding of the lattice frequencies in the far infrared.

ACKNOWLEDGMENTS

The polished crystal plates were obtained through the kind cooperation of Elias Burstein of the Naval Research Laboratory, Washington, D. C., and Dr. Hans Jaffe of the Brush Development Company, Cleveland, Ohio. We are greatly indebted to Mr. Burstein and to Paul H. Egli of the Metallurgy Division, Naval Research Laboratory, for making the reflectance-measuring apparatus available to New York University.

The authors wish to express their sincere gratitude to Professor R. S. Halford of Columbia University, New York, New York, for his interest throughout the course of this work and for his many valuable suggestions.

Finally, we wish to thank A. R. Dennett of the Eppley Laboratory, Newport, Rhode Island, for his help and advice.

Polarization Effects in the Ionic Conductivity of Silver Bromide

ROBERT J. FRIAUF*†
Department of Physics,‡ University of Chicago, Chicago 37, Illinois
(Received August 26, 1953)

Alternating current impedance measurements on samples of silver bromide with silver and with gold electrodes show the presence of polarization effects. These effects appear as a capacitive component of the impedance and a slight dependence of the resistance on the frequency of the measurement, and their dependence on temperature, frequency, pressure, voltage, and impurity content has been investigated. A macroscopic theory is developed to describe the motion of the mobile charge carriers (ionic defects) which exist in AgBr at elevated temperatures. The general equations contain the effects of conduction and diffusion currents, space charge, and formation and recombination. Since these equations are nonlinear, an approximation procedure is developed, which is valid for small values of the applied voltage. The results of the theory with appropriate boundary conditions give semiquantitative agreement with the temperature and frequency dependence of the observed results and afford a good qualitative description of all of the observed effects. It is concluded that Frenkel defects are responsible for the polarization effects and that the formation and recombination rate is smaller than might at first be expected.

I. INTRODUCTION

THE purpose of the experiments to be described has been to study the ionic defects which occur in AgBr. In order to facilitate the description of the experiments and the accompanying theory, it will be convenient to summarize the current state of information about the defects in AgBr. Recent investigations of the ionic conductivity of pure AgBr and of AgBr with small amounts of divalent impurities indicate that the conductivity can be adequately described, at least for temperatures below 300°C, by assuming that Frenkel defects exist for the silver ions.[1,2] An analysis of the measurements yields values for the equilibrium concentration of defects and for the mobilities of each of the two types of charge carriers. A number of other properties of AgBr, however, have led many investigators to suggest that at least some Schottky defects must also exist. At temperatures near the melting point there are anomalous increases in ionic conductivity,[1] specific heat,[3,4] and thermal expansion.[5,6] From studies of the absorption spectrum of AgBr with small amounts of Ag_2S, several writers have concluded that Schottky defects are present to a lesser or greater extent.[7,8] Finally there are scattered reports of diffusion of bromine in AgBr.[9–11] At the present time it appears that the presence of some Schottky defects in AgBr is suggested by many experiments but has not been definitely proved by any.

In view of this situation it was thought that a study of the polarization effects associated with the ionic conductivity might lead to further information about the possible presence of some Schottky defects. The polarization effects appear experimentally in the following way. When an alternating voltage is applied to a sample of AgBr with silver electrodes, the electrical behavior of the sample is not entirely equivalent to that of an ideal resistance. There is also a capacitive component in the current flowing through the sample, and both this and the resistance depend on frequency. It is these deviations from the behavior as an ideal resistance that form the object of interest for these investigations.

A qualitative explanation of these effects may be given as follows. Imagine the ionic defects to be mobile charge carriers moving in a continuous medium. When an ac voltage is applied to the sample, the charge carriers in the interior will move back and forth in phase with the applied voltage and thus contribute to the bulk conductivity of the sample. When charge carriers arrive at the electrodes, however, some of them may not be able to carry their charge out of the sample. In this case charge carriers will pile up at the electrodes and thus produce a capacitive effect. The electric field produced by the piled-up charges will also hinder the approach of additional charge carriers and hence tend to increase the resistance. On the basis of this picture

---

* U. S. Atomic Energy Commission Predoctoral Fellow, 1951–1953.

† Present address: Department of Physics and Astronomy, University of Kansas, Lawrence, Kansas.

‡ The experimental work was performed in the Institute for the Study of Metals and was supported in part by the U. S. Office of Naval Research. This paper is taken from a thesis which was presented in partial fulfillment of the requirements for the degree of Doctor of Philosophy.

[1] S. Kurnick, J. Chem. Phys. **20**, 218 (1952).
[2] J. Teltow, Ann. Physik **5**, 63, 71 (1949).
[3] R. Christy and A. Lawson, J. Chem. Phys. **19**, 517 (1951).
[4] H. Kanzaki, Phys. Rev. **81**, 884 (1951).
[5] A. Lawson, Phys. Rev. **78**, 185 (1950).
[6] C. Berry, Phys. Rev. **82**, 422 (1951), disagrees with Lawson's interpretation.
[7] O. Stasiw, Ann. Physik **5**, 151 (1949); Z. Physik **127**, 522 (1950); **130**, 39 (1951).
[8] J. W. Mitchell, Phil. Mag. **40**, 249, 669 (1949).
[9] A. Murin and Yu. Taush, Doklady Akad. Nauk S.S.S.R. **80**, 579 (1951).
[10] A. Langer, J. Chem. Phys. **11**, 11 (1943).
[11] T. B. Grimley, *Fundamental Mechanisms of Photographic Sensitivity*, edited by J. W. Mitchell (Butterworths Scientific Publications, London, 1951), p. 46. The interpretation of the results described by Langer and Grimley has been disputed by K. E. Zimen, *ibid.*, p. 53.

it is to be expected that the anomalous effects will be larger at low frequencies, and this behavior is observed.

Since it seems probable that bromine ion vacancies, if any are present in AgBr, would be more likely to pile up at silver electrodes than either silver ion vacancies or interstitial silver ions, it was originally hoped that the polarization effects observed in AgBr with silver electrodes could be ascribed to bromine ion vacancies. In this case a study of the polarization effects would provide information about the Schottky defects in AgBr. An analysis of the theory corresponding to the above picture, however, indicates that Frenkel defects are primarily responsible for these effects, as they are for the conductivity itself.

II. EXPERIMENTAL PROCEDURE

AgBr was prepared by precipitation from $AgNO_3$ and HBr obtained from Mallinckrodt Chemical Works. Spectroscopic analysis indicated no more than a few parts in 10^5 of polyvalent impurities, and measurements of conductivity at room temperature confirmed this analysis. For the earlier work powdered AgBr obtained from Goldsmith Brothers Company, Chicago, was used. Single crystals were grown by withdrawing from the melt at a rate of 2 in. per hr (Czochralski method). These were machined in a lathe to cylinders about $\frac{3}{8}$ in. in diameter and $\frac{1}{4}$ in. long; several thousandths of an in. was then removed by etching, and the samples were annealed at 390°C for about 20 hr. For the earlier work polycrystalline samples were prepared by pouring molten AgBr into a pellet die and applying a pressure of 10 000 kg/cm²; the average grain size was about 1 mm. Electrodes of silver or of gold were applied by evaporation of the metal in a vacuum; for the silver electrodes a coating of Du Pont silver paint was added. Pieces of solid silver or gold were held against these electrodes by a light spring pressure of about 5 g/mm² during measurements. Temperature was measured with a Chromel P-Alumel thermocouple with an error of not more than 0.5°C. The sample holder was designed so that the lead wires contained no screw contacts in the high temperature region in order to avoid any possible copper oxide rectifying effects.

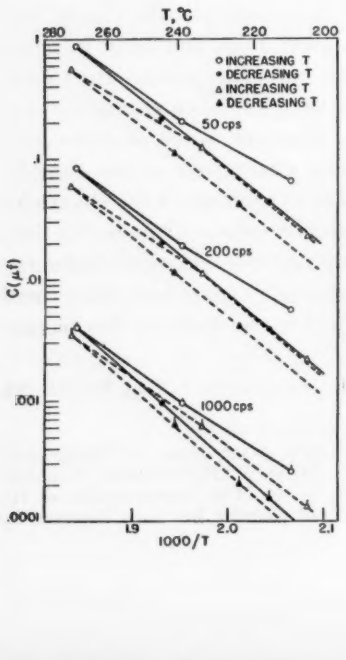

FIG. 1. Capacity as a function of temperature for No. 6a (silver electrodes). The dotted curves represent a second series of measurements. Vertical lines at 1000 cps indicate the possible error caused by the residual inductances in the measuring circuits.

For the ac impedance measurements a General Radio Type 716-C capacitance bridge was used as an equal arm bridge, with a General Radio Type 602-M resistance box and various condensers placed in parallel with the variable condenser in the bridge. The alternating voltage was supplied by an audio oscillator, the frequency of which was constant within 1.5 percent, and a tuned amplifier and oscilloscope served as a null detector. Because of the large conductivity of AgBr the phase angles encountered ranged from 1 to 10^{-5} radian compared to a pure resistance; in order to measure such small phase angles in the presence of a low resistance, considerable care was necessary to avoid spurious effects. The residual capacity in the resistance box and the leakage capacity in the leads and sample holder, collectively amounting to about 60 $\mu\mu$f, had to be subtracted from the measured values; for this reason values of capacity less than 100 $\mu\mu$f were not considered reliable. The residual inductance in the resistance box and in the lead wires, of the order of 1 μh in both cases, led to a more serious effect at low resistances. A negative equivalent capacity $\Delta C = -L/R^2$ was introduced, and since $\Delta C \sim 100$ $\mu\mu$f even for $R = 100$ ohms, it was not possible to obtain reliable capacity measurements when the resistance was less than 100 ohms. Within the range of conditions mentioned above the error in the capacity measurements was less than 1.5 percent or 10 $\mu\mu$f, with the resistance measurements much more accurate.

III. EXPERIMENTAL RESULTS

The electrical behavior of the samples is represented at each frequency by an equivalent parallel combination of resistance and capacity. Table I shows a summary of the capacity measurements. The high frequency conductivity of the single-crystal samples has a temperature dependence corresponding to an activation energy of 17.8 kcal/mole and is in good agreement with previous observations.[1,2]

It will be seen from Fig. 1 that the magnitude of the measured capacity depends somewhat on the thermal history of the sample. It is believed that this behavior, along with similar variations in magnitude of capacity between different samples with supposedly identical electrodes, is caused by changes in the precise conditions of the electrodes. The possibility for such changes, especially at the higher temperatures, arises because there is a time of at least 2 hr, and sometimes as long as 16 hr, between measurements at successive temperatures. The slopes of the curves obtained with decreasing temperature are quite reproducible, however, as is shown by the two different series of measurements in Fig. 1. It therefore appears that the changes of capacity which occur with decreasing temperature are caused by

TABLE I. Summary of experimental results for capacity. Values in parentheses are considered less reliable than the other values. Samples No. 3a–6b are single crystals prepared from Mallinckrodt chemicals. Samples No. 14–29 are polycrystalline and are prepared from Goldsmith Brothers AgBr; Nos. 28 and 29 have 0.1 percent (mole) $CdBr_2$ added. All samples except Nos. 5a and 6b have silver electrodes; these two have gold electrodes.

Sample	l (cm)	C (μf/cm^2) $T=253°C$ $f=200$ cps	Temperature slope (kcal/mole) 50 cps	200 cps	1000 cps	Frequency slope (T as shown)		
							241°	*267°*
5b*	0.592	0.02–0.008	(29.5)	(31.5)			(1.55)	(1.40)
6a*	0.570	0.03–0.005	(25.6)	(26.0)			(1.62)	(1.33)
						216°		*270°*
5b	0.592	0.038	29.3	29.8	31.7	1.76		1.72
6a	0.570	0.048	29.5	30.5	32.0	1.79		1.71
						223°	*241°*	*271°*
5b	0.592	0.02–0.006	[a]	[a]	[a]	(1.46)	(1.50)	(1.40)
6a	0.570	0.031	29.1	30.0	32.0	1.70	1.67	1.61
						223°	*241°*	*271°*
3a*	0.585	0.02–0.008	(26.7)	(27.0)	(25.5)	1.46	1.40	1.46
3b*	0.597	0.01–0.006	(24.0)	(25.2)	(26.7)	1.50	1.46	1.42
						219°	*241°*	*266°*
3a	0.585	0.023	(28.2)	(27.5)	(25.4)	1.50	1.58	1.60
3b	0.597	0.017	(29.3)	(27.8)	(27.2)	1.61	1.64	1.70
						219°	*244°*	*266°*
5a*	0.661	0.21	30.0	29.8	29.6	1.62	1.68	1.66
6b*	0.674	0.17	29.4	29.8	29.4	1.60	1.63	1.60
						210°		*267°*
20	1.224	0.042	20.0	20.9	21.8	1.35		1.38
21	1.277	0.033	(21.9)	(23.6)	(26.1)	1.49		1.37
22	1.243	0.036	(15.8)	(16.9)	(20.4)	1.52		1.28
						210°		*267°*
23	0.632	0.040	(19.6)	21.4	23.3	1.33		1.29
26	0.634	0.072	16.5	17.8	20.6	1.43		1.36
27	0.624	0.091	17.8	20.0	20.1	1.36		1.33
						210°		*267°*
28	0.696	0.12	20.8	25.1	28.6	1.59		1.43
29	0.688	0.17	19.8	23.4	26.1	1.55		1.44
						210°	*245°*	*292°*
14	1.245	0.0024	(20.4)	(18.0)	(20.3)	1.60	1.61	1.51
15	0.506	0.028	(19.5)	(20.6)	(21.8)	1.50	1.42	1.37

* Annealed without electrodes. In all other cases samples were annealed with electrodes.
[a] A dc voltage was applied to this sample a number of times.

changes in the density and mobilities of the ionic charge carriers in AgBr; this temperature dependence can be represented by an activation energy, which is listed in Table I. It should also be mentioned that the treatment of the samples after the electrodes have been applied has some influence on the magnitude of the observed capacity. For samples which are not annealed after the electrodes are applied, the magnitude of the capacity is less by as much as a factor ten, and the changes during a series of measurements are considerably larger than those in Fig. 1. In relation to this effect, observation of samples after annealing with electrodes shows two noticeable effects: (a) Since no spring pressure acts on the electrodes during annealing, the silver paint tends to pull together, creating ridges and thin spots. (b) There is a reddish coloration of the AgBr for a distance of about 1 mm from the electrodes.

The frequency dependence of the observed capacity, as is shown in Fig. 2, can be represented by $C=\text{const}/f^n$; n is given as the frequency slope in Table I. Measurements are made for a complete set of frequencies at a fixed temperature, the whole frequency range being covered in about 15 min. Figure 3 shows the general behavior of the excess resistance $\Delta R(f)=R(f)-R_0$, where R_0 is the normal bulk resistance which is observed at high frequencies.

Since the theory to be developed indicates that the sample is a nonlinear circuit element, it was advisable to investigate the effect of varying the amplitude of the applied voltage. As is shown in Fig. 4, the value of capacity measured at 0.1 volt rms, which was used for all measurements, is within 2 percent of the limiting value at zero voltage.

Table II shows the results of measurements made on

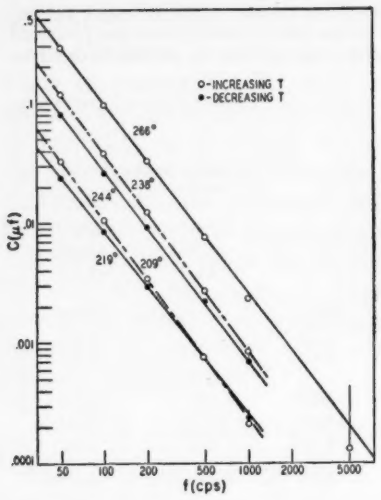

FIG. 2. Capacity as a function of frequency for No. 3a (silver electrodes). Vertical lines at 1000 and 5000 cps indicate the possible error caused by the residual inductances in the measuring circuits.

two polycrystalline samples which were subjected to hydrostatic pressures up to 7500 kg/cm². The pressure dependence of the conductivity, $\Delta V = 11.1$ cm³/mole at 245°C, is in good agreement with previous values.[1] The frequency dependence of the capacity is not affected

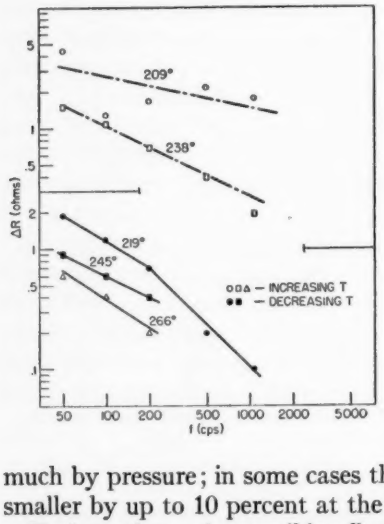

FIG. 3. Excess resistance as a function of frequency for No. 3a (silver electrodes).

much by pressure; in some cases the frequency slope is smaller by up to 10 percent at the higher pressures.

To investigate the possible effects of impurities, two polycrystalline samples were prepared with 0.1 percent (mole) $CdBr_2$ added to the melt. Since the general behavior of these samples (Nos. 28 and 29 in Table I) is not greatly altered, the effects observed for the pure AgBr are presumably characteristic of the ideally pure substance.

When 0.1 volt dc is applied to samples with silver electrodes, the dc resistance is about 5±5 percent larger than the high frequency ac resistance, with occasional erratic effects. After a small direct current (about one Coulomb) has passed through the sample, there is often a decrease of the ac capacity by amounts comparable to those in Fig. 1. For samples with gold electrodes the dc resistance is much larger than the high frequency ac resistance—20 times at 15 sec and 100 times at 3 min—and appears to increase indefinitely with time.

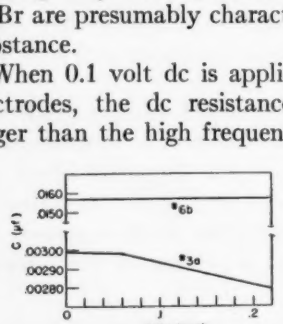

FIG. 4. Variation of capacity with applied voltage for No. 3a (silver electrodes) and No. 6b (gold electrodes) at $T = 218$°C and $f = 200$ cps.

IV. THEORY

A. Differential Equations and Boundary Conditions

To develop a macroscopic mathematical theory, the ionic defects in AgBr are considered as mobile charge carriers in a continuous medium with dielectric constant K. For each type of charge carrier the equilibrium concentration, mobility, and rate constants for formation and recombination are supposed to have known values, depending only on the temperature. The equations are developed and solved for the case of two types of charge carriers, positive (interstitial silver ions) and negative (silver ion vacancies), with the same equilibrium concentration c_0 but different mobilities μ_p and μ_n. (The Einstein relation $\mu/D = e/kT$ between mobility and diffusion coefficient is assumed to be valid, especially for Frenkel defects.) For the case of plane parallel electrodes the differential equations relating the actual concentrations p of positive and n of negative charge carriers and the electric field E are[12]

$$\frac{\partial p}{\partial t} = -\mu_p \frac{\partial (pE)}{\partial x} + D_p \frac{\partial^2 p}{\partial x^2} + k_1(c_0^2 - pn);$$

$$\frac{\partial n}{\partial t} = \mu_n \frac{\partial (nE)}{\partial x} + D_n \frac{\partial^2 n}{\partial x^2} + k_1(c_0^2 - p_n); \qquad (1)$$

$$\frac{\partial E}{\partial x} = \frac{4\pi e}{K}(p - n).$$

The rate constants for formation and recombination of Frenkel defects have been combined into a single constant k_1 by a detailed balance argument, neglecting a

TABLE II. Variation of capacity with pressure. The pressure dependence is represented as $C(T,P) = C(T,0)\exp(-P\Delta V/RT)$.

Sample	T°C	ΔV (cm³/mole) 50 cps	200 cps	1000 cps
14	210	11.7	11.0	
	245	13.3	13.4	
	292	14.6	13.8	
15	210	11.7	12.7	12.1
	245	12.7	12.3	11.0
	292	11.2	10.2	8.5

[12] G. Jaffé, Ann. Physik **16**, 217, 249 (1933).

small term in the first two equations of $k_1c_0^2(n/N)$, where N is the total number of ion pairs per unit volume.

Because of the nonlinear terms in Eqs. (1), it has been necessary to linearize the equations by making two approximations: (a) Since the applied voltage is given by $V(t)=V_0+V_1e^{j\omega t}$, it is assumed that the dependent variables can be represented as[13]

$$p(x,t)=p_0(x)+p_1(x)e^{j\omega t}. \tag{2}$$

(b) The dc solution for zero external dc voltage is taken to be

$$p_0(x)=c_0, \quad n_0(x)=c_0, \quad \text{and} \quad E_0(x)=0. \tag{3}$$

A set of linear, homogeneous equations is then obtained, and these can be solved in a straightforward manner.[14]

$$j\omega p_1=-\mu_p c_0\frac{dE_1}{dx}+D_p\frac{d^2p_1}{dx^2}-k_1c_0(p_1+n_1);$$

$$j\omega n_1=\mu_n c_0\frac{dE_1}{dx}+D_n\frac{d^2n_1}{dx^2}-k_1c_0(p_1+n_1); \tag{4}$$

$$\frac{dE_1}{dx}=\frac{4\pi e}{K}(p_1-n_1).$$

The use of the above approximations is dictated more by necessity than by appropriateness. The omission of terms in $e^{sj\omega t}$ with $s=-1, \pm2, \ldots$, in the Fourier time expansion of Eq. (2) removes the nonlinear features of the theory. The neglect of the nonlinear dependence on voltage is justified if $eV_1/kT\ll1$, however, which is approximately satisfied experimentally, and the higher harmonics are removed from the measurements by the tuned amplifier. Furthermore Eq. (3) does not represent the actual state of affairs very well near a free surface of AgBr[15] or near a contact with metallic silver.[16] Nonetheless the approximation procedure does have the advantage that none of the terms in Eqs. (1) have been discarded. Thus the solutions of Eqs. (4) can be expected to show, at least qualitatively, all of the interesting effects arising from the interactions of the different processes involved—the interplay of the conduction and diffusion currents, the influence of one type of charge carrier on the motion of the other type through space-charge effects, and the role of formation and recombination. A somewhat different approach to this problem has also been presented,[13,17] but has the disadvantage, among others, of making the motion of each type of charge carrier independent of all other types.

One of the boundary conditions is always

$$\int_{-L}^{L}Edx=V,$$

where the origin has been placed at the middle of the sample of length $2L$. The other boundary conditions specify the nature of current flow at the electrodes and will be stated for positive charge carriers. One possible extreme is that no current can flow at all; the other is that current can flow freely:

$$i_p(\pm L,t)=0, \tag{5}$$

or

$$\Delta p(\pm L,t)=0, \tag{6}$$

where Δp is the change in concentration from that existing for zero external voltage. A way of considering intermediate possibilities is to write[17]

$$i_p(\pm L,t)=\pm(eD_p/L)r_p\Delta p(\pm L,t). \tag{7}$$

A possible physical significance for the blocking parameter r_p may be seen by supposing a symmetrical potential barrier of height W to exist at the electrode. Then it is found that $r_p=aL\nu_0D_p^{-1}\exp(-W/kT)$, where a is the interionic distance and ν_0 is the vibrational frequency of an ion in the lattice. With appropriate values for AgBr ($D_p=10^{-4}$ cm^2/sec, $\nu_0=10^{13}$ sec^{-1}), r_p varies from 5×10^{-5} to 2×10^4 for $W=1.4$ to 0.5 ev; this range of values is large enough to give either complete blocking ($r_p\sim0$) or completely free passage ($r_p\sim\infty$) for the experimental range of frequencies. One disadvantage of Eq. (7), however, is that it is not possible to represent any rectifying action at the electrodes with this type of condition even though some rectification probably does occur.

B. General Solution

The general solution of Eqs. (4) for symmetrical boundary conditions is represented by

$$p_1(x)=A_1\sinh a_1x+A_2\sinh a_2x. \tag{8}$$

The polarization effects arise in layers near the electrodes with characteristic lengths determined by.

$$\left\{\begin{matrix}2a_1^2\\2a_2^2\end{matrix}\right\}=(\alpha_p^2+\alpha_n^2)+(\nu_p'+\nu_n')\mp[(\alpha_p^2+\alpha_n^2)^2+(\nu_p'-\nu_n')^2+2(\alpha_p^2-\alpha_n^2)(\nu_p'-\nu_n')]^{\frac{1}{2}},$$

where

$$\alpha_p^2=\alpha^2-\lambda_p, \quad \nu_p'=\nu_p+2\lambda_p,$$
$$\alpha_n^2=\alpha^2-\lambda_n, \quad \nu_n'=\nu_n+2\lambda_n,$$

and

$$\alpha^2=\frac{4\pi e}{K}\frac{e}{kT}c_0, \qquad \begin{matrix}\nu_p=j\omega/D_p, & \lambda_p=k_1c_0/D_p,\\ \nu_n=j\omega/D_n, & \lambda_n=k_1c_0/D_n.\end{matrix}$$

[13] G. Jaffé, Phys. Rev. **85**, 354 (1952).

[14] After most of the work in this paper had been completed, the writer learned that J. R. Macdonald had developed a similar procedure for solving the same differential equations. A private discussion showed that his approximate equations are identical to the ones described here, as are his results for the boundary conditions that he considers (both carriers blocked). See J. R. Macdonald, Phys. Rev. **92**, 4 (1953).

[15] J. Frenkel, *Kinetic Theory of Liquids* (Oxford University Press, London, 1946), pp. 36–40.

[16] T. B. Grimley and N. F. Mott, Discussions Faraday Soc. **1**, 3 (1947).

[17] H. C. Chang and G. Jaffé, J. Chem. Phys. **20**, 1071 (1952).

The significance of the characteristic lengths can be more easily appreciated from the simpler formulas valid for equal mobilities.

$$a_1^2=\nu+2\lambda=(j\omega+2k_1c_0)/D;\quad a_2^2=2\alpha^2+\nu. \tag{9}$$

Except at very high frequencies, $1/a_2=1/\sqrt{2}\alpha$ is the Debye length which appears in the Debye-Hückel theory of strong electrolytes. When formation is not important, $1/|a_1|=(D/\omega)^{\frac{1}{2}}$ is closely related to the rms distance the charge carriers can diffuse during a half-cycle, $(2\pi D/\omega)^{\frac{1}{2}}$. For the conditions encountered in AgBr the two lengths are of the order of 5×10^{-7} cm and 1×10^{-4} cm, respectively.

When the arbitrary constants in Eq. (8) have been determined by application of a certain set of boundary conditions, the remaining step is to calculate the total current flowing through the sample for comparison to the experimentally determined current per unit area,

$$I=(1/R+j\omega C)(V_1/A). \tag{10}$$

By using $i_p=e\mu_pc_0E_1-eD_p(dp_1/dx)$, etc., which is consistent with Eqs. (4), the total current may be calculated as the space average of the conduction and displacement currents to be

$$I=(e\mu_pc_0/2L)V_1+\Delta I_p+(e\mu_nc_0/2L)V_1 +\Delta I_n+(j\omega K/8\pi L)V_1,$$

with

$$\begin{aligned}\Delta I_p&=-(eD_p/2L)[p_1(L)-p_1(-L)];\\ \Delta I_n&=\ (eD_n/2L)[n_1(L)-n_1(-L)].\end{aligned} \tag{11}$$

C. Results for Special Cases

When both types of charge carriers are blocked (Eq. [5]), the total current is given by Eq. (11) with

$$\Delta I_p=-(e\mu_pc_0/2L)V_1(1-F)S;$$

$$\Delta I_n=-\frac{e\mu_nc_0}{2L}V_1\left(-\frac{\alpha_p^2+\nu_p'-a_2^2}{\alpha_p^2} +\frac{\alpha_p^2+\nu_p'-a_1^2}{\alpha_p^2}F\right)S, \tag{12}$$

where

$$F=\frac{(a_1^2-\nu_n'+\alpha_p^2-\alpha_n^2)a_2\coth a_2L}{(a_2^2-\nu_n'+\alpha_p^2-\alpha_n^2)a_1\coth a_1L};$$

$$\frac{1}{S}=\left[\left(1-\frac{\alpha^2}{\alpha_p^2}\frac{a_2^2-\nu_p'}{a_2^2}\right)a_2L\coth a_2L+\frac{\alpha^2}{\alpha_p^2}\frac{a_2^2-\nu_p'}{a_2^2}\right] -\left[\left(1-\frac{\alpha^2}{\alpha_p^2}\frac{a_1^2-\nu_p'}{a_1^2}\right)a_1L\coth a_1L+\frac{\alpha^2}{\alpha_p^2}\frac{a_1^2-\nu_p'}{a_1^2}\right]F.$$

For the situations encountered in AgBr terms of the order of ν/α^2 and $\lambda/\alpha^2(<0.001)$ and $F(<0.01)$ may be neglected; then the parameters of the equivalent circuit can be expressed as

$$-\Delta\left(\frac{1}{R}\right)=\frac{1}{R_0}\frac{1}{1+(\omega\tau)^2};\quad C=\frac{C_0}{1+(\omega\tau)^2}, \tag{13}$$

where $R_0=2L/[e(\mu_p+\mu_n)c_0]$ is the high-frequency bulk resistance, $C_0=K\alpha/(4\pi\sqrt{2})$ is the low-frequency limiting capacity, and $\tau=R_0C_0=\sqrt{2}L/[\alpha(D_p+D_n)]$ is the Debye relaxation time. (At 253°C in AgBr $C_0=3.9\,\mu$f/cm^2, and $\omega\tau=1$ at 300 cps.) The effect of formation and recombination in this case is negligible.

For another case of interest, negative carriers blocked (Eq. [5]) and positive carriers free (Eq. [6]), it is found that

$$\Delta I_p=0,\quad \Delta I_n=-(e\mu_nc_0/2L)V_1[(a_2^2-a_1^2)/\alpha_p^2]S, \tag{14}$$

where

$$\frac{1}{S}=\left(\frac{a_2^2-\nu_n'}{\alpha_p^2}-\frac{\alpha^2\nu_p'}{\alpha_p^2a_1^2}+\frac{\alpha^2-\alpha_n^2}{\alpha_p^2}\right)a_1L\coth a_1L +\frac{\alpha^2}{\alpha_p^2}\frac{\nu_p'(a_2^2-a_1^2)}{a_1^2a_2^2}-\left(\frac{a_1^2-\nu_n'}{\alpha_p^2}-\frac{\alpha^2\nu_p'}{\alpha_p^2a_2^2}+\frac{\alpha^2-\alpha_n^2}{\alpha_p^2}\right) \times a_2L\coth a_2L.$$

The results for the opposite case can be obtained by interchanging the subscripts p and n throughout. Again terms of the order of ν/α^2 and λ/α^2 may be neglected; if the last term in $1/S$ (which contributes <1 percent) is also neglected and it is supposed that formation and recombination are unimportant ($k_1c_0=0$), the equivalent parallel quantities can be expressed as

$$-\Delta\left(\frac{1}{R}\right)=\omega C=\frac{e\mu_nc_0}{\sqrt{2}L^2}\left(\frac{D_p+D_n}{2D_p}\right)^{\frac{1}{2}}\left(\frac{D_n}{\omega}\right)^{\frac{1}{2}}. \tag{15}$$

C now varies as $1/\omega^{\frac{1}{2}}$ and $\Delta(1/R)$ as $1/\omega^{\frac{1}{2}}$ in contrast to the $1/\omega^2$ dependence of both quantities at high frequency in the previous case. There is an appreciable effect from formation and recombination in this case when k_1c_0 is comparable to or larger than ω.

It will be seen that there is a considerable difference between these two cases; this occurs because a new physical process enters into the second case. In the first case the capacity is caused primarily by the piling up of charge carriers at the electrodes; only the Debye length is involved. In the second case this same effect is present for the negative carriers, but in addition the positive carriers carry a sizable current through the electrodes, and phase changes in this, caused by interaction with the space charge of the piled-up negative carriers, also lead to a capacitive effect. At very low frequencies the second effect would predominate, giving a limiting capacity $(K/4\pi)(\alpha^2L/12)\sim1$ farad/cm^2 for $f<10^{-7}$ cps in AgBr at 253°C. For audio-frequencies the two effects are comparable and combine to give the

results of the preceding paragraph, in which the diffusion length is the important distance.

The results for intermediate boundary conditions (Eq. [7]) have been calculated only when formation and recombination are unimportant ($k_1c_0=0$).

$$\Delta I_p=-(e\mu_p c_0/2L)V_1(1-F)S;$$

$$\Delta I_n=-\frac{e\mu_n c_0}{2L}V_1\left(-\frac{\alpha^2+\nu_p-a_2^2}{\alpha^2}+\frac{\alpha^2+\nu_p-a_1^2}{\alpha^2}F\right)S, \quad (16)$$

where

$$F=\frac{(a_1^2-\nu_n)a_2L\coth a_2L+\alpha^2r_p+(\alpha^2+\nu_p-a_2^2)r_n}{(a_2^2-\nu_n)a_1L\coth a_1L+\alpha^2r_p+(\alpha^2+\nu_p-a_1^2)r_n};$$

$$S^{-1}=[(\nu_pL/a_2)\coth a_2L+r_p+(a_2^2-\nu_p)/a_2^2]$$
$$-[(\nu_pL/a_1)\coth a_1L+r_p+(a_1^2-\nu_p)/a_1^2].$$

These formulas usually give results intermediate to those obtained for the previous cases. For a given value of r_p, for instance, the positive carriers appear almost completely blocked at high frequencies and almost completely free at low frequencies; if $r_p<5$, however, the blocking is apparent even for $\omega=0$.

D. Estimates of the Formation and Recombination Rates

In order to determine whether formation and recombination occur rapidly enough to affect the polarization effects appreciably, it is necessary to obtain at least an estimate of the rate constant k_1c_0. The formation process involves the jumping of a silver ion from a normal lattice site to an interstitial position, leaving a vacancy; the energy required is the energy E_F required to form a pair of Frenkel defects plus an energy something like the energy U_i for the mobility of an interstitial ion. By comparison to the formation terms in Eqs. (1),

$$k_1c_0=\nu_0\exp[-(\tfrac{1}{2}E_F+U_i)/kT], \quad (17)$$

where ν_0 is the vibrational frequency of a silver ion in the lattice.[18] With the values of E_F and U_i determined from conductivity measurements[1] and $\nu_0=10^{13}$ sec^{-1}, it is found that $k_1c_0=2\times10^5$ sec^{-1} at 253°C. Although this value does not seem unreasonable,[19] it is large enough to produce a major change in the theoretical results for some cases. Since the experimental results do not indicate any such effect, it is interesting to consider whether there is any reason for a slower formation and recombination rate.

In the previous calculation the energy E_F determined for the equilibrium condition has been used; in this case part of the energy initially required for the formation of the defects has been compensated by the subsequent relaxation of the ions in the neighborhood of the defects. It seems very likely, however, that during formation the jumping ion must practically complete its jump before all of the relaxation of the surrounding ions can occur; hence, Eq. (17) should be replaced by

$$k_1c_0=\nu_0\exp[-(E_F^*+U_i-\tfrac{1}{2}E_F)/kT], \quad (18)$$

where E_F^* is larger than E_F by at least some of the relaxation energy. According to calculations for several alkali halides,[20] the relaxation energy is largely due to the change in energy of the electric polarization of the lattice; a rough calculation of this change using the Jost model[21] gives 20 kcal/mole for the relaxation energy of a pair of Frenkel defects.

A lower limit for k_1c_0 may be estimated from recent rapid specific heat measurements on AgBr[22] if it is assumed that the defects which contribute to the anomalous rise in specific heat above 350°C are Frenkel defects. Since equilibrium is apparently established in less than 5×10^{-4} sec, a lower limit for k_1c_0 at 350°C is 4000 sec^{-1}. By using this value in Eq. (18), it is found that $E_F^*-E_F=8.5$ kcal/mole, and this leads to $k_1c_0=70$ sec^{-1} at 253°C.

V. COMPARISON OF THEORETICAL AND EXPERIMENTAL RESULTS

A. Theoretical Results

Typical theoretical curves, Figs. 5–8, show the capacity in excess of the geometrical capacity $KA/8\pi L$ and the resistance in excess of the bulk resistance R_0.

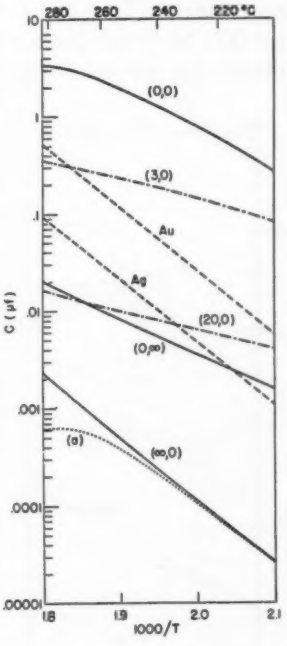

FIG. 5. Theoretical curves of log$C$ *vs* $1/T$ at 200 cps. The values of the blocking parameters are shown in parentheses as (r_p,r_n). The various labels mean the following: (0,0) Both charge carriers blocked. $(0,\infty)$ Positive carriers blocked, negative carriers free. $(\infty,0)$ Positive carriers free, negative carriers blocked. (3,0) and (20,0) Positive carriers partially blocked, negative carriers blocked. (a) The effect of formation and recombination on the $(\infty,0)$ curve is shown. *Ag:* Experimental results for a sample with silver electrodes. *Au:* Experimental results for a sample with gold electrodes.

[18] J. Frenkel, *Kinetic Theory of Liquids* (Oxford University Press, London, 1946), pp. 17–27.

[19] A roughly similar value of $k_1c_0=10$ sec^{-1} at room temperature (the calculations here give $k_1c_0=1$ sec^{-1}) is given by F. Seitz, Revs. Modern Phys. **23**, 328 (1951).

[20] N. F. Mott and M. J. Littleton, Trans. Faraday Soc. **34**, 485 (1938).

[21] W. Jost, J. Chem. Phys. **1**, 466 (1933).

[22] T. E. Pochapsky, J. Chem. Phys. **21**, 1539 (1953).

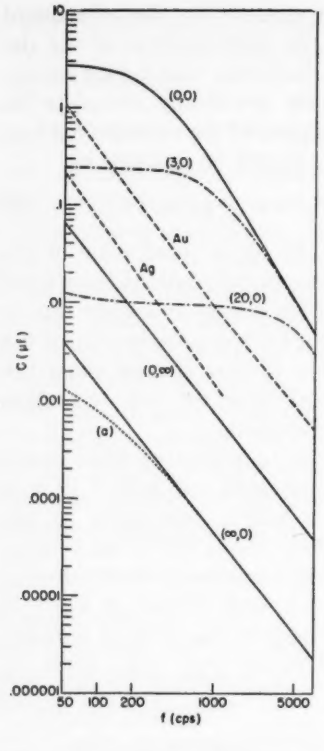

FIG. 6. Theoretical curves of log$C$ *vs* log$f$ at 253°C. Notation as in Fig. 5.

These curves have been calculated for a sample with dimensions $2L=0.61$ cm and $A=0.71$ cm^2 by using the values of c_0, μ_p, and μ_n reported by Kurnick.[1] The effect of formation and recombination has been included only for the dotted curves (a); for these curves fairly large values of k_1c_0 have been chosen by taking $k_1c_0=4000$ sec^{-1} at 350°C (see Sec. IV D) and using Eq. (17) to obtain values at lower temperatures. Although this procedure gives larger values than those

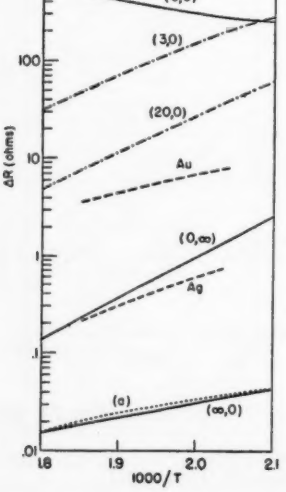

FIG. 7. Theoretical curves of logΔR *vs* $1/T$ at 200 cps. Notation as in Fig. 5.

which would be obtained by using Eq. (18), the change in the curves is not tremendous. The effect of these values of k_1c_0 on the $(0,\infty)$ curves would be about the same; there would not be any noticeable effect on the (0,0) curves.

The solid curves represent the cases with extreme boundary conditions; for purposes of comparison to the experimental results the slopes of the theoretical capacity curves for these cases are given in Table III. For the calculation of the curves with intermediate boundary conditions the possible temperature dependence of r_p (see discussion following Eq. [7]) has not been taken into account because of the peculiar frequency dependence of these curves. Rough calculations for the cases (3,3) and (0,20) show that both these curves lie fairly close to the (3,0) curve and have the same general shape.

B. Comparison of Observed and Calculated Curves

The writer would like to propose that the most nearly correct explanation of the experimental results is contained in the $(\infty,0)$ curves. The calculated magnitudes are rather small for this case, but there is good agreement between the calculated and observed slopes in Figs. 5–8. The calculated magnitudes are in better accord with the observed ones for the opposite case $(0,\infty)$, but there is quite a difference in the calculated and observed temperature dependence of the capacity. Since the slopes are more reproducible experimentally than the magnitudes, this seems to be a serious fault. The calculated magnitudes for the (0,0) case are larger than the observed ones, but neither of the expected low-frequency effects—saturation of capacity and rapid rise of excess resistance—is observed experimentally. In addition the dc resistance measurements indicate that there is by no means complete blocking with silver electrodes. The calculated curves for intermediate boundary conditions have much more curvature than the observed curves.

The smallness of the calculated results for the $(\infty,0)$ case is not especially serious for two reasons. First, according to Eq. (15) it should be found that $\omega C=|\Delta(1/R)|$ for this case; since the ratio of observed to calculated magnitudes for samples with silver electrodes is 40 for capacity and 15 for excess resistance, this condition is roughly satisfied. For the samples with gold electrodes the two ratios are 240 and 160, respectively, in even better agreement. Secondly, there are several reasons for expecting larger results than those given by the theory. One is that the surfaces next to the electrodes are rough compared to the characteristic length of 10^{-4} cm; the actual area of contact is therefore probably larger than the nominal area of the sample by a factor of 2 to 5. Another reason is that even with no applied field there are a large number of vacancies near the electrodes; according to Grimley and Mott the con-

TABLE III. Summary of theoretical results for capacity. Boundary conditions are represented by values of the blocking parameters r_p and r_n.

r_p	r_n	C (μf/cm^2) $T=253$°C $f=200$ cps	T slope (kcal/mole) 50 cps	200 cps	1000 cps	f slope 227°C	253°C	283°C	P slope $\left(\frac{\text{cm}^3}{\text{mole}}\right)$
0	0	1.95	8.7	21.4	28.5	1.97	1.95	1.82	18.0
0	∞	0.0084	16.9	16.9	16.8	1.50	1.50	1.50	9.5
∞	0	0.00050	29.4	29.4	29.4	1.50	1.50	1.50	19.1

centration of vacancies is increased by a factor 100 for a distance of one Debye length near the electrodes.[16] Although it has not been possible to take this excess concentration into account in the theory, it seems likely that there will be some enhancement of the polarization effects.

It seems quite unlikely that the observed polarization effects are primarily due to the motion of bromine ion vacancies, which presumably would be completely blocked at the electrodes, with both silver ion vacancies and interstitial silver ions free at the electrodes. The calculations for this case would be similar to those for the $(0,\infty)$ case and would lead to poor agreement with the observed results in two respects. In the first place, the activation energies for formation and mobility of bromine vacancies are supposed to be considerably larger than the corresponding energies for silver vacancies; the theoretical temperature slopes would thus be considerably larger than the observed ones. Secondly, since the bromine vacancies contribute less than 1/300 of the total conductivity for the temperature range considered,[23] the calculated magnitudes of the polarization effects would be even smaller than those calculated for the silver vacancies. Thus even if bromine vacancies do make a small contribution, their presence is completely masked by the silver vacancies and interstitials.

On the basis of the dc resistance measurements it would appear that the samples with gold electrodes should show a behavior more like the completely blocked case (0,0). It is observed that the polarization effects are larger by about a factor ten with gold electrodes; the character of the curves, however, is nearly the same as for the samples with silver electrodes.

The experimental curves do not show any of the curvature exhibited by the curves (a); hence it must be concluded, since the $(\infty,0)$ curves appear to be appropriate for describing the experimental results, that the formation and recombination rate is somewhat smaller than the value used to calculate the curves (a). A value smaller by a factor ten would cause the curves (a) to lie very close to the solid curves for the $(\infty,0)$ case and would not be especially inconsistent with Pochapsky's experiment.[22]

C. Other Aspects of the Results

Another indication that the actual state of affairs corresponds to some sort of partial blocking at the electrodes is the fact that the observed capacity decreases as the external voltage increases, Fig. 4. The opposite behavior would be expected for the completely blocked case: physically, an increase of voltage would cause more charge to pile up at the electrodes during a half cycle; mathematically, an increase of capacity with voltage has been found in the exact solution for a constant applied voltage.[12] For the cases with one carrier free and the other blocked, on the other hand, it appears reasonable that an increase of voltage tends to keep the current which flows through the electrodes more nearly in phase with the applied voltage, thus causing a decrease of capacity.

The dependence of the magnitude of the observed capacity on the treatment of the electrodes described in Sec. III can now be qualitatively explained. Since the electrodes appear to deteriorate somewhat during annealing, as described, this treatment apparently increases the blocking at the electrodes and hence causes larger values of capacity. While the samples are subjected to a moderate spring pressure during measurement, on the other hand, it is probable that plastic flow of the silver bromide tends to improve the contact with the metal electrodes. Also the passage of a direct current

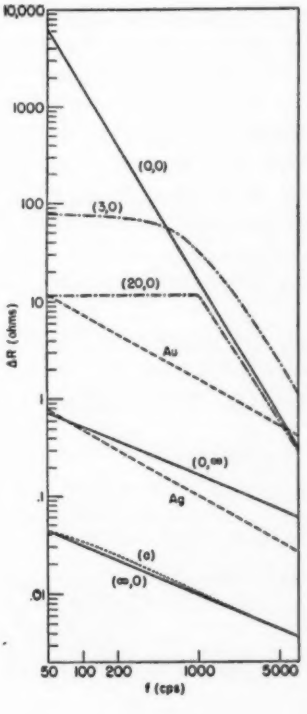

FIG. 8. Theoretical curves of logΔR *vs* log$f$ at 253°C. Notation as in Fig. 5.

[23] C. Tubandt, Handb. exptl. Physik, Vol. XII, Part 1, 1932.

would seem to improve the contact at the electrodes. Thus the slow decrease of capacity in these situations, especially at the higher temperatures, is explained.

The pressure dependence of the capacity has been calculated with the approximate formulas of Eqs. (13) and (15) by using the free volumes given by Kurnick;[1] the slopes are listed in Table III. It will be seen by comparison to Table II that the calculated pressure slopes are somewhat large for the (0,0) and $(\infty,0)$ cases and slightly small for the $(0,\infty)$ case. This is the same situation that exists for the temperature slopes of the polycrystalline samples, and the numbers are even approximately proportional. Hence, the pressure dependence appears to be in substantial agreement with the temperature dependence.

For the (0,0) case at high frequencies and for the $(\infty,0)$ and $(0,\infty)$ cases at all frequencies, the capacity should vary as $1/L^2$. Because of problems associated with the electrical measurements, it was not possible to vary the length a great deal, but some samples were used with about twice the length of the others. As can be seen from Table I the capacity is somewhat less for these samples; the factor looks more like 2 than 4, but the change is in the proper direction.

D. Conclusions

Despite some necessary approximations, the theory predicts a number of interesting polarization effects, and many of these are observed, at least qualitatively, in the experiments. Since polarization effects have been known for many years, it is interesting to have even a semiquantitative explanation starting from the fundamental laws of physics. Although the measurements were hampered by the large bulk conductivity of AgBr and some uncertainty about the boundary conditions, the results agree reasonably well with the theory. It appears that the polarization effects are due to the motion of Frenkel defects, with probably the silver vacancies blocked at the electrodes. Since there is no indication in the experimental results of the effects which would be caused by a fast formation and recombination rate, it is concluded that the rate constant for these processes is smaller than might be expected on the basis of a simple picture.

It is a pleasure for the author to acknowledge the constant encouragement of his sponsor, Professor A. W. Lawson, and the many stimulating discussions with the personnel of the Institute for the Study of Metals.

Electronic Structures of the CH Radical

JIRO HIGUCHI
Laboratory of Physical Chemistry, Tokyo Institute of Technology, Ookayama, Meguro-ku, Tokyo
(Received November 30, 1953)

The electronic states and the molecular constants of the ground and lower excited states of the CH radical are calculated by the Heitler-London method and the LCAO-SCF method. In the former, s^2p^2, sp^3, and p^4 configurations of the carbon atom are taken into account for the wave function, and in the latter LCAO-SCF MOs are calculated for the ground and lower excited states. The interactions between all electrons are considered, but the orthogonal relationship between the 1*s* orbitals of carbon and hydrogen is assumed. As much as possible, the energy integrals were computed from SCF AOs. The results are in general agreement with the observations and Mulliken's prediction. It is concluded that without configuration interaction no satisfactory LCAO-SCF calculation can be made to determine the ground state of the radical as well as of the electronic levels of the carbon atom.

I. INTRODUCTION

THE observed electronic states of the CH radical are $^2\Sigma^+$, $^2\Sigma^-$, $^2\Delta$, and $^2\Pi$, and its ground state has been considered to be $^2\Pi$.[1,2] Mulliken[3] showed from molecular orbital considerations that the not yet observed state $^4\Sigma^-$ is probably close above the $^2\Pi$ state or it may lie lower and be the ground state. A few calculations,[4,5] in which the atomic orbital method is used, lead to the same conclusion, but the approximations used, like disregard of overlap integrals or use of an approximate Hamiltonian, may affect the result considerably. In the present work the electronic properties of the ground and lower excited states of the CH radical are newly investigated by using both the methods of molecular orbitals and atomic orbitals, complemented in these points.

The molecular orbital treatment adopted here is the LCAO self-consistent field (SCF) method developed by Roothaan.[6] This method has already been applied by several authors[7–9] to the ground states of molecules in which each orbital is filled with electrons having paired spins. In the present work, the method is applied to the electronic states of the CH radical which have non-closed shells. The energy levels of the lower excited states are computed by use of the ground state MOs and compared with the observed values and also with the results obtained by use of the corresponding state MOs and by the atomic orbital treatment. It is believed that these results will be useful for a test of the LCAO-SCF method.

The calculation is performed by taking the six atomic orbitals *c*, *s*, σ, π_+, π_-, and *h* into consideration, which mean 1*s*, 2*s*, 2*p*σ, 2*p*π_+, 2*p*π_- orbitals of carbon atom and 1*s* of hydrogen atom, respectively. The interactions between all electrons have been explicitly included but the orthogonality between *c* and *h* is assumed, because its overlap integral is considerably smaller than the others.[10]

II. ATOMIC ORBITALS AND ENERGY INTEGRALS

It is desirable for the calculation to choose atomic orbitals which can give reasonable energy values. In ordinary calculations the simple Slater AOs[11] have been used, but these orbitals are not necessarily accurate in the following points: for instance, the kinetic energy of the 2*s* orbital is only one-third of that of the 2*p* orbital, and the Coulomb integral between two 2*s* orbitals is identical with that between the 2*s* and 2*p* orbitals.

To correct these points an orthogonal 2*s* function is generally used, but these orbitals are still inaccurate in the case of the molecule or free radical as well as in the free atom. For example, the energy difference between the ^1D state and the ^3P state of the carbon atom, and between the $^2\Sigma^+$ state and the $^2\Delta$ state of the CH radical, assuming the single configuration, is theoretically $K_{\pi_+\pi_-}$. This is the one-center integral of carbon, and its value is calculated as 1.82 ev by Slater AOs, while the observed value is 1.26 ev[12] for the atom and 1.07 ev[1] for the radical. The calculated value is considered to be too large, even if the configuration interaction is included.

In view of these facts, it is desirable to use the SCF AOs of Hartree[13,14] or Hartree-Fock[15] instead of the Slater AOs. In this case better results are obtained for the free atom, and the calculated value of the above-mentioned integral $K_{\pi_+\pi_-}$ is not too large as in the case of Slater AOs.

If the Hartree-Fock SCF AOs are chosen for the carbon atom in the $^2\Pi$ state, these AOs must satisfy the following Fock equations of the valence state $V_2(\sigma\pi)$ in

[1] G. Herzberg, *Molecular Spectra and Molecular Structure* (D. Van Nostrand Company, Inc., New York, 1950), second edition, Vol. I, p. 518.
[2] H. Sponer, *Molekülspektren* (Verlag Julius Springer, Berlin, 1935), I. Tabellen, p. 26.
[3] R. S. Mulliken, Revs. Modern Phys. **4**, 1 (1932).
[4] K. Niira and K. Oohata, J. Phys. Soc. Japan **7**, 61 (1952).
[5] J. Higuchi, Bull. Chem. Soc. Japan **26**, 1 (1953).
[6] C. C. J. Roothaan, Revs. Modern Phys. **23**, 69 (1951).
[7] R. G. Parr and R. S. Mulliken, J. Chem. Phys. **18**, 1338 (1950).
[8] J. F. Mulligan, J. Chem. Phys. **19**, 347 (1951).
[9] R. G. Parr and G. R. Taylor, J. Chem. Phys. **19**, 497 (1951).
[10] For example, $S_{ch}=0.07$ while $S_{sh}=0.56$ and $S_{\sigma h}=0.48$ at the internuclear distance of 1.124 A.
[11] $c=(\delta'^3/\pi)^{\frac{1}{2}}\exp(-\delta' r)$, $s=(\delta^5/3\pi)^{\frac{1}{2}}r\exp(-\delta r)$, $\sigma=(\delta^5/\pi)^{\frac{1}{2}}r\times\exp(-\delta r)\cos\theta$, $\pi_\pm=(\delta^5/\pi)^{\frac{1}{2}}r\exp(-\delta r)\sin\theta\exp(\pm i\varphi)$ and $h=(1/\pi)^{\frac{1}{2}}\exp(-r)$. In the present calculation δ and δ' are chosen as 1.59 and 5.6875, respectively.
[12] R. F. Bacher and S. Goudsmit, Phys. Rev. **46**, 948 (1934); W. Moffitt, Proc. Roy. Soc. (London) **A202**, 534 (1950).
[13] C. C. Torrance, Phys. Rev. **46**, 388 (1934).
[14] C. W. Ufford, Phys. Rev. **53**, 568 (1938).
[15] A. Jucys, Proc. Roy. Soc. (London) **A173**, 59 (1939).

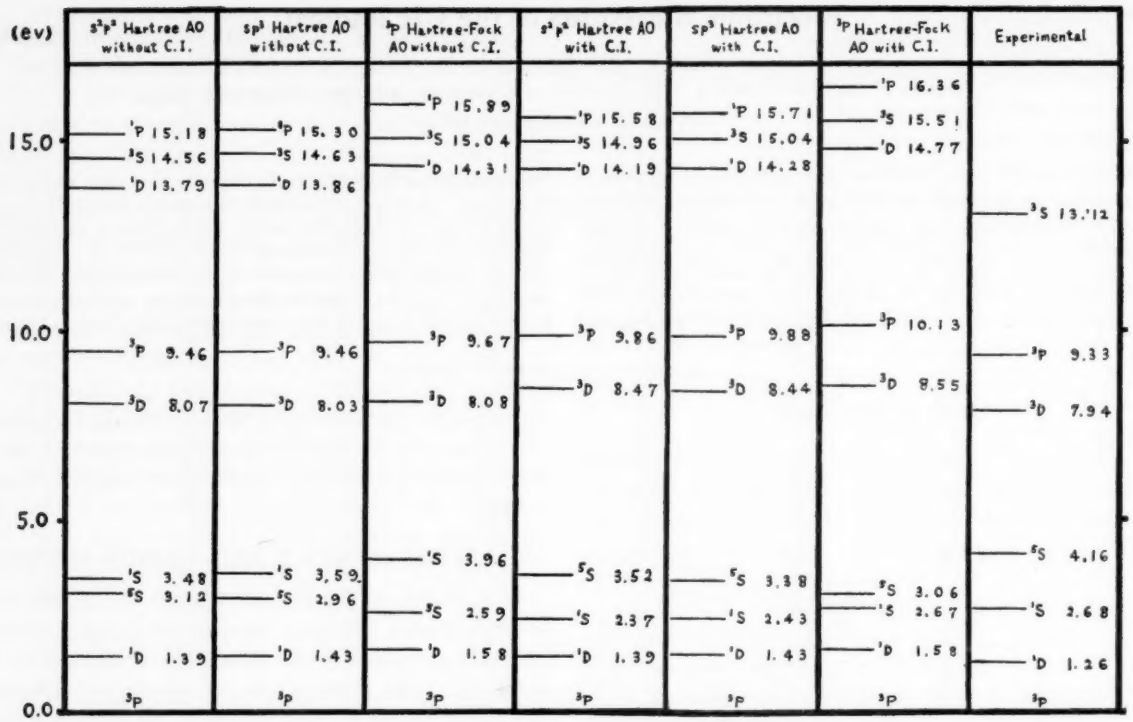

FIG. 1. Electronic levels of the carbon atom.

the s^2p^2 configuration of the carbon atom, for the bonding property in the $^2\Pi$ state is generally considered as being of $2p$ type.[16]

$$(I+2J_c-K_c+2J_s-K_s+J_\sigma-\tfrac{1}{2}K_\sigma+J_\pi-\tfrac{1}{2}K_\pi)s = (I_s+2J_{cs}-K_{cs}+J_{s\sigma}-\tfrac{1}{2}K_{s\sigma}+J_{s\pi}-\tfrac{1}{2}Ks_\pi)s \quad (1)$$

$$(I+2J_c-K_c+2J_s-K_s+J_\pi-\tfrac{1}{2}K_\pi)\sigma = (I_\sigma+2J_{c\sigma}-K_{c\sigma}+2J_{s\sigma}-K_{s\sigma}+J_{\sigma\pi}-\tfrac{1}{2}K_{\sigma\pi})\sigma. \quad (2)$$

Here

$$I=-\tfrac{1}{2}\Delta_\mu-\frac{6}{r_{C\mu}} \quad (3)$$

$$J_i{}^\mu\phi^\mu=\left(\int\bar{\phi}_i{}^\nu\frac{1}{r^{\mu\nu}}\phi_i{}^\nu dv^\nu\right)\phi^\mu \quad (4)$$

$$K_i{}^\mu\phi^\mu=\left(\int\bar{\phi}_i{}^\nu\frac{1}{r^{\mu\nu}}\phi^\nu dv^\nu\right)\phi_i{}^\mu \quad (5)$$

and

$$I_i=\int\bar{\phi}_i{}^\mu\left(-\tfrac{1}{2}\Delta_\mu-\frac{1}{r_{C\mu}}\right)\phi_i{}^\mu dv^\mu \quad (6)$$

$$J_{ij}=\int\bar{\phi}_i{}^\mu\bar{\phi}_j{}^\nu\frac{1}{r^{\mu\nu}}\phi_i{}^\mu\phi_j{}^\nu dv^{\mu\nu} \quad (7)$$

$$K_{ij}=\int\bar{\phi}_i{}^\mu\bar{\phi}_j{}^\nu\frac{1}{r^{\mu\nu}}\phi_j{}^\mu\phi_i{}^\nu dv^{\mu\nu}, \quad (8)$$

where $r_{C\mu}$ is the distance between the carbon nucleus and the μth electron, and $r^{\mu\nu}$ is the distance between the μth and the νth electron.

But in practice, the SCF AOs which satisfy Eqs. (1) and (2) have not been obtained, and therefore in the present paper it is assumed that the Hartree SCF AOs for the s^2p^2 configuration satisfy these equations. Consequently one-center integrals calculated by Ufford[14] were used. This assumption has errors due to the exchange terms, but they may not be large, because the differences between the electronic levels of the carbon atom, calculated by the SCF AOs of Hartree on the one hand and Hartree-Fock on the other hand, are small as shown in Fig. 1. The majority of the two-center integrals are, however, difficult to calculate, and it is therefore assumed that the use of Slater AOs instead of the SCF AOs gives satisfactory approximations of the two-center integrals. They are taken from the table by Kotani and Amemiya[17] which is calculated by using Slater AOs of s, σ, π, and h. The core-field energies are, however, obtained from Eqs. (1) and (2), because for those cases the Slater AOs are not good approximations.

In the present paper the electronic states of the CH radical are calculated by using these energy values, although the valence state of carbon is not $V_2(\sigma\pi)$ in the states other than the II state. This approximation may be allowed, because the values are almost identical with those using the other valence state. The contributions from the electronic configuration of carbon are not the

[16] W. Moffitt, Proc. Roy. Soc. (London) **A202**, 548 (1950).

[17] M. Kotani and A. Amemiya, Proc. Phys. Math. Soc. Japan **22**, Extra No. I (1940).

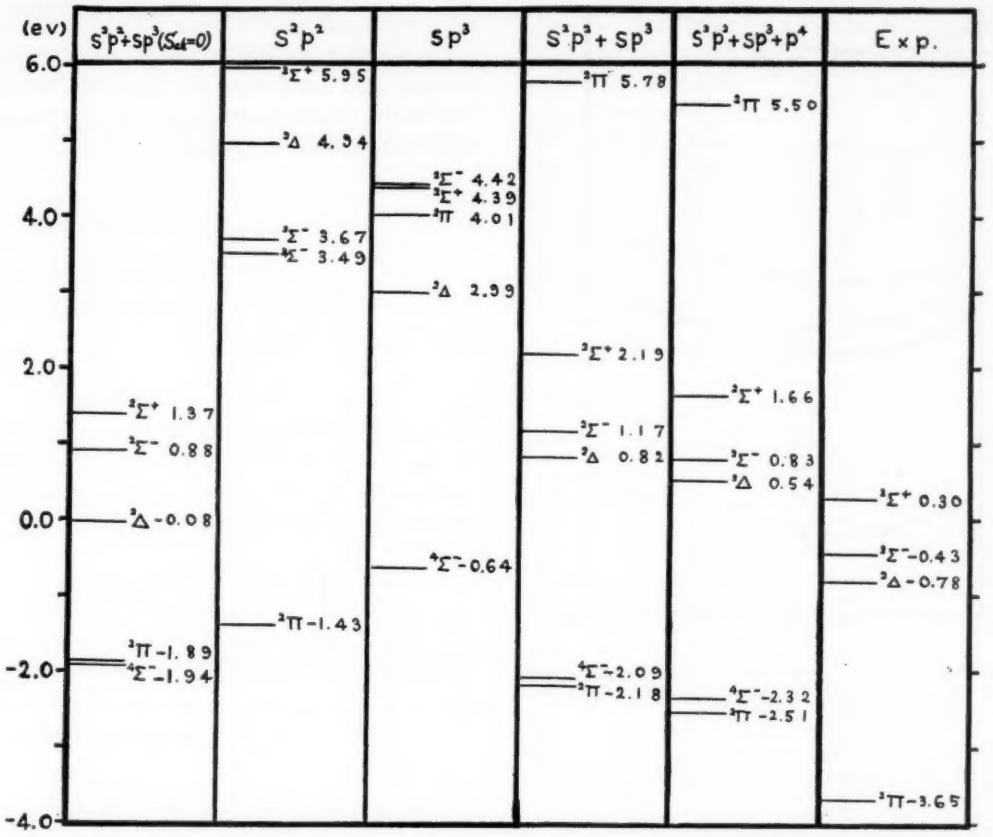

FIG. 2. Electronic levels calculated by the Heitler-London method for the various atomic configurations at the internuclear distance of 1.124 A. The origin of energy is chosen to be $C(^3P)+H(^2S)$ with configuration interaction. The left side shows the levels which are calculated by disregarding the nonorthogonality and by including the influence of 1*s* orbital of carbon.

same in the different states. It is more desirable to use the SCF AOs for sp^3, especially in the $^4\Sigma^-$ state, in which the contribution of sp^3 is prominent. In the present calculation, however, this point is not considered, because there is little difference between the energies calculated with s^2p^2 and sp^3 AOs as shown in Fig. 1.

III. ATOMIC ORBITAL CALCULATION

The ground and lower excited states ($^2\Pi$, $^4\Sigma^-$, $^2\Delta$, $^2\Sigma^-$, $^2\Sigma^+$ and $^2\Pi$) of the CH radical are investigated by the Heitler-London method. In the calculation of the CH radical the role of both the s^2p^2 and sp^3 configurations of carbon is very important.[5] The effect of p^4 configuration is of some significance in the relationship between the ^5S state and the ^1S state of the carbon atom. Therefore, in the present calculation, the s^2p^2, sp^3 and p^4 configurations of carbon are taken in, whereas all ionic structures are disregarded. Thus, there are twelve possible kinds of the electronic orbital wave functions for the entire radical, which are given by the products of atomic orbitals:

$$\begin{aligned}\Psi^A&=(c)(c)(s)(s)(\sigma)(\sigma)(h)\\ \Psi^B&=(c)(c)(s)(s)(\pi_+)(\pi_-)(h)\\ \Psi^C&=(c)(c)(s)(s)(\sigma)(\pi_\pm)(h)\\ \Psi^D&=(c)(c)(s)(s)(\pi_\pm)(\pi_\pm)(h)\end{aligned}\qquad(9)$$

in the s^2p^2 configuration,

$$\begin{aligned}\Psi^E&=(c)(c)(s)(\sigma)(\pi_+)(\pi_-)(h)\\ \Psi^F&=(c)(c)(s)(\sigma)(\sigma)(\pi_\pm)(h)\\ \Psi^G&=(c)(c)(s)(\pi_\pm)(\pi_\pm)(\pi_\mp)(h)\\ \Psi^H&=(c)(c)(s)(\sigma)(\pi_\pm)(\pi_\pm)(h)\end{aligned}\qquad(10)$$

in the sp^3 configuration, and

$$\begin{aligned}\Psi^I&=(c)(c)(\sigma)(\sigma)(\pi_+)(\pi_-)(h)\\ \Psi^J&=(c)(c)(\pi_+)(\pi_+)(\pi_-)(\pi_-)(h)\\ \Psi^K&=(c)(c)(\sigma)(\pi_\pm)(\pi_\pm)(\pi_\mp)(h)\\ \Psi^L&=(c)(c)(\sigma)(\sigma)(\pi_\pm)(\pi_\pm)(h)\end{aligned}\qquad(11)$$

in the p^4 configuration.

Since the spatial symmetry of the CH radical belongs to the symmetry group $C_{\infty v}$ and the electronic terms with different multiplicity or symmetry do not interact, the basic wave functions for this radical, which are constructed from (9), (10), and (11) to fit the Pauli principle, can be classified by the irreducible representations of $C_{\infty v}$ (Σ^+, Σ^-, Π, and Δ). Thus, there are 6, 5, 8, 4, and 5 basic wave functions belonging to the types of $^2\Sigma^+$, $^2\Sigma^-$, $^2\Pi$, $^2\Delta$, and $^4\Sigma^-$, respectively, which can be

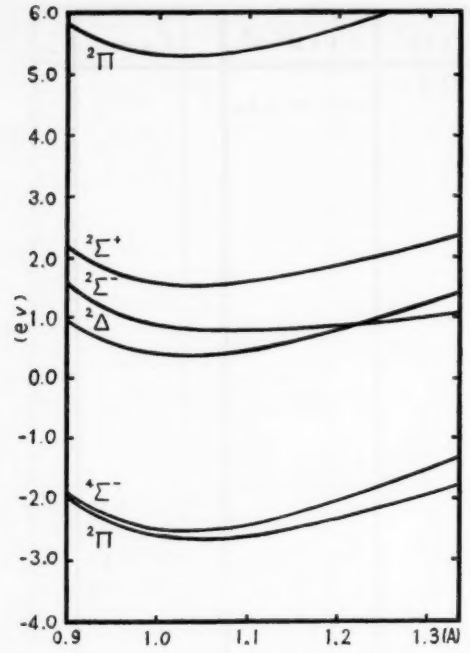

FIG. 3. Potential curves calculated by the Heitler-London method. The origin of energy is chosen to be $C(^3P)+H(^2S)$ with configuration interaction.

constructed by the method of Serber,[18] Yamanouchi,[19] and Kotani and Siga.[20]

The Hamiltonian of this system should be given by

$$\mathbf{H}=\sum_{\mu=1}^{7}\left(-\tfrac{1}{2}\Delta_\mu-\frac{6}{r_{C\mu}}-\frac{1}{r_{H\mu}}\right)+\tfrac{1}{2}\sum_{\substack{\mu,\nu=1\\ \mu\neq\nu}}^{7}\frac{1}{r^{\mu\nu}}. \tag{12}$$

Thus, the secular equations can be set up by using these antisymmetrized basic wave functions as follows:

$$\det.|H_{mn}-S_{mn}E|=0.^{21} \tag{13}$$

By evaluating the necessary integrals the electronic energies can be calculated.

Figure 2 shows the electronic levels calculated by assuming the various atomic configurations at the internuclear distance of 1.124 A which is very close to the equilibrium internuclear distance of the $^2\Pi$ state (1.120 A),[1] and Fig. 3 shows the potential curves obtained by solving the secular equations including all nonpolar configurations. Table I gives the vibrational frequencies ω_e's, the equilibrium internuclear distances r_e's and the electronic levels at the equilibrium points for each state, and Table II gives the contributions from the s^2p^2, sp^3, and p^4 configurations for these states.

[18] R. Serber, Phys. Rev. **45**, 461 (1934); J. Chem. Phys. **2**, 697 (1934).
[19] T. Yamanouchi, Proc. Phys. Math. Soc. Japan **18**, 623 (1936).
[20] M. Kotani and M. Siga, Proc. Phys. Math. Soc. Japan **19**, 471 (1937).
[21] Formulas for all the matrix elements are obtainable from the author upon request.

IV. LCAO-SCF CALCULATION

LCAO-MO ϕ's which are formed by the six atomic orbitals χ_p's are chosen so that they belong in sets to irreducible representations of the symmetry $C_{\infty v}$ of the CH radical, and they are reduced to

$$\begin{aligned} &K(\sigma)=c,\\ &1\sigma=a_{11}s+a_{12}\sigma+a_{13}h,\\ &2\sigma=a_{21}s+a_{22}\sigma+a_{23}h,\\ &3\sigma=a_{31}s+a_{32}\sigma+a_{33}h,\\ &1\pi_+=\pi_+,\\ &1\pi_-=\pi_-. \end{aligned} \tag{14}$$

Here, in the $i\sigma$ orbitals, the order of increasing number i is the order of increasing orbital energy. And the coefficients a_{ip} of atomic orbitals χ's are chosen to satisfy the orthonormality conditions:

$$\int\bar{\phi}_i{}^\nu\phi_j{}^\nu dv^\nu=\sum_{p,q}\bar{a}_{ip}S_{pq}a_{jq}=\delta_{ij}, \tag{15}$$

where the overlap integrals S_{pq} are defined by

$$S_{pq}=\bar{S}_{qp}=\int\bar{\chi}_p\chi_q dv. \tag{16}$$

The electronic structure of the lowest $^2\Pi$ state is given as resulting from configuration $(1\sigma)^2(2\sigma)^2(1\pi)^1$ by Mulliken. The total seven electron normalized wave

TABLE I. Molecular constants.

Method	State	D_e(ev)[a]	E_e(ev)[b]	ω_e(cm^{-1})	r_e(A)
Heitler-London	$^2\Pi$		7.93	3.5×10^3	1.04
	$^2\Sigma^+$		4.15	3.5×10^3	1.05
	$^2\Sigma^-$		3.41	2.6×10^3	1.10
	$^2\Delta$		2.99	3.6×10^3	1.04
	$^4\Sigma^-$		0.12	3.7×10^3	1.04
	$^2\Pi$	2.60	0.00	3.4×10^3	1.06
LCAO SCF without C.I.	$^2\Pi$		6.77	3.3×10^3	1.13
	$^2\Sigma^+$		3.70	3.4×10^3	1.09
	$^2\Sigma^-$		3.08	3.1×10^3	1.14
	$^2\Delta$		2.30	3.4×10^3	1.09
	$^4\Sigma^-$		−0.21	3.7×10^3	1.07
	$^2\Pi$	(2.70)	0.00	3.3×10^3	1.09
LCAO SCF with C.I.	$^2\Pi$		7.09	3.1×10^3	1.14
	$^2\Sigma^+$		3.65	3.2×10^3	1.11
	$^2\Sigma^-$		3.07	3.1×10^3	1.13
	$^2\Delta$		2.75	3.3×10^3	1.10
	$^4\Sigma^-$		0.09	3.5×10^3	1.08
	$^2\Pi$	2.98	0.00	3.1×10^3	1.09
Experimental[c]	$^2\Pi$		...	...	...
	$^2\Sigma^+$		3.94	2.8×10^3	1.11
	$^2\Sigma^-$		3.21	2.5×10^3	1.19
	$^2\Delta$		2.87	2.9×10^3	1.10
	$^4\Sigma^-$		...	...	...
	$^2\Pi$	3.65	0.00	2.9×10^3	1.12

[a] The energy of the $C(^3P)$ is calculated by including the interaction of the p^4 configuration; therefore the value by the LCAO SCF method without configuration interaction is not correct dissociation energy.
[b] Excitation energies are relative to the lowest $^2\Pi$ state.
[c] See reference 1.

function Φ for this state is then built up as an antisymmetrized product of these LCAO MOs and the energy of the state is given by

$$E=\int\bar{\Phi}\mathbf{H}\Phi dv. \tag{17}$$

Introducing the notations

$$H_i=\int\bar{\phi}_i{}^{\nu}\left(-\tfrac{1}{2}\Delta_{\nu}-\frac{6}{r_{C\nu}}-\frac{1}{r_{H\nu}}\right)\phi_i{}^{\nu}dv^{\nu} \tag{18}$$

and

$$H'_i=H_i+2J_{ci}-K_{ci}, \tag{19}$$

one obtains

$$\begin{aligned}E=2H_c+J_{cc}+2H'_{1\sigma}+2H'_{2\sigma}+H'_{1\pi}+J_{1\sigma1\sigma}\\+4J_{1\sigma2\sigma}-2K_{1\sigma2\sigma}+2J_{1\sigma1\pi}-K_{1\sigma1\pi}\\+J_{2\sigma2\sigma}+2J_{2\sigma1\pi}-K_{2\sigma1\pi}.\end{aligned} \tag{20}$$

To obtain the 1σ and 2σ orbitals, a variational procedure is carried out for the energy of state (17), subject to the orthonormality conditions of the MOs (15). It can be shown that this variational process leads to the following equation for the orbital:

$$(\mathbf{H}'+\mathbf{G})\mathbf{a}_i=\epsilon_{ii}\mathbf{S}\mathbf{a}_i. \tag{21}$$

Here the column vectors $\mathbf{a}_i$'s give the coefficients of the AOs in the $i\sigma$ orbitals. $\mathbf{S}$ is a Hermitian matrix with elements given by (16); $\mathbf{H}'$ is the core-field energy matrix with elements

$$\begin{aligned}H'_{pq}=\overline{H'}_{qp}=\int\bar{\chi}_p{}^{\nu}\left(-\tfrac{1}{2}\Delta_{\nu}-\frac{6}{r_{C\nu}}-\frac{1}{r_{H\nu}}\right)\chi_q{}^{\nu}dv^{\nu}\\+2(pq:cc)-(pc:cq),\end{aligned} \tag{22}$$

where

$$(pq:rt)=\int\bar{\chi}_p{}^{\mu}\bar{\chi}_r{}^{\nu}\frac{1}{r^{\mu\nu}}\chi_q{}^{\mu}\chi_t{}^{\nu}dv^{\mu\nu}. \tag{23}$$

$\mathbf{G}$ is the electronic interaction matrix with elements

$$G_{pq}=\bar{G}_{qp}=\sum_{n=1}^{7}d_nD_{pq}{}^{(n)}, \tag{24}$$

where the d_n's and $D_{pq}{}^{(n)}$'s are given by

$$\begin{aligned}d_1&=a_{11}{}^2+a_{21}{}^2\\d_2&=a_{11}a_{12}+a_{21}a_{22}\\d_3&=a_{11}a_{13}+a_{21}a_{23}\\d_4&=a_{12}{}^2+a_{22}{}^2\\d_5&=a_{12}a_{13}+a_{22}a_{23}\\d_6&=a_{13}{}^2+a_{23}{}^2\\d_7&=\tfrac{1}{2}\end{aligned} \tag{25}$$

TABLE II. Contributions from the s^2p^2, sp^3, and p^4 configurations.[a]

State	$R(A)$ / Configuration	0.920	1.022	1.124	1.226	1.328
$^2\Sigma^+$	s^2p^2	0.49	0.50	0.55	0.63	0.73
	sp^3	0.47	0.46	0.41	0.33	0.23
	p^4	0.04	0.04	0.04	0.04	0.04
$^2\Sigma^-$	s^2p^2	0.67	0.66	0.71	0.78	0.85
	sp^3	0.29	0.31	0.26	0.20	0.13
	p^4	0.04	0.03	0.03	0.02	0.02
$^2\Delta$	s^2p^2	0.46	0.47	0.52	0.59	0.68
	sp^3	0.51	0.50	0.46	0.39	0.30
	p^4	0.03	0.03	0.02	0.02	0.02
$^4\Sigma^-$	s^2p^2	0.30	0.31	0.34	0.38	0.44
	sp^3	0.68	0.67	0.64	0.60	0.54
	p^4	0.02	0.02	0.02	0.02	0.02
$^2\Pi$	s^2p^2	0.93	0.90	0.90	0.91	0.93
	sp^3	0.05	0.08	0.08	0.07	0.05
	p^4	0.02	0.02	0.02	0.02	0.02

[a] These values correspond to the contribution from the electronic configuration of the carbon atom at infinite separation.

and

$$\begin{aligned}D_{pq}{}^{(1)}&=2(pq:ss)-(ps:sq)\\D_{pq}{}^{(2)}&=4(pq:s\sigma)-(ps:\sigma q)-(p\sigma:sq)\\D_{pq}{}^{(3)}&=4(pq:sh)-(ps:hq)-(ph:sq)\\D_{pq}{}^{(4)}&=2(pq:\sigma\sigma)-(p\sigma:\sigma q)\\D_{pq}{}^{(5)}&=4(pq:\sigma h)-(p\sigma:hq)-(ph:\sigma q)\\D_{pq}{}^{(6)}&=2(pq:hh)-(ph:hq)\\D_{pq}{}^{(7)}&=2(pq:\pi\pi)-(p\pi:\pi q).\end{aligned} \tag{26}$$

Thus, the H'_{pq}'s, $D_{pq}{}^{(n)}$'s, and S_{pq}'s corresponding to the atomic orbitals p and q are obtained. The procedure followed in the calculation is to assume values of the $\mathbf{a}_i$'s consistent with the orthonormality conditions (15), compute the G_{pq}'s by (25) and (24), solve Eq. (21) for ϵ_{ii} and a new set of $\mathbf{a}_i$'s, and repeat until self-consistency is attained.

In the same way the LCAO-SCF calculations are performed for the following lower excited states:

$$\begin{aligned}^4\Sigma^-:\ E=2H_c+J_{cc}+2H'_{1\sigma}+H'_{2\sigma}+2H'_{1\pi}+J_{1\sigma1\sigma}\\+2J_{1\sigma2\sigma}-K_{1\sigma2\sigma}+4J_{1\sigma1\pi}-2K_{1\sigma1\pi}+2J_{2\sigma1\pi}\\-2K_{2\sigma1\pi}+J_{1\pi_+1\pi_-}-K_{1\pi_+1\pi_-}.\end{aligned} \tag{27}$$

$$\begin{aligned}^2\Delta:\ E=2H_c+J_{cc}+2H'_{1\sigma}+H'_{2\sigma}+2H'_{1\pi}+J_{1\sigma1\sigma}\\+2J_{1\sigma2\sigma}-K_{1\sigma2\sigma}+4J_{1\sigma1\pi}-2K_{1\sigma1\pi}+2J_{2\sigma1\pi}\\-K_{2\sigma1\pi}+J_{1\pi_\pm1\pi_\pm}.\end{aligned} \tag{28}$$

$$\begin{aligned}^2\Sigma^-:\ E=2H_c+J_{cc}+2H'_{1\sigma}+H'_{2\sigma}+2H'_{1\pi}+J_{1\sigma1\sigma}\\+2J_{1\sigma2\sigma}-K_{1\sigma2\sigma}+4J_{1\sigma1\pi}-2K_{1\sigma1\pi}+2J_{2\sigma1\pi}\\+K_{2\sigma1\pi}+J_{1\pi_+1\pi_-}-K_{1\pi_+1\pi_-}.\end{aligned} \tag{29}$$

$$\begin{aligned}^2\Sigma^+:\ E=2H_c+J_{cc}+2H'_{1\sigma}+H'_{2\sigma}+2H'_{1\pi}+J_{1\sigma1\sigma}\\+2J_{1\sigma2\sigma}-K_{1\sigma2\sigma}+4J_{1\sigma1\pi}-2K_{1\sigma1\pi}+2J_{2\sigma1\pi}\\-K_{2\sigma1\pi}+J_{1\pi_+1\pi_-}+K_{1\pi_+1\pi_-}.\end{aligned} \tag{30}$$

TABLE III. Self-consistent solutions.[a]

		State	The lowest $^2\Pi$	Lower excited $^2\Pi$	State	$^4\Sigma^-$	$^2\Delta$	$^2\Sigma^-$	$^2\Sigma^+$
S_{ss}	1.00000	G_{ss}	1.8716	1.9632	$G^{(1)}{}_{ss}$	1.9452	1.9306	1.9066	1.9306
$S_{\sigma\sigma}$	1.00000	$G_{\sigma\sigma}$	1.9144	2.2241	$G^{(1)}{}_{\sigma\sigma}$	2.0369	2.0543	2.0824	2.0543
S_{hh}	1.00000	G_{hh}	1.6849	1.7838	$G^{(1)}{}_{hh}$	1.7392	1.7357	1.7328	1.7357
$S_{s\sigma}$	0.00000	$G_{s\sigma}$	0.0619	−0.0456	$G^{(1)}{}_{s\sigma}$	−0.0010	0.0022	0.0145	0.0022
S_{sh}	0.55987	G_{sh}	1.0022	1.0077	$G^{(1)}{}_{sh}$	1.0124	1.0067	1.0048	1.0067
$S_{\sigma h}$	0.46758	$G_{\sigma h}$	0.8149	0.9667	$G^{(1)}{}_{\sigma h}$	0.8732	0.8827	0.8990	0.8827
$S_{\pi\pi}$	1.00000	$G_{\pi\pi}$	1.7835	1.8382	$G^{(2)}{}_{ss}$	1.4429	1.5204	1.6953	1.5204
H'_{ss}	−2.6862			1.8638	$G^{(2)}{}_{\sigma\sigma}$	1.6864	1.7454	1.8429	1.7454
$H'_{\sigma\sigma}$	−2.3742	$\epsilon_{1\sigma 1\sigma}$	−0.8962	−0.8344	$G^{(2)}{}_{hh}$	1.3894	1.4066	1.4460	1.4066
H'_{hh}	−2.3103	$\epsilon_{2\sigma 2\sigma}$	−0.4966		$G^{(2)}{}_{s\sigma}$	−0.0552	−0.0501	−0.0356	−0.0501
$H'_{s\sigma}$	−0.1711	$\epsilon_{1\pi 1\pi}$	−0.4626	−0.4079	$G^{(2)}{}_{sh}$	0.7177	0.7560	0.8497	0.7560
H'_{sh}	−1.6107			−0.3823	$G^{(2)}{}_{\sigma h}$	0.7151	0.7441	0.7940	0.7441
$H'_{\sigma h}$	−1.2868				$G_{\pi\pi}$	1.7596	1.8376	1.8159	1.8888
$H'_{\pi\pi}$	−2.2461				$\epsilon_{1\sigma 1\sigma}$	−0.8456	−0.8596	−0.8639	−0.8596
					$\epsilon_{2\sigma 2\sigma}$	−0.6587	−0.5828	−0.5020	−0.5828
					$\epsilon_{1\sigma 2\sigma}$	0.1313	0.0512	−0.0925	0.0512
					$\epsilon_{1\pi 1\pi}$	−0.4865	−0.4085	−0.4301	−0.3573

[a] Overlap integrals are dimensionless. The other terms have dimension of energy; their values are given in atomic units. 1 atomic unit = 27.204 ev.

$$^2\Pi:\quad E=2H_c+J_{cc}+2H'_{1\sigma}+3H'_{1\pi}+J_{1\sigma 1\sigma}+6J_{1\sigma 1\pi}-3K_{1\sigma 1\pi}+J_{1\pi_\pm 1\pi_\pm}+2J_{1\pi_+ 1\pi_-}-K_{1\pi_+ 1\pi_-}. \quad (31)$$

In these calculations, except for the lower excited $^2\Pi$ state (31), the procedures are considerably troublesome because the variational procedures are carried out for the energies of the states (27)–(30), in which the 2σ orbital is occupied by one electron only, subject to the orthonormality conditions of MOs (15). These processes lead to the following simultaneous equations instead of Eq. (21):

$$\begin{aligned}(\mathbf{H}'+\mathbf{G}^{(1)})\mathbf{a}_1&=\epsilon_{11}\mathbf{S}\mathbf{a}_1+\tfrac{1}{2}\epsilon_{12}\mathbf{S}\mathbf{a}_2\\(\mathbf{H}'+\mathbf{G}^{(2)})\mathbf{a}_2&=\epsilon_{12}\mathbf{S}\mathbf{a}_1+\epsilon_{22}\mathbf{S}\mathbf{a}_2.\end{aligned} \quad (32)$$

TABLE IV. LCAO SCF MOs for the ground and lower excited states.[a]

$$(1\sigma)=\begin{Bmatrix}0.758\\0.698\\0.804\\0.698\\0.631\\0.719\end{Bmatrix}(s)+\begin{Bmatrix}0.211\\0.260\\0.140\\0.260\\0.332\\0.219\end{Bmatrix}(\sigma)+\begin{Bmatrix}0.286\\0.329\\0.259\\0.329\\0.358\\0.326\end{Bmatrix}(h)$$

$$(2\sigma)=-\begin{Bmatrix}0.686\\0.642\\0.572\\0.642\\0.701\\0.647\end{Bmatrix}(s)+\begin{Bmatrix}0.602\\0.707\\0.673\\0.707\\0.686\\0.677\end{Bmatrix}(\sigma)+\begin{Bmatrix}0.523\\0.326\\0.474\\0.326\\0.277\\0.399\end{Bmatrix}(h)$$

$$(3\sigma)=\begin{Bmatrix}0.790\\0.878\\0.834\\0.878\\0.884\\0.857\end{Bmatrix}(s)+\begin{Bmatrix}1.030\\0.948\\0.997\\0.948\\0.941\\0.980\end{Bmatrix}(\sigma)-\begin{Bmatrix}1.335\\1.387\\1.358\\1.387\\1.390\\1.368\end{Bmatrix}(h)$$

$$(1\pi_\pm)=\pi_\pm$$

$$\text{for the}\begin{Bmatrix}^2\Pi & (1\sigma)^2(1\pi_\pm)^2(1\pi_\mp)^1\\ ^2\Sigma^+ & (1\sigma)^2(2\sigma)^1(1\pi_+)^1(1\pi_-)^1\\ ^2\Sigma^- & (1\sigma)^2(2\sigma)^1(1\pi_+)^1(1\pi_-)^1\\ ^2\Delta & (1\sigma)^2(2\sigma)^1(1\pi_\pm)^2\\ ^4\Sigma^- & (1\sigma)^2(2\sigma)^1(1\pi_+)^1(1\pi_-)^1\\ ^2\Pi & (1\sigma)^2(2\sigma)^2(1\pi_\pm)^1\end{Bmatrix}\text{state, respectively.}$$

[a] These MOs are calculated at the internuclear distance of 1.124 A.

Here, $\mathbf{H}'$ and $\mathbf{S}$ matrices are identical with those given in Eqs. (22) and (16), respectively, but the elements of $\mathbf{G}^{(i)}$'s are as follows:

$$G^{(1)}{}_{pq}=\overline{G^{(1)}}_{qp}=\sum_{n=1}^{6} d^{(1)}{}_n D_{pq}{}^{(n)}+2(pq:\pi\pi)-(p\pi:\pi q)$$

$$G^{(2)}{}_{pq}=\overline{G^{(2)}}_{qp}=\sum_{n=1}^{6} d^{(2)}{}_n D_{pq}{}^{(n)}+2(pq:\pi\pi) \quad (33)$$

$$+\begin{Bmatrix}-2\\-1\\+1\end{Bmatrix}(p\pi:\pi q)\ \text{for the}\begin{Bmatrix}^4\Sigma^-\\ ^2\Delta\ \text{or}\ ^2\Sigma^+\\ ^2\Sigma^-\end{Bmatrix}\text{state,}$$

where $D_{pq}{}^{(n)}$'s are given in Eqs. (26), and $d^{(i)}{}_n$'s are given by

$$\begin{aligned}d^{(1)}{}_1&=a_{11}{}^2+\tfrac{1}{2}a_{21}{}^2\\d^{(1)}{}_2&=a_{11}a_{12}+\tfrac{1}{2}a_{21}a_{22}\\d^{(1)}{}_3&=a_{11}a_{13}+\tfrac{1}{2}a_{21}a_{23}\\d^{(1)}{}_4&=a_{12}{}^2+\tfrac{1}{2}a_{22}{}^2\\d^{(1)}{}_5&=a_{12}a_{13}+\tfrac{1}{2}a_{22}a_{23}\\d^{(1)}{}_6&=a_{13}{}^2+\tfrac{1}{2}a_{23}{}^2\end{aligned} \quad (34)$$

and

$$\begin{aligned}d^{(2)}{}_1&=a_{11}{}^2\\d^{(2)}{}_2&=a_{11}a_{12}\\d^{(2)}{}_3&=a_{11}a_{13}\\d^{(2)}{}_4&=a_{12}{}^2\\d^{(2)}{}_5&=a_{12}a_{13}\\d^{(2)}{}_6&=a_{13}{}^2.\end{aligned} \quad (35)$$

The calculation for the lower excited $^2\Pi$ state is easily performed in like manner as for the lowest $^2\Pi$ state. Table III gives the self-consistent solutions obtained by such procedures at the internuclear distance of 1.124 A, and Table IV gives the LCAO MOs of the lowest

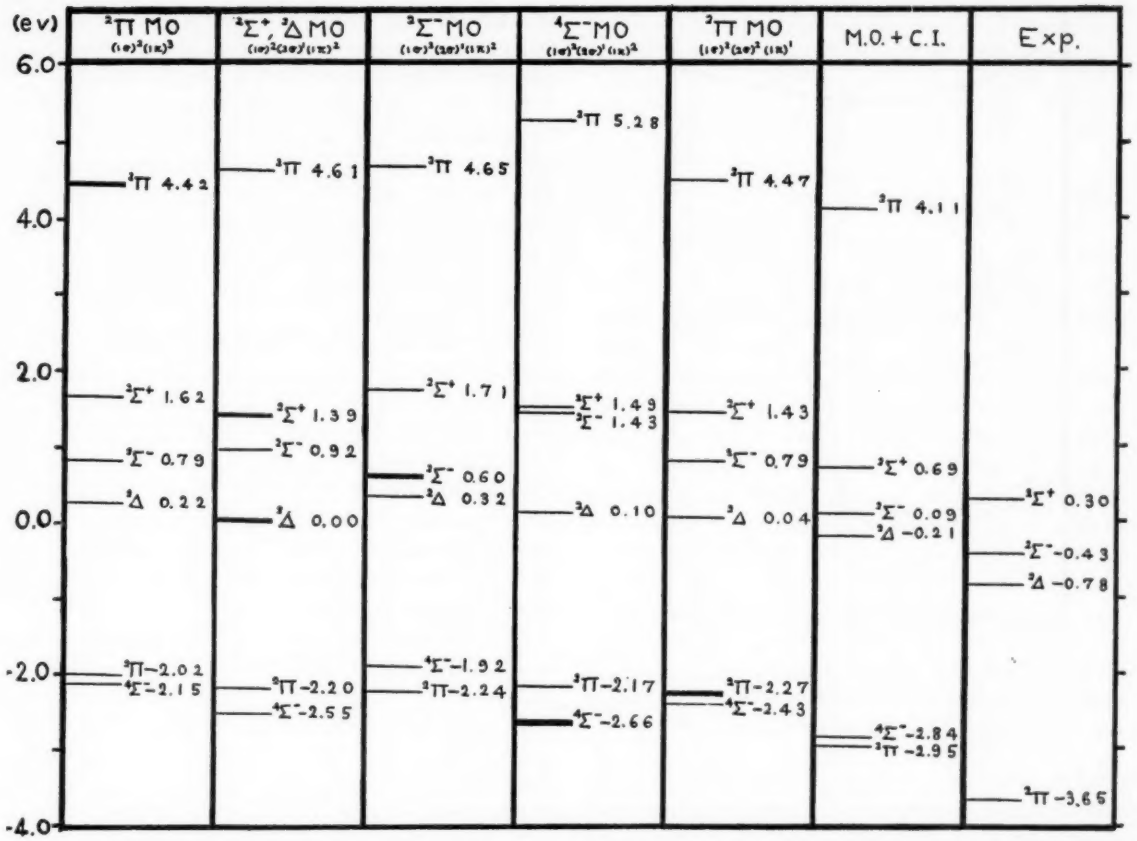

FIG. 4. Electronic levels calculated by the various LCAO-SCF MOs at the internuclear distance of 1.124 A. The origin of energy is chosen to be $C(^3P)+H(^2S)$ with configuration interaction. The bold line shows the level in which the energy is minimized.

energies of these states. From the LCAO MOs the electronic levels are calculated as shown in Fig. 4.

In the electronic levels of these states, assuming the single configuration, the energies calculated by using the lowest $^2\Pi$ state MOs are good approximations of those calculated by using the MOs which minimize the energy of each state. Accordingly, the calculations for several internuclear distances are carried out for the lowest $^2\Pi$ state only, and the LCAO MOs for this state at several internuclear distances are given in Table V. The potential curves of the states are calculated from these LCAO MOs without configuration interaction and are shown in Fig. 5, and the molecular constants calculated by using these values are given in Table I.

The influence of configuration interaction is generally very significant; therefore all the electronic configurations, which are obtained by the excitations of electrons except from the inner shell, must be taken in. Thus, there are 18, 9, 8, 9, and 14 basic wave functions belonging to the types of $^2\Pi$, $^4\Sigma^-$, $^2\Delta$, $^2\Sigma^-$, and $^2\Sigma^+$, respectively. In the present calculation, however, the electronic energies of these states are calculated by second order perturbation. The potential curves obtained in such a manner are shown in Fig. 6, and the molecular constants are given in Table I, together with the above results.

V. LCAO MOs

As shown in Tables IV and V the LCAO MOs of the lowest energy obtained by the SCF procedure are considerably changed according to each state, but they

TABLE V. LCAO SCF MOs for the lowest $^2\Pi$ state.

$$(1\sigma)=\begin{Bmatrix}0.596\\0.665\\0.719\\0.767\\0.811\end{Bmatrix}(s)+\begin{Bmatrix}0.253\\0.244\\0.219\\0.189\\0.157\end{Bmatrix}(\sigma)+\begin{Bmatrix}0.400\\0.354\\0.326\\0.301\\0.277\end{Bmatrix}(h)$$

$$(2\sigma)=-\begin{Bmatrix}0.766\\0.701\\0.647\\0.596\\0.542\end{Bmatrix}(s)+\begin{Bmatrix}0.638\\0.665\\0.677\\0.682\\0.684\end{Bmatrix}(\sigma)+\begin{Bmatrix}0.404\\0.388\\0.399\\0.424\\0.453\end{Bmatrix}(h)$$

$$(3\sigma)=\begin{Bmatrix}1.242\\1.024\\0.857\\0.725\\0.619\end{Bmatrix}(s)+\begin{Bmatrix}1.165\\1.056\\0.980\\0.925\\0.884\end{Bmatrix}(\sigma)-\begin{Bmatrix}1.729\\1.524\\1.368\\1.247\\1.152\end{Bmatrix}(h)$$

$(1\pi_\pm)=\pi_\pm$

at the internuclear distance of $\begin{Bmatrix}0.920\\1.022\\1.124\\1.226\\1.328\end{Bmatrix}$ A.

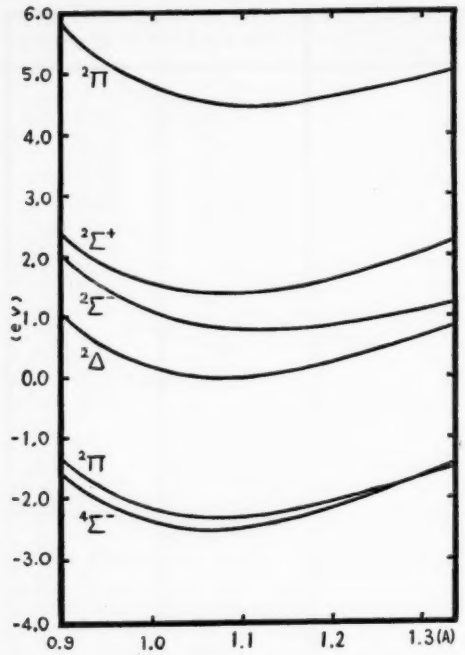

FIG. 5. Potential curves calculated by the lowest $^2\Pi$ state SCF MOs without configuration interaction. The origin of energy is chosen to be $C(^3P)+H(^2S)$ with configuration interaction.

correspond to the results of the AO method, and can be considered as the reasonable MOs. Therefore, the nature of these orbitals may represent those of the real CH radical. The nature of $i\sigma$ orbitals can be made to correspond to those of CO_2.[8] That is, the 1σ orbital indicates strongly bonding property, for the coefficient of s is much larger than the others, but the 2σ and 3σ orbitals are weakly bonding due to strong s-p mixing in the carbon orbitals of these MOs, for the coefficient of s is nearly equal to that of σ. But the 1π orbital of the CH radical is almost nonbonding, because the orbital is formed by only one atomic orbital of the carbon atom.[22]

On the other hand, these bonding properties of the CH radical are shown by the experimental results that the removal of an electron from the 2σ orbital to form the $^1\Pi$ state of CH^+ changes the internuclear distance from 1.12 A to 1.23 A. And the removal of an electron from the 1π orbital to form the $^1\Sigma^+$ state of CH^+ changes the internuclear distance only from 1.12 A to 1.13 A.[1]

It may be recognized from these results that the nature of the $i\sigma$ orbital scarcely changes in a molecule or in a free radical, and the σ orbital of the lowest energy except that of inner shell is strongly bonding, but the σ orbitals of higher energies are weakly bonding.

It is seen that the coefficient of s in the 1σ orbital increases with the internuclear distance while others decrease, but in the 2σ orbital this relation is reversed. This accords with the fact that the decomposition products of the $^2\Pi$ state are $C(^3P)$ and $H(^2S)$,[2,23] and the contribution from the s^2p^2 configuration increases with the internuclear distance in the atomic orbital calculation (see Table II).

The "LCAO orbital energies" given in Table III represent good approximations to the ionization energies of corresponding electron shells. However, the calculated value of 1π orbital is 12.72 ev which is the minimum ionization energy at the equilibrium internuclear distance calculated in the $^2\Pi$ state. This value corresponds to the removal of an electron from 1π orbital, and is somewhat greater than the observed value of 11.1 ev.[24] However, this result may be sufficiently good to explain the experimental fact.

Using these LCAO MOs without configuration interaction the dipole moment for the corresponding state can be calculated as shown in Table VI. These values are very large and the direction is in reverse compared with the ordinary CH bond, for example in methane.[25] However, the CH radical is not a stable molecule; therefore the nature of the bond may be changed by the existence of the nonclosed shells or the lone-pair electrons (2σ electrons) which exist in the direction of the CH bond.

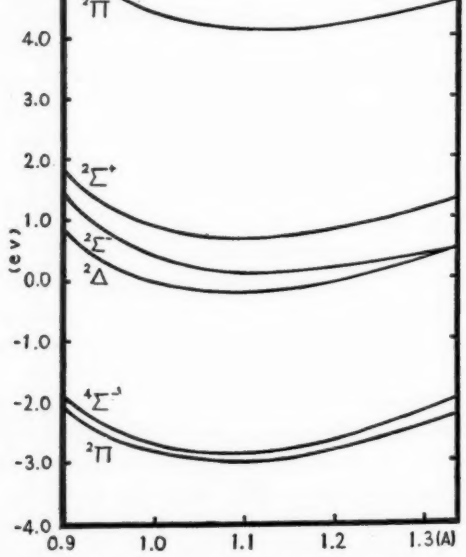

FIG. 6. Potential curves calculated by the lowest $^2\Pi$ state SCF MOs with configuration interaction. The origin of energy is chosen to be $C(^3P)+H(^2S)$ with configuration interaction.

[22] If the electronic energies of the CH^+ radical can be approximately calculated by using the $^2\Pi$ state MOs of the CH radical without configuration interaction, the equilibrium internuclear distances of the CH^+ radical are obtained as follows:

orbital of the removed electron	state	electronic configuration	equilibrium internuclear distance (A)
1σ	$^1\Pi$	$(1\sigma)^1(2\sigma)^2(1\pi)^1$	(>1.30 if existing)
	$^3\Pi$	$(1\sigma)^1(2\sigma)^2(1\pi)^1$	(>1.30 if existing)
2σ	$^1\Pi$	$(1\sigma)^2(2\sigma)^1(1\pi)^1$	1.30
	$^3\Pi$	$(1\sigma)^2(2\sigma)^1(1\pi)^1$	1.21
1π	$^1\Sigma^+$	$(1\sigma)^2(2\sigma)^2$	1.16

The relative values may explain the bonding property of the CH radical.

[23] If the single configuration is assumed, the decomposition products of the state are $C(V_2)$ and $H(^2S)$.

[24] See reference 1, p. 459.

[25] C. R. Mueller and H. Eyring, J. Chem. Phys. **19**, 193 (1951).

VI. ELECTRONIC STATES AND ELECTRONIC ENERGIES

The electronic levels calculated by both the AO and MO methods given in Table I satisfactorily explain the observed values. This is, of course, due to confining the calculation to the ground and lower excited states only, in which the influence of higher states is very small. Especially, there is little more than 0.2 ev difference between the results of the AO or the MO method with configuration interaction and the observed values. In view of these facts, the influence of ionic structures is almost equal in these states except in the lower excited $^2\Pi$ state.

The ground state of the radical is determined as $^2\Pi$ by both the AO and the MO method with configuration interaction, but the not yet observed state $^4\Sigma^-$ is close above the $^2\Pi$ state and the difference is about 0.1 ev. Therefore, considering the errors of the calculations it cannot conclusively be determined which state is the ground state. However, the calculations, in which the ground state is taken to be $^4\Sigma^-$, involved comparatively more errors than these two calculations. Accordingly, the ground state is probably the $^2\Pi$ state as shown in Mulliken's prediction.[3]

Comparing the various results of the AO method (see Fig. 2), it is necessary for calculations of carbon compounds that at least both the s^2p^2 and sp^3 configurations are taken in, but the contribution from the p^4 configuration does not exceed five percent, so this influence may be much less significant in other cases. The effect of nonorthogonality is very significant. That is, if the overlap integrals are not included, the integrals having considerable value, which are not cancelled by this assumption, will be ignored. Consequently, some errors may result, especially due to the off-diagonal terms which include the exchange integrals between s or σ and h in the secular determinant. Hence, the energies of the higher states are much lowered by these terms as shown in Fig. 2. This influence may not be significant only in the qualitative discussion, for the magnitude of this error increases with the energy value.

In the results by the LCAO-SCF method given in Fig. 4, the minimum energies calculated by the variational procedure are hardly different from those calculated by the MOs which minimize the energy of the other state; therefore the change of the coefficients in the LCAO MOs may not sharply affect the total energy value. The results calculated by using certain MOs without configuration interaction are qualitatively as satisfactory as those calculated by the AO method ignoring the overlap integrals.

The equilibrium internuclear distances r_e's in the calculations agree well with the observed values, but the results of the AO method are slightly smaller than those of the LCAO-SCF method. This is contrary to the consideration that there might be further decrease of internuclear distance if the ionic structures were brought in, but it may be due to the errors which are essentially caused by the methods and the assumptions used.

TABLE VI. Dipole moment.[a]

State	The lowest $^2\Pi$	$^4\Sigma^-$	$^2\Delta$	$^2\Sigma^-$	$^2\Sigma^+$	Lower excited $^2\Pi$
Dipole moment (D. C^-H^+)	1.97	1.07	1.41	1.89	1.41	1.19

[a] These values are calculated at the internuclear distance of 1.124 A, and the values of integrals used are as follows: $(s|rc|\sigma)=0.9078$, $(s|rc|h)=0.5749$ and $(\sigma|rc|h)=0.9492$ (in atomic units).

The vibrational frequencies ω_e's are somewhat different from the observed values as compared with the other results. However, they can qualitatively explain the observed values, and the differences may be produced by using the Slater AOs which reduce the electronic interactions at a large internuclear distance.

In view of these points, the present calculations are generally in good agreement with both the observed values and Mulliken's prediction. But only in the not yet observed lower excited $^2\Pi$ state, the vibrational frequency is not small and the equilibrium internuclear distance is hardly different from that in other states. In the single configuration approximation, however, the potential curve of this state crosses with that of the upper $^2\Pi$ state at the internuclear distance smaller than 1.4 A. Consequently, the real curve probably has a maximum point, in which the main configuration changes from $(1\sigma)^2(1\pi)^3$ to $(1\sigma)^2(2\sigma)^1(1\pi)^1(3\sigma)^1$, and decreases with nuclear separation beyond the point. Therefore, the state is unstable and may not be observed.

VII. DISCUSSION

The results in the present calculation are qualitatively satisfying, but the numerical values obtained are in no sense final. These points, in part, have been discussed by Mulligan in his calculation of CO_2,[8] but in the present paper there are several problems which have not been discussed. In the first place, it must be considered that the wave functions used are the Hartree SCF-AOs for the one-center integrals in spite of the assumption of Fock's Eqs. (1) and (2). As shown in Fig. 1, however, this influence is small in the electronic levels of the atom, and then may be also slight in the radical, for the Hartree-Fock energy parameters (inside of the bracket on the right hand in Eqs. (1) and (2)) do not make a large difference between those calculated by the Hartree and Hartree-Fock SCF AOs. The use of simple Slater AOs in the two-center integrals instead of the SCF AOs increases the electronic interaction of $2s$ orbital too much at the small internuclear distance, but this influence becomes small in separating both nuclei. In such a choice of energy integrals, however, the atomic energies are in good agreement with the observations; therefore, the modification by Moffitt[26] is hardly neces-

[26] W. Moffitt, Proc. Roy. Soc. (London) **A210**, 224 (1951).

sary. But strictly speaking, the Hartree-Fock SCF AOs of the valence states must be used, which correspond to each state of the radical, and the errors arising from the selection of atomic orbitals may affect the total energy in some degree.

The assumption of the 1*s* electron of carbon in the inner shell is not quite valid, especially at the small internuclear distance, but is acceptable in separating both nuclei. Considering the result of H_2O by Ellison and Shull,[27] this assumption is acceptable in some degree; therefore it is not considered that this may cause unreasonable results.

The configuration interaction calculated by the second order perturbation does not always give a good approximation, due to some overestimation of energy. In the present calculation, however, the first order perturbation coefficients of the interacting basic wave functions are usually very small and scarcely exceed 0.1, so the influence is not significant in the discussion of the electronic levels.

If reasonable energy values are used, the approximation of LCAO-SCF method is of the same degree and according to circumstances more convenient as compared with the AO method in which the overlap integrals are disregarded, even if the excited states are calculated by using either the ground state MOs or the lower excited state MOs. In the present calculation the influence of the configuration interaction is not very large; for example in the lowest $^2\Pi$ state the contribution from the electronic configuration $(1\sigma)^2(2\sigma)^2(1\pi)^1$ is 96 percent, so the assumption of the single configuration is rather correct. However, for a rigorous discussion of the electronic states, the configuration interaction is very significant in the case of molecules as well as in atoms. The energy depression by configuration interaction in the present calculation is smaller than in others,[28] and this is due to the fact that the CH radical is a simple radical, and moreover the energy integrals calculated by the SCF AOs are used in the one-center integrals. That is, the latter is almost identical with the modification by Moffitt.[29]

In brief, the good results of the calculation are due to the fact that the CH radical is a simple heteronuclear radical[30] and that the selection of energy integrals is fairly good. Therefore, if such reasonable energy values, especially in the many-center integrals, are used in large molecules, reasonable results may be expected as in the present calculation.

VIII. ACKNOWLEDGMENT

The author wishes to thank Dr. S. Shida and Mr. Y. Mori of this Laboratory, and Dr. K. Niira and Mr. K. Oohata of the Laboratory of Physics for their kind discussions and suggestions.

[27] F. O. Ellison and H. Shull, J. Chem. Phys. **21**, 1420 (1953).

[28] Coulson, Craig, and Jacobs, Proc. Roy. Soc. (London) **A206**, 297 (1951).

[29] M. Wolfsberg, J. Chem. Phys. **21**, 943 (1953).

[30] W. Moffitt, Proc. Roy. Soc. (London) **A196**, 510 (1949).

A Treatment of Chemical Kinetics with Special Applicability to Diffusion Controlled Reactions

RICHARD M. NOYES
Department of Chemistry, Columbia University, New York, New York
(Received December 4, 1953)

If a molecule is produced in a medium containing molecules able to react with it, its instantaneous reactivity is a function of the time since its formation. At very short times the reactivity is determined by the conventional "true" rate constant k, which is the product of the rate constant for encounters and the probability of reaction during an encounter. At long times (10^{-9} sec or greater in many liquids), the reactivity falls to a value determined by the "long-time" rate constant k'. The constants k and k' differ by the factor $1-\beta'$, where β' is the probability that a specific pair of molecules separating from a nonreactive encounter will ultimately react with each other. If β' is small either because there is little chance of reaction per encounter (activation control), or because there is little chance the specific pair will undergo a subsequent encounter (as in gas phase), the two rate constants are virtually identical and conventional kinetics apply.

Equations are developed for the time dependence of the reactivity of a molecule in such a system, and a model is suggested for evaluating the necessary parameters in terms of the relative diffusion coefficient, the encounter diameter, and the root-mean-square displacement distance during diffusion. Application of available kinetic data indicates that diffusive displacements in liquids are of the order of a molecular diameter and take place with a frequency of the order of 10^{11} sec^{-1}.

In the quenching of fluorescence and other processes where reactive molecules are produced singly, experimental measurements have given the "long-time" rate constant, k'. When reactive molecules are produced in pairs, the recombination process in a thermal equilibrium is described by the "true" rate constant, k; but k' has been obtained from all rate measurements on the recombination of pairs produced photochemically. Experiments are suggested for obtaining information on systems during the short time in which the apparent rate constant is changing.

I. INTRODUCTION

IF a reference molecule is produced in a homogeneous medium containing a random distribution of molecules capable of reacting with it, conventional treatments assume that its subsequent instantaneous reactivity is a function only of the concentration of potential reactants and is independent of the time since its formation. Actually, the existence of the reference molecule for a finite time without reacting *ipso facto* eliminates certain possible initial configurations of the system, and the probability of finding a potential reactant near the reference molecule is less than it was initially, or than it still is near a random position in the bulk of the medium. Collins and Kimball[1] were the first to point this out and to show that the instantaneous reactivity of such a reference molecule falls with time to a limiting value.

Another way to look at this effect is to note that two molecules that have separated after an encounter are still so close that there is a significant probability that they will make additional encounters with each other. The longer a reference molecule has existed without reacting, the greater the fraction of its encounters that take place with molecules it has previously encountered. If the medium contains both inert (solvent) molecules and potential reactants, the fact that a reference molecule has not yet reacted indicates the probability that more than a normal statistical average of its previous encounters took place with inert molecules. Therefore, as the fraction of re-encounters increases, the probability of reaction in any specific time interval drops below the value calculated from a random distribution of reactants.

Fortunately, the reactivity varies only negligibly with time if there is high probability either that two molecules will not react during a specific encounter (conventional activation controlled reactions) or that two molecules separating from an encounter will never re-encounter each other (homogeneous reactions in gases at pressures less than tens of atmospheres). However, the variation in reactivity may be significant for diffusion controlled reactions as between highly reactive molecules in liquid phase or condensations on aerosol droplets having diameters at least of the order of the mean free path in the surrounding gas. In the present paper we show that, regardless of the detailed molecular model that is assumed, deviations from conventional kinetic treatments can be described in terms of the probability two molecules will react during an encounter and the time-dependent probability that two molecules separating from an encounter will re-encounter each other.

The subsequent discussion emphasizes the distinction in condensed phases between collisions and encounters. Collisions have fairly definite significance in gases but are not clearly defined in liquids. Roughly, a *collision* occurs whenever two molecules come into contact and approach until the repulsive forces overcome the inertial forces and dr/dt (where r is the intermolecular distance) changes from a negative to a positive value. *Encounters* arise as a result of the diffusion process, which involves randomly directed displacements of the order of a molecular diameter. When two molecules are thus brought into adjacent positions, they are said to have undergone an encounter whose duration is determined by the time until one or the other undergoes a diffusive displacement. During an encounter, the molecules may undergo several collisions which are quasi-vibrational in

[1] F. C. Collins and G. E. Kimball, J. Colloid Sci. 4, 425 (1949).

character and result from motions that do not contribute to diffusion. In the gas phase, collisions and encounters are identical, and the words may be used interchangeably.

Rabinowitch[2] discussed a liquid of rigid molecules and concluded that the average frequency of collisions between solute molecules is of the same order but somewhat larger than the frequency that would be observed for the same concentration of molecules in gas phase. This conclusion is consistent with the observation that the rate constants for several reactions have comparable frequency factors in gas phase and in nonpolar solvents. However, collisions in the gas phase are randomly distributed in time, while Rabinowitch and Wood[3] pointed out that collisions in solution occur in sets, each set corresponding to an encounter as defined above.

It does not appear to have been recognized that encounters also show a smaller tendency to occur in sets. We have previously[4] examined a model in which diffusive displacements are of the order of molecular dimensions, and have found a probability of the order of 0.5 that two molecules separating from an encounter will subsequently re-encounter each other. Moreover, except in very concentrated solutions, the time between encounters by the same molecules is very short compared to the time until an encounter with another solute molecule.

In Sec. II below, we show how the time-dependent probability for a first re-encounter between a specific pair of molecules can be used to calculate the change with time of the reactivity of a single reactive molecule produced at random in a solution. In Sec. III, we attempt to develop a model for calculating this time-dependent probability of a re-encounter in terms of diffusion coefficient, frequency of diffusive displacements, and ratio of encounter diameter to root-mean-square displacement distance, and we discuss experimental evidence on the magnitudes of these quantities. Finally, in Sec. IV, we discuss some interesting consequences of this treatment in real systems and present evidence from the literature and suggestions for experimental tests.

NOMENCLATURE

$f(t)$ = time-dependent probability for a first subsequent encounter between a pair of inert molecules that have undergone an encounter at time zero.

$g(t)$ = time-dependent probability for any subsequent encounter between such molecules.

$h(t)$ = time-dependent reaction probability for a pair of potentially reactive molecules that have undergone a nonreactive encounter at time zero.

k = "true" rate constant.

k' = "long-time" rate constant.

k_{ex} = "experimental" rate constant.

N = number of relative diffusive displacements since zero time.

$P_{reac}(t)$ = time-dependent probability of reaction by a reference molecule.

P_s = *a priori* probability per unit time for any encounter by an inert reference molecule.

$S(t)$ = probability molecule produced at zero time is not reacted at time t.

$X(r,N)$ = probability particle lies distance r from origin after N random displacements.

$Y(r)$ = probability molecule at distance r will undergo encounter at next displacement.

α = probability two molecules will react during an encounter.

β = probability two molecules separating from an encounter will undergo at least one more encounter with each other.

β' = probability two molecules separating from an encounter will subsequently react with each other.

$\gamma = \rho/\sigma$.

ν = frequency of diffusive displacements.

ρ = encounter diameter.

σ = root-mean-square displacement distance.

II. VARIATION OF REACTIVITY WITH TIME

The detailed treatment of the situation involves the behavior of a specific pair of molecules subsequent to an encounter. Let us assume an effectively infinite volume of solution containing an inert solute such as argon, and let a specific pair of solute molecules undergo an encounter at zero time. This pair may subsequently undergo one or more additional encounters with each other, but they need not necessarily do so. Let β be the probability that they will make subsequent encounters with each other, and let $f(t)dt$ be the probability that they make their *first* subsequent encounter between times t and $t+dt$. It is clear that

$$\int_0^\infty f(t)dt = \beta. \qquad \text{(II-1)}$$

Let $g(t)dt$ be the probability the same pair will make *any* subsequent encounter between t and $t+dt$. The probability the pair will undergo encounters subsequent to a specific one is independent of the number of previous encounters, if any; so we can relate $f(t)$ and

[2] E. Rabinowitch, Trans. Faraday Soc. **33**, 1225 (1937).
[3] E. Rabinowitch and W. C. Wood, Trans. Faraday Soc. **32**, 1381 (1936).
[4] R. M. Noyes, J. Chem. Phys. **18**, 999 (1950).

$g(t)$ by

$$g(t)=f(t)+\int_0^t f(t-t')f(t')dt' + \int_0^t f(t-t'')\int_0^{t''} f(t''-t')f(t')dt'dt'' + \int_0^t f(t-t''')\int_0^{t'''} f(t'''-t'') \times \int_0^{t''} f(t''-t')f(t')dt'dt''dt'''+\ldots, \quad \text{(II-2)}$$

where t', t'', and t''' are times of first, second and third encounters, respectively, taking place between 0 and t. The terms given are the probabilities of first, second, third and fourth subsequent encounters at time t. If we use Eq. (II-1) and consider the meaning of $g(t)$, we see that

$$\int_0^\infty g(t)dt=\beta+\beta^2+\beta^3+\beta^4+\ldots=\beta/(1-\beta). \quad \text{(II-3)}$$

Now, instead of an inert solute, let the solution contain a single pair of potentially reactive molecules behaving identically with the inert molecules considered above, except that there is probability α they will react during an encounter. If $\alpha<1$, let the two molecules undergo a nonreactive encounter at time zero. If $\alpha=1$, let the initial configuration of the system be that observed for two inert molecules that have just separated after an encounter at zero time.[5] Let $h(t)dt$ be the probability this pair of molecules will react between t and $t+dt$. Since these molecules can react only once with each other, we obtain

$$h(t)=\alpha f(t)+\alpha(1-\alpha)\int_0^t f(t-t')f(t')dt' + \alpha(1-\alpha)^2\int_0^t f(t-t'')\int_0^{t''} f(t''-t')f(t')dt'dt'' + \alpha(1-\alpha)^3\int_0^t f(t-t''')\int_0^{t'''} f(t'''-t'') \times \int_0^{t''} f(t''-t')f(t')dt'dt''dt'''+\ldots. \quad \text{(II-4)}$$

For truly diffusion controlled reactions where $\alpha=1$, $h(t)=f(t)$; while for activation controlled reactions where $\alpha\ll1$, $h(t)=\alpha g(t)$. There is no simple relationship for intermediate values of α. If β' is the probability that the specific pair will ever react,

$$\int_0^\infty h(t)dt=\beta'=\alpha\beta+\alpha(1-\alpha)\beta^2+\alpha(1-\alpha)^2\beta^3 +\ldots=\alpha\beta/(1-\beta+\alpha\beta). \quad \text{(II-5)}$$

The above paragraphs considered the behavior of a specific *pair* of molecules. Let us now consider a *single* reference molecule in a solution containing other solute molecules. If the molecule is inert and is selected at random in space and time, let $P_s dt$ be the *a priori* probability it will undergo an encounter with any other solute molecule between t and $t+dt$. The value of P_s depends upon concentration, but in a particular solution it is a constant independent of time as long as no information is available about the history of previous encounters by the reference molecule.

If the reference molecule is not inert but may react with some solute molecules, let it be produced at time zero in a random position in the solution and let $P_{\text{reac}}dt$ be the probability it will react between t and $t+dt$. The argument of Sec. I indicates that P_{reac} is a function of time since the formation of the molecule. To derive the time dependence, we have used a model suggested by the work of Collins and Kimball.[1] Assume an ensemble of n systems in each of which a reference molecule is created at zero time at a random position in a random distribution of potentially reactive molecules.[6] If a reaction occurs in any system, discard it and immediately create a prototype system identical with the original one at the time of reaction except that the molecules behave as though they had undergone an encounter without reacting. If a reaction occurs in a prototype system, create another prototype system and so *ad infinitum*. The sum of real and prototype systems is always n, but n_t, the number of real systems at time t, will steadily decrease.

The total distribution with time of encounters in all systems, real and prototype, is the same as it would be in an ensemble of n systems each containing an inert reference molecule like that discussed above. Then $n\alpha P_s$ is the total rate of reactions in all systems, and it is independent of time. The rate of reactions in real systems at time t is $n_t P_{\text{reac}}$ by definition. Reactions in prototype systems belong in two classes. Some are reactions with molecules that have never before reacted with the reference molecule either in a real or prototype system; the rate of these reactions is $(n-n_t)P_{\text{reac}}$. The other reactions in prototype systems are with molecules that reacted with the reference molecule in either a real or prototype system at time $t-t'$ and have not reacted with it again until time t; the rate of these reactions is

[5] The condition of having just separated from an encounter does not necessarily correspond to a unique intermolecular distance. We can handle the situation by taking an ensemble of systems in which the distribution of intermolecular distances is the same as the distribution right after terminations of encounters between inert molecules.

[6] These potential reactants may be chemically identical with the reference molecule (as in the recombination of halogen atoms), or they may be different (as in a reaction between unlike radicals or between an amine and a substituted borane). The argument in this section is the same for every case provided potential reactivity is defined only with relation to the reference molecule.

$\int_0^t n\alpha P_s h(t')dt'$. Then,

$$n\alpha P_s = n_t P_{reac} + (n-n_t)P_{reac} + n\alpha P_s \int_0^t h(t')dt' \quad \text{(II-6)}$$

$$P_{reac}(t) = \alpha P_s \left(1 - \int_0^t h(t')dt'\right). \quad \text{(II-7)}$$

Equation (II-7) is the fundamental expression describing the behavior of P_{reac} with time. If a reference molecule is produced at zero time in a random position, the customary kinetic treatment is to assume its subsequent instantaneous reactivity is αP_s independent of time. This is indeed the initial reactivity, but a molecule that has lived sufficiently long will appear to obey standard kinetic expressions except the apparent rate constant obtained from experimental measurements is $1-\beta'$ of the initial "true" rate constant based on the rate constant for encounters in an inert system. Since $\beta'=\alpha\beta/(1-\beta+\alpha\beta)$, the discrepancy is unimportant for small values either of α (activation controlled reactions) or of β (reactions in gas phase). However, for diffusion controlled reactions in liquids where α may be unity and β may be of the order of 0.5, the factor of $1-\beta'$ may cause discrepancies between experimental rate constants and values calculated from diffusion coefficients or similar data but neglecting the effect discussed here.

The quantity P_{reac} measures instantaneous reaction probability and must be proportional to the concentration[7] of potentially reactive molecules in the immediate vicinity of the reference molecule. Since P_{reac} falls with time to a limiting value that is $1-\beta'$ of the initial value, a gradient must be established in the concentration of potentially reactive molecules. This gradient was discussed by Collins and Kimball[1] and has been mentioned in Sec. I; it arises because the existence of the reference molecule without reacting since time zero has exerted an *a posteriori* influence on the probability of finding another molecule in the immediate neighborhood. At distances greater than molecular dimensions, the gradient is like any that arises where Fick's law can be applied to diffusion into a sink, and dc/dr varies inversely as r,[2] where c is local concentration and r is distance from the center of the reference molecule.

The argument presented above assumes P_s is independent of time during the lifetime of a specific reference molecule. This requirement is strictly satisfied only when a steady-state concentration is maintained by simultaneous production and reaction of molecules. Actually, the bulk concentration of potential reactants needs to remain virtually constant only during a time sufficient for the integral of $h(t)$ to reach its limiting value. We shall show below that this time is of the order of 10^{-9} second for small molecules in ordinary liquids, and P_s will be constant during this interval except for some problems in radiation chemistry where a large number of reactive species are produced in a localized region. At longer times, the reactivity of the reference molecule will vary with concentration of potential reactants as predicted by conventional kinetics except that the apparent rate constant will be $1-\beta'$ of the value given by the customary model.

[7] "Concentration" cannot be used in the strict sense when applied to microscopic regions in a single system. The word is used here to describe the probability of finding a potentially reactive molecule in a particular volume element.

III. APPROXIMATE EVALUATION OF PARAMETERS

Deviations in the kinetics of molecules at long times since formation can be described in terms of the quantities α and β; the description at all times also requires one of the functions $f(t)$ and $h(t)$. These parameters are not generally experimentally determinable, but several theoretical procedures are available for estimating β and $f(t)$. Any such procedure will be based on some model of the microscopic detail of the region surrounding the reference molecule, and at present any tractable model of detailed structure in the liquid state apparently involves assumptions that are open to question. The object of this section is to briefly discuss possible models and to show how to obtain satisfactory approximate values for $f(t)$ and β. Even if these calculations are invalidated by subsequent refinement of our understanding of liquids, the equations derived in the proceeding sections should still be valid.

Two additional parameters appear to be needed for any foreseeable model of these systems. Let σ be the root-mean-square distance traversed by a molecule during a diffusive displacement, and let ρ be the encounter diameter or the separation of the centers of two molecules when encounter between them has become inevitable. In gas phase, ρ will equal the collision diameter, but in solution it may be somewhat larger than the sum of the radii of the individual molecules because surrounding solvent molecules may tend to force together two molecules that have approached to a certain minimum separation.[2] Let $\gamma=\rho/\sigma$; this ratio will be important in many of the subsequent equations.

A. Estimation of $f(t)$ or $g(t)$

The function $f(t)$ is the instantaneous probability of a *first* subsequent encounter between a pair of molecules that encountered at time zero. If it and α are known, Eqs. (II-4) and (II-7) permit calculation of the variation of P_{reac} with time. Although $f(t)$ is the function of interest, many theoretical treatments yield $g(t)$, the instantaneous probability of *any* subsequent encounter.

For a model, we have used the theory of random flights and for the sake of simplicity have assumed the displacement distance σ to be constant. If a particle starts at the origin and makes N displacements randomly oriented with respect to each other, let $X(r,N)dr$ be the probability the particle will lie between the distances r and $r+dr$ of the origin. An approximation valid

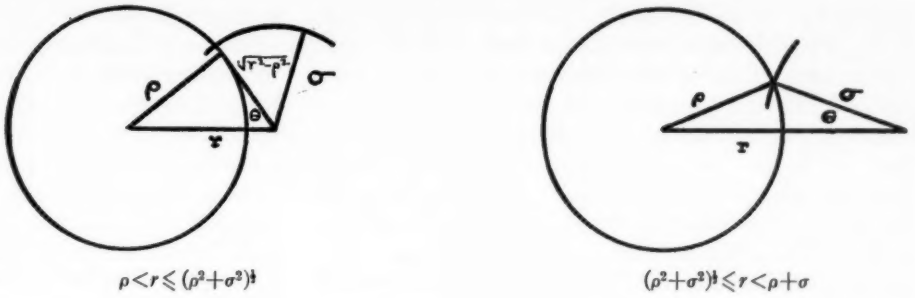

$\rho<r\leqslant(\rho^2+\sigma^2)^{\frac{1}{2}}$ $\qquad$ $(\rho^2+\sigma^2)^{\frac{1}{2}}\leqslant r<\rho+\sigma$

FIG. 1. Displacement at maximum angle leading to an encounter.

at large N is[8]

$$X(r,N)=\frac{4}{\pi^{\frac{1}{2}}}\left(\frac{3}{2N\sigma^2}\right)^{\frac{3}{2}}r^2\exp(-3r^2/2N\sigma^2). \quad \text{(III-1)}$$

For small values of r, this approximation is valid to a few percent even for values of N as small as 5.[9] If r is of the same order of magnitude as σ, the exponential term in Eq. (III-1) will differ negligibly from unity after a few tens of displacements.

Let ρ be the encounter diameter for a reference molecule at the origin and r be the distance to the center of another molecule undergoing displacements in random directions. Two molecules located near each other in a liquid will be influenced by solvent molecules and will not make relative displacements in completely random directions. However, the assumption made here is probably no worse than the other extreme of assuming that directions are determined by sites in a regular lattice. Let θ be the maximum angle between the direction to the origin and the direction of a displacement such that the trajectory will intersect the sphere defined by the encounter diameter. The situation is illustrated in Fig. 1. We see that

$$\begin{aligned}\cos\theta&=\frac{(r^2-\rho^2)^{\frac{1}{2}}}{r} && \rho<r\leqslant(\rho^2+\sigma^2)^{\frac{1}{2}}\\ &=\frac{r^2+\sigma^2-\rho^2}{2r\sigma} && (\rho^2+\sigma^2)^{\frac{1}{2}}\leqslant r<\rho+\sigma.\end{aligned} \quad \text{(III-2)}$$

Let $Y(r)$ be the probability these molecules will undergo an encounter at the next displacement. Then $Y(r)=\frac{1}{2}(1-\cos\theta)$, where $0<\theta<\pi/2$.

$$\begin{aligned}Y(r)&=\frac{r-(r^2-\rho^2)^{\frac{1}{2}}}{2r} && \rho<r\leqslant(\rho^2+\sigma^2)^{\frac{1}{2}}\\ &=\frac{\rho^2-(r-\sigma)^2}{4r\sigma} && (\rho^2+\sigma^2)^{\frac{1}{2}}\leqslant r<\rho+\sigma.\end{aligned} \quad \text{(III-3)}$$

Let $g(N)$ be the probability that an inert molecule will undergo an encounter with the reference molecule on the $(N+1)st$ displacement after a previous encounter. If ρ is sufficiently small compared to σ, we can use the Chandrasekhar model and neglect the fact that it permits the physically impossible situation of $r<\rho$. Then,

$$g(N)=\int_{\rho}^{\rho+\sigma}X(r,N)Y(r)dr. \quad \text{(III-4)}$$

This function is not generally integrable for the approximation in Eq. (III-1), but if N is large enough that the exponential term is negligibly different from unity, then

$$g(N)=\left(\frac{27}{8\pi}\right)^{\frac{1}{2}}\left(\frac{\rho}{\sigma}\right)^2\frac{1}{N^{\frac{1}{2}}}=\frac{1.036\gamma^2}{N^{\frac{1}{2}}}. \quad \text{(III-5)}$$

At shorter times, it is probably a fair approximation to multiply this value of $g(N)$ by $\exp(-3\gamma^2/2N)$.

Let ν be the frequency with which a molecule makes diffusive displacements; then 2ν is the frequency of relative displacements between two molecules. Since $t=N/2\nu$ and $g(t)=2\nu g(N)$, then, to the extent that Eq. (III-5) is valid,

$$g(t)=\frac{1.036\gamma^2}{(2\nu)^{\frac{1}{2}}t^{\frac{1}{2}}}. \quad \text{(III-6)}$$

Although these expressions for $g(t)$ are probably good for small values of γ, they are certainly unsatisfactory for γ much greater than unity. Moreover, $f(t)$ is the function of real interest. This function can also be expected to vary inversely as $t^{\frac{1}{2}}$ at long times. Since at short times $f(t)=g(t)$, and since $\int_0^\infty f(t)dt=(1-\beta)\times\int_0^\infty g(t)dt$, at long times $f(t)<(1-\beta)g(t)$. We do not know of any procedure other than iterative calculations for estimating $f(t)$ for the model we have chosen. We have performed such calculations to obtain $f(N)$ for the special case $\rho=\sigma$ $(\gamma=1)$. The initial distribution of molecules separating from an encounter was taken to be $r^2Y(r)/\int_\rho^{\rho+\sigma}r^2Y(r)dr$. This distribution is suggested by the principle of microscopic reversibility and is the same as the probability distribution of the distances from which a molecule would undergo encounters if it were immersed in a uniform density of other molecules. We then evaluated the probability distribution of molecules for fifteen successive displacements, considering only the distribution for those molecules that had not undergone encounters and using $Y(r)$ to determine the

[8] S. Chandrasekhar, Revs. Modern Phys. **15**, 1 (1943). The $X(r,N)$ given here is greater by a factor of $4\pi r^2$ than the $W(r,N)$ calculated by Chandrasekhar as a density probability.

[9] M. H. Quenouille, Proc. Cambridge Phil. Soc. **43**, 581 (1947).

probability of an encounter on each displacement. After only four displacements, the data could be fitted within the accuracy of the calculations by the expression $f(N)=0.2390/(N+0.442)^{\frac{1}{2}}$, and the calculations were converging on a value of $\beta=0.520$. This result suggests that $f(t)$ varies inversely as $t^{\frac{1}{2}}$ at much shorter times than $g(t)$ attains this type of behavior and that in this special case $f(t)=0.481(1-\beta)g(t)$ when $g(t)$ is defined by Eq. (III-6). We plan to carry out additional calculations to determine the variation of this numerical factor with γ, and to test the generality of the observation that in this special case $f(t)=(1-\beta)^2g(t)$ at long times.

B. Estimation of β

The quantity β denotes the probability a pair of molecules separating from an encounter will undergo at least one more encounter with each other. From Eq. (II-3) and Sec. III(a),

$$\frac{\beta}{1-\beta}=\int_0^\infty g(t)dt=\sum_1^\infty g(N)$$

$$=\int_\rho^{\rho+\sigma} Y(r)\int_0^\infty X(r,N)dNdr. \quad \text{(III-7)}$$

If we use Eq. (III-1) as an approximation for $X(r,N)$,

$$\int_0^\infty X(r,N)dN=6r/\sigma^2. \quad \text{(III-8)}$$

If we use the model leading to Eq. (III-3) for $Y(r)$, we get

$$\frac{\beta}{1-\beta}=\frac{3}{2}\gamma^2\ln\frac{1+(1+\gamma^2)^{\frac{1}{2}}}{\gamma}+\gamma^3-\frac{1}{2}$$

$$-\frac{3}{2}\gamma^2(1+\gamma^2)^{\frac{1}{2}}+\frac{1}{2}(1+\gamma^2)^{\frac{1}{2}}. \quad \text{(III-9)}$$

Equation (III-9) can be expanded in series if γ is not unity. For $\gamma<1$,

$$\frac{\beta}{1-\beta}=\frac{3}{2}\gamma^2\ln\frac{2}{\gamma}-\frac{3}{4}\gamma^2+\gamma^3-\frac{3}{16}\gamma^4$$

$$+\frac{1}{64}\gamma^6-\frac{1}{256}\gamma^8+\ldots. \quad \text{(III-10)}$$

For $\gamma>1$,

$$\frac{\beta}{1-\beta}=\frac{3}{2}\gamma-\frac{1}{2}+\frac{1}{8\gamma}-\frac{1}{80\gamma^3}+\ldots. \quad \text{(III-11)}$$

In Table I we present values of β calculated for different γ.

Equation (III-9) is based on the approximation from Eq. (III-1) for $X(r,N)$. We can see two objections to the use of this approximation. First, although the approximation is good after N is more than a few units, a large fraction of the molecules that ever undergo subsequent encounters do so during the first two or three displacements, while the approximation is poor. Second, the model for Eq. (III-1) permits molecules to be located anywhere in space, while the reference molecule excludes a sphere of radius ρ in the real case. At least the second objection can be met by noting that Eq. (III-9) is not concerned in any way with the distribution of encounters in time. The quantity $\beta/(1-\beta)$ is the total number of subsequent encounters, and $6rdr/\sigma^2$ from Eq. (III-8) is the total number of times that a molecule starting its diffusion at the origin will end a displacement at a distance between r and $r+dr$. If molecules separating from an encounter are distributed in space the same way as molecules undergoing their first diffusive displacement outward through a hypothetical spherical shell of radius ρ, then Eq. (III-9) will be valid even though Eq. (III-1) is a very poor approximation during the times that the encounters actually occur. We are convinced that Eq. (III-9) is very good for large values of γ. Small values of γ are not of interest because they correspond to the gas phase situation where β is small and the reactivities do not differ significantly from values given by standard kinetic theory expressions. However, since the validity of the equation may be questioned for γ near unity, we have examined other models.

Iterative calculations furnish the most laborious but direct check. The calculations described in Sec. III(a) for estimating $f(t)$ for $\rho=\sigma(\gamma=1)$ were converging clearly to $\beta=\sum_1^\infty f(N)=0.520$. This answer is in excellent agreement with the 0.527 given by Eq. (III-9), and at least some of the difference may arise from repeated use of approximation methods for numerical integrations in the calculations.

Iterative calculations to estimate β [but not $f(t)$] can be greatly simplified by the use of equations developed previously.[4] These equations show that if it is possible to calculate the probability two molecules will attain a specified finite separation without undergoing another encounter, then it is possible to calculate the probability they will ever undergo an encounter. Numerical results depend upon the model chosen for the behavior of two molecules when close together. In

TABLE I. Values of β calculated from Eq. (III-9).

γ	β
0.01	0.000720
0.03	0.00500
0.1	0.0370
0.2	0.104
0.5	0.308
1	0.527
2	0.719
5	0.875
10	0.9355
30	0.9780
100	0.99336
1000	0.999334

the previous paper, we used a rather crude model involving jumps between adjacent sites in a closest packed lattice, and assumed that molecules separating from an encounter were distributed uniformly in available sites between ρ and $\rho+\sigma$. This treatment gave $\beta=0.56$ for the case $\rho=\sigma$, and use of the model presented in this paper should lead to still better agreement with the value from Eq. (III-9).

A different approach valid for large γ is suggested by Wijsman.[10] He used an expansion in spherical harmonics on the Boltzmann transport equation to obtain $P(r)$, the probability two molecules initially separated by distance r will ultimately undergo an encounter. In terms of the nomenclature used in this paper, the solution is

$$P(r)=\left(1+\frac{2}{3\gamma}+\frac{1}{2\gamma^2}\right)^{-1}\rho/r. \qquad \text{(III-12)}$$

If two molecules separating from an encounter are only infinitesimally removed from each other before diffusion begins, $P(r)$ can be identified with β and expansion of $\beta/(1-\beta)$ gives $3\gamma/2-9/8$ in good agreement with the $3\gamma/2-1/2$ in Eq. (III-11).

In addition to these rather direct methods for evaluating β, it is also possible to use the conclusion of Sec. II that for a completely diffusion controlled reaction the ratio of the initial to the long-time reactivity of a molecule is $1/(1-\beta)$. Collins and Kimball[11] used a random walk model to estimate the instantaneous reactivity at very short times after formation and then used Fick's limiting law for diffusion into a sink to estimate the reactivity at long times. Their results at large γ are clearly converging to $\beta/(1-\beta)=3\gamma/2$, but at $\rho=\sigma$ they get $\beta=0.27$ in bad disagreement with the values given by our independent treatments. We believe that most of the discrepancy arises from the use of Fick's limiting law for the long-time reactivity. The use of this law is equivalent to a treatment which passes to a limit of increasing ν and decreasing σ such that D remains constant.

We can propose another method for calculating the long-time reactivity without requiring this limiting treatment. The diffusion coefficient of a single molecule is given by

$$D=\tfrac{1}{6}\nu\sigma^2. \qquad \text{(III-13)}$$

Since two molecules undergo relative displacements with a frequency of 2ν, the diffusion coefficient for relative motion is $2D$. The rate at which molecules strike a surface of unit area is $\bar{v}c/4$ where $\bar{v}$ is the average speed and c is the concentration (assumed temporarily to be without a gradient) in the vicinity of the surface. If the average and root-mean-square displacements in solution do not differ greatly, the average speed of a solute molecule is $\nu\sigma$; and if one molecule is regarded as stationary, the average relative speed of the other is $2\nu\sigma$. Then, in a solution of inert molecules, the rate at which a molecule undergoes encounters is

$$P_s=4\pi\rho^2\frac{2\nu\sigma}{4}c=\frac{12\pi D\rho^2 c}{\sigma}. \qquad \text{(III-14)}$$

If the molecules are not inert but react at every encounter, the long-time reactivity of a molecule is $(1-\beta)P_s$ and is given by

$$P=12\pi D\gamma\rho(1-\beta)c. \qquad \text{(III-15)}$$

For large γ, $(1-\beta)=2/3\gamma$, and Eq. (III-15) reduces to $8\pi D\rho c$ in agreement with the value predicted by Fick's limiting law for a relative diffusion coefficient of $2D$. For smaller γ, Eq. (III-15) predicts that the long-time reactivity is $\frac{3}{2}\gamma(1-\beta)$ of the value calculated from Fick's limiting law. If the reactivity ratios of Collins and Kimball are divided by this factor with the use of β values from Table I, the agreement with our treatment is greatly improved. Thus, at $\gamma=1$ the ratio of initial to long-time reactivity is raised from 1.37 to 1.93 in much more reasonable agreement with the value of 2.11 calculated from Table I. The corrected Collins and Kimball reactivity ratios agree with ours to 4 percent at $\gamma=2$, and get progressively better as γ increases.

C. Magnitudes in Real Systems

The magnitudes of the effects discussed here depend upon the nature of the diffusion process in liquids. Some treatments[2,4] have assumed that only displacements of the order of a molecular diameter contribute to diffusive motion, while others[1] have assumed smaller displacements at higher frequency. For small molecules in nonpolar liquids, D is frequently of the order of 3×10^{-5} cm^2/sec, but some additional type of experimental measurement is necessary to evaluate the quantities ν and σ. Two types of information on iodine atoms seem to support the concept of displacements of the order of molecular diameters.

If molecular iodine in hexane at 25° is dissociated by light of 4358 A, the quantum yield is 0.66 for the production of atoms that escape their original partners.[12] This figure and previous measurements of relative quantum yield,[13] indicate that the yield is 0.41 at 5780 A. If all of the molecules undergo dissociation in the primary process, and if the separation attained is about the same as when nonreactive molecules separate from an encounter, these quantum yields can be equated to $1-\beta'$. If, as seems probable, recombination takes place at virtually every encounter between atoms, then $\beta'=\beta$ and the values in Table I indicate that the displacement distance is very nearly the same magnitude as the encounter diameter. The argument is not con-

[10] R. A. Wijsman, Bull. Math. Biophys. **14**, 121 (1952).
[11] F. C. Collins and G. E. Kimball, Ind. Eng. Chem. **41**, 2551 (1949).
[12] F. W Lampe and R. M. Noyes, J. Am. Chem. Soc. **76**, 2140 (1954).
[13] J. Zimmerman and R. M. Noyes, J. Chem. Phys. **18**, 658 (1950).

clusive because the energy of the quantum is in excess of the strength of the bond that is broken, and the excess energy may cause an initial separation much larger than the average displacement in normal diffusion. If this initial separation is of the order of two molecular diameters, Eq. (III-12) indicates that about half of the atoms could escape their original partners even if the displacement distance for diffusion were much smaller than a molecular diameter.

Our studies[12,13] and those of Marshall and Davidson[14] indicate a rate constant of about 2×10^{10} liter/mole sec for the process $I+I\rightarrow I_2$ in hexane. This rate constant is measured for iodine atoms that have lived long enough to establish the limiting conditions described above, and it is $1-\beta'$ of the rate constant that would apply for encounters if the atoms were inert. We do not see how any theory involving small diffusive displacements can give a rate constant for encounters greater than 6×10^{10}, the rate constant for gas phase collisions calculated with the van der Waals diameter of 4.3 A. This means that β' (and hence β) cannot be more than about 0.7, and Table I shows that this situation corresponds to a displacement distance at least half the encounter diameter.

We regard these figures as strong evidence that diffusive displacements in liquids are of the order of a few Angstrom units. Wang[15] has reached the same conclusion about water by assuming that the same activation processes are involved in self-diffusion, dipole orientation, and viscous flow.

If we use Eq. (III-13) with $D=3\times10^{-5}$ cm^2/sec and $\sigma^2=10^{-15}$ cm^2, ν is about 2×10^{11} sec^{-1}. Then the argument in Sec. III(a) above indicates that $f(t)$ will vary inversely as $t^{\frac{3}{2}}$ even at times less than 10^{-10} sec. By about 10^{-9} sec, $f(t)$ will have fallen to 0.1 percent of its initial value, and $\int_0^t f(t)dt$ will have effectively reached its limiting value of β. The reference molecule has then reached its limiting reactivity.

IV. APPLICATIONS TO KINETIC PROBLEMS

These effects are only significant for diffusion controlled reactions in which the encounter diameter is comparable to or greater than the displacement distance. Since diffusion controlled reactions take place as rapidly as the molecules can undergo encounters, they cannot be studied by techniques in which solutions of potential reactants are mixed, but they can be studied by techniques in which reactive molecules are generated homogeneously—frequently by the action of some form of radiation. The generating process often causes formation of two or more reactive species in proximity, and in these cases the initial concentration of potentially reactive molecules is greater near a molecule that has just been produced than it would be if all molecules were distributed at random. Consequently, the reactivity of a molecule that has just been produced may vary even more strongly with time than in the situation already discussed. In this Section, we discuss the kinetic treatment of some of the more common situations and suggest experiments for obtaining additional information. The peculiar features encountered emphasize the care necessary when using the term "rate constant."

A. Reactive Molecules Produced Singly

Development of Kinetic Equations

In bimolecular reactions, the two molecules either are or are not chemically distinguishable. These types may be designated

$$A+A\rightarrow\text{Products} \qquad \text{(IV-1)}$$

$$A+B\rightarrow\text{Products.} \qquad \text{(IV-2)}$$

If R is the rate per unit volume of the process as written,

$$R=k_{ex}c_A{}^2 \qquad \text{(IV-3)}$$

for type (IV-1), and

$$R=k_{ex}c_Ac_B \qquad \text{(IV-4)}$$

for type (IV-2). The "experimental" rate constant k_{ex} is defined by these equations. In kinetic work, k_{ex} is customarily assumed independent of concentration changes that do not affect the activity coefficients of reactants or transition states; we shall see that this assumption may not be justified.

Let molecules of type A be produced singly at a constant rate in a solution containing a concentration c of potentially reactive molecules, all of which are either type A or B. This situation is encountered in the quenching of fluorescence and in condensation phenomena. Let $P_{\text{reac}}(\text{av})$ be the average value of P_{reac} for all A molecules in the solution. If the reaction is of type (IV-1),

$$P_{\text{reac}}(\text{av})=2k_{ex}c_A, \qquad \text{(IV-5)}$$

where the factor of 2 enters because $P_{\text{reac}}(\text{av})c_A$ is twice the total rate of reaction per unit volume. If the reaction is of type (IV-2),

$$P_{\text{reac}}(\text{av})=k_{ex}c_B. \qquad \text{(IV-6)}$$

The subsequent development applies to reactions of type (IV-2); the results will be applicable to reactions of type (IV-1) if $2c_A$ is substituted for c_B.

Let

$$\alpha P_s=kc_B. \qquad \text{(IV-7)}$$

Here, k is α times the rate constant that would be applicable for encounters if the molecules were inert; we shall refer to it as the "true" rate constant. Finally, let

$$k'=(1-\beta')k \qquad \text{(IV-8)}$$

where k' is the rate constant that would apply if all A molecules have lived long enough for P_{reac} to fall to its limiting value; we shall refer to it as the "long-time"

[14] R. Marshall and N. Davidson, J. Chem. Phys. **21**, 2086 (1953).

[15] Wang, Robinson, and Edelman, J. Am. Chem. Soc. **75**, 466 (1953).

rate constant. These rate constants apparently have not been distinguished previously, but most authors have thought they could equate k_{ex} with k even when k_{ex} was really equal to k'.

From Eqs. (II-7) and (II-5) with the above,

$$P_{\text{reac}}(t)=kc_B\left(1-\int_0^t h(t')dt'\right)$$

$$=c_B\left[k'+k\left(\beta'-\int_0^t h(t')dt'\right)\right]. \quad \text{(IV-9)}$$

Let S be the probability that a molecule produced at zero time is still not reacted at time t. Since $-dS/dt = P_{\text{reac}}S$,

$$S(t)=\exp(-kc_Bt)\exp\left(kc_B\int_0^t\int_0^{t'} h(\tau)d\tau dt'\right)$$

$$=\exp(-k'c_Bt)\exp\left[-kc_B\int_0^t\left(\beta'-\int_0^{t'} h(\tau)d\tau\right)dt'\right], \quad \text{(IV-10)}$$

where t' is a time between zero and t and τ is between zero and t'. From the definition of $P_{\text{reac}}(\text{av})$, we can write

$$P_{\text{reac}}(\text{av})=\frac{\int_0^\infty P_{\text{reac}}(t)S(t)dt}{\int_0^\infty S(t)dt}. \quad \text{(IV-11)}$$

If these equations are combined with (IV-6), k_{ex} can be evaluated in terms of k and β'. Although the exact solution is cumbersome, there are two limiting cases, only one of which can be attained experimentally.

As one limiting case, let $S(t)$ fall to a very small value before $P_{\text{reac}}(t)$ differs significantly from its initial value of kc_B. In this case, $k_{ex}=k$ and experiments give the "true" rate constant. However, the estimates in Sec. III(c) above indicate $\int_0^t h(t')dt'$ may become significant compared to unity within 10^{-11} sec after formation, and if S is to have dropped to 0.01 in this time, then kc_Bt must be as large as 5 when t is 10^{-11} sec. Since k can hardly be more than a few times 10^{10} liter/mole sec, c_B must be of the order of 10 M to attain this limiting case. This means that we can attain the "true" rate constant only when molecules are produced in a medium containing a high mole fraction of molecules with which they react on every encounter, and measurements of rate constant are impossible under such circumstances.

In the other limiting case, most of the contributions to the integrals in Eq. (IV-11) are made after P_{reac} has fallen to its limiting value of $k'c_B$; then $k_{ex}=k'$. Since this time is about 10^{-9} sec, the average lifetime should be at least ten times this, and $k'c_B$ should be no more than 10^8 sec^{-1}. Since the rate constant for encounters is of the order of 10^{10} liter/mole sec, c_B should be less than $0.01/\alpha$ M if this limiting case is to hold.

In conclusion, when c_B is less than 0.01 M, the system will obey standard kinetic expressions, but the rate constant obtained is k', the "long-time" value. At higher concentrations, the experimental rate constant may increase for reasons that arise because of deviations from truly random spatial distribution. These effects are distinct from those ordinarily leading to changes in thermodynamic activity coefficients.

Quenching of Fluorescence

When very reactive species are produced singly, there are no general techniques for measuring the steady-state concentration or obtaining k_{ex}. However, rate constants are measurable by competition methods in the special case of the quenching of fluorescence. Let k_f be the rate constant for fluorescence by an excited molecule (corrected if necessary for time-independent quenching by solvent), and let k_q be the "true" rate constant for quenching by a species in concentration c_q.

$$-\frac{dS}{dt}=(k_f+P_{\text{reac}})S. \quad \text{(IV-12)}$$

If the concentration of quencher is less than 0.01 M, $P_{\text{reac}}=k_q'c_q$, and studies of the concentration dependence of fluorescent intensity will permit evaluation of k_q' if k_f can be estimated. These studies will not measure k_q unless there is an independent method for evaluating β' for the reaction between an excited molecule and a quencher. Measurements at higher concentration of quencher might provide information on the form of $h(t)$, but they would be difficult to interpret and we do not believe they offer as much promise as studies in which reactive molecules are produced in pairs.

Curme and Rollefson[16] studied the quenching of fluorescence of β-naphthylamine by carbon tetrachloride in gas phase and in cyclohexane and isoöctane. The average lifetime of a fluorescing molecule in solution was estimated at 2×10^{-8} sec, so the values of k_q reported are really k_q' and should be divided by $1-\beta'$ for comparison with quenching constants in gas phase. A very interesting feature of the data is that the pre-exponential terms in the Arrhenius equation for k_q' are four or more times as large as the temperature independent k_q measured in gas phase, and dividing the liquid rate constants by $1-\beta'$ will serve to increase this factor. The authors regard this order of magnitude agreement as indicating that collisions occur at comparable frequencies in gas and liquid phases; however, they are really comparing collisions in the gas with encounters in the liquid. We propose that the agreement requires that the encounter diameter in liquid is

[16] H. G. Curme and G. K. Rollefson, J. Am. Chem. Soc. 74, 3766 (1952).

larger than the collision diameter in gas. This idea was first presented by Rabinowitch[2] and arises because the probable distribution of solvent molecules will tend to force together two molecules that have approached to a certain minimum separation at which they are not yet in contact. Confirmation of this effect will require additional studies of the temperature dependence of diffusion controlled reactions.

Condensation Phenomena

These equations could also be modified to apply to the growth of droplets or crystallites from nuclei formed in supersaturated media. In these cases, ρ would be a function of time; Frisch and Collins[17] have presented a treatment of this situation. In liquid with moderate α, the particles would soon grow large enough to use Fick's limiting law to describe the reactivity. These phenomena provide the only gas phase situation in which the equations of this paper differ significantly from standard kinetic expressions. When growing aerosol droplets are comparable in size to the mean free path in the gas, diffusion control will become important, and studies of rate of growth as a function of droplet size and pressure of inert gas might permit an evaluation of the accommodation coefficient for molecules striking the surface of the growing drop.

B. Reactive Molecules Produced in Pairs

Thermal Equilibria

If a dissociative equilibrium is established in a medium, the rates of dissociation and combination are equal. Some of the fragments recombine with their original partners and some of them diffuse apart and combine with fragments from other dissociations. The principle of microscopic reversibility requires that fragments separating from a dissociation have the same average kinetic energy as fragments approaching each other and about to undergo combination. Therefore, for every two fragments that combine, a pair of fragments is produced somewhere else by an operation that is the exact reverse of combination.[18] Then, the distribution of nearest neighbors among fragments is the same as it would be in a solution containing the same concentration of inert molecules behaving identically except that the encounters were nonreactive. The total rate of formation or combination in the reactive solution will be α times the rate of encounters in the inert solution, and the kinetics of combination are described by the "true" rate constant k regardless of how long the fragments live.

If the concentration of fragments is less than 0.01 M, the same result is obtained by noting that a fraction β' of the fragments recombine rapidly with their original partners, and a fraction $1-\beta'$ diffuse apart. The rate constant for the combination of those that diffuse apart is k', which is $(1-\beta')$ of k. The average lifetime of all fragments is that predicted with the use of k, and the average lifetime of those that escape their original partners is predicted with k'. Actually, the equilibrium can be described satisfactorily with either constant according as the rate constant for dissociation includes or excludes those processes in which original partners ultimately recombine.

Nonequilibrium Situations

In some systems, the fragments from a dissociation may react with species chemically distinguishable from their original partners, or they may be produced by a process like absorption of light that is not the reverse of combination. During photochemical dissociation in a liquid, some of the potential fragments may be oriented with respect to solvent molecules so that their kinetic energy is dissipated without ever attaining a separation of one displacement distance, and they undergo "primary recombination."[3] Since the energy in the absorbed quantum often exceeds that of the bond that is broken by more than average thermal kinetic energy, some of the fragments that escape primary recombination may not start random diffusive motion until they have attained a separation somewhat greater than that at the termination of a nonreactive encounter. Although a significant fraction of these will undergo diffusive "secondary recombination"[4] with their original partners, the fraction is probably less than β'. Because of these effects operating in opposite directions, the quantum yield for fragments escaping their original partners may be greater or less than $1-\beta'$.

If the net quantum yield could be identified with $1-\beta'$, a conventional kinetic treatment of the rate of absorption of radiation and the stationary concentration of fragments would give k, the "true" rate constant for combination. However, studies of the kinetics of combination[13,14] follow only those fragments that escape from their original partners, and their reaction is described by the smaller "long-time" rate constant k'. Previous publications, including our own, have not appreciated this fact.

Information presented in Sec. III(c) above indicates that k' for the combination of iodine atoms in hexane at 25° is about a third of the rate constant for collisions in the gas phase, and k must be even larger. Since the rate constant in solution must contain a temperature dependent term corresponding to the activation energy for diffusion, we believe that these data like those of Curme and Rollefson[16] indicate the encounter diameter in liquid is greater than the collision diameter in gas. We are currently studying the temperature dependence of k' in this system.

[17] H. L. Frisch and F. C. Collins, J. Chem. Phys. **21**, 2158 (1953).

[18] The author is indebted to Dr. A. O. Allen of the Brookhaven National Laboratory for suggesting the argument in this paragraph.

Possible Experimental Tests

If a molecule formed by combination of fragments is distinguishable from one that has not dissociated, it may be possible to learn something about β'. The azobisnitriles are possible compounds, and a test is suggested by the work of Overberger and Berenbaum[19] who caused simultaneous decomposition of compounds of the type

$$R_2C(CN)-N=N-(CN)CR_2$$

and

$$R_2'C(CN)-N=N-(CN)CR_2'.$$

They found some of the unsymmetrical product

$$R_2C(CN)-(CN)CR_2',$$

indicating that some radical fragments escaped their original partners. However, the unsymmetrically coupled products appeared to be in lower yield than predicted from a random distribution of radicals. This observation could be explained by a unimolecular loss of nitrogen from the original azonitrile, by a primary recombination of the radical fragments, or by a diffusive secondary recombination of a fraction β'. If the latter interpretation is correct, the system offers possibilities for estimating β'.

Still more information can be obtained with scavengers which react with fragments from a dissociation. Under exceptionally favorable conditions, scavengers may be efficient enough to catch some fragments that would otherwise react with their original partners, and studies at different scavenger concentrations may even give information on the form of $h(t)$. Such a possibility is suggested by the work of Arnett and Peterson.[20] They let an azobisnitrile decompose in the presence of a polymerizable monomer which caught the radicals produced. In methyl methacrylate, only one polymer chain was started for each molecule of nitrogen evolved. They concluded that the molecule dissociated into dissimilar radicals, only one of which was able to initiate polymerization. We suggest as an alternative that about half the radicals that are produced react with their original partners, and the other half diffuse apart and initiate polymerization. This suggestion is supported because with more reactive monomers the same azobisnitrile is able to initiate up to two chains per molecule of nitrogen evolved. The data for vinyl acetate suggest that the efficiency of chain initiation is decreased by dilution of the bulk monomer with ethanol, while dilution of methyl methacrylate has no effect on the lower efficiency with this monomer. Studies with a reactive monomer like vinyl acetate might furnish interesting information on the form of $h(t)$.

[19] C. G. Overberger and M. B. Berenbaum, J. Am. Chem. Soc. **73**, 4883 (1951).

[20] (a) L. M. Arnett, J. Am. Chem. Soc. **74**, 2027 (1952); (b) L. M. Arnett and J. H. Peterson, J. Am. Chem. Soc. **74**, 2031 (1952).

Finally, the work of Rutenberg and Taube[21] may illustrate scavengers that are and are not catching fragments that would otherwise recombine with their original partners. In the concentration range 0.001 to 0.01 M, manganous and cerous ions apparently catch all long-lived halogen atoms produced by photochemical dissociation in aqueous solution. Halide ions in concentration up to at least 2 M steadily increase the quantum yield for the production of fragments that can subsequently oxidize manganous ion. The authors postulate an activated X_3^- ion that may be deactivated without dissociation but whose dissociation is facilitated by an X^- ion. Alternatively, the absorption of a quantum may produce an X atom and an X_2^- ion which could recombine by diffusion. Reaction of X with X^- to form another X_2^- would reduce the chance of recombination of original partners for electrostatic and perhaps for other reasons.[22]

It will be difficult to interpret the action of scavengers at high concentrations because the rate constant for the reaction between scavenger and fragment will be changing with time since the fragment was produced. However, we believe it may be possible to obtain information at least substantiating that $h(t)$ varies as $t^{-\frac{1}{2}}$.

C. Several Reactive Molecules Produced Simultaneously

When high-energy particles or photons pass through matter, large numbers of ions and radicals are produced along the tracks. These highly reactive species subsequently react with each other and with the unaffected molecules of the surrounding medium. Because these species are produced in local regions of abnormally high concentration of similar species and because they may diffuse out of these regions before they react, their instantaneous reactivities vary greatly with the time since formation. The details of this situation are beyond the scope of the present paper.

ACKNOWLEDGMENT

This work was supported in part by the United States Atomic Energy Commission under Contract No. AT(30-1)-1314.

The author is indebted to Dr. J. M. Miller and Dr. F. C. Collins for much stimulating discussion and criticism. He is especially indebted to Dr. A. O. Allen and other members of the staff of the Brookhaven National Laboratory for helpful criticism that revealed some fallacies in preliminary work on this subject.

[21] A. C. Rutenberg and H. Taube, J. Am. Chem. Soc. **72**, 5561 (1950); and **73**, 4426 (1951).

[22] Dr. W. H. Hamill of the University of Notre Dame has independently arrived at the same conclusion and has carried out quantitative calculations tending to confirm it.

Chemical Synthesis from Free Radicals Produced in Microwave Fields

R. L. McCarthy
E. I. du Pont de Nemours and Company, Inc., Engineering Department, Engineering Research Laboratory, Wilmington, Delaware

(Received January 21, 1954)

Although much attention has been given to the physics of a microwave glow discharge, substantially less information is available regarding the chemical effects upon a gas undergoing such excitation. We have studied the chemical effects of a 2450-Mc/sec glow discharge on several gases and have made quantitative measurements on a few simple molecular systems, e.g., N_2, H_2, O_2, air, CH_4. A fundamental relationship has been found to exist between the yield in simple chemical systems and the controllable variables of electric field strength, contact time, and pressure. Analytical expressions for these relationships have been obtained.

INTRODUCTION

THE work herein reported crosses the conventional boundaries of research in physics and chemistry and brings together the techniques and knowledge of microwave engineering with those of atomic and free-radical reactions. In this work, energy supplied to a gas from a commercially-available ultra high frequency (2450-Mc) magnetron oscillator sustained a microwave glow discharge. The production of free radicals in this discharge and their chemical activity are the subjects of this study.

UNIQUE FEATURES OF MICROWAVE GAS DISCHARGES

Microwave gas discharges differ essentially in many respects from low frequency and direct-current electrical discharges.

1. As is well known, the emission spectrum of a microwave glow shows a much more extensive band structure than that of a 60-cps glow discharge in the same gas. This indicates increased molecular excitation and, hence, greater potentiality for energy transfer from the electric field to the molecules and from molecule to molecule. For example, even the helium-molecule ion spectrum has been analyzed by several observers.

2. Not reported heretofore is the fact that the luminous microwave discharge, after being initiated at a low absolute pressure (5 to 30 mm Hg), will persist as a glow discharge although the pressure is raised to greater than atmospheric. This greatly increases the possible material throughout for a given apparatus.

3. We have found that the production of free radicals per unit of energy input in a microwave gas discharge is approximately 10 times that for low-frequency or direct-current discharges. (A free radical is here defined as an uncharged atom or group of atoms containing an unpaired electron.)

ELECTRICAL CHARACTERISTICS OF THE MICROWAVE DISCHARGE

The microwave gas discharge, which is a luminous electrodeless discharge, took place in a partially evacuated quartz tube placed in a microwave cavity. Microwave power was drawn from a generator obtained from the Raytheon Manufacturing Company, and the cavity resonators were designed and built by us (Figs. 1 and 2). The electrical parameters which influence chemical reactions are the Q of the loaded cavity, the shunt impedance, and the voltage gradient during discharge. These have been measured for the systems studied, and their effect on yield has been computed.

The microwave generator which was used throughout these experiments delivered up to 1500 w of microwave power at an exact frequency of 2464 Mc/sec. Since this was a fixed frequency unit, there was no possibility of investigating the effect of frequency on chemical yield.

A more significant variable than the carrier frequency is the manner in which power is delivered to the cavity, i.e., whether it is pulsed or continuous (C.W.) power.

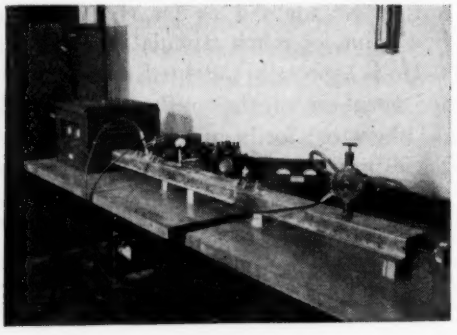

FIG. 1. The Raytheon Model N-1650 microwave generator.

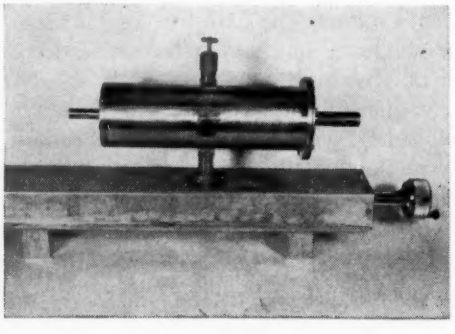

FIG. 2. Cavity *B*.

In the generator as delivered from Raytheon, the microwave power output was pulsed at a repetition rate of 120 pps with a ratio of on-time to off-time of 3:8. When this power was delivered to a cavity in which a glow discharge was maintained, the intensity of the luminous discharge was a faithful reproduction of the pulses of input power, and the discharge went on and off 120 times/sec. When a filter was added to the power supply, the power output retained some ripple but no longer returned to zero 120 times/sec (Fig. 3).

The limiting pressures and field strengths at which a glow discharge could be maintained in air in one specific cavity resonator were as follows:

(a) Without filter, at a power input of 320 w: 37 mm Hg, 350 v/cm.

(b) With filter, at a power input of 320 w: 63 mm Hg, 250 v/cm.

Hence, although the field strength was less, the pressure at which the discharge could be maintained was greater for the pure C.W. system. This advantage, however, is not convertible into an increased yield of free radicals by using a C.W. source. A series of tests on the production of free radicals from nitrogen using C.W. power gave a yield of nitrogen atoms one half of that recorded with the pulsed microwave source under the same conditions of power input, pressure, and contact time. No attempt was made to determine optimum pulse width and repetition rate.

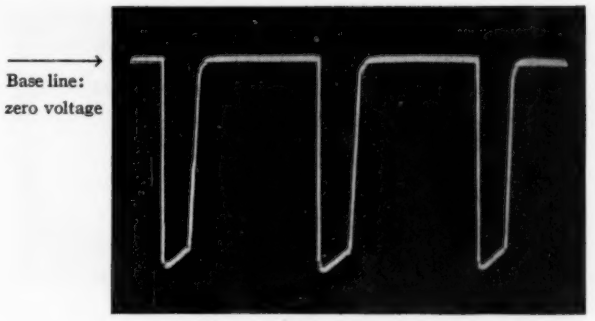

(a) Light intensity without filter.

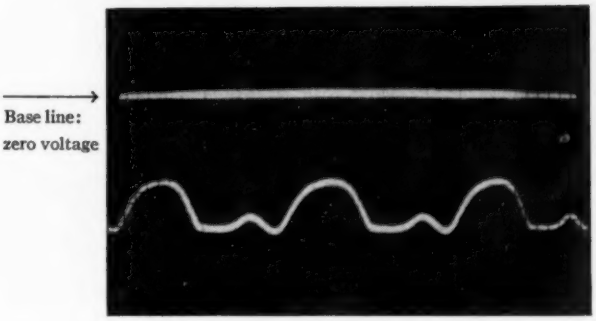

(b) Light intensity with filter.

FIG. 3. Light emission from discharge.

PRODUCTION, MEASUREMENT, AND YIELD OF FREE RADICALS

1. Evidence for the Production of Free Radicals

Knowledge of the composition of the effluent gas stream from a microwave discharge is of great importance in understanding the chemical reactions which take place. It may be composed of ions, free radicals, excited molecules or atoms, or neutral ground-state molecules, or any combination of these. The following evidence leads to the conclusion that the effluent gas contains an appreciable concentration of free radicals.

(a) It was possible to activate oxygen in the microwave field, pass it into a stream of nitrogen outside the cavity, and thus produce nitric oxide. Consequently, the emergent gas stream cannot be made up solely of neutral ground-state molecules. Under certain conditions the effluent stream from an oxygen discharge gave off a yellow light, persisting as much as 30 to 50 cm downstream of the discharge zone; the discharge zone, by contrast, had a purple color. At no point outside the cavity was the luminous oxygen stream deflected toward the walls of a Pyrex glass vessel by a unidirectional electric field of 8000 v/cm, or a magnetic field of 4000 gauss. Hence, the luminous particles present outside the discharge zone were not charged.

(b) Chemical evidence for the existence of free radicals in the effluent of the microwave discharge was also obtained. This is based on the observation that ethane and ethylene were produced in significant amounts from methane only when the effluent stream from a microwave discharge was allowed to impinge directly on a liquid-nitrogen-cooled wall (Table I). If only stable molecules had been formed in the discharge zone, the cold wall would not have altered the products.

Several measurements indicate that the free radicals do not recombine instantly but persist as free radicals for some time after leaving the discharge zone.

TABLE I. Decomposition of methane.[a]

Test	Cavity	Condition[a]	Exposure time, sec	Methane reacted, %	Percent of reacted methane as C_2H_2	C_2H_4	C_2H_6
159–21–1	*A*	a	1.8×10^{-2}	26	72	16	9
159–20–3	*A*	b	4.1×10^{-2}	17	67	···	···
58–50–2	*A*	a	6.6×10^{-2}	29	34	21	11
159–20–1	*A*	b	1.5×10^{-2}	32	48	···	···
11–50–7	*B*	b	1.2	95	95	···	···
11–50–11	*B*	b	12	25	85	···	···
10–3–3	*D*	b	2.6	100	95	···	···
10–4–2	*D*	b	3.4	50	93	···	···

[a] Conditions: (a) Collected on liquid-nitrogen-cooled wall. (b) Collected sample of gas from line downstream of discharge.

2. Yield of Simple Free Radicals

Free radical studies were conducted with nitrogen, oxygen, hydrogen, air, and water vapor as separate input materials. The free-radical flux was measured by measuring the linear portion of the time–temperature-rise curve of a stainless steel block of known mass placed directly in the effluent stream from the microwave discharge. It is well known that the collision of

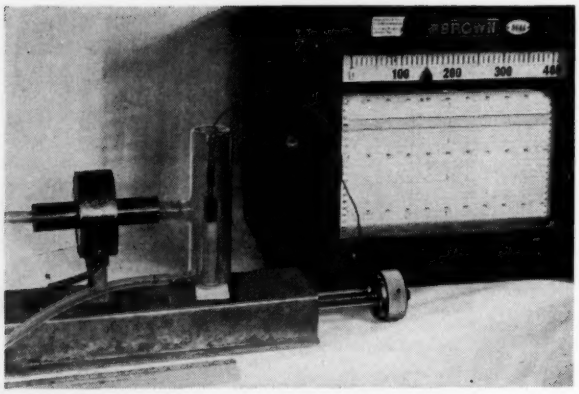

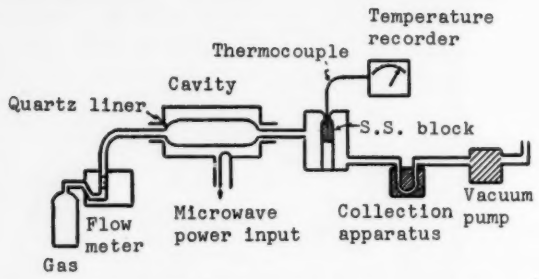

FIG. 4. (a). Cavity *A* and steel block calorimeter. (b). Free-radical calorimeter.

two free radicals in the gas phase does not produce a stable molecule, since the total energy content of the two atoms is greater than the energy of the molecule in any stationary state. Hence, a molecule is formed only if a third body capable of accepting this liberated energy is present at the time of collision. In the experiments described, a stainless steel block of sufficiently large size to intercept the gas stream was placed a few centimeters downstream of the discharge zone. Recombination of free radicals on this surface raised the temperature of the block (Fig. 4). From the time–temperature-rise curve, the specific heat of the block, and the known binding energies of the molecules, the number of atoms recombining per unit time was determined. Since the microwave power absorbed in the cavity was known, the yield in gram atoms per kilowatt-hour was readily computed. Although the steel block rose as much as 130°C, a point in the gas stream 4 cm downstream of the block rose only 6° to 8°C above the temperature of the inlet gas. This proves that a large fraction (>90 percent) of the heat imparted to the steel block was due to the recombination of free radicals and not due to the impact of a thermally hot gas stream.

3. Yield of Free Radicals

Measurement of the production of simple free radicals and atoms was made over the widest range of process variables available with the cavity used in these tests. The yield was computed for nitrogen, oxygen, and hydrogen atoms, and is plotted in Figs. 5, 6, and 7 as a function of a parameter α, where $\alpha=E^2p/\tau Z_s$; E=the electric field strength, v/cm; p=the absolute pressure, mm of Hg absolute; τ=the time of flight, i.e., the time for a molecule in the gas stream to pass from the discharge zone to the steel block where recombination is measured, sec; and Z_s=the shunt impedance, ohms.

The parameter α uniquely determines the yield, through the relationship given by Eq. (1)

$$Y=A-B\exp(-h\alpha^r), \qquad (1)$$

where Y=yield, gram atoms per kilowatt-hour; and B, h, r=empirically determined constants for each gas.

The asymptote A represents the highest yield available in the range of variables examined, which represents the limits of available apparatus. These highest yield values where 1.0 g atom/kw-hr for hydrogen, 0.80 g atom/kw-hr for oxygen, and 0.58 g atom/kw-hr for nitrogen (Figs. 5, 6, 7). The range of the individual variables studied was E, 150 to 300 v/cm; p, 16 to 200 mm Hg; τ, 0.005 to 0.5 sec; and Z_s, 2×10^5 to 2×10^6 ohms.

Tests similar to those designed to measure free-radical yields from nitrogen, oxygen, and hydrogen were made using helium, a monatomic gas, as input material. A luminous glow discharge of about the same intensity as that of the diatomic gases was observed, but only a very slight temperature rise of the calorimeter was recorded, e.g., 1.7°C/min for helium as contrasted with 22°C/min for nitrogen under the same conditions. This heating could be accounted for by the 0.2 percent N_2 impurity in the helium, giving, as is expected, no energy release for recombination in helium.

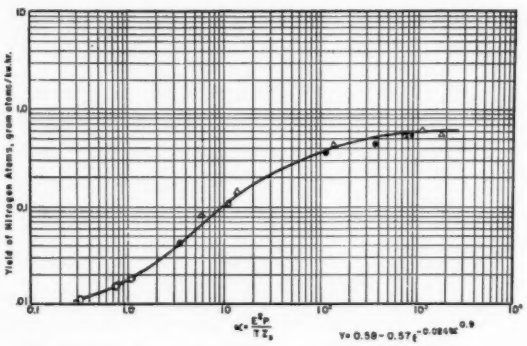

FIG. 5. Yield of nitrogen atoms. ● Discharge in nitrogen in cavity *A*. ○ Discharge in nitrogen in cavity *D*. ▲ Discharges in air cavities *A* and *D*.

SYNTHESIS OF SIMPLE CHEMICAL COMPOUNDS

Two simple chemical systems, one inorganic and the other organic, have been studied extensively. These are the synthesis of nitric oxide from nitrogen and oxygen and the production of acetylene from methane.

1. Synthesis of Nitric Oxide

(*a*) *Production and Analysis of Nitric Oxide* (*NO*)

Experiments have been performed on the production of nitric oxide from mixtures of nitrogen and oxygen.

While dry air has been the principal raw material, equal volumes of nitrogen and oxygen as well as large excesses of nitrogen and of oxygen have been used. Pressures greater than 1 atmosphere have been used.

The products of the discharge were collected in a gas sample bottle downstream from the discharge and subjected to mass spectrometer analysis. Nitrogen, oxygen, nitric oxide, and nitrogen dioxide were the only significant products. By converting all the nitric oxide to nitrogen dioxide an accurate determination of the yield was obtained.

(*b*) *Yield of Nitrogen Dioxide* (NO_2) *from Air*

Although the primary product of an air discharge is principally nitric oxide, the yield of nitrogen dioxide was measured since the conversion of nitric oxide to nitrogen dioxide in the presence of oxygen requires no additional energy. The yield of nitrogen dioxide in gram moles per kilowatt-hour *versus* the empirical parameter β is given in Fig. 8.

$$Y=0.15\exp(0.016\beta^{\frac{1}{2}}), \qquad (2)$$

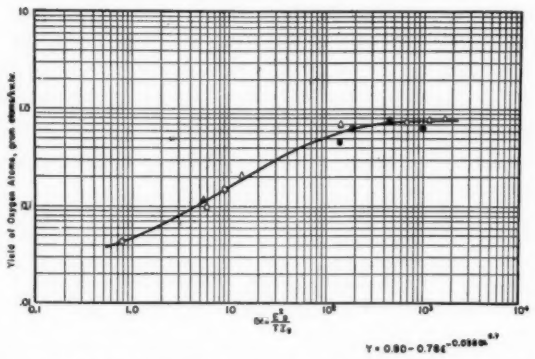

FIG. 6. Yield of oxygen atoms. ● Discharge in oxygen in cavity *A*. ○ Discharge in oxygen in cavity *D*. △ Discharges in air in cavities *A* and *D*.

where $\beta=pZ_s/E^2t$; p=the absolute pressure, mm Hg absolute; E=the electric field strength, v/cm; t=the contact time, i.e., the average time a molecule spends in the discharge zone, sec; and Z_s=the shunt impedance, ohms. The range of the variables studied was p, 30 to 760 mm Hg; E, 60 to 400 v/cm; t, 0.02 to 4 sec; and Z_s, 4×10^4 to 2×10^6 ohms. Note that parameters governing yield in Eqs. (1) and (2) are not identical

$$\alpha=E^2p/\tau Z_s; \quad \beta=pZ_s/E^2t.$$

An explanation of the physical situation causing this follows. In both α and β, time appears in the denominator. In α, τ refers to the time of flight, i.e., the time necessary for the gas to flow from the discharge zone to the point at which the free-radical concentration is measured. Since the free radicals are lost through recombination along the walls of the tube during this time, both α and Y increase as τ decreases. The expression for β, t refers to the time the molecules spend in the glow discharge. For most efficient production, the molecule should be dissociated and then removed from the discharge zone. This should take place in a time comparable with breakdown or ionization time in the gas. This is very small (of the order of 100 μsec) compared with any available exposure time in our system. Longer exposure times result in some wasteful decomposition of the product molecules, hence the yield increases as t decreases.

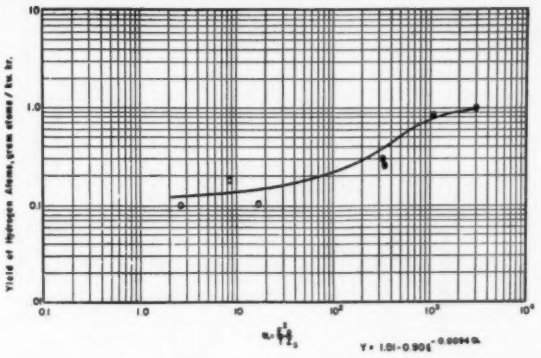

FIG. 7. Yield of hydrogen atoms. ● Discharge in hydrogen in cavity *A*. ○ Discharge in hydrogen in cavity *D*.

In both α and β, the gas pressure appears in the numerator, since for zero gas pressure the yield must go to zero. For the simple free radicals, essentially this occurred, as can be seen from Figs. 5, 6, and 7, which indicate a wide range of validity of the parameter α. For the more complicated molecular systems of nitric oxide and acetylene, the yield decreased with decreasing pressure, but did not go to zero for zero pressure (Fig. 8). This indicates the more limited applicability of the parameter β and the influence of apparatus limitations and measurement techniques on the results.

In α, the square of the field gradient E^2 appears in the numerator, while in β it appears in the denominator. An explanation of this can be advanced as follows. In the studies of simple free radicals in which α

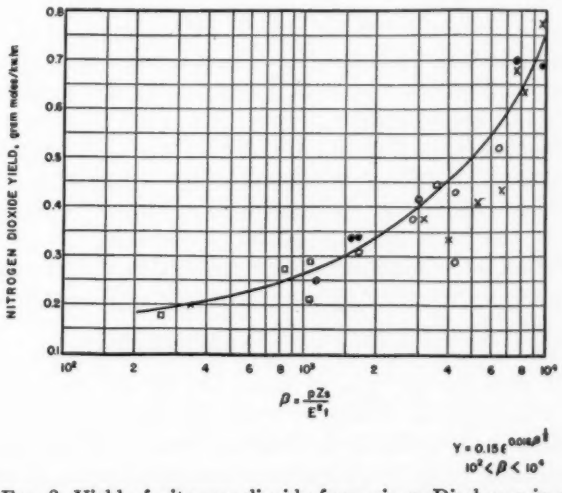

FIG. 8. Yield of nitrogen dioxide from air. ● Discharge in air in cavity *A*. × Discharge in air in cavity *B*. □ Discharge in air in cavity *C*. ○ Discharge in air in cavity *D*.

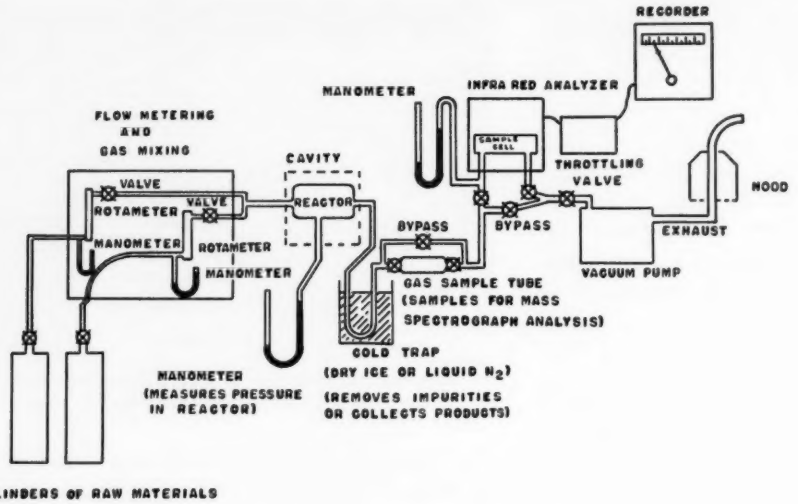

FIG. 9. Microwave glow discharge system.

appears, the only reaction is one of dissociation of the input molecules. The kinetic energy of the electrons which produce dissociation is proportional to the square of the voltage gradient, hence the yield Y increases as the field strength E increases. In β, the square of the field strength appears in the denominator; hence, as E decreases, the yield increases. This is believed to arise from the fact that the reaction studied is not a simple one of dissociation, but it includes free-radical recombination to form a desirable product, plus subsequent decomposition of this product. Even though the free radicals recombine to form the same product molecule, it represents a waste of energy, hence, a reduced yield. It appears reasonable that increasing E^2 will reduce the yield when the weakest chemical bond of the product molecule has a higher dissociation energy than at least one bond in the raw material. This is true for nitric oxide and acetylene, since NO (150 kcal/mole)$>O_2$ (117 kcal/mole) and C_2H_2 (123 kcal/mole for C$\equiv$C) $>CH_4$ (87 kcal/mole for C$-$H). The cavity impedance Z_s is simply an electrical parameter which relates power input to voltage across the cavity. Since power is approximately equal to $\sim E^2/Z_s$, E^2 must always be multiplied by $1/Z_s$ to yield comparative data for all cavities. For this reason, Z_s appears in the denominator of α and the numerator of β.

Since all the glow discharge reactions are threshold reactions, a certain electron energy level must be reached before the discharge takes place. No matter what the value of any individual variable, the yield remains zero unless glow takes place. Hence, the range of α and β are limited by the apparatus available and are specified for the studies made.

The highest yield of nitrogen dioxide observed was 0.77 mole/kw-hr. This occurred for the highest value of β at which a discharge could be maintained. The yield Y in gram moles per kilowatt-hour increases with increasing values of β, reaching its highest value at the point where the glow is on the verge of extinction. Physically, this means that the process is most efficient when the energy supplied to the electrons from the microwave field is just sufficient to sustain the discharge. At this point, the number of electrons produced in the gas per unit time equals the number lost through diffusion to the walls. When the number lost exceeds the number produced in unit time, the glow is extinguished and chemical reaction ceases. On the other hand, production of an excessive number of electrons reduces the efficiency of the process, since many strike the walls with high energy and others dissociate product molecules.

(c) *Molecular Dynamics in the Formation of Nitric Oxide*

The low yields of nitric oxide in terms of the theoretical maximum (only 13 percent) raise the question of the molecular dynamics involved in the production and recombination of nitrogen and oxygen atoms.

The theoretical maximum yield of nitric oxide for the glow discharge is much less than the calculated thermochemical yield. In the latter it is assumed that all the energy put into the system does useful chemical work. This cannot be true for the glow discharge, as will be discussed now.

With the energy transfer involved, it becomes difficult to predict a yield from even so simple a system as the synthesis of nitric oxide from nitrogen and oxygen. For a safe theoretical maximum, the following assumptions seem justified. Nitric oxide is formed by a three-body collision involving a nitrogen atom and an oxygen atom. This three-body collision is assumed to take place only at the wall, since three-body collisions in the gas are so infrequent. If two atoms (N and O), both in the ground state, collide at the wall to form an NO molecule, they must give up their binding energy to the wall as heat. If the atoms are in excited states, they can either form an excited molecule or give up all their energy to the wall to form a ground-state molecule. In any case energy must be dissipated as heat at the rate of 150 kg cal for every mole of nitric oxide formed, for this is the binding energy which is given up to the

wall. This is independent of any way in which energy is transferred prior to the formation of the nitric oxide molecule. If only 150 kg cal/mole of nitric oxide formed were lost, we would obtain our maximum theoretical yield for the microwave discharge, namely, 5.7 g moles/kw-hr; the statistics of recombination to reform molecular oxygen and nitrogen would reduce this to 3.8 g moles/kw-hr. The theoretical yield based on this mechanism is much lower than that derived from a thermochemical calculation, since heat is not a useful form of energy in the microwave discharge and once the microwave energy has been degraded to heat through molecular energy transfer it is permanently lost to the system. This is true since the reactions in the microwave discharge depend upon the electron temperature and not upon the molecular temperature. The two are not in equilibrium but differ by several thousand degrees. The electron temperature depends almost entirely on the field strength and the molecular bond strengths; the translational molecular velocity influences it very little. Hence, when energy is transferred from electrons to molecules and this energy is partitioned into translational molecular velocity, it cannot be returned to the electrons, which are the principal source of chemical activity.

The problem of molecular dynamics in the formation of nitric oxide has been attacked experimentally with the following results:

(1) When dry air, which contains four nitrogen molecules for every oxygen molecule, was passed through the microwave discharge, thirteen oxygen molecules were dissociated for every five nitrogen molecules dissociated.

(2) On the average only one-half of the collisions of a nitrogen atom with an oxygen atom on a third body produced nitric oxide, normalized against one collision of two nitrogen atoms to form molecular nitrogen or one collision of two oxygen atoms to form molecular oxygen.

The data from which these conclusions are drawn are taken from the measurements of the free-radical yield from nitrogen and oxygen discharges and the observed yields of nitrogen dioxide from air.

2. Synthesis of Acetylene from Methane

(a) *Production and Analysis of Acetylene*

The production of acetylene from methane has been investigated. As in all other cases, the glow was initiated at low pressure and maintained at a higher pressure by increasing the flow of raw material. Discharges were maintained up to a $\frac{1}{2}$ atmos absolute pressure.

Particularly convenient control of the process was achieved by inserting a Beckman Model IR2 infrared spectrophotometer in the discharge stream (Fig. 9). The acetylene concentration was recorded continuously on a chart, and the effect of process variables was readily seen. The complete chemical analysis was obtained by extracting a gas sample from the effluent stream and subjecting it to mass spectrometer analysis. From the pressure, flow rate, input power, and chemical analysis, the yield of acetylene in gram moles per kilowatt-hour was readily determined. For tests on the production of acetylene, the methane used was prepared by the Matheson Company; its composition was 98.8 percent CH_4, 0.7 percent C_2H_6, less than 0.05 percent C_2H_2, and the remainder higher paraffins.

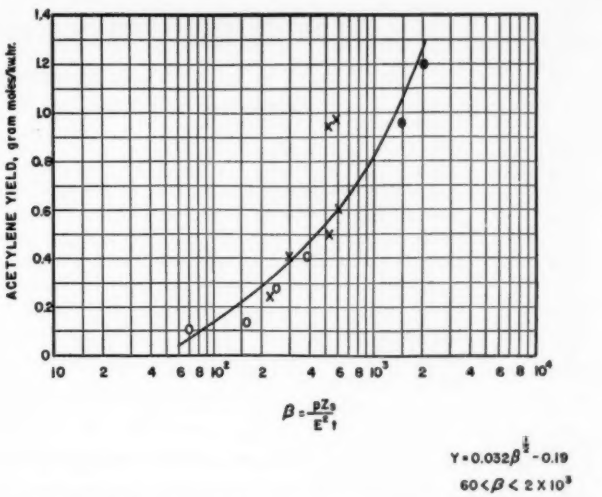

FIG. 10. Yield of acetylene from methane. ● Discharge in methane in cavity *A*. × Discharge in methane in cavity *B*. ○ Discharge in methane in cavity *D*.

(b) *Yield of Acetylene*

The yield of acetylene is plotted *versus* β in Fig. 10, where β again equals pZ_s/E^2t. The yield Y is for the range of the individual variables as follows: E, from 150–310 v/cm; p, from 16–220 mm Hg; t, from 1×10^{-2} to 10 sec; Z_s from 4×10^4 to 2×10^6 ohms.

The yield increased with increasing values of β to the highest value observed at which the flow could be maintained; this yield was 1.2 g moles/kw-hr. The maximum theoretical yield for acetylene according to the mechanism previously described is 2.0 g moles/kw-hr.

ACKNOWLEDGMENTS

The author wishes to acknowledge the cooperation and extensive contributions throughout a large portion of this program of L. M. Magner of the Engineering Research Laboratory, and T. A. Ford of the Chemical Department, E. I. du Pont de Nemours and Company.

The United Atom-Separated Atom Treatment of H_2^+ †

J. R. STREETMAN AND F. A. MATSEN
Departments of Chemistry and Physics, University of Texas, Austin, Texas
(Received January 29, 1954)

A trial wave function consisting of a linear combination of 1*S* orbitals centered on the nuclei and on a point half-way between them was used in a variational treatment of H_2^+. A one-electron three-center integral with nonequal charges which arises in the course of this treatment was evaluated. The effective nuclear charges for minimum energy were found approximately by calculating energies for a range of values of the separated atom charge and of the united atom charge. The lowest energy calculated, −0.5969 au, occurred where both effective nuclear charges are equal at 1.25. The energy value should be compared with −0.6031 au, the exact value, and with −0.6001 au obtained by hybridizing 1*S* and 2*Pz* orbitals on the separated nuclei. The ratio of the united atom coefficient to separated atom coefficient was found to be 0.3501 for the energy value mentioned.

THE hydrogen molecule ion can be thought of as being formed by the approach and interaction of a hydrogen atom and a proton. This viewpoint is expressed in the most familiar treatment[1] which consists of using as trial wave function a linear combination of atomic orbitals on each of the two nuclei. The hydrogen molecule ion can also be thought of as being formed from He^+ by the separation of the doubly charged nucleus into two singly charged nuclei. This viewpoint is expressed in the united atom treatment[2] in which the trial wave function consists of a single atomic orbital arising from a point midway between the nuclei.

Since the real molecule would be expected to occupy a position somewhat in between these two extremes, it would appear that a combination of the two treatments would be better than either of them separately. In this paper the two treatments are combined, and the trial wave function used is

$$\psi = C_{ab}\phi_{ab} + C_2\phi_2$$
$$\phi_{ab} = \phi_1 + \phi_3 = (z^3/\pi)^{\frac{1}{2}}(e^{-za} + e^{-zb})$$
$$\phi_2 = (z'^3/\pi)^{\frac{1}{2}} e^{-z'u},$$

since symmetry requires that the two separated atom orbitals have the same coefficient. The coordinates are

a, the distance to nucleus *A*; *b*, the distance to nucleus *B*; and *u*, the distance to the point halfway between the nuclei. Elliptical and spherical coordinates are defined about these points in the usual ways.

The secular determinant can be written

$$\begin{vmatrix} 2[H_{11}+H_{13}-E(1+S_{13})] & 2(H_{12}-ES_{12}) \\ 2(H_{12}-ES_{12}) & H_{22}-E \end{vmatrix} = 0.$$

The Hamiltonian for the hydrogen molecule ion is

$$H = -\tfrac{1}{2}\nabla^2 - 1/a - 1/b + 1/R,$$

so that after some elementary integrations in spherical coordinates there is obtained:

$$H_{11} = z^2/2 - z - [z^3/\pi]\int e^{-2za}(1/b)dV + 1/R$$

$$H_{12} = -(z^2/2)S_{12} + (z-1)[(zz')^{\frac{3}{2}}/\pi]\int e^{-z'u}(1/a)e^{-za}dV - [(zz')^{\frac{3}{2}}/\pi]\int e^{-za}(1/b)e^{-z'u}dV + S_{12}/R$$

$$H_{13} = (1/R - z^2/2)S_{13} + (z-2)(z^3/\pi)\int e^{-za}(1/b)e^{-zb}dV$$

$$H_{22} = z'^2/2 + 1/R - 2(z'^3/\pi)\int e^{-2z'u}(1/a)dV,$$

where *R* is the internuclear distance in atomic units as are all distances in this paper.

By the use of elliptical coordinates

$$(z^3/\pi)\int e^{-2za}(1/b)dV = (z^3R^2/2)(A_1B_0 + A_0B_1)_{(Rz)}^{(Rz)}$$

$$(z^3/\pi)\int e^{-za}(1/b)e^{-zb}dV = z^3R^2A_1(Rz)$$

$$(2z'^3/\pi)\int e^{-2z'u}(1/a)dV = R^2(z'^3/4)(A_1B_0 + A_0B_1)_{(Rz'/2)}^{(Rz'/2)}$$

$$S_{13} = (z^3R^3/2)(A_2 - \tfrac{1}{3}A_0)_{(Rz')}$$

$$S_{12} = (zz')^{\frac{3}{2}}(R^3/32)(A_2B_0 - A_0B_2)_{(\beta)}^{(\alpha)}$$

$$[(zz')^{\frac{3}{2}}/\pi]\int e^{-z'u}(1/a)e^{-za}dV = (zz')^{\frac{3}{2}}(R^2/8)(A_1B_0 - A_0B_1)_{(\beta)}^{(\alpha)},$$

† This work was supported by Contract DA-23-072-ORD-774 of the U. S. Office of Ordnance Research.

[1] L. Pauling, Chem. Revs. **5**, 173 (1928).

[2] See F. A. Matsen, J. Chem. Phys. **21**, 928 (1953), and other references given there.

for z' greater than z. For z greater than z', the elliptical coordinates must be redefined to keep β positive. The result will be the same for all the integrals in the foregoing except for the last which will give the result

$$(zz')^{\frac{1}{2}}(R^2/8)(A_1B_0+A_0B_1)_{(\beta)^{(\alpha)}}.$$

For z' greater than z,

$$\alpha=(z'+z)R/4$$
$$\beta=(z'-z)R/4.$$

For z greater than z',

$$\alpha=(z'+z)R/4$$
$$\beta=(z-z')R/4.$$

$A_i(x)$ and $B_i(x)$ are tabulated in Kotani.[3] The evaluation of the three-center integral

$$[(zz')^{\frac{1}{2}}/\pi]\int e^{-za}(1/b)e^{-z'u}dV$$

is given in the appendix.

The energies for a number of values of α and β are given in Table I. Minimizing E with respect to α and β will minimize it with respect to z and z'.[4]

An attempt was made to find the minimum more exactly by means of four-point Lagrangian interpolation. This indicated that the minimum should lie (as closely as the interpolation could determine), at $\alpha=1.25$, $\beta=0$. The energy value was therefore calculated for these values of α and β by the same method used for the calculation of the energies in Table I. The results of combining united atom and LCAO treatments can be seen from this comparison:

	Energy (au)	
LCAO	−0.556	for $z=1$, $R=2$
LCAO	−0.583	for $z=1.29$, $R=2$
LCAO including $2Pz$ orbitals	−0.6001	
Exact	−0.6031	
United Atom+LCAO	−0.5969	for $z=z'=1.25$, $R=2$.

The ratio C_2/C_{ab} at $z=z'=1.25$, $R=2$ is 0.3510.

[3] M. Kotani, Proc. Phys.-Math. Soc. Japan, **20**, 57 (1938). The notation $(A_iB_j\pm A_jB_i)_{(\beta)^{(\alpha)}}$ used above means $(A_i(\alpha)B_j(\beta)\pm A_j(\alpha)B_i(\beta))$.

[4] The condition for E to be a minimum with respect to z is

$$\left(\frac{\partial E}{\partial z}\right)_{z'}=\left(\frac{\partial E}{\partial \alpha}\right)_\beta\left(\frac{\partial \alpha}{\partial z}\right)_{z'}+\left(\frac{\partial E}{\partial \beta}\right)_\alpha\left(\frac{\partial \beta}{\partial z}\right)_{z'}=0.$$

Since

$$\left(\frac{\partial \alpha}{\partial z}\right)_{z'}=\frac{R}{4},\quad \left(\frac{\partial \beta}{\partial z}\right)_{z'}=-\frac{R}{4},\quad \left(\frac{\partial E}{\partial \alpha}\right)_\beta-\left(\frac{\partial E}{\partial \beta}\right)_\alpha=0.$$

Similarly, the condition for z' reduces to

$$\left(\frac{\partial E}{\partial \alpha}\right)_\beta+\left(\frac{\partial E}{\partial \beta}\right)_\alpha=0.$$

Therefore the requirement for minimization with respect to z and z' simultaneously is

$$\left(\frac{\partial E}{\partial \alpha}\right)_\beta=0,\quad \left(\frac{\partial E}{\partial \beta}\right)_\alpha=0.$$

TABLE I. Energy in atomic units.

	$-E$			
α	0.5	1.0	1.5	2.0
β				
0	0.275995	0.559116	0.572960	0.351593
0.25	0.456648	0.499494	0.594338	0.460466
0.50		0.377974	0.564263	0.553917
$\alpha=1.25$, $\beta=0$	0.596889			

If z is held constant at 1 and z' at 2, the energy varies with internuclear distance as shown in the figure, which also serves to tabulate the variation of C_2^2 with R under the same restrictions on z and z'.

APPENDIX

The method used[5] to evaluate the three-center integral was to express a and u in elliptical coordinates and $1/b$ in terms of these by the Neuman expansion. The first six terms (to $k=5$) of the expansion give accuracy to six or seven significant figures.

The method used here was, for the most part, equivalent to a more general method of treating three-center integrals.[6] The following integrals are defined:

$$M_k(3,n,\alpha)=\int_1^\infty e^{-\alpha f}Q_k(f_+)P_k(f_-)f^n df$$

$$=Q_k(3)\int_1^3 e^{-\alpha f}P_k(f)f^n df+P_k(3)\int_3^\infty e^{-\alpha f}Q_k(f)f^n df$$

$$G_k(n,1,3,\alpha)=\int_1^3 e^{-\alpha f}f^nP_k(f)df$$

$$f_k(n,3,\infty,\alpha)=\int_3^\infty e^{-\alpha f}f^nQ_k(f)df.$$

Above, use has been made of the fact that the coordinates of the point B are $f=3$, $g=$either 1 or -1 (depending on the sense in which the elliptical coordinates

TABLE II. Mixing coefficient for united atom wave function.

α	0.5	1.0	1.5	2.0
β				
0	−4.32421	0.410864	0.395731	0.530081
0.25	−10.3225	1.10025	0.170661	0.228548
0.50		1.35961	0.168380	0.0921084
$\alpha=1.5$, $\beta=0$	3.5102			

[5] J. R. Streetman, Master of Arts thesis, University of Texas (May, 1953).

[6] R. S. Barker and H. Eyring, J. Chem. Phys. **21**, 912 (May, 1953).

TABLE III. $G_k(n,1,3,\alpha)$.

n	$k=0$	1	2	3	4	5
			$\alpha=0.5$			
0	0.7668009991	1.40788236	3.8589713	13.2220	51.52	217.61
1	1.407882357	2.82824787	8.4963386	31.0930	126.8	
2	2.828247866	6.13351987	19.787078	76.0826	321.0	1435.3
3	6.133519870	14.1341343	48.102960	191.916	831.2	
4	14.13413434	34.1131469	120.80351	495.581		
5	34.11314691	85.2470508	310.99411			
6	85.24705081	218.700452				
7	218.7004524					
			$\alpha=1$			
0	0.3180923728	0.536610609	1.3304794	4.201783	15.41	62.224
1	0.5366106088	0.993017043	2.7357143	9.37509	36.44	
2	0.9930170435	2.00267973	6.0222602	21.99311	89.37	388.35
3	2.002679726	4.34584580	13.996936	53.6468	225.5	
4	4.345845805	9.99885085	33.926395	134.869		
5	9.998850850	24.0662117	84.921139			
6	24.06621170	59.9470428				
7	59.94704282					
			$\alpha=1.5$			
0	0.1413474424	0.220767075	0.49400962	1.42311	4.854	18.550
1	0.2207670753	0.376455561	0.94217040	2.98550	10.94	
2	0.3764555615	0.701702625	1.9418842	6.65414	25.79	108.17
3	0.7017026253	1.42007463	4.2731658	15.5711	63.05	
4	1.420074628	3.082678094	9.9107029	37.8613		
5	3.082678094	7.08049350	23.949870			
6	7.080493498	16.9941395				
7	16.99413948					
			$\alpha=2$			
0	0.0664282655	0.097163646	0.19730122	0.516054	1.622	5.8062
1	0.0971636460	0.153676903	0.34849794	1.01128	3.455	
2	0.1536769029	0.264719842	0.66823834	2.12365	7.772	31.197
3	0.2647198415	0.496717861	1.3800809	4.72753	18.28	
4	0.4967178613	1.00829390	3.0352073	11.0346		
5	1.008293905	2.18904419	7.024063			
6	2.189044187	5.01880679				
7	5.018806791					

are defined). The sense in which the elliptical coordinates are defined depends on whether z or z' is greater, and is such as to make β positive in the following breakdown:

$$[(zz')^{\frac{1}{2}}/\pi]\int e^{-z\alpha}(1/b)e^{-z'u}dV$$
$$=\sum_k (zz')^{\frac{1}{2}}(g_B)^k\frac{4(2k+1)}{R\pi}\int_1^\infty e^{-\alpha f}Q_k(f_+)P_k(f_-)$$
$$\times\int_{-1}^1 e^{-\beta g}P_k(g)(R/4)^3(f^2-g^2)dg\int_0^{2\pi}d\phi.$$

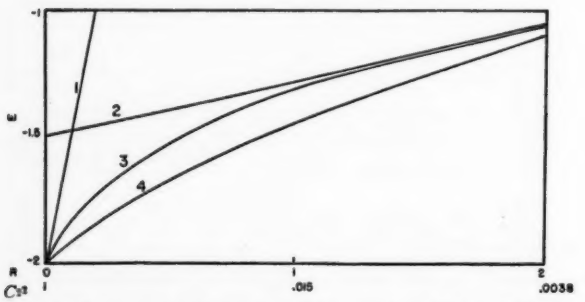

FIG. 1. Energy as a function of internuclear distance, both in atomic units. (1) United atom ($z'=2$); (2) Separated atom ($z=1$); (3) United atom-separated atom ($z'=2$, $z=1$); C_1^2 is the fractional contribution of the united atom; (4) Exact.

Substituting $R=2$, the equilibrium values and rearranging

$$=\tfrac{1}{2}(zz')^{\frac{1}{2}}\sum_k (g_B)^k(2k+1)$$
$$\times\left[\int_1^\infty e^{-\alpha f}f^2Q_k(f_+)P_k(f_-)df\int_{-1}^1 e^{-\beta g}P_k(g)dg\right.$$
$$\left.-\int_1^\infty e^{-\alpha f}Q_k(f_+)P_k(f_-)df\int_{-1}^1 e^{-\beta g}g^2P_k(g)dg\right]$$
$$=\tfrac{1}{2}(zz')^{\frac{1}{2}}\sum_k (g_B)^k(2k+1)$$
$$\times[M_k(3,2,\alpha)G_k(0,\beta)-M_k(3,0,\alpha)G_k(2,\beta)]$$

$z<z'$	$z>z'$
$\alpha=(z'+z)R/4$	$\alpha=(z'+z)R/4$
$\beta=(z'-z)R/4$	$\beta=(z-z')R/4$
$g_B=-1$	$g_B=1$,

$G_k(n,\beta)$ is the familiar Kotani G.

The following recursion formulas and their proofs for $G_k(n,1,3,\alpha)$ and $f_k(n,3,\infty,\alpha)$ are given by Barker and

TABLE IV. $f_k(n,3,\infty,\alpha)$.

n	$k=0$	1	2	3	4	5
			$\alpha=0.5$			
0	1.022222714^{-1}	8.4839518^{-3}	8.9903775^{-4}	1.0680^{-4}	1.378^{-5}	-7.6291^{-6}
1	4.547442721	3.4673449^{-2}	3.4576590^{-3}	3.932	4.323^{-5}	
2	2.265975049^{0}	1.5388653^{-1}	1.41052855^{-2}	1.50655^{-3}	-5.321^{-4}	-6.3642^{-2}
3	1.309543581^{1}	7.6472854	6.2458545	5.74109	-3.469^{-2}	
4	9.046305286	4.4067843^{0}	3.0933607^{-1}	6.9468		
5	7.581404664^{2}	3.0360575^{1}	1.76688818^{0}			
6	7.676138819^{3}	2.5389141^{2}				
7	9.232855971^{4}					
			$\alpha=1$			
0	1.339680926^{-2}	1.24297121^{-3}	1.4251217^{-4}	1.79228^{-5}	2.345^{-6}	-6.0788^{-6}
1	5.103003959	4.5606112	5.0794216	6.24164	4.589	
2	2.037088843^{-1}	1.73486413^{-2}	1.8616944^{-3}	2.20312^{-4}	2.807^{-5}	-7.9587
3	8.637288031	6.9144091	7.0716434	8.13911	9.349	
4	3.952535434^{0}	2.9262403^{-1}	2.8145983^{-2}	3.08413^{-3}		
5	1.985894272^{1}	1.3362758^{0}	1.1890009^{-1}			
6	1.112661224^{2}	6.6989143^{0}				
7	7.025727898					
			$\alpha=1.5$			
0	2.134153283^{-3}	2.08519134^{-4}	2.48804135^{-5}	3.22731^{-6}	4.445^{-7}	-7.9254^{-7}
1	7.614516825	7.2797137	8.53440375	1.09171^{-5}	9.941^{-7}	
2	2.788329625^{-2}	2.5950683^{-3}	2.97738775^{-4}	3.71440	4.800^{-6}	-4.6104^{-5}
3	1.054561475^{-1}	9.4929246	1.06031375^{-3}	1.30345^{-4}	-9.105^{-6}	
4	4.151770182	3.5858925^{-2}	3.87537690	4.49217		
5	1.717569099^{0}	1.4097592^{-1}	1.46131005^{-2}			
6	7.546333613	5.8226510				
7	3.560267423^{1}					
			$\alpha=2$			
0	3.712434012^{-4}	3.7402463^{-5}	4.5749454^{-6}	6.05625^{-7}	8.298^{-8}	4.04^{-8}
1	1.276778552^{-3}	1.26797764^{-4}	1.532436^{-5}	2.00811^{-6}	2.916^{-7}	
2	4.464614074	4.3580909	5.192397	6.7342	8.545	-4.2966^{-6}
3	1.592801030^{-2}	1.52282067^{-3}	1.7836415^{-4}	2.27414^{-5}	6.06	
4	5.822427705	5.4282462	6.227731	7.6788		
5	2.192206182^{-1}	1.98232744^{-2}	2.2173714^{-3}			
6	8.554726210	7.4551787				
7	3.485005514^{0}					

Eyring.

$$G_k(n,1,3,\alpha)=\frac{2k-1}{k}G_{k-1}(n+1,1,3,\alpha)-\frac{k-1}{k}G_{k-2}(n,1,3,\alpha) \quad \text{for} \quad k>0$$

$$G_0(n,1,3,\alpha)=(1/\alpha)(nG_0(n-1,1,3,\alpha)+e^{-\alpha}-3^ne^{-3\alpha}) \quad \text{for} \quad n>0$$

$$f_k(n,3,\infty,\alpha)=\frac{2k-1}{k}f_{k-1}(n+1,3,\infty,\alpha)-\frac{k-1}{k}f_{k-2}(n,3,\infty,\alpha) \quad \text{for} \quad k>1$$

$$f_1(n,3,\infty,\alpha)=f_0(n+1,3,\infty,\alpha)-3^{n+1}A_n(3\alpha).$$

With these and the obvious relations

$$G_0(0,1,3,\alpha)=\frac{1}{\alpha}(e^{-\alpha}-e^{-3\alpha})$$

$$f_0(0,3,\infty,\alpha)=\frac{1}{2\alpha}\{[-E_i(-4\alpha)]e^{\alpha}-[-E_i(-2\alpha)]e^{-\alpha}+e^{-3\alpha}\ln 2\}$$

$$f_0(1,3,\infty,\alpha)=\frac{e^{\alpha}}{2}(1/\alpha^2-1/\alpha)[-E_i(-4\alpha)]-\frac{e^{-\alpha}}{2}(1/\alpha^2+1/\alpha)[-E_i(-2\alpha)]+\tfrac{1}{2}(1/\alpha^2-1/\alpha)e^{-3\alpha}\ln 2,$$

there is needed only a recursion formula for $f_0(n,3,\infty,\alpha)$. Barker and Eyring recommend breaking this last function down three times more into simpler functions, but for systems having so much symmetry and giving such simple integrals as the one considered in this paper, it seemed easier to use a recursion formula the derivation of which parallels rather closely that of Rosen's formula[7]

TABLE V. Values of three-center integral.

β $\alpha=$	0.5	1.0	1.5	2.0
0	3.87521^{-1}	5.00574^{-1}	4.70136^{-1}	3.93358^{-1}
0.25	2.68101	4.86032	4.79802	4.19064
0.50		3.79144	4.54899	4.06992

[7] P. Rosen, Phys. Rev. **38**, 2108 (1931).

for his $f_0(n,\alpha)$.

$$f_0(n,3,\infty,\alpha)=f_0(n-2,3,\infty,\alpha)+1/\alpha[nf_0(n-1,3,\infty,\alpha)-(n-2)f_0(n-3,3,\infty,\alpha)-3^{n-1}A_{n-2}(3\alpha)+4\cdot 3^{n-2}e^{-3\alpha}\ln 2] \quad \text{for} \quad n>1.$$

Since the integrals $f_k(n,3,\infty,\alpha)$ and $G_k(n,1,3,\alpha)$ are basic to calculations of one-electron 3-center integrals, the values calculated are given in Tables III and IV.

The calculated values of the 3-center integral are given in Table V.

THE JOURNAL OF CHEMICAL PHYSICS VOLUME 22, NUMBER 8 AUGUST, 1954

The Ferrous Sulfate Radiation Dosimeter: A Calorimetric Calibration with Gamma Rays*†

R. M. Lazo, H. A. Dewhurst, and Milton Burton
Department of Chemistry, University of Notre Dame, Notre Dame, Indiana

(Received January 25, 1954)

The ferrous sulfate radiation dosimeter (herein called the Fricke dosimeter) has been recalibrated by a calorimetric method in which assumptions regarding energy absorbed in the glass and the heat capacity of the calorimeter have been eliminated. The 100-ev yield, $G(Fe^{++}\rightarrow Fe^{+++})$, is 15.8 ± 0.3 for Co^{60} gamma radiation in agreement with the Hochanadel-Ghormley value. The result is compared with other G values reported in the literature and it is recommended that the low value be adopted for Co^{60} gamma radiation and for electrons in the 1–2 Mev range.

1. INTRODUCTION

THE oxidation of ferrous sulfate in aerated $0.8N$ sulfuric acid solution by ionizing radiations[1] satisfies most of the requirements of an aqueous dosimeter.[2] Unfortunately, general adoption of this system is prevented by serious discrepancies in the 100-ev yield[3] reported by different authors (Table I).

The reasons for these discrepancies[4–10] have not heretofore been understood. Suggested explanations have included (i) dose-rate dependence at high dose rates, (ii) organic impurities in the dosimeter solution, and (iii) errors in absolute measurement of the energy absorbed. The recent work of Miller[11] has shown that the oxidation yield is independent of dose rate up to 100 000 r/min, provided the solution contains dissolved oxygen. Therefore, unless the solution becomes oxygen-depleted, dose-rate dependence cannot be considered a serious source of error. In aerated solutions many organic impurities enhance the oxidation yield.[12] Their presence can be ascertained by the addition of sodium chloride to the dosimeter solution.[12] This technique was recently applied by Hart[13] in a redetermination of the absolute yield with tritium-beta particles. He found that addition of sodium chloride decreased the yield from 15.5 to 12.8. Hochanadel and Ghormley[6] reported that with polystyrene irradiation cells the oxidation yield depended on the time the solution was in contact with the cell. They suggest that the higher yields obtained with polystyrene cells at low dose rates may result from dissolved organic matter. Miller[14] has recently found that on prolonged irradiation (>24 hours) in the presence of Lucite the oxidation yield increased about 5 percent; this increase was eliminated by addition of sodium chloride. In agreement with his previous observations,[2] and contrary to Hochanadel and Ghormley, Miller found that polystyrene had no effect on the oxidation yield. Perhaps the disagreement is to be attributed to differences in the polystyrene samples used. Large errors, which are difficult to detect, may occur in the absolute determination of the absorbed energy. The techniques usually employed for evaluation of the energy absorbed

* Contribution from the Radiation Project of the University of Notre Dame, supported in part under U. S. Atomic Energy Commission contract AT(11-1)-38 and U. S. Navy equipment loan contract Nonr-06900.

† Abstract from a thesis submitted by R. M. Lazo in partial fulfillment of the requirements for the degree of Doctor of Philosophy at the University of Notre Dame.

[1] Hereafter referred to as the "Fricke dosimeter," this system was first investigated by H. Fricke and S. Morse, Am. J. Roentgenol. Radium Therapy **18**, 430 (1927); Phil. Mag. **7**, 129 (1929).

[2] N. Miller and J. Wilkinson, Discussions Faraday Soc. **12**, 50 (1952).

[3] The 100-ev yield, $G=G(Fe^{++}\rightarrow Fe^{+++})$, is defined as number of Fe^{2+} ions oxidized, or Fe^{3+} ions produced, per 100 ev absorbed in the solution.

[4] N. Miller, J. Chem. Phys. **18**, 79 (1950).

[5] T. J. Hardwick, Can. J. Chem. **30**, 17, 39 (1952).

[6] C. J. Hochanadel and J. A. Ghormley, J. Chem. Phys. **21**, 880 (1953).

[7] Cormack, Hummel, Johns, and Spinks, J. Chem. Phys. **22**, 6 (1954). The values in Table I given by them have been brought into question by Dr. N. Miller who has recalculated their $Co^{60}\gamma$ values and obtained $G\sim17.3$ or 17.8 with a further small correction for absorption of $Co^{60}\gamma$ radiation in the irradiated solution (private communication February 9, 1954).

[8] Davison, Goldblith, Proctor, Karel, Kan, and Bates, Nucleonics **11**, No. 7, 22 (1953).

[9] C. B. Amphlett, Discussions Faraday Soc. **12**, 272 (1952).

[10] J. Saldick and A. O. Allen, J. Chem. Phys. **22**, 438 (1954).

[11] N. Miller, Nature **171**, 688 (1953).

[12] H. A. Dewhurst, Trans. Faraday Soc. **48**, 905 (1952).

[13] E. J. Hart (private communication).

[14] N. Miller (private communication).

are (i) ionization chamber measurement, (ii) power input (i.e. current and voltage) measurement of a low-current electron beam, and (iii) calorimetric measurement.

The absolute oxidation yields given in Table I are summarized according to the method used to evaluate the energy absorbed. The published ionization chamber G values vary over such a wide range that establishment of a most probable value on such basis is impossible. The power-input measurements tend to favor a relatively low value for the yield. The calorimetric data give values at both extremes and nothing between. Because of the convenience and extensive use of the Fricke dosimeter the importance of establishment of the absolute yield is evident. In this laboratory we have repeated and extended the calorimetric calibration of the dosimeter both for selection of a most probable G value and for comprehension of the discrepancy in the heretofore reported calorimetric measurements.

TABLE I. Calibration of Fricke dosimeter.

Authority	Radiation	G
Ionization method		
Fricke and Morse[a]	x-rays	18.0
Miller[b]	Ra γ rays	19.9
	1.2-Mev x-rays	21.1±1.3
Hardwick[c]	Co^{60} γ rays	20.4±0.3
	$P^{32}\beta^-$	21.1±0.5
	$S^{35}\beta^-$	20.2±0.9
Hochanadel and Ghormley[d]	Co^{60} γ rays	16.7
Cormack, Hummel, Johns, and Spinks[e]	24.5-Mev x-rays	15.5 or 16.4
	Co^{60} γ rays	15.8 or 16.0
Calorimetric method		
Hochanadel and Ghormley[d]	Co^{60} γ	15.6±0.3
Davison *et al.*[f]	Co^{60} γ	20.2
Hardwick[c]	$P^{32}\beta^-$	21.1±0.5

Authority	Electron energy Mev	Beam current μamp	G
Power input method			
Amphlett[g]	0.92	0.001	17
Hochanadel and Ghormley[d]	1.33	0.065–1.5	16.8
Davison *et al.*[f]	3.0	not given	~20
Saldick and Allen[h]	1–2	6×10^{-5}–0.5	15.6±0.5

[a] See reference 1.
[b] See reference 4.
[c] See reference 5.
[d] See reference 6.
[e] See reference 7.
[f] See reference 8.
[g] See reference 9.
[h] See reference 10.

2. EXPERIMENTAL

2.1 Materials

All solutions were prepared with triply distilled water, i.e., laboratory distilled water further purified by distillation from acid dichromate and then from alkaline permanganate in an all-Pyrex apparatus.

Baker's cp analyzed ferrous ammonium sulfate was used without further purification. It has been reported that recrystallization does not affect the yield.[6] Known amounts of the ferrous ammonium sulfate were dissolved in the purified water made 0.8N in sulfuric acid (Bakers cp analyzed reagent). Concentration of ferrous ion ranged from $5\times10^{-4}M$ to $10^{-3}M$. Addition of $10^{-3}M$ sodium chloride (Merck reagent) to these solutions did not change the yield.

2.2 Analytical Method

Amount of ferric ion produced was determined spectrophotometrically by its own absorption in 0.8N H_2SO_4 at 305mμ using a Beckman model DU spectrophotometer equipped with thermostated hydrogen lamp. Optical density measurements (in 1.0-cm silica cells) were made at a temperature of 22.5±0.1°C approximately one-half hour after irradiation. This method requires accurate control of the solution temperature because the measured extinction coefficient increases about 0.8 percent per degree C. Separate determination of the decadic molar extinction coefficient yielded a value of 2160±10 liters $mole^{-1}$ cm^{-1} at 22.5°C.

2.3 Apparatus

An approximately 300-curie cobalt-60 source similar to that described by Hochanadel and Ghormley[15] was used. The experimental arrangement, shown in Fig. 1, consisted of a brass source positioner (for ensurance of reproducible geometry), cavity heater, and adiabatic calorimeter. The cavity heater was made of nichrome ribbon wound on a triangular framework which almost completely filled the cavity; its function was to maintain the temperature of the calorimeter surroundings equal to that of the water in the calorimeter bulb. The adiabatic calorimeter consisted of a cylindrical brass jacket on the exterior surface of which an insulated nichrome heater was wound and on the interior of which was located a Pyrex bulb containing a water sample. The space between jacket and bulb was continuously evacuated at less than 1 mm measured pressure with a mechanical pump during all experiments.

To ensure uniform wall thickness calorimeter bulbs were made on a glass lathe. The size of each suitable bulb was modified to obtain desired glass fraction and volume. During use (in all calorimetric calibration, either electrical or irradiation) the calorimeter bulb was sealed at the neck (through which all electric connections to the water were made) with a droplet of apiezon wax. The neck is as shown in Fig. 1; the bulb was hung by the electric connections to water thermocouple and heater (weight of both 0.028 g) during all experiments.

Temperatures of water, calorimeter jacket, and cavity were measured with copper-constantan thermo-

[15] C. J. Hochanadel and J. A. Ghormley, Rev. Sci. Instr. **22**, 473 (1951).

couples with the reference junctions at 0°C. A Rubicon high-precision potentiometer (No. 40077) in conjunction with a Rubicon spotlight galvanometer of 0.0012 microampere/mm sensitivity was used for measurement of thermocouple potential differences. To facilitate the temperature balance readings of cavity, jacket, and water, the thermocouple circuit was arranged so that the voltage outputs were in opposition with a resultant zero deflection when the temperatures were equal. Heater currents were adjusted manually with fine-control circuits and all temperatures were read and maintained equal to the nearest half microvolt.

For electrical calibration a small resistance heater with copper leads was totally immersed in the water. A 6-volt heavy-duty storage battery continuously charged through a constant voltage transformer supplied current to the heater. Through suitably arranged precision resistors (calibrated against a Wheatstone bridge in turn calibrated against Bureau of Standards calibrated resistors), it was possible to obtain with a single reading on a Rubicon precision potentiometer a voltage corresponding to both current through the heater and voltage across it.[16] The heating time was recorded with an electrical timer actuated by a relay switch connected to the heating circuit.

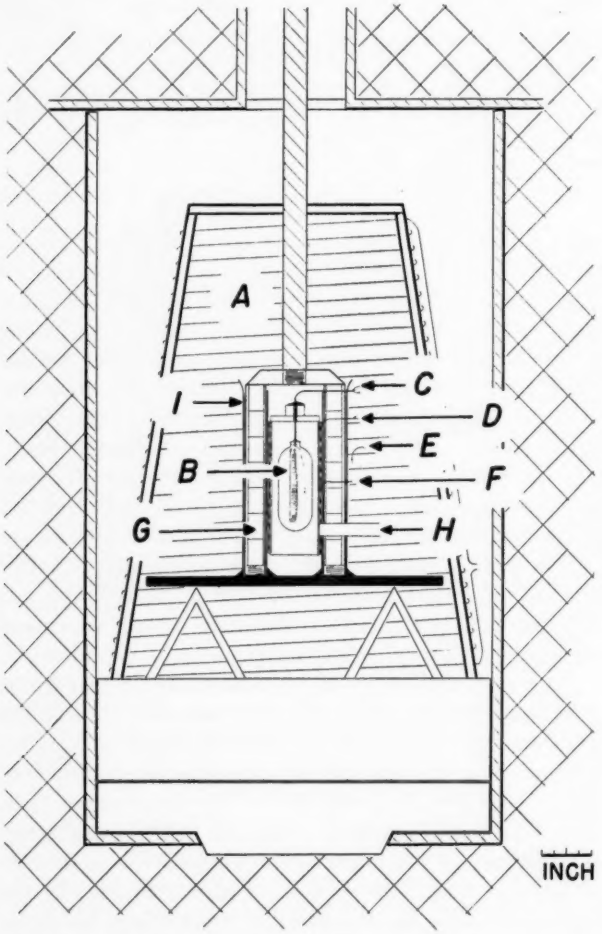

FIG. 1. Layout of calorimeter in Co^{60} source. Legend: *A*, cavity heater; *B*, calibration heating filament; *C*, water thermocouple; *D*, jacket heater; *E*, cavity thermocouple; *F*, jacket thermocouple; *G*, cobalt in wall of brass cylinder; *H*, to vacuum system; *I*, brass source positioner.

2.4 Calorimetric Method

The adiabatic calorimetric method is particularly suited to the measurement of the very small temperature rise caused by absorption of γ-ray energy. These measurements are necessarily of long duration (i.e. up to four hours) and it is essential therefore that thermometric and calorimetric errors be accurately known or entirely eliminated. Such errors were eliminated by the method of comparative measurements[17] employing electrical calibration.

The calorimeter was calibrated electrically by measurement of temperature rise as a function of time at constant rate of energy input. From the relation energy input $=EIt=E^2t/R$ joules, the energy equivalent of the calorimeter was obtained from the equation

$$\Delta Q/\Delta t=H_c(\Delta T/\Delta t) \quad (1)$$

where $\Delta Q/\Delta t$ is the rate of electrical energy input in ev/min, $\Delta T/\Delta t$ the measured rate of temperature rise in microvolts/min, and H_c the energy equivalent of the calorimeter in ev/microvolt. The rate of γ-ray energy absorption by the calorimeter, $(\Delta Q/\Delta t)_\gamma$, was then calculated from the following equation,

$$(\Delta Q/\Delta t)_\gamma=H_c(\Delta T/\Delta t)_\gamma. \quad (2)$$

To determine the amount of γ-ray energy absorbed by the ferrous sulfate solution it was necessary to correct for (i) energy absorbed by the glass and (ii) energy absorbed in 0.8*N* sulfuric acid. The correction for (i) was made empirically (see section 3.2) and for (ii) it was assumed that the energy absorbed in 0.8*N* sulfuric acid was greater than that in water by the ratio of their densities; i.e., 1.025.

All γ-ray measurements were made inside the cylindrical cobalt source (Fig. 1), introduced from the movable turret above.[15] Prior to the temperature measurements the water samples were irradiated for

TABLE II. Effect of cavity heating. Weight of water = 7.103 g; weight of glass = 1.418 g.

	Cavity heating		Without cavity heating	
Energy input joule/min	Heating rate, μvolts/min	Calibration, μvolts/joule	Heating rate, μvolts/min	Calibration, μvolts/joule
0.193	0.258	1.337	0.188	0.974
0.979	1.301	1.328	1.034	1.056
1.922	2.545	1.324	2.250	1.171
3.309	4.375	1.322	4.150	1.254
5.275	7.000	1.327	6.850	1.298
8.468	11.23	1.326	11.22	1.325

[16] W. P. White, *Modern Calorimeter* (The Chemical Catalog Company, Inc., New York, 1928), p. 134.
[17] W. Swietoslowski, *Microcalorimetry* (Reinhold Publishing Corporation, New York, 1946).

TABLE III. Correction for glass fraction.

Weight water, grams	Glass fraction	Calibration, 10^{18}ev/μvolt	γ heating, μvolt/min	γ energy 10^{17}ev/cc-min	Fe^{2+} oxidized, 10^{15} ions/cc-min	G(apparent)
10.99	0.320	10.8[a]	0.383[a]	3.76	41.8	10.8
11.02	0.220	7.40	0.467	3.14	39.8	12.4
11.25	0.156	10.5[a]	0.317[a]	2.96	40.7	13.4
10.90	0.121	7.13	0.426	2.79	39.7	13.9
11.14	0.059	9.84[a]	0.299[a]	2.64	40.3	14.9
				Graphical extrapolation		15.8

[a] In these very early experiments voltage readings were made in arbitrary units and not in true microvolts. The fact in no way affects the results because in such runs energy input calculations for electrical and radiation input experiments were based on the same arbitrary units. Variations in yield/cc-min are largely chronological in origin and reflect decay of the source.

sixteen hours. This technique ensured that steady-state concentrations of decomposition products (H_2, H_2O_2, O_2) were attained, thus eliminating any error due to heat of chemical reaction. The temperature of the water was recorded every ten minutes for a period of one to three hours. In every case the temperature-time plots were linear.

For determination of G values in a bulb after an energy-input calibration, the bulb was withdrawn from the irradiation chamber and the heater element, thermocouple and apiezon seal were removed. The bulb was carefully cleaned, filled with dosimeter liquid and returned to position in, as nearly as possible, the same geometry in which it had been calibrated. In such an experiment the bulb was mounted in an approximately half-inch diameter cork-stopper support cut and hollowed out to accommodate the bulb in almost exactly the desired position. Since it was independently established that there was no volume effect on the extrapolated true G value (Sec. 3.2), this method of supporting the sample introduced no error into the subsequent determinations. Irradiation was according to the usual procedure with this type of source.[6,15]

In this type of source an effort is made to have a nearly homogeneous gamma-radiation field in the region of exposure but it is known, from experiment, that such an objective is not achieved. To satisfy the question whether local inhomogeneities in the field might affect the G values, calorimetric calibrations were performed in various positions with the smallest volume calorimeter bulb. The G values so obtained did not vary by more than experimental error.

3. CALIBRATION OF DOSIMETER

The calibration of the Fricke dosimeter by Hochanadel and Ghormley was based on a calculated heat capacity for the calorimeter and on the assumption that the amount of energy absorbed by the glass was proportional to its weight-fraction. Neither of these assumptions is necessary for interpretation of the data herein reported.

3.1 Effect of Cavity Heating

For reconciliation of the results of Hochanadel and Ghormley and of Davison *et al.* it was necessary to study the effect of cavity heating on the calorimetric measurements. The former authors used a cavity heater to obtain adiabatic conditions whereas the latter used a heater wound directly on the calorimeter jacket.

In these experiments energy was introduced by electrical heating at known and constant rate into a calorimeter bulb of known weight containing a known weight of water. Temperature rise per unit energy input was studied as a function of rate of energy input. In every case linear temperature-time plots were obtained. The results are summarized in Table II. With cavity heating, the calibration, expressed as the ratio microvolts temperature rise per joule input, remained essentially constant whereas in the absence of cavity heating (jacket heating only) the ratio increased slowly with increased rate of energy input. It is noteworthy that at the highest rate of energy input in absence of cavity heating the ratio became equal to that with cavity heating, while at the low rate, comparable to the γ-ray heating rate, the ratio was about 35 percent lower. The conclusion was that with jacket heating only, heat leakage would be an important consideration in our experiments. The rate of temperature rise in the irradiation experiments was $\sim 0.01°$ min^{-1} while the rate in the electric-heating experiments varied in the range 0.005–0.27° min^{-1}. The temperature-time plots at steady-state conditions were always linear. Furthermore, since in the latter experiments the calibration was not affected by rate of energy input, it may be concluded that temperature gradients within the sample were insufficient to affect the fundamental assumption of a linear relationship between temperature at the water thermocouple and amount of energy input.

Because of space limitations Davison *et al.* were forced to use a jacket heater which covered the wall and bottom of the calorimeter jacket. The top of their calorimeter was not heated and the possibility of heat leakage should be considered. Such an effect may account in part for the high yield obtained by

these authors. However, the jacket heating they employed was probably more efficient than that used in our experiments because both top and bottom of our calorimeter were unheated.

In some of our early experiments we calibrated electrically at a heating rate corresponding to the gamma-ray heating rate. Under such conditions the G values established were in good agreement with those obtained using cavity heating. In the experiments used as a basis for the results here reported (i.e., in what we consider our most reliable work) we used a combination of both cavity and jacket heating.

3.2 Glass Fraction Correction

The correction for energy absorbed by the glass was made by varying the glass weight fraction at constant volume and extrapolating to zero glass weight fraction. A typical example is shown in Table III. G(apparent) was calculated from the total energy absorbed in the calorimeter and includes the density correction. Table III contains the pertinent data from which G(apparent) was calculated. These results were analyzed by the method of least squares which gave the equation,

$$G(\text{apparent}) = 15.8 \pm 0.3 - (15.5 \pm 0.3) W_g \quad (3_{11})$$

where W_g is the glass weight fraction and the subscript in (3_{11}) refers to the volume of solution in ml. Both standard deviations are estimated (see Sec. 3.3) and are greater than those calculated by superficial application of least-square theory. Equation (3_{11}) gives experimental confirmation to the assumption made by Hochanadel and Ghormley that the amount of energy absorbed in the glass is proportional to its weight fraction.

The results obtained at several volumes are presented in Fig. 2, which shows G(apparent) as a function of the glass weight fraction. The individual groups of points are expressed by Eq. (3_{11}) and the following similar equations

$$G(\text{apparent}) = 15.7 \pm 0.3 - (16.1 \pm 0.5) W_g \quad (3_4)$$

$$G(\text{apparent}) = 15.8 \pm 0.3 - (15.4 \pm 0.3) W_g \quad (3_7)$$

$$G(\text{apparent}) = 15.8 \pm 0.3 - (15.8 \pm 0.3) W_g. \quad (3_{15})$$

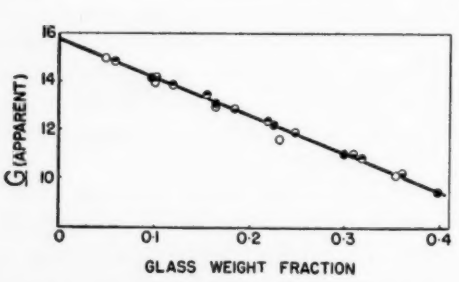

FIG. 2. G (apparent) as a function of glass weight fraction in the calorimeter for calorimeter bulbs of different volume. Legend: ○ 4 ml; ● 7 ml; ◓ 11 ml; ◒ 15 ml.

Within the precision of the work the yield is independent of the volume with an extrapolated value 15.8 ± 0.3 in agreement with the calorimetric measurements of Hochanadel and Ghormley.

3.3 Precision

An analysis was made of the precision (standard deviation) of the electrical calibration measurements, the γ-ray energy determinations and the chemical measurements. It was estimated that the precision of the resistor resistances in the electrical calibration circuit was 0.2 percent. The precision of the potentiometer used in this circuit was estimated as 0.1 percent by the manufacturer with resultant 0.2 percent precision for the electrical calibration energy input. A standard deviation of 0.4 percent for the temperature measurements was obtained from a least-squares analysis of a typical set of temperature-time results. The precision of the chemical measurements was estimated to be 1.2 percent (this value includes uncertainty in the extinction coefficient, optical density, and reproducibility of irradiation conditions).

The quantities associated with the aforementioned precisions enter into the calculation of G as either factors or divisors. Since all but one of these precisions have been estimated, it is proper to sum them (instead of taking the square root of the sum of their squares) in order to arrive at the precision of G(apparent).[18] This summation results in a precision of ± 2.0 percent.

3.4 Accuracy

The method of successive comparative measurements chosen has eliminated nearly all the systematic thermometric and calorimetric corrections. These include (i) the change in measured reading with temperature of the thermocouple, (ii) the heat developed by the electric current which passes through the wires of the thermocouple, (iii) radiative heat losses, (iv) heat exchange of the calorimeter with the evacuated air space between the calorimeter and the jacket, (v) small deviations of the temperature of the jacket when compared with that of the calorimeter, and (vi) corrections associated with measuring the temperature increase and energy equivalent of the calorimeter.

Any question about possible effect of temperature inhomogeneity in the calorimeter bulb has been answered experimentally (Sec. 3.1). If the reading of the water thermocouple is a function of its position, then the heat input into the bulb may be compounded of two sources: radiation or internal electrical heater input and external heat from the calorimeter jacket, provided that the jacket heater is at some temperature different from that of the wall of the bulb. As to the

[18] T. K. Sherwood and C. E. Reed, *Applied Mathematics in Chemical Engineering* (McGraw-Hill Book Company, Inc., New York, 1939), p. 380.

former sources of energy the internal electrical heater might be expected to raise the temperature of the thermocouple to some value higher than that of the glass wall while under certain circumstances it may be imagined (e.g. for reasons discussed in the succeeding paragraphs) that radiation will raise the temperature of the surface of the bulb to a value higher than that of the thermocouple. Effects so resultant are uncompensating and would be sensitive to the precise position of the thermocouple and the actual dimensions of the bulb. Experimentally, as related in Sec. 3.1, with the very small rate of temperature rise employed no such sensitivity was observed and it is concluded that such an effect, if existent, is negligibly small and that in these experiments the temperature throughout the bulb is essentially uniform.

The suggestion has been made that an important source of error can reside in low-energy electrons scattered from the inner brass jacket and absorbed exclusively in a very thin layer of the glass bulb. Such absorption, according to the suggestion, cannot be revealed by extrapolation to zero glass fraction because it appears as a constant added component unaffected by wall thickness in the range of glass fraction studied. The effect of such an unassignable added energy component is to raise the measured energy input by a fixed amount and thus to decrease the apparent G by a corresponding amount. A question is raised as to the amount of this effect. The following argument shows that this contribution cannot exceed 0.24 percent of the total energy input to the calorimeter.

According to the suggestion of the previous paragraph the electrons of interest are those which cannot penetrate the minimum thickness of glass bulb-wall employed in these experiments. Such bulbs were not uniform in thickness but varied in the range 0.0025–0.005 cm. We adopt the maximum value, corresponding to 12.5 mg cm^{-2} of Pyrex glass. The electrons of such maximum range have an energy $\gtrsim$0.09 Mev.[19] From data on initial distribution of Compton electrons,[20] it follows that 0.6 percent of the total energy of Compton recoils from ~1.2-Mev gammas is in that range.

We are concerned with the total number of such electrons produced in the brass per unit time in a thickness from which they can emerge and the fraction of such emergent electrons which "see" the bulb. All such electrons are absorbed in the bulb wall but the energy they expand therein is <0.09 Mev by an amount determined by the thickness of brass through which they have emerged. A complete calculation of the fraction which "see" the bulb and of their average energy is unnecessarily tedious. Instead we note that to the total energy so expended in a wall of thickness $\gtrsim$0.005 cm must be added the energy expended by similar low-energy electrons in the glass, whether they arise in the glass or in the water. The simplest assumptions are (a) that the electron flux in the region of the glass wall is isotropic and (b) that the maximum energy expended by electrons of energy $\gtrsim$0.09 Mev in the glass wall no matter where they originate is adequately given by the assumption that it is equal to the total energy of all such electrons produced in the glass with energy $\gtrsim$0.09 Mev. As a reasonable approximation the total energy expended in the glass is E_g

$$E_g = W_g E_{\text{cal}}$$

where E_{cal} is total energy expended in the calorimeter. The maximum total energy undetectable by the method of extrapolation to zero wall thickness E_g' is given by

$$E_g' \sim 0.006 W_g E_{\text{cal}}.$$

For $W_g = 0.4$ as in the bulbs of smallest glass fraction $0.006 W_g = 2.4 \times 10^{-3}$, i.e., the maximum fraction of energy produced in the glass and unrevealed by extrapolation to zero wall thickness. A reasonable conclusion is that in the experimental method herein described, energy loss unrevealed by extrapolation to zero wall thickness makes negligible contribution to any error in the method.

4. CONCLUSION

Although the calorimetric method of absolute energy determination is essentially sound and should provide a reliable technique for dosimeter calibration, precaution must be taken to avoid uncompensated heat losses.

Of the determinations of G for the Fricke dosimeter heretofore made in this way, only the Hochanadel-Ghormley Co^{60} work appears to adopt adequate precautions against such loss and is thus considered inherently more reliable. This view is strengthened by the nature of the agreement shown in Table I with the more recent results of Saldick and Allen, who used the power-input method for 1–2 Mev electrons from a Van de Graaff generator.

In the Hochanadel-Ghormley determinations assumptions were made in regard to glass fraction correction and heat capacity of the system. In the determination herein reported, these assumptions were eliminated. The values, respectively $G = 15.6 \pm 0.3$ and $G = 15.8 \pm 0.3$, are within the limits of error the same as the Saldick-Allen value 15.6 ± 0.5.

On the basis of these results it may be concluded that the low G value for the Fricke dosimeter is correct.

The authors express their appreciation to Dr. C. J. Hochanadel, Dr. J. A. Ghormley, Mr. A. Kuppermann, and Dr. R. W. Hummel for many valuable discussions.

[19] See L. E. Glendenin, Nucleonics **2**, No. 1, 16 (1948).
[20] Johns, Cormack, Denesuk, and Whitmore, Can. J. Phys. **30**, 556 (1952).

The Germanium-Oxygen System*

MICHAEL HOCH AND HERRICK L. JOHNSTON
The Cryogenic Laboratory and The Department of Chemistry, The Ohio State University, Columbus, Ohio
(Received February 8, 1954)

High-temperature x-ray diffraction patterns of germanium plus germanium oxide GeO_2 between 750° and 1400°C, showed that germanium monoxide GeO is not a stable compound. At elevated temperatures germanium can dissolve up to 60 atom percent of oxygen. The oxygen causes first a slight expansion and then a contraction of the Ge lattice. At 850° and 930°C, the x-ray pattern of a germanium-oxygen compound, consisting of equimolecular quantities of germanium and oxygen, showed only the germanium pattern. At 1000° and higher (above the melting point of pure germanium, 965°C), the germanium pattern disappears, and liquid-like structure is visible, though the sample is still solid (melting point 1430°C). When the temperature is lowered again to 930°C, the germanium pattern reappears. The electrical resistivity of the Ge and GeO_2 mixture shows a sharp break at 970°C. In the germanium-oxygen compound we thus have a disordering of the germanium lattice above the melting point of pure germanium.

INTRODUCTION

THE work of Buess and Wartenberg[1] and of Jolly and Latimer[2] showed that, when a mixture of germanium and germanium dioxide is heated in vacuum, germanium monoxide vaporizes. The solid is, as Jolly and Latimer point out, germanium plus germanium dioxide. A solid compound having the germanium-to-oxygen ratio of 1:1 can be prepared by precipitation from an aqueous solution of divalent germanium with alkali; this compound however is amorphous and thermodynamically unstable.

We proposed to investigate the possibility that GeO has a thermodynamically stable solid phase. For this purpose, we photographed x-ray diffraction patterns of a mixture of Ge and GeO_2 at various temperatures. If GeO is stable at any temperature, then the reaction $Ge(s)+GeO_2(s)\rightleftarrows 2GeO(s)$ proceeds to the right. The x-ray diffraction patterns of germanium and germanium dioxide should disappear, and a new pattern, that of GeO, should appear. This, however, was not the case.

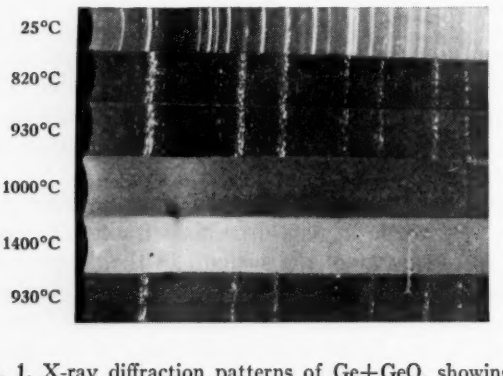

FIG. 1. X-ray diffraction patterns of Ge+GeO, showing the dissolution of O in Ge and the disordering of the Ge lattice above the melting point of pure Ge (965°C).

We found that oxygen is very soluble in germanium, and therefore determined the lattice parameter of germanium as a function of the oxygen content.

Finally, we measured the electrical resistivity as a function of temperature for pure germanium dioxide and for the germanium-germanium dioxide mixture.

EXPERIMENTAL PROCEDURE

The method of obtaining the high-temperature x-ray diffraction patterns has been described elsewhere.[3] We want to emphasize that the x-ray samples are compressed rods, 0.03 in. in diameter, 0.25 in. long, which are not contained in a holder but stand by themselves.

For the determination of the lattice constants, the mixture of germanium and germanium dioxide was heated in a helium atmosphere for two hours at 750°C, then rapidly quenched. An x-ray diffraction pattern was photographed in a Norelco 119-mm diameter camera, using Ni-filtered copper K_α radiation. The lattice constants of germanium were determined from the [4, 4, 4] and [7, 1, 1] lines by the method suggested by Cohen.[4]

For the electrical resistivity measurements, the finely pulverized materials were pressed into a quartz tube, 1.25 in. long, 0.60 in. i.d. Two platinum wires serving as leads were pushed into the ends of the material. A Pt−PtRh thermocouple was fastened onto the outside of the quartz tube. This assembly was placed

TABLE I. Lattice constants of germanium as a function of the oxygen contents.

Atomic ratio Ge:O	a_{00} in A units
1:0.000	5.6447±0.0004
1:0.2575	5.6454±0.0004
1:0.495	5.6461±0.0004
1:0.81	5.6466±0.0004
1:1.02	5.6461±0.0004
1:1.32	5.6455±0.0004

* This work was supported in part by the U. S. Office of Naval Research under contract with The Ohio State University Research Foundation.

[1] W. Buess and H. V. Wartenberg, Z. anorg. u. allgem. Chem. **266**, 281 (1951).

[2] W. L. Jolly and W. M. Latimer, J. Am. Chem. Soc. **74**, 5757 (1952).

[3] M. Hoch and H. L. Johnston, J. Am. Chem. Soc. **75**, 5224 (1953).

[4] M. U. Cohen, Rev. Sci. Instr. **6**, 68 (1935).

into a larger quartz tube, through which helium or air could be passed. The heating was done in a muffle furnace, and the heating and cooling speeds were 5° per minute between 700° and 1000°C. The resistance was measured with a Leeds and Northrup resistance box.

The germanium and germanium oxide were obtained from the Fairmount Chemical Company.

EXPERIMENTAL RESULTS

The GeO_2 was in the hexagonal form and heating it to 900°C for 24 hours, in the presence of a small amount of germanium, did not transform it into the tetragonal form. X-ray diffraction patterns obtained at 870°C, 975°C, and 1090°C showed only the GeO_2 diffraction lines.

Figure 1 shows the x-ray diffraction patterns of a 1:1 mixture of Ge and GeO_2 obtained at various temperatures. At 25°C the Ge and GeO_2 lines are both present. At 850° and 930°C only the Ge diffraction pattern is visible. In the patterns taken at 1000° and 1400°C (above the melting point of pure germanium), a liquid-like structure is visible, although the sample is solid. (A liquid sample would melt and crumble down, because the sample is self-supported.) When the temperature is lowered again to 930°C, the germanium diffraction pattern reappears. The melting point taken in the x-ray camera was found to be 1430°C. The rate of solution of GeO_2 in Ge is strongly temperature-dependent. At 750°C, 1½ hours are needed to obtain complete solution (disappearance of GeO_2 diffraction lines); at 850°C the solution is completed in 30 minutes.

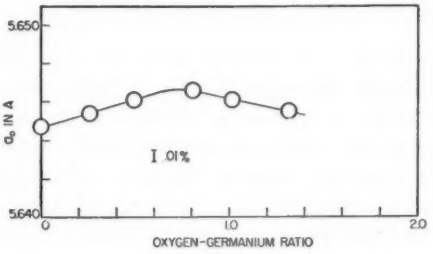

FIG. 2.

Table I contains the measured lattice constants of germanium for various oxygen contents, and the data are plotted in Fig. 2. Germanium can dissolve up to 60 atom percent oxygen interstitially.

Figure 3 shows the results of the resistivity measurements; $\log R$ is plotted against $1/T$. The data on $Ge+GeO_2$ were taken in a helium atmosphere; the data on GeO_2 were taken in air to avoid loss of oxygen from the GeO_2. One set of measurements (not shown) was taken on GeO_2 in a helium atmosphere. The curve had two breaks, similar to that of $Ge+GeO_2$. The low-temperature break, present in both GeO_2 and $Ge+GeO_2$, occurs at 920°C; the high-temperature break is present in $Ge+GeO_2$ and occurs at 970°C.

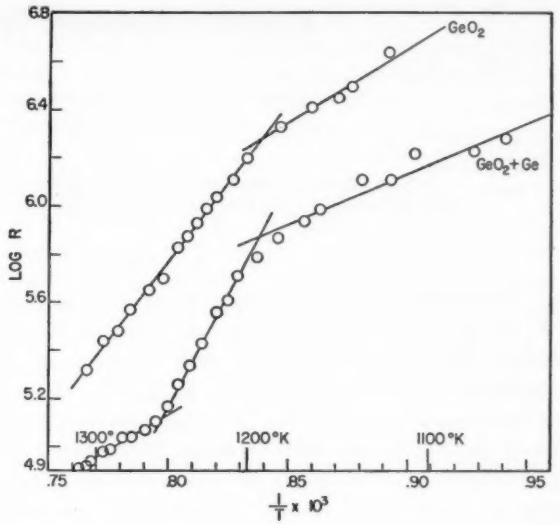

FIG. 3.

DISCUSSION OF RESULTS

The high-temperature x-ray diffraction patterns show that, in the temperature range 850°–1400°C, solid germanium monoxide is not a stable compound. From the work of Jolly and Latimer it follows that below 600° solid GeO is not stable either. The solid solution of oxygen in germanium melts at 1430°C. We can conclude from this that solid GeO has no stability range. From the disappearance of the GeO_2 x-ray diffraction pattern (when $Ge+GeO_2$ are heated together) it follows that above 750°C Ge can dissolve up to 60 atom percent of oxygen. The oxygen first causes a slight expansion of the germanium lattice, but when its concentration increases, a contraction occurs because of strong attracting forces between the germanium and oxygen.

The disappearance of the germanium lattice in x-ray diffraction patterns of a compound with a composition Ge:O=1:1, taken above 965°C (the melting point of pure Ge), indicates that a transition or disordering of the Ge lattice takes place. It may be a random change of place between the germanium and oxygen atoms in the lattice. This change of place, if rapid and frequent enough, would destroy any x-ray diffraction patterns. It is very probable that the frequency of exchange of places increases strongly at the melting point of pure germanium. The break in the resistivity curve of GeO_2+Ge, occurring at 970°C (melting point of germanium) substantiates the reasoning mentioned in the foregoing. The break in the resistivity, occurring at 920°C and present in pure GeO_2, is probably due to the oxygen and therefore would not show up in the x-ray diffraction pattern.

Hyperfine Splittings in Polyatomic Free Radicals*

S. I. WEISSMAN
Department of Chemistry and Physics, Washington University, St. Louis 5, Missouri
(Received February 9, 1954)

The hyperfine interaction in polyatomic molecules in doublet states is investigated. It is demonstrated that for molecules undergoing rapid and jittery tumbling the dipolar part of the interaction vanishes.

A NUMBER of instances of hyperfine splittings in the paramagnetic resonance absorption of dilute solutions of free radicals have been reported. In the following paragraphs, some of the features of the relation between these splittings and the electronic structures of the free radicals are presented. Ideas which have previously been applied to hyperfine interactions in atoms and ions and to nuclear magnetic resonance phenomena in liquids and solids[1] are extended to cover hyperfine interactions in polyatomic molecules.

Choose a coordinate system (x,y,z) fixed in the molecule with origin at the nucleus in question. The coordinates of the electrons are given in this system. The Hamiltonian for the interaction between the magnetic moment of one electron and the nucleus is

$$g_e g_n\left\{\frac{\mathbf{S}_e\cdot\mathbf{S}_n}{r^3}-\frac{3(\mathbf{S}_e\cdot\mathbf{r})(\mathbf{S}_n\cdot\mathbf{r})}{r^5}-\tfrac{2}{3}\delta(r)\mathbf{S}_e\cdot\mathbf{S}_n\right\},$$

g_e and g_n are the gyromagnetic ratios of electron and nucleus, respectively, $\mathbf{S}_e$ and $\mathbf{S}_n$ are their spin operators, and $\mathbf{r}$ is the vector position of the electron.

A more complete Hamiltonian would include terms representing interaction of the orbital motion of the electron with the magnetic field of the nucleus and a term representing spin-orbit interaction. However, since for the nondegenerate orbits which are encountered in polyatomic molecules, the first type of interaction leads to equal shifts in the pairs of levels between which transitions are observed and the second is frequently very small, neither will be considered here.

Expansion of the Hamiltonian in x, y, z coordinates leads to

$$g_e g_n\Big\{r^{-3}\Big[S_{ex}S_{nx}\Big(1-\frac{3x^2}{r^2}\Big)+S_{ey}S_{ny}\Big(1-\frac{3y^2}{r^2}\Big)+S_{ez}S_{nz}\Big(1-\frac{3z^2}{r^2}\Big)-3(S_{ex}S_{ny}+S_{ey}S_{nx})\frac{xy}{r^2}-3(S_{ex}S_{nz}+S_{ez}S_{nx})\frac{xz}{r^2}-3(S_{ey}S_{nz}+S_{ez}S_{ny})\frac{yz}{r^2}\Big]-\tfrac{2}{3}\delta(r)(S_{ex}S_{nx}+S_{ey}S_{ny}+S_{ez}S_{nz})\Big\}.$$

The last term, involving the delta function, leads to a splitting only when $\psi(0,0,0)^2$ (where $\psi(x,y,z)$ is the orbital part of the electronic wave function) is nonvanishing. Contributions to hyperfine splitting from this term occur in all states of a molecule in which $\psi(0,0,0)^2$ is nonvanishing. The other terms have been studied in many connections. Although the complete expression (including space and spin dependence) is totally symmetric with respect to the symmetry group of the problem, the space dependent part is not necessarily totally symmetric. Of the six space dependent terms,

$$1-\frac{3x^2}{r^2},\quad 1-\frac{3y^2}{r^2},\quad 1-\frac{3z^2}{r^2},\quad \frac{xy}{r^2},\quad \frac{xz}{r^2},\quad \text{and}\quad \frac{yz}{r^2},$$

five are linearly independent since the sum of the first three vanishes. Five independent linear combinations may be chosen to transform—in spherical symmetry—according to the five-dimensional representation D_+^2. In lower symmetries various linear combinations will transform according to the irreducible representations of the corresponding group. (The symmetry group corresponds to the site symmetry about the nucleus under consideration.)

Decision as to the possibility of contribution to the hyperfine interaction is made by the standard methods. D_+^2 is decomposed into its irreducible components in the appropriate symmetry group. If the orbital state under consideration belongs to the representation Γ_k, nonvanishing components of the interaction may occur only if $\Gamma_k\times\Gamma_k$ contains at least one of the components into which D_+^2 is decomposed.[2]

Results of calculations of the kind described above[3] are here summarized for some of the frequently encountered point groups.

In the cubic groups O_h, O, T_d, T, all components of the interaction in nondegenerate orbital states vanish. In all the degenerate orbital states nonvanishing components are permitted.

In the lower symmetries (all of those whose character tables are given in Herzberg's *Infrared and Raman*

* Assisted by the joint program of the U. S. Office of Naval Research and the U. S. Atomic Energy Commission.

[1] See for instance, A. Abragam and M. H. L. Pryce, Proc. Roy. Soc. (London) **205**, 1935 (1951); Bloembergen, Purcell, and Pound, Phys. Rev. **71**, 466 (1947); **73**, 679 (1948).

[2] In case spin-orbit interaction is large enough to produce significant admixture of more than one orbital species, similar arguments apply to the direct products $\Gamma_i\times\Gamma_j$ where i and j range over all the orbital species included in the state. ($i=j$ is included).

[3] Such calculations are formally identical with those which have done for determination of selection rules in Raman spectra and for nuclear quadrupole couplings.

Spectra) nonvanishing components of the interaction may occur in all orbital states.

FIXED MOLECULES AND TUMBLING MOLECULES

Many studies of paramagnetic resonance are made at high magnetic fields[4] with free radicals in liquid or crystalline solution. In high fields the almost correct spin functions are simple product spin functions of electron and nucleus, with very little mixing between products of the same M_z value. The Z axis is the direction of the external field. Under these conditions the only components of the Hamiltonian which need be considered are those which give diagonal elements among the set of product spin functions. The Hamiltonian is transformed to a laboratory coordinate system XYZ and only terms in $S_{ez}S_{nz}$ are retained.

These operations lead to a Hamiltonian of the form:

$$S_{ez}S_{nz}g_e g_n\left\{\frac{\cos^2\alpha}{r^3}\left(1-\frac{3x^2}{r^2}\right)+\frac{\cos^2\beta}{r^3}\left(1-\frac{3y^2}{r^2}\right)\right.$$
$$+\cos^2\gamma\left(1-\frac{3z^2}{r^2}\right)-\frac{6xy}{r^5}\cos\alpha\cos\beta-\frac{6xz}{r^5}\cos\alpha\cos\gamma$$
$$\left.-\frac{6yz}{r^5}\cos\beta\cos\gamma-\tfrac{2}{3}\delta(r)(\cos^2\alpha+\cos^2\beta+\cos^2\gamma)\right\},$$

where $\cos\alpha$, $\cos\beta$, $\cos\gamma$ are the direction cosines of the Z axis in the molecular x, y, z system.

In all cases the delta-function term is independent of $\cos\alpha$, $\cos\beta$, $\cos\gamma$. The other terms for fixed molecules lead to a contribution whose dependence on $\cos\alpha$, $\cos\beta$, $\cos\gamma$ is determined by the diagonal matrix elements of

$$\frac{1}{r^3}\left(1-\frac{3x^2}{r^2}\right),\quad \frac{1}{r^3}\left(1-\frac{3z^2}{r^2}\right)$$

etc., in the orbital electronic state in question. For rapidly tumbling molecules, the contribution of these terms is obtained by averaging $\cos^2\alpha$, $\cos^2\beta$, etc. over a spherically symmetrical set of orientations. These averages are $\langle\cos^2\alpha\rangle=\langle\cos^2\beta\rangle=\langle\cos^2\gamma\rangle=\frac{1}{3}$; $\langle\cos\alpha\ \cos\beta\rangle=\langle\cos\alpha\cos\gamma\rangle=\langle\cos\beta\cos\gamma\rangle=0$.

Averaging over all angles at this point is equivalent to the statement that the time average of the magnetic field of the nucleus at the electron determines the nature of the observed levels. It has been recognized that such averaging adequately explains the sharpness of nuclear magnetic resonance lines in liquids. This averaging in time is proper if within the precession period of nuclear spin and electronic spin about each other the angles α, β, γ, undergo many excursions through all values corresponding to an isotropic distribution. In terms of a perturbation description the situation may be stated somewhat as follows: Consider the effects of two perturbations on the paramagnetic molecule. The first perturbation is the interaction between the molecule and its surroundings, the second the dipolar part of the hyperfine interaction. Let the rotation of the molecule be described by a linear combination of stationary state rotational wave functions. These will have amplitude corresponding to the square roots of the appropriate Boltzmann factors and statistical weights. Further, the amplitudes will be time dependent with random phase factors. The interaction with the surroundings induces transitions between the various rotational states. If the matrix elements of this "rotational" interaction are large compared with the matrix elements of the dipolar part of the hyperfine interaction, its effect must first be calculated. The dipolar part of the interaction is then calculated as a perturbation of the wave functions appropriate for the rotational interaction. The relevant feature of the latter wave functions is the spherical symmetry of the averaged angular distribution. The statement that the matrix elements of the "rotational" interaction are large compared with those of the dipolar part of the hyperfine interaction is, of course, equivalent to the statement that the tumbling frequency is large compared with the hyperfine frequency.

The phenomena are well displayed by the free radical ion peroxylamine disulfonate, $ON(SO_3)_2^{=}$. The hyperfine interaction with the nitrogen nucleus exhibits a large anisotropy; the interval between adjacent lines varies from 6 to 27 oersteds as a single crystal, dilute in the paramagnetic ion, is rotated in the external field. In fluid media of low viscosity, the spectrum consists of three sharp lines, each less than 0.4 oersted wide. In highly viscous solvents, (which contribute small "rotational" matrix elements) the spectrum is very broad, being approximately the superposition of the spectra from many crystals randomly oriented.

For liquids, the Hamiltonian then becomes

$$S_{ez}S_{nz}g_e g_n\left\{\frac{1}{r^3}-\frac{x^2+y^2+z^2}{r^5}-\tfrac{2}{3}\delta(r)\right\}.$$

The quantity in the brackets is averaged over the orbital electronic function.

Since the diagonal elements of

$$\frac{1}{r^3}-\frac{x^2+y^2+z^2}{r^5}$$

vanish for all orbits, only the delta-function term contributes to the hyperfine splitting in rapidly tumbling molecules.

ACKNOWLEDGMENT

I am indebted to Professor Henry Primakoff for suggestions concerning the description of the rotational behavior of molecules in liquids.

[4] Fields in which the electron-field interaction is large compared with the electron-nucleus interaction.

Stark Effect in the Microwave Spectra of KCl and NaCl†

P. A. TATE* AND M. W. P. STRANDBERG
Research Laboratory of Electronics and Department of Physics, Massachusetts Institute of Technology, Cambridge, Massachusetts

(Received February 8, 1954)

Some further lines in the microwave spectrum of KCl have been observed at frequencies predicted by the rotational constants given by recent molecular beam work. Measurements have been made on the Stark patterns of the $J=2\rightarrow3$, $v=0$ line of $K^{39}Cl^{35}$ and the $J=1\rightarrow2$, $v=0$ line of $Na^{23}Cl^{35}$. The dipole moments of these molecules have been determined to be 10.1 ± 0.2 Debye units for KCl and 8.5 ± 0.2 Debye units for NaCl. The KCl value is in fair agreement with the results of molecular beam investigations.

INTRODUCTION

UNTIL recent years there have been few accurate values of the electric dipole moments of alkali halide molecules in the literature. More data are now available from the very precise techniques of modern molecular beam electric resonance experiments. A fairly accurate method of measuring molecular dipole moments is afforded by measuring the Stark displacements of a line in the microwave spectrum. This has been done for KCl and NaCl and will be reported in this paper.‡

EXPERIMENTAL

The measurements were made on molecules in the gas phase at around 700°C. The instrument used was a Stark-modulation microwave spectrometer of simple construction specially designed for the high temperatures needed. It will be more fully described elsewhere.

THEORY

The nuclear electric quadrupole hyperfine splitting in the molecular energy levels of most of the alkali halides with nuclear spin ≥1 is of the order of or less than, several megacycles per second. This is mainly because of the low internal electric field gradients at the nuclei. Fortunately something is known about the quadrupole coupling constants for the nuclei in KCl and NaCl from molecular beam measurements. The simultaneous Stark and quadrupole effects can therefore be calculated to give a complete picture of the line splitting. Two different methods were used to perform this calculation.

The first method is very direct. The Hamiltonian consists of three parts: a rotational part, a Stark energy part, and a quadrupole coupling part. Bardeen and Townes[1] have given the matrix elements for quadrupole interaction of a single nucleus in the $(IJFM_F)$ representation. The matrix elements of the Stark energy (i.e., of $-\mu\cdot\mathfrak{E}$ where μ is the dipole moment vector and $\mathfrak{E}$ is the electric field vector) were calculated using the methods of Condon and Shortley.[2] The matrix elements of rotational energy are well known. All three matrices making up the total Hamiltonian are diagonal in M_F. Thus the Hamiltonian for a given M_F consists of a matrix in I, J, F with elements both on and off the diagonal. Because diagonal elements with the same J but different F have very nearly the same energy ordinary second-order perturbation theory cannot be used here. However, the elements off-diagonal in J can be reduced to positions diagonal in J by use of the following formula:

$$(JF|\Delta E|JF')=-\sum_{J''F''}\frac{(JF|E|J''F'')(J''F''|E|JF')}{(J'|W|J'')-(J'|W|J)},$$

where $(JF|E|J''F'')$ is an energy matrix element off-diagonal in J; $(JF|\Delta E|JF')$ is the correction to be added to the matrix element $(JF|E|JF')$ upon removal of elements off-diagonal in J; and $(J|W|J)$, $(J''|W|J'')$ are diagonal matrix elements.

This formula may be verified by operations on rows and columns of the secular determinant, neglecting terms like

$$\frac{(JF|E|J'F')(J''F''|E|J'''F''')}{(J'''|W|J''')-(J|W|J)}$$

when they are off-diagonal in J and making other evident approximations. It reduces the matrix to a series of square blocks of elements along the diagonal with all elements in a block having the same J. The separate J blocks may now be factored out and diagonalized exactly by any convenient procedure because they are of low order, in this work not more than four.

The foregoing method is applicable to problems involving arbitrary field strengths. If the Stark field is strong enough so that the splitting due to Stark effect is large compared with the splitting due to nuclear quadrupole effect but small compared with the energy difference between adjacent rotational levels, a simpler approximate method may be used. Fano[3] has given

† This work was supported in part by the U. S. Signal Corps the Air Materiel Command, and the U. S. Office of Naval Research.

* Now at the National Research Council of Canada, Ottawa.

‡ Preliminary report of this work was given in Phys. Rev. **91**, 464A (1953).

[1] J. Bardeen and C. H. Townes, Phys. Rev. **13**, 97 (1948).

[2] E. U. Condon and G. H. Shortley *Theory of Atomic Spectra* (Cambridge University Press, Cambridge, 1951).

[3] U. Fano, R. P. 1866, J. Research Natl. Bur. Standards **40**, 215 (1948).

explicit formulas for the diagonal elements of the Hamiltonian matrix under these conditions for the case of two nuclei with a quadrupole moment as well as for the case of just one nucleus in the molecule having a quadrupole moment. The $(I_1I_2JM_JM_{I1}M_{I2})$ representation, in which the matrix is approximately diagonal, was used. The case where $M_J=\pm1$ requires special treatment because the Stark energy elements $(M_J=-1|M_J=-1)$ and $(M_J=+1|M_J=+1)$ are equal but are connected by off-diagonal $(M_J=\mp1|M_J=\pm1)$ elements of the quadrupole interaction. The off-diagonal elements of the total Hamiltonian are therefore not small compared with the difference between diagonal elements, and perturbation theory cannot be used. This case was treated by factoring out a secular determinant for $M_J=\pm1$ and solving it separately.

The selection rules are given in the ordinary way by the nonzero elements of the dipole moment matrix in the representation in which the Hamiltonian matrix is diagonal. In the spectrograph used the E vector of the rf field was in the direction of the Stark field, i.e., the

TABLE I. Microwave absorption lines in KCl.

Molecule	Transition	Observed[a]	SHT[b]	Calculated[c]
$K^{39}Cl^{35}$	$J=2\rightarrow3$, $v=0$	23 067.5±0.5	23 066±10	23 067.25
	1	22 925.4±0.5	22 918±10	22 925.78
	2	22 785.2±1.0	···	22 784.90
	3	22 644.0±2.0	22 646±10	22 644.69
	4	···	22 504±10	22 504.94
$K^{39}Cl^{37}$	$J=2\rightarrow3$, $v=0$	22 410.3±1.5	···	22 411.54
	1	22 278.0±3.0	···	22 276.05

[a] The units are Mc/sec.
[b] See reference 5.
[c] See reference 6.

Z direction. Thus we are only concerned with the component μ_Z of the dipole moment. If we exclude $M_J=\pm1$ for the moment the wave functions are those of the unperturbed problem slightly modified by the perturbations of quadrupole coupling and Stark effect. Thus the matrix elements of μ_Z are very nearly those of the unperturbed problem. In the unperturbed $(I_1I_2JM_JM_{I1}M_{I2})$ representation, μ_Z is diagonal in M_J, $M_{I1}M_{I2}$ and has $(J, J\pm1)$ elements in J. For $|M_J|\neq1$ in absorption we have $\Delta M_J=0$, $\Delta M_{I1}=0$, $\Delta M_{I2}=0$, and $\Delta J=+1$. When $M_J=\pm1$ we still have $\Delta J=+1$ but the wave functions are in general rather complete mixtures of the wave functions of the unperturbed problem. Fortunately, the Hamiltonian matrix for $M_J=\pm1$ can be split up into a product of several submatrices[3] some with only one element, and considerable simplification results. Transitions that actually occur can only do so between states that lie in the same submatrix.

Zero field levels for the case of two nuclear quadrupole moments were calculated in a $(I_1I_2JF_1F)$ representation as described by Bardeen and Townes. Intensities were taken from the tables of Robinson and Cornwell[4] for identical nuclear coupling.

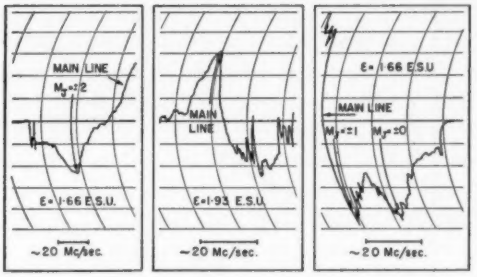

FIG. 1. Recorder traces of the Stark components of the KCl $J=2\rightarrow3$ line.

RESULTS

A. Potassium Chloride

A few lines in KCl were observed that have not previously appeared in the literature. Table I summarizes the observed lines and compares them with those observed by Stitch, Honig, and Townes[5] designated by "SHT." The values marked "Calculated" were calculated from the molecular constants reported by Fabricand, Carlson, Lee, and Rabi[6] from molecular beam methods. The constants calculated from our observations are

for $K^{39}Cl^{35}$: $B_e=3856.10\pm0.40$ Mc/sec,
$\alpha_e=23.64\pm0.10$ Mc/sec,
and for $K^{39}Cl^{37}$: $B_e=3746.07\pm0.60$ Mc/sec,
$\alpha_e=22.05\pm0.75$ Mc/sec.

These agree within the experimental error with the molecular beam values.

Measurements were made on the Stark effect of the $J=2\rightarrow3$, $v=0$ line in $K^{39}Cl^{35}$. Figure 1 shows records of the main line and its Stark components taken with an Esterline-Angus recorder. Quadrupole structure contributed to broadening the lines but was not resolved.

The theoretical splitting of the $J=2\rightarrow3$ line together with experimental points is plotted against the parameter $\mu^2\mathcal{E}^2/h^2$ in Fig. 2. For the calculated splitting eqQ was taken to be -5.656 Mc/sec for the K^{39} nucleus. This is the value found in the molecular beam work of Fabricand, Carlson, Lee, and Rabi.[6] The corresponding quantity for the Cl^{35} nucleus from the same work is less than 0.050 Mc/sec and can be neglected. The calculations were made by the first method described under "Theory." The zero field lines are indicated on the vertical axis in Fig. 2. The experimental points, represented by short vertical lines, are fitted for a value of $\mu=10.07$ Debye units.

[4] G. W. Robinson and C. D. Cornwell, J. Chem. Phys. **21**, 1436 (1953).
[5] Stitch, Honig, and Townes, Phys. Rev. **86**, 607 (1952).
[6] Lee, Fabricand, Carlson, and Rabi, Phys. Rev. **91**, 1395 (1953).

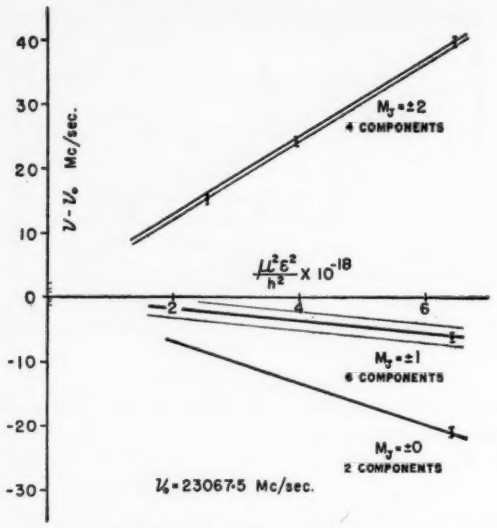

FIG. 2. Theoretical Stark-quadrupole splitting of the KCl $J=2\rightarrow3$ line with experimental points. The weak nuclear electric quadrupole interaction causes the splitting of each M_J value.

Sources of error in the value of μ lie in inaccurate frequency measurement and inaccurate measurement of the Stark field. The measurement of frequency was good to ±1 Mc/sec. A further but unknown error in position of the line maximum was caused by the presence of frequency-dependent "guide noise." This is a spurious signal or background response caused by the audio-modulated Stark field setting up mechanical vibrations in the Stark septum or wave-guide walls which modulated the transmitted power and hence could produce a response in the detection system. This condition distorted the line shape and gave the appearance of a frequency shift. The Stark voltage could be measured to about one percent. It is known that the Stark electrode was not exactly centered to the extent of several thousandths of an inch. The effect of this is second order and could hardly exceed 0.5 percent even in an extreme case. The average electrode spacing was known to better than 1 percent. The total known error in μ is estimated at two percent. The result $\mu=10.1\pm0.2$ does not agree completely with the molecular beam value of 10.48 ± 0.05 Debye units.[6] This discrepancy may possibly be ascribed to the effects of "guide noise."

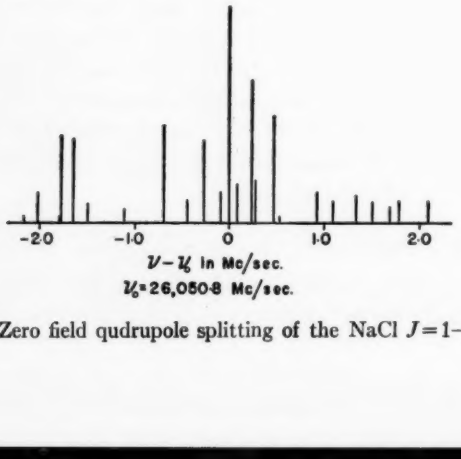

FIG. 3. Zero field qudrupole splitting of the NaCl $J=1\rightarrow2$ line.

B. Sodium Chloride

Stark effect measurements were made on the $J=1\rightarrow2$, $v=0$ line of $Na^{23}Cl^{35}$. This line has been reported at 26,051.1±0.75 Mc/sec by Stitch, Honig, and Townes.[7] Our measurements gave 26 050.8±1.0 Mc/sec, in agreement with theirs.

The simultaneous Stark and quadrupole splitting for this line was calculated by the second method described in the section on theory. The quadrupole coupling constant, eqQ, for Na was taken from Coté and Kusch to be −5.67 Mc/sec.[8] The magnitude of eqQ for Cl^{35} has been measured by Nierenberg and Ramsey[9] by the molecular beam magnetic resonance technique and found to be 5.58 Mc/sec. The sign of this quantity is not known but is most probably negative.[10] These magnitudes and signs were assumed

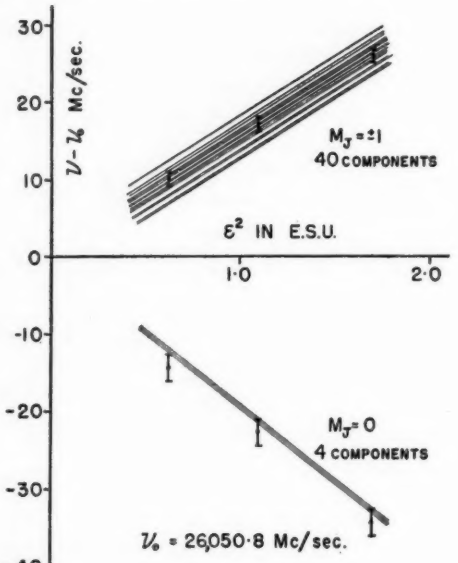

FIG. 4. Theoretical Stark-quadrupole splitting of the NaCl $J=1\rightarrow2$ line with experimental points. The weak nuclear electric quadrupole interaction causes the splitting of each M_J value.

in the calculation. Splitting at zero field was also worked out and is shown in Fig. 3.

The Stark-quadrupole splitting is plotted against the square of the Stark field in Fig. 4. Two main Stark components corresponding to $M_J=0$ and $M_J=\pm1$ are shown. The $M_J=\pm1$ component is very complicated owing to the more liberal selection rules in force here. It consists in fact of 40 lines not all of which could be plotted in the graph. The central components are intense while the outer ones are quite weak so that the line is not broadened as much as might be thought. Experimentally no quadrupole splitting could be

[7] Stitch, Honig, and Townes, Phys. Rev. **86**, 813 (1952).
[8] R. E. Coté and P. Kusch, Phys. Rev. **90**, 103 (1953).
[9] W. A. Nierenberg and N. F. Ramsey, Phys. Rev. **72**, 1075 (1947).
[10] Logan, Coté, and Kusch, Phys. Rev. **86**, 280 (1952).

resolved. Under these conditions the $M_J=0$ line appeared the more diffuse on the spectrograph perhaps because of a flatter peak and it was preferred to make measurements on the $M_J=\pm1$ line.

The short vertical lines plotted in Fig. 4 represent experimental points fitted for $\mu=8.48$ Debye units. Because of the difficulty experienced in setting the frequency standard on the $M_J=0$ component the dipole moment value is based on the $M_J=\pm1$ measurements only. The measurement error in the value of μ for NaCl is the same as for KCl, namely ±2 percent. However, there was "guide noise" present in the NaCl case also, and with due regard to the discrepancy between the measured and molecular beam value for KCl we may expect some further error from this cause. This gives 8.5 ± 0.2 Debye units for the dipole moment of $Na^{23}Cl^{35}$.

THE JOURNAL OF CHEMICAL PHYSICS VOLUME 22, NUMBER 8 AUGUST, 1954

Rotational Spectrum of PH_3†

HARALD H. NIELSEN
Department of Physics and Astronomy, The Ohio State University, Columbus, Ohio

(Received February 8, 1954)

Lines in the rotational spectrum of PH_3, indentifiable with the rotation of the molecules in the first excited states of the frequencies ν_2 and ν_4, allow an independent test to be made of the Coriolis interaction between these states as calculated from the vibrational-rotational band spectrum. It is shown that the B values observed from the rotational spectrum for these states are consistent with those obtained from the information derivable from the vibrational-rotational spectrum.

THE first excited vibrational states of the frequencies ν_2 and ν_4 in the PH_3 and AsH_3 molecules are respectively perturbed through Coriolis interaction. One of these frequencies is perpendicular while the other is parallel and the perturbation cannot, therefore, be treated in the simple manner possible when the perturbing frequencies both are perpendicular.[1] The problem has been discussed by the author[2] who has given approximate energy relations for the states ν_2 with $K=0$ and for ν_4 with $K+1=J$ and $K+1=J-1$,* respectively. These energy relations, which have been used to interpret anomalies in the vibrational-rotational bands ν_2 and ν_4 in the spectra of PH_3 and AsH_3 make possible an evaluation of the $B^{(xx)}$ values of these states.

The recent work by Stroup, Oetjen, and Bell[3] on the pure-rotational spectrum of PH_3 provides an independent test of the theory proposed by the author for the energies of these perturbed states. Their work shows that in addition to the regular rotational lines in the spectrum, certain other much weaker lines are present. These may be arranged in two series, one series which yields a B value larger, and another series which yields a B value smaller, than the B value of the molecule in its normal vibrational state. This suggests that these lines may be identified with the molecule rotating in the first excited vibrational states of ν_2 and ν_4, respectively. With this identification, we shall proceed to calculate from Nielsen's theory, and from other data on the PH_3 molecule,[4] what the B values of the molecule may be expected to be.

The permanent electric moment lies along the axis of symmetry of the molecule and the selection rules must, therefore, be $\Delta J=+1$ with $\Delta K=0$. Applying these to Eqs. (5) and (5a) in reference 2, one may derive the following relations for the frequencies of the lines in the rotational spectrum of the molecule in the first excited states of ν_2 and ν_4, respectively.

$$\nu_2=2JB_e^{(xx)}\{1-4[B_e^{(xx)}(\zeta_{2,4}^{(x)})^2/\delta]\}, \tag{1}$$

$$\nu_4=-4[(B_e^{(xx)}\zeta_{2,4}^{(x)})^2/\delta]+2JB_e^{(xx)}\{1+2[B_e^{(xx)}(\zeta_{2,4}^{(x)})^2/\delta]\}.$$

It will be seen from Eqs. (1) that in one instance the B value has decreased by an amount, say ΔB, where $\Delta B=-4B_e^{(xx)}[B_e^{(xx)}(\zeta_{2,4}^{(x)})^2/\delta]$ and in the other instance the B value has increased by an amount, say $\Delta B'$ where $\Delta B'=2B_e^{(xx)}[B_e^{(xx)}(\zeta_{2,4}^{(x)})^2/\delta]$. Taking for $B_e^{(xx)}$ the value of B in the normal vibrational state and the value of $2[(B_e^{(xx)}\zeta_{2,4}^{(x)})^2/\delta]=0.09$ as given in reference 4, one obtains the values $\Delta B=-0.18K$ and $\Delta B'=+0.09K$. The experimental values[3] for these are, respectively, $\Delta B=0.12\,K$ and $\Delta B'=-0.15\,K$. We regard the agreement between experiment and theory to be satisfactory for the following reasons: Each line, as measured, is in reality composed of $J+1$ components, a component for each value of K. For ν_2 our computations have been made only for $K=0$, but for ν_4 they have been made for the values $K+1=J$ and $K+1=J-1$. The

† This work was assisted by the U. S. Office of Naval Research under contract No. N6 onr-22526, NR 019-123 with the Ohio State University Research Foundation.

[1] H. H. Nielsen, J. Chem. Phys. **5**, 818 (1938).

[2] H. H. Nielsen, J. Chem. Phys. **21**, 142 (1953).

* The last two terms in Eqs. (5) and (5a) in reference 2 should respectively be $-2J\zeta_4Be^{(xx)}[1-2(\zeta_{2,4}^{(x)})^2(Be^{(xx)2}/\zeta_4\delta Be^{(xx)}]$ and $-2(J-1)\zeta_4Be^{(xx)}[1-4(\zeta_{2,4}^{(x)})^2(Be^{(xx)})^2/\zeta_4\delta Be^{(xx)}]$.

[3] Stroup, Oetjen, and Bell, J. Opt. Soc. Am. **43**, 1096 (1953).

[4] V. M. McConaghie and H. H. Nielsen, J. Chem. Phys. **21**, 1836 (1953).

maximum of the composite of the several components must be between $K=0$ and $K=J$ and to make a fair comparison of the ΔB's the same value of K, intermediate between $K=0$ and $K=J$, should have been chosen in both cases. The following argument may be helpful: Consider the case of ν_2 where the calculated ΔB is larger than the measured value. The perturbation which gives rise to ΔB has its largest value for $K=0$, which was used to estimate ΔB. Hence, for some value of K between $K=0$ and $K+1=J$, ΔB would have a somewhat smaller value. Likewise consider the case of ν_4, where the calculated value of $\Delta B'$ is smaller than the measured value. The perturbation which gives rise to $\Delta B'$ is a minimum for the values $K+1=J$ and $K+1=J-1$; hence, for some value of K between $K+1=J$ and $K=0$, $\Delta B'$ would have somewhat larger values. It is, therefore, probably more significant to compare the values of $\Delta B'-\Delta B$, obtained theoretically, with this difference, obtained experimentally. If this is done it will be seen that the value $\Delta B'-\Delta B=0.27$ is obtained in each case.

It may be seen further from the experimental data that the set of lines attributed to the rotation of the molecule in the excited state ν_2 is somewhat more intense than the set attributed to the molecule rotating in the state ν_4. This effect is beyond the scope of this discussion, but it is believed to be associated with the fact that the wave functions of the perturbed states ν_2 and ν_4 are hybrid functions of the wave functions of the unperturbed states ν_2 and ν_4, the coefficients depending in an involved manner on the rotational quantum numbers and upon the frequency difference δ between ν_4 and ν_2.

THE JOURNAL OF CHEMICAL PHYSICS VOLUME 22, NUMBER 8 AUGUST, 1954

Techniques in the Study of Emission Spectra of Polyatomic Molecules—The Spectra of Benzaldehyde and Acetophenone*

G. Wilse Robinson†
Department of Chemistry, University of Rochester, Rochester, New York
(Received February 9, 1954)

A rather simple method is presented for obtaining the electrodeless discharge emission spectra of polyatomic molecules. The spectra obtained for benzaldehyde and acetophenone were of very high intensity and without a trace of spectral impurities. It was possible in the case of benzaldehyde to detect over a hundred sharp bands in the region 3688–5433 A, and to observe some structure in the "broad" emission bands of acetophenone. In both these molecules there is strong evidence that the emission involves the same upper state as does the long-wave absorption. The (0,0) band of benzaldehyde is assigned at 26914 cm^{-1} and that of acetophenone at 27501 cm^{-1}. The possibility of extending the techniques to other molecules is discussed.

I. INTRODUCTION

ELECTRODELESS discharge techniques using high-frequency excitation have had their greatest success in the study of the spectra of diatomic molecules. The ability to reach rather high excitation conditions coupled with the advantages inherent in the use of a system not contaminated by metal electrodes was ideal for many problems.

Since, in a high-frequency discharge, an electron avalanche is not necessary to sustain excitation, it was thought that conditions would be milder than in the ordinary dc or low-frequency discharge, and thus would be more suitable for the study of polyatomic molecules. The method has usually failed because conditions, even in the electrodeless discharge, proved so severe that the polyatomic molecule dissociated strongly, and the spectrum obtained was much confused by the overlying spectra of fragments. In many instances, no doubt, the spectrum of the polyatomic molecule itself was so weak in comparison to that of the impurities that it was completely overlooked.

It has been found here that by carefully controlling in various special ways the conditions in an electrodeless discharge, spectra of very high intensity without any trace of impurity could be obtained for a number of aldehydes and ketones. The purpose of this paper is to describe the methods used and to discuss the spectra of two of the molecules thus far studied, especially in relation to the long-wave absorption, fluorescence, and vibrational frequencies. The possible extension of the technique to other molecules also is discussed.

II. EXPERIMENTAL

The Oscillator

A very simple two-tube 60-w variable frequency Hartley-type oscillator‡ was used to obtain the

* This work was supported in part by the Office of Ordnance Research under Contract DA-30-115-ORD-295 with the University of Rochester.

† Post-doctoral fellow, 1952–1954. Present address: Department of Chemistry, The Johns Hopkins University, Baltimore, Maryland.

‡ Circuit diagrams can be found in nearly all texts of elementary electronics.

excitation. The two 807 tetrodes were connected in a push-pull arrangement. Since the spectra are little affected by slight frequency instability or voltage irregularities, facilities for frequency or voltage stabilization were omitted. The oscillator operated in the neighborhood of 10 Mc/sec but could be varied within a rather wide range by means of a variable tuning condenser. The power output of the oscillator was adjusted by means of a variac controlling the input to the 807 screen-plate supply. A heavy copper coil was made to fit over 25-mm diameter Pyrex tubing which served as the discharge tube. Although many schemes were tried, the most effective arrangement for transferring the energy from the oscillator was obtained when this external coil was used as the tank coil.

Conditions in the Discharge

A series of papers by Schüler and his collaborators[1] has described some methods of controlling the conditions in an electric discharge, and a review of the theory of the behavior of gases in a high-frequency discharge has recently been presented by Morgan.[2] The mechanism of the discharge, as usual, is one of ionization of some molecules, excitation of the resulting electrons and ions in the electromagnetic field, and subsequent bombardment of other molecules by the excited particles. The energy conditions depend strongly on the ionization potential of the gas and the pressure at which the discharge is maintained. The lower the ionization potential, the lower can the average energy of the excited particles be in order to sustain the discharge. The higher the pressure, the larger is the fraction of excited particles which does not have the opportunity, under the influence of the electromagnetic field, to gain high kinetic energies between collisions. The chance of dissociation thus is decreased if the molecule has a relatively low ionization potential and if the discharge is maintained at the highest pressure possible.

The high-pressure limit, where fewer than necessary of the discharge-sustaining or high-energy particles are present, depends upon the power of the oscillator used, the advantage of using a higher-powered oscillator being largely one of increased intensity. If too much power is used, increasing the pressure to optimum can be brought about only by decreasing the pumping speed, and too low a pumping speed will give rise to impurities in the spectrum because of the inefficient removal of products of decomposition. Even though the oscillator was capable of 60-w output, it was never found desirable to use more than half of this. For condensable gases, a high pumping speed was maintained by means of two very large liquid nitrogen traps (500-cc bulbs) in series, the first being only partially immersed. This arrangement was used in conjunction with a high-speed mechanical pump so that noncondensable dissociation products also were rapidly removed. A diffusion pump was not found necessary. The flow rate could be controlled by means of the vapor pressure of the substance or merely by adjusting an appropriately placed stopcock or needle valve. A good pumping rate was found to be about 200 ml/hr of the liquid. The fresh gas entered the spectrograph-end of the discharge tube so that the quartz window (sealed on with wax) was kept clear of decomposition products.

The apparent limitations of the method are threefold: (1) the molecule of interest may have too high an ionization potential; (2) the vapor pressure of the substance may be too low to maintain a high pressure in the discharge; or (3) only a limited supply of the material may be available. In some cases these limitations can be simultaneously overcome by a very simple procedure—namely, maintainence of the discharge not with the molecule to be studied but with some other substance. This substance should have a reasonably low ionization potential, preferably below 10 ev, and a vapor pressure of at least 10 mm at room temperature. It also must be chemically inert towards the molecule to be studied, and spectroscopically inert in that its emission or absorption spectrum does not interfere with that of the molecule of interest. Benzene can fulfill these conditions in a great many instances. Whether the resulting low-energy electrons themselves or excited benzene molecules are the more instrumental in producing the molecular excitation has not been determined, but in either case a "low-energy bath" is produced which suppresses dissociation. Benzene is not useful below about 3200 A, the region where its own emission and absorption are moderately strong. Reagent quality benzene without further purification was found adequate for this purpose.§

The spectrograph used for this work was a Bausch and Lomb large Littrow quartz type having a reciprocal dispersion of about 25 A/mm at 5250 A and about 8 A/mm at 3700 A, the approximate region covered in the investigation. Eastman 103a-G plates were used.

III. RESULTS

Benzaldehyde

Besides the shorter wavelength absorption systems in benzaldehyde, there exists a region of sharp bands from 3160–3750 A. This absorption has been interpreted as arising from excitation of a nonbonding electron localized in the carbonyl group.[3] The system was first studied by Almasy[4] and subsequently has been inves-

[1] For a review of this work see H. Schüler and L. Reinebeck, Z. Naturforsch. **5A**, 657 (1950), and H. Schüler, Spectrochim. Acta 4, 85 (1950).

[2] G. D. Morgan, Science Progr. **41**, 22 (1953).

§ Using a slit width of 0.15 mm, a 45-mm exposure of the benzene emission alone revealed no spectra in the region above about 3200 A. Effectively this was an exposure time at least 5 times longer than any which were used in the study of benzaldehyde or acetophenone.

[3] H. L. McMurry, J. Chem. Phys. **9**, 241 (1941).

[4] F. Almasy, J. chim. Phys. **30**, 528, 634, 713 (1933).

TABLE I. Observed bands of benzaldehyde.

I[a]	λ_{air}	ν_{vac}[c]	v', v''
vw	3688.1A	27 106 cm^{-1}	188, 0
vw	3691.3	27 083	2×188, 218
vw	3694.9	27 056	3×188, 2×218
vw	3702.9	26 998	?
vw	3706.6	26 971	?
w	3710.5	26 943	?
m	3714.4	26 914	0, 0
w	3718.6	26 884	188, 218
vw	3745	26 697	0, 218
vw	3749	26 667	188, 2×218
w	3778[b]	26 462	0, 452
w	3792[b]	26 363	0, 551
w	3820[b]	26 170	0, 744
w	3859[b]	25 907	0, 1004
w	3885[b]	25 732	0, 1168
vw	3904	25 607	425, 1732
w	3922[b]	25 489	0, 1425
m	3940.4	25 370	188, 1732
m	3945.1	25 340	2×188, 1732+218
w	3950.9	25 303	3×188, 1732+(2×218)
vs	3969.8	25 182	0, 1732
s	3974.8	25 150	188, 1732+218
m	3979.2	25 123	2×188, 1732+(2×218)
m	3983.9	25 093	3×188, 1732+(3×218)
m	3988.3	25 065	4×188, 1732+(4×218)
w	3992.4	25 040	5×188, 1732+(5×218)
m	4004.5	24 965	0, 1732+218
m	4009.3	24 935	188, 1732+(2×218)
w	4014.3	24 904	2×188, 1732+(3×218)
w	4039.1	24 751	0, 1732+(2×218)
w	4043.3	24 725	188, 1732+(3×218)
w	4056.6	24 644	0, 1732+538
w	4065.3	24 591	0, 1732+591
w	4071.4	24 555	188, 1732+591+218
w	4098.6	24 392	0, 1732+790
w	4104.7	24 355	188, 1732+790+218
w	4115.2	24 293	0, 1732+889
w	4120.2	24 264	188, 1732+889+218
m	4134.8	24 178	0, 1732+1004
m	4139.2	24 152	188, 1732+1004+218
m	4163.1	24 014	0, 1732+1168
m	4168.8	23 981	188, 1732+1168+218
w	4188.9	23 866	0, 3048
w	4193.7	23 838	188, 3048+218
w	4202.0	23 791	0, 1732+1168+218
w	4207.0	23 763	188, 1732+1168+(2×218)
vw	4213.7	23 725	0, 1732+1458
vw	4220.8	23 685	188, 1732+1458+218
m	4228.2	23 644	188, 1732+1726
m	4233.7	23 613	2×188, 1732+1726+218
m	4237.6	23 591	0, 1732+1592
vs	4262.6	23 455	0, 1732+1726
vs	4597.1	21 749	0, (1706)
s	4985.0	20 054	0, (1695)
m	5433	18 401	0, (1653)

[a] Visual estimate.
[b] Broad.
[c] Error about ±5 cm^{-1} except where λ is given to only four figures in which case error is about ±10 cm^{-1}.

tigated by Garg[5] and by Imanishi and his co-workers.[6] Garg reports additional absorption between 5198–3970 A which he ascribes to benzaldehyde, but which possibly belongs to an impurity.|| The (0,0) band of the 3160–3750 A transition is tentatively assigned by these authors to 26915 cm^{-1}, but Imanishi *et al.* point out that if the electronic transition is a "forbidden" one because of approximate C_{2v} symmetry,[3] 26915 cm^{-1} may correspond to a transition involving nontotally symmetric vibrations.

The fluorescence spectrum of flowing benzaldehyde has been studied by Prileshajewa[7] who reports bands at 4580 A, 4270 A, and 3960 A. The emission spectrum in an electric discharge has been reported by Schüler and Reinebeck[8] as an impurity in the spectra of certain aromatic molecules. These authors give few details of the spectrum itself but observe emission near 3715 A which they believe to correspond to the same transition as the absorption in this region. Somewhat more recently the spectrum has been reported by Asundi and his co-workers.[9] Because of the low vapor pressure of the substance, however, high pressures evidently could not be maintained in the discharge with the result that many of their bands were broad and diffuse. With a 5-hr exposure, which implies low oscillator power and a narrow slit width, they were able in the region 3940–5443 A to observe 17 bands, only five of which were classed as *sharp*.

Because of interference by a CO band in the 3715 A region, the absence of this band in the work of Asundi *et al.*,[9] and the apparent lack of sharpness of the bands reported by all previous workers, it was felt that a reinvestigation of benzaldehyde would be worth while. In the present work, without using benzene to sustain the discharge, the author was able to improve somewhat on the results of Asundi and his co-workers[9] as long as the excitation conditions were kept very mild. Furthermore, in agreement with Schüler and Reinebeck,[8] bands were found in the 3715 A region. Because of the low intensity of the emission, however, long exposure times were required. A much better spectrum of very much higher intensity could be obtained when the discharge was sustained with benzene. The liquid benzene and a small amount of benzaldehyde were simply premixed in the sample reservoir. Using this technique it was possible to increase the intensity at least tenfold without introducing a trace of the CO spectrum or other impurities. Accordingly the slit width could be reduced, and this, in addition evidently to a decrease in rotational excitation, caused the bands to become very much sharper and more well resolved. In contrast with earlier work, more than 100 sharp bands were found in the region 3688–5433 A. Using a slit width of 0.03 mm, convenient exposure times ranged from 1 min for the stronger bands to 30 min for the weak bands around 3715 A.

A tabulation of the bands is given in Table I along with their most probable vibrational origin. The error

[5] S. N. Garg, J. Sci. Research Banares Hindu Univ. **2**, 153 (1951–52).
[6] Imanishi, Ito, Semba, and Anno, J. Chem. Phys. **20**, 532 (1952); Bull. Chem. Soc. Japan **25**, 150 (1952).
|| The author using liquid benzaldehyde was unable to find in this region any absorption which could be compared with Garg's observations.

[7] N. Prileshajewa, Acta Physicochim. U.R.S.S. **3**, 195 (1935).
[8] H. Schüler and L. Reinebeck, Z. Naturforsch. **5A**, 448 (1950).
[9] Asundi, Bhattacharya, and Appalanarasimham, Current Sci. (India) **21**, 273 (1952).

is estimated as not more than 5 cm^{-1} except in those cases where the wavelength is given to only four significant figures. Intensities are visual estimates. Because the vibrational pattern is repeated only as combinations with various quanta of the C=O stretching frequency, a complete tabulation of the observed bands is not given for $\nu < 23455$ cm^{-1}. The stronger of the bands appear identical with those observed in fluorescence and previous electrodeless discharge work. Additional emission bands of similar character extend toward the red beyond the sensitivity of the type-G plates.

Because of the lack of information from other sources concerning the various vibrations in benzaldehyde it would be meaningless to do more than merely point out possible connections between the frequencies found here and those found in infrared and Raman investigations.[10] These relationships are expressed in Table II along with an interpretation of the vibration in those cases where it seems definitely established.[11] The common occurrence of the C=O stretching frequency and its combination bands is not surprising in view of the fact that the electronic transition is quite localized in the carbonyl grouping. The frequencies which are doubly degenerate in benzene are split in benzaldehyde, modes involving large-amplitude vibrations of the relatively heavy CHO group being lowered appreciably from the parent value. Some of the lower frequencies are probably of this origin. The 218 cm^{-1} frequency is in all probability a skeletal bending mode; its corresponding value in the upper electronic state is 188 cm^{-1}, the difference being responsible for the 30-cm^{-1} frequency observed throughout the system. The nature of the 425-cm^{-1} excited state frequency is unknown. Of 744 cm^{-1} and 790 cm^{-1}, one is probably the C−C−C bending vibration originally of species b_{1u} in benzene. Frequencies of this magnitude are observed in nearly all substituted benzenes where the D_{6h} symmetry has been destroyed.

Although, according to Table I, the (0,0) band is assigned at 26914 cm^{-1}, the presence of the unexplained bands at slightly higher frequencies makes this assignment somewhat doubtful. Some of these bands also occur in absorption and may be due to a very low-frequency mode in the upper electronic state, but it seems more than coincidence that their separation is just 30 cm^{-1}, the commonly occuring difference frequency. On the other hand, if the (0,0) band were taken at a higher frequency, it would have been difficult to explain the other observed bands in the spectrum. This question might be answered by a study of the temperature dependence of the absorption bands.

What is more interesting than a knowledge of the exact position of the (0,0) band is the fact that the long-wave absorption and the emission (including fluorescence) almost certainly involve the identical upper and lower electronic states. This is borne out by the fact that four of the absorption bands in the 3715 A region[6] are duplicated within experimental error in emission. The weakness in emission of this group as compared to the longer wavelength bands is attributed to a Franck-Condon phenomenon, although the (0,0) band is reported as *very strong* in absorption.[6] Upholding the Franck-Condon explanation, however, is the notion that, as has been fairly well established for formaldehyde,[12] the C=O bond length might be substantially increased in the upper electronic state. For example, it is certainly not impossible that the 1310-cm^{-1} frequency observed in the long-wave absorption[6] of benzaldehyde is the upper state C=O stretching frequency.¶ Self-absorption as a reason for the decreased emission intensity was discounted.

Acetophenone

The fluorescence spectrum of flowing acetophenone vapor was first studied by Prileshajewa.[7] Recently, Vanselow and Duncan[13] studied the fluorescence spectrum of the vapor, the solid solution, and the microcrystalline solid, as well as the absorption spectrum of the vapor and liquid. These authors observed in the fluorescence of the vapor three very broad bands with indications of others at longer wavelengths. The apparent lack of any structure within the bands compelled them to measure the intensity maxima

TABLE II. Vibrational frequencies in the emission spectrum of benzaldehyde.

This work	Infrared[a]	Raman[a]	Assignment[b]
188 cm^{-1}	———	upper state ———	
425	———	upper state ———	
218	...	248	
452	...	441	
538	...	...	
551	...	...	
591	...	617	C−C−C bending; e_{2g}
744	745	748	
790	...	...	
889	...	...	
1004	1002	1000	C−C stretching; a_{1g}
1168	1179	1168	C−H bending; e_{2g}
1425	...	...	
1458	1451	1459	
1592	1605	1598	C−C stretching; e_{2g}
1732	1715	1701	C=O stretching
3048	3077	3068	C−H stretching

[a] Values taken from reference 4.
[b] Includes original benzene species in the case of ring vibrations.

[10] A summary of this work can be found in reference 6.
[11] See for example M. J. Murray and F. F. Cleveland, J. Chem. Phys. **9**, 129 (1941); or K. S. Pitzer and D. W. Scott, J. Am. Chem. Soc. **65**, 803 (1943).
[12] See, for example, H. Sponer and E. Teller, Revs. Modern Phys. **13**, 75 (1941).
¶ This notion is in disagreement with reference 6 where 1310 cm^{-1} is tentatively assigned as a ring vibration. An indication that 1310 cm^{-1} may be the C=O stretching vibration in the upper state is that it occurs so commonly both in progressions and combinations in the long-wave absorption (localized C=O) but evidently not at all in the shorter wavelength region (localized ring-π).
[13] R. D. Vanselow and A. B. F. Duncan, J. Am. Chem. Soc. **75**, 829 (1953).

TABLE III. Observed bands of acetophenone.

λ_{air}	ν_{vac}	v', v''
3635 A	27 501 cm^{-1}	0, 0[a]
3863	25 879	90, 1715
3877	25 786	0, 1715
3881	25 755	90, 1715+120
3893	25 679	0, 1715+120
4078	24 515	0, 1715+1271
4135	24 177	90, 1715+1712
4152.6	24 074	0, 1715+1712
4157.6	24 045	90, 1715+1712+120
4465	22 390	0, (1684)
4825	20 719	0, (1671)
5237	19 090	0, (1629)

[a] Calculated from 25786-cm^{-1} band.

which were found to lie at 23600 cm^{-1}, 21930 cm^{-1}. and 20500 cm^{-1}. In solid solution the entire spectrum was shifted by about 500 cm^{-1} to the violet and new band centers appeared at 25500 cm^{-1}, 19250 cm^{-1}, and 17600 cm^{-1}.

Previous study of the emission spectrum of acetophenone in an electric discharge[14] revealed an identical spectrum to that obtained in fluorescence, but likewise there was no possibility of determining the exact position of any of the bands because of their diffuse character.

By employing the same technique as was described for benzaldehyde it was possible not only to observe some structure in these "broad bands" of acetophenone, but also to extend the spectrum to shorter wavelengths. A tabulation of the bands and their assignment is given in Table III, but because of the diffuse background, the measurements are somewhat less reliable than those for benzaldehyde. The assignment is in disagreement with that of Vanselow and Duncan.[13] The 1400-cm^{-1} frequencies labeled v_2 and v_2' by these authors are possibly 1700-cm^{-1} frequencies, the difference being caused by the error sometimes involved in the measurement of intensity maxima.

The low frequency, about 120 cm^{-1} in the ground state and 90 cm^{-1} in the upper state, is probably analogous to the lowest frequency observed in benzaldehyde. The value for the ground state is about 40 cm^{-1} less than the lowest Raman frequency[15] but this was also true in benzaldehyde. The 1271-cm^{-1} mode is probably a CH_3 bending vibration.

The (0,0) band given in Table III was extrapolated from the 25786-cm^{-1} band assuming a C=O stretching frequency of 1715 cm^{-1}. Although the emission in this neighborhood was brought out well on long exposures, no really definite structure was found in contrast to that at longer wavelengths, and it was thought that the least error would be introduced by such an estimate. Because of the fact that emission does occur in this region and because of the analogy with the similar molecule benzaldehyde, it is very likely that the (0,0) band is near this estimated frequency. In like manner, one might also conclude that this is the origin of both the emission and long-wave absorption in acetophenone, the intensity being reduced for a reason similar to that in benzaldehyde. This reasoning lacks confirmation because of an apparent absence of sharp absorption in the 27501-cm^{-1} region, but the long-wave limit of the absorption of the liquid and the vapor does seem to lie at about 3600 A.[13] A low-pressure absorption study employing a long path length might more firmly bear out these points.

IV. CONCLUSIONS

One of the most interesting aspects of this work is the demonstration that in both molecules the long-wave absorption and emission very probably involve the same two electronic states. The relatively large absorption coefficients[3] indicate that the upper states are singlet states. The phosphorescence spectra of the two molecules lie in about the same region as the discharge emission and, at least in the case of benzaldehyde, seem to exhibit a similar vibrational pattern. This phosphorescence has been interpreted by Lewis and Kasha[16] as resulting from a triplet-singlet transition. If this is true the lowest excited singlet state and the triplet state have about the same energies. Since it would be expected that both processes could occur simultaneously it would be interesting to compare in these two molecules the "fast" and the "slow" spectra observed under identical environmental conditions.

The means of extending the techniques to other molecules should be apparent from what has been said in the foregoing. In many cases, no doubt, the methods will not work as well as they have for benzaldehyde and acetophenone. Preliminary work on some unconjugated aldehydes and ketones, however, has shown very promising results.[17] Benzene as a discharge-sustaining substance should find quite a few applications especially in the study of substances having low vapor pressures. Unfortunately the benzene spectrum will interfere in a number of interesting cases. It is not to be inferred, however, that benzene must be used in all instances. Actually, if the rules of high pressure and fast pumping speed are followed, benzene may not be necessary. It would be very convenient of course to find a substitute for benzene that can be used down to about 2000 A.

In conclusion I would like to acknowledge Professor A. B. F. Duncan for introducing me to this problem and for his help and encouragement throughout the course of the work.

[14] H. Schüler and A. Woeldike, Physik. Z. **42**, 390 (1941).
[15] Murray, Cleveland, and Saunders, J. Am. Chem. Soc. **64**, 1181 (1942).
[16] G. N. Lewis and M. Kasha, J. Am. Chem. Soc. **66**, 2100 (1944).
[17] G. W. Robinson, J. Chem. Phys. **22**, 1147 (1954).

The Photographic Latent Image. III. Dimensional Changes in Silver Bromide Following Exposure*

MAURICE L. HUGGINS
Research Laboratories, Eastman Kodak Company, Rochester, New York
(Received February 16, 1954)

Using previously tested equations and constants, calculations are made of the dimensional changes to be expected in AgBr crystals as a result of the presence of varying proportions of uncharged bromine atom and silver-ion vacancy defects. The results depend to a considerable extent on the unknown degree of ordering of these defects. With reasonable assumptions as to this degree of ordering and as to the magnitudes of the other unknown and approximately known quantities involved, the experimentally observed behavior—a lattice constant decrease, followed by a return to approximately the original value on further exposure—is quantitatively accounted for.

INTRODUCTION

BERRY[1] has recently reported decreases in the lattice dimensions of the crystal grains, essentially silver bromide, in certain photographic emulsions after irradiation with x-rays. These changes may be attributed either to the formation, in the interior of each crystal, of latent-image regions of slightly smaller dimensions than those in the remainder of the crystal, or to dimensional changes in the latter, nonlatent-image regions. The second type of explanation seems to this writer to be the more probable.

The primary process, when a light or x-ray quantum is absorbed by the crystal, is customarily assumed to be the emission of a photoelectron from one of the ions, usually a bromide ion. This electron is assumed to be trapped almost immediately at some irregularity within the crystal or on the surface; it then serves, in many cases at least, as a nucleus for the growth of a latent-image speck. The bromine atom, left uncharged as a result of its loss of the photoelectron, is not itself mobile. It can, however, readily add an electron from one of its neighbor Br^- ions, leaving the latter uncharged. By repetition of this process, the site of the uncharged atom (sometimes called "the positive hole") can move around with a considerable degree of freedom, until it becomes neutralized by a free electron, reaches the surface, or is caught in a trap in the interior of the crystal. The rapidity with which these processes occur depends, of course, on various factors, such as the crystal size, space charge effects, trap concentrations, etc.[2,3] The instantaneous concentration of positive holes under a given set of circumstances is still a matter of speculation. In spite of this, and because of this, it is of interest to compute the dependence of the lattice dimensions in the interior of the crystal on this concentration. The author realizes that the existence of appreciable concentrations of isolated positive holes for appreciable times is quite questionable, under most experimental conditions, at least. Calculation of the density changes to be expected from the presence of positive holes trapped in various ways or paired with silver-ion vacancies (giving "V-centers") would be prohibitively difficult, however. It is hoped that the results for the relatively simple case dealt with here will be useful in estimating the magnitudes of the dimensional changes in more complicated situations. For example, in the absence of a better procedure, one might reasonably assume that the removal of the net charge from a bromide ion to give a bromine atom produces the same effect on the crystal dimensions if the ion is in a region of irregularity (a trap) in the interior of the crystal as if it is in a regular portion of the structure, as assumed in the present work.

The usual theories of latent-image formation also involve the transfer of silver ions from the body of the crystal to latent-image sites. The process might be by a Grotthus chain mechanism or by motion of interstitial ions, assumed always to be present to a slight extent. In either case, the net result is the production of vacancies in the crystal structure where in the perfect crystal there would be Ag^+ ions. Such vacancies would also affect the lattice dimensions, and it would be of interest to compute the magnitude of the effect.

The production of either of these two types of defect without the other, or in unequal amounts, would result in an over-all "space charge"; this would also affect the lattice dimensions. The space charge would be modified by the presence of latent-image sites having net charges and by charges at the surface of the crystal. It should be useful, nevertheless, to deduce the magnitude of the dimensional changes to be expected as a function of the relative number of unbalanced charges, assuming a uniform distribution and neglecting latent-image and surface charges.

Another pertinent calculation which can be made is that of the change in dimensions resulting from the presence in equal amounts of the two types of defect mentioned, assuming them to be distributed in the body of the crystal in the manner which would result in greatest stability.

* Communication No. 1644 from the Kodak Research Laboratories.

[1] C. R. Berry, Royal Photographic Society Centenary Conference, London, September, 1953.

[2] L. P. Smith, in *Semiconducting Materials*, edited by H. K. Henisch (Butterworths Scientific Publications Ltd., London, 1951), p. 114.

[3] F. Seitz, Revs. Modern Phys. **23**, 328 (1951).

The present paper reports the methods and results of calculations of the magnitudes of the four effects just discussed. In spite of the approximations which must necessarily be introduced, it is believed that the results obtained will contribute to more intelligent discussion of latent-image processes.

GENERAL PROCEDURE

The present work is based on the lattice energy treatment of Born and Mayer[4] and its extension to interatomic distance calculations by Huggins and Mayer.[5,6] Various constants used in previous computations involving silver halide crystals by Mayer[7] and by Huggins[8,9] are utilized.

The rate of change of the equilibrium value of the shortest interatomic distance (r) with a certain energy function ψ is first computed. The change in the magnitude of this function with the relative number (x_1) of uncharged bromine ions (positive holes) is then calculated. The product of these two differentials then gives the desired rate of change of equilibrium interatomic distance with the number of defects of this sort,

$$\frac{dr_0}{dx_1}=\frac{dr_0}{d\psi}\frac{d\psi}{dx_1}. \tag{1}$$

A similar procedure is followed with regard to the defects of the other kind under consideration—vacancies caused by removal of Ag^+ ions—and likewise with regard to the effect of uncompensated charges in the body of the crystal and the effect of equal numbers of charges of the two types.

It is convenient to define the function ψ by means of the equation

$$\psi\equiv r\frac{dE}{dr}-\frac{3vT\alpha_T}{\beta}. \tag{2}$$

Here, E is the potential energy of the crystal per pair of Ag^+ and Br^- ions; v is the volume per pair of ions, equal to $2r^3$; T is the absolute temperature; α_T and β are the coefficients of expansion and compressibility, respectively. At equilibrium,

$$r=r_0 \tag{3}$$

and

$$\psi=0. \tag{4}$$

THE PERFECT CRYSTAL

As in the previous work in this field, referred to above, the potential energy at the absolute zero can be taken as the sum of three separate parts: the Coulomb energy (E_C), the van der Waals attraction energy (E_W), and the overlap repulsion energy (E_R).

$$E=E_C+E_W+E_R. \tag{5}$$

These can be expressed as functions of the distance (r) between closest atoms by the following equations:

$$E_C=\sum_{ij}\frac{\epsilon_i\epsilon_j e^2}{r_{ij}}=-\frac{\alpha_M e^2}{r}. \tag{6}$$

$$E_W=-\sum_{ij}\frac{c_{ij}}{r_{ij}^6}-\sum_{ij}\frac{d_{ij}}{r_{ij}^8}=-\frac{C}{r^6}-\frac{D}{r^8}. \tag{7}$$

$$\begin{aligned}10^{12}E_R&=\sum_{ij}k_{ij}\exp[a(r_i+r_j-r_{ij})]\\&=6k_{\mathrm{AgBr}}\exp[a(r_{\mathrm{Ag}}+r_{\mathrm{Br}}-r)]\\&\quad+6k_{\mathrm{BrBr}}\exp[a(2r_{\mathrm{Br}}-\sqrt{2}r)]\\&\quad+6k_{\mathrm{AgAg}}\exp[a(2r_{\mathrm{Ag}}-\sqrt{2}r)].\end{aligned} \tag{8}$$

The summations are over all the interatomic distances (r_{ij}) between ions. As indicated, however, only the closest pairs of unlike ions and the closest pairs of like ions contribute significantly to the summation of Eq. (8). The constants concerned are collected in Table I.

Substitution into Eqs. (6) to (8), into (5), and finally into (2) gives ψ as a function of r. Then

$$\frac{dr_0}{d\psi}=-1\Big/\left(\frac{d\psi}{dr}\right)_{r=r_0} \tag{9}$$

$$=-164. \tag{10}$$

POSITIVE-HOLE DEFECTS

If there were no shifts of the relative positions of neighboring ions as a result of the removal of an electron from a bromide ion, the energy change associated with that process and, from that, the change in equilibrium distance could be readily evaluated. The neighboring ions would in fact move, however, changing considerably the magnitude of the lattice energy and equilibrium interatomic distance changes.

A complete calculation of the ionic displacements around each uncharged bromine atom would be very difficult. As an approximation, believed to be sufficiently accurate for the purpose, it will be assumed that no ions shift, except the six Ag^+ ions closest to the uncharged atom.[16] The magnitude of this displacement (s) will now be computed.

We consider a single one of these Ag^+ ions and express the energy of its interaction with other ions and with

[4] M. Born and J. E. Mayer, Z. Physik **75**, 1 (1932).
[5] M. L. Huggins and J. E. Mayer, J. Chem. Phys. **1**, 643 (1933).
[6] M. L. Huggins, J. Chem. Phys. **5**, 143 (1937); J. Chem. Phys. **15**, 212 (1947).
[7] J. E. Mayer, J. Chem. Phys. **1**, 327 (1933).
[8] M. L. Huggins, J. Chem. Phys. **11**, 412 (1943).
[9] M. L. Huggins, "Transitions in Silver Halides," in *Phase Transformations in Solids*, edited by Smoluchowski, Mayer, and Weyl (John Wiley and Sons, Inc., New York, 1951).

[16] In justification of this approximation, calculation of the equilibrium positions of the six closest Br^- ions, on the assumption that the closest Ag^+ ions are shifted in accordance with Eq. (17), places them only 0.01A away (toward the uncharged Br) from their normal positions.

the adjacent uncharged Br atom as a sum of Coulomb, van der Waals, overlap repulsion, and polarization energy (E_P') terms. We then differentiate with respect to s and find the value of s which makes the differential equal to zero. This is the equilibrium value, s_0.

$$E'=E_C'+E_W'+E_R'+E_P' \tag{11}$$

$$\left(\frac{dE'}{ds}\right)_{s=s_0}=0. \tag{12}$$

The Coulomb energy, van der Waals attraction energy, and overlap repulsion energy required here are sums of the interaction energies of these types for interaction between the specified silver ion and the other ions in the crystal:

$$E_C'=e^2\sum_j \frac{E_j}{r_{\mathrm{Ag},j}}. \tag{13}$$

$$E_W'=-\sum_j\left(\frac{c_{\mathrm{Ag},j}}{r_{\mathrm{Ag},j}^6}+\frac{d_{\mathrm{Ag},j}}{r_{\mathrm{Ag},j}^8}\right). \tag{14}$$

$$E_R'=\sum_j k_{\mathrm{Ag},j}\exp[a(r_{\mathrm{Ag}}+r_j-r_{\mathrm{Ag},j})]. \tag{15}$$

The summations need to be carried only to the value of r, beyond which the differential with respect to s is negligible. For these three summations 279, 18, and 18 terms, respectively, are found to be sufficient.

The specified shifting silver ion is in an unsymmetrical Coulomb field of force, both because of the removal of the charge on one of its neighboring bromide ions and because of its displacement from its normal symmetrical location. The polarization energy is related to the magnitude of the force field F and to the polarizability α_{Ag^+} by the equation

$$E_P'=-\frac{\alpha_{\mathrm{Ag}^+}}{2}F^2; \tag{16}$$

F is the vector sum of the Coulomb forces between the specified silver atom and the surrounding ions. For present purposes, 549 terms suffice.

Differentiating the above energy contributions with respect to s, summing for trial values of s, and plotting the sum against s, lead to the result [by Eq. (12)]:

$$s_0=0.23\cdot10^{-8}\text{ cm}. \tag{17}$$

For this value of s, the computed values of the Coulomb, van der Waals, overlap repulsion, and polarization energy contributions (each times 10^4) to dE'/ds are, respectively: -1.98, -0.53, 2.30, and 0.205.

The energy of the crystal per pair of Ag^+ and Br^- ions is equal to its value (E_0) for a perfect crystal, plus the change in energy resulting from the removal of the charge from a fraction (x_1) of the bromide ions, with the resulting displacements of the ions surrounding them. We may write

$$E=E_0+\Delta E_C+\Delta E_W+\Delta E_R+E_P. \tag{18}$$

Assuming all defects to be sufficiently removed from each other that their mutual interactions can be neglected, each of the energy-change terms is proportional to x_1. Hence,

$$E=E_0+x_1\left(\frac{\Delta E_C}{x_1}+\frac{\Delta E_W}{x_1}+\frac{\Delta E_R}{x_1}+\frac{E_P}{x_1}\right), \tag{19}$$

and, from Eqs. (1) and (2),

$$\frac{d\psi}{dx_1}=r\frac{d}{dr}\left(\frac{\Delta E_C}{x_1}+\frac{\Delta E_W}{x_1}+\frac{\Delta E_R}{x_1}+\frac{E_P}{x_1}\right). \tag{20}$$

The Coulomb energy change per defect is the sum of a term for removal of the charge at the center of the defect and terms for changes in Coulomb interaction energy due to the shifts of the six close Ag^+ ions:

$$\frac{\Delta E_C}{x_1}=\frac{\alpha_M e^2}{2r}+e^2\sum_j \epsilon_j\left(\frac{1}{r_{\mathrm{Ag},j}}-\frac{1}{r_{\mathrm{Ag},j}^0}\right). \tag{21}$$

Here, $r_{\mathrm{Ag},j}$ is the distance from one of the shifted silver ions to another ion (j) and $r_{\mathrm{Ag},j}^0$ is the corresponding distance, if no shift occurred. The summation should include terms for the mutual interactions between the six displaced silver ions and all non-negligible terms for interaction between these and other ions. In the present calculations, 591 terms were included.

For the van der Waals attraction energy per defect, we can write, similarly,

$$\frac{\Delta E_W}{x_1}=-\sum_j\left\{c_{\mathrm{Ag},j}\left[\frac{1}{r_{\mathrm{Ag},j}^6}-\frac{1}{(r_{\mathrm{Ag},j}^0)^6}\right]+d_{\mathrm{Ag},j}\left[\frac{1}{r_{\mathrm{Ag},j}^8}-\frac{1}{(r_{\mathrm{Ag},j}^0)^8}\right]\right\}. \tag{22}$$

TABLE I. Constants.

		Ref			Ref
r_0	$2.887\cdot10^{-8}$ cm	a	C	$967\cdot10^{-60}$ erg cm^6	b
α_T	$1.04\cdot10^{-6}$	b	D	$1410\cdot10^{-76}$ erg cm^8	b
β	$2.75\cdot10^{-12}$ cm^2/dyne	b	k_{AgBr}	0.9305	e
ϵ_{Ag^+}	+1		k_{BrBr}	0.750	e
ϵ_{Br^-}	−1		k_{AgAg}	1.111	e
e	$4.8024\cdot10^{-10}$ esu	c	a	$4.00\cdot10^8$ cm^{-1}	f
α_M	1.7476	d	r_{Ag}	$1.00\cdot10^{-8}$ cm	f
c_{AgBr}	$109\cdot10^{-60}$ erg cm^6	b	r_{Br}	$1.62\cdot10^{-8}$ cm	f
c_{BrBr}	$208\cdot10^{-60}$ erg cm^6	b	α_{Ag^+}	$1.72\cdot10^{-24}$ cm^3	b
c_{AgAg}	$67\cdot10^{-60}$ erg cm^6	b	α_{Br^-}	$4.47\cdot10^{-24}$	b
d_{AgBr}	$199\cdot10^{-76}$ erg cm^8	b	S_4'	10.198	g
d_{BrBr}	$475\cdot10^{-76}$ erg cm^8	b	S_4''	6.335	g
d_{AgAg}	$91\cdot10^{-76}$ erg cm^8	b	α_M'	1.7627	d
			κ	13.1	h

[a] C. R. Berry, Phys. Rev. 82, 422 (1951).
[b] See reference 7.
[c] F. D. Rossini *et al.*, Selected values of chemical thermodynamic properties, Circ. Nat. Bur. Standards 500, U. S. Govt. Printing Office, Washington, D. C., 1952.
[d] J. Sherman, Chem. Revs. 11, 93 (1932).
[e] L. Pauling, Z. Krist. 67, 377 (1928).
[f] See reference 9.
[g] J. E. Jones and A. E. Ingham, Proc. Roy. Soc. (London) A107, 636 (1925).
[h] K. Højendahl, Kgl. Danske Videnskab. Selskab, Math.-fys. Medd. 16, No. 2 (1938).

It is found that 72 terms, taking account of the interactions between the six shifting Ag^+ ions and their closest like and unlike neighbors, are sufficient.

Strictly, a correction should be made for differences in the van der Waals constants applicable to interactions between a bromine *ion* and other ions, and those applicable to interactions between an uncharged bromine *atom* and ions of other elements. Since a good basis for estimating this correction is lacking, it has been omitted. It is believed, however, that this omission does not introduce any serious error.

The change in overlap repulsion energy per defect is

$$\frac{\Delta E_R}{x_1}=\sum_{ij}\{k_{ij}\exp[a(r_i+r_j-r_{ij})]-k_{ij}^0\exp[a(r_i+r_j+r_{ij}^0)]\}, \quad (23)$$

where k_{ij}^0 is the same as k_{ij}, except when one of the two atoms (i,j) concerned is the uncharged bromine atom, in which case it is unity. For this summation, 108 terms, covering the interactions of the seven central atoms and their close unlike and like neighbors, are enough.

The polarization energy per defect can be expressed by the following equation:

$$\frac{E_P}{x_1}=-\sum_i\frac{\alpha_{Ag^+}}{2}\left(\frac{e}{r_{Br,i}^2}\right)^2-\sum_j\frac{\alpha_{Br^-}}{2}\left(\frac{e}{r_{Br,j}^2}\right)^2+\frac{6\alpha_{Ag^+}e^2}{2r^4}+6E_P'. \quad (24)$$

The first two terms on the right represent the energy of polarization of all of the silver ions (i) and bromide ions (j) in the structure as a result of the removal of the charge at the center of the defect (equivalent to the insertion of a charge, e, at that location). The third term subtracts the contributions of the six shifting silver ions from the first summation. The final term adds the polarization energies of these ions again, in their shifted positions (with $S=S_0$), as already computed.

This equation can be simplified to the following, in which S_4' and S_4'' have values given in Table I:

$$\frac{E_P}{x_1}=-[(S_4'-6)\alpha_{Ag^+}+S_4''\alpha_{Br^-}]\frac{e^2}{2r^4}+6E_P'. \quad (25)$$

Differentiating the above expressions for the energy changes per defect with respect to r and performing the summations yield the result [by Eq. (20)]

$$\left(\frac{d\psi}{dx_1}\right)_{r=r_0}=6.77\cdot10^{-12}. \quad (26)$$

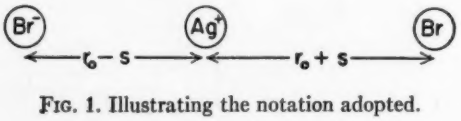

FIG. 1. Illustrating the notation adopted.

(The Coulomb, van der Waals, overlap repulsion, and polarization energy contributions to this total, in units of 10^{-12} erg, are, respectively: -1.24, $+3.34$, -19.19, and $+23.85$.) Combining this with Eq. (10), we obtain

$$\frac{dr_0}{dx_1}=-0.11\cdot10^{-8}. \quad (27)$$

The fractional change in lattice constant per defect is then

$$\frac{1}{r_0}\frac{dr_0}{dx_1}=-0.038. \quad (28)$$

SILVER-ION VACANCIES

The case of a crystal from which a few of the silver ions have been removed can be treated similarly. All other ions are assumed, as an approximation, to remain in their relative positions, except the six bromide ions immediately surrounding each vacancy. These are calculated to be shifted 0.13A away from the vacancy. At this distance, the computed Coulomb, van der Waals, overlap repulsion, and polarization energy contributions to dE'/ds are, respectively (each times 10^4): -2.27, -0.58, $+2.23$, and $+0.61$.

Proceeding as before, except for the changes obviously necessary, we obtain

$$\frac{d\psi}{dx_2}=9.86\cdot10^{-12}. \quad (29)$$

(The Coulomb, van der Waals, overlap repulsion, and polarization energy contributions, in 10^{-12} erg, are, respectively: -3.71, -15.23, $+6.33$, and $+22.47$.)

$$\frac{dr_0}{dx_2}=-0.16\cdot10^{-8} \quad (30)$$

$$\frac{1}{r_0}\frac{dr_0}{dx_2}=-0.056. \quad (31)$$

THE "SPACE CHARGE" EFFECT

The crystal dimensions would obviously be affected by the presence of uncompensated charges resulting, for example, from an excess of positive-hole defects over silver-ion vacancy defects. To estimate the magnitude of this effect, a uniform distribution of these unbalanced charges throughout the crystal at the points of a cubic close-packed (face-centered cubic) lattice may be assumed. If the crystal contains m AgBr pairs and $n=ym$ unbalanced charges, the Coulomb energy per charge, due to repulsion between these unbalanced charges, is

$$\frac{E_U}{y}=\frac{e^2}{\kappa n}\sum_{ij}\frac{1}{r_{ij}}=\frac{e^2k_n}{\kappa A}, \quad (32)$$

where r_{ij} is the distance between a pair of the charges, A is the edge of the unit cube of their assumed lattice, and κ is the dielectric constant of the crystal. A is related to r, the distance between adjacent Ag^+ and Br^- ions in the structure, by the equation

$$A=\frac{2r}{y^{\frac{1}{3}}}. \tag{33}$$

For small values of n, k_n is readily computed by direct summation. Graphically, it is found (Fig. 2) to follow quite closely the relation

$$k_n=-1.67+1.50n^{\frac{1}{3}}. \tag{34}$$

When n is not too small, the constant term can be neglected. The unbalanced charge energy per pair of ions is then

$$E_U=\frac{0.75e^2m^{\frac{1}{3}}y^2}{\kappa r}. \tag{35}$$

From this and Eqs. (1), (2), and (10),

$$\frac{d\psi}{dy}=-\frac{1.50e^2m^{\frac{1}{3}}y}{\kappa r}, \tag{36}$$

$$=-0.915\cdot10^{-12}m^{\frac{1}{3}}y \quad \text{for} \quad r=r_0 \tag{37}$$

$$\frac{dr_0}{dy}=0.0150\cdot10^{-8}m^{\frac{1}{3}}y, \tag{38}$$

$$\frac{1}{r_0}\frac{dr_0}{dy}=0.0052m^{\frac{1}{3}}y. \tag{39}$$

The volume of the crystal, V_{cr}, is related to m by the equation

$$V_{cr}=mv=m\cdot2r_0^3=48.1\cdot10^{-24}m. \tag{40}$$

Therefore,

$$\frac{dr_0}{dy}=0.00113\cdot10^8V_{cr}^{\frac{1}{3}}y \tag{41}$$

$$\frac{1}{r_0}\frac{dr_0}{dy}=3.926\cdot10^{12}V_{cr}^{\frac{1}{3}}y \tag{42}$$

if the volume of the crystal is in cm^3.

THE DEFECT INTERACTION EFFECT

Defects of the uncharged Br type are equivalent, at some distance away, to excess positive charges; defects of the Ag^+ vacancy type are likewise equivalent to excess negative charges. If both are present in equivalent amounts and are sufficiently mobile, they will tend to assume relative locations like those of the ions in an ionic crystal. Greatest stability would be obtained with the CsCl arrangement, each type of defect being surrounded symmetrically by the maximum number (8) of the other type. If such an arrangement is assumed,

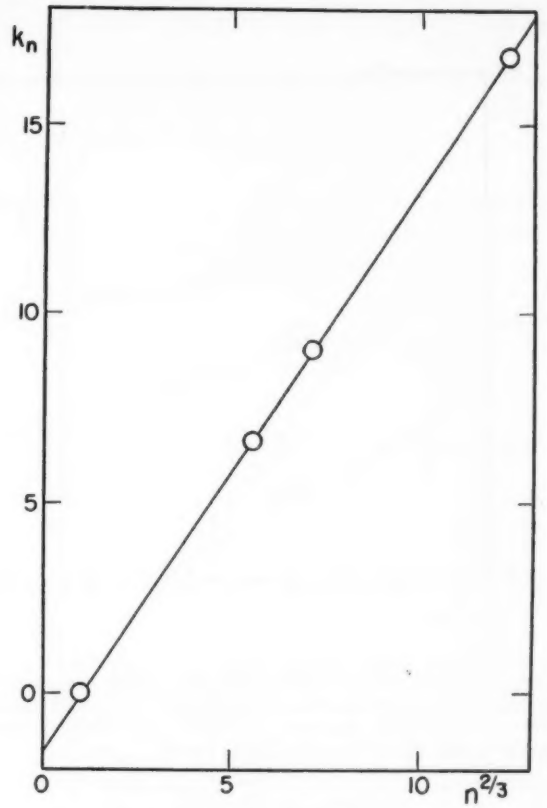

FIG. 2. Illustrating the agreement with Eq. (34).

there will be an additional contribution to the crystal energy, not already considered, and so an effect on the equilibrium interatomic distance. Calculation of the magnitude of this effect, on the assumption that this arrangement exists, is easy. The result may be considered to be an upper limit for the effect in actual crystals, in which the tendency toward the most stable distribution might be only partially satisfied.

In crystals with unequal numbers of the two types of defects being considered, each type would still tend to surround itself most closely by defects of the other type. One might approximate the situation (assuming sufficient mobility) by adding together the attraction energy just discussed, calculated for equal numbers ($z=x_2$; assuming $x_2<x_1$) of the two types, and the repulsion energy considered in the last section, computed considering only the excess of one type over the other ($y=x_1-x_2$).

Taking z defects of each kind per pair of Ag^+ and Br^- ions, in a CsCl-like arrangement, the energy of defect interaction is

$$E_{DI}=-\frac{z\alpha_M'e^2}{\kappa r_{+-}}, \tag{43}$$

where α_M' is the Madelung constant for the CsCl structure and r_{+-} is the shortest distance between unlike defects. Designating the volume per pair of defects

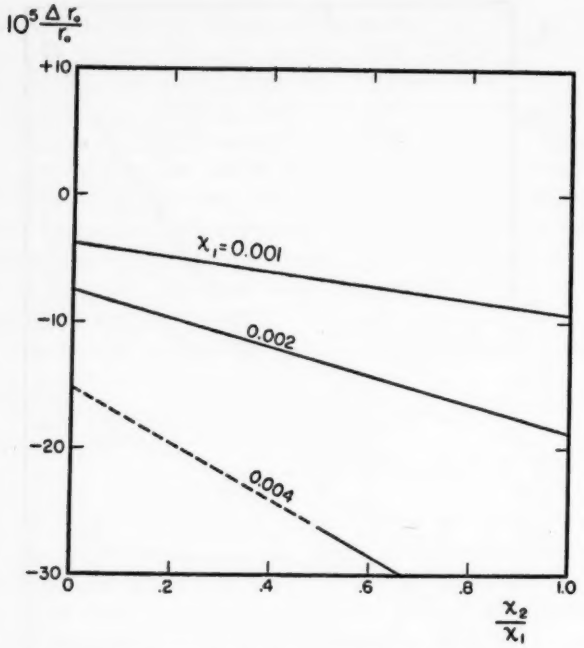

FIG. 3. Dependence of the fractional change in dimensions on the ratio (x_2/x_1) of silver-ion vacancies to uncharged bromine atoms, for a particle diameter of 5×10^{-6} cm, assuming perfect disorder in the distribution of defects ($\gamma=0$).

as v_{+-},

$$r_{+-}=\frac{3^{\frac{1}{2}}v_{+-}^{\frac{1}{2}}}{2}=\frac{3^{\frac{1}{2}}}{2}\frac{v^{\frac{1}{2}}}{z^{\frac{1}{2}}}=\frac{3^{\frac{1}{2}}}{2^{\frac{1}{2}}}\frac{r}{z^{\frac{1}{2}}}. \tag{44}$$

Hence,

$$E_{DI}=-\frac{2^{\frac{1}{2}}}{3^{\frac{1}{2}}}\frac{\alpha' e^2 z^{4/3}}{\kappa r} \tag{45}$$

$$\frac{d\psi}{dz}=\frac{2^{8/3}}{3^{3/2}}\frac{\alpha' e^2 z^{\frac{1}{2}}}{\kappa r}=\frac{3.79\cdot10^{-20}z^{\frac{1}{2}}}{r} \tag{46}$$

$$\frac{dr_0}{dz}=-\frac{0.815\cdot10^{-16}z^{\frac{1}{2}}}{\kappa r_0}=-0.0215\cdot10^{-8}z^{\frac{1}{2}} \tag{47}$$

$$\frac{1}{r_0}\frac{dr_0}{dz}=-0.00746z^{\frac{1}{2}}. \tag{48}$$

COMPARISON WITH EXPERIMENT

The foregoing results may be summarized by the following equation:

$$\frac{\Delta r_0}{r_0}=-0.038x_1-0.056x_2 +26\cdot10^{12}\gamma_1 V_{cr}^{\frac{1}{2}}(x_1-x_2)^2-0.073\gamma_2 x_2^{4/3}, \tag{49}$$

where γ_1 and γ_2 are fractions measuring the efficiency of ordering of the defects.

Berry[1] observed a fractional lattice change $(\Delta r_0/r_0)$ of $-2.6\cdot10^{-5}$ in crystals in which he estimated that the fraction of silver ions converted to silver was 0.002. The value of x_1 should be less than 0.002, since electrons reaching the surface or trapped in latent-image centers or other irregularities would produce metallic silver but would not contribute to the lattice contraction. Also, x_2 should be somewhat less than x_1, perhaps very much less. The crystal grains averaged about $5\cdot10^{-6}$ cm in diameter, or $65\cdot10^{-18}$ cm^3 in volume. Hence,

$$26\cdot10^{12}V_{cr}^{\frac{1}{2}}=422.$$

Somewhat longer exposures, giving a fraction of silver ions converted to silver of the order of 0.005, showed no significant lattice contraction. For a theory to account for the observed behavior, therefore, it must explain both the lattice contraction at low exposures and the absence of such contraction, within the limits of error of the experiments, at higher exposures.

Figures 3 to 8 show the relative lattice change to be expected, according to Eq. (49), as a function of various parameters. For simplicity, γ_1 and the much less important γ_2 have been assumed to be equal, and are designated γ.

It seems reasonable to assume that the charge density in the crystal cannot have a value greater than a certain unknown minimum (which might be a function of the time after the production of the photoelectrons), since the greater this charge density, the greater would be the rate of diffusion of the positive holes to the surface or to other traps, where they would be ineffective in modifying the internal dimensions of the crystal structure. In the figures, portions of the curves for which x_1-x_2, which is a measure of the charge density,

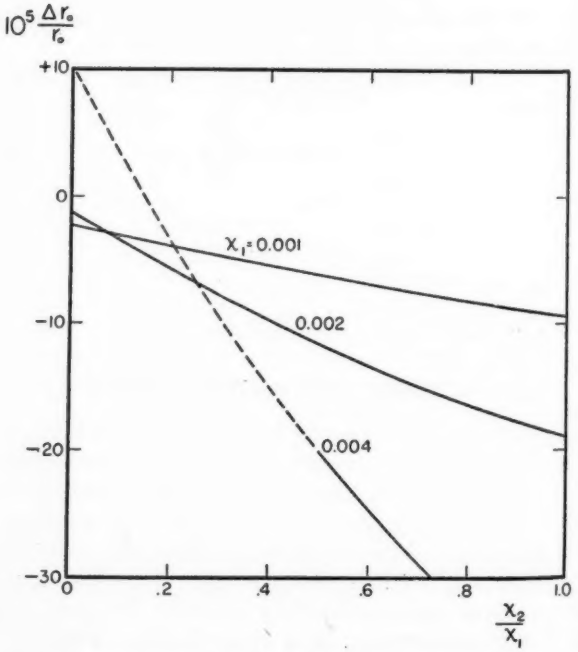

FIG. 4. Same as Fig. 3, except that the ordering efficiency coefficient (γ) is taken equal to 0.5.

exceeds the arbitrary limit 0.002, have been indicated by dashed lines.

It also seems reasonable to assume that the total number of unbalanced charges in the crystal n cannot exceed a certain limit (in a given crystal, a given time after exposure). The higher the value of n, the faster would electrons be trapped in latent-image sites and elsewhere. The limiting value would be expected to increase with the size of the crystal, but not proportionally. To indicate this limitation on n, portions of the curves in Fig. 7 which correspond to n greater than 10 000 (a purely arbitrary limit) have been dotted. The n value corresponding to a given value of D can be computed from the following equation, deducible from Eq. (40):

$$n=\frac{10^{24}|x_1-x_2|V_{cr}}{48.1}=10.886\cdot 10^{21}|x_1-x_2|D^3. \quad (50)$$

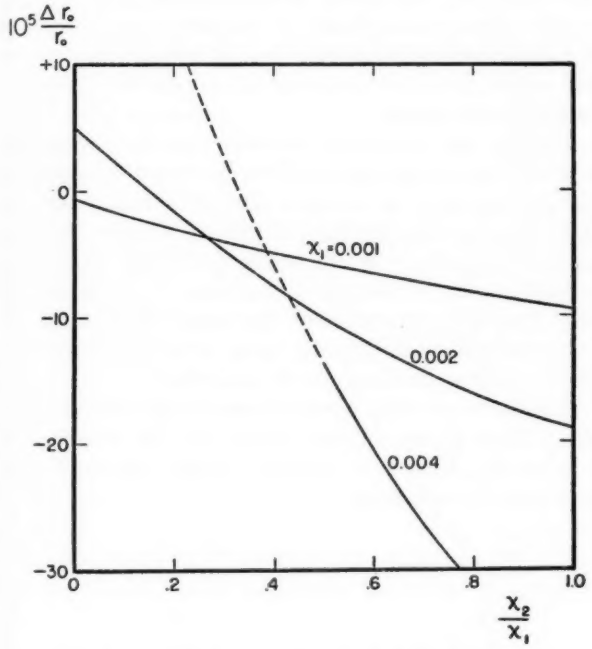

FIG. 5. Same as Figs. 3 and 4, except that the ordering efficiency coefficient (γ) is taken as 1.0.

The magnitude of γ for a given set of experimental conditions is impossible to estimate, on the basis of present knowledge. It is doubtless dependent on time, temperature, and other factors. Since the lattice dimensional changes depend markedly on this unknown factor, the graphs have been made for several γ values.

Figures 3, 4, and 5 show that the lattice dimensions decrease as the number (x_2) of silver-ion vacancies increases, for a constant number (x_1) of uncharged bromine atoms. The rate of decrease is greater the larger the value of x_1 and the larger the value of the efficiency of ordering (γ).

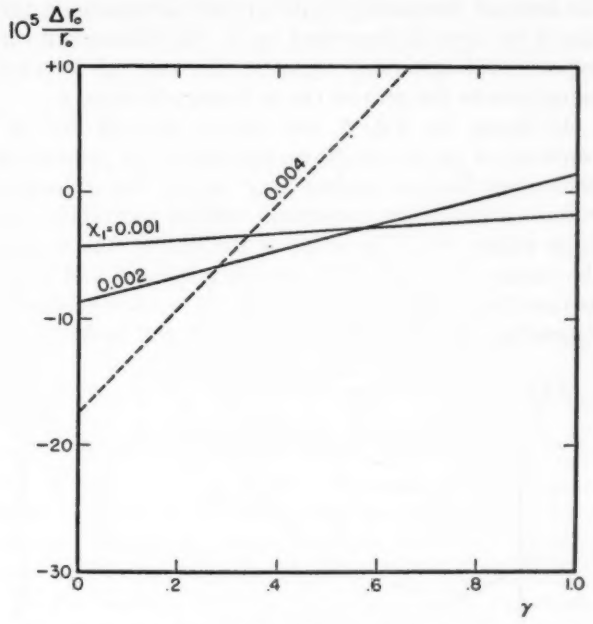

FIG. 6. Dependence of the fractional change in dimensions on the ordering efficiency coefficient, for crystals of diameter 5×10^{-6} cm, with the ratio (x_2/x_1) of silver-ion vacancies to uncharged bromine atoms equal to 0.1.

Figure 6 shows that, for a fixed ratio (x_2/x_1) of silver-ion vacancies to uncharged bromine atoms, the lattice dimensions increase with γ, the efficiency of ordering of the charges, the rate of increase being greater the greater the number of (x_1) of uncharged bromine atoms.

Figure 7 shows that, for fixed values of x_1 and x_2,

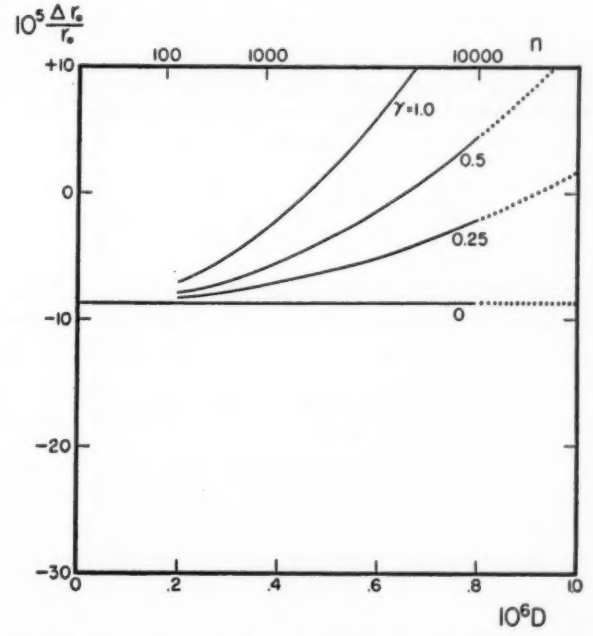

FIG. 7. Dependence of the fractional change in dimensions on the particle diameter, assuming that the fraction (x_1) of bromine atoms which are uncharged is 0.002 and the fraction (x_2) of silver-ion sites which are vacant is 0.0002.

the internal dimensions of the crystal increase with the size of the crystal (measured by D, the diameter of the hypothetical spherical crystal), the rate of increase being greater the greater the ordering efficiency γ.

As shown by Fig. 8, the curves showing the dependence of the lattice dimensions on x_1, the number of uncharged bromine atoms (and so on the exposure, at least if this is not too great), exhibit a minimum for finite values of γ. The shape of the curve, determining the values of x_1 and of Δr_0 at the minimum and at an assumed maximum charge density (x_1-x_2), is markedly dependent on the values of γ and the ratio x_2/x_1.

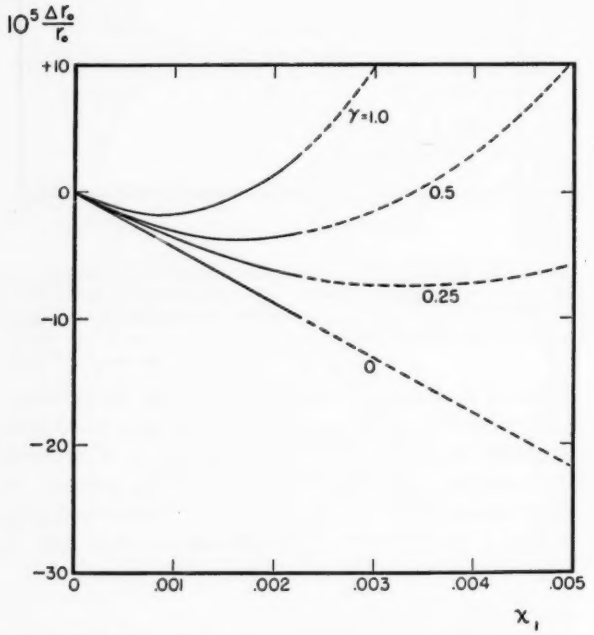

FIG. 8. Dependence of the fractional change in dimensions on the fraction (x_1) of bromine atoms which are uncharged, for a particle diameter of 5×10^{-6} cm, and a ratio, x_2/x_1 of 0.1.

Arbitrary values of these unknowns can readily be chosen which will lead to the observed experimental results. The latter, however, are insufficient to determine these quantities uniquely, without further data from other sources.

SUMMARY AND CONCLUSION

Using ideas, equations, and constants which have been previously tested, calculations have been made of the change in lattice dimensions to be expected as a function of the concentrations of lattice defects of the two kinds considered, their degree of ordering, and the size of the crystal grains. By appropriate choice of the unknown parameters, the dimensional changes observed by Berry following x-ray exposure can be quantitatively accounted for. This cannot be considered as evidence for the existence in the crystals, at the time of the measurements, of defects of the specific kinds assumed in these calculations, since (as already noted) other related but more complex types would have similar dimensional effects. It does show, however, that it is unnecessary to assume that the observed changes are related in any way to the structural dimensions in latent-image regions.

Despite the necessary indefiniteness of the conclusions which can be drawn directly from the results of the present study, it is hoped that these results will aid in evaluating the dimensional effects of the more complex irregularities undoubtedly existing in actual crystals under various circumstances. It is also hoped that they will encourage further study of dimensional changes in silver halide and other crystals as functions of the experimentally variable quantities.

The author is glad to acknowledge help received from discussions of the subject matter of this paper with Chester R. Berry and Charles Duboc of the Kodak Research Laboratories.

Approximate Method of Evaluating Lattice Sums of r^{-n} for Graphite

A. D. CROWELL
Amherst College, Amherst, Massachusetts
(Received February 15, 1954)

The graphite lattice is approximated by a set of planes in which the carbon atoms are assumed to be distributed with uniform density. It is shown that the lattice sums of r^{-n} taken over the graphite planes can then be expressed directly in terms of tabulated functions. The results of the approximation are compared with the results obtained by direct summation.

I. INTRODUCTION

THE calculation of the energy of interaction between a given atom or molecule and a crystal lattice often involves the summation of a long range central force of the form μr^{-n} over the lattice sites of the crystal. Hove and Krumhansl[1] have recently described a method for evaluating such sums for cubic crystals in which the periodic distribution of atoms in the crystal is represented by a Fourier series and the sums are obtained by an application of Fourier transforms. Young and the author[2] calculated the heat of adsorption of argon on graphite assuming that the energy of interaction between an argon atom and a carbon atom in the graphite lattice could be expressed in the form $(\nu r^{-12}-\mu r^{-6})$. Lattice sums of r^{-6} and r^{-12} were obtained by direct summation over the nearest hundred carbon atoms and by integration over the remainder of the lattice. These calculations were carried out for varying positions of the argon atom above three different sites on the basal plane of graphite. The calculations showed that the sums were nearly independent of the site over which the argon atom was located. Because of the labor involved it would seem desirable to establish a technique for calculating sums of this type without recourse to direct summation. Such a technique would not only greatly simplify the extension of these calculations to the absorption of other atoms on graphite and graphite-like substances but would also make it possible to readily investigate interactions of the form μr^{-n} for other values of n.

A method such as that of Hove and Krumhansl is somewhat complicated for graphite because of the hexagonal structure of the basal plane. The graphite lattice consists of a laminar structure of basal planes in which the carbon atoms are hexagonally arranged. The distance between nearest neighbors in the basal plane is 1.418A and the separation of the basal planes is 3.348A.[3] The relatively close spacing of the carbon atoms in the basal plane as compared to the separation of the planes suggests that a useful approximation would result from considering the carbon atoms to be uniformly distributed in the planes. The results of Crowell and Young are consistent with this suggestion. It will be shown that this approximation leads to an expression for the sum of r^{-n} over an infinite lattice in terms of tabulated functions. A comparison with the results obtained by direct summation will be made in the case of $n=6$. A similar approximation has been made by Brennan[4] in calculating the interlayer binding energy in graphite, but the relationship to tabulated functions in the general case and a detailed comparison with the results of direct summation were not presented.

II. EVALUATION OF THE SUMS

If we assume that the energy of interaction between an atom over a basal plane of graphite and a carbon atom in the graphite lattice can be represented by by μr^{-n}, then the total energy may be calculated by evaluating $\mu\sum r^{-n}$ over the lattice. It is proposed to approximate this summation by integrating over the planes and then forming the sum of the resulting terms. The graphite lattice is thus represented by a set of horizontal planes separated by a distance d. The value of r is the distance from the location of the external atom at point P to a point on one of the planes. The point P will be taken external to the lattice and its distance to the nearest plane will be denoted by z. If one lets S_m be the approximate value of the summation of r^{-n} over the mth plane from P, one finds

$$S_m=2\pi\sigma\int_0^\infty((z+md)^2+\alpha^2)^{-n/2}\alpha d\alpha,$$

where σ is the number of atoms per unit area in the basal plane. This gives the approximate expression for the lattice sum as

$$\sum r^{-n}=\sum S_m=2\pi\sigma(n-2)^{-1}d^{2-n}\sum_{m=0}^{\infty}(x+m)^{2-n},$$

where $x=z/d$. The summation of $(x+m)^{2-n}$ is the generalized Riemann zeta function of x and $n-2$. These functions have been tabulated as derivatives of $\Psi(x)=(d/dx)\ln\Gamma(x)$. In particular it can be shown that the kth derivative of $\Psi(x)$ is

$$\Psi^{(k)}(x)=(-1)^{k+1}k!\sum_{m=0}^{\infty}(x+m)^{-k-1}.$$

[1] J. Hove and J. A. Krumhansl, Phys. Rev. **92**, 569 (1953).
[2] A. D. Crowell and D. M. Young, Trans. Faraday Soc. **49**, 1080 (1953).
[3] H. Lipson and A. R. Stokes, Proc. Roy. Soc. (London) **A181**, 101 (1942).
[4] R. O. Brennan, J. Chem. Phys. **20**, 40 (1952).

TABLE I. Values of lattice sums of r^{-6} over a graphite lattice for varying positions of an external atom over the basal plane. Summations are given for several values of z the distance from the external atom to the nearest basal plane.

z (A)	Values of r^{-6} by direct summation $(A)^{-6}$ Site A	Site B	Site C	Values of r^{-6} by approximation $(A)^{-6}$ $(2\pi\sigma/24d^4)\Psi^{(3)}(x)$	$(\pi\rho/6z^3)$
2.127		0.03077	0.03125	0.0303	0.0620
2.836	0.009562	0.009798	0.009806	0.00983	0.00261
3.545	0.004097	0.004105	0.004112	0.00413	0.00134
4.254	0.001993	0.002040	0.002049	0.00209	0.000774
4.963		0.001136	0.001142	0.00118	0.000488

These relationships are given and the derivatives tabulated by Davis[5] for values of k up to 4. Thus the lattice sum may be expressed as

$$\sum r^{-n}=\frac{2\pi\sigma(-1)^n}{(n-2)d^{n-2}(n-3)!}\Psi^{(n-3)}(x).$$

As the lattice sum converges for values of $n>3$, values of the summation are readily obtained in terms of tabulated functions for values of n between 3 and 8.

III. EXAMPLES AND APPLICATIONS

As an example of the use of the above approximation the results obtained by Crowell and Young in the study of the heat of adsorption of argon on graphite will be compared with those found by the present method. Crowell and Young evaluated lattice sums of r^{-6} over three different sites on the basal plane for values of z from 2.127A to 4.963A. For $n=6$ the above approximation for the lattice sum becomes $\sum r^{-6}=(2\pi\sigma/24d^4)\Psi^{(3)}(x)$. The results obtained from this expression, where $d=3.35$A and $\sigma=0.382$ atom/A^2, are compared with those obtained by direct summation in Table I. The first column gives the value of z for which the summation is obtained. The next three columns give the results for direct summation over the nearest hundred carbon atoms and integration over the remainder of the lattice. The external atom was placed over the center of a lattice hexagon (site A), over the midpoint between two adjacent carbon atoms (site B), and over a carbon atom (site C). The fourth column shows the results of the present method, and the final column shows the values that are obtained if one makes the approximation that the carbon atoms are uniformly distributed throughout the lattice, giving the approximate result $\sum r^{-6}=\pi\rho/(6z^3)$, where ρ is the number of carbon atoms per unit volume. We see from the table that the values of the direct summations vary only slightly from site to site and differ by only a few percent from the values obtained by the approximation described in this paper. We note that the approximation of a continuous distribution of carbon atoms is by no means as satisfactory.

Not only is the approximation useful for obtaining the values of lattice sums, but it greatly facilitates the solution of problems where the form of the sum as a function of z is of interest. As an example we consider the use of the results just obtained in calculating the heat of adsorption of argon on graphite. Expressing the energy of interaction between the graphite lattice and an argon atom as $\Phi(z)=-\mu\sum r^{-6}+\nu\sum r^{-12}$, Crowell and Young[2] determined μ by the Kirkwood-Muller formula. As there is no similar expression for ν in the case of argon atoms and carbon atoms in graphite, the value of ν was arbitrarily selected by the requirement that $\Phi(z)$ be a minimum for $z=3.60$A when the argon atom is over site C. This value is half the sum of the interlaminar separation in graphite and the equilibrium separation of a pair of argon atoms. The differentiation of $\Phi(z)$ to obtain the conditions for a minimum required the use of elaborate interpolation formulas and gave a value of $\nu/\mu=2.21\times10^3$ (A)^6. By direct differentiation of the Ψ functions, keeping only the first term in the sum of r^{-12}, one obtains a ratio of $\nu/\mu=2.32\times10^3$ (A)^6. Using this result to calculate the value of $\Phi(z)_{\min}$, one obtains the results shown in Table II. The success of the approximation in this example where the results of direct summation are known gives one considerable confidence in the use of the method in similar problems.

The method may also be applied to the calculation of the energy of interaction with an infinite lattice of an atom located between the graphite planes. Such an atom is in effect acted upon by two external lattices, one at a distance z from the atom and the other at a distance $d-z$ from the atom. The previous results can at once be extended to give

$$\sum r^{-n}=\frac{2\pi\sigma(-1)^n}{(n-2)d^{n-2}(n-3)!}[\Psi^{(n-3)}(x)+\Psi^{(n-3)}(1-x)].$$

This expression may be greatly simplified in the event that n is even, since it can be shown[5] that $\Psi^{(k)}(x)+(-1)^{k+1}\Psi^{(k)}(1-x)=(-1)^k\pi(d^k/dx^k)\cot\pi x$. Thus in the important case of $n=6$, we obtain $\sum r^{-6}=(\pi^5\sigma/6d^4)\times(\csc^2\pi x)(3\csc^2\pi x-2)$. If the atom were midway between the basal planes, we would have $x=\frac{1}{2}$ and $\sum r^{-6}=(\pi^5\sigma/6d^4)$.

Since the approximation ignores the structure of the basal planes of graphite, its usefulness decreases when the atom whose interaction with the lattice is desired is close to the basal plane compared to the interatomic spacing of carbon atoms in the plane. For this reason the method is of greatest value when the

Table II. Values of the equilibrium energy of interaction $\Phi_{\min}$ of an argon atom over a basal plane of graphite as obtained by direct summation and by the present approximation.

Description	$-\Phi_{\min}$ (erg/atom) $\times10^{12}$
Direct sum for site A	0.1253
Direct sum for site B	0.1233
Direct sum for site C	0.1230
Present approximation	0.123

[5] H. T. Davis, *Tables of Higher Mathematical Functions* (Principia Press, Inc., Bloomington, 1933).

atom is at least a few interatomic spacings from the surface of the graphite or, in the case of an interlaminar atom, nearly midway between the adjacent planes. However, even in cases where the approximation is not sufficiently accurate for the problem at hand, it does provide a useful means for estimating the relative contribution to the total sum of the nearest planes and a ready method for obtaining the contributions from the more distant planes. It should perhaps be remarked that the assumption of a uniform density of carbon atoms in the basal planes may be a better model for the graphite lattice in some problems than the more detailed structure because of the presence of the conducting electrons in the planes.

IV. CONCLUSIONS

The value of lattice sums of r^{-n} over a graphite lattice may be approximated to within a few percent by assuming a uniform distribution of carbon atoms in the basal planes of graphite. The approximation enables one to express the summations directly in terms of tabulated functions for several useful values of n. The method has been applied to the determination of the heat of adsorption of argon on graphite as an illustration of the use and accuracy of the technique. It is hoped that this approximation will be of value in similar adsorption problems and in any other problems where the lattice sums of r^{-n} for graphite are required.

THE JOURNAL OF CHEMICAL PHYSICS VOLUME 22, NUMBER 8 AUGUST, 1954

Hydrogen Bonding in Sodium Trifluoroacetate-Trifluoroacetic Acid Compounds

WILLIAM KLEMPERER AND GEORGE C. PIMENTEL
Department of Chemistry and Chemical Engineering, University of California, Berkeley, California

(Received February 16, 1954)

The dissociation pressure of trifluoroacetic acid over two compounds with sodium trifluoroacetate has been measured from 25° to 40°C. One compound is $CF_3COONa \cdot 2CF_3COOH$, and the other is probably $CF_3COONa \cdot CF_3COOH$. The infrared spectra of $CF_3COONa \cdot 2CF_3COOH$, $CF_3COONa \cdot 2CF_3COOD$, and CF_3COONa have been measured in the spectral region 4000 to 650 cm^{-1}. The stability of these salt-acid compounds is attributed to strong hydrogen bonding. The heat of dissociation of $CF_3COONa \cdot 2CF_3COOH$ is +14 kcal per mole of monomeric trifluoroacetic acid, and the OH stretching frequency is found 1150 cm^{-1} below its location in the monomeric acid.

INTRODUCTION

MANY of the carboxylic acids form compounds with their salts. In some cases there are two compounds, for example, the sodium acetate-acetic acid system has the compounds $CH_3COONa \cdot CH_3COOH$ and $CH_3COONa \cdot 2CH_3COOH$.[1]

Recently, Speakman has determined by x-ray analysis the structure of a carboxylic acid-salt compound, potassium hydrogen phenylacetate.[2] He found the abnormally short oxygen-oxygen distance 2.55A, which is indicative of a strong hydrogen bond between the carboxyl and carboxylate groups.

The present work is a study of the sodium trifluoroacetate-trifluoroacetic acid system. For studies of the type presented here, this system has advantages over other carboxylic acid-salt systems. Trifluoroacetic acid has the highest vapor pressure of any of the carboxylic acids, permitting relatively rapid, reversible formation of the addition compounds. Secondly, the absence of carbon hydrogen motions simplifies the interpretation of the infrared spectrum. The formation of acid-salt compounds was detected by measurement of the pressure of trifluoroacetic acid in equilibrium with a solid, made with varying proportions of sodium trifluoroacetate and trifluoroacetic acid. The heat of formation of these compounds was then determined from the temperature coefficient of the dissociation pressure. In order to gain more intimate knowledge of the structure of the compounds, the infrared spectrum was measured.

[1] A. W. Davidson and W. H. McAllister, J. Am. Chem. Soc. **52**, 507 (1930).
[2] J. C. Speakman, J. Chem. Soc. 3357 (1949).

EXPERIMENTAL

Materials

Sodium Trifluoroacetate

Halogen Chemicals, Inc., sodium trifluoroacetate was used. Water in the bulk material amounted to 2.4 percent by weight, and it was removed by exposing the solid to a high vacuum for about 24 hours.

Trifluoroacetic Acid

This compound was prepared from sodium trifluoroacetate and "Baker's Analyzed" concentrated sulfuric acid. The preparation and subsequent handling were done under vacuum.

Deuterotrifluoroacetic Acid

Trifluoroacetic anhydride was prepared from trifluoroacetic acid by contact with phosphorus pentoxide. Deuterotrifluoroacetic acid was prepared from equimolar

TABLE I. The pressure of trifluoroacetic acid over sodium trifluoroacetate as a function of the amount of trifluoroacetic acid absorbed.

Mole ratio CF_3COOH	Stationary pressure in mm Absorbing	Desorbing
0.409	0.91	
0.401		0.85
0.389		0.81
0.511	1.05	
0.5		0.89
0.63	1.18	
0.578		0.88
0.975		0.99
1.07		1.04
1.43	1.61	
1.42		0.96
1.80		0.98
1.98		1.20
1.95		0.93

amounts of the anhydride and deuterium oxide. All handling was done under vacuum.

Acetonitrile

Eastman Kodak "White Label" acetonitrile was first refluxed with anhydrous potassium carbonate, then refluxed and distilled from phosphorus pentoxide.

Dissociation Pressure Measurements

A weighed sample of sodium trifluoroacetate was put in contact with a fixed amount of gaseous trifluoroacetic acid. Pressure measurements were taken at intervals until successive measurements indicated constancy for a period of several hours. The sample was then removed and weighed. The vacuum line was evacuated and the sample replaced. As before, pressure measurements were continued until no more drift was evident. The equilibrium pressure is bracketed by these measurements. The results are summarized in Table I. After the sample reached a composition of 1.98 moles of acid per mole of salt, it did not change in weight when in contact with trifluoroacetic acid at a pressure of 50 mm for 5 hours. The absorbing and desorbing gases were shown to be the same by their infrared spectra. The gas was shown to be trifluoroacetic acid by comparison to the published spectrum of trifluoroacetic acid.[3] During these pressure measurements, the sample was at room temperature, 24±3°C.

The same sample of material was then used for the determination of the temperature coefficient of the dissociation pressure. Its composition was 2 moles trifluoroacetic acid per mole sodium trifluoroacetate. A second sample of different composition, namely 0.34 moles of trifluoroacetic acid per mole of sodium trifluoroacetate, was subsequently used in these measurements. The first four columns of pressures in Table II refer to these samples.

During the course of the above measurements, the second sample was heated to 55°C. Upon cooling it no longer reproduced its previous dissociation pressure. The last two columns in Table II refer to the sample after the heating.

With the one indicated exception all measurements in Table II are by desorption. The pressures in Tables I and II are estimated to be accurate to 0.05 mm. The thermostat used maintained the temperature constant within 0.1°.

TABLE II. Dissociation pressure of trifluoroacetic acid over compounds with sodium trifluoroacetate.

T °C	Sample 1[a,b] P_t mm	P_m	Sample 2[a,c] P_t mm	P_m	Sample 3[a,d] P_t mm	P_m
24.15	1.10	0.87				
29.95	1.90	1.49				
36.01	3.10	2.41				
24.20			1.07	0.84		
30.15			1.85	1.46		
34.84			2.66	2.10		
24.86					0.58	0.51
29.82					0.88	0.76
34.72					1.31	1.14
39.80					2.05	1.77
					2.44[e]	

[a] P_t is the measured pressure; and P_m is the pressure of trifluoroacetic acid monomer computed from the measured pressure by the dimerization constant of Lundin, Harris, and Nash, J. Am. Chem. Soc. **74**, 4654 (1952).
[b] Sample 1: 1.95 moles CF_3COOH per mole CF_3COONa.
[c] Sample 2: 0.34 mole CF_3COOH per mole CF_3COONa before heating to 55°C.
[d] Sample 3: Sample 2 after heating to 55°C.
[e] Stationary pressure measured by absorption.

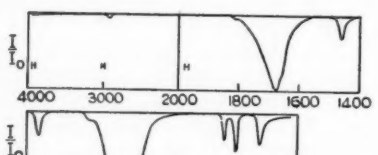

FIG. 1. The infrared spectrum of CF_3COONa.

Infrared Measurements

A Perkin-Elmer model 21 double-beam infrared spectrophotometer, equipped with sodium chloride optics, was used to obtain the spectra. The cells used were 7 mm in length. The cells could be opened to introduce samples directly onto the windows.

Sodium trifluoroacetate was dissolved in acetonitrile. Solution was put onto the cell window, and the cell was then closed. These operations were performed in a dry box. The cell was connected to a vacuum line and the acetonitrile was rapidly boiled off by evacuation. The last traces of solvent were removed by prolonged pumping with high vacuum. The infrared spectrum of sodium trifluoroacetate is shown in Fig. 1. This spectrum is more detailed than that given in reference 3, and differs slightly in the spectral region near 1200 cm^{-1}.

The compound $CF_3COONa \cdot 2CF_3COOH$ was studied in the infrared, and its spectrum is shown in Fig. 2. The

[3] Fuson, Josien, Jones, and Lawson, J. Chem. Phys. **20**, 1627 (1952).

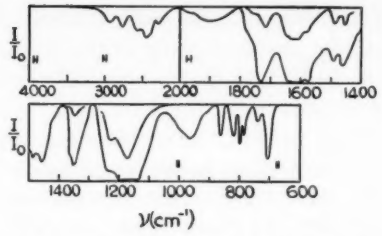

FIG. 2. The infrared spectrum of $CF_3COONa \cdot 2CF_3COOH$.

spectroscopic sample was prepared from the above sodium trifluoroacetate sample, by contacting this sample with trifluoroacetic acid at 40 mm pressure for 1 to 5 minutes. The pressure was then reduced to 7 mm and left for one hour. Before the spectrum was determined, the pressure was reduced to 2 mm. The samples of $CF_3COONa \cdot 2CF_3COOD$ were made in the same manner using CF_3COOD. The spectrum of the deuterated acid-salt compound is shown in Fig. 3.

The infrared absorption maxima of the three compounds CF_3COONa, $CF_3COONa \cdot 2CF_3COOH$, and $CF_3COONa \cdot 2CF_3COOD$, are presented in Table III. Unfortunately, the samples scattered light appreciably, and to different extents. This scattering precluded accurate intensity measurements.

DISCUSSION

The data in Table I indicate the formation of a compound between trifluoroacetic acid and sodium trifluoroacetate with formula $CF_3COONa \cdot 2CF_3COOH$. The data in Table II for sample 2, before and after heating to 55°C, indicate that actually two compounds exist. By analogy to the sodium acetate-acetic acid system where two compounds are also known, it seems probable that the second compound is $CF_3COONa \cdot CF_3COOH$. Sample 2 was prepared by reacting sodium trifluoroacetate with trifluoroacetic acid at a pressure of 50 mm. Since the dissociation pressures of the two compounds at room temperature differ by only one half a millimeter, it is reasonable to expect the formation of substantial amounts of $CF_3COONa \cdot 2CF_3COOH$, which might be converted to $CF_3COONa \cdot CF_3COOH$ only very slowly. In such a case, both salts would be present and the higher dissociation pressure will be measured.

The dissociation reaction for $CF_3COONa \cdot 2CF_3COOH$ is

$$\tfrac{1}{2}CF_3COONa \cdot 2CF_3COOH = \tfrac{1}{2}CF_3COONa + CF_3COOH. \quad (1)$$

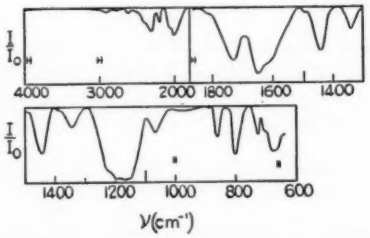

FIG. 3. The infrared spectrum of $CF_3COONa \cdot 2CF_3COOD$.

In Fig. 4, the natural logarithm of the pressure of monomeric CF_3COOH is plotted against the reciprocal of the absolute temperature. The slope gives the heat of reaction (1), $\Delta H = +14 \pm 2$ kcal per mole of monomeric CF_3COOH. The heat of the assumed reaction, $CF_3COONa \cdot CF_3COOH = CF_3COONa + CF_3COOH$, is $\Delta H = +16 \pm 2$ kcal per mole of monomeric CF_3COOH. These values may be compared to the heat of the gas phase reaction $\frac{1}{2}(CF_3COOH)_2 = CF_3COOH$, $\Delta H = +7.0$ kcal per mole of monomeric CF_3COOH.[4]

The infrared spectrum of $CF_3COONa \cdot 2CF_3COOH$ (Fig. 2), shows a broad, complex band in the 3000- to 2000-cm^{-1} region. This absorption must be caused by hydrogen vibrations, as shown by its absence in the deuterated compound and in sodium trifluoroacetate. The poorly defined center of this band is taken to be

TABLE III. Infrared absorption bands of CF_3COONa, $CF_3COONa \cdot 2CF_3COOH$, and $CF_3COONa \cdot 2CF_3COOD$.

CF_3COONa Frequency cm^{-1}	$CF_3COONa \cdot 2CF_3COOH$ Frequency cm^{-1}	$CF_3COONa \cdot 2CF_3COOD$ Frequency cm^{-1}
2920 (1)	2910 (3)	2630 (1)
1680 (10)	2760 (4)	2400 (*sh*)
1457 (4)	2560 (2)	2310 (3)
1218 (8)	2430 (5)	2190 (4)
1190 (2)	2310 (2)	2060 (*sh*)
1145 (10)	2200 (1)	1975 (5)
896 (4)	1900 (2)	1738 (8)
806 (6)	1780 (*sh*)	1655 (9)
725 (5)	1730 (8)	1590 (*sh*) broad
	1625 (9) broad	1445 (7)
	1570 (*sh*)	1350 (3)
	1488 (6)	ca 1200 (10)
	1456 (6)	1075 (3)
	1352 (6)	862 (3)
	1230 (*sh*)	797 (7)
	1175 (10)	733 (2)
	965 (4)	705 (*sh*)
	864 (3)	675 (6)
	818 (3)	
	797 (4)	
	785 (2)	
	736 (2)	
	710 (6)	

(Relative intensities are indicated in parentheses.)

the most intense feature at 2450 cm^{-1}. In gaseous monomeric trifluoroacetic acid the OH stretch is located at 3587 cm^{-1}, while the center of the broad OH stretch in the dimer is near 3000 cm^{-1}.[3] The low frequency of the OH vibration in the acid-salt is indicative of strong hydrogen bonding. Lord and Merrifield[5] and Rundle and Parasol[6] have shown that the shift in OH frequency upon hydrogen bond formation is correlated with shortening of the oxygen-oxygen distance. Use of the linear relation of Lord and Merrifield[5] and a frequency shift of 1150 cm^{-1} yields an oxygen-oxygen distance of 2.63A, reasonably close to the oxygen-oxygen dis-

[4] Lundin, Harris, and Nash, J. Am. Chem. Soc. **74**, 4654 (1952).
[5] R. C. Lord and R. E. Merrifield, J. Chem. Phys. **21**, 166 (1952).
[6] R. E. Rundle and M. Parasol, J. Chem. Phys. **20**, 1487 (1951).

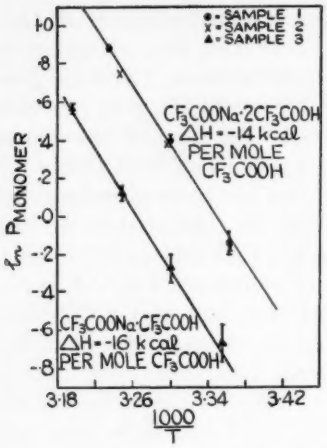

FIG. 4. The dissociation pressure as a function of temperature.

tance found in potassium hydrogen phenylacetate by Speakman.[2]

As in potassium bifluoride,[7,8] the measured heats of reaction cannot be related directly to energy of the hydrogen bond in $CF_3COONa \cdot 2CF_3COOH$ since there will undoubtedly be differences in the lattice energies of the above compound and sodium trifluoroacetate. It seems reasonable to expect the lattice energy of the acid-salt to be lower than that of the neutral salt because of reduced coulombic interaction in the expanded lattice. Thus the measured heat is probably a lower limit of the hydrogen bond energy.

Large spectral changes are observed in the carbonyl stretch region on going from CF_3COONa to $CF_3COONa \cdot 2CF_3COOH$. The strong 1680 cm^{-1} band of CF_3COONa disappears in $CF_3COONa \cdot 2CF_3COOH$. In the acid-salt there are two intense bands in this region, one centered at 1730 cm^{-1}, the other a broad band centered at 1625 cm^{-1}.

The strong absorption of sodium trifluoroacetate at 1680 cm^{-1} is caused by carboxylate stretching motions. Since normally the carbonyl stretching frequency is lowered when it becomes hydrogen bonded, the broad 1625 cm^{-1} band of the acid-salt is assigned to the bonded carboxylate stretching motion. The acid-salt presumably involves bonding as in Fig. 5. In monomeric trifluoroacetic acid the carbonyl stretching frequency occurs at 1826 cm^{-1}. There is no band present at this frequency in $CF_3COONa \cdot 2CF_3COOH$. The nearest intense band to 1826 cm^{-1} is located at 1730 cm^{-1}. Assigning this 1730 cm^{-1} band to the carbonyl vibration indicates a surprisingly large shift, 100 cm^{-1}. Since it is unlikely that the carbonyl group of the acid is hydrogen bonded, it is suggested that when trifluoroacetic acid forms the hydrogen bond, the proton moves away from the acid oxygen toward the carboxylate oxygen. This movement of the proton is similar to ionization of the trifluoroacetic acid except that the proton is not removed completely. In this process the carboxyl group acquires carboxylate ion character with a resulting weakening of the carbonyl bond.

The broad band at 965 cm^{-1} of $CF_3COONa \cdot 2CF_3COOH$ is absent in both CF_3COONa and $CF_3COONa \cdot 2CF_3COOD$. The only band of similar width and intensity present in the deuterated acid-salt below 1000 cm^{-1} is located at 675 cm^{-1}. If these two bands correspond to similar motions, the isotopic shift is 1.43, which cannot be accounted for with an oscillator whose potential function is harmonic and invariant under isotopic substitution.[9]

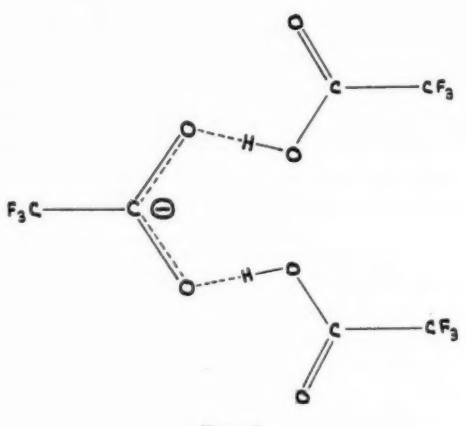

FIG. 5.

CONCLUSIONS

1. Two acid-salt compounds of trifluoroacetic acid and sodium trifluoroacetate are stable and have a high heat of formation. The average $\Delta H = -15$ kcal per mole of monomeric trifluoroacetic acid.

2. Evidence for strong hydrogen bonds is found in the infrared spectrum of $CF_3COONa \cdot 2CF_3COOH$ where the O—H stretching mode shifts by 1150 cm^{-1} from its location in the monomeric gaseous acid.

3. There is some evidence that a carboxylic acid acquires carboxylate ion character when it forms a hydrogen bond.

[7] E. F. Westrum and K. S. Pitzer, J. Am. Chem. Soc. **71**, 1940 (1949).
[8] J. A. A. Ketelaar, Rec. Trav. Chim. **60**, 523 (1941).
[9] For further discussion, see W. A. Klemperer, Ph.D. thesis (1954), University of California, Berkeley, California.

Infrared Absorption Investigation on the Rotational Isomerism of 1,1,2-Trichloroethane

KENJI KURATANI AND SAN-ICHIRO MIZUSHIMA
Institute of Science and Technology and Faculty of Science, Tokyo University, Tokyo, Japan
(Received March 1, 1954)

The energy difference between the rotational isomers of 1,1,2-trichloroethane has been determined in the gaseous and liquid states by the infrared absorption measurements. In the solid state, only one of the rotational isomers has been found to be stable. The different behavior in rotational isomerism between 1,1,2-trichloroethane and 2-methylbutane, both having the same skeletal configuration, has been explained in terms of the difference in the electrostatic part of the hindering potential.

IT was concluded by Thomas and Gwinn[1] that a large energy difference existed (greater than 2300 cal/mole) between the rotational isomers of 1,1,2-trichloroethane Cl_2HC-CH_2Cl from the gaseous dipole moment, while Sheppard and Szasz[2] found almost no energy difference between the isomers of 2-methylbutane $(CH_3)_2HC-CH_2CH_3$, which has a skeletal configuration similar to that of 1,1,2-trichloroethane. The different behavior of these two substances is very important in the understanding of the nature of the hindering potential to internal rotation.[3] We have, therefore, made an infrared investigation on 1,1,2-trichloroethane in the gaseous, liquid, and solid states in order to obtain more exact values of the energy difference between the rotational isomers reported in our previous paper.[4]

The infrared spectra were measured with a Baird spectrophotometer. Absorption bands in the region from 2000 to 630 cm^{-1} were recorded with the NaCl prism, and those in the region from 800 to 400 cm^{-1} with the KBr prism. The results obtained are shown in Table I, where the notations *s*, *m*, and *w* denote, respectively, strong, medium, and weak intensities of absorption bands, and *sh* indicates a shoulder of the absorption curve. The sample used in the measurement was redistilled through a column of 30 theoretical plates, bp, 113° at 760 mm.

TABLE I. The infrared absorption bands of 1,1,2-trichloroethane (cm^{-1}).

Solid	Liquid	Vapor
...	525 *m*	526 *w*
640 *m*	640 *m*	...
663 *s*	661 *s*	669 *s*
...	700 *m*	...
727 *s*	729 *s*	735 *s*
772 *s*	777 *s*	782 *s*
784 *w*	784 *w*	790 *sh*
929 *s*	930 *s*	929 *s*
...	937 *w*	937 *sh*
...	1008 *m*	1007 *sh*
1050 *m*	1050 *m*	1049 *m*
1159 *m*	1157 *m*	1157 *m*
1208 *s*	1208 *s*	1204 *s*
...	1236 *m*	1242 *sh*?
1259 *s*	1261 *s*	1259 *s*
1302 *m*	1304 *m*	1303 *s*
1428 *s*	1430 *s*	1430 *s*
...	2860 *w*	2860 *w*
2985 *m*	2980 *m*	2985 *m*
3010 *m*	3010 *m*	...

The maximum number of observable fundamental infrared bands in the frequency region from 1500 to 500 cm^{-1} for one molecular form is ten, including three C−Cl stretching, one C−C stretching, four CH_2 deformation frequencies, and two CH deformation frequencies, The number of infrared bands actually observed in the liquid state is larger than this value (see Table I). This may be considered a result of the fact that some of these bands are to be assigned to overtones or combination tones. However, as we have observed the disappearance of several bands (1236, 1008, 700, and 525 cm^{-1}), on solidification, it is probable to assume two rotational isomers in the liquid state and only one of them in the solid state, just as in the case of 1,2-dihalogenoethanes, whose rotational isomerism has been studied conclusively.[5] The number of stronger infrared bands observed in the solid state becomes small enough to be explained from a single configuration.

The bands at 1236 and 700 cm^{-1} which were observed only in the liquid state increase their relative intensities in a polar solution and decrease them in a nonpolar solution when compared with the bands at 1208 and 729 cm^{-1}, which are observed in both the liquid and solid states (see Table II). From this solvent effect it is

TABLE II. Ratio of the optical densities D_m/D_l observed for the two bands at 1236 and at 1208 cm^{-1} in various solvents.

Solvent	$D(1236)/D(1208)$
liquid state	0.34
carbon tetrachloride	0.15
carbon disulfide	0.24
acetonitrile	0.52

[1] J. R. Thomas and W. D. Gwinn, J. Am. Chem. Soc. **71**, 2785 (1949).
[2] N. Sheppard and G. J. Szasz, J. Chem. Phys. **18**, 145 (1950).
[3] Mizushima, Morino, and Shimanouchi, J. Phys. Chem. **56**, 324 (1952). See also reference 1.
[4] Kuratani, Miyazawa, and Mizushima, J. Chem. Phys. **21**, 1411 (1953).
[5] For the summary of the work on 1,2-dihalogenoethanes see, e.g., S. Mizushima, *The Reilly Lectures* (University Press, Notre Dame University, Notre Dame, Indiana, 1951) Vol. V. and *Internal Rotation*, (Academic Press, New York, 1954). See also Mizushima, Morino, Watanabe, Shimanouchi, and Yamaguchi, J. Chem. Phys. **17**, 591 (1949).

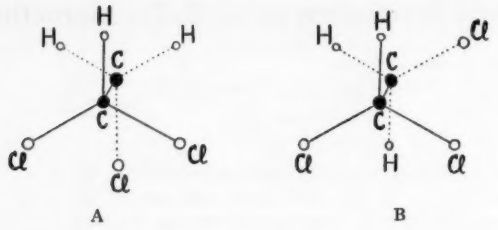

FIG. 1. Stable molecular forms of 1,1,2-trichloroethane. A, more polar form; B, less polar form.

readily seen that the bands at 1236 and 700 cm^{-1} are to be assigned to the more polar form (Fig. 1) which becomes relatively more stable in a polar solvent.[6] Therefore, we can assign the more polar form to the isomer which exists only in the liquid state and disappears on solidification and assign the less polar form (Fig. 1) to the isomer which is found in both the liquid and solid states.

In the gaseous state at lower temperature the intensity of the bands at 1236, 1008, 700, and 525 cm^{-1}, assigned to the more polar form, becomes so weak as to escape detection, and at higher temperatures only one of them with a peak at 526 cm^{-1} is detectable. This means that the more polar form becomes less stable in the gaseous state in agreement with the explanation presented in our previous paper.[6]

Let us next discuss the energy difference ΔE of rotational isomers in the liquid and gaseous states which can be obtained from the temperature dependence of the intensity ratio of two absorption bands, one assigned to the less polar form and the other to the more polar form. The equilibrium ratio of these two kinds of molecules is given by

$$\frac{N_l}{N_m}=\text{const}\, e^{\Delta E/RT}, \tag{1}$$

where $\Delta E=E_m-E_l$ is the energy difference and N_l and N_m are the number of the less polar and the more polar molecules, respectively. Let k be the molecular absorption coefficient and D the optical density; we have

$$\frac{D_l}{D_m}=\frac{k_l N_l}{k_m N_m}=\text{const}\frac{k_l}{k_m}e^{\Delta E/kT}. \tag{2}$$

If, therefore, we observe the ratio of optical densities D_l/D_m at different temperatures, we can calculate the value of ΔE from Eq. (2), assuming ΔE and k to be constant in the temperature range in which we have made our measurements. If we take into account induced emission (Einstein[7]), Eq. (2) becomes

$$\frac{D_l}{D_m}=\frac{B_l\nu_l(1-e^{-h\nu l/kT})\cdot N_l}{B_m\nu_m(1-e^{-h\nu m/kT})\cdot N_m},$$

which we can rewrite as

$$\frac{D_l'}{D_m'}=\frac{D_l/(1-e^{-h\nu l/kT})}{D_m/(1-e^{-h\nu m/kT})}=\text{const}\frac{B_l}{B_m}\frac{\nu_l}{\nu_m}e^{\Delta E/kT}, \tag{3}$$

where D_l' and D_m' are the corrected optical densities, and B_l and B_m are the transition probability coefficients which are independent of temperature. From this equation we can evaluate ΔE, using the corrected ratio D_l'/D_m' at different temperatures. The observed and the corrected ratios of optical densities are shown in Table III, where the correction for the induced emission was not made for the data obtained in the liquid state, since at lower temperatures the correction becomes negligibly small.

From the experimental data shown in Table III we can calculate the value of ΔE and the probable error by the method of least squares. The results are shown in Table IV, where the third and fourth columns refer to the wave numbers of the bands used in the intensity measurements.

The large values of ΔE obtained in the gaseous state are consistent with the result of the gaseous dipole measurement by Thomas and Gwinn,[1] and by Shirai,[8] who observed almost a constant moment in a wide range of temperature. The small value of ΔE in the liquid state is also consistent with the experimental results of Malherbe and Bernstein.[9]

TABLE III. Observed and corrected ratios of optical densities D_l/D_m at different temperatures. (The numbers in parentheses refer to wave numbers of the bands used in the intensity measurements).

(a) Liquid

t°C	$D_l(1208)/D_m(1236)$	t°C	$D_l(777)/D_m(700)$
27	2.75	27	1.06
27	2.84	74	1.01
52	2.74	98	0.96
61	2.64	98	0.96
80	2.63		
80	2.59		
102	2.59		

(b) Vapor

t°C	$D_l(669)/D_m(526)$	$D_l'(669)/D_m'(526)$	$D_l(782)/D_m(526)$	$D_l'(782)/D_m'(526)$
97	23.1	21.7	20.5	18.7
125	17.7	16.5	15.2	13.7
155	13.7	12.7	12.5	11.2
155	13.3	12.3	12.1	10.8

[6] Watanabe, Mizushima, and Masiko, Sci. Papers Inst. Phys. Chem. Research (Tokyo) **40**, 425 (1943). S. Mizushima and H. Okazaki, J. Am. Chem. Soc. **71**, 3411 (1949). Morino, Mizushima, Kuratani, and Katayama, J. Chem. Phys. **18**, 754 (1950).

[7] See, for example, E. C. Kemble, *The Fundamental Principles of Quantum Mechanics* (McGraw-Hill Book Company, Inc., New York, 1937) p. 462.

[8] M. Shirai, private communication.

[9] F. E. Malherbe and H. J. Bernstein, J. Am. Chem. Soc. **74**, 1859 (1952).

It should be realized that some of the bands of the less polar form may overlap those of the more polar form in the liquid state and that in consequence there may be some uncertainty as to the value of the energy difference obtained in the liquid state. This uncertainty cannot be great, since we did not observe an appreciable change in the relative intensity of bands assigned to the less polar form on solidification. In the gaseous state the uncertainty in the value of ΔE due to the overlapping of bands is far less than that in the liquid state, because, as was mentioned before, the number of molecules in the more polar form is very small as compared with that in the less polar form. A simple estimation tells us that the uncertainty is less than 50 cal/mole, which is within the limit of experimental error shown in Table IV.

The small energy difference between the rotational isomers of 1,1,2-trichloroethane in the liquid state seems to be in agreement with that of 2-methylbutane. However, it should be realized that the former does not refer to the energy difference in the free state, while the latter can be regarded as such, because in the case of nonpolar substance such as 2-methylbutane the energy difference in the gaseous state is almost the same as in the liquid state.[6] Therefore, we have to conclude that the behavior of 1,1,2-trichloroethane is quite different from that of 2-methylbutane.

As shown in our previous paper,[3] the most important element in determining the hindering potential to internal rotation is the steric repulsion, and therefore the stable molecular forms should correspond approximately to the minima of the steric repulsive potential. In these minima the repulsive force may become of the same order of magnitude as the electrostatic force: in other words, in the energy difference between the two potential minima (i.e., ΔE referred to above) the electrostatic potential may play a significant role. Therefore, even if there is no difference in the steric repulsive potential between 1,1,2-trichloroethane and 2-methylbutane, the values of energy difference ΔE of these two substances can differ considerably from each other, since in the former there is large electrostatic potential due to the large bond moment of C—Cl, while there is no such potential in the latter. In this way we can understand the difference of the value of ΔE between these two substances.

TABLE IV. The energy difference ΔE in cal/mole.

	$\Delta E = E_m - E_l$ (cal/mole)	Absorption bands used in the measurement	
		Less polar form	More polar form
Liquid	220±30	1208	1236
	290±60	777	700
Vapor	2900±100	669	526
	3000±100[a]		
	2750±150	782	526
	2850±150[a]		

[a] Corrected for the induced emission.

We would like to note the difference in the value of ΔE between 1,1,2-trichloroethane and 1,2-dichloroethane, which was also discussed by Thomas and Gwinn.[1] If the carbon valence was tetrahedral, charge distributions in the bonds were the same, and the azimuthal angle of the more stable form was different from that of the less stable form by 120°, ΔE of these two substances should be equal to each other. However, there is a difference of ΔE amounting to 2900−1200 = 1700 cal/mole[10] which would mainly be due to the strong repulsive force between two chlorine atoms, one linked to one carbon atom and the other to another carbon atom. This force shifts the equilibrium position of one chlorine atom with respect to the other so that the difference in the azimuthal angle between the two isomers becomes smaller for 1,2-dichloroethane[11] and larger for 1,1,2-trichloroethane than the ideal value of 120°. In consequence the energy of the less stable form of 1,2-dichloroethane and that of the more stable form of 1,1,2-trichloroethane are decreased as compared with the ideal energy value referred to above. This results in the smaller value of ΔE for 1,2-dichloroethane and the larger value for 1,1,2-trichloroethane.

[10] Watanabe, Mizushima, and Morino, Sci. Papers Inst. Phys. Chem. Research (Tokyo) **39**, 401 (1942). See also reference 5.

[11] J. Ainsworth and J. Karle, J. Chem. Phys. **20**, 425 (1952).

The Surface Migration of Carbon on Tungsten*

RALPH KLEIN†
Explosives and Physical Sciences Division, Bureau of Mines, Pittsburgh, Pennsylvania
(Received March 8, 1954)

The surface migration of carbon on tungsten was observed with the field-emission microscope technique. The tungsten point was shadowed with carbon and heated to a given temperature; observations of the emission patterns were made at room temperature at various time intervals. The migration occurs at a measurable rate starting about 850°K. It is characterized by a sharp boundary of a form which clearly shows that the (011) and (121) planes are avoided. An activation energy of 55±7 kcal/mole was calculated for the process by application of the theory of diffusion with a sharp moving boundary.

IN a previous paper[1] the results of a study of the oxygen-carbon surface reaction on a tungsten surface with the field-emission microscope[2] indicated that a more extended interpretation required knowledge of the migration of both carbon and oxygen on the tungsten lattice. This paper concerns the migration of carbon on tungsten, which, apart from its pertinence to the carbon-oxygen surface reaction on tungsten, is of intrinsic interest.

The mobility of the surface layer on tungsten has been investigated for such substances as the alkali metals, barium, and thorium by utilizing the changes in thermionic or photoelectric emission during the course of the migration.[3] The field-emission microscope has been used to follow the surface migration of tungsten over its own lattice,[4] barium over tungsten,[5,6] and oxygen on tungsten.[7] The advantages of the field-emission microscope technique in studying surface migration phenomena are twofold; the surface under consideration can be well defined with respect to geometry and freedom from contaminants, and observations of almost atomic dimensions may be made in detail. The direct observation of the migration process is possible because of changes effected in the work function of the emitting surface. As has been noted previously,[1] carbon, in contrast to barium (which is highly electropositive with respect to tungsten) or oxygen (which is highly electronegative), changes the work function of a tungsten surface only very slightly. However, there is a small increase of the work function, which is sufficient to enable the surface migration to be observed.

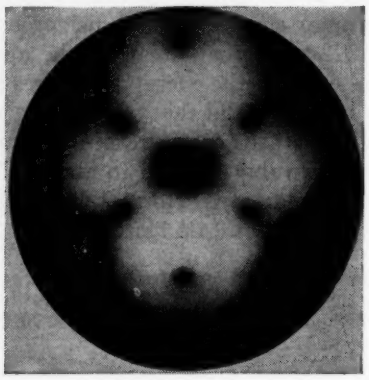

FIG. 1. Clean tungsten. 5600 volts; 5 microamperes.

EXPERIMENTAL

The apparatus used was the same as previously described,[1] with minor modifications. A side tube containing a tantalum filament was added to the system. This provided, in addition to the pumping action of the ionization gauge, the gettering action of a tantalum film evaporated onto the walls of the tube. In order to attain an ultra-high vacuum, considerable care was required in the method of mounting of the 0.005-inch diameter graphite filament used as the source of carbon. Best results were obtained when carbon clamping paste was avoided. The filament was held with a spring clip made from 0.04-inch nickel wire.

After a 450°C bakeout and outgassing of filaments (including 5 hours of outgassing of the graphite filament at 2200°C as measured by a micro-optical pyrometer), a final vacuum was attained which, exclusive of helium, was estimated to be better than 10^{-12} mm of mercury. After the point was flashed, the emission pattern for clean tungsten was observed. Seven days later, with no flashing of the filament, the pattern had not changed perceptibly, even on the (111) zones or the (121) planes, which indicate the progress of contamination by darkening and enlarging.[8]

The graphite filament (the source of carbon) was 10 mm from the emitting point in a plane 1 mm behind the point and perpendicular to the tip. Carbon was evaporated by heating the filament to 2300°C for 3 to

* This research is a part of the work being done at the Bureau of Mines on Order No. CS-670-54-9, supported by Headquarters, Air Research and Development Command, Office of Scientific Research, through Project SQUID.

† Physical chemist; Acting Chief, Kinetics Section, Explosives and Physical Sciences Division, Bureau of Mines, Pittsburgh, Pennsylvania.

[1] R. Klein, J. Chem. Phys. **21**, 1177 (1953).
[2] E. W. Müller, Physik. Z. **37**, 838 (1936).
[3] For references, see R. M. Barrer, *Diffusion In and Through Solids* (Cambridge University Press, Cambridge, 1941), Chapter VIII.
[4] E. W. Müller, Z. Physik **126**, 642 (1949).
[5] E. W. Müller, Z. Physik **108**, 668 (1938).
[6] J. A. Becker, Bell System Tech. J. **30**, No. 4, 907 (1951).
[7] R. Gomer and J. K. Hulm, J. Am. Chem. Soc. **75**, 4114 (1953).
[8] M. K. Wilkinson, J. Appl. Phys. **24**, 1203 (1953).

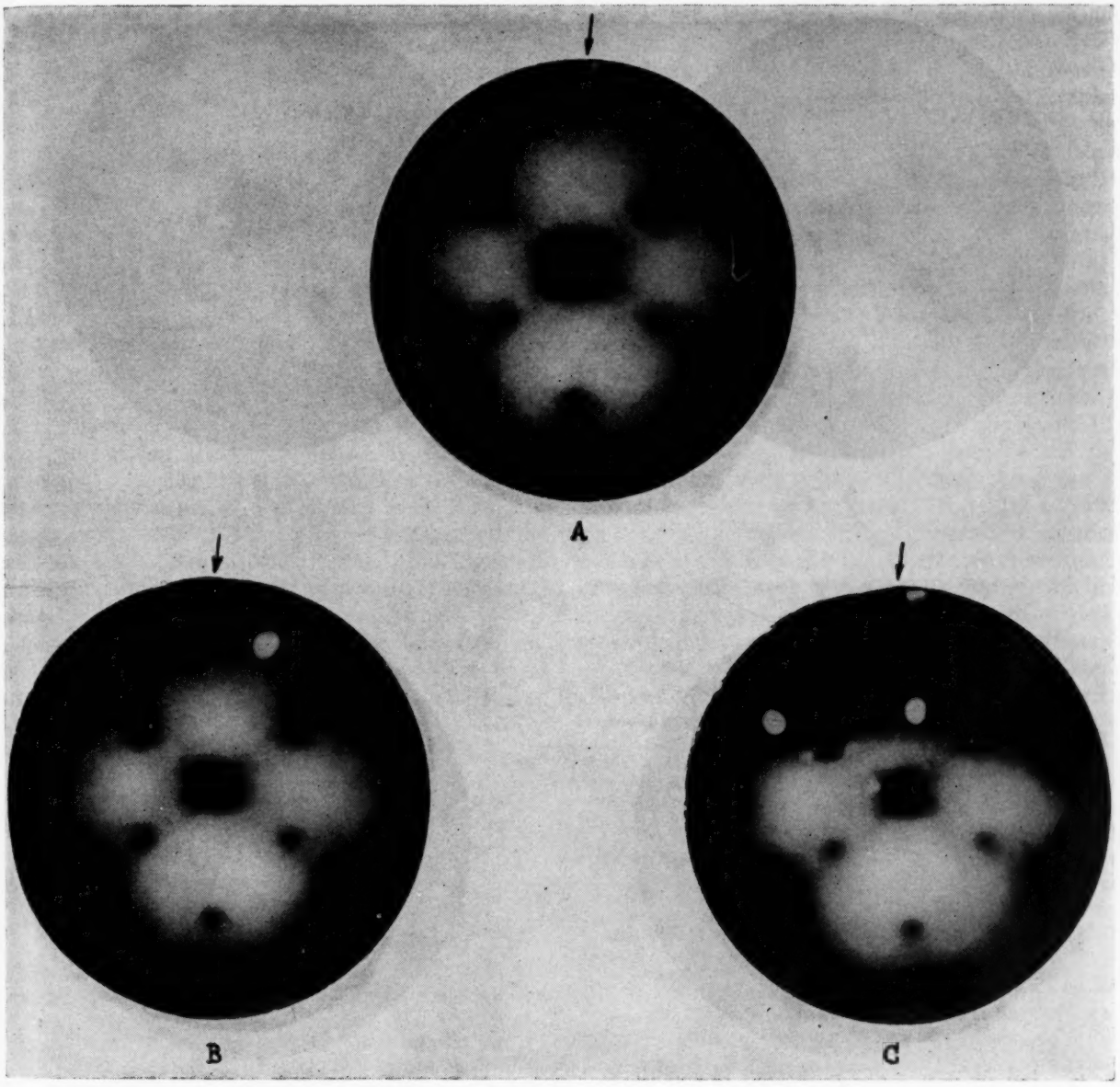

FIG. 2. Tungsten shadowed with carbon. Direction of evaporation shown by arrow. Ratio of amounts of carbon: A. 1, B. 5, C. 20.

60 seconds onto the tungsten tip, maintained at room temperature. No pressure rise was detectable during the evaporation of carbon. Surface migration was followed by heating the point to various temperatures for measured time intervals with the field off. To minimize the uncertainty due to heatup time, large initial currents were supplied by a circuit consisting of an amplifier and two thyratrons. The loop, to which the emitting tip was attached, was one arm of a bridge circuit. With a feedback arrangement, a high current could be supplied initially, so that the temperature-time curve for the tip approximated a square wave. Temperatures were determined with a micro-optical pyrometer, suitable emissivity corrections being applied.

Figure 1 is the well-known pattern for clean tungsten. The sharp shadow on the right is that of the filament holder. A potential of 5600 volts was required for a 5-microampere emission current. All patterns were taken at this current level. Whether the tungsten tip was partly or completely covered, or even if clustering had occurred, the voltage required for the 5-microampere emission was always within about 5 percent of 5600 volts.

SURFACE MIGRATION

The initial patterns, in which the tungsten tip is shadowed with carbon, are shown in Fig. 2. The times of evaporation from the graphite filament, hence the

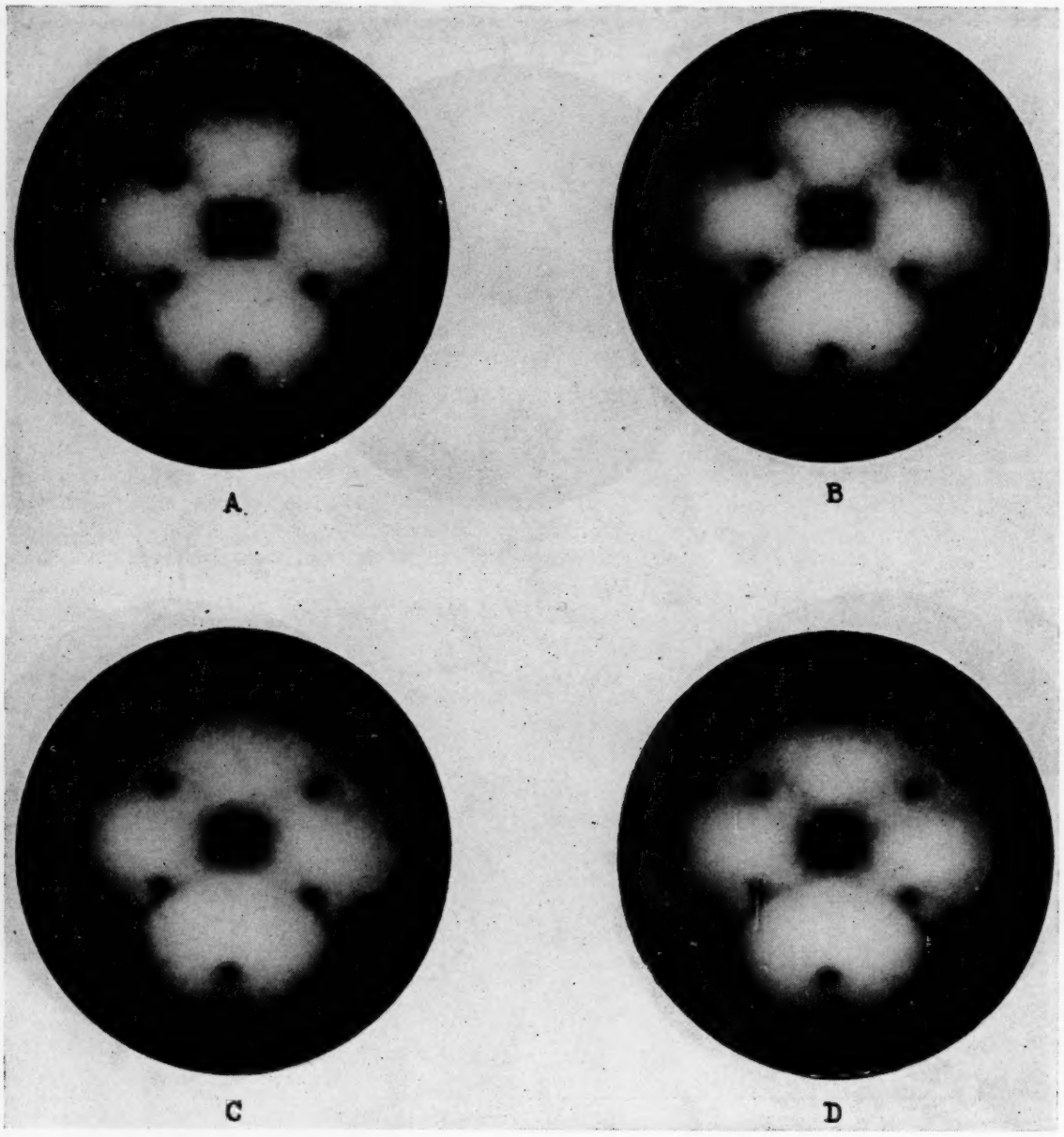

FIG. 3. Carbon migration at 850°K. A. 15 seconds, B. 3½ minutes, C. 55 minutes, D. 85 minutes.

amounts deposited on the tip, are in the ratio 1:5:20. There is only a slightly decreased emission with increasing deposition of carbon. The presence of the surface layer is indicated, in addition to darkening, by a slight graininess of the pattern on the areas covered. It is to be noted that there are no distinct boundaries before heating. This is further evidence that adsorbed carbon has very little effect on the work function of a tungsten surface.

In Fig. 3(A), a tungsten point shadowed with carbon has been heated to 850°K for 15 seconds. Figure 3(B) is the pattern after 3½ minutes further heating at 850°K. The remarkable effect is the formation of a sharp boundary, which, at this temperature, moves only very slowly. This is illustrated by Figs. 3(C) and 3(D), where the total heating time was 55 and 85 minutes, respectively, at 850°K. It is evident that below the boundary, the normal clean tungsten pattern is characterized by a slightly higher emission than the corresponding carbon covered surface at the top of the pattern. The work function of a tungsten surface is therefore decreased very slightly by adsorbed carbon. This effect is small, however.

There are several possible explanations for the formation of a sharp boundary layer in this diffusion process. First, there may be a sharp inflection in the surface concentration-work function curve, the sharp boundary being an isoconcentration line corresponding to the

inflection point. Second, there may be a strong dependence of diffusion coefficient on concentration. Third, the carbon may become fixed to the substrate either by the formation of a surface carbide or by strong adsorptive forces. The first hypothesis is ruled out because the patterns before temperature treatment show no sharp boundaries. The second requires, in the case of a rapidly increasing coefficient of diffusion with concentration, the existence of strong, lateral, repulsive forces. This is consistent neither with the clustering of the carbon which occurs in later stages of the temperature-time history, nor with the known carbon-carbon bond strengths. It is probable that the sharp boundary occurs as a result of strong lateral carbon-carbon interaction, with possible surface carbide formation.

The characteristics of the migration at a given temperature can be observed in detail by freezing the pattern at convenient time intervals. Figure 4 shows a sequence of patterns at 975°K. The sharp boundary line forms an umbrella-shaped curve as the migration proceeds. The slightly rounded cusps of this curve are in the direction of the center of the (011) and (121) planes. It is unlikely that the pattern changes are due to migration into and out of the lattice, for an unusual anistropy for the volume diffusion would have to be assumed. Undoubtedly, the process is that of true surface migration. To interpret the shape of the boundary line in terms of a mechanism, it is suggestive to consider the problem of heat flow from a linear constant temperature source at the edge of a semi-infinite plane containing a circular hole, the plane being initially at a uniform temperature lower than that of the source. The curve of an isothermal on the far side of the hole with respect to the line source, but not too far removed, can be shown, at least experimentally, to almost parallel the source, except in the immediate vicinity of the hole. There it develops a rounded cusp, the center of which is on a perpendicular from the line source through the center of the circular cutout. From the similarity between the isothermals and the corresponding sharp boundary in the pattern of the carbon migration on tungsten, one must conclude that the (011) and (121) planes correspond to the circular holes in the two-dimensional heat-flow case. Therefore the areas are avoided in the migration process. The tungsten surface over which the carbon migration occurs is spherical, as has been shown by electron-microscope observations. It is not inconsistent with a Wulff construction that the characteristic spots in the clean tungsten emission pattern, consisting of low-indexed planes, are flats on the spherical surface.[9] Since the sphere, considered atomically, is built up in lattice steps, the potential

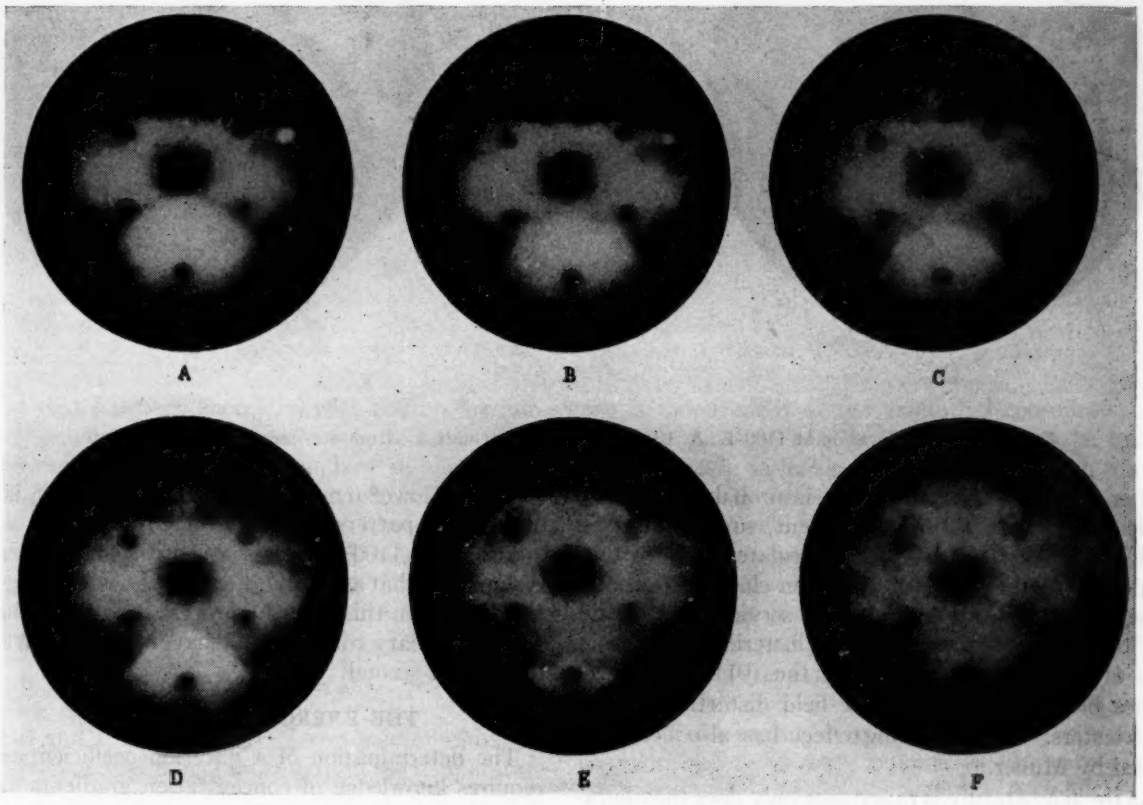

FIG. 4. Carbon migration at 975°K. A. 45 seconds, B. 2 minutes 45 seconds, C. 5 minutes 45 seconds, D. 11 minutes, E. 21 minutes, F. 56 minutes.

[9] C. Herring, Phys. Rev. 82, 87 (1951).

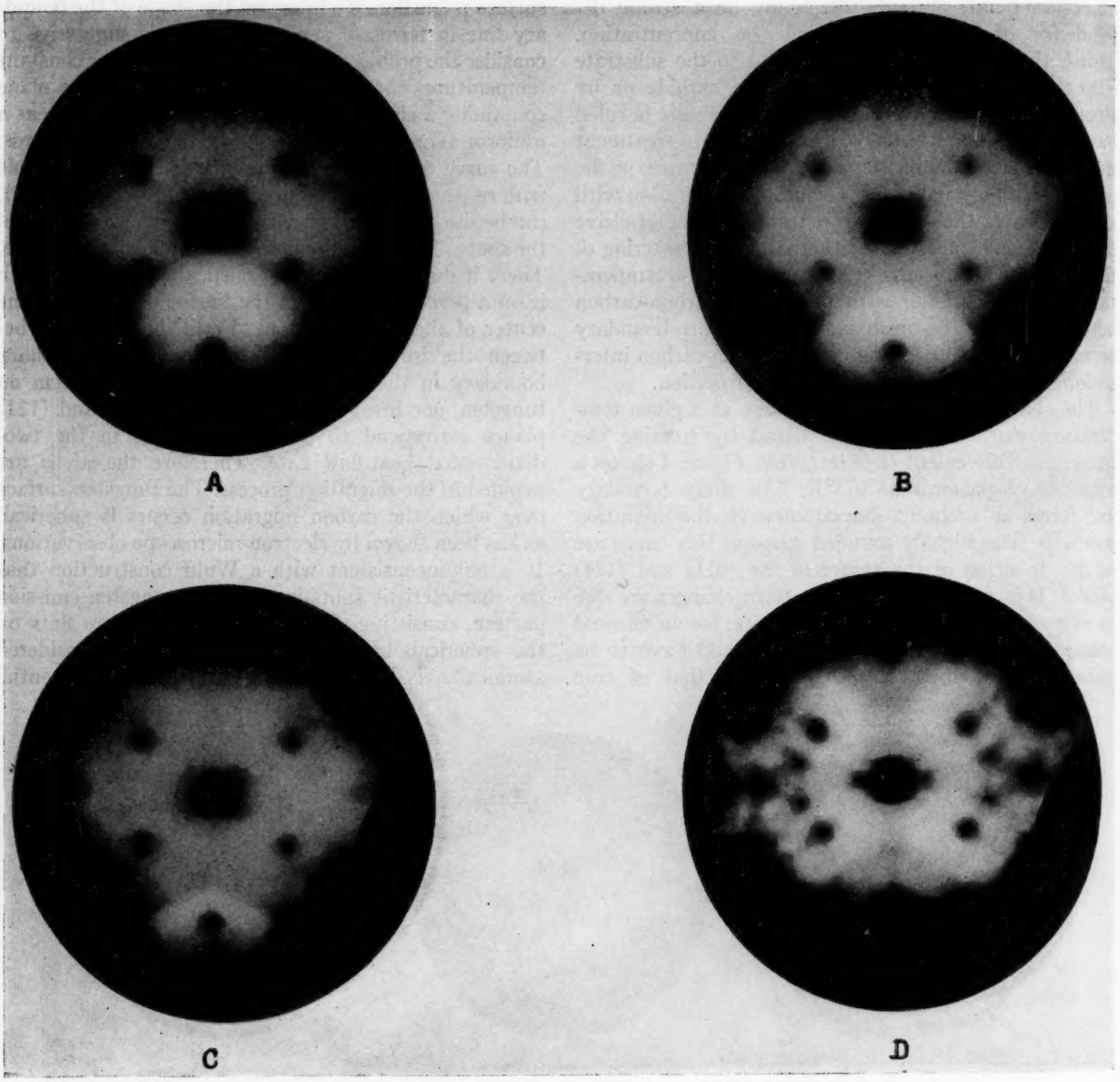

FIG. 5. Carbon migration at 1100°K. A. 10 seconds, B. 37 seconds, C. 1 minute 7 seconds, D. 22 minutes.

barrier to the migration process is probably due to a lattice step, several atoms in extent, surrounding the (011) and (121) planes. This postulate gains further support from the evidence of carbon clustering around these planes, the re-entrant edges serving to nucleate the three-dimensional growth. Clustering is seen in Fig. 4(C), the emission around the (011) and (121) planes being enhanced by the field distortion due to the clusters. This clustering effect has also been observed by Müller.[10]

As the temperature is raised, not only does the migration occur at a more rapid rate, but the final quasi-steady-state pattern differs in detail from those characteristic of lower-temperature regions. Figure 5 is a set of emission patterns showing the course of the surface migration at 1100°K. The shape of the sharp boundary is similar to that at 975°K. Figure 6 shows the migration at 1250°K. In this case the process is so rapid that the sharp boundary completes its traverse of the pattern in less than 1 second.

THE ENERGY OF ACTIVATION

The determination of a diffusion coefficient usually requires knowledge of concentration gradients in relationship to mass flow. Since carbon affects the work function of a tungsten surface only very slightly, it is impossible to calculate the surface concentration of carbon by measuring changes in work function, a

[10] E. W. Müller, Ergeb. exakt. Naturw. **27**, 290–360 (1953).

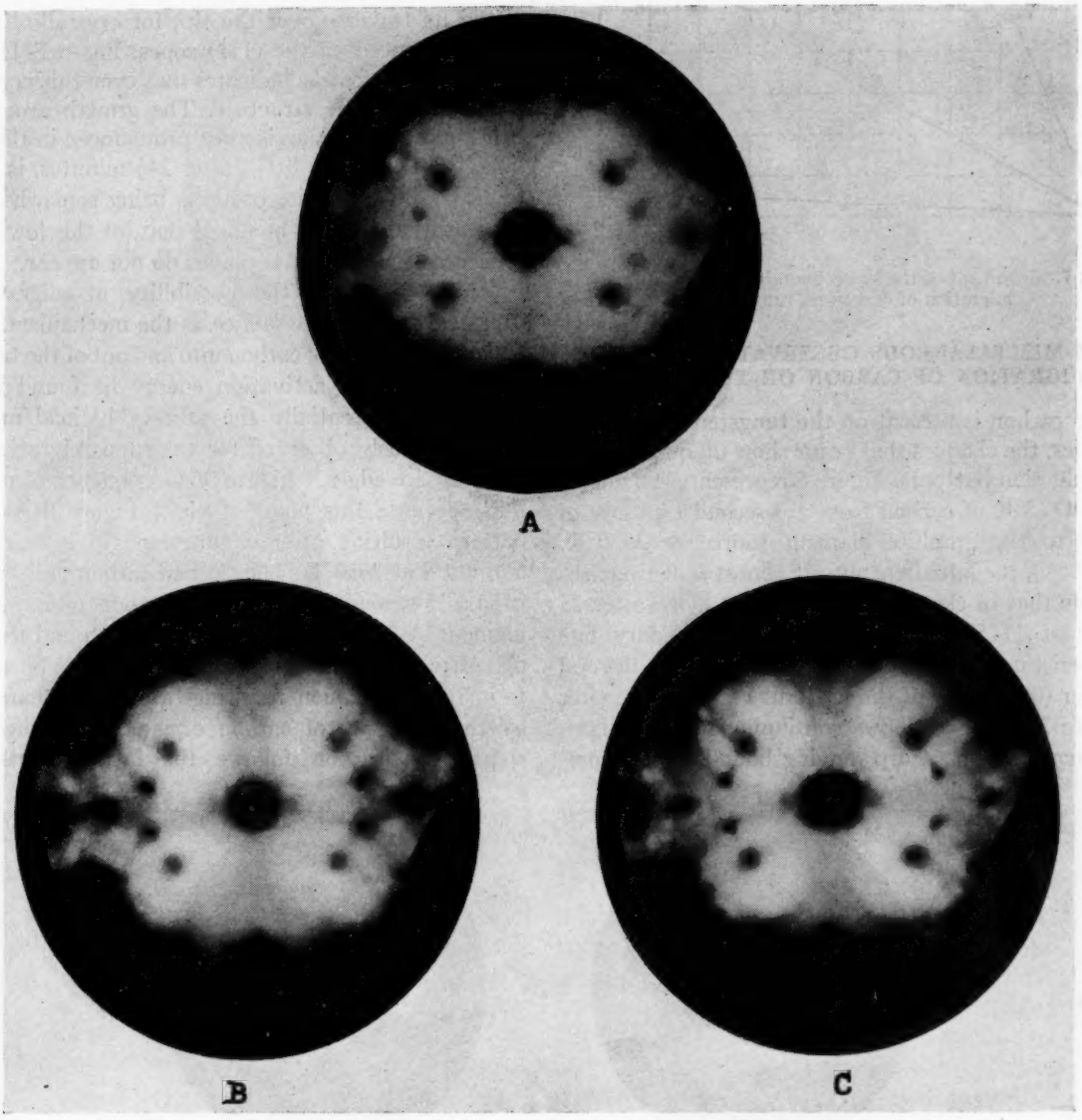

FIG. 6. Carbon migration at 1250°K. A. 5 seconds, B. 15 seconds, C. 45 seconds.

method that has been successful with cesium, barium, and oxygen, where the changes are quite large. From the movement of the sharp boundary in the surface migration of carbon on tungsten an activation energy can be calculated. For migration on the surface of a sphere, assuming concentration-independent diffusion coefficients,

$$\frac{\partial c}{\partial t}=\frac{D}{a^2}\left[\frac{\partial^2 c}{\partial\theta^2}+\operatorname{ctn}\theta\frac{\partial c}{\partial\theta}+\csc^2\theta\frac{\partial^2 c}{\partial\varphi^2}\right]+D'\frac{\partial^2 c}{\partial r^2}\bigg|_{r=a},$$

where D and D' refer to surface and volume diffusion, respectively. Experiments show that, in the temperature regions where the surface migration occurs, volume diffusion is negligible in the time intervals involved. If the coordinate system is oriented so that the initial carbon boundary is at $\theta=\pi/2$ and if the carbon boundary is independent of the azimuthal coordinate, then $(\partial c/\partial t)=(D/a^2)(\partial^2 c/\partial\theta^2)$. The process may be treated approximately as linear diffusion with a sharp moving boundary in a semi-infinite medium. In this case $\xi/\sqrt{t}=K\sqrt{D}$, where ξ is the distance the boundary has moved perpendicular to itself in time t, K is a constant, and D the surface diffusion coefficient.[11] The plots of ξ *versus* $t^{\frac{1}{2}}$ are linear, as shown in Fig. 7. The energy of activation is determined by $E=R[d\ln(\xi^2/t)/d(-1/T)]$ if K is assumed to be independent of temperature. This gives 55 ± 7 kcal/mole for the activation energy of the surface migration of carbon on tungsten characterized by a sharp boundary. The value calculated is sensitive to the slope of the $\xi-t^{\frac{1}{2}}$ plots, and relatively small differences in these slopes from run to run account for the uncertainty in the activation energy.

[11] H. Fujita, J. Chem. Phys. **21**, 700 (1953).

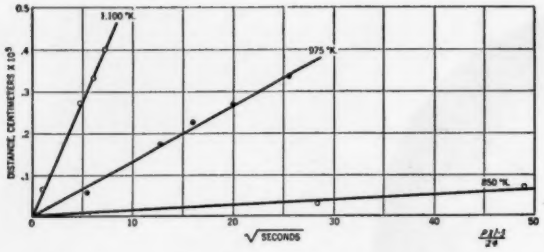

FIG. 7. Movement of the sharp boundary in the surface migration of carbon on tungsten.

SOME MISCELLANEOUS OBSERVATIONS ON THE MIGRATION OF CARBON ON TUNGSTEN

When carbon is present on the tungsten tip in small quantities, the changes that occur show up quite clearly in the emission patterns. Figure 8 represents the migration at 1175°K of carbon from a 3-second exposure of the tip to the graphite filament source at 2570°K. Figure 8(A), the initial pattern, is almost indistinguishable from that of clean tungsten. Figure 8(B), after 25 seconds at 1175°K, shows the sharp boundary line characteristic of the carbon migration. It is just beyond the lower (001) plane of the pattern. Figure 8(C), after 1 minute 25 seconds, shows continuing surface migration, even after the sharp moving boundary has completed its traverse over the tip, for crystallite growth has commenced on the (111) zones. Figure 8(D), after 6 minutes 50 seconds, indicates that even this crystallite growth has a fine structure. The growth around the (011) and (121) planes is most pronounced in the direction of (001). Figure 8(E), after 24½ minutes, is similar to 8(D), the crystallite patterns being somewhat more concentrated. It may be noted that, at this low carbon concentration, the (334) planes do not appear.

Müller suggested the possibility of migration of tungsten over its own lattice as the mechanism for the apparent diffusion of carbon into and out of the tungsten lattice, since the activation energy he found for the process was essentially the same (110 kcal/mole) as that previously observed for tungsten migration over (011) lattice edges.[10] Figure 9 is a sequence of patterns that supports this point of view. Figure 9(A) is the pattern resulting after a tungsten tip is heated for 6 minutes at 2050°K. The tip had carbon on its surface from a 15-second exposure to the vapor from a graphite filament at 2570°K. The lattice steps around the (011) plane are sharply outlined. These lines are to be ascribed to increased emission resulting from field enhancement by the piling up of carbon crystallites in the lattice steps. The carbon follows the lattice steps when

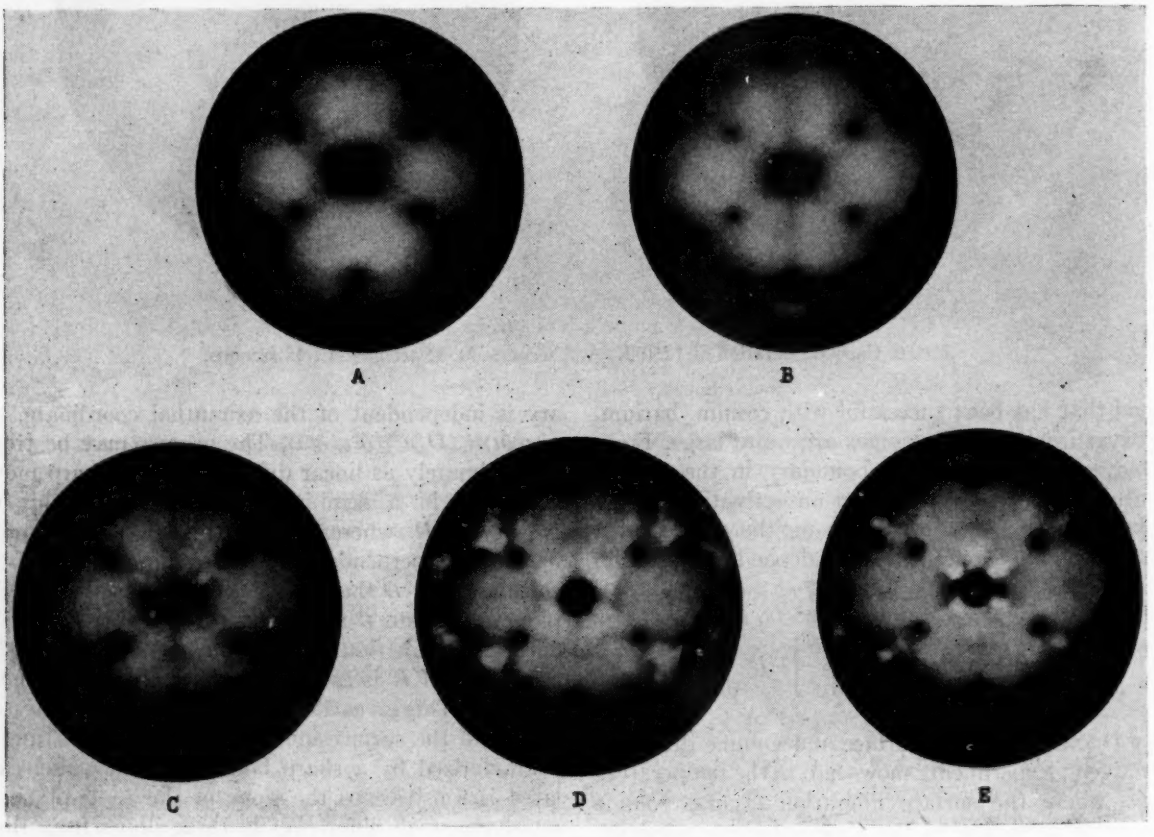

FIG. 8. Carbon migration at 1175°K. The total amount of carbon is ⅓ that in the previous figures. A. Initial, B. 25 seconds, C. 1 minute 25 seconds, D. 6 minutes, E. 24½ minutes.

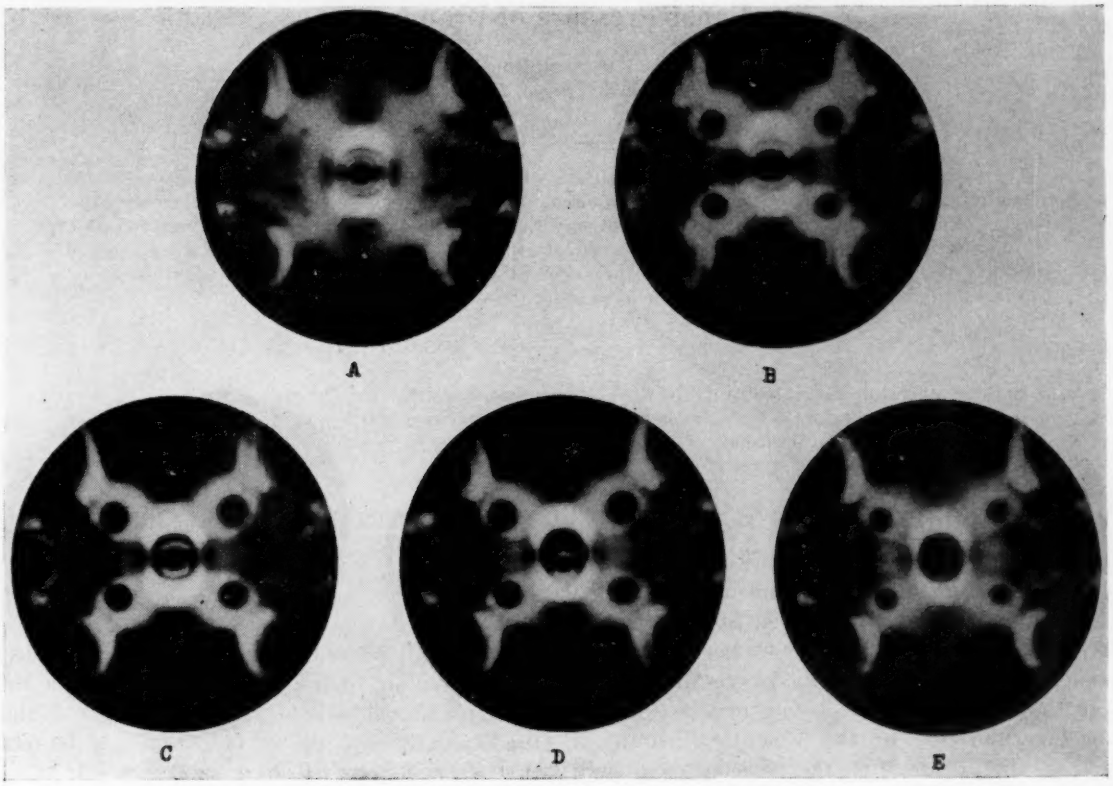

FIG. 9. Carbon migration at 2050°K. A. 6 minutes, B. 2 minutes, C. 6½ minutes, D. 12 minutes, E. 17 minutes. (B, C, D, and E have twice the amount of carbon of A.)

tungsten atoms migrate. This is inferred from the patterns of Fig. 9. Figure 9(B) is the pattern of a tip with twice the amount of carbon of 9(A); 9(C) shows that migration is occurring, as evidenced by the separation of the innermost lattice step from its neighbors. Later stages are shown in 9(D) and 9(E). The explanation for the off-center effect is not immediately apparent, but it is probably related to a chance variation of the inhibiting effect of the carbon crystallites in the lattice steps on the tungsten migration.

It is evident from the data that surface migration of carbon on tungsten occurs in stages. First there is a migration characterized by a sharp boundary. This boundary has been observed only over the surface containing the (001) plane delineated by the (111) zones. Whether or not it is peculiar to this surface will be determined in future experiments by changing the geometry of the shadowing process. After the boundary movement, with the surface uniformly covered with a carbon layer, there occurs, second, a three-dimensional growth or clustering of the carbon in the (111) zones and lattice steps surrounding the (011) planes and, to a more limited extent, around the (121) planes. The patterns are then stable up to the higher temperature regions when tungsten migration over its own lattice is observed. Eventually diffusion of the carbon into the lattice, as well as evaporation from the surface, takes place.

Vapor Pressure of Uranium

EVERETT G. RAUH AND ROBERT J. THORN
Chemistry Division, Argonne National Laboratory, Lemont, Illinois
(Received March 17, 1954)

The vapor pressures and the heat of vaporization of liquid uranium have been measured by collecting a known fraction of the vapor effusing from a Knudsen cell. The deposits were "weighed" by comparing the number of fissions upon thermal neutron irradiation with the fissions from a standard. The measured rate of vaporization is extremely sensitive to the residual pressure of oxygen in the vacuum at background pressures of the order of 10^{-7} mm Hg. With the aid of a theoretically derived expression the effusion rate can be extrapolated to zero oxygen pressure to yield for the vapor pressure the result that

$$\log p(\text{mm}) = -\frac{(23330 \pm 21)}{T} + (8.583 \pm 0.011),$$

over the temperature range 1630 to 1970°K. This expression, together with heat capacity data for solid uranium, yields a value of 116.6 kcal/mole for the heat of sublimation at 0°K and predict a value of about 4.7 kcal/mole for the heat of fusion.

I. INTRODUCTION

An inspection of a summary[1] of the determinations of the vapor pressure of uranium revealed that a more careful and complete investigation of this property was necessary before its value could be established. The most recent measurements by Derge and Cefola[2] are subject to error for the following reasons: (1) No accurate determination of the weights of uranium deposited on the targets from the effusion oven could be made because the α counts of the deposits were about the same as the background count. (2) The residual pressure in the system was of the order of 10^{-4} mm Hg. (3) No correction was made for the solubility of the crucible material in liquid uranium. (4) The authors did not examine their data for internal consistency. Such an analysis would have shown that their data predict an unreasonable value for the heat of fusion.

Since techniques are now available which permit the elimination of these sources of error, the vapor pressure has been redetermined over a temperature range from 1630 to 1970°K. As in the previous measurements the Knudsen effusion method[3] was used but refinements giving greater precision were employed. First, a more sensitive method which is independent of any quantity such as half-life was employed to "weigh" the deposit. This method of weighing the deposit involved fission counting and resulted in 10^4 times greater sensitivity. Second, the experimental conditions were more nearly ideal. Not only was the residual pressure in the vacuum system lower (10^{-7} mm Hg or better), but a quantitative determination of the effect of oxygen was made. Third, the data were analyzed for internal consistency with the aid of recently reported auxiliary data pertaining to the entropies of the vapor and solid.

[1] J. J. Katz and E. Rabinowitch, *The Chemistry of Uranium* (McGraw-Hill Book Company, Inc., New York, 1951), p. 152.
[2] G. Derge and M. Cefola, Atomic Energy Commission Document CT-2277, October 22, 1944.
[3] M. Knudsen, Ann. Physik **29**, 179 (1909).

II. EXPERIMENTAL MEASUREMENTS

A. Method

1. Vapor Pressure

The vapor pressure was determined by collecting a known fraction of the vapor effusing from a Knudsen cell. In this method the vapor pressure is found from the kinetic theory and the cosine law,[4] to be related to the weight collected W by the relation

$$p = (2\pi RT/M)^{\frac{1}{2}}(d/\rho)^2 W/\pi r^2 t, \qquad (1)$$

in which d is the orifice-to-collimator distance, r is the radius of the collimator, ρ is the radius of the orifice, t is the time of collection, and R, T, M have their usual significance. In the derivation of this expression the assumptions are made that the area of the orifice is small compared with the area of the collimator, and the square of the collimator radius is small compared with the square of the orifice-to-collimator distance. Since $r^2/d^2 \cong 0.001$ and $\rho^2/r^2 \cong 0.002$ for the measurements reported herein, these assumptions are certainly justified. The quantities d and ρ were measured at room temperature and corrected for the expansion of the effusion cell at the temperatures of effusion.

The deposits of uranium metal on the targets were weighed by comparing the number of fissions upon thermal neutron irradiation in the thermal column of the Argonne heavy water reactor with the fissions from a standard, both plates being counted simultaneously in a twin chamber counter. The amount of uranium on the standard plates was about 10^{-9} g.

2. Heat of Vaporization (and Sublimation)

In addition to the usual interest in the heat of vaporization, in this case this quantity provides a means of examining the data for internal consistency. This is made possible by comparing the value obtained from

[4] R. G. J. Fraser, *Molecular Rays* (The Macmillan Company, New York, 1931), pp. 14–15.

the Clapeyron equation,

$$\Delta H_v = -RT[d \ln p/d(1/T)], \quad (2)$$

with that obtained from the second and third laws of thermodynamics. From statistical mechanical relations one finds for the heat of sublimation (at 0°K) of a crystalline solid to a perfect monatomic gas

$$\Delta H_0^0 = T\left\{-R \ln p + R \ln\left[\frac{(2\pi k)^{3/2}}{h^3 N_0^{5/2}}\right] + R \ln T^{5/2} M^{3/2} + R \ln RQ + \frac{H_s^0}{T} - S_s^0 - 1/T \int_p^1 V_s dp\right\}, \quad (3)$$

in which p is the vapor pressure at a temperature T, Q is the electronic partition function for the gas, H_s^0 is the heat content of the solid, S_s^0 is the entropy of the solid, and the other symbols have their customary significance. From the heat of sublimation and the heat of fusion one can then calculate a heat of vaporization to compare with that calculated from Eq. (2). At the melting point, 1406°K, Eq. (3) becomes

$$\Delta H_0^0 = 1.406(-R \ln p_m + 46.280) \text{ kcal/mole}. \quad (4)$$

In the evaluation of the constant in this equation the last term in Eq. (3) was neglected. The partition function was evaluated from data by Kiess, Humphreys, and Laun,[5] and the heat content and entropy of the solid have been calculated from data reported by Ginnings and Corruccini.[6] These data also interrelate the heat of sublimation at the melting point ΔH_{1406} and that at 0°K.

$$\Delta H_{1406} = \Delta H_0 - 5.2 \text{ kcal/mole}.$$

Since $\Delta H_{1406} = \Delta H_v + \Delta H_f$ in which ΔH_f is the heat of fusion, one finds that the heat of sublimation can also be calculated from Eq. (2) by the expression

$$\Delta H_0 = \Delta H_v + 5.2 + \Delta H_f. \quad (5)$$

B. Apparatus and Procedure

Aside from some minor alterations, the apparatus was identical to the one used by Erway and Simpson.[7] A shutter was provided to protect the optical window between pyrometer readings. A variable leak was provided at the throat of the divergent nozzle mercury vapor pump. This consisted of a brass Hoke needle valve controlled by a 600:1 reducing drive. With this control the pressure at the ion gauge could be changed by as little as 10 percent at 10^{-7} mm Hg with a full atmosphere of pressure behind the valve. The position of the drive was not reproducible, but the pressure remained constant for a given setting for long periods of time. The tantalum effusion cell (orifice area = 0.2247 ±0.0008 cm²; orifice-to-collimator distance = 7.883 ±0.005 cm) was also the same as that described by Erway and Simpson[7] except that the inner nested cups were drawn from sheet tantalum. Unfortunately, even tantalum may not be the most desirable material to use for a crucible to contain uranium. Although there is no evidence that the two materials form solid solutions, tantalum is soluble in liquid uranium. However, the solubility has been determined[8] as a function of temperature and as shown later the correction for the solubility is not sufficiently large to cause an appreciable error in either the vapor pressure or the heat of vaporization.

The platinum disks (0.75×0.005 inch) on which the vapor condensed were cleaned chemically with nitric acid and then heated to about 500°C just prior to their introduction into the apparatus. As determined by actual measurement the target *in situ* attained a temperature of less than 200°C with the oven at the highest temperature. Although this would appear to be a sufficiently low temperature to condense all of the uranium, a further test of the fraction condensing was carried out. A 0.5-inch hole was drilled through one target holder and this holder was loaded with two platinum disks with 0.25-inch holes through their centers. The target behind the altered holder was then also exposed to the uranium beam; any atoms reflected from the third target would condense on the back of the second. As shown by fission counting there was no uranium on the middle target. Hence all the uranium arriving at a target must have condensed.

The temperature was measured with a disappearing filament pyrometer which was standardized against a calibrated band lamp. All readings were corrected for the transmissivity of interposed window and prism.

The uranium in the form of wire containing about 93 percent U^{235} was cleaned anodically in an electrolyte of 46 percent concentrated sulfuric acid and 6 percent glycerin. Within one hour after the metal (77.6 mg) was cleaned it was placed in the apparatus and the latter was evacuated.

C. Experimental Data

Since preliminary experiments had indicated a possible effect of the residual gases of the vacuum, a series of exposures was made to measure this effect quantitatively. In the first series of exposures the uranium was evaporated with the lowest obtainable background pressure. In three subsequent series (Exposure Series *b* through *d*) oxygen was admitted at successively greater pressures. These four series of exposures were prepared on successive days, and throughout this period liquid nitrogen was maintained

[5] Kiess, Humphreys, and Laun, J. Research Natl. Bur. Standards 37, 57 (1946).

[6] D. C. Ginnings and R. J. Corruccini, Atomic Energy Commission Document MDDC-589, January 23, 1947.

[7] N. D. Erway and O. C. Simpson, J. Chem. Phys. 18, 953 (1950).

[8] Schramm, Gordon, and Kaufmann, Atomic Energy Commission Document AECD-2686, August 26, 1949.

in that part of the apparatus surrounding the targets and collimator. The last series of exposures was prepared after a lapse of three days during which time the liquid nitrogen was not maintained in this container. The pressure in the vacuum system during the last series was about the same as during the first series. In all these experiments the pressure in the system was sufficiently low so that scattering of the beam could be neglected.

The data which are presented in Fig. 1 give the values summarized in Table I.

III. DISCUSSION OF DATA

A. Internal Consistency

As stated previously, the calculation of the heat of vaporization and/or sublimation by two different procedures and a knowledge of the heat of fusion enables one to examine the measurements for internal consistency. Although the heat of fusion of uranium has not been measured, one can make an estimate of a value which is sufficiently accurate for the present purpose. Unless uranium is vastly different from the other elements it should have an entropy of fusion of about 2 or 3 eu and hence a heat of fusion of about 4 kcal/mole. Examination of the values for this quantity listed in Table I shows that in only the cases of the extremely good vacuum does the calculated heat of fusion agree with this estimation. Even in the absence of a more complete analysis of the data, it would seem reasonable to accept the first series as representative of pure uranium. However, as shown below it is possible to derive a relation which describes the data quantitatively in such a manner that exposure series *b*, *c*, *d*, and *e* extrapolate to exposure series *a* and a reasonable value for the heat of fusion.

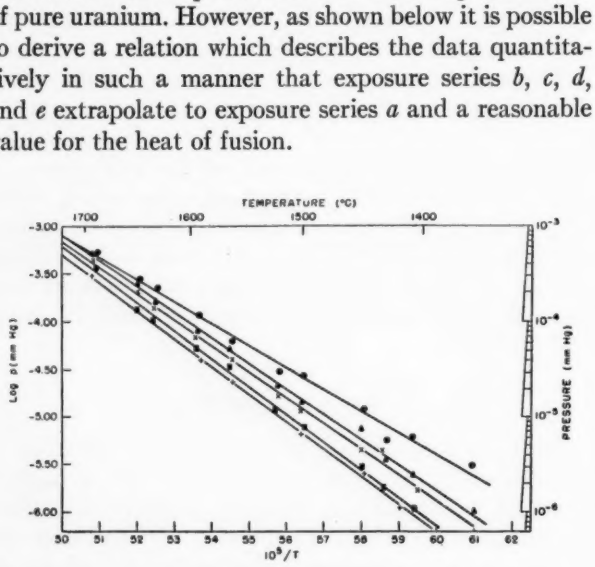

FIG. 1. Experimental vapor pressure *vs* reciprocal temperature at varying residual pressures in vacuum system.

	Pressure in vacuum system with oven cold
● Series *a*	4×10^{-8} mm
▲ Series *b*	4×10^{-7} mm
× Series *c*	1×10^{-6} mm
■ Series *d*	5×10^{-6} mm
+ Series *e*	4×10^{-8} mm

B. Role of Oxygen

As shown by preliminary experiments the presence of both oxidized metal in the oven and oxygen in the vacuum vessel suppresses the rate of effusion of uranium from the oven. Hence it appeared to be obvious that the role of oxygen present in the vacuum system is to produce an oxide of uranium. One can, however, suggest several mechanisms by which an oxide could produce the observed effect.

(1) An oxide may form which is soluble in liquid uranium.

(2) The uranium may become completely oxidized so that the dissociation pressure (i.e., the partial pressure of uranium over an oxide) is measured.

(3) The oxide may form a high electronic work function surface so that an appreciable number of uranium ions leave the orifice. These may or may not be collected.

(4) An impervious oxide film may form on the liquid uranium surface and suppress the rate of evaporation of the metal.

The first mechanism seems unlikely for the following reason. For an unsaturated solution (i.e., unsaturated with oxide) the effusion rate for a given amount of oxide should depend upon the amount of metal in the effusion cell. An experimental comparison, however, showed that the suppression of the effusion rate is independent of the amount of metal. For a saturated solution the oxide solubility would probably increase with increasing temperature and hence would cause a decrease in the numerical value of the slope of log p *vs* $1/T$ with increasing oxygen or oxide whereas the observed effect is a decrease in the slope.[9] The second suggested mechanism is not indicated by the data since a logarithmic plot of the experimental vapor pressure *vs* the oxygen pressure is not linear. At present the authors are not prepared to examine the third mechanism listed above. However, it appears doubtful that there were any appreciable number of positive uranium ions collected in exposure series *a* at least for reasons which will be discussed later. Although one might infer that the presence of the oxide film would not decrease the vapor pressure measured by the Knudsen method, a detailed examination of the quantitative influence of an impervious oxide layer reveals that the rate of effusion will be suppressed and that the mechanism listed last is quite plausible.

The role of the oxygen can be formulated as follows. One considers a Knudsen cell containing oxygen gas, liquid uranium, gaseous uranium, solid uranium oxide, and gaseous uranium oxide. The partial pressures are sufficiently low so that the frequency of gaseous collisions is extremely small compared with the frequency

[9] This second statement follows from the Raoult's law with dN_u/dT negative. Therefore

$$|d\ln p_s/d(1/T)| < |d\ln p_u/d(1/T)|.$$

of collision at the wall. If the oxide is insoluble in the liquid, it will form a layer over a part of the metal (assumed to cover the entire inside of the cell) so that the rate of evaporation of the metal through the oxide will be negligible. (It is assumed that a monolayer is sufficient to suppress the evaporation of the metal.) One can then assume that in a relatively short time a steady-state condition is attained in which at a given temperature and pressure of oxygen in the vacuum vessel the number of moles of each gaseous species (i.e., O_2, U, and UO_x) and the fraction of the surface covered are constant with time. A detailed balancing of each of these molecular forms requires that (1) the rate of change of the oxygen in the cell equals the rate of effusion into the cell from the vacuum minus the rate of effusion out of the cell minus the net rate of reaction with the liquid metal and the impervious oxide phase; (2) the rate of change of uranium in the gas phase equals the rate of evaporation minus the rate of condensation minus the rate of effusion out of the orifice; (3) the rate of change of the oxide in the gas phase equals the rate of evaporation minus the rate of condensation minus the rate of effusion out of the orifice; and (4) the rate of change of a layer of the oxide in the solid phase equals the rate of formation plus the rate of condensation minus the rate of evaporation.

These statements can be written as algebraic equations if one defines:

A = the initial area of liquid metal before oxidation;
s = area of the orifice in the cell;
f = fraction of A covered with oxide;
p_u = vapor pressure of uranium metal;
p_x = vapor pressure of some oxide UO_x;
p_0 = pressure of oxygen in the vacuum vessel;
π_u = steady-state partial pressure of uranium in the cell;
π_x = steady-state partial pressure of oxide in the cell;
π_0 = steady-state partial pressure of oxygen in the cell;
T_0 = temperature of oxygen in the vacuum vessel, and
n = number of moles of oxide formed per mole of oxygen reacting

(i.e., $n\mathrm{U}+\mathrm{O}_2=n\mathrm{UO}_x$ or $\mathrm{n}=2/x$).

In the same order as listed above the expressions are

$$\frac{dN_0}{dt}=\frac{p_0 s}{(2\pi M_0 RT_0)^{1/2}}-\frac{\pi_0 s}{(2\pi M_0 RT)^{1/2}}-\frac{\pi_0 A}{(2\pi M_0 RT)^{1/2}}, \quad (6)$$

$$\frac{dN_u}{dt}=\frac{p_u A(1-f)}{(2\pi M_u RT)^{1/2}}-\frac{\pi_u A}{(2\pi M_u RT)^{1/2}}-\frac{\pi_u s}{(2\pi M_u RT)^{1/2}}, \quad (7)$$

$$\frac{dN_x}{dt}=\frac{p_x A f}{(2\pi M_x RT)^{1/2}}-\frac{\pi_x A}{(2\pi M_x RT)^{1/2}}-\frac{\pi_x s}{(2\pi M_x RT)^{1/2}}, \quad (8)$$

TABLE I. Summary of results.

Exposure series	A[a]	B[a]	Heat of vaporization[b] (kcal/mole)	Heat of sublimation by third law[b] (ΔH_0^0) (kcal/mole)	Heat of fusion (kcal/mole)
a	23 031±492	8.378±0.275	106.8	116.6	4.6
b	26 846±238	10.293±0.133	124.2	121.7	−7.7
c	27 069±459	10.335±0.253	125.2	122.5	−7.9
d	29 376±303	11.444±0.167	135.8	125.9	−15.1
e	29 082±106	11.211±0.056	134.5	126.0	−13.7

[a] $\mathrm{Log}p(\mathrm{mm})=(-A/T)+B$.
[b] Corrected for the solubility of tantalum in liquid uranium: $\log N_u=(313/T)-0.215$.

and

$$\frac{d(\mathrm{UO}_x)}{dt}=\frac{n\pi_0 A(1-f)}{(2\pi M_0 RT)^{1/2}}+\frac{\pi_x A}{(2\pi M_x RT)^{1/2}}-\frac{p_x A f}{(2\pi M_x RT)^{1/2}}. \quad (9)$$

In writing these expressions we have assumed that all reaction, condensation, and vaporization coefficients are unity. Upon comparing Eqs. (6) and (9) one might infer that a term to account for the reaction of the oxygen with the oxide has been omitted from the latter. However, since it has been assumed that a monolayer is sufficient to suppress the evaporation of the metal, this reaction is not effective and hence should not be included. In other words the assumption is made that the oxygen reacts with the oxide without increasing the fraction of the surface covered with oxide. In view of the fact that the rate of oxidation of a metal such as uranium does not decrease appreciably until a thick coating relative to a few atomic layers has formed, it also does not appear to unreasonable to assume that the fraction of the oxygen reacting with the oxide is unity.

According to the assumption regarding the steady-state condition the left side of each of these equations is zero. Hence one can eliminate f and π_0 from the expressions to obtain the relations for π_u and π_x. These are

$$\pi_u=p_u[A/(A+s)-\pi_x/p_x], \quad (10)$$

and

$$\pi_x=\frac{np_0p_x(TM_x/T_0M_0)^{1/2}[A/(A+s)]}{np_0(TM_x/T_0M_0)^{1/2}+p_x}. \quad (11)$$

Since the experimental vapor pressures p_e were calculated on the basis of the assumption that all the uranium is in the form of atomic uranium, one writes that

$$p_e=\pi_u+(M_u/M_x)^{1/2}\pi_x. \quad (12)$$

If the values of π_u and π_x as given by Eqs. (10) and (11) are substituted into Eq. (12) one finds that

$$p_e=[A/(A+s)]\{p_u-[p_u/p_x-(M_u/M_x)^{1/2}]\times p_x[p_0/(p_0+P)]\}, \quad (13)$$

in which

$$P=(p_x/n)(T_0M_0/TM_x)^{1/2}. \quad (14)$$

Qualitatively Eq. (13) predicts the observed data. If $p_u>p_x$ then the experimental vapor pressure will decrease with increasing oxygen pressure. To find rigorously whether the data agree quantitatively with Eq. (13), a knowledge of the parameter P is required. Unfortunately, a number of the quantities contained in Eq. (14) are not known with any great accuracy. For example, the exact values of p_x, n, A, M_x, and T_0 are not known with reasonable certainty. However P can be treated as an experimental parameter which is determined from Eq. (13) for each temperature by minimizing the sum of the squares of the residuals.

To effect this analysis one must know the partial pressure of the oxygen in the vacuum vessel. Since the residual gases in a vacuum system are mostly carbon dioxide and water and/or perhaps carbon monoxide and hydrogen in the presence of hot tantalum, one cannot accept the ion gauge reading as representing the oxygen pressure. Therefore, with a residual pressure of the order of 5×10^{-8} mm Hg a tenable assumption is that the partial pressure of oxygen is of the order of 10^{-8} and that this value may be considered as being zero for all practical purposes when compared with pressures of the order of 4×10^{-7} mm Hg or greater. On this basis then the partial pressures of oxygen in exposure series *b*, *c*, and *d* are obtained by subtracting the ion gauge readings in exposure series *a* from the corresponding readings (i.e., at corresponding temperatures) in these three cases. In other words the data are analyzed on the basis of the oxygen admitted into the system.

As shown in Fig. 2 the experimental vapor pressure p_e does appear to depend upon $p_0/(p_0+P)$ in a linear manner. Furthermore, the value of P is of the order expected since a value in the range of 10^{-6} mm Hg is indicated according to Eq. (14). In addition one can show that the values for the experimental vapor pressure obtained in exposure series *e* agree with the proposed mechanism. Since the vapor pressure of the oxide is less than that of the metal for all temperatures employed in this investigation and since the rate of formation of the oxide is comparable with the rate of effusion, the oxide cannot be vaporized out of the oven without also distilling out the metal. Therefore one cannot expect that the effect of the oxygen can be removed in a short time by evacuating the oxygen from the system. In view of this and the fact that the oven was exposed to the water vapor which had accumulated on the liquid nitrogen trap at the top of the apparatus, further oxidation of the metal could have occurred between exposure series *d* and *e*. Hence the authors believe that the vapor pressures measured in exposure series *e* should correspond to the values for large oxygen pressure or a value of $p_0/(p_0+P)$ very close to unity. Inspecting Fig. 2 one observes that the deviations of the values for exposure series *e* from the extrapolated values at $p_0(p_0+P)=1$ for exposure series *a*, *b*, *c*, and *d* are not unreasonable. Moreover, a statistical comparison of these values shows that these points agree with the others.

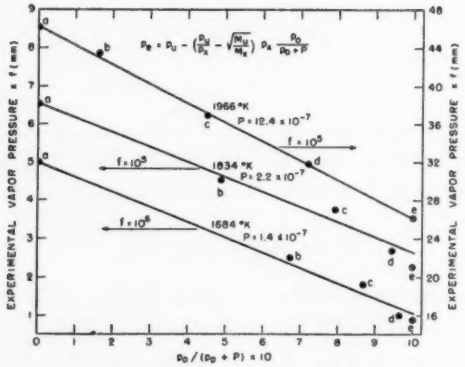

FIG. 2. Test of Eq. (13).

In view of the agreement discussed above, the authors believe that the theory is a reasonably correct one and therefore the partial pressure of uranium above a solution of uranium and tantalum is given by the extrapolated value of p_e at $p_0/(p_0+P)=0$. Extrapolations were carried out at ten different temperatures. The least squares equation for these values is

$$\log p_e(\text{mm})=-\frac{(23017\pm21)}{T}+(8.3683\pm0.011). \quad (15)$$

Some of the difficulties involved in the determination of the vapor pressure of an easily oxidized metal which has a low volatility at temperatures of measurement can be more readily ascertained now by the mechanism described. For example as shown in Fig. 3 the experimentally measured vapor pressure is extremely sensitive to the oxygen pressure if the vapor pressure is as small as ten times the oxygen pressure. Even if the vapor pressure is 10^3 times the oxygen pressure, the measurements are affected by the residual oxygen in the vacuum system. It is important to observe that the sensitivity decreases with increasing oxygen pressure, so that at a pressure in the range of 10^{-6} to 10^{-5} mm Hg the effect is not great. These statements are true if the vapor pressure of the oxide is less than that of the metal as is usually the case for the lower oxides such as UO or UO_2. At higher oxygen pressures the higher oxides may form such as UO_3, and since in the case of uranium, tantalum, and tungsten at least these have a vapor pressure which is higher than the metal, $p_u/p_x>(M_u/M_x)^{1/2}$, and as shown by Eq. (13) the experimental vapor pressure will increase with increasing oxygen. This explains the fact that the vapor pressures reported by Derge and Cefola[2] were in general larger than the ones reported here. To circumvent completely these difficulties in the case of uranium it would be

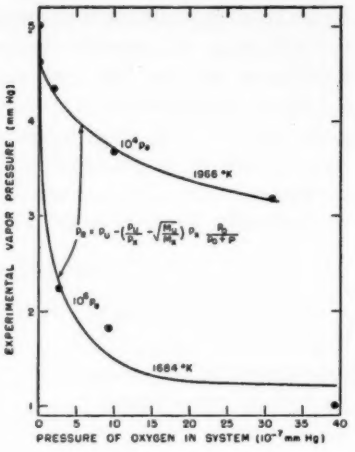

FIG. 3. Effect of oxygen on experimental vapor pressure.

desirable to make measurements at a temperature of about 2200°K in a vacuum of 10^{-8} mm Hg.

C. Correction for Tantalum

As stated previously, Schramm, Gordon, and Kaufmann[8] have determined the solubility of tantalum in liquid uranium. Since one would not expect the logarithm of the mole fraction of the uranium in the solution to be a linear function of reciprocal temperature, the presence of the tantalum should have introduced a curvature in the log p_e *vs* $1/T$ curves. However, the total effect is so small compared with the scatter of the data that one cannot expect to detect this curvature. This fact enables one to make a first-order correction without correcting the individual vapor pressure measurements. A plot of experimental values for logarithm of mole fraction of uranium *vs* $1/T$ is actually linear in the region of interest. The authors believe, however, that this is a "fortuitous" accident caused by an experimental error. Nevertheless, we accept the experimental curve so that the solubility of tantalum in uranium is represented by the equation

$$\log N_u = 313/T - 0.2145.$$

Since the vapor pressure of the uranium can be estimated by Raoult's law,

$$p_e = N_u p_u,$$

one finds that

$$\log p_u = \log p_e - 313/T + 0.2145. \qquad (16)$$

Comparing this equation with the values of the slope and intercept in Table I, one observes that the corrections for the tantalum solubility are of the same order as the errors. Therefore, a more accurate correction is not necessary.

D. Errors

A total probable error of ±0.3 percent was assigned to the inherent uncertainties in R and M and to the systematic uncertainties in ρ, r, d, and $\langle w_M' \rangle_{Av}$. The total probable error in the statistical uncertainties in t and in the counting varied from 1.1 percent to 4.8 percent for the shortest and longest exposures respectively. The scatter of the data, however, indicates some basic errors which were not determined specifically. It is quite probable that one basic error is associated with the oxide film. For example, it is possible that the surface oxide had broken momentarily during a part or all of an exposure causing p_e to be high relative to the others. However, because of the large number of exposures made, the over-all effect must be small. This is in evidence by the small probable error in the least squares treatment of the data.

Also considered was the possible source of error introduced by positive uranium ions. The more complete system which should be considered in these experiments is as follows:

$$U_s = U_g.$$
$$e_s = e_g.$$
$$U_g = U_g^+ + e_g.$$

If one collects on the platinum plates only the neutral uranium atoms U_g, then one needs no knowledge concerning the positive ions and one calculates the true vapor pressure and heat of vaporization. On the other hand, if one collects both neutral atoms and positive ions then the ratio of their partial pressures is given by the expression

$$p_+/p = (Q_+/Q) \exp[(\phi - I)/RT],$$

in which the Q's are the partition functions, I is the ionization potential of uranium, and ϕ is the work function of the surface from which the ions are evaporating. At 1406°K, $Q = 19.63$ and $Q_+ = 26.90$. The ionization potential of uranium has been estimated by Hubbard and Meggers[10] to be 4 ev. The question now arises as to the more nearly correct value of ϕ to be employed. Since there are essentially no collisions in the gas phase at pressures of the order of 10^{-5} mm Hg, each uranium atom or ion must suffer its last contact with the condensed uranium and/or uranium oxide surface before leaving the oven. If there is no oxide present (exposure series *a*), then the value of ϕ may be as low as 3.27 ev.[11] This corresponds to a value of $p_+/p = 3.4 \times 10^{-3}$ and indicates that in this case there is no appreciable error because of positive ions. In the presence of oxide, however, ϕ may be as large as 5.94 ev,[12] in which event $p_+/p = 6.3 \times 10^6$ and there may or may not be an error because of positive ions. From these estimates one concludes that the value for the vapor pressure and heat of vaporization obtained in

[10] H. D. Hubbard and W. F. Meggers, *Key to Periodic Chart of the Atoms* (W. M. Welch Scientific Company, Chicago, Illinois, 1950).
[11] W. L. Hole and R. W. Wright, Phys. Rev. **56**, 785 (1939).
[12] E. G. Rauh and R. J. Thorn, unpublished data.

exposure series *a* are probably not in error because of positive ions, but that the interpretation of Exposure Series *b*, *c*, *d*, and *e* may be only partially complete.

IV. SUMMARY

In view of the fact that all the data in Table I can be interpreted quantitatively in terms of an impervious oxide film and because the extrapolated values are internally consistent, the authors conclude that the vapor pressure of uranium metal is represented by the equation

$$\log p_u(\text{mm}) = -\frac{(23330\pm 21)}{T} + (8.583\pm 0.011). \quad (17)$$

From this we conclude a value of 106.7±0.1 kcal/mole for the heat of vaporization, a value of 116.6±0.1 kcal/mole for the heat of sublimation at 0°K, and 4.7±0.2 kcal/mole for the heat of fusion. The error given for the last quantity is a statistical error only. Since there is considerable uncertainty in the partial pressures of oxygen, the error in the heat of fusion is undoubtedly larger than 0.2 kcal/mole.

ACKNOWLEDGMENTS

The authors are indebted to W. C. Bentley for the fission counts of the uranium deposits, to O. C. Simpson for suggesting the measurements, and to G. H. Winslow for helpful discussions.

THE JOURNAL OF CHEMICAL PHYSICS VOLUME 22, NUMBER 8 AUGUST, 1954

High-Temperature Equation of State by a Perturbation Method. I. Nonpolar Gases*

ROBERT W. ZWANZIG
Sterling Chemistry Laboratory,† Yale University, New Haven, Connecticut

(Received March 2, 1954)

A theoretical study is made of the equations of state of argon and nitrogen, at high temperatures and densities. The intermolecular potential used is of the Lennard-Jones form, with an adjustable rigid sphere cutoff. A perturbation theory is developed, by which the thermodynamic properties of one system may be related to those of a slightly different system and to the difference in the intermolecular potentials of the two systems. In this article, the unperturbed system is a rigid sphere fluid, and the Lennard-Jones potential is the perturbation. The results are in fair agreement with experiment, and also lead to an experimental test of the theoretical rigid sphere equation of state.

I.

At very high temperatures, the equation of state of a gas is determined largely by the forces of repulsion between its component molecules. At somewhat lower temperatures, it should be possible to obtain the equation of state by considering forces of attraction as perturbations on the forces of repulsion. In this article, we shall investigate the equations of state of argon and nitrogen from this point of view. (The results will first be obtained in a form applicable to all gases whose molecules interact with a certain type of potential.)

The experimentally available PVT data on the noble gases may be represented, at least at high temperatures, by the equation

$$\frac{pv}{RT} = \Phi_0(v) + \frac{a_1(v)}{RT} + \frac{a_2(v)}{(RT)^2} + \cdots. \quad (1)$$

In the cases of argon and nitrogen, this equation reproduces the data satisfactorily over the temperature range 0°C to 150°C, and up to a density of six or seven hundred amagat units. Figure 1 illustrates this agreement in the case of argon. At temperatures below 0°C the $1/T^2$ term becomes important. At temperatures above 150°C, there is not much available data with which this equation may be tested; therefore, extrapolation to extremely high temperatures is unsafe. However, the assumption that the equation linear in $1/T$ is valid at high temperatures is a useful working hypothesis, and is supported to some extent by the results to be described in this article.

We shall choose for the repulsion a rigid sphere potential with an appropriate diameter, and for the attraction the Lennard-Jones potential. Then, we are able to predict the high-temperature limit $\Phi_0(v)$ for argon and nitrogen within an error of five or ten percent over the entire density range. We can also predict the limiting slope $a_1(v)$, with less accuracy. A virial expansion, containing second and third virial coefficients, is not at all accurate at the high end of this density range.

The parameters of the Lennard-Jones potential are determined by an analysis of experimental second virial coefficient data. The diameter of the rigid spherical core is kept as an adjustable parameter. The high temperature limit $\Phi_0(v)$ is not sensitive to the exact value of this diameter, over a reasonable range of variation, but the

* This work was supported by the U. S. Office of Naval Research, under Contract Nonr-410(00) with Yale University.
† Contribution No. 1218.

slope $a_1(v)$ is quite sensitive. The comparison between our theory and experiment provides a partial experimental verification of the theoretical equation of state of a gas composed of rigid spheres, which was developed by Kirkwood, Maun, and Alder,[1] up to a density of about half that of close packed spheres.

II.

The theoretical results described in this article are obtained by performing a perturbation expansion on the partition function of the system. Special cases of this expansion have been used in various contexts, e.g., in the theory of order-disorder in binary solid solutions[2] and in the theory of the equation of state of molecules interacting with multipole electrostatic potentials.[3] (We shall describe numerical calculations on the latter theory in a future article.) Also, the theory of conformal solutions developed by Longuet-Higgins[4] may be obtained in this way, although actually he used a different procedure. Since the general results of this perturbation expansion appear to be widely useful, we shall describe its derivation in some detail.

The thermodynamic properties of a system may be obtained from its partition function. Since we are interested specifically in the equation of state of a system which obeys classical statistical mechanics, we need only the configurational contribution to the partition function. The system consists of N molecules in a volume v, and its total potential energy is V_N. The configurational free energy $\bar{A}_N$ is given by

$$\exp(-\beta\bar{A}_N)=Q_N=\frac{1}{N!}\int_v\cdots\int_v \times\exp(-\beta V_N)d\tau_1\cdots d\tau_N \quad (2)$$

$$\beta=1/kT.$$

V_N is a function of the configuration of each molecule, and $\int d\tau_i$ is an integral over the entire configuration space of the ith molecule. At this point, we make no assumptions about the coordinates needed to specify completely the configuration of a molecule.

We assume that the potential energy may be separated into two parts,

$$V_N=V_N^{(0)}+V_N^{(1)}, \quad (3)$$

where $V_N^{(0)}$ is the potential energy of an unperturbed system, and $V_N^{(1)}$ is the perturbation. The partition function of the unperturbed system is

$$\exp(-\beta\bar{A}_N^{(0)})=Q_N^{(0)}=\frac{1}{N!}\int\cdots\int \times\exp(-\beta V_N^{(0)})d\tau_1\cdots d\tau_N. \quad (4)$$

The probability of any particular configuration of the unperturbed system is

$$P_0^{(N)}=\exp\beta(\bar{A}_N^{(0)}-V_N^{(0)});$$

$$\int\cdots\int P_0^{(N)}d\tau_1\cdots d\tau_N=1. \quad (5)$$

When Eq. (2) is multiplied and divided by $Q_N^{(0)}$, we get

$$Q_N=Q_N^{(0)}\int\cdots\int P_0^{(N)}\exp(-\beta V_N^{(1)})d\tau_1\cdots d\tau_N \quad (6)$$

or

$$\exp-\beta(\bar{A}_N-\bar{A}_N^{(0)})\equiv\exp(-\beta\bar{A}_N^{(1)}) =\langle\exp(-\beta V_N^{(1)})\rangle_0 \quad (7)$$

where $\bar{A}_N^{(1)}$ is the contribution to the free energy from the perturbation, and the average of $\exp(-\beta V_N^{(1)})$ is performed over the unperturbed ensemble,

$$\langle\exp(-\beta V_N^{(1)})\rangle_0=\int\cdots\int P_0^{(N)} \times\exp(-\beta V_N^{(1)})d\tau_1\cdots d\tau_N. \quad (8)$$

We wish to express the perturbation free energy as a power series in β,

$$\bar{A}_N^{(1)}=\sum_{n=1}^{\infty}\frac{\omega_n}{n!}(-\beta)^{n-1} \quad (9)$$

so that

$$\begin{aligned}\exp(-\beta\bar{A}_N^{(1)})&=\exp\left(\sum_{n=1}^{\infty}\frac{\omega_n}{n!}(-\beta)^n\right)\\&=\langle\exp(-\beta V_N^{(1)})\rangle_0\\&=\sum_{k=0}^{\infty}\frac{(-\beta)^k}{k!}\langle\alpha^k\rangle_0;\\ V_N^{(1)}&\equiv\alpha,\end{aligned} \quad (10)$$

where we have temporarily replaced $V_N^{(1)}$ by α, for the sake of convenience in notation. Equation (10) defines the ω_n in terms of the $\langle\alpha^k\rangle_0$. This relationship may be obtained by using the theory of Thiele semi-invariants.[5] Since this theory is not widely known, we shall outline a procedure which leads to the desired relations.

When $\exp(-\beta\bar{A}_N^{(1)})$ is expanded, and the multinomial expansion theorem is used, we get

$$\exp(-\beta\bar{A}_N^{(1)})=\sum_{k=0}^{\infty}\frac{1}{k!}\left[\sum_{n=1}^{\infty}\frac{\omega_n}{n!}(-\beta)^n\right]^k$$

$$=\sum_{k=0}^{\infty}\frac{1}{k!}\sum_{\substack{n_j\\(\Sigma n_j=k)}}k!\prod_{j=1}^{\infty}\frac{1}{n_j!}\left[\frac{(-\beta)^j\omega_j}{j!}\right]^{n_j}$$

[1] Kirkwood, Maun, and Alder, J. Chem. Phys. **18**, 1040 (1950).
[2] J. G. Kirkwood, J. Chem. Phys. **6**, 70 (1938).
[3] J. A. Pople, Proc. Roy. Soc. (London) **215A**, 67 (1952).
[4] H. C. Longuet-Higgins, Proc. Roy. Soc. (London) **205A**, 247 (1951).
[5] H. Cramér, *Mathematical Methods of Statistics* (Princeton University Press, Princeton, 1946), p. 185.

where the summation $\sum n_j$ is a multiple sum over all values of $n_1, n_2, \cdots$ subject to the restriction $\sum_1^\infty n_j = k$. When powers of β are collected, we obtain

$$\exp(-\beta \bar{A}_N^{(1)}) = \sum_{k=0}^{\infty} \sum_{\substack{n_j \\ (\Sigma n_j = k)}} (-\beta)^{\Sigma j n_j} \prod_{j=1}^{\infty} \frac{1}{n_j!} \left(\frac{\omega_j}{j!}\right)^{n_j}$$

$$= \sum_{k=0}^{\infty} \sum_{s=0}^{\infty} (-\beta)^s \sum_{\substack{n_j \\ (\Sigma n_j = k) \\ (\Sigma j n_j = s)}} \prod_{j=1}^{\infty} \frac{1}{n_j!} \left(\frac{\omega_j}{j!}\right)^{n_j} \tag{11}$$

$$= \sum_{s=0}^{\infty} (-\beta)^s \sum_{\substack{n_j \\ (\Sigma j n_j = s)}} \prod_{j=1}^{\infty} \frac{1}{n_j!} \left(\frac{\omega_j}{j!}\right)^{n_j}.$$

The summation over s leads to the restriction $\sum j n_j = s$ and the summation over k removes the restriction $\sum n_j = k$. Since Eqs. (10) and (11) contain expansions in powers of β of the same quantity, we may equate coefficients of like powers of β, and get

$$\langle \alpha^k \rangle_0 = k! \sum_{\substack{n_j \\ (\Sigma j n_j = k)}} \prod_{j=1}^{\infty} \frac{1}{n_j!} \left(\frac{\omega_j}{j!}\right)^{n_j}. \tag{12}$$

For the first few values of k, we have

$$\begin{aligned} \langle \alpha \rangle_0 &= \omega_1 \\ \langle \alpha^2 \rangle_0 &= \omega_2 + \omega_1^2 \\ \langle \alpha^3 \rangle_0 &= \omega_3 + 3\omega_2\omega_1 + \omega_1^3 \\ \langle \alpha^4 \rangle_0 &= \omega_4 + 4\omega_3\omega_1 + 3\omega_2^2 + 6\omega_2\omega_1^2 + \omega_1^4. \end{aligned} \tag{13}$$

These may be inverted to give the desired expressions

$$\begin{aligned} \omega_1 &= \langle \alpha \rangle_0 \\ \omega_2 &= \langle \alpha^2 \rangle_0 - \langle \alpha \rangle_0^2 \\ \omega_3 &= \langle \alpha^3 \rangle_0 - 3\langle \alpha^2 \rangle_0 \langle \alpha \rangle_0 + 2\langle \alpha \rangle_0^3 \\ \omega_4 &= \langle \alpha^4 \rangle_0 - 4\langle \alpha^3 \rangle_0 \langle \alpha \rangle_0 - 3\langle \alpha^2 \rangle_0^2 + 12\langle \alpha^2 \rangle_0 \langle \alpha \rangle_0^2 - 6\langle \alpha \rangle_0^4 \end{aligned} \tag{14}$$

which are the first four cases of the general result

$$\omega_j = j! \sum_{\substack{n_s \\ (\Sigma s n_s = j)}} (-1)^{\Sigma n_s - 1} (\Sigma n_s - 1)! \times \prod_{s=1}^{\infty} \frac{1}{n_s!} \left(\frac{\langle \alpha^s \rangle_0}{s!}\right)^{n_s}. \tag{15}$$

(The proof that this is equivalent to Eq. (12) is somewhat involved, and will not be presented here.)

Thus we have shown that at high temperatures, the free energy is

$$\begin{aligned} \bar{A}_N &= \bar{A}_N^{(0)} + \omega_1 - \omega_2/2kT + O(1/kT)^2 \\ \omega_1 &= \langle V_N^{(1)} \rangle_0 \\ \omega_2 &= \langle (V_N^{(1)})^2 \rangle_0 - \langle V_N^{(1)} \rangle_0^2. \end{aligned} \tag{16}$$

Let us now consider the case where the perturbation may be expressed as a sum of pair potentials

$$V_N^{(1)} = \tfrac{1}{2} \sum_{i \neq j}^{N} V^{(1)}(i,j). \tag{17}$$

(We use the letters i, j to represent the coordinates of the molecules i and j in their configuration spaces.) Then,

$$\omega_1 = \tfrac{1}{2} \sum_{i \neq j}^{N} \langle V^{(1)}(i,j) \rangle_0. \tag{18}$$

The probability distribution function in the configuration space of molecules 1 and 2 is

$$P_0^{(2)}(1,2) = \int \cdots \int P_0^{(N)} d\tau_3 \cdots d\tau_N. \tag{19}$$

If all the molecules are identical, we obtain

$$\omega_1 = \tfrac{1}{2} N(N-1) \int\int V^{(1)}(1,2) P_0^{(2)}(1,2) d\tau_1 d\tau_2. \tag{20}$$

In order to express ω_2 in terms of reduced distribution functions, we must evaluate

$$\begin{aligned} \langle (V_N^{(1)})^2 \rangle_0 &= \tfrac{1}{4} \langle \sum_{i \neq j}^{N} \sum_{k \neq l}^{N} V^{(1)}(i,j) V^{(1)}(k,l) \rangle_0 \\ &= \tfrac{1}{4} \sum_{ijkl}{}' \langle V^{(1)}(i,j) V^{(1)}(k,l) \rangle_0 \\ &\quad + \sum_{ijk}{}' \langle V^{(1)}(i,j) V^{(1)}(j,k) \rangle_0 \\ &\quad + \tfrac{1}{2} \sum_{ij}{}' \langle [V^{(1)}(i,j)]^2 \rangle_0, \end{aligned} \tag{21}$$

where the summation sign $\sum'$ represents a summation over all the indicated indices, with no two of the indices allowed to be equal. We now define the distribution functions $P_0^{(3)}$ and $P_0^{(4)}$,

$$P_0^{(3)}(1,2,3) = \int \cdots \int P_0^{(N)} d\tau_4 \cdots d\tau_N \tag{22}$$

$$P_0^{(4)}(1,2,3,4) = \int \cdots \int P_0^{(N)} d\tau_5 \cdots d\tau_N. \tag{23}$$

Again, if all the molecules are identical, we obtain

$$\begin{aligned} \langle (V_N^{(1)})^2 \rangle_0 &= \frac{1}{4} \frac{N!}{(N-4)!} \int\int\int\int P_0^{(4)} V^{(1)}(1,2) \\ &\quad \times V^{(1)}(3,4) d\tau_1 d\tau_2 d\tau_3 d\tau_4 + \frac{N!}{(N-3)!} \\ &\quad \times \int\int\int P_0^{(3)} V^{(1)}(1,2) V^{(1)}(2,3) d\tau_1 d\tau_2 d\tau_3 \\ &\quad + \frac{1}{2} \frac{N!}{(N-2)!} \int\int P_0^{(2)} [V^{(1)}(1,2)]^2 d\tau_1 d\tau_2. \end{aligned} \tag{24}$$

Therefore, in the limit that N is very large, we get

$$\omega_2=\tfrac{1}{4}N^4\int\int\int\int[P_0^{(4)}(1,2,3,4)-P_0^{(2)}(1,2)P_0^{(2)}(3,4)]V^{(1)}(1,2)V^{(1)}(3,4)\times d\tau_1 d\tau_2 d\tau_3 d\tau_4+N^3\int\int\int P_0^{(3)}(1,2,3)\times V^{(1)}(1,2)V^{(1)}(2,3)d\tau_1 d\tau_2 d\tau_3+\tfrac{1}{2}N^2\int\int P_0^{(2)}(1,2)[V^{(1)}(1,2)]^2 d\tau_1 d\tau_2. \quad (25)$$

In this article we shall use only the correction ω_1. In the theory of a dipole gas, ω_2 also is needed. The higher-order terms are progressively more complicated.

III.

We shall now apply this perturbation theory to the calculation of the high-temperature behavior of a gas of molecules which interact with the potential

$$V(R)=V^{(0)}(R)+V^{(1)}(R)$$
$$V^{(0)}(R)=\begin{cases}\infty & (R\leq ca)\\ 0 & (R>ca)\end{cases} \quad (26)$$
$$V^{(1)}(R)=4\epsilon\left[\left(\frac{a}{R}\right)^{12}-\left(\frac{a}{R}\right)^{6}\right],$$

where c is a number between zero and one. This is a modified Lennard-Jones potential, whose well has a depth ϵ, which crosses the R axis at $R=a$, and which suddenly becomes infinitely steep at $R=ca$. The unperturbed system is a gas composed of rigid spheres of diameter ca. The advantage of introducing the parameter c is that we may make use of the special properties of a rigid sphere fluid, and still preserve the essential features of the Lennard-Jones potential. This could be accomplished by selecting a fixed value of c, say $c=1$. By allowing c to vary, we may consider a family of potentials whose repulsive parts vary in hardness. For argon and nitrogen, at the temperatures with which we are concerned, the Boltzmann factor $\exp(-V(R;c)/kT)$ for c about 0.9 or smaller is numerically almost exactly the same as the Boltzmann factor for the unmodified Lennard-Jones potential.

The free energy of the system is

$$\bar{A}_N=\bar{A}_N^{(0)}+\omega_i+O(1/kT) \quad (27)$$

where

$$\exp(-\beta\bar{A}_N^{(0)})=\frac{1}{N!}\int_v\cdots\int_v\times\exp(-\beta\textstyle\sum V^{(0)}(R_{ij}))d^3R_1\cdots d^3R_N \quad (28)$$

and

$$\omega_1=\tfrac{1}{2}N^2\int_v\int_v V^{(1)}(R_{12})P_0^{(2)}(R_1,R_2)d^3R_1 d^3R_2. \quad (29)$$

The radial distribution function $g_0^{(2)}$ is defined by

$$g_0^{(2)}(R_{12};v)=\frac{1}{v^2}P_0^{(2)}(\mathbf{R}_1,\mathbf{R}_1+\mathbf{R}_{12};v). \quad (30)$$

When surface effects are neglected, the integral of Eq. (29) may be transformed to the form

$$\omega_1=\frac{2\pi N^2}{v}\int_0^\infty R^2V^{(1)}(R)g_0^{(2)}(R;v)dR. \quad (31)$$

It is convenient to express the various quantities in these equations in terms of the properties of a fluid of rigid spheres with unit diameter, contained in a volume Nv^*. Therefore, we use the reduced units

$$x=R/ac$$
$$v^*=v/Na^3c^3$$
$$p^*=p(a^3c^3/\epsilon) \quad (32)$$
$$T^*=Tk/\epsilon.$$

The free energy per molecule of this reference fluid is $A_0(v^*)$. Then, the free energy of the unperturbed system is

$$\bar{A}_N^{(0)}=NA_0\left(\frac{v}{Na^3c^3}\right). \quad (33)$$

The radial distribution function of the reference fluid will be denoted by $g_0^{(2)}(x;v^*)$. Since

$$V^{(1)}(R)=V^{(1)}(acx)=\epsilon\left\{\frac{1}{c^6}\left(\frac{4}{x^{12}}-\frac{4}{x^6}\right)+\frac{1}{c^6}\left(\frac{1}{c^6}-1\right)\frac{4}{x^{12}}\right\} \quad (34)$$

we obtain

$$\frac{\omega_1}{N\epsilon}=\frac{2\pi}{v^*}\frac{1}{c^6}\left\{I_0(v^*)+\left(\frac{1}{c^6}-1\right)I_1(v^*)\right\} \quad (35)$$

where

$$I_0(v^*)=\int_0^\infty x^2\left(\frac{4}{x^{12}}-\frac{4}{x^6}\right)g_0^{(2)}(x;v)dx \quad (36)$$

and

$$I_1(v^*)=\int_0^\infty x^2\frac{4}{x^{12}}g_0^{(2)}(x;v)dx. \quad (37)$$

The factor c has been separated out, so that the integrals involve only properties of the fluid of rigid spheres with *unit* diameter. To calculate the pressure, we differentiate the free energy with respect to volume, and obtain

$$p^*=p_0^*-\frac{\partial}{\partial v^*}\frac{\omega_1}{N\epsilon}+O\left(\frac{1}{T^*}\right) \quad (38)$$

TABLE I. Reduced perturbation free energy $-\omega_1/N\epsilon$ on B−G and K basis.

$1/v^*$	$1/c$	1.00	1.02	1.04	1.06	1.08	1.10
0	B−G	0	0	0	0	0	0
	K	0	...	...	...	...	0
0.2	B−G	1.221	1.278	1.316	1.326	1.301	1.229
	K	1.164	...	...	...	...	1.229
0.4	B−G	2.621	2.715	2.757	2.728	2.607	2.364
	K	2.330	...	...	...	...	2.150
0.6	B−G	4.171	4.272	4.272	4.138	3.828	3.294
	K	3.553	...	...	...	...	2.972
0.8	B−G	5.845	5.918	5.827	5.517	4.924	3.968
	K	4.813	...	...	...	...	3.589
1.0	B−G	7.618	7.622	7.378	6.809	5.818	4.228
	K	6.185	...	...	...	...	4.070

or

$$\frac{pv}{RT}=\Phi=\Phi_0(v^*)+\frac{a_1^*(v^*)}{T^*}+O\left(\frac{1}{T^*}\right)^2 \tag{39}$$

where $\Phi_0=p_0^*v^*/T^*$ is the equation of state for the unperturbed system, and

$$a_1^*(v^*)=-v^*\frac{\partial}{\partial v^*}\frac{\omega_1}{N\epsilon}. \tag{40}$$

Equation (39) is of the same form as Eq. (1), since Φ_0 and a_1^* are functions of volume only.

Kirkwood, Maun, and Alder[1] have calculated $\Phi_0(v^*)$ and $g_0^{(2)}(x;v^*)$ by numerically solving a certain integral equation. This equation arises from the application of the superposition approximation to two different but equivalent and exact sets of equations, derived by Kirkwood and by Born and Green, for the probability densities $P_0^{(n)}$. The effect of the approximation is that both theories lead to an integral equation of the same form, but that this equation contains a parameter λ which depends on v^* differently in the two theories. By solving this integral equation in terms of λ, Kirkwood, Maun, and Alder thus obtained two sets of solutions in terms of v^*. We shall refer to these as the solutions with λ(K) and with λ(B−G). We have used their numerical results to evaluate $\omega_1/N\epsilon$ and $a_1(v^*)$. The results of our computations are presented in Tables I and II, along with $\Phi_0(v^*)$ which was interpolated from the tables in reference 1.

TABLE II. $\Phi_0(v^*)$ and $-a_1^*(v^*)$ on B−G and K basis.

		$-a_1^*(v^*)$						
$1/v^*$	$1/c$	1.00	1.02	1.04	1.06	1.08	1.10	$\Phi_0(v^*)$
0	B−G	0	0	0	0	0	0	1.00
	K	0	...	...	...	...	0	1.00
0.2	B−G	1.33	1.37	1.39	1.38	1.33	1.21	1.54
	K	1.16	...	...	...	...	1.07	1.52
0.4	B−G	2.95	3.00	2.97	2.83	2.55	2.10	2.43
	K	2.36	...	...	...	...	1.79	2.22
0.6	B−G	4.86	4.84	4.62	4.19	3.47	2.39	3.73
	K	3.79	...	...	...	...	2.17	3.18
0.8	B−G	6.89	6.71	6.23	5.37	4.03	2.11	5.40
	K	5.10	...	...	...	...	2.13	4.37

TABLE III. Second virial coefficient for modified Lennard-Jones potential.

	$-B^*(T^*,c)$				
$1/T^*$	0.2	0.4	0.6	0.8	1.0
c					
0	−0.0812	0.1042	0.3214	0.5680	0.8462
0.80	−0.0812	0.1042	0.3214	0.5680	0.8462
0.84	−0.0813	0.1042	0.3214	0.5680	0.8462
0.88	−0.0832	0.1040	0.3214	0.5680	0.8462
0.92	−0.0920	0.1014	0.3205	0.5677	0.8461
0.96	−0.1130	0.0886	0.3126	0.5626	0.8428
1.00	−0.1471	0.0581	0.2852	0.5379	0.8203

IV.

In order to compare the results of this calculation with experiment, we must find suitable values of a and ϵ. These parameters are most easily obtained from an analysis of the second virial coefficient of the gas. Since the assumed intermolecular potential depends upon a parameter c, the a and ϵ obtained by this analysis will depend on what value of c is used.

We define the second virial coefficient, in reduced units, by

$$B^*=B/2\pi a^3c^3=\int_{0x^2}^{\infty}(1-\exp(-\gamma(x)/T^*))dx \tag{41}$$

where

$$\gamma(x)=\begin{cases}\infty & (x\leq c)\\ 4\left(\dfrac{1}{x^{12}}-\dfrac{1}{x^6}\right) & (x>c).\end{cases} \tag{42}$$

Therefore,

$$B^*(T^*;c)=B^*(T^*;0)+\int_{0x^2}^{c}\exp\left[-4\left(\frac{1}{x^{12}}-\frac{1}{x^6}\right)\Big/T^*\right]dx. \tag{43}$$

$B^*(T^*;0)$ is the second virial coefficient for the ordinary Lennard-Jones potential, and is readily available. The integral in Eq. (43) is easily evaluated by numerical integration, and the resulting second virial coefficient is given in Table III. The special case, where $c=1$, has already been studied.[6]

Over the presently useful temperature range, $B^*(T^*;c)$ has practically the same shape as $B^*(T^*;0)$.

TABLE IV. Conversion factors for the Lennard-Jones parameters.

c	$\epsilon(c)/\epsilon(0)$	$a(0)/a(c)$
0	1.000	1.000
0.80	1.000	1.000
0.84	1.000	1.000
0.88	1.003	1.004
0.92	1.022	1.019
0.96	1.077	1.053
1.00	1.183	1.099

[6] Kirkwood, Lewinson, and Alder, J. Chem. Phys. 20, 929 (1952).

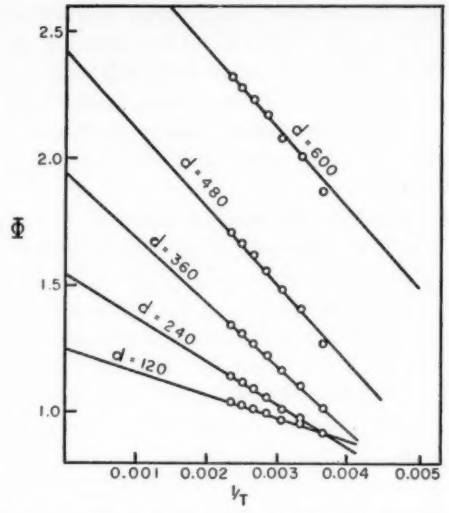

FIG. 1. Experimental data on argon. Density d in amagat units.

By comparing the positions of the Boyle temperature for various values of c, we can easily obtain $\epsilon(c)/\epsilon(0)$. Then, by comparing the magnitudes of B^* at some other point, we can obtain $a(c)/a(0)$. The values of the ratios obtained in this way are given in Table IV.

V.

We shall now compare the results of the theory with experimental data on argon[7] and nitrogen.[8] The experimental pv/RT was plotted as a function of $1/T$, and the linear part of the curve was extrapolated to infinite temperature. The limiting intercepts Φ_0 and slopes $a_1(v)$ are shown as functions of $1/v$ in Figs. 2 to 5.

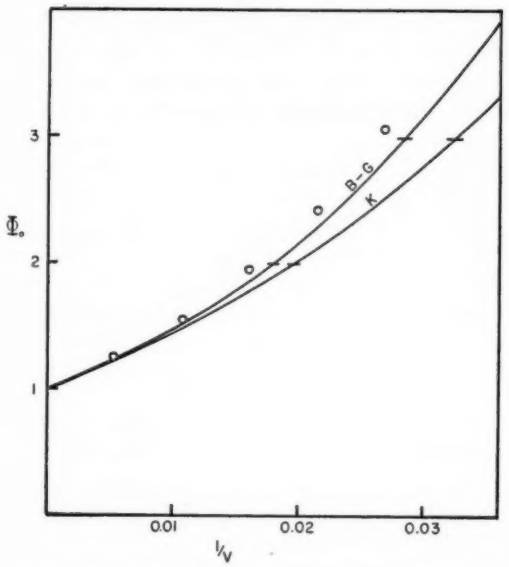

FIG. 2. Intercepts $\Phi_0(v)$ for argon, with the λ(B−G) and the λ(K) correlations. Horizontal lines indicate the effect of variation of c.

[7] Michels, Wijker, and Wijker, Physica **15**, 627 (1949).
[8] Michels, Lunbeck, and Wolkers, Physica **17**, 801 (1951).

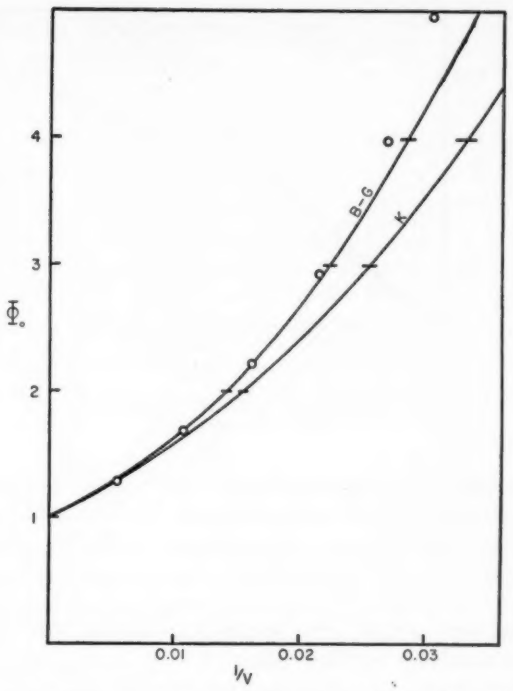

FIG. 3. Intercepts $\Phi_0(v)$ for nitrogen, with the λ(B−G) and the λ(K) correlations. Horizontal lines indicate the effect of variation of c.

The parameters a and ϵ for argon[7] and nitrogen[9] have been determined for the ordinary Lennard-Jones potential, $c=0$. They are

$$\begin{aligned} \text{Argon:}\quad & \epsilon(0)/k = 119.8^\circ\text{K} \\ & a(0) = \ 3.405\text{A} \\ \text{Nitrogen:}\quad & \epsilon(0)/k = \ 95.05^\circ\text{K} \\ & a(0) = \ 3.698\text{A}. \end{aligned}$$

These values, when corrected according to Table IV, may be used to convert our theoretical results from reduced units to experimental units. This conversion was performed using both the λ(K) and the λ(B−G) correlations. In the B−G case, they were carried out

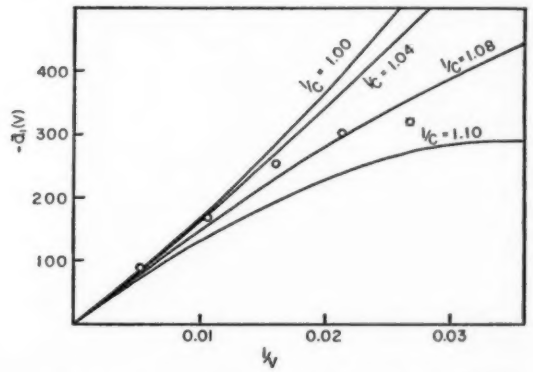

FIG. 4. Limiting slopes $a_1(v)$ for argon, with the λ(B−G) correlation.

[9] Michels, Wouters, and De Boer, Physica **1**, 587 (1934).

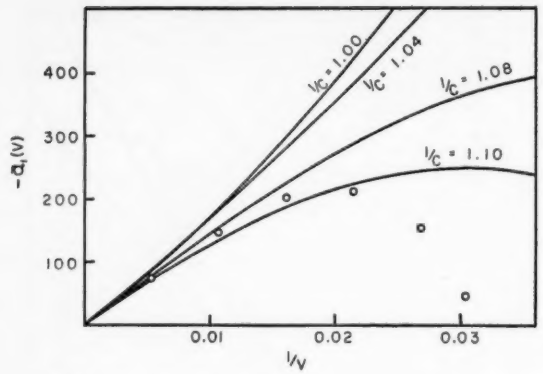

FIG. 5. Limiting slopes $a_1(v)$ for nitrogen, with the $\lambda(B-G)$ correlation.

for a number of values of c: in the K case, they were carried out only for $1/c=1.0$ and 1.1. Figures 2 to 6 contain comparisons of our theory with the experimental data. In Figs. 2 and 3, the intercepts $\Phi_0(v)$ are plotted against $1/v$. The experimental values are represented by circles; the theoretical values should be represented by families of curves, one for each value of c. Since these curves lie close together, we show instead a mean curve, and then indicate the variation in Φ_0 due to a variation in c by horizontal lines. The variation in c is from $1/c=1$ to $1/c=1.1$, and the ensuing change in Φ_0 is small. Results calculated with $\lambda(B-G)$ agree with experiment somewhat better than those with $\lambda(K)$. Deviations between theory and experiment increase with density in the same way for both argon and and nitrogen.

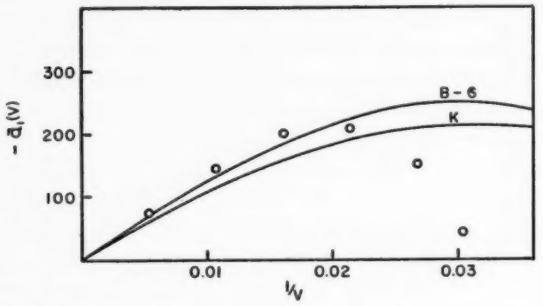

FIG. 6. Limiting slopes $a_1(v)$ for nitrogen, with the $\lambda(B-G)$ and the $\lambda(K)$ correlations, at $c=1/1.1$.

In Figs. 4 and 5, the limiting slopes $a_1(v)$ are plotted against $1/v$. The experimental values are represented by circles. In these two figures, only the $\lambda(B-G)$ correlation was used. The effect of a change in c from $1/c=1$ to $1/c=1.1$ is considerable. At low densities, $1/c=1.08$ appears to give the best fit, and at high densities $1/c=1.1$ is somewhat better. For both argon and nitrogen, the experimental curves turn downward more sharply than the theoretical ones.

Figures 6 contains a comparison of the experimental $a_1(v)$ with theory, calculated with $\lambda(B-G)$ and with $\lambda(K)$, at $1/c=1.1$ only, for nitrogen. The $\lambda(B-G)$ correlation fits this experimental data somewhat better at low densities; however, both the $\lambda(B-G)$ and the $\lambda(K)$ results deviate considerably at high densities.

We estimate that the over-all accuracy with which this theory predicts values of pv/RT is about five to ten percent, with the poorer accuracy at the higher densities. The results shown in Figs. 2 and 3 may be regarded as an experimental test of the theoretically predicted rigid sphere equation of state. The highest densities involved are about half the density of a system of close-packed spheres.

ACKNOWLEDGMENT

The application of the perturbation theory to nonpolar gases, utilizing rigid sphere radial distribution functions for the unperturbed system, was suggested by Professor John G. Kirkwood. A large part of the computational work was performed by Theodore Einwohner and Richard J. Plock.

Second-Order Quadrupole Effects in Asymmetric Tops. The Microwave Spectrum of Vinyl Iodide

H. W. MORGAN AND J. H. GOLDSTEIN
Stable Isotope Research and Production Division, Oak Ridge National Laboratory, Oak Ridge, Tennessee*
(Received March 23, 1954)

The $J=3\rightarrow4$ transition of the asymmetric rotor, vinyl iodide, has been observed in the region 24 000–26 000 Mc. The groupings $3_{12}\rightarrow4_{13}$ and $3_{13}\rightarrow4_{14}$ have been studied, and the quadrupolar hyperfine patterns, arising from the iodine nucleus, have been fitted to second-order theory with an average error of ±0.12 Mc.

The values determined for the coupling parameters are $\chi_{aa}=-1656$ Mc and $\chi_{bb}=+770$ Mc, each to within ±10 Mc. On the assumption that the C–I bond is a principal axis of the χ tensor, χ_{zz} the value along the C–I bond, was found to be -1877 Mc, and χ_{ab} to equal -765 Mc. Assuming planarity, and neglecting centrifugal distortion, the following values of the rotational constants were obtained: $(b+c)=6325.41\pm0.03$ Mc, $(b-c)=192.03\pm0.05$ Mc, and $\kappa=-0.9921554\pm0.0000031$.

INTRODUCTION

VINYL iodide is a planar molecule of near prolate symmetry, with a rotational spectrum similar to those of several vinyl derivatives recently studied.[1–3] The presence of the iodine nucleus, however, with its large quadrupole coupling constant, indicates that second-order hyperfine structure effects should be observable. These second-order effects allow in principle a more complete characterization of the symmetry of the charge distribution in the vicinity of the quadrupolar nucleus.

Preliminary calculations of the rotational spectrum were based on the following electron diffraction data:[4]

$$r_{CI}=2.03\pm0.04 \text{ A},$$
$$r_{CC}=1.34\pm0.04 \text{ A},$$
$$\text{and } \angle CCI=122°\pm2°.$$

In addition, the following values were assumed:

$$r_{CH}=1.09 \text{ A},$$
$$\text{and } \angle HCH=120°.$$

The rotational constants calculated from this model indicated that the $J=3\rightarrow4$ transition should occur at $24\,000\pm600$ Mc. Each transition corresponding to $\Delta K=0$ is split by the nuclear quadrupole effect into a hyperfine pattern covering 200 to 300 Mc. Because of the experimental difficulties in resolving the spectrum in regions where these multiplets overlap, only the well separated $3_{12}\rightarrow4_{13}$ and $3_{13}\rightarrow4_{14}$ patterns were selected for study.

EXPERIMENTAL

The vinyl iodide used was a commercially available preparation[5] with a reported purity of approximately 95 percent and was stabilized by the addition of 10-ppm tertiary butyl catechol. No further purification was attempted before use. The sample was protected from light and oxygen and showed no signs of decomposition over a period of several months.

All observations were made with a Stark effect spectrograph employing square wave modulation. A 100-kc repetition rate was used for visual study, and a 4-kc rate for presentation on a recorder. Frequencies were measured in the conventional manner by comparison with harmonics of a 10-Mc crystal, calibrated and continuously monitored against WWV. Each reported frequency represents the average of a series of measurements made over an interval of several months and is estimated to be accurate to ±0.05 Mc.

Initial assignments were made with the aid of an approximate pattern based on assumed values of the coupling parameters and then verified by Stark effect patterns and by relative intensity measurements

TABLE I. Observed microwave spectrum of vinyl iodide.

Assignment $J\rightarrow J'$	Assignment $F\rightarrow F'$	Frequency Mc	Relative intensity Theoretical	Relative intensity Observed[a]	$\frac{I_{-70°C}}{I_{+20°C}}$ ($\pm20\%$)
$3_{12}\rightarrow4_{13}$	5/2→ 7/2	25 641.14	40	36	2.3
	3/2→ 5/2	25 650.43	28	28	2.5
	7/2→ 9/2	25 657.34	56	50	2.4
	9/2→ 9/2	25 657.89	15	13	2.6
	9/2→11/2	25 685.91	76	70	2.5
	1/2→ 3/2	25 688.71	18	20	2.5
	11/2→13/2	25 709.28	100	100	2.5
	7/2→ 7/2	25 752.80	16	15	2.3
	5/2→ 5/2	25 788.26	14	15	2.0
	3/2→ 3/2	25 793.83	10	10	2.3
$3_{13}\rightarrow4_{14}$	11/2→11/2	24 683.33	10	12	2.4
	5/2→ 7/2	24 869.49	40	44	2.3
	3/2→ 5/2	24 877.60	28	33	2.8
	7/2→ 9/2	24 888.45	56	61	2.6
	9/2→ 9/2	24 889.69	15	20	2.4
	1/2→ 3/2	24 918.05	18	21	2.7
	9/2→11/2	24 919.85	76	75	2.5
	11/2→13/2	24 942.47	100	100	2.5
	7/2→ 7/2	24 991.87	16	15	2.3
	5/2→ 5/2	25 029.18	14	11	2.4
	3/2→ 3/2	25 034.06	10	10	2.3

[a] Taken at −70°C, values ±10 percent.

* This paper is based on work performed for the U. S. Atomic Energy Commission by Carbide and Carbon Chemicals Company, a Division of Union Carbide and Carbon Corporation, at the Oak Ridge National Laboratory.

[1] J. H. Goldstein and J. K. Bragg, Phys. Rev. **75**, 1453 (1949).
[2] C. D. Cornwell, J. Chem. Phys. **18**, 1118 (1950).
[3] W. S. Wilcox and J. H. Goldstein, Phys. Rev. **87**, 172 (1952).
[4] Hugill, Coop, and Sutton, Trans. Faraday Soc. **34**, 1518 (1938).
[5] Supplied by Monomer-Polymer, Inc., Leominister, Massachusetts.

taken at −70°C on the recording system. The ratio of intensity at −70°C to that at +20°C was obtained for all the lines studied and was used to exclude extraneous lines from consideration. The data obtained, together with assignments, are presented in Table I. Because of their very low intensities, the $\Delta F=-1$ transitions were not all observed and so are not included in this study. The line corresponding to $J=3_{12}\rightarrow 4_{13}$, $F=11/2\rightarrow 11/2$ was obscured by a transition arising from another multiplet and could not be observed.

SECOND-ORDER QUADRUPOLE EFFECTS—THEORY

For an asymmetric top, the matrix elements of the quadrupolar Hamiltonian, H_Q, have the form:[6]

$$(J\tau F/H_Q/J'\tau'F')=f(JIF)(J\tau J/\chi_{ZZ}/J'\tau'J), \quad (1)$$

where $f(JIF)$ is a function of the quantum numbers, including numerical factors, and $\chi_{ZZ}=eQ\nabla E_{ZZ}$, referred to an axis system fixed in space. J' may assume the values J, $J\pm1$, and $J\pm2$. The allowed values of τ' will be discussed below. Only the evaluation of the off-diagonal elements of (1) required for second-order calculations will be discussed.

The evaluation of (1) requires that χ_{ZZ} be expressed in terms of components in the principal axis system of the molecule as shown in the following equation:

$$\chi_{ZZ}=\alpha_{Zx}^2\chi_{xx}+\alpha_{Zy}^2\chi_{yy}+\alpha_{Zz}^2\chi_{zz}+2\alpha_{Zy}\alpha_{Zz}\chi_{yz}, \quad (2)$$

where α_{Zm} is the appropriate direction cosine, Z is in the space-fixed axis system, and y and z are the in-plane axes of the principal inertial system of the molecule. Employing the correspondence $xyz\rightarrow cba$, appropriate to prolate tops, and the properties of χ and α, (2) may be expressed in the form

$$\chi_{ZZ}=\tfrac{1}{2}(3\alpha_{Za}^2-1)\chi_{aa}+(\alpha_{Zb}^2-\alpha_{Zc}^2)\epsilon+2\alpha_{Zb}\alpha_{Za}\chi_{ab}, \quad (3)$$

where $\epsilon=(\chi_{bb}-\chi_{cc})$ measures the departure of χ from cylindrical symmetry.

The selection rules for the index τ, used in setting up the matrix elements of (3), may be obtained by group theory. Table II gives the species and characters of the V group, the classifications of the direction cosine terms, and the asymmetric rotor states.[6]

Thus, for a nonvanishing matrix element of $(\alpha_{zi}\alpha_{zj})$ to exist between two states $J\tau$ and $J'\tau'$, it is necessary that

$$R(\tau)\times R(\tau')=R(\alpha_{zi}\alpha_{zj}). \quad (4)$$

TABLE II. Characters and species for the V group.

Direction cosines	K_{-1}, K_{+1}	Species	E	C_2^a	C_2^b	C_2^c
α_{Zc}^2, α_{Zb}^2, α_{Za}^2	ee	A	1	1	1	1
$\alpha_{Zc}\alpha_{Zb}$; α_{Za}	eo	B_a	1	1	−1	−1
$\alpha_{Zc}\alpha_{Za}$; α_{Zb}	oo	B_b	1	−1	1	−1
$\alpha_{Za}\alpha_{Zb}$; α_{Zc}	oe	B_c	1	−1	−1	1

[6] J. K. Bragg, Phys. Rev. **74**, 533 (1948).

The left-hand side of this equation denotes the direct product of the two representations. Two states, therefore, may couple through either the first two terms of (3), or through the last term, but cannot couple through both. Moreover, the element χ_{ab} cannot couple the nearly degenerate states of identical K_{-1} in a near prolate top. Thus, its accurate evaluation through second-order effects is possible only in the unlikely event of accidental degeneracy between states of appropriate symmetry and J.

Limiting symmetric rotor wave functions were used as a basis for evaluating the matrix elements:[7]

$$S(JKM\gamma)=(\tfrac{1}{2})^{\frac{1}{2}}[\psi^{\times}(JKM)+(-1)^{\gamma}\psi^{\times}(J-KM)] \quad (5)$$

$$S(JOMO)=\psi^{\times}(JOM). \quad (6)$$

This choice appears reasonable inasmuch as κ is quite close to −1 for this molecule, and since the second-order effects are relatively small. By this procedure, the various elements of (3) were obtainable by matrix multiplication of symmetric top direction cosine elements already available.[7] In the symmetric rotor limit, the matrix elements of the second term in (3) vanish unless $K_{-1}=1$ for both states. Also, the off-diagonal elements of unity, in the first term of (3), vanish by virtue of orthogonality.

Since no near degeneracies were encountered, the expressions for the perturbations of each sublevel were obtained, by the usual methods of second-order perturbation theory, in terms of the parameters χ_{aa}, ϵ and χ_{ab}.

ANALYSIS OF DATA

Final values of the quadrupolar coupling constants were obtained by a method of successive approximation.

TABLE III. Quadrupole coupling parameters for vinyl iodide.

$\chi_{aa}=-1656$ Mc
$\chi_{bb}=+770$ Mc
$\epsilon=-116$ Mc
$\chi_{ab}=-765$ Mc

The hyperfine splittings were first fitted by first-order theory using least squares to yield preliminary values of χ_{aa} and χ_{bb}. From these, a value was obtained for ϵ. Although the deviations from first-order theory were evident, they were too small to allow the calculation of χ_{ab}. Therefore, an indirect procedure was employed. The assumption was made that the C−I axis was a principal axis of χ. χ_{ab} was then determined by carrying out the transformation which carries the principal axis system into the bond-axis system in the molecule. Using these preliminary values of χ_{aa}, ϵ, and χ_{ab}, and energy level values computed from experimental rotational constants, second-order corrections were determined and applied to the observed frequencies.

[7] King, Hainer, and Cross, J. Chem. Phys. **11**, 27 (1943).

TABLE IV. Observed and calculated hyperfine structure.

Transition	Component	Δ(obs)	Calculated Δ(1st order)	Observed −1st order	2nd order correction	Final error
$3_{12}\rightarrow 4_{13}$	11/2→13/2	+ 20.57	+ 19.84	+0.73	+0.59	+0.14
	11/2→11/2[a]		−219.29			
	9/2→11/2	− 2.80	− 2.29	−0.51	−0.61	+0.10
	9/2→ 9/2	− 30.82	− 31.20	+0.38	+0.37	+0.01
	7/2→ 9/2	− 31.37	− 31.20	−0.17	−0.16	−0.01
	7/2→ 7/2	+ 64.09	+ 63.40	+0.69	+0.54	+0.15
	5/2→ 7/2	− 47.57	− 47.08	−0.49	−0.46	−0.03
	5/2→ 5/2	+ 99.55	+100.10	−0.55	−0.49	−0.06
	3/2→ 5/2	− 38.28	− 38.01	−0.27	−0.42	+0.15
	3/2→ 3/2	+105.12	+106.52	−1.40	−1.03	−0.37
	1/2→ 3/2	0	0	0	0	0
$3_{13}\rightarrow 4_{14}$	11/2→13/2	+ 24.42	+ 23.22	+1.20	+0.93	+0.27
	11/2→11/2	−234.72	−236.55	+1.83	+1.65	+0.18
	9/2→11/2	+ 1.80	+ 1.76	+0.04	−0.14	+0.18
	9/2→ 9/2	− 28.36	− 29.65	+1.29	+0.85	+0.44
	7/2→ 9/2	− 29.60	− 29.65	+0.05	+0.12	−0.07
	7/2→ 7/2	+ 73.82	+ 73.12	+0.70	+0.61	+0.09
	5/2→ 7/2	− 48.57	− 48.20	−0.37	−0.36	−0.01
	5/2→ 5/2	+111.13	+111.66	−0.53	−0.40	−0.13
	3/2→ 5/2	− 40.45	− 40.01	−0.44	−0.43	−0.01
	3/2→ 3/2	+116.01	+116.98	−0.97	−0.78	−0.19
	1/2→ 3/2	0	0	0	0	0

[a] Not observed.

With these corrected frequencies, and a refined value for κ, a second least squares fit was made to first-order theory. Second-order corrections were again made using the new values, and analysis of these corrected frequencies showed no significant change in χ_{aa} and χ_{bb}. These final values for the coupling parameters are given in Table III.

The observed frequencies, corrected for second-order effects, were subjected to a graphical analysis to determine the ranges of χ_{aa} and χ_{bb}. For the $3_{12}\rightarrow 4_{13}$ grouping, these ranges were −1646 to −1662 Mc and +770 to +775 Mc, respectively, and for the $3_{13}\rightarrow 4_{14}$ grouping, −1646 to −1664 Mc and +748 to +778 Mc, respectively. From this, it is thus concluded that the values for χ_{aa} and χ_{bb} have been determined to within ±10 Mc.

The value of χ_{zz}, the component of χ along the C−I bond, was obtained by transforming the tensor from the principal axis system to the bond axis system, using the previously mentioned orthogonal transformation. The value so obtained is −1877 Mc, which is slightly less than the value −1934 Mc reported for methyl iodide.[8] The values of the other components in the bond axis system are $\chi_{xx}=+886$ Mc and $\chi_{yy}=+991$ Mc, where the x axis is taken perpendicular to the plane of the molecule. The corresponding value of the asymmetry parameter, $\eta=(\chi_{yy}-\chi_{xx})/\chi_{zz}$, is thus 0.060. The departure from cylindrical symmetry indicated by these results is consistent with the double bond character usually attributed to vinyl halide bonds.

In Table IV are presented the predicted hyperfine patterns, to both first and second order, calculated with the parameters of Table III. The displacements are measured relative to the $F=\frac{1}{2}\rightarrow\frac{3}{2}$ transition frequency, chosen as a reference because it is subject to virtually no second-order effect.

The application of second-order theory to the nineteen frequency differences listed in Table IV, has reduced the mean difference between observed and predicted splittings from 0.67 Mc to 0.12 Mc. Of interest is the fact that two pairs of transitions, degenerate in first-order theory, occur with observed spacings of 0.55 Mc and 1.24 Mc, compared with second-order predictions of 0.53 Mc and 0.71 Mc, respectively.

The zero-order frequencies averaged over all hyperfine components, together with the rotational constants, calculated on the assumption of planarity and neglecting centrifugal distortion, are given in Table V.

TABLE V. Rotational constants of vinyl iodide.

$(b+c)=$	6325.41	±0.03 Mc
$(b-c)=$	192.03	±0.05 Mc
$\kappa=$	−0.9921554	±0.0000031
$\delta=$	+0.0039222	±0.0000015
$\nu_0 3_{12}\text{—}4_{13}=$	25 684.57	±0.10 Mc
$\nu_0 3_{13}\text{—}4_{14}=$	24 916.46	±0.10 Mc

ACKNOWLEDGMENTS

The authors are indebted to Mr. A. L. Southern for a preliminary study of the spectrum and to Dr. J. R. McNally for helpful discussions and for checking the manuscript.

[8] Gordy, Simmons, and Smith, Phys. Rev. **74**, 243 (1948).

Conjugation of Several Phenyl Radicals Bonded to a Single Central Atom

H. H. JAFFÉ
Venereal Disease Experimental Laboratory, U. S. Public Health Service, School of Public Health, University of North Carolina, Chapel Hill, North Carolina

(Received March 18, 1954)

Spectroscopic evidence is used to show that phenyl radicals are only weakly conjugated with central atoms (S, P, As, Sb, Si, Sn, Pb) not having unshared valence electrons. No resonance interaction is encountered between several phenyl radicals attached to such a central atom, and each phenyl radical makes an independent contribution to the molar extinction coefficients. If the central atom (S, N, P, As, Sb, Bi) has an unshared pair of electrons, extensive conjugation between the phenyl radicals occurs and leads to spectra in sharp contrast to those of simple benzene derivatives. No simple relation exists between the spectra of closely related compounds with different numbers of phenyl radicals attached to the same central atom. The near ultraviolet absorption spectra of dimethylaniline, methyldiphenylamine, triphenylamine, triphenylarsine, triphenylstibine, triphenylbismuthine, triphenylarsine oxide, and triphenylstibine dichloride are reported and compared with those of related compounds of phosphorus, sulfur, and group IVA elements.

IN recent years considerable evidence has been accumulated which indicates that the elements of the second and higher rows of groups IVA to VIA of the periodic system are able to expand their valence shell of electrons beyond the octet.[1] Much of this evidence depends on the demonstration of resonance interaction between a central atom belonging to the specified group of elements and an unsaturated or aromatic organic radical attached to this central atom. Although such resonance interaction has been demonstrated by chemical means,[2] most of the evidence consists of spectroscopic data.[3]

In the present paper we shall examine the extent of conjugation between several phenyl radicals attached to a single central atom capable of expansion of its valence shell.[4] In particular, we shall be interested in a comparison between the conjugation through a central atom possessing unshared valence electrons, and conjugation which can arise only by expansion of the valence shell of the central atom. The comparisons will be based on the ultraviolet absorption spectra of several series of closely related compounds, especially of the phenyl derivatives of the elements of group VA in the "trivalent" and "pentavalent" states. The spectra of a number of phosphorus compounds have been reported in previous papers from this laboratory.[5] The spectra of several analogous compounds of nitrogen, arsenic, antimony, and bismuth have been determined in the present investigation, and the relevant data are reported in Table I. The same table includes data for the phosphorus compounds discussed here, and for some related compounds of sulfur[3a,b,6] and of group IVA elements.[7]

MONOPHENYL COMPOUNDS

Before discussing the conjugation between several phenyl radicals attached to a single atom, we wish to examine the evidence for resonance interaction between a central sulfur, phosphorus, or arsenic atom and a single phenyl radical attached to it. Substitution of a methylsulfonyl ($-SO_2CH_3$), phosphono ($-PO_3H_2$), hydroxyphosphinyl ($-HPO_2H$), hydroxyethylphosphinyl ($-P(C_2H_5)O_2H$), or arsono ($-AsO_3H_2$) group in the benzene ring produces a bathochromic shift and hyperchromic effect on the "secondary" band,[8] but leaves the general appearance of the spectrum, and particularly its vibrational structure essentially unchanged (see Fig. 1). It is very likely that the bathochromic shift and the hyperchromic effect should be ascribed to weak resonance interaction between the ring and the central atom, and that the magnitude of this interaction decreases in the order S>As>P. The effects resemble those observed on substitution of benzene by a halogen atom or a carboxy group.[9] They differ, however, both quantitatively and qualitatively from the effects resulting from substitution by such radicals as the methylmercapto (CH_3S-), amino, hydroxy, or arsenoso groups ($O=As-$).[10] The latter groups completely suppress all vibrational structure of the "secondary" band of benzene and lead to a much

[1] A complete bibliography documenting this statement is beyond the scope of this paper. References 2–4 have some bearing on this point, and refer to other papers on the same subject.

[2] See F. G. Bordwell and G. D. Cooper, J. Am. Chem. Soc. **74**, 1058 (1952); H. Zollinger, Helv. Chim. Acta **36**, 1711 (1953).

[3] E.g., (a) E. A. Fehnel and M. Carmack, J. Am. Chem. Soc. **71**, 84 (1949); (b) **71**, 231 (1949); (c) **71**, 2889 (1949), **72**, 1292 (1950); (d) H. P. Koch, J. Chem. Soc. **1949**, 387, 394, 401, 408.

[4] A theoretical treatment of this problem has been given by H. H. Jaffé, J. Phys. Chem. **58**, 185 (1954); see also H. P. Koch and W. Moffitt, Trans. Faraday Soc. **47**, 7 (1951).

[5] H. H. Jaffé and L. D. Freedman, J. Am. Chem. Soc. **74**, 1069, 2930 (1952). Two errors in the first of these papers should be corrected: In the last column of Table I, under $(C_6H_5)_3PO$, the entry should read 1962; the ordinate of Fig. 2 should be marked $\epsilon \times 10^{-4}$; and the ordinate coordinates for the left-hand portion of Fig. 3 should read 10 and 20.

[6] A. Mangini and R. Passerini, Boll. sci. fac. chim. ind. Bologna **8** (1950). Chem. Abstracts **45**, 3241*d* (1951).

[7] G. Milazzo, Gazz. chim. ital. **71**, 73 (1941).

[8] The term "secondary" band is used in accordance with the definition of L. Doub and J. M. Vandenbelt, J. Am. Chem. Soc. **69**, 2714 (1947).

[9] See data in reference 8.

[10] Unfortunately, the spectrum of phenylphosphine ($C_6H_5PH_2$) could not be obtained since the compound was too readily oxidized. Preliminary data, however, suggested that its spectrum resembles that of the aniline.

greater increase in the intensity of the absorption. Hence, it must be concluded that the groups not possessing unshared electron pairs produce only a relatively minor perturbation of the π-electron system of benzene. Substituents with a central sulfur, phosphorus, or nitrogen atom possessing an unshared pair, on the other hand, completely change the π-electron system, and lead to entirely different spectral characteristics.

TABLE I. Ultraviolet absorption spectra of some organic compounds of elements of groups IVA to VIA.

Compounds	λ_{max} ($m\mu$)	$\epsilon_{max} \times 10^{-4}$
a. Central atoms with an unshared pair of electrons		
$(C_6H_5)_3N$	228, 297	0.729, 2.21
$(C_6H_5)_2NCH_3$	245, 291	0.851, 1.17
$C_6H_5N(CH_3)_2$	252, 298	1.13, 0.171
$(C_6H_5)_3P$[a]	261	1.10
$(C_6H_5)_3As$	248	1.23
$(C_6H_5)_3Sb$	256	1.17
$(C_6H_5)_3Bi$	(248, 280)[b]	(1.29, 0.426)
C_6H_5AsO[c]	(232)[b], 264, 270	(1.09), 0.275, 0.237
$(C_6H_5)_2S$[c]	250, 277	1.2, 0.58
$C_6H_5SCH_3$[c]	254, (275)[b]	0.96, (0.14)
$(C_6H_5)_2SO$[d]	232, (262)[b]	1.4, (0.24)
b. Central atoms without unshared electrons		
$(C_6H_5)_3PO$[a]	224.5, (255),[b] 260, 265.5, 272.5	214, (0.105), 0.152, 0.196, 0.162
$(C_6H_5)_3AsO \cdot H_2O$	221, (253.5),[b] 258, 263, 270	2.16, (0.102), 0.140, 0.172, 0.137
$(C_6H_5)_3SbCl_2$	218, (252),[b] 259.5, 263.5, 269.5	2.90, (0.107), 0.130, 0.146, 0.106
$C_6H_5AsO_3H_2$	214, (245, 251),[b] 256.5, 262, 269	0.67, (0.0243, 0.0385), 0.0564, 0.0738, 0.0612
$C_6H_5AsO_3H^-$[e]	(250),[b] 255.5, 261.5, 268	(0.0334), 0.0481, 0.0606, 0.0493
$C_6H_5AsO_3^=$[e]	(245),[b] 251, 256.5, 261, 267.5	(0.0226), 0.0298, 0.0371, 0.0394, 0.0298
$(C_6H_5)_2SO_2$[f]	235, (254),[b] 260, 266, 274	3.8, —, 0.18, 0.21, 0.15
$C_6H_5SO_2CH_3$[f]	217, (253),[b] 258, 264, 271	0.68, —, 0.066, 0.098, 0.081
$(C_6H_5)_4Si$[g]	237, 254, 260, 265, 271	0.17, 0.11, 0.14, 0.14, 0.11
$(C_6H_5)_4Sn$[g]	251, 259, 265	0.09, 0.11, 0.09
$(C_6H_5)_4Pb$[g]	248, 259, 266, 270	0.40, 0.20, 0.11, 0.055

[a] From reference 5.
[b] Numbers in parenthesis represent inflection points.
[c] From reference 3a.
[d] From reference 6.
[e] The solvent used was water.
[f] From reference 3b.
[g] From reference 7.

POLYPHENYL COMPOUNDS

The conclusions reached above for compounds having a single phenyl radical linked to a central sulfur, nitrogen, phosphorus, or arsenic atom are equally valid for compounds in which several phenyl radicals are bonded to such a central atom. The spectra of triphenylamine [$(C_6H_5)_3N$], -phosphine [$(C_6H_5)_3P$], -arsine [$(C_6H_5)_3As$], -stibine [$(C_6H_5)_3Sb$], and -bismuthine [$(C_6H_5)_3Bi$] are shown in Fig. 2. Triphenylamine has an absorption band at longer wavelengths and of greater intensity than the other compounds, probably because first row elements have a greater tendency for double

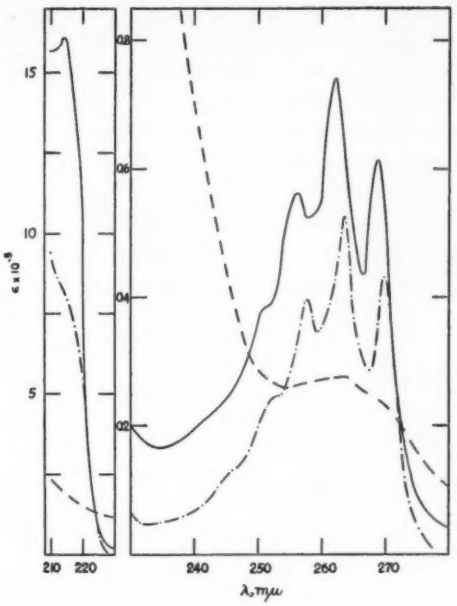

FIG. 1. The spectra (in 95 percent ethanol) of $C_6H_5AsO_3H_2$———; C_6H_5AsO– – –; $C_6H_5PO_3H_2$–·–·–.

bond formation than do elements of higher rows of the periodic system. The spectrum of triphenylbismuthine does not show a band near 250 mμ, i.e., in the region where the spectra of the analogous compounds of phosphorus, arsenic, and antimony have the main bands. However, the inflection point near 248 mμ indicates the existence of an electronic transition giving rise to absorption in this region. Diphenyl sulfide

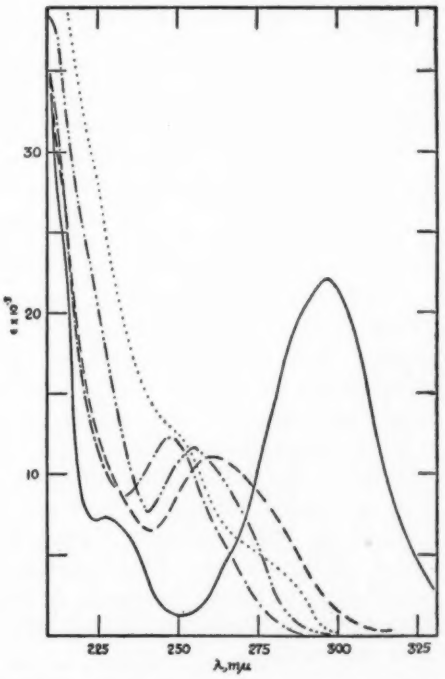

FIG. 2. The spectra (in 95 percent ethanol) of $(C_6H_5)_3N$———; $(C_6H_5)_3P$– – –; $(C_6H_5)_3As$–·–·–; $(C_6H_5)_3Sb$–·–·–·–; $(C_6H_5)_3Bi$ ·····.

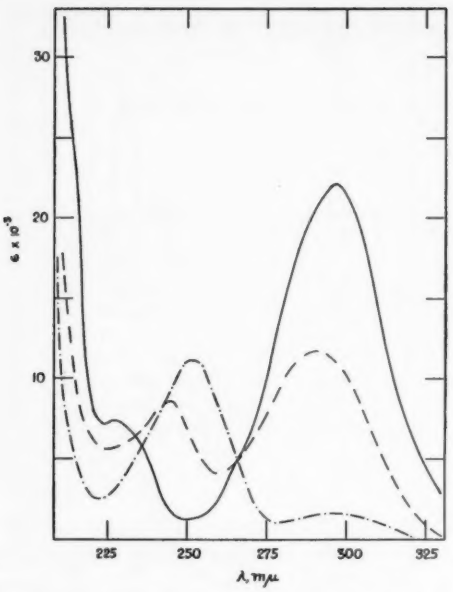

FIG. 3. The spectra (in 95 percent ethanol) of $(C_6H_5)_3N$———; $(C_6H_5)_2NCH_3$– – –; $C_6H_5N(CH_3)_2$–·–·–.

$[(C_6H_5)_2S]$ and diphenyl sulfoxide $[(C_6H_5)_2SO]$ have two phenyl radicals attached to a central sulfur atom possessing an unshared pair of electrons. Both compounds have structureless intense absorption bands in the near ultraviolet region.[3a,6]

Figure 3 compares the spectra of dimethylaniline $[C_6H_5N(CH_3)_2]$, N-methyldiphenylamine $[(C_6H_5)_2NCH_3]$, and triphenylamine $[(C_6H_5)_3N]$. All three compounds show two broad structureless bands, one between 225 and 250 mμ, the other around 290–300 mμ. The position of the latter band does not greatly depend on the number of phenyl groups present in the compound, but the intensity increases sharply with this number. The band at 225–250 mμ, on the other hand is shifted distinctly toward shorter wavelengths and decreases slightly in intensity with an increase in the number of phenyl radicals. These facts are understandable only if the transitions in the polyphenyl compounds involve electrons delocalized over the entire molecule, i.e., if the phenyl radicals are conjugated.

The spectra of triphenylphosphine oxide $[(C_6H_5)_3PO]$, triphenylarsine oxide $[(C_6H_5)_3AsO\cdot H_2O]$,[11] and triphenylstibine dichloride $[(C_6H_5)_3SbCl_2]$ are shown in Fig. 4. They closely resemble one another and also the spectrum of diphenylsulfone.[3b] All four spectra show the well-defined vibrational structure characteristic of unperturbed or weakly perturbed benzene rings. The same is true of the tetraphenyl derivatives of silicon, tin, and lead. Hence, it may be concluded that the several phenyl rings in these compounds do not greatly perturb each other, and thus are not appreciably conjugated with one another.

[11] The compound occurs with one mole of water, but it is not known whether the structure is

$(C_6H_5)_3AsO\cdot H_2O$ or $(C_6H_5)_3As(OH)_2$.

The lack of conjugation of the individual rings in the above compounds is further confirmed by an examination of the effect of successive introduction of phenyl radicals around a central atom. Each phenyl radical appears to make an independent contribution to the molar extinction coefficient of corresponding peaks. Thus the ratio of the ϵ values for corresponding maxima of the "secondary" bands in triphenylphosphine oxide, diphenylphosphinic acid $[(C_6H_5)_2PO_2H]$, phenylethylphosphinic acid $[(C_6H_5)(C_2H_5)PO_2H]$, and phenylphosphonous acid $C_6H_5PO_2H_2$ is approximately equal to the ratio of the number of phenyl radicals in these compounds, namely 3:2:1:1.[5] Similarly, the ratios of ϵ_{max} for diphenyl sulfone and phenyl methyl sulfone $[(C_6H_5)CH_3SO_2]$[3b] and for triphenylarsine oxide and benzenearsonic acid $(C_6H_5AsO_3H_2)$ are approximately 2:1 and 3:1, respectively. A similar relation has been noted in the compounds $(C_6H_5)_nCH_{4-n}$,[12] in which no conjugation between the phenyl rings is possible. The relation between the spectra of symmetrical and unsymmetrical phosphinic acids[5] is also strong evidence for lack of conjugation of the individual rings in these compounds.

There appears to be little systematic variation of the characteristics of the "secondary" band with the nature of the central atom. However, the absorption at shorter wavelengths (<240 mμ) seems to depend strongly on the central atom. The end absorption (or short wavelength band) is the more intense the lower the central atom is located in the periodic system,

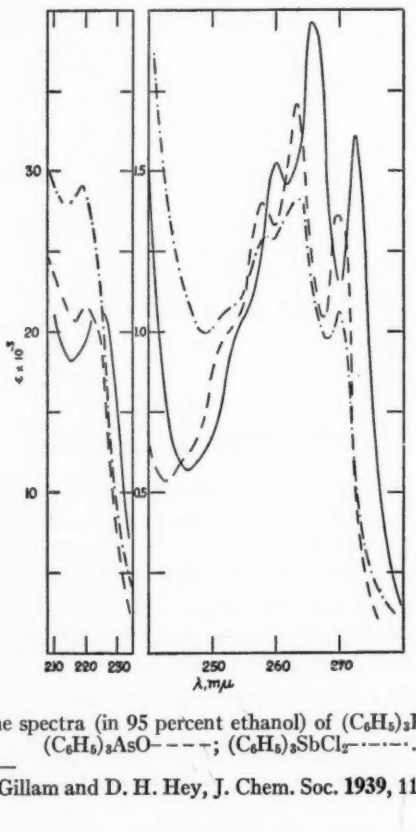

FIG. 4. The spectra (in 95 percent ethanol) of $(C_6H_5)_3PO$———; $(C_6H_5)_3AsO$– – –; $(C_6H_5)_3SbCl_2$–·–·–.

[12] E. A. Gillam and D. H. Hey, J. Chem. Soc. **1939**, 1170.

provided comparisons are made only between closely related compounds. This observation suggests that the central atom is strongly involved in the transition concerned. Although the data presented here are insufficient to make a decision on this point, it is not unlikely that the end absorption corresponds to a dissociation process, as Milazzo has proposed.[7]

EXPERIMENTAL

All compounds were either obtained from commercial sources or prepared in this laboratory by known methods. Commercial samples were purified by recrystallization or distillation. Unless otherwise indicated, the spectra were determined in solution in commercial 95 percent ethanol which was transparent above 210 mμ. A Beckman DU spectrophotometer and 1 cm quartz cells were used throughout. The concentrations of the solutions were so chosen as to obtain optical densities between 0.3 and 0.7 at the absorption maxima, and no optical density data below 0.15 were used.

THE JOURNAL OF CHEMICAL PHYSICS VOLUME 22, NUMBER 8 AUGUST, 1954

Molecular Orbital Theory of Orientation in Aromatic, Heteroaromatic, and Other Conjugated Molecules

KENICHI FUKUI, TEIJIRO YONEZAWA, CHIKAYOSHI NAGATA, AND HARUO SHINGU
Faculty of Engineering, Kyoto University, Kyoto, Japan

(Received March 31, 1953)

As to the LCAO MO treatment of the orientation problem in chemical reactions of π-electron systems, the *frontier* electron concept which has been previously introduced by the authors for explaining the reactivities in aromatic hydrocarbons is subjected to an extension in the sense that the *frontier orbitals* are specified according to the type of reaction. Thus, *fundamental postulates* relating to the reactivities of π-electron systems are set up, which are believed to include general principles involved in the mechanism of both substitution and addition of electrophilic, nucleophilic, or radical type. On the basis of these postulates it is possible to predict the position of attack in conjugated molecules in all the three types of substitution as well as addition in a consistent manner. There is a nearly perfect agreement between the theoretical conclusions and experimental results hitherto reported.

1. INTRODUCTION

ONE of the recent successes achieved by quantum mechanics in the field of physical organic chemistry is the development of the theory in explaining the orienting effect of substituents in aromatic molecules. The quantitative treatments of this problem so far reported may be roughly classified into two groups. The one,[1] which may be called the "static method," is based on the hypothesis that the position of higher (or lower) calculated density of total π electrons is more easily attacked by electrophilic (or nucleophilic) reagents. The other,[2] which may be called the "localization method," is related to the calculation of the difference in unsaturation energy of the hypothetical transition complexes.

Prominence of the latter method should be admitted in that it is capable of explaining the reactivity in all the three types, i.e., electrophilic, nucleophilic, and radical type, of substitution from a unified standpoint, whereas by means of the former method it is difficult to account for the point of attack in the radical substitution, and in this respect the "free valency method"[5] serves as filling up that defect of the static method.

In this paper it is shown that another unifying method can also be established on the basis of the "*frontier electron*" concept which has been previously introduced by some of the present authors in the case of electrophilic substitution in condensed aromatic hydrocarbons.[3] On treating the orientation problem in substituted atomatic and other related molecules, it is found that the concept should naturally be extended in the sense that the *frontier orbitals* are specified according to the type of reaction. Thus, we are led to set up the *fundamental postulates*, in the light of which the position of attack by electrophilic, nucleophilic, and radical reagents can be predicted not only for substitution but also for addition in an excellent agreement with experiment.

[1] E. Hückel, Z. Physik **72**, 312 (1931); Z. physik. Chem. **B35**, 163 (1937); Z. Elektrochem. **43**, 827 (1937); G. W. Wheland and L. Pauling, J. Am. Chem. Soc. **57**, 2086 (1935); T. Ri, Rev. Phys. Chem. Japan **17**, 1, 16 (1943) (in Japanese); M. J. S. Dewar, Trans. Faraday Soc. **42**, 764 (1946); H. C. Longuet-Higgins and C. A. Coulson, Trans. Faraday Soc. **43**, 87 (1947); C. A. Coulson and H. C. Longuet-Higgins, Proc. Roy. Soc. (London) **A191**, 39; **A192**, 16 (1947); A. Pullman, Rev. sci. **86**, 219 (1948); A. Pullman and J. Metzger, Bull. soc. chim. France **1948**, 1021 (1948); H. C. Longuet-Higgins and C. A. Coulson, J. Chem. Soc. (London) **1949**, 971 (1949); C. Sandorfy, Bull. soc. chim. France **1949**, 615 (1949); H. C. Longuet-Higgins, J. Chem. Phys. **18**, 283 (1950); Orgel, Cottrel, Dick, and Sutton, Trans. Faraday Soc. **47**, 113 (1951); J.-I. F. Alonso, Compt. rend. **233**, 403 (1951); L. Szabö, Compt. rend. **233**, 625 (1951).

[2] G. W. Wheland, J. Am. Chem. Soc. **64**, 900 (1942); H. C. Longuet-Higgins, J. Chem. Phys. **18**, 283 (1950); M. J. S. Dewar, J. Chem. Soc. (London) **1949**, 463 (1949); C. A. Coulson, Research **4**, 307 (1951); M. J. S. Dewar, J. Am. Chem. Soc. **74**, 3355, 3357 (1952).

[3] Fukui, Yonezawa, and Shingu, J. Chem. Phys. **20**, 722 (1952).

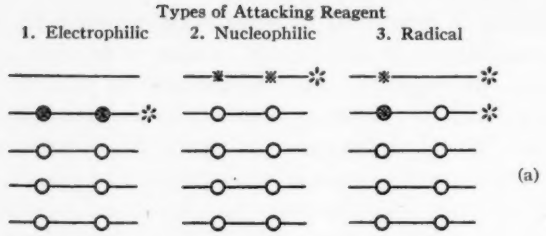

FIG. 1. Frontier electrons and frontier orbitals. (a) Even π-electron system. (b) Odd π-electron system.

2. FUNDAMENTAL POSTULATES

As a general characteristic of chemical activation it may be assumed that in the vicinity to the transition state the electrons in the reagent as well as those in the reactant molecule will be delocalized and a transfer of electrons will occur between the reagent and the reactant. From the standpoint of the *frontier* electron concept we suppose that the *frontiers* are most susceptible to the electron transfer and that this transfer of electrons, which may serve to lower the energy of the activated complex, will form the essential part of the electronic interaction in question. *Two* electrons should be characterized in this connection as *frontiers* in that they are most closely related to the formation of a covalent σ bond between the π-electron system and the reagent, and these two are provided either from the highest occupied orbital in the π-electron system to the reagent in an electrophilic reaction, or from the reagent to the lowest empty orbital in the π-electron system in a nucleophilic reaction, and in a radical reaction one electron is provided from the reagent and the other from the π-electron system.

From this point of view, in order to make reference to the reactivity in terms of the electron distribution in an *isolated* π-electron system, it is convenient to define a new concept of *frontier orbital* in relation to the isolated π-electron system as characterized by partial occupation by the *frontier* electron in case of the electron transfer at the transition state, according to the type of reaction.

On the basis of these considerations, the following *fundamental postulates* are set up, which enable us to predict the reactivity of π-electron system in a most general and consistent manner:

1. *In case of the reaction with an electrophilic reagent, that position is more susceptible to attack which has the higher density of the two electrons occupying the highest molecular orbital in the ground state.*

2. *In case of the reaction with a nucleophilic reagent, that position is more susceptible to attack which would have the higher density of the two electrons assumed to occupy the lowest unoccupied orbital of the ground state.*

3. *In case of the reaction with a radical reagent, that position is more susceptible to attack which would have the higher density of the two electrons, one occupying the highest orbital and the other occupying the lowest unoccupied orbital of the ground state.*

As a consequence of these postulates we can classify the *frontier* electrons and orbitals for various types of reactants and reagents, which is illustrated in Fig. 1, including the cases of even and odd π-electron systems. In the latter case where the π-electron system is a radical, the above postulates should be somewhat modified as shown in Fig. 1(b). Also in the case of an excited state of the π-electron system, e.g., in the case of a diradical state, the principle involved in the postulates may be correspondingly applicable.

3. ELECTROPHILIC SUBSTITUTION

Substitution in Heterocyclic Compounds

For the quantum-mechanical treatment of reactivity in heterocyclic compounds several parameters representing the influence of heteroatom as to the Coulomb and exchange integrals have been introduced by several authors[1,2] from some empirical or theoretical arguments.

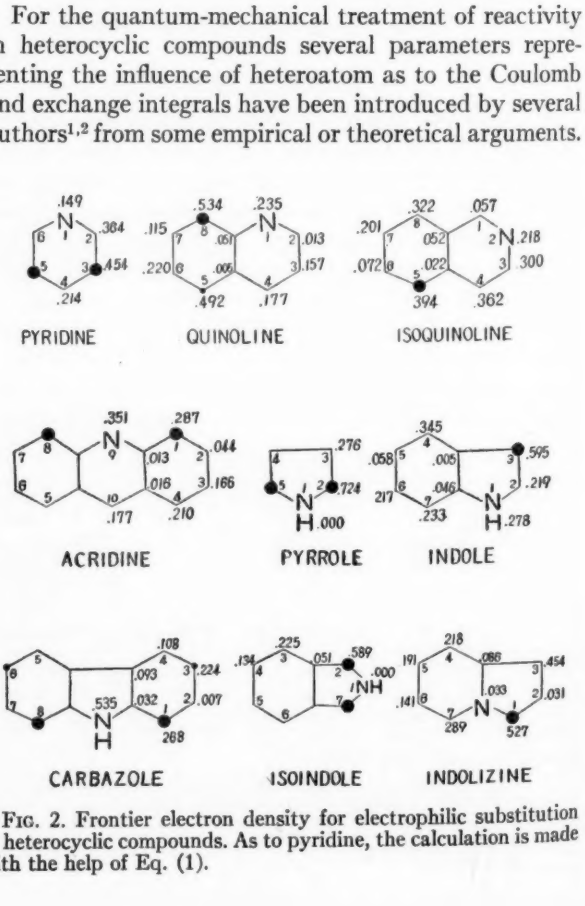

FIG. 2. Frontier electron density for electrophilic substitution in heterocyclic compounds. As to pyridine, the calculation is made with the help of Eq. (1).

TABLE I. Coulomb and exchange integrals for heteromolecules containing nitrogen atom.

Type of nitrogen atom	Pyridine type					Pyrrole type				
	Coulomb[a,b,c]			Exchange[d]		Coulomb			Exchange	
Integrals	α_1	α_2	α_r	β_{12}	β_{rs}	α_1	α_2	α_r	β_{12}	β_{rs}
Wheland-Pauling[e] Longuet-Higgins-Coulson (1947)[e] Pullman[e]	$\alpha+2\beta$	$\alpha+\frac{1}{4}\beta$	α	β	β	$\alpha+2\beta$	$\alpha+\frac{1}{4}\beta$	α	β	β
Orgel *et al.*[e]	$\alpha+\beta$	$\alpha+\frac{1}{10}\beta$	α	β	β	$\alpha+2\beta$	$\alpha+\frac{1}{3}\beta$	α	β	β
Dewar[e]	...	...	...	...	...	α	α	α	0.55β	β
Present authors	$\alpha+\beta$	α	α	β	β	$\alpha+\beta$	α	α	β	β

[a] Subscript 1: nitrogen atom.
[b] Subscript 2: carbon atom adjacent to nitrogen.
[c] Subscript r: other carbon atoms.
[d] Subscript rs: any pair of mutually adjacent atoms except 12 (exchange integrals between nonadjacent atoms and all overlap integrals neglected entirely).
[e] See reference 1.

These parameters are tabulated in Table I together with those which are adopted by the present authors.*

The calculated densities of *frontier* electrons in pyridine, quinoline, isoquinoline, acridine, pyrrole, indole, carbazole, isoindole, and indolizine are indicated in Fig. 2, and the reaction products of halogenation, nitration, and sulfonation are tabulated in Table II. The agreement between calculated and experimental results is almost satisfactory.

Nuclear Substitution in Benzene Derivatives

In this paragraph the object of calculation is restricted to mono-substituted benzenes.† The twofold degeneracy of *frontier* orbitals in nonsubstituted benzene is removed by the influence of the substituent. If the perturbation is small, two separate orbitals, the corresponding energies of which are in close proximity, are produced as the result of the removal of degeneracy. In such a case, the contribution of the density of electrons in the lower orbital must be taken into account in the calculation of the *frontier* electron density.

In order to evaluate the degree of contribution of the lower orbital the following Eq. (1) is assumed as giving the *frontier* electron density for the electrophilic reaction at the rth atom in the molecule $f_r^{(E)}$:

$$f_r^{(E)}=2\cdot\frac{|C_r^{(1)}|^2+|C_r^{(2)}|^2e^{-D\Delta\lambda}}{1+e^{-D\Delta\lambda}}, \qquad (1)$$

where $\Delta\lambda$ is the energy difference between the two orbitals in units of β and $C_r^{(1)}$, $C_r^{(2)}$ are the coefficients of LCAO MO at the rth atom corresponding to the highest and the next orbital respectively, and D is a constant which determines the degree of contribution of the lower MO to the *frontier* electron density. Throughout the present paper‡ the value of D is taken, tentatively, to be 3 in consideration of the complete agreement between calculation and experiment which has been obtained[3] in aromatic hydrocarbons without considering the contribution of the next orbital.

In regard to LCAO MO treatment, mono-substituted benzenes are classified into several types of *isoaromatic*§ hydrocarbon, that is, benzene type, benzyl anion type, styrene type, and 2-phenylpropenyl anion type (Fig. 3), and other types.

Benzene Type

To this type belong, for example, *t*-butyl benzene and benzene sulfonic acid in which the effect of substituent is only inductive. This effect can be represented after Sandorfy[1] and Dewar[2] (1949) by two parameters a and ϵ in Eq. (2).

$$\alpha_r=\alpha+\epsilon^{r-1}a\beta, \qquad (2)$$

TABLE II. Products of electrophilic substitution in heterocyclic compounds.

Compounds	Predicted position	Structure of reaction products: Halogenation	Nitration	Sulfonation
Pyridine	3,5	3-Cl[a] 3-Br[a]	3-NO_2[l]	3-SO_3H[p]
Quinoline	8,(5)	5-I[b]	5-NO_2, 8-No_2[j]	5-SO_3H, 8-SO_3H[q]
Isoquinoline	5	...	5-NO_2, 8-NO_2[k]	...
Acridine	1	...	1-NO_2, 3-NO_2[l] 1,3-di-NO_2[m]	...
Pyrrole	2,5	2-Cl[c] 2,5-di-Cl[d]	...	...
Indole	3	2,3-di-Cl[e] 3-I[f]	3-NO_2[n]	...
Carbazole	1,(3)	3-Cl[g] 3-Br[h]	1-NO_2, 3-NO_2[o]	...

[a] H. J. Den Hertog and J. P. Wibaut, Rec. trav. chim. **51**, 382, 940 (1932).
[b] W. La Coste, Ber. deut. chem. Ges. **18**, 781 (1885).
[c] G. Mazzara and A. Borgo, Gaz. chim. ital. **35** II, 20 (1905).
[d] G. Mazzara and A. Borgo, Gaz. chim. ital. **35** I, 477 (1905).
[e] G. Mazzara and A. Borgo, Gaz. chim. ital. **35** II, 536 (1905).
[f] H. Pauly and K. Gunderman, Ber. deut. chem. Ges. **41**, 4006 (1908).
[g] Mazzara, Lamberti, and Zanardi, Gaz. chim. ital. **26** II, 238 (1896).
[h] W. Vaubel, Z. angew. Chem. **14**, 784 (1901).
[i] P. Schorigin and A. Toptschiew, Ber. deut. chem. Ges. **69**, 1874 (1936).
[j] W. Koenigs, Ber. deut. chem. Ges. **12**, 449 (1879).
[k] Ad. Claus and K. Hoffmann, J. prakt. Chem. (2) **47**, 253 (1893).
[l] C. Graebe and H. Caro, Ann. Chem. **158**, 275 (1871).
[m] K. Lehmsteat, Ber. deut. chem. Ges. **65**, 834 (1924).
[n] F. Angelico and G. Velardi, Gaz. chim. ital. **34** II, 60 (1904).
[o] H. Lindemann, Ber. deut. chem. Ges. **57**, 557 (1924).
[p] O. Fischer, Ber. deut. chem. Ges. **15**, 62 (1882).
[q] A. Kaufmann and H. Hüssig, Ber. deut. chem. Ges. **41**, 1735 (1908).

* As it is intended in the present paper to examine the general validity of the frontier electron theory using the smallest number of uncertain parameters, the effect of the heteroatom on the Coulomb integral of the adjacent carbon atom is neglected, as is shown in Table I.

† For di- or polysubstituted aromatic systems the present method can be also useful, but especially in benzene derivatives it becomes important to consider the steric circumstances.

‡ Also in nucleophilic or radical reaction, the equation similar to Eq. (1) is necessary, if any orbital lies in close proximity to the frontier orbitals.

§ See H. C. Longuet-Higgins, J. Chem. Phys. **18**, 283 (1950).

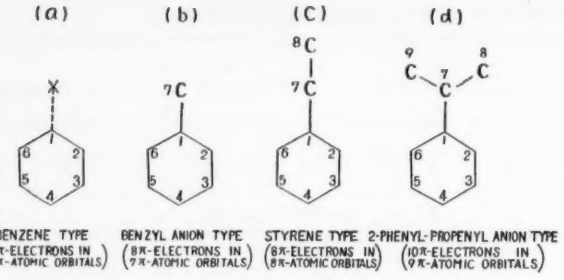

FIG. 3. Characteristic types of π-electron system in mono-substituted benzenes.

in which α_r is the Coulomb integral at the rth carbon atom (in Fig. 3). The parameter a is negative for the substituent which repells the σ electrons in the X−C σ bond, and positive for the substituent which attracts the σ electrons. The parameter ϵ, which represents the diminishing factor of the inductive effect, is taken here to be zero.|| In Fig. 4, the *frontier* electron densities at *ortho*-, *meta*-, and *para*-positions are given for various values of a ranging from -1 to $+1$. Qualitatively the results are as satisfactory as that obtained by other methods.[1,2]¶

Benzyl Anion Type

Halogenobenzenes, phenol, aniline, etc., belong to this type. Two parameters a and b** in Eq. (3) are adopted here as being characteristic of each substituent.

$$\alpha_1=\alpha+a\beta, \qquad \alpha_7=\alpha+b\beta. \tag{3}$$

In Fig. 5, the calculated *frontier* electron densities are plotted for various values of a and b. In halogenobenzenes, phenol, and aniline, the values of a are assumed to be positive and small, so that, as is shown in Fig. 5 (b), the substituents are *ortho-para* directing.

The reactivity of toluene has been hitherto understood by considering the hyperconjugation†† or, otherwise, the purely inductive effect.‡‡ In consideration of the possible contribution of the structure

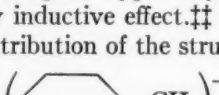

to the electronic state, it seems reasonable that toluene may be put into the class of benzyl anion type, where b is taken to be a large positive value and a a small negative value.§§

Styrene Type

Molecules which have the following substituents belong to this type:

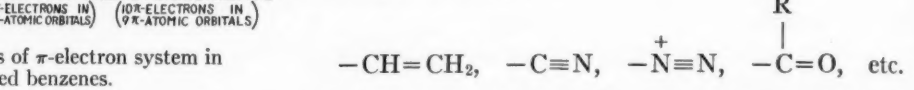

In this type another similar parameter c in addition to a and b in Eq. (3), is considered concerning the side-chain atom C_8. The calculated results are shown in Fig. 6. If $a\simeq 0$ and b, $c\ll 1$, the substituent is *ortho-para* directing, and when $a\simeq 0$ and $c>1$, it is *meta*-directing. In Fig. 6(a) the *frontier* electron density at C_8 atom in styrene is seen to be very large in conformity with the high reactivity of ω position of that compound.

2-Phenyl-propenyl Anion Type

Nitrobenzene, benzoate anion, benzoic esters, etc., belong to this type, and parameters a, b, d, and d' are adopted relating to the C_1, C_7, C_8, and C_9 atom, respectively. Calculated result for nitrobenzene is shown in Fig. 6(c).

Other Types

Diphenyl, stilbene, azobenzene, etc., belong to none of the above four types. These conjugated systems may be treated separately without classification. Calculated *frontier* electron densities for some of these molecules are shown in Fig. 6(d), (e), and (f).

Substitution in Substituted Condensed Aromatics

It is, in principle, possible to apply here the same method as used in the case of substituted benzenes,|| ||

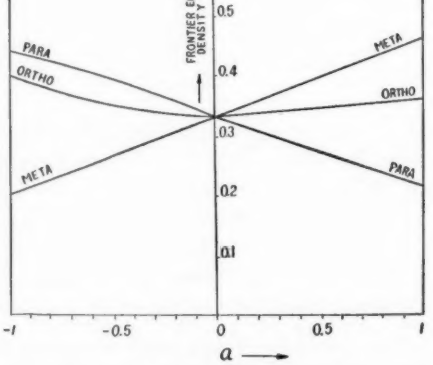

FIG. 4. Frontier electron density *vs* a in benzene type molecules.

|| For some appropriate values of ϵ which are not equal to zero the calculation is also carried out, but the results remain unchanged as to whether *ortho-para* directing or *meta*-directing effect is concluded.

¶ We reserve here the detailed discussions on the problem of $o:p$ ratio, as it seems hopeless to expect any valuable result, having neither sufficient knowledge for determining the exact values of a and ϵ nor a quantitative method of taking into account the influence of steric factors.

** According to Sandorfy (reference 1), Dewar (reference 2), and Jaffé [J. Chem. Phys. **20**, 279 (1952)], the relation between a and b is represented by $a=\epsilon b$, but it may not always be necessary to adhere to this relation when, as in this case, phenolate ion and other anions are also included in the benzyl anion type.

†† For example, Wheland (reference 2) considered

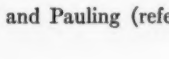

type.

‡‡ E.g., see Wheland and Pauling (reference 1) and Longuet-Higgins (reference 2).

§§ As an example, if $b=5$ and $a=-0.1$, following frontier electron densities are obtained: *ortho*=0.3442, *para*=0.3697, and *meta*=0.2820.

|| || For example, in 1-vinyl naphthalene, the positions ω and 4 are predicted to be most susceptible to attack, and in 2-vinyl

but this requires rather tedious calculations. Here we make use of a simplification similar to that adopted by Longuet-Higgins as to the treatment of substituted condensed aromatics.[4] Namely, the electronic effect of a substituent is represented by only one parameter, either a or b which are given by $\alpha_C=\alpha+a\beta$, and $\alpha_X=\alpha+b\beta$ (X: substituent; C: adjacent carbon). For the electron-repelling¶¶ substituents, we take $a<0$ or $b\geqq 0$, and for the electron-attracting, $a>0$ or $b<0$.*** Thus the calculation is carried out as to the following three cases:

(1) The effect is purely inductive and small (the parameter a ($|a|\ll 1$) is adopted),
(2) The effect is mesomeric and small ($|b|\gg 1$),
(3) The effect is mesomeric and large ($b=0$).

The perturbation method is applied in the cases (1) and (2).

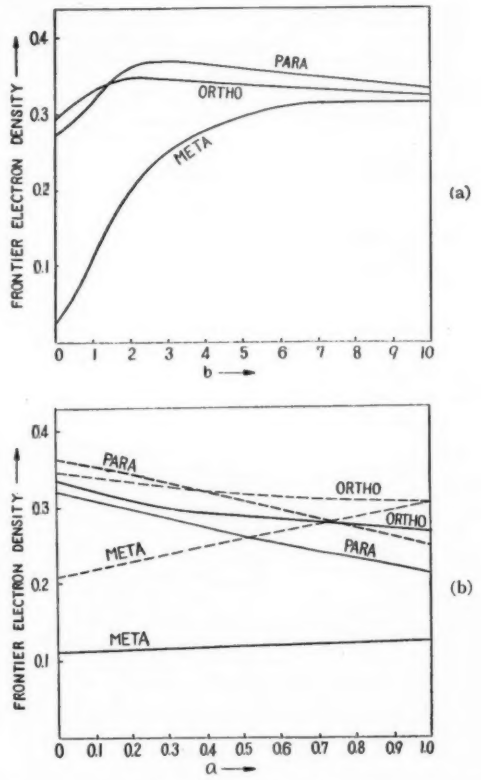

FIG. 5. Frontier electron density in benzyl anion types. (a) Frontier electron density *vs* b when $a=0$. (b) Frontier electron density *vs* a (>0) when $b=1$ (full line curves) and $b=2$ (dotted curves).

naphthalene, the positions 1 and ω. These predicted positions are identical for electrophilic, nucleophilic, and radical reactions.

[4] H. C. Longuet-Higgins (see reference 2); A. and B. Pullman, Rev. sci. **84**, 145 (1946). Longuet-Higgins attempted to explain the orientation in 2-naphthylamine by calculating the densities of total π electrons, taking $\alpha_N\equiv\alpha$. He considered that the effect of amino group was approximately the same as that of $-CH_2$ group in the corresponding isoaromatic system.

¶¶ Here, the substituents which in *benzene* derivatives are *ortho-para*-directing are referred to as electron-repelling substituents, and those which are *meta*-directing, as electron-attracting substituents.

*** The case $b=0$ is omitted for the convenience of calculation.

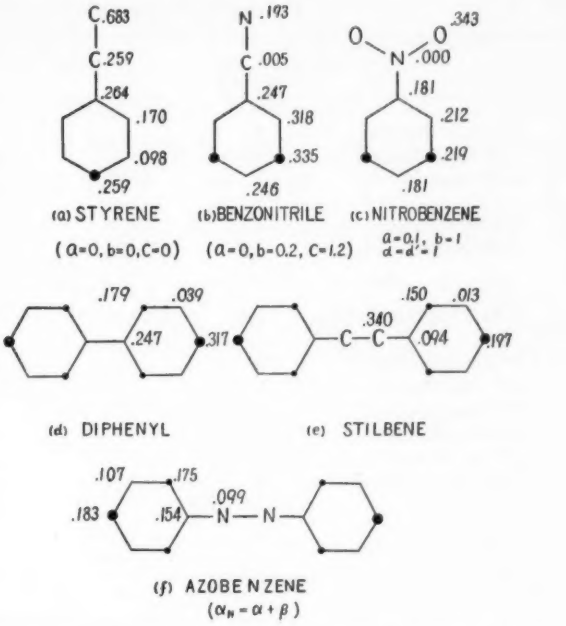

FIG. 6. Frontier electron density in some styrene type and 2-phenyl-propenyl anion type molecules, and in some complex benzene derivatives. Experimental results:

Compound	Reaction	Products
styrene	nitration	ω-NO_2[a]
benzonitrile	nitration	3-NO_2[b]
diphenyl	nitration	2-NO_2, 4-NO_2[c]
stilbene	...	...
azobenzene	nitration	p-NO_2, p,p'-di-NO_2[d]

[a] E. Simon, Ann. Chem. **31**, 269 (1839).
[b] M. Schöpff, Ber. deut. chem. Ges. **18**, 1063 (1885).
[c] Schultz, Schmidt, and Strasser, Ann. Chem. **207**, 352 (1881).
[d] A. Werner and E. Stiasny, Ber. deut. chem. Ges. **32**, 3268 (1899).

As to 1- and 2-substituted naphthalenes the results of calculation are shown in Fig. 7. As can be seen in the figure the *frontier* electron distributions in the case $|b|\gg 1$ coincides exactly with that in the case $|a|\ll 1$ if a is taken to be $-1/b$. The coincidence can be easily proved mathematically for any aromatic hydrocarbon. Thus *the two effects, mesomeric and inductive, may be discussed quite indiscriminately if they are small and in the same direction.*

In Table III experimental results as to the orientation in substituted naphthalenes are compared with the predictions obtained from Fig. 7. The agreement is good, when, as for electron-repelling substituents, b is taken to be zero for amino and hydroxyl and to be large for halogen and methyl and when, as for electron-attracting substituents, a as well as b is assumed to be small. The results of similar treatments of other substituted condensed aromatics are tabulated in Table IV, showing a good agreement of the theory with experiment.

4. NUCLEOPHILIC SUBSTITUTION

The nucleophilic substitution treated here is restricted to the direct replacement of a hydrogen atom with

TABLE III. Products of electrophilic substitution in substituted naphthalenes.

(a) Electron-repelling substituents

Compounds	Predicted position	Structure of the reaction products: Chlorination	Bromination	Nitration	Sulfonation
1-F-naphthalene	4	...	4-Br[h]	...	4-SO_3H[h]
1-Cl-naphthalene	4	4-Cl[a]	4-Br[i]	4-NO_2[s]	4-SO_3H, 5-SO_3H[ee]
1-Br-naphthalene	4	4-Cl[b]	4-Br[j] 5-Br[k]	...	4-SO_3H[dd]
1-I-naphthalene	4	4-Cl[c]	4-Br[l]	...	...
1-OH-naphthalene	2,4	2-Cl[d] 4-Cl[e] 2,4-di-Cl[e]	...	2-NO_2[t] 2,4-di-NO_2[u]	2-SO_3H[ee] 4-SO_3H[ff] 2,4-di-SO_3H[ee]
1-NH_2-naphthalene	2,4	4-Cl[f]	2,4-di-Br[m]	(4-NO_2, 5-NO_2, 8-NO_2[v])	4-SO_3H[gg] 2,4-di-SO_3H[gg]
1-CH_3-naphthalene	4	...	4-Br[n]	4-NO_2[w]	4-SO_3H[hh]
2-F-naphthalene	1,8	...	...	1-NO_2[h]	...
2-Cl-naphthalene	1,8	...	...	...	8-SO_3H, 6-SO_3H[ii]
2-Br-naphthalene	1,8	...	...	1-NO_2, 3-NO_2[x]	8-SO_3H[jj]
2-I-naphthalene	1,8	...	1-Br[o]	...	8-SO_3H[jj]
2-OH-naphthalene	1	1-Cl[g]	1-Br[p] 8-Br[q] 1,6-di-Br[p]	1-NO_2[y] 1,6-di-NO_2[z]	1-SO_3H[kk] 6-SO_3H[ll]
2-NH_2-naphthalene	1	...	1,6-di-Br[r]	(8-NO_2, 5-NO_2[aa])	(5-SO_3H, 8-SO_3H[mm])
2-CH_3-naphthalene	1,8	...	...	1-NO_2[bb]	6-SO_3H[hh]

(b) Electron-attracting substituents

Compounds	Predicted position	Structure of the reaction products: Halogenation	Nitration	Sulfonation
1-COOH-naphthalene	8,5	5-Cl[nn] 8-Cl[nn] 5-8-di-Cl[oo] 5-Br[pp]	5-NO_2[aaa] 8-NO_2[aaa]	5-SO_3H[ggg] 6-SO_3H[ggg] 7-SO_3H[ggg]
1-NO_2-naphthalene	8,5	5-Cl[qq] 8-Cl[qq] 5,8-di-Cl[rr] 5-Br[ss]	5-NO_2[bbb] 8-NO_2[bbb]	5-SO_3H[hhh]
1-SO_3H-naphthalene	8,5	5-Br[tt]	4-NO_2[ccc] 5-NO_2[ccc] 8-NO_2[ccc]	5-SO_3H[iii]
1-CHO-naphthalene	8,5	5-Br[uu]	...	...
1-CN-naphthalene	8,5	5-Cl[vv] 5-Br[ww]	5-NO_2[ddd]	...
2-COOH-naphthalene	5,4	5,8-di-Cl[xx] 5-Br[yy]	5-NO_2[eee] 8-NO_2[eee]	5-SO_3H[jjj] 8-SO_3H[kkk]
2-NO_2-naphthalene	5,4	...	...	5-SO_3H[lll] 8-SO_3H[lll]
2-SO_3H-naphthalene	5,4	5-Cl[zz] 8-Cl[zz]	5-NO_2[fff] 8-NO_2[fff]	5-SO_3H[iii] (6 and 7-SO_3H[mmm])

[a] H. E. Armstrong, Chem. News **66**, 189 (1892).
[b] I. Guareschi and P. Biginelli, Chem. Zentr. **1877**, 518 (1877).
[c] C. Willgerodt and P. Schlöser, Ber. deut. chem. Ges. **33**, 693 (1900).
[d] R. Lesser and G. Gad, Ber. deut. chem. Ges. **56**, 972 (1923).
[e] P. T. Cleve, Ber. deut. chem. Ges. **21**, 894 (1886).
[f] P. Seidler, Ber. deut. chem. Ges. **11**, 1201 (1878).
[g] Ioffe, Kuznetzov, and Litovskii, J. Gen. Chem. (U.S.S.R.) **5**, 1685 (1935).
[h] Schieman, Gueffroy, and Wikelmüller, Ann. Chem. **487**, 270 (1931).
[i] I. Guareschi and P. Biginelli, Gaz. chim. ital. **16**, 152 (1886).
[j] C. Glaser, Ann. Chem. **135**, 42 (1865).
[k] Yu. S. Zalkind and S. B. Faermann, J. Russ. Phys.-Chem. Soc. **62**, 1021 (1930).
[l] H. Hirtz, Ber. deut. chem. Ges. **29**, 1409 (1896).
[m] R. Condon and J. Kenyon, J. Chem. Soc. (London) **1935**, 1591.
[n] L. F. Fieser and M. Fieser, *Organic Chemistry* (D. C. Heath and Company, Boston, 1950), second edition, p. 792.
[o] H. Hirtz, Ber. deut. chem. Ges. **29**, 1409 (1896).
[p] Verma, Mozumdar, and Rajah, J. Indian. Chem. Soc. **10**, 591 (1933).
[q] K. Fries and K. Schimmelschmidt, Ber. deut. chem. Ges. **58**, 2840 (1925).
[r] L. Michaellis, Ber. deut. chem. Ges. **26**, 2196 (1893).
[s] A. Atterberg, Ber. deut. chem. Ges. **9**, 927 (1876).
[t] H. H. Hodgson and E. W. Smith, J. Chem. Soc. (London) **1935**, 671 (1935).
[u] J. Schmidt, Ber. deut. chem. Ges. **33**, 3245 (1900).
[v] R. Meloda and J. Streatfeld, J. Chem. Soc. (London) **63**, 1055 (1893).
[w] R. Lesser, Ann. Chem. **402**, 11 (1914).
[x] Yu. Zalkind and F. Filinov, J. Gen. Chem. (U.S.S.R.) **4**, 979 (1943).
[y] A. Pictet de Krijanowski, Chem. Zentr. **1903**, II, 1109 (1903).
[z] J. Schmidt, Ber. deut. chem. Ges. **33**, 3246 (1900).
[aa] P. Friedländer and St. Szymanski, Ber. deut. chem. Ges. **25**, 2076 (1892).
[bb] H. E. Fierz-David and E. Mannhart, Helv. Chim. Acta **20**, 102 4(1937).
[cc] H. E. Armstrong and W. P. Wynne, Chem. News **61**, 285 (1890).
[dd] H. E. Armstrong and S. Williamson, Chem. News **54**, 256 (1886).
[ee] M. Conrad and W. Fischer, Ann. Chem. **273**, 105 (1893).
[ff] K. Holdermann, Ber. deut. chem. Ges. **39**, 1225 (1906).
[gg] W. H. Hunter and M. M. Sprung, J. Am. Chem. Soc. **53**, 1432 (1931).
[hh] L. F. Fieser and M. Fieser, *Organic Chemistry* (D. C. Heath and Company, Boston, 1950), second edition, p. 793.
[ii] H. E. Armstrong and W. P. Wynne, Chem. News **55**, 91 (1887).
[jj] H. E. Armstrong and W. P. Wynne, Chem. News **60**, 58 (1889).
[kk] H. E. Armstrong, Ber. deut. chem. Ges. **15**, 202, 207 (1882).
[ll] L. Schaeffer, Ann. Chem. **152**, 296 (1869).
[mm] H. Erdmann, Ann. Chem. **275**, 280 (1893).
[nn] A. G. Ekstrand, J. prakt. Chem. **38**, 148 (1888).
[oo] A. G. Ekstrand, J. prakt. Chem. **38**, 151, 153 (1888).
[pp] O. Gausmann, Ber. deut. chem. Ges. **9**, 1520 (1875).
[qq] A. G. F. Anilinf, Germ. Pat. 99, 758; Chem. Zentr. **1899** I, 463 (1899).
[rr] Bayer & Co. Germ. Pat. 293, 318; Chem. Zentr. **1916** II, 359.
[ss] I. Guareschi, Ann. Chem. **222**, 291 (1884).
[tt] L. Darmstaedter and H. Wichelhaus, Ann. Chem. **152**, 303 (1869).
[uu] P. Ruggli and R. Preus, Helv. Chim. Acta **24**, 1345 (1941).
[vv] A. G. Ekstrand, J. prakt. Chem. **38**, 147 (1888).
[ww] O. Hausmann, Ber. deut. chem. Ges. **9**, 1516 (1876).
[xx] A. G. Ekstrand, Ber. deut. chem. Ges. **17**, 1605 (1884).
[yy] H. Goldstein and R. Matthey, Helv. Chim. Acta **21**, 62 (1938).
[zz] Chr. Rudolf, Germ. Pat. **101**, 348; Chem. Zentr. **1899** I, 960 (1899).
[aaa] A. G. Ekstrand, J. prakt. Chem. **38**, 156, 241 (1888).
[bbb] P. Friedländer, Ber. deut. chem. Ges. **32**, 3531 (1899).
[ccc] H. Erdmann and C. Süvern, Ann. Chem. **275**, 231 (1893).
[ddd] Fr. Graeff, Ber. deut. chem. Ges. **16**, 2246 (1833).
[eee] A. G. Ekstrand, J. prakt. Chem. **42**, 273 (1890).
[fff] H. E. Armstrong and W. P. Wynne, Chem. News **59**, 94 (1889).
[ggg] M. Stumpf, Ann. Chem. **188**, 10 (1877).
[hhh] H. Erdmann, Ann. Chem. **247**, 311 (1888).
[iii] A. E. Armstrong and W. P. Wynne, Chem. News **55**, 136 (1887).
[jjj] M. Stumpf, Ann. Chem. **188**, 10 (1877).
[kkk] M. Stumpf, Ann. Chem. **188**, 12 (1877).
[lll] H. Kappeler, Ber. deut. chem. Ges. **45**, 633 (1912).
[mmm] H. E. Armstrong, Ber. deut. chem. Ges. **15**, 204 (1882).

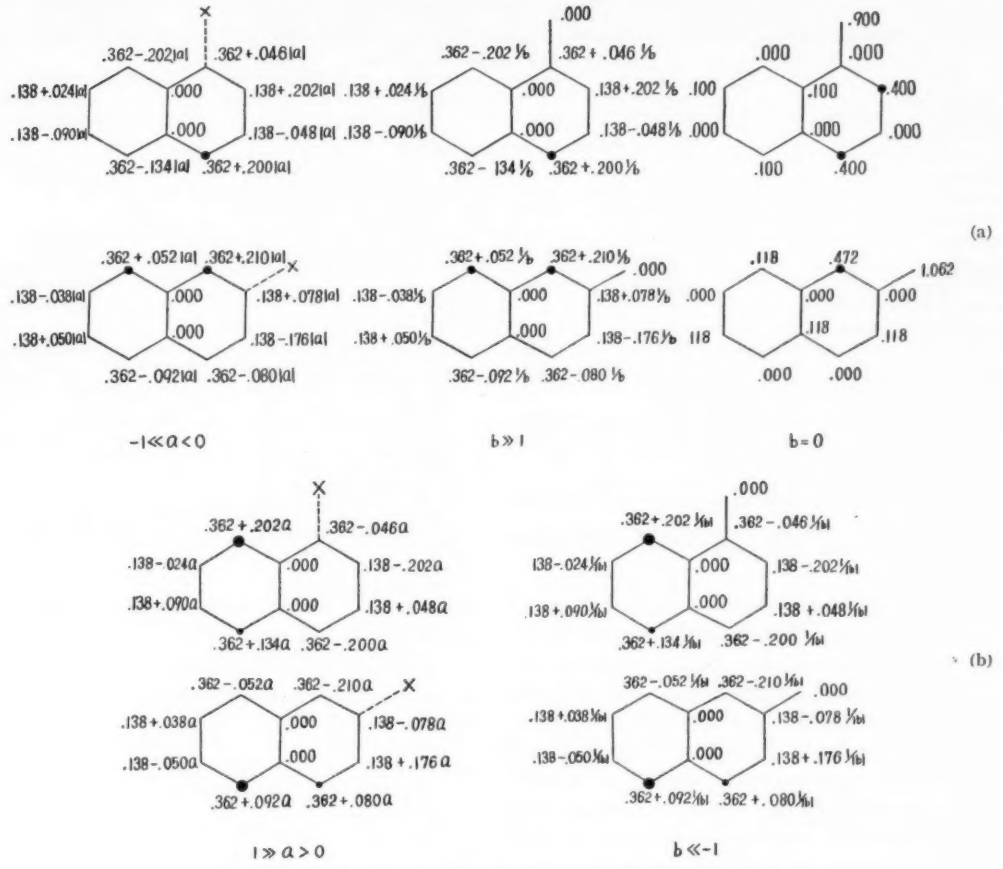

FIG. 7. The frontier electron densities in 1- and 2-substituted naphthalenes.
(a) Electron-repelling substituent. (b) Electron-attracting substituent.

nucleophilic reagents such as OH^- and NH_2^-.††† The results of the calculation as to the five known cases, are shown in Fig. 8 together with the experimental results.

5. RADICAL SUBSTITUTION

The calculated *frontier* electron densities‡‡‡ as to the reactivity in radical substitution in several aromatic and

††† A typical example of the nucleophilic substitution in conjugated systems may be the hydrolysis of aryl halides, which, however, cannot be the object of the present treatment, because in such a reaction the point of attack is originally fixed. Of course it is possible, by means of the frontier electron method, to predict which one of all the possible mono-halogeno-derivatives is most liable to hydrolysis.

‡‡‡ In this calculation the contributions of two unpaired electrons in different two orbitals are assumed to be in equal weight.

TABLE IV. Products of electrophilic substitution in substituted condensed aromatic hydrocarbons.

(a) Electron-repelling substituents

Compounds	Predicted position	Structure of the reaction products: Halogenation	Nitrosation or nitration	Sulfonation
9-Cl-anthracene	10	10-Cl[a]	...	...
9-Br-anthracene	10	10-Br[b]	...	...
9-OH-anthracene	10	10-Br[c]	...	...
1-OH-anthracene	2,4	...	2-NO, 4-NO[m]	...
2-OH-anthracene	1	...	1-NO[m]	...
9-Cl-phenanthrene	10	10-Cl[d]	...	...
9-Br-phenanthrene	10	...	10-NO_2[n]	(2-SO_3H[p])
9-OH-phenanthrene	10	10,3-di-Br[e]	...	...
2-Cl-chrysene	8	8-Cl[f]	8-NO_2[o]	...
2-Br-chrysene	8	...	8-NO_2[o]	...
3-Br-pyrene	5,8	5,8-di-Br[g]	...	...
3-NH_2-pyrene	5,8	5-Cl[h]	...	5-SO_3H, 8-SO_3H[q]
12-Cl-naphthacene	5	5-Cl[i], 6-Cl[j]	...	...
12-Br-naphthacene	5	5-Br[i], 6-Br[j]	...	...
3-Cl-perylene	10	9-Cl[k]	...	...
3-Br-perylene	9,10	9-Br, 10-Br[l]	...	...

(TABLE IV. *Continued on next page with footnotes.*)

TABLE IV—*Continued.*

(b) Electron-attracting substituents

Compounds	Predicted position	Structure of the reaction products: Halogenation	Nitration	Sulfonation
9-NO_2-anthracene	10	...	10-NO_2[e]	...
9-COOH-anthracene	10	10-Br,10-Cl[r]	...	...
2-NO_2-chrysene	8	...	8-NO_2[t]	...
2-CN-chrysene	8	...	8-NO_2[t]	...
2-COOH-chrysene	8	...	8-NO_2[t]	...
3-SO_3H-pyrene	5	...	...	5-SO_3H[v]
3-NO_2-perylene	4,(9)	...	(10-NO_2[u])	...
3-SO_3H-perylene	4,(9)	...	...	(9-SO_3H, 10-SO_3H[w])
12-substituted naphthacene	11	...	...	...
13-substituted pentacene	6	...	...	...

[a] Ed. Lippmann and I. Pollack, Ber. deut. chem. Ges. **34**, 2768 (1901).
[b] C. Graebe and C. Liebermann, Ber. deut. chem. Ges. **1**, 186 (1868).
[c] Fr. Goldmann, Ber. deut. chem. Ges. **20**, 2437 (1887).
[d] H. Sandqvist and A. Hagelin, Ber. deut. chem. Ges. **51**, 1521 (1919).
[e] J. Schimel and O. Spoun, Ber. deut. chem. Ges. **43**, 1802 (1910).
[f] Soc. Pour. L'ind. Chim. à Bâle, Swiss Pat. 204, 239 (July 17, 1939).
[g] E. Clar, Ber. deut. chem. Ges. **69**, 1671 (1936).
[h] Corell, Vollman, and Becker, U.S.P. 2,185,661 (Jan. 2, 1939).
[i] I. J. Postovskii and R. G. Beyles, Compt. Rend. Acad. Sci. U.R.S.S. **39**, 102 (1943).
[j] C. Marschalk and C. Stumm, Bull. soc. chim. France **1948**, 418 (1948).
[k] Zinke, Funke, and Pongratz, Ber. deut. chem. Ges. **58**, 330 (1925).
[l] Zinke, Kinner, and Wolfbauer, Ber. deut. chem. Ges. **58**, 328 (1925).
[m] R. Anschütz, *Chemie der Kohlenstoffverbindungen* (1935), p. 702.
[n] R. K. Callow and J. M. Gulland, J. Chem. Soc. (London) **1929**, 2424.
[o] I. G. Farbenind. A.-G. Fr. Pat., 794, 534 (February 19, 1936).
[p] L. E. May and E. Mosettig, J. Org. Chem. **11**, 15 (1946).
[q] M. Corell, U.S.P. 2,046,249 (June 30, 1936).
[r] G. Behla, Ber. deut. chem. Ges. **20**, 704 (1887).
[s] J. Meisenheimer, and E. Connerade, Ann. Chem. **330**, 167 (1904).
[t] I. G. Farbenind. A.-G. Fr. Pat., 794,534 (Feb. 19, 1936).
[u] Zinke, Hirsch, and Brozek, Monatshefte Chem. **51**, 205 (1929).
[v] E. Tietze and O. Bayer, Ann. Chem. **540**, 189 (1939).
[w] C. Marschalk, Chem. Zentr. **1927 I**, 1833 (1927).

heteroaromatic molecules are shown in Fig. 9 together with experimental results. The agreements of theory with experiment are satisfactory. (Similar results are obtainable by means of the localization method[2] and also by computing the free valency number.[5] The latter method has been developed by Daudel, Vroelant, and Coulson *et al.*[5] and most recently examined experimentally by Kooyman and Farenhorst,[6] and Roitt and Waters.[7] It can, however, be pointed out that the free valency method contains an ambiguity in evaluating

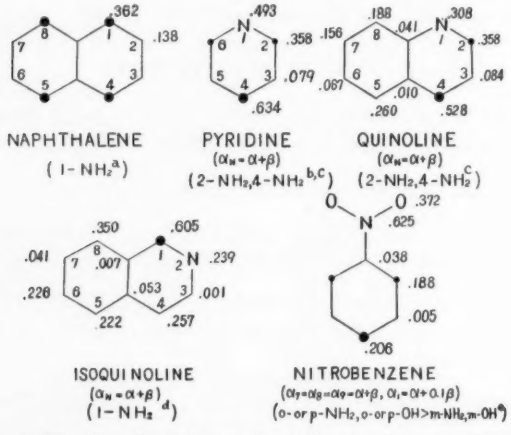

FIG. 8. The frontier electron densities for the case of nucleophilic substitution. (Experimental results are shown in brackets. The parameters used are the same as before.)

Literatures cited in Fig. 8:

[a] F. Sachs, Ber. deut. chem. Ges. **39**, 3006 (1906); C. Graebe, *ibid.* **34**, 1778 (1901).
[b] A. E. Chichibabin, Ber. deut. chem. Ges. **56**, 1879 (1923).
[c] A. E. Chichibabin, J. Russ. Phys.-Chem. Soc. **46**, 1216 (1914).
[d] M. T. Leffler, *Organic Reaction* (1942), p. 91.
[e] A. Wohl, Ber. deut. chem. Ges. **32**, 3486 (1899); Bergstrom, Granare, and Erickson, J. Organ. Chem. **7**, 98 (1942).

[5] C. Vroeland and R. Daudel, Bull. soc. chim. France **16**, 217 (1949); Buu-Hoi, Daudel, and Vroelant, Bull. soc. chim. France **16**, 211 (1949); Daudel, Sandorfy, Vroelant, Yvan, and Chalvet, Bull. soc. chim. France **19**, 66 (1950); Burkitt, Coulson, and Longuet-Higgins, Trans. Faraday Soc. **47**, 553 (1951).

[6] E. C. Kooyman and E. Farenhorst, Nature **169**, 153 (1952).

[7] I. M. Roitt and W. A. Waters, J. Chem. Soc. (London) **1952**, 2695 (1952).

N_{max} and requires a most laborious calculation of bond order in larger organic molecules.)

In *alternant* hydrocarbons,[8] the electron distribution in the lowest unoccupied orbital is identically the same

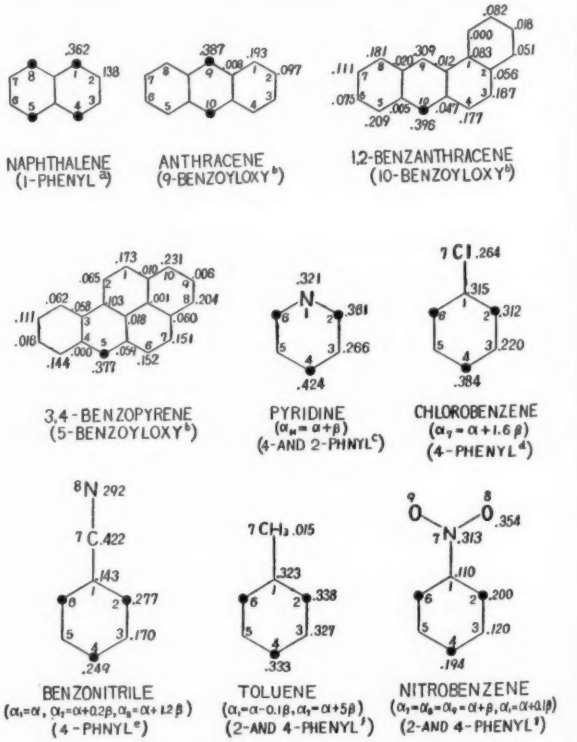

FIG. 9. The frontier electron densities for the case of radical substitution.

Literatures cited in Fig. 9:

[a] W. A. Waters, J. Chem. Soc. (London) **1939**, 864 (1939).
[b] See reference 7.
[c] Haworth, Heilbron, and Hey, J. Chem. Soc. (London) **1940**, 349 (1940).
[d] D. H. Hey, J. Chem. Soc. (London) **1934**, 1966.
[e] M. Gomberg and W. E. Bachmann, J. Am. Chem. Soc. **46**, 2389 (1924).
[f] M. Gomberg and J. C. Pernert, J. Am. Chem. Soc. **48**, 1372 (1926).
[g] D. Detar and H. Scheifele, Jr., J. Am. Chem. Soc. **73**, 1442 (1951).

[8] See C. A. Coulson and H. C. Longuet-Higgins, Proc. Roy. Soc. (London) **A192**, 16 (1947).

Frontier electron density for primary addition:

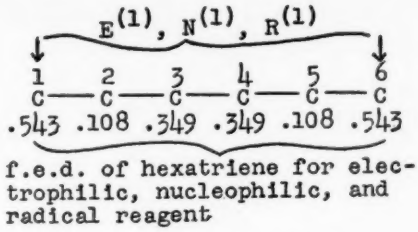

f.e.d. of hexatriene for electrophilic, nucleophilic, and radical reagent

Frontier electron densities for secondary addition:

a. $E^{(1)}$-$N^{(2)}$ type addition

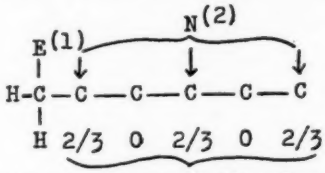

f.e.d. of pentadienyl cation for nucleophilic reagent

b. $E^{(1)}$-$R^{(2)}$ type addition

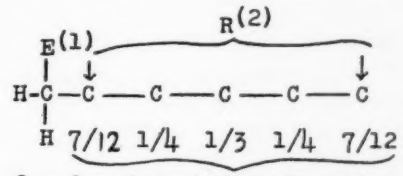

f.e.d. of pentadienyl cation for radical reagent

c. $N^{(1)}$-$E^{(2)}$ type addition

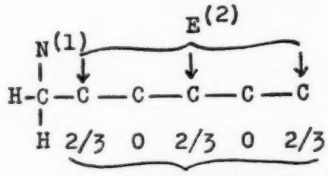

f.e.d. of pentadienyl anion for electrophilic reagent

d. $N^{(1)}$-$R^{(2)}$ type addition

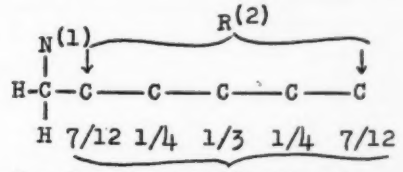

f.e.d. of pentadienyl anion for radical reagent

e. $R^{(1)}$-$E^{(2)}$ type addition

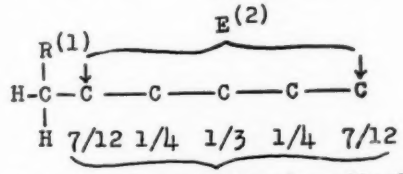

f.e.d. of pentadienyl radical for electrophilic reagent

f. $R^{(1)}$-$N^{(2)}$ type addition

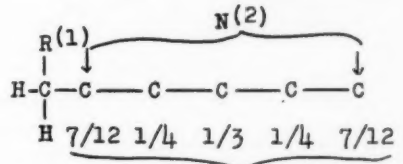

f.e.d. of pentadienyl radical for nucleophilic reagent

g. $R^{(1)}$-$R^{(2)}$ type addition

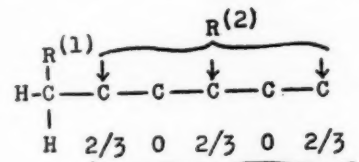

f.e.d. of pentadienyl radical for radical reagent

FIG. 10. The frontier electron densities for addition to hexatriene (f.e.d. = frontier electron density).

as in the highest occupied orbital,[9] so that the predicted points of attack are identical in any of electrophilic, nucleophilic, and radical substitution. In most of hydrocarbons treated there predicted positions agree very well with the points of the maximum free valency number, the values of which are found by Kooyman and Farenhorst[6] to be parallel with the rates of radical substitution.

[9] See our previous paper (reference 3).

6. ADDITION

Addition reactions to a conjugated system may be considered to proceed successively through the transition state similar to that of substitution. (Brown[10] and Dewar[11] assumed a simultaneous addition in their treatment of the Diels-Alder diene synthesis. But, from the reaction-kinetical standpoint, successive mechanism

[10] R. D. Brown, J. Chem. Soc. (London) **1950**, 691, 2720, 3249 (1950).

[11] M. J. S. Dewar, J. Am. Chem. Soc. **74**, 3357 (1952).

TABLE V. Comparison of predicted structures of addition products with experimental results.

Conjugated molecules	Predicted positions	Experimental results
butadiene	1:2, 1:4	1:2, 1:4
hexatriene	1:2, 1:4, 1:6	1:2, 1:6[a]
styrene	$\alpha:\omega$	$\alpha:\omega$
stilbene	$\alpha:\alpha'$	$\alpha:\alpha'$
anthracene	9:10	9:10
phenanthrene	9:10	9:10

[a] Farmer, Laroria, Switz, and Thorpe, reference 12.

is naturally to be preferred.) Then we can apply here the *frontier* electron method analogously, using the same classification into three types, *viz.*, electrophilic (E), nucleophilic (N), and radical (R).

In discussing the reactivity in polyene and some aromatic molecules, seven cases§§§ of successive addition are to be considered according to the type of reagent, which are indicated in Fig. 10.

Taking hexatriene as an example, the primary attack is predicted to occur at the terminal carbon atom, in any case of $E^{(1)}$, $N^{(1)}$, and $R^{(1)}$. In the secondary attack, as one atomic π orbital at the terminal carbon has disappeared as a result of the primary addition, the point of attack is now controlled by the *frontier* electron density of a conjugated system consisting of five carbon atoms. From the results shown in Fig. 10, it can be concluded that the structures of the addition products are predicted to be 1:2, 1:4, or 1:6, taking all the possible cases of addition into consideration. Experimentally, addition product of bromine to hexatriene is reported to be a mixture of 1:2- and 1:6-dibromide.[12]

Similar calculations for all the possible modes of addition are carried out as to butadiene, stilbene, styrene, anthracene, and phenanthrene. The results are in a complete agreement with experiment, as is shown in Table V.|| || ||

It is possibly of importance in obtaining a knowledge of the true feature of activated complexes to consider the theoretical foundation of the fundamental postulates, which, however, is omitted in the present paper and will be published elsewhere.

The authors are grateful to the Education Ministry of the Japanese Government for a grant-in-aid.

§§§ Combining the three types of primary attack, *viz.*, $N^{(1)}$, $E^{(1)}$, and $R^{(1)}$, with three types of secondary attack, *viz.*, $E^{(2)}$, $N^{(2)}$, and $R^{(2)}$, we have nine varieties of mode of addition. But the two among these, $E^{(1)}-E^{(2)}$ and $N^{(1)}-N^{(2)}$ type additions, which are not likely to happen, are left out of consideration.

[12] Farmer, Laroria, Switz, and Thorpe, J. Chem. Soc. (London) **1927**, 2937 (1927).

|| || || The frontier electron method is also useful in the treatment of cationoid, anionoid, and radical polymerization, which will be published elsewhere.

THE JOURNAL OF CHEMICAL PHYSICS VOLUME 22, NUMBER 8 AUGUST, 1954

Contributions of Vibrational Anharmonicity and Rotation-Vibration Interaction to Thermodynamic Functions

R. E. PENNINGTON* AND K. A. KOBE
Department of Chemical Engineering, University of Texas, Austin, Texas

(Received March 23, 1954)

Certain correction terms applying to the rigid-rotator harmonic-oscillator approximation for the thermodynamic functions have been worked out in a general form. Tables of the functions which appear in these correction terms are presented. These results have been applied in the calculation of the thermodynamic properties of nitrous oxide. A comparison of the present procedure and that of Mayer and Mayer for diatomic molecules is given.

I. INTRODUCTION

MORE detailed knowledge of the spectra of polyatomic molecules is gradually becoming available. With the determination of the anharmonicity and interaction constants of a molecule it becomes possible to improve the statistically calculated thermodynamic functions by taking these effects into account. Several papers[1–3] have dealt with this problem in some detail. The calculations for determining these corrections are rather lengthy. Therefore, approximations to a generalized partition function and its derivatives have been worked out, and tables of the functions which appear in the correction terms have been compiled. These tables were used to calculate the thermodynamic functions of nitrous oxide at selected temperatures.

II. THE PARTITION FUNCTION

For the present purposes, it is assumed that the energy levels of some molecule of interest may be represented in the nomenclature of Herzberg[4] in the following

* Present address: Bureau of Mines Petroleum Experiment Station, Bartlesville, Oklahoma.

[1] A. R. Gordon, J. Chem. Phys. **3**, 259 (1935).

[2] L. S. Kassel, Chem. Rev. **18**, 277 (1936).

[3] Stockmayer, Kavanagh, and Mickley, J. Chem. Phys. **12**, 408 (1944).

[4] G. Herzberg, *Infrared and Raman Spectra of Polyatomic Molecules* (D. Van Nostrand Company, Inc., New York, 1945).

manner:

$$T-G_0=\sum_i \nu_i v_i+\sum_i x_{ii}v_i(v_i-1)+\sum_{i<j} x_{ij}v_iv_j+\sum_i g_{ii}(l_i^2-v_i)+F_v. \quad (1)$$

The term F_v stands for the rotational levels and takes different forms depending on the structure of the molecule: for linear molecules[5]

$$F_v=B_v[J(J+1)-l^2]-DJ^2(J+1)^2, \quad (2)$$

for spherical top molecules

$$F_v=B_vJ(J+1) \quad (3)$$

for symmetric top molecules

$$F_v=B_vJ(J+1)+(A_v-B_v)K^2 \quad (4)$$

for asymmetric top molecules

$$F_v=\tfrac{1}{2}(B_v+C_v)J(J+1)+[A_v-\tfrac{1}{2}(B_v+C_v)]W_\tau^v. \quad (5)$$

In each of these representations of the rotational levels the effective inertial quantities are used, i.e.,

$$B_v=B_0-\sum_i \alpha_i^B v_i \quad (6)$$

and similarly for A_v and C_v. In what follows, the form

$$B_v=B_0(1-\sum_i b_iv_i), \quad (7)$$

etc., will be more convenient to employ.

It is only in the case of linear molecules that a centrifugal distortion term has been included. Sufficient spectroscopic data for the inclusion of such terms for the other cases are not usually available.[4] Wilson[6] has proposed a method whereby the effects of centrifugal distortion on the thermodynamic functions of nonlinear molecules may be estimated. He has shown these effects to be significant for such light hydrogen-containing molecules as water and ammonia. It is to be noted also that none of representations (1)–(5) takes into account Coriolis splitting or Fermi resonance. The effect of Coriolis splitting on the thermodynamic functions should be very small.[7] No generalized representation of the energy levels which takes into account the effects of Fermi resonance *a priori* is available. However, except in the case of a close resonance in some of the lower-lying levels, this effect should also produce a small contribution to the thermodynamic functions. These limitations should be kept in mind in the application of results based on Eqs. (1)–(5).

If Eq. (1) is used to represent the energy levels, a "generalized" internal partition function may be written as

$$Q=Q_0^0Q_v'Q_lQ_R(v,l)$$

$$Q_0^0=\exp(-hcG_0/kT)$$

$$Q_v'=\sum_v \exp[-\sum_i u_iv_i+\sum_i X_{ii}'u_iv_i(v_i-1)+\sum_{i<j} X_{ij}(u_iu_j)^{\frac{1}{2}}v_iv_j \quad (8)$$

$$Q_l=\sum_l \exp[-\sum_i G_{ii}u_i(l_i^2-v_i)].$$

These expressions have been abbreviated by the shorthand

$$u_i=hcv_i/kT \quad X_{ij}=-x_{ij}/(\nu_i\nu_j)^{\frac{1}{2}}$$
$$X_{ii}'=-x_{ii}/\nu_i \quad G_{ii}=g_{ii}/\nu_i. \quad (9)$$

Rotational Sums

The form of $Q_R(v,l)$ depends on the molecular structure. For linear molecules

$$Q_R(v,l)=[\exp(\beta_vl^2)]\sum_{J=l}^{J=\infty}(2J+1)\times\exp[-\beta_vJ(J+1)][1-\delta J(J+1)], \quad (10)$$

with

$$\beta_v=(1-\sum_i b_iv_i)B_0hc/kT=(1-\sum_i b_iv_i)\beta_0$$
$$\delta=D/B_0. \quad (11)$$

By introducing the asymptotic Euler-Maclaurin expansion first given by Mulholland[8] and neglecting second-order terms in v and l, this relation may be reduced to

$$Q_R(v,l)=(1-\sum_i b_iv_i)^{-1}(1+2\delta/\beta_0)Q_R^0$$
$$Q_R^0=\sigma^{-1}\beta_0^{-1}(1+\beta_0/3+\beta_0^2/15+\cdots), \quad \beta_0<1 \quad (12)$$

σ = symmetry number.

The expression for Q_R^0 will be satisfactory except for large values of β_0 (i.e., very low temperatures or an extremely large value of B_0). The treatment of Mayer and Mayer[9] of the rotational partition function for diatomic molecules is equally applicable to this case and they give equations and tables for Q_R^0 for large β_0. One further operation on $Q_R(v,l)$ will make it more useful when substituted back into Q. This consists of the expansion,

$$(1-\sum_i b_iv_i)^{-1}\approx 1+\sum_i (b_i+b_i^2)v_i+\sum_i b_i^2v_i(v_i-1)+2\sum_{i<j} b_ib_jv_iv_j, \quad (13)$$

[5] Note that the term $-B_vl^2$ has not been taken into the vibrational formula.
[6] E. B. Wilson, J. Chem. Phys. **4**, 526 (1936).
[7] E. B. Wilson, J. Chem. Phys. **7**, 948 (1939).
[8] H. P. Mulholland, Proc. Cambridge Phil. Soc. **24**, 280 (1928).
[9] J. E. Mayer and M. G. Mayer, *Statistical Mechanics* (John Wiley and Sons, Inc., New York, 1940).

TABLE I. Rotational constants in the correction terms.

Linear	Spherical top
$s=2Dk/B_e^2hc$ $r_i=b_i+b_i^2$	$s=0$ $r_i=3b_i/2+15b_i^2/8$
Symmetrical top	**Asymmetrical top**
$s=0$ $r_i=b_i+a_i/2+b_i^2+a_ib_i/2+3a_i^2/8$	$s=0$ $r_i=(a_i+b_i+c_i)/2+(a_i^2+b_i^2+c_i^2)/4+(a_i+b_i+c_i)^2/8$

and the neglect of purely second-order terms. Similar expressions may be derived for the other cases.[1,2] Actually, the leading term in the expansion of Q_R^0 for these other cases, is, at room temperature and higher, almost always a sufficient approximation. This is the classical partition function for rotation and is given by

$$Q_R^0=\sigma^{-1}[\pi(kT/hc)^3/ABC]^{\frac{1}{2}}, \tag{14}$$

where for symmetrical top molecules $C=B$ and for spherical top molecules $C=A=B$. A general expression for $Q_R(v,l)$ may therefore be taken as

$$Q_R(v,l)\approx(1+\sum_i r_iv_i)(1+2\delta/\beta_0)Q_R^0, \tag{15}$$

in which the r_i are the combinations of the rotation-vibration interaction constants given in Table I and $\delta\neq0$ only for linear molecules.

Vibrational Angular Momentum Sums

The quantum numbers l_i of the degenerate vibrations take on the values v_i, v_i-2, $\cdots$, v_i-2v_i. The summation over the l_i represented by Q_l may be accomplished in the following manner. For a particular l_i

$$\sum_{l_i}\exp[-G_{ii}u_i(l_i^2-v_i)]\approx\sum_{l_i}[1-G_{ii}u_i(l_i^2-v_i)]$$

$$\sum_{l_i}1=v_i+1$$

$$\sum_{l_i}(l_i^2-v_i)=(v_i+1)(v_i)(v_i-1)/3 \tag{16}$$

$$\sum_{l_i}\exp[-G_{ii}u_i(l_i^2-v_i)]\approx[v_i+1][1-G_{ii}u_iv_i(v_i-1)/3]\approx[v_i+1]\exp[-G_{ii}u_iv_i(v_i-1)/3].$$

TABLE II. The functions ${}^n\varphi$.

u	${}^1\varphi$	${}^2\varphi$	${}^3\varphi$	${}^4\varphi$	${}^5\varphi$	${}^6\varphi$	${}^7\varphi$	${}^8\varphi$	${}^9\varphi$	${}^{10}\varphi$	${}^{11}\varphi$
0.20	4.5167	4.9834	10.0000	8.1600	9.8465	19.9874	2.0199	0.6033	0.9967	0.9033	1.7078
0.25	3.5208	3.9792	8.0000	6.1980	7.8120	15.9798	1.7604	0.6302	0.9948	0.8802	1.5087
0.30	2.8583	3.3084	6.6664	4.9022	6.4463	13.3058	1.5656	0.6575	0.9925	0.8575	1.3502
0.35	2.3862	2.8281	5.7138	3.9858	5.4619	11.3895	1.4117	0.6852	0.9898	0.8352	1.2197
0.40	2.0333	2.4669	4.9996	3.3076	4.7188	9.9522	1.2860	0.7133	0.9868	0.8133	1.1096
0.45	1.7596	2.1851	4.4437	2.7867	4.1344	8.8277	1.1804	0.7418	0.9833	0.7918	1.0151
0.50	1.5415	1.9589	3.9990	2.3762	3.6629	7.9248	1.0900	0.7708	0.9794	0.7708	0.9327
0.55	1.3638	1.7730	3.6350	2.0459	3.2738	7.1830	1.0114	0.8001	0.9752	0.7501	0.8603
0.60	1.2164	1.6176	3.3316	1.7756	2.9469	6.5620	0.9422	0.8298	0.9705	0.7298	0.7959
0.65	1.0923	1.4854	3.0748	1.5510	2.6677	6.0326	0.8806	0.8600	0.9655	0.7100	0.7382
0.70	0.9864	1.3716	2.8544	1.3623	2.4262	5.5749	0.8253	0.8905	0.9602	0.6905	0.6863
0.75	0.8953	1.2725	2.6633	1.2022	2.2155	5.1755	0.7753	0.9214	0.9544	0.6714	0.6393
0.80	0.8160	1.1854	2.4959	1.0653	2.0300	4.8235	0.7298	0.9528	0.9483	0.6528	0.5966
0.85	0.7465	1.1081	2.3481	0.9472	1.8651	4.5095	0.6882	0.9845	0.9419	0.6345	0.5576
0.90	0.6851	1.0390	2.2165	0.8449	1.7179	4.2281	0.6500	1.0166	0.9352	0.6166	0.5218
0.95	0.6306	0.9769	2.0986	0.7556	1.5854	3.9734	0.6147	1.0491	0.9281	0.5991	0.4890
1.00	0.5820	0.9207	1.9923	0.6774	1.4659	3.7420	0.5820	1.0820	0.9207	0.5820	0.4587
1.05	0.5383	0.8695	1.8959	0.6085	1.3573	3.5300	0.5516	1.1152	0.9130	0.5652	0.4307
1.10	0.4990	0.8227	1.8081	0.5477	1.2585	3.3353	0.5233	1.1489	0.9050	0.5489	0.4048
1.15	0.4634	0.7798	1.7277	0.4938	1.1682	3.1554	0.4969	1.1828	0.8967	0.5328	0.3807
1.20	0.4310	0.7401	1.6538	0.4458	1.0854	2.9884	0.4722	1.2172	0.8882	0.5172	0.3584
1.25	0.4016	0.7035	1.5856	0.4031	1.0093	2.8331	0.4490	1.2519	0.8794	0.5019	0.3376
1.30	0.3746	0.6695	1.5224	0.3649	0.9393	2.6880	0.4271	1.2870	0.8703	0.4870	0.3182
1.35	0.3500	0.6378	1.4637	0.3307	0.8746	2.5520	0.4066	1.3224	0.8610	0.4724	0.3001
1.40	0.3273	0.6082	1.4089	0.3000	0.8149	2.4244	0.3873	1.3582	0.8515	0.4582	0.2831
1.45	0.3065	0.5805	1.3577	0.2724	0.7596	2.3043	0.3690	1.3944	0.8418	0.4444	0.2673
1.50	0.2872	0.5546	1.3097	0.2475	0.7082	2.1909	0.3518	1.4308	0.8318	0.4308	0.2525
1.55	0.2694	0.5301	1.2645	0.2250	0.6606	2.0838	0.3354	1.4676	0.8217	0.4176	0.2386
1.60	0.2530	0.5071	1.2220	0.2048	0.6163	1.9823	0.3200	1.5048	0.8114	0.4048	0.2255
1.65	0.2377	0.4854	1.1817	0.1864	0.5751	1.8861	0.3053	1.5422	0.8010	0.3922	0.2133
1.70	0.2235	0.4649	1.1437	0.1699	0.5368	1.7948	0.2914	1.5800	0.7904	0.3800	0.2017
1.75	0.2103	0.4455	1.1075	0.1548	0.5010	1.7079	0.2782	1.6181	0.7796	0.3681	0.1909
1.80	0.1980	0.4270	1.0731	0.1412	0.4677	1.6254	0.2657	1.6564	0.7687	0.3565	0.1807
1.85	0.1866	0.4096	1.0404	0.1288	0.4366	1.5467	0.2538	1.6952	0.7577	0.3452	0.1711
1.90	0.1759	0.3929	1.0092	0.1175	0.4076	1.4718	0.2424	1.7342	0.7466	0.3342	0.1620
1.95	0.1659	0.3771	0.9793	0.1073	0.3806	1.4004	0.2316	1.7734	0.7354	0.3234	0.1535
2.00	0.1565	0.3620	0.9507	0.0980	0.3553	1.3324	0.2214	1.8130	0.7241	0.3130	0.1454

TABLE II—*Continued.*

u	${}^{1}\varphi_{1}\varphi$	${}^{2}\varphi_{2}\varphi$	${}^{3}\varphi_{3}\varphi$	${}^{4}\varphi_{4}\varphi$	${}^{5}\varphi_{5}\varphi$	${}^{6}\varphi_{6}\varphi$	${}^{7}\varphi_{7}\varphi$	${}^{8}\varphi_{8}\varphi$	${}^{9}\varphi_{9}\varphi$	${}^{10}\varphi_{10}\varphi$	${}^{11}\varphi_{11}\varphi$
2.10	0.1395	0.3340	0.8970	0.0818	0.3096	1.2052	0.2022	1.8930	0.7013	0.2930	0.1306
2.20	0.1246	0.3083	0.8473	0.0683	0.2698	1.0894	0.1848	1.9741	0.6783	0.2741	0.1174
2.30	0.1114	0.2848	0.8012	0.0571	0.2349	0.9837	0.1690	2.0563	0.6552	0.2563	0.1056
2.40	0.0998	0.2633	0.7581	0.0478	0.2044	0.8874	0.1546	2.1394	0.6320	0.2394	0.0951
2.50	0.0894	0.2436	0.7178	0.0400	0.1778	0.7995	0.1414	2.2236	0.6089	0.2236	0.0856
2.60	0.0802	0.2253	0.6799	0.0335	0.1546	0.7194	0.1294	2.3086	0.5859	0.2086	0.0772
2.70	0.0720	0.2085	0.6442	0.0280	0.1342	0.6464	0.1184	2.3945	0.5631	0.1945	0.0696
2.80	0.0647	0.1930	0.6104	0.0235	0.1165	0.5801	0.1083	2.4813	0.5405	0.1813	0.0627
2.90	0.0582	0.1787	0.5785	0.0197	0.1010	0.5198	0.0992	2.5688	0.5182	0.1689	0.0566
3.00	0.0524	0.1654	0.5483	0.0165	0.0875	0.4651	0.0908	2.6572	0.4963	0.1572	0.0511
3.10	0.0472	0.1531	0.5195	0.0138	0.0758	0.4155	0.0831	2.7462	0.4747	0.1462	0.0461
3.20	0.0425	0.1418	0.4922	0.0116	0.0656	0.3707	0.0760	2.8360	0.4536	0.1360	0.0416
3.30	0.0383	0.1312	0.4662	0.0097	0.0567	0.3303	0.0696	2.9264	0.4330	0.1264	0.0376
3.40	0.0345	0.1214	0.4414	0.0081	0.0489	0.2938	0.0637	3.0174	0.4129	0.1174	0.0339
3.50	0.0311	0.1124	0.4178	0.0068	0.0422	0.2610	0.0582	3.1090	0.3933	0.1090	0.0307
3.60	0.0281	0.1040	0.3953	0.0057	0.0364	0.2315	0.0533	3.2011	0.3743	0.1011	0.0277
3.70	0.0254	0.0962	0.3739	0.0048	0.0313	0.2050	0.0488	3.2938	0.3558	0.0938	0.0250
3.80	0.0229	0.0889	0.3535	0.0040	0.0270	0.1813	0.0446	3.3870	0.3380	0.0870	0.0226
3.90	0.0207	0.0822	0.3340	0.0033	0.0232	0.1601	0.0408	3.4806	0.3207	0.0806	0.0204
4.00	0.0187	0.0760	0.3154	0.0028	0.0199	0.1412	0.0373	3.5746	0.3041	0.0746	0.0185
4.20	0.0152	0.0649	0.2809	0.0019	0.0146	0.1094	0.0312	3.76	0.2726	0.0639	0.0151
4.40	0.0124	0.0554	0.2497	0.0014	0.0108	0.0844	0.0261	3.95	0.2436	0.0547	0.0124
4.60	0.0102	0.0472	0.2214	0.0009	0.0079	0.0647	0.0218	4.15	0.2170	0.0467	0.0101
4.80	0.0083	0.0402	0.1960	0.0007	0.0057	0.0494	0.0182	4.34	0.1928	0.0398	0.0083
5.00	0.0068	0.0341	0.1731	0.0005	0.0042	0.0375	0.0152	4.53	0.1707	0.0339	0.0068
5.20	0.0055	0.0290	0.1525	0.0003	0.0030	0.0284	0.0126	4.73	0.1508	0.0288	0.0055
5.40	0.0045	0.0246	0.1341	0.0002	0.0022	0.0214	0.0105	4.92	0.1329	0.0245	0.0045
5.60	0.0037	0.0209	0.1177	0.0002	0.0016	0.0161	0.0088	5.12	0.1168	0.0208	0.0037
5.80	0.0030	0.0177	0.1031	0.0001	0.0011	0.0120	0.0073	5.32	0.1025	0.0176	0.0030
6.00	0.0025	0.0149	0.0901	0.0001	0.0008	0.0090	0.0061	5.51	0.0897	0.0149	0.0025
6.50	0.0015	0.0098	0.0639	0.0000	0.0004	0.0042	0.0038	6.01	0.0637	0.0098	0.0015
7.00	0.0009	0.0064	0.0448		0.0002	0.0020	0.0024	6.51	0.0448	0.0064	0.0009
7.50	0.0006	0.0042	0.0312		0.0001	0.0009	0.0015	7.00	0.0312	0.0042	0.0006
8.00	0.0003	0.0027	0.0215		0.0000	0.0003	0.0010	7.50	0.0215	0.0027	0.0003
8.50	0.0002	0.0017	0.0147			0.0000	0.0006	8.10	0.0147	0.0017	0.0002
9.00	0.0001	0.0011	0.0100				0.0004	8.50	0.0100	0.0011	0.0001
9.50	0.0001	0.0007	0.0068				0.0002	9.00	0.0068	0.0007	0.0001
10.00	0.0000	0.0004	0.0045				0.0001	9.50	0.0045	0.0004	0.0000

With this result Q_l may be put in a convenient form for substitution into the partition function.

$$Q_l=\prod_i \binom{v_i+d_i-1}{v_i} \exp[-G_{ii}u_iv_i(v_i-1)/3]. \quad (17)$$

Vibrational Sums

Application of the results for $Q_R(v,l)$ and Q_l will reduce the over all partition function to a series of sums over the vibrational quantum numbers only. This form is

$$Q=Q_0{}^0Q_R{}^0(1+2\delta/\beta_0)Q_v$$

$$Q_v=\sum_v\left[\prod_i\binom{v_i+d_i-1}{v_i}\right][1+\sum_i r_iv_i]$$

$$\times\exp[-\sum u_iv_i+\sum_i X_{ii}u_iv_i(v_i-1) \quad (18)$$

$$+\sum_{i<j} X_{ij}(u_iu_j)^{\frac{1}{2}}v_iv_j]$$

$$X_{ii}=X_{ii}'-G_{ii}/3=-(x_{ii}+g_{ii}/3)/\nu_i.$$

To carry out the summation of Q_v analytically it is necessary to expand the small exponentials in X_{ii} and X_{ij}. Use is then made of the relations[2]

$$\sum_v \exp(-uv)=(1-e^{-u})^{-1}$$

$$\sum_v v\exp(-uv)=e^{-u}(1-e^{-u})^{-2} \quad (19)$$

$$\sum_v v^n\exp(-uv)=\frac{(-1)^nd^n}{du^n}\sum_v\exp(-uv).$$

If second-order terms are neglected, the algebra is not too difficult and the end result is that

$$\ln Q=\ln Q_0{}^0+\ln Q_R{}^0+\ln Q_v{}^0+\ln Q_c$$

$$\ln Q_v{}^0=-\sum_i d_i\ln(1-e^{-u_i}) \quad (20)$$

$$\ln Q_c=2\delta/\beta_0+\sum_i d_ir_i{}^1\varphi_i$$

$$+\tfrac{1}{2}\sum_i d_i(d_i+1)X_{ii}{}^A\varphi_i+\sum_{i<j}d_id_jX_{ij}{}^7\varphi_i{}^7\varphi_j.$$

The expression for $\ln Q_v{}^0$ is the harmonic oscillator result. The small corrections are given in terms of the

functions ${}^n\varphi_i$, which are tabulated in Eqs. (24). Stockmayer, Kavanagh, and Mickley[3] obtained the last two terms in $\ln Q_e$ without, however, taking into account the l_i splitting of the degenerate levels ($g_{ii}\neq 0$) and the resulting adjustment of the "effective" X_{ii}. This effect may become significant at higher temperatures.

III. THE THERMODYNAMIC FUNCTIONS

In terms of Eq. (20) for $\ln Q$ the thermodynamic functions may be obtained as the sum of three parts: (a) a rigid-rotator contribution calculated with inertial quantities for the vibrationless ground state; (b) a harmonic oscillator contribution computed from observed fundamentals; and (c) a number of small corrections. These last are evaluated here. The corrections are given in terms of the functions ${}^n\varphi$ and constants characteristic of the molecule. The contributions to the thermodynamic functions are

$$-F_c/RT=sT+\sum_i d_i\gamma_i{}^1\varphi_i+\tfrac{1}{2}\sum_i d_i(d_i+1)X_{ii}{}^4\varphi_i+\sum_{i<j} d_id_jX_{ij}{}^7\varphi_i{}^7\varphi_j \quad (21)$$

$$E_c/RT=sT+\sum_i d_i\gamma_i{}^2\varphi_i+\tfrac{1}{2}\sum_i d_i(d_i+1)X_{ii}{}^5\varphi_i+\sum_{i<j} d_id_jX_{ij}{}^7\varphi_i{}^7\varphi_j({}^8\varphi_i+{}^8\varphi_j) \quad (22)$$

$$C_c/R=2sT+\sum_i d_i\gamma_i{}^3\varphi_i+\tfrac{1}{2}\sum_i d_i(d_i+1)X_{ii}{}^6\varphi_i+\sum_{i<j} d_id_jX_{ij}{}^7\varphi_i{}^7\varphi_j\times[({}^8\varphi_i+{}^8\varphi_j)^2+{}^{10}\varphi_i+{}^{10}\varphi_j-1]. \quad (23)$$

For these relations the ${}^n\varphi$ and vibrational constants are defined as follows:

$${}^1\varphi=(e^u-1)^{-1}$$
$${}^2\varphi=ue^u(e^u-1)^{-2}$$
$${}^3\varphi=u^2e^u(e^u+1)(e^u-1)^{-3}$$
$${}^4\varphi=2u(e^u-1)^{-2}$$
$${}^5\varphi=2u(2ue^u-e^u+1)(e^u-1)^{-3}$$
$${}^6\varphi=4u^2e^u(2ue^u-2e^u+u+2)(e^u-1)^{-4}$$
$${}^7\varphi=u^{\frac{1}{2}}(e^u-1)^{-1}$$
$${}^8\varphi=\tfrac{1}{2}(2ue^u-e^u+1)(e^u-1)^{-1}$$
$${}^9\varphi=u^2e^u(e^u-1)^{-2}=(C/R)_{HO}$$
$${}^{10}\varphi=u(e^u-1)^{-1}=(E/RT)_{HO}$$
$${}^{11}\varphi=-\ln(1-e^{-u})=(-F/RT)_{HO}$$
$$u_i=hc\nu_i/kT$$
$$X_{ii}=(-x_{ii}-g_{ii}/3)/\nu_i$$
$$X_{ij}=-x_{ij}/(\nu_i\nu_j)^{\frac{1}{2}}.$$

The constants in the centrifugal stretching and rotation-vibration terms depend on the structure of the molecule, the various forms are given in Table I.

The evaluation of the ${}^n\varphi$ for several frequencies at a number of temperatures is a lengthy computation. To facilitate the calculation of the correction terms a compilation of the ${}^n\varphi$ for a wide range of the argument u, is given in Table II. The values of the argument are those used by Mayer and Mayer[9] in their tabulation of the harmonic oscillator functions. The last three ${}^n\varphi$ are, respectively, the heat capacity, the internal energy, and the free energy, functions for a harmonic oscillator. These entries agree closely with the tables of Mayer and Mayer and exactly with those of Johnston, Savedoff, and Belzer.[10]

IV. NITROUS OXIDE

The original analysis of the spectrum of nitrous oxide for the anharmonicity coefficients was made by Plyler and Barker[11] and corrected by Barker.[12] A number of calculations of various thermodynamic functions of nitrous oxide have been published.[13] Some of these were based on the earlier-published[11] slightly erroneous representation of the energy levels, while in others the harmonic oscillator approximation was used. Kobe and Pennington used the corrected assignment and a satisfactory approximation to the partition function. However, the numerical differentiation used by them to calculate the other functions produced serious error. Thermodynamic functions have been calculated for nitrous oxide using the tables given here and the data

TABLE III. Molal thermodynamic functions of nitrous oxide in the ideal-gas state.

T °K	$-(F^0-E_0^0)/T$ cal deg^{-1}	$H^0-E_0^0$ cal	S^0 cal deg^{-1}	C_p^0 cal deg^{-1}	C_v cal deg^{-1}
273.16	44.211	2062.2	51.760	8.952	0.004
298.16	44.876	2290.9	52.556	9.232	0.005
300	44.925	2307.0	52.615	9.253	0.005
400	47.208	3281.7	55.412	10.207	0.011
500	49.091	4341.8	57.775	10.965	0.018
600	50.713	5470.6	59.831	11.590	0.030
700	52.149	6656.5	61.658	12.110	0.043
800	53.442	7889.6	63.304	12.542	0.058
900	54.622	9162.5	64.803	12.903	0.073
1000	55.710	10469	66.179	13.206	0.092
1100	56.721	11802	67.450	13.458	0.108
1200	57.665	13158	68.630	13.671	0.125
1300	58.551	14535	69.732	13.854	0.142
1400	59.386	15929	70.764	14.009	0.159
1500	60.177	17336	71.734	14.142	0.175

[10] Johnston, Savedoff, and Belzer, *Contributions to the Thermodynamic Functions by a Planck-Einstein Oscillator in One Degree of Freedom* (U. S. Government Printing Office, Washington, 1949).

[11] E. K. Plyler and E. F. Barker, Phys. Rev. **38**, 1827 (1931).

[12] E. F. Barker, Phys. Rev. **41**, 369 (1932).

[13] W. H. Rodebush, Phys. Rev. **40**, 113 (1932); R. M. Badger and S. C. Woo, J. Am. Chem. Soc. **54**, 3523 (1932); L. S. Kassel, *ibid.* **56**, 1838 (1934); R. W. Blue and W. F. Giaque, *ibid.* **57**, 991 (1935); A. R. Gordon, J. Chem. Phys. **3**, 259 (1935); E. Justi, Gebiete Ingenieurw. **A5**, 134 (1934); K. A. Kobe and R. E. Pennington, Petroleum Refiner **29**, No. 7, 129 (1950).

of Herzberg and Herzberg.[14] These data included the rotation-vibration interaction constants which had not been available before. Since it is as yet not possible to eliminate completely the effects of Fermi resonance from the vibrational constants, the assignment of Herzberg and Herzberg which best reproduced the lower-lying levels was chosen for use in these latest calculations. The resulting thermodynamic data are presented in Table III. The correction terms exert their greatest effect on the heat capacity, and these contributions are included in the tabulation.

V. DISCUSSION

The correction terms in Eq. (20) are to the first order only. In the derivation of these results an effort was made to carry all second- and some third-order terms. The number of such terms is of course much greater, and the functions involved are more complicated. After taking a second derivative to obtain the contributions to the heat capacity, the completely general result becomes prohibitively complicated. An estimate of the second-order contributions to the heat capacity of water at 1500°K indicated a value of about 0.1 percent of the total C_p^0. The water molecule was chosen specifically for its very large rotation-vibration interaction. In the case of nitrous oxide, with a fairly low-frequency degenerate fundamental (588 cm^{-1}), the second-order contributions to the heat capacity at 1000°K are somewhat less than 0.1 percent though increasing rapidly. Since at such high temperatures the extrapolation of the anharmonicity and interaction coefficients (to the now important higher vibration levels) usually becomes somewhat uncertain and the effects of Fermi resonance become more pronounced, an error of 0.1 percent in the most sensitive function does not seem too serious.

For the case of diatomic molecules the results given here become particularly simple. The expression for $\ln Q_e$ reduces to exactly the same function as was obtained for this case by Mayer and Mayer.[9] They, however, give series expansions for the corrections to the thermodynamic functions. These expansions are proposed for use at "moderately small" values of u only. A comparison of the correction terms for the heat capacities of two molecules, O_2 and HBr, is given in Table IV. As should be expected, the expansion fails badly at $u=5.0$. It is also slightly smaller than the function given here at lower values of u. The temperatures corresponding to these values of u are included in the table.

TABLE IV. Correction terms for the heat capacities of diatomic molecules cal deg^{-1} $mole^{-1}$.

	O_2			HBr	
u	T, °K	P & K[a]	M & M[b]	T, °K	P & K[a]	M & M[b]
10.0	223	0.004	...	367	0.010	...
5.0	446	0.010	−0.048	733	0.032	−0.068
3.0	744	0.030	+0.014	1232	0.080	+0.046
2.0	1114	0.056	0.050	1834	0.150	0.136
1.5	1489	0.084	0.080	2450	0.215	0.207
1.0	2228	0.132	0.128	3667	0.340	0.330
0.5	4456	0.271	0.267	7334	0.697	0.679

[a] This method.
[b] Mayer and Mayer (see reference 9).

It is to be expected that deviations from the representation of energy levels, equation (1), used here will arise. In the case of HCN it has been found necessary to add a cubic term, $y_{333}v_3(v_3^2-1)$, to obtain a satisfactory fit to the observed spectrum.[15] The inclusion of such terms in $\ln Q_e$ is not difficult. When expanded in Q_v this particular term would appear as

$$\sum_v Y_3 v_3(v_3^2-1)\exp(-u_3 v_3)=6Y_3{}^1\varphi_3{}^2\varphi_3(1-e^{-u_3})^{-1}, \quad (24)$$

where Y_3 is y_{333}/ν_3, and the relations in Eq. (19) have been applied. If the harmonic oscillator term, $(1-e^{-u})^{-1}$, is factored out, the resulting addition to $\ln Q_e$ is just the quantity $6Y_3{}^1\varphi_3{}^2\varphi_3$. This function and its derivatives may be evaluated conveniently from information in Table II.

In some cases it becomes necessary or desirable to make an empirical adjustment for anharmonicity in very complicated molecules. Expressions which have been used for fitting anharmonicity as determined by comparison with calorimetric data are[16]

$$\begin{aligned} C_e &= \tfrac{1}{2}Z^6\varphi \\ E_e/T &= \tfrac{1}{2}Z^5\varphi \\ -F_e/T &= \tfrac{1}{2}Z^4\varphi. \end{aligned} \quad (25)$$

In these expressions (Z) serves as an adjustable degeneracy-anharmonicity constant and the arbitrary frequency for which the ${}^n\varphi$ are evaluated provides an additional adjustable parameter. The information in Table II is useful in such calculations.

[14] G. Herzberg and L. Herzberg, J. Chem. Phys. **18**, 1551 (1950).

[15] E. Lindholm, Z. Physik **108**, 454 (1938).

[16] McCullough, Finke, Hubbard, Good, Pennington, Messerly, and Waddington, J. Am. Chem. Soc. (to be published).

The Box Model and Electron Densities in Conjugated Systems

JOHN R. PLATT
Physics Department, University of Chicago, Chicago, Illinois
(Received March 15, 1954)

Part I describes the pi-electron density distributions of some conjugated systems, computed by generalizing Schmidt's model, with the electrons free to move in a properly shaped box of constant potential. Only products and sums of sine functions are needed for rectangular boxes (polyacenes, porphine) and Bessel functions for circular (coronene) or circular-sector boxes (phenanthrene). Plaster models of the pi-electron density surface are shown for 10 molecules. In aromatics, ring-shaped regions of high density are found at the same locations as the rings of the carbon skeleton.

In Part II it is shown that the density maxima in the boxes usually coincide with the high-order bonds or high-density atoms predicted by resonance theory or LCAO theory or the free-electron-network theory, with similar correspondence for low-density bonds or atoms. This suggests that the common success of these three other theories rests not on their various special assumptions, but on primitive general requirements of wave continuity and orthogonality in space.

In Part III this point is elaborated into a theorem that the density and transition energy of a closed-shell system are stable under large changes in the one-particle potential function if the changes occur below the highest-filled orbital. Taken together with electron repulsion and antisymmetrization, this helps explain why Coulomb and short-range forces can be successfully approximated by the smoothed-potential model of the nucleus and the free-electron model of metals and molecules.

In Part IV it is shown that the box model leads to a "periodic table" of stabilities of convex conjugated hydrocarbons. Their possible spectral types are discussed. Some new hydrocarbons are described which may be stable.

I. ELECTRON DENSITIES FROM THE BOX MODEL

A MECHANICAL model was described earlier,[1] which represented the pi-electron density distribution given by the free-electron network theory[2,3] of conjugated systems.

Another free-electron theory—the Schmidt box model[4]—can be developed to give the ground-state density distributions represented by the plaster surfaces shown in Figs. 1 to 4 for 10 molecules. The pi-electrons are confined to a three-dimensional box of suitable shape with constant potential inside. The z motion is supposed independent of x and y and constant for all conjugated systems, and it may be separated, leaving the two-dimensional wave equation

$$\nabla^2\psi+\frac{8\pi^2m}{h^2}E'\psi=0$$

with "square-well" boundary conditions suitable for infinite vertical potential walls.

For rectangular and circular (or semicircular) boxes, this equation then has the textbook solutions

$$\psi_{n_xn_y}=\frac{2}{(lw)^{\frac{1}{2}}}\sin 2\pi n_x\frac{x}{l}\sin 2\pi n_y\frac{y}{w}$$

$$E'=\frac{h^2}{8m}\left(\frac{n_x^2}{l^2}+\frac{n_y^2}{w^2}\right)=154\left(\frac{n_x^2}{l^2}+\frac{n_y^2}{w^2}\right)\text{ kilokaysers},$$

where l and w are the length and width of the rectangle; and

$$\psi_{qt}=A_{qt}J_q\left(u_{qt}\frac{r}{a}\right)\begin{Bmatrix}\sin q\varphi\\ \cos q\varphi\end{Bmatrix},$$

$$E'=\frac{h^2}{8\pi^2m}\frac{u_{qt}^2}{a^2}=15.7\frac{u_{qt}^2}{a^2}\text{ kilokaysers},$$

(see Fig. 7) where a is the radius of the circle and u_{qt} is the tth root of the Bessel function $J_q(x)$. The numerical values give the two-dimensional energy contribution E' in kilokaysers (10^3 cm^{-1}) when l, w, or a are in units of the average C=C bond length, 1.40A. Solutions for boxes of other shapes are mathematically formidable.

The plaster surfaces show the value of the ground-state electron density for N electrons,

$$q(x,y)=2\sum^{N/2}\psi_{jk}^2$$

where j and k stand for the appropriate indices of ψ summed over their values in the lowest $N/2$ orbitals, with 2 electrons in each orbital.

Where possible, the boundaries of the box were taken to pass through the fictitious carbon atoms which would be adjacent to the conjugated network if the hexagonal lattice were extended. In some cases this condition could be satisfied only approximately (pyrene, phenanthrene) and the results are less satisfactory; and they seem least satisfactory for molecules with indented perimeters (phenanthrene, biphenyl, perylene) which the simple box shapes do not follow. Of course the network plays no part in the solutions except to determine the box shape. Thus, a change of box size by a

[1] J. R. Platt, J. Chem. Phys. **21**, 1597 (1953).
[2] K. Ruedenberg and C. W. Scherr, J. Chem. Phys. **21**, 1565 (1953), Theory; bibliography of original papers of Bayliss, Kuhn, Simpson, and others. The network model was independently developed by Y. Ooshika, Researches Chem. Phys, Japan **29**, 16 (1950).
[3] C. W. Scherr, J. Chem. Phys. **21**, 1582 (1953). Calculations.
[4] (a) O. Schmidt, Z. physik. Chem. **B39**, 59 (1938); (b) **B42**, 83 (1939); (c) **B44**, 185, 194 (1939); (d) **B47**, 1 (1940).

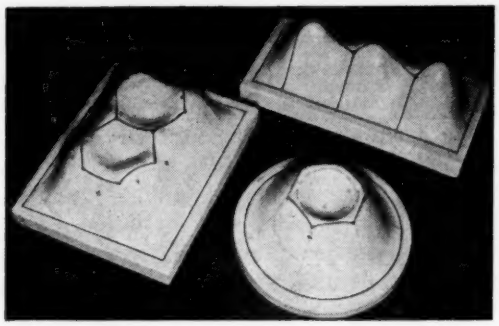

FIG. 1. Density surfaces for naphthalene, benzene, hexatriene.

constant scale factor changes the density-distribution scale by the same factor and does not affect the sequence of the orbitals.

The box dimensions, indices of filled orbitals, and predicted and observed spectroscopic transitions are given in Table I. The two-dimensional benzene density was given correctly by O. Schmidt.[4a] (The naphthalene density was computed incorrectly by his collaborator, H. Schmidt,[4b] and the transition energies in both cases were computed incorrectly, because wave functions were included which do not have the proper symmetry for pi electrons.) The energy predictions here, like those of the free-electron network model, are absolute and have no adjustable parameters except the almost unalterable dimensions of the boxes.

Dimensional Analysis and Energy Predictions

In molecular calculations, some agreement, say within a factor of two, will always be found between predicted and observed frequencies as a result of dimensional considerations, regardless of the model or approximation used. The optical electrons in an atom or molecule have velocities of the order of that in the first orbit of hydrogen $c/137$ or less, say one-half this on the average. The wavelength of the first resonance frequency of a system of diameter d is then not the classical antenna wavelength $\lambda \simeq 2d$ which is derived for photons traveling across the system with the speed of light; but it is instead about $\lambda \simeq 500d$, since the particles travel across with these smaller velocities. This is a general result for *any* quantum-mechanical formulation if the electrons have such velocities throughout the system. The predicted lowest absorption frequencies for some of the molecules of Table I by this formula would be: hexatriene 24, naphthalene 28, anthracene 21, biphenyl 20, benzene 36, coronene 20 kilokaysers. (The sigma-electron spectra are at higher frequencies because these electrons have higher velocities and probably move in a potential field with more marked periodicities so that their classical limit of motion may not extend through the whole molecule. See Part III.)

The success of a frequency prediction for a molecule is therefore not by itself a critical test of the merit of the structure assumed for the molecule or of the approximation used, because it is simply not very sensitive to these variables; this is especially true when other variable parameters are also introduced. Such successes merely show that the fundamental constants e, m, and h were inserted somewhere in the calculations.

On the other hand, the failure of a frequency prediction (by more than, say, a factor of two) is a correspondingly serious blow to a theory.

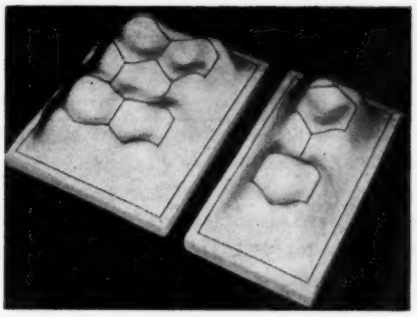

FIG. 3. Density surfaces for perylene, biphenyl.

Point-Lattice, Network, and Surface Wave Functions

The free-electron network wave functions described earlier[2,3] satisfied a differential equation in the multiply-connected 1-dimensional network. Their values at the atoms (in the Dewar modification,[5] with the network

FIG. 2. Density surfaces for phenanthrene, anthracene, pyrene.

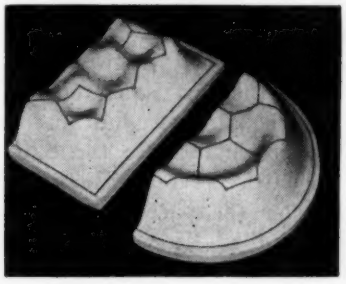

FIG. 4. Density surfaces for porphine, coronene.

[5] K. Ruedenberg and N. S. Ham, J. Chem. Phys. (to be published).

TABLE I. Box model orbitals and spectra.

	w[a]	l[a]	N	Filled orbitals n_y; n_x	Pred. first transitions (center of gravity) and polarizations	First obs. singlets (of same polarization)
Rectangular Boxes						
Hexatriene	$2\frac{1}{2}$	$7j$	6	1;1,2,3	1,3−1,4 x 29 kK[b] 1,2−1,4 *forb* 50	38 kK[b] 52
Naphthalene or Azulene	4	$6j$	10	1;1,2,3 2;1,2	1,3−2,3 y 29 2,2−2,3 x 28 1,3−1,4 x 40 2,2−1,4 y 39	Na 35 Az 15 32 29 45 36 59 52
Anthracene	4	$8j$	14	1;1–4 2;1–3	2,3−1,5 y 22 2,3−2,4 x 22 1,4−1,5 x 29 1,4−2,4 y 29	27 (29) 39 53
Porphine	$8j$	$8j$	26	1;1–4 2;1–4 3;1–3 4;1,2	2,4−3,4 } x,y 16 4,2−4,3 } 3,3−3,4 } x,y 23 3,3−4,3 }	17 (c.g.) 25 (c.g.)
Biphenyl (nonconvex)	$4j$	7	12	1;1–4 2;1,2	2,2−2,3 x 16 1,3−2,3 y 39 1,4−1,5 x 28 1,4−2,4 y 39	40 41 50 53?
Perylene (nonconvex)	$6j$	7	20	1;1–4 2;1–4 3;1,2	3,2−3,3 x 16 1,4−1,5 x 28 2,4−2,5 x 28 2,3−3,3 y 29 2,4−3,4 y 29	23 26 40 ? ?
Pyrene (approx)	4.7	6.5	16	1;1–4 2;1–3 3;1	1,4−2,4 y[c] 21 2,3−2,4 x 26 1,4−3,3 x 30 2,3−3,3 y 35	27 30 37 42
Circular Boxes		a	N	l;q		
Benzene		2	6	1;0,1	1,1−1,2 x,y, x,y 46	48 (c.g.)
Coronene		3.61	24	1;0–4 2;0,1	1,4−1,5 x,y, x,y 23	29 (c.g.)
Phenanthrene (approx; semicirc.)		4.15	14	1;1s−5s[d] 2;1s,2s	1,5−2,3 y 17 1,5−1,6 x 20 2,2−2,3 x 22 2,2−1,6 y 26	28 33 39 53

[a] j=cos30°. [b] kK=kilokayser=1000 cm^{-1}. [c] Highest filled u-orbital pair to lowest unfilled g-orbital pair. [d] Sine functions only.

extended beyond the perimeter so that every carbon is at a branch point) also satisfy rigorously a finite-difference equation which leads to a secular equation identical with the interacting-lattice-point type of secular equation used in LCAO theory. If we look for a similar connection between the two-dimensional differential equation of the box model and the finite-difference lattice-point equation, we find that the latter still gives a first approximation to the differential wave function at the lattice points.[6] This approximation is best, of course, when the space boundary passes through adjacent points of the lattice, which was the preferred condition in the calculations here. But the difference-values and the two-dimensional differential values are not identical as in the one-dimensional treatment, except in special cases (e.g., certain orbitals of triphenylene in a triangular box). The relations between the lattice, network, and surface wave functions are discussed more fully by Coulson and Frost.[7]

What is important for the present purpose is that there is a one-to-one correspondence between the lower orbitals obtained with any of the models, with respect to symmetry character and approximate energy sequence; with close agreement in the spatial location of nodes and antinodes and relative amplitudes at the atomic positions for corresponding wave functions. This correspondence holds throughout the filled orbitals, giving close agreement in the descriptions of the ground

[6] R. V. Southwell, *Relaxation Methods in Theoretical Physics* (Clarendon Press, Oxford, 1946).

[7] C. A. Coulson, Proc. Phys. Soc. (London) **66A**, 652 (1953); A. A. Frost, J. Chem. Phys. (to be published).

state. Serious differences in orbital energy sequence between the different models begin to appear only when we reach orbitals whose wavelengths approach the dimensions of the aromatic rings in the network. This limit is in the vicinity of the Nth orbital, the last in the LCAO group of p-pi orbitals. It seems possible that up to this point the differences in energy sequence between different methods may be less important in describing the molecule than the large correction and interaction terms which are omitted in all these simple one-electron descriptions.

Characteristics of the Density Surfaces

The density surfaces of Figs. 1 to 4 show several unexpected features. Probably the most surprising is that at the position of every aromatic ring there is a ring of high pi-electron density surrounding a central valley, *in spite of the fact that the rings played no part in the density calculations!* The pyrrole rings of porphine are similarly marked. (The outer valleys of coronene are smeared together by the artificial degeneracy introduced by the circular box.) This suggests that particular ring configurations are stabilized not merely by the hexagonal framework of the trigonal sigma bonds, but also by the self-consistent coincidence of the nuclear positions with the rings of high pi-electron density which are formed by the semifree pi-electron motion limited by the gross molecular shape.

Thus, the fact that naphthalene and azulene are stable while cyclodecapentaene presumably is not, may be partly because 10 electrons confined to a small oblong area form double rings with regions where the density is higher than it would be if the electrons were spread out into a circle.

We can understand the formation of these density rings a little better if we compare anthracene and pyrene (Table I). Anthracene has four maxima (at the cross links) on the x axis, contributed by the four $n_y=1$ functions with $n_x=1, 2, 3, 4$, which have an antinode on the x axis. It has three maxima at each side from the strong addition of the three $n_y=2$ functions with $n_x=1, 2, 3$, which all have nodes on the x axis. This combination of 4 maxima on the x axis with 3 on either side, gives rise to the three rings of high density. In pyrene, in the rectangular box approximation, the box is wider, but the same orbitals are filled and we would again get 3 rings along the long axis, except that we now have an additional orbital filled, $n_x=1$, $n_y=3$, with three maxima on the y axis, one of them in the center. This added central density splits the anthracenic central minimum into two, and so creates the four rings of pyrene. Pyrene may be fitted about as well by a square box, in which case the four rings form a symmetrical clover-leaf pattern.

With the linear fused polyacenes, naphthalene, anthracene, and so on, it is easy to make a general proof[8] for the rectangular box model that there is always a minimum lying within every ring of the skeleton, a ridge of high density at every cross link, and a zigzag ridge of high density corresponding to the C—C zigzag along each long edge of the box. With the rectangular boundary, the densities at the different carbon atoms are almost, but not exactly identical. They are identical in the LCAO theory and in the Dewar modification of the free-electron-network theory for alternant hydrocarbons. It is an interesting mathematical question whether a different choice of boundary (such as more pointed ends on the box?) would also produce constant atom densities here.

Exploratory studies have been made of the sigma-electron density distribution using the box model. Patterns are also found in this case which bear some resemblance to the molecular framework, but the more numerous orbitals give distributions much more sensitive to the shape of the box; and, with boundary shapes of uncertain merit, there is more of a problem in choosing which of the numerous top orbitals to fill.

II. DENSITY MAXIMA: RELATION TO OTHER THEORIES

When we turn to considering the pi-electron density maxima in more detail, we see that they occur at those positions which are already known to give high bond order or electron density in valence-bond resonance theory, in LCAO theory, and in free-electron network theory. Thus the box model maxima are where the 1–2 bonds would be in naphthalene, anthracene, and the other polyacenes; and near the 1, 3, 5, 7 positions in azulene. The electron densities in the different naphthalene bonds on the box model are in the same sequence as those given by the other theories, with 1–2 strongest and 9–10 weakest.

These resemblances were somewhat to be expected, though perhaps not such exact fidelity of detail, from the lattice-network-surface mathematical relationships already noted. But they illuminate the common success of these three other theories, which has already been shown to be due to the properties of a secular determinant common to all three.[2,9–11]

The fact that we can obtain both the azulene and naphthalene density predictions with the same box shows that the spatial distribution of the electrons does not depend critically on the detailed structure of the network. The further fact that we obtain agreement with the three other theories shows that the distribution does not depend on the different special assumptions of the different theories. Just as the success of molecular theories in predicting transition energies is the result of dimensional considerations; so their success in predicting electron distribution is simply the result

[8] C. W. Scherr (unpublished).

[9] H. C. Longuet-Higgins, J. Chem. Phys. **18**, 265 (1950).

[10] M. J. S. Dewar and H. C. Longuet-Higgins, Proc. Roy. Soc. (London) **A214**, 482 (1952).

[11] N. S. Ham, (in preparation).

of primitive general requirements of wave continuity and orthogonality in space.

In several cases in the Figures, $N/2$ maxima may be discerned (hexatriene, phenanthrene, pyrene, perylene). Some of these evidently represent regions of high double-bond character with weak adjacent bonds, i.e., almost isolated C=C pi-electron pairs with low resonance. In such cases, the representation of the molecule as a sum of such pairs packed together is evidently a good approximation. It is an interesting mathematical question why some box shapes and some values of N favor such strong well-separated maxima while others do not.

III. STABILITY OF DENSITY AND TRANSITION ENERGY WITH CHANGING POTENTIALS

But the resemblances between the results of the different theories involve something more than mathematical resemblances between lattice and network and surface wave functions, because there are large differences between these theories in the one-electron potential function assumed, from the flat-bottomed well of the box theory to the implied strong local Coulomb fields of the LCAO theory. Figure 5 suggests why the density distribution and transition energy should also be insensitive to these differences. Compare the system on the left in Fig. 5, having a flat-bottomed one-electron potential with the system on the right having an irregular stepped one-electron potential, under the condition that the limits of motion and the energy of the highest filled orbital are the same in both cases.

The difference of the first transition energies in these cases is less than 20 percent, and there is only about 20 percent root-mean-square difference in electron densities summed over the filled states; in spite of the fact that the root-mean-square change of potential is over 60 percent of the highest orbital energy and the change is distributed in a particularly unfavorable way, so that one pair of electrons is substantially bound locally, like inner-shell electrons, in one part of the box. (Infinite potential walls were assumed for simplicity in calculating these diagrams, but it is obvious that a Coulomb or other shape of potential function, if it were the same in both diagrams *above* the highest filled orbital, would not alter these qualitative resemblances.)

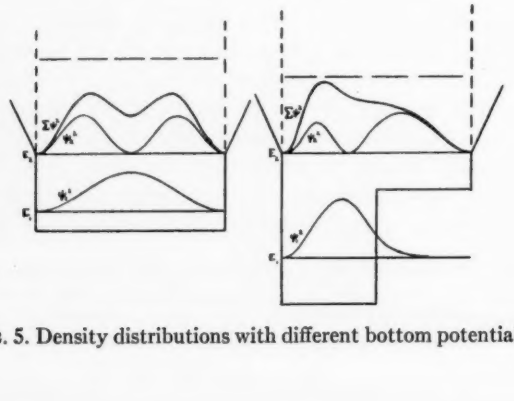

FIG. 5. Density distributions with different bottom potentials.

With more orbitals filled, the changes in density and transition energy would have been still smaller.

We see that a change of potential produces changes in electron distribution in different orbitals which largely compensate each other, provided the change in potential does not alter the classical limit of motion or boundary of the top orbital. It is easy to see why this is so: the density maxima of different orbitals are kept apart because they are orthogonal; or, what is the same thing, if one orbital is bound to one region and has a maximum amplitude there, some other orbitals must have their highest kinetic energy there and so spend the least time and have the least amplitude in that vicinity. These compensations get better with increasing number of orbitals, so that we may say that the root-mean-square change of total density δq in a system with n filled orbitals is of the order of n times smaller than the change in the density of any one orbital:

$$\delta q \sim \frac{\delta(\psi_i^2)}{n}.$$

The relative change of density is smaller by another factor of n:

$$\frac{\delta q}{q} \sim \frac{\delta(\psi_i^2)}{n\sum\psi_i^2} \sim \frac{1}{n^2}\frac{\delta(\psi_i^2)}{\psi_i^2}.$$

We may express this more rigorously by thinking of the perturbed ψ's as being expanded in the complete set of the original ψ's:

$$\psi_i+\delta\psi_i=\sum a_{ij}\psi_j.$$

But the sum can be broken into two parts, one over the filled orbitals and the other over the empty orbitals:

$$\psi_i+\delta\psi_i=\sum_{j=1}^{n} a_{ij}\psi_j+\sum_{j=n+1}^{\infty} a_{ij}\psi_j.$$

Now in the first sum the $a_{i1}\cdots a_{in}$ are the coefficients of a linear transformation among the filled orbitals; and it is well known that such a transformation does not alter the density; so the density must have the form

$$q'=q_0+\sum_{k=1}^{\infty}\sum_{j=n+1}^{\infty} b_{jk}\psi_j\psi_k.$$

The change in density is limited to the high-frequency terms under the sum, which are presumably small, and which presumably get smaller as the lower limit of the j sum rises with increasing n.

The stability of charge density on changing the potential shape at the bottom of the well is paralleled by the stability of the transition energies. The potential energy of the highest-filled orbital is some kind of average over its region of motion; and the lowest empty orbitals must make similar averages over the same region, the averages becoming more alike the larger

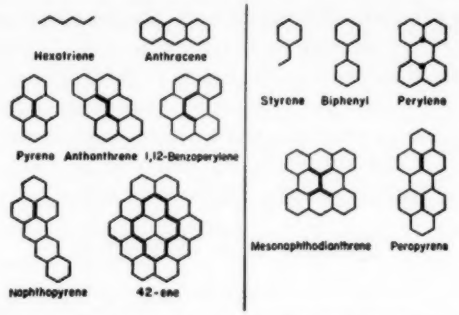

FIG. 6. Perimetral dissection of convex and nonconvex hydrocarbons. (Successive perimeters are indicated alternately by light and heavy lines.)

the number of nodes, which increases with n. (An exception is the important case where the periodicity of the nodes is close to a periodicity of the potential and we are in the vicinity of a Brillouin zone boundary.)

This theorem, that charge density in closed-shell systems is almost independent of what we may call the bottom shape of the potential, depends on orthogonality. It is supported by two other powerful forces pressing toward a uniform distribution of charge in real physical systems: 1) electron repulsion, which includes the shielding of cores by inner electrons; and 2) antisymmetrization of the total state wave function. These both act to prevent electron density from piling up in any region; and the latter, as Margenau has pointed out,[12] is similar in quantum mechanics to the classical doctrine that two bodies cannot be in the same place at the same time. Collectively, these reasons make understandable the success of the simple smoothed-potential models of the nucleus and the free-electron models of hydrocarbons. As with an ocean, many of the important observables of a sea of electrons depend only on the total content and the surface shape and level; and for these observables, the bottom details and the distribution and energy of low orbitals are almost irrelevant mathematical fictions and may be replaced indifferently by a flat-bottom assumption in the calculations.

In molecular theory, there may be other such observables besides the density and transition energy whose calculation is thus invariant to the sophistication of our physical assumptions and mathematical apparatus, and where consequently it may be extremely hard to determine what physical interactions and correction terms are most important to introduce in trying to improve on the first approximations.

IV. THE PERIODIC TABLE OF CONVEX CONJUGATED HYDROCARBONS

Every different type of one-electron potential function generates a different periodic table. The Coulomb law generates the Mendeleef table. A spherical hole "square-well" potential generates the nuclear shell, or "magic-number" table. A one-dimensional "square-well" generates the polyenes. A one-dimensional loop generates the cata-condensed hydrocarbons.[13] So a convex two-dimensional "square-well" potential like those in Part I generates a periodic table of "convex" conjugated hydrocarbons.

We define this group of hydrocarbons as follows. Every planar conjugated system has certain carbon atoms at the edge of the system which we may call "perimeter carbons." In a cata-condensed system or in a polyene, every carbon is on the perimeter (Fig. 6, hexatriene, anthracene). In a pericondensed system such as pyrene, there are additional carbons inside. If the perimeter carbons were removed, some or all of these additional carbons would lie on the new perimeter. These we may call "second-perimeter carbons." If the system is large enough, we may remove these carbons also, and have "third-perimeter carbons" within, and so on.

A convex hydrocarbon is then one in which the perimeter and every inner-perimeter is a connected unbranched even-membered loop with $2(2m+1)$ carbons, except for the last inner perimeter which may be a connected unbranched even-membered chain with $2n$ carbons (Fig. 6, left side). The reason for the restriction on the number of members will be seen below. Conjugated hydrocarbons which do not have this property may be odd-ring compounds, such as fluoranthene and rubicene. Or they may be even-ring compounds in which some perimeter or inner-perimeter is either broken or branched (Fig. 6, right side).

The relation of some of the convex compounds to the two-dimensional potential problem may be seen from Fig. 7, which gives the two-dimensional orbital energies

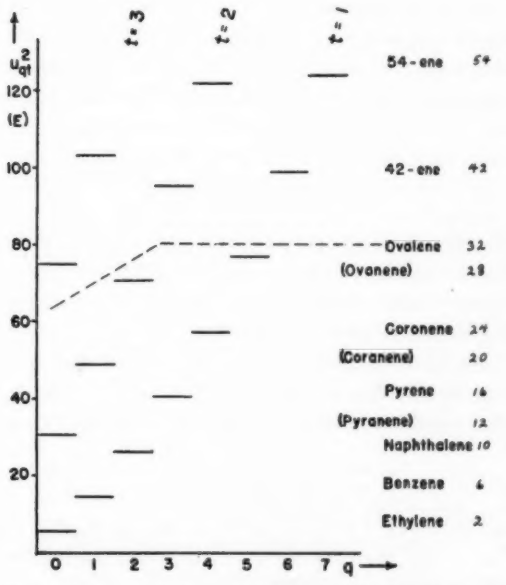

FIG. 7. Energy shells and periodic table of a circular box potential.

[12] H. Margenau, *The Nature of Physical Reality* (McGraw-Hill, Book Company, Inc., New York, 1950), Chapter 20.

[13] J. R. Platt, J. Chem. Phys. **17**, 484 (1949).

of a circular box. Two quantum numbers, here q and t, are required to specify the r,φ-dependence of the wavefunction. The number q is the "orbital ring quantum number" which was found useful in classifying the orbitals of cata-condensed hydrocarbons.[13,14] Only one quantum number was needed, since each of these molecules could be regarded to a certain approximation as a one-dimensional loop. In the present case, q gives the number of nodal planes of the wave function which pass through the axis of the cylindrical box. The number t is a new "radial ring quantum number" which must now be added in classifying the orbitals of peri-condensed convex hydrocarbons, since these are necessarily two-dimensional systems in all our approximations. It is one more than the number of cylindrical nodal surfaces in the wave function.

Values of u_{qt}^2, which are proportional to the energies of the orbitals, are plotted against q in Fig. 7. The orbitals are all doubly degenerate except those for which $q=0$. They will be filled in the order of increasing energy by the available pi electrons, one for every carbon in the conjugated system. Two electrons may be placed in each $q=0$ state, four in each other state, by the Pauli principle. The filling of each additional orbital shell gives us a new, stable, approximately round molecule. Some of these convex molecules are indicated at the right side of Fig. 7 opposite their last filled levels. The total number of pi electrons required to fill up to any level is also given. These molecules are the closed-shell "rare gases" of the pillbox potential. Schmidt also discussed this building-up principle, but with more emphasis on the simple connection of ethylene, benzene, and naphthalene units.

Pyrene is the first of these molecules to require a filled orbital with a radial node ($t=2$, $q=0$). Coronene has two such filled orbitals ($t=2$, $q=0,1$). It is as if we created a single $t=2$ orbital for the central ethylene in pyrene, and two of them for the central benzene ring in coronene. As a convenient method of bookkeeping, in fact, we may think of the filled $t=1$ orbitals as those required to take care of all the pi electrons of the perimeter carbons; of the $t=2$ orbitals as those required for the second-perimeter carbons; of the $t=3$ orbitals (with two radial nodes) as those required for the third-perimeter carbons; and so on. The highest value of t will give radial nodes approximately separating each inner perimeter from the next.

Mathematically, these orbitals of different t are as distinct as the K-, L-, and M-shell orbitals of an atom and for much the same reason, although we are grouping the subshells differently here. So the two concentric rings of high density in coronene in Fig. 3, which are symbolized in the chemical structure by the inner ring and the perimeter of coronene, arise largely from the $t=2$ and $t=1$ orbitals, respectively, and denote inner and outer electron shells as real and distinct as the different Hartree density shells of an atom.

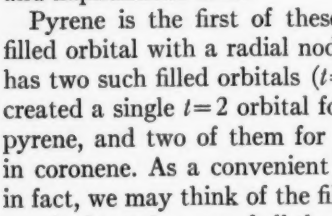

FIG. 8. Possible new stable hydrocarbons.

[14] W. Moffitt, J. Chem. Phys. 22, 320 (1954).

Possible New Molecules

Several nonconvex molecules may be identified with some of the closed shells of Fig. 7. Thus, biphenyl might be thought of in a certain approximation as the first molecule with $t=2$, with 2 inner carbons and a broken perimeter of 10 carbons on the outside. But our arguments so far suggest that there may also be a stable molecule with 2 inner carbons, and a continuous perimeter of 10 carbons. We might call it "pyranene" in view of its necessary resemblance to pyrene. If the sigma-bond angle strain is not too great, we may predict from Fig. 7 several such almost-round compounds, with 12, 20, and 28 conjugated carbons, having 2, 6, and 10 of these, respectively, on an inner perimeter. Possible structures and names for three compounds of this type are given in Fig. 8. The carbon skeletons of these compounds are isomeric with biphenyl, perylene, and *meso*-naphthodianthrene (Fig. 6), respectively, but they are relatively poorer in hydrogen than these 6-ring compounds. Each of the indicated structures has four 5-rings, corresponding to the removal of four CH groups from each of the molecules pyrene, coronene, and ovalene, respectively.

Geometrical construction indicates that sigma-bond angles as low as 80° and as high as 160° would be required in pyranene. These deviations from the trigonal 120° angles of the 6-ring systems are about three times as large as the deviations found in the fulvenes and azulenes, which are stable. But they are not as large as the deviations from the tetrahedral 109° angle to the 60° angle in cyclopropane, which is also fairly stable. The sigma-bond strain is less serious in the other compounds of Fig. 8.

Several Kekulé structures can be written for each compound, and density calculations for pyranene and coranene with the box model show minima in the ring centers as with ordinary aromatics. So it seems just possible that some or all of these compounds may be stable in spite of the sigma-bond strain.

The presence of the odd rings, and the fact that the highest filled levels will be of $t=2$ type in each case, would undoubtedly make their spectra and chemical behavior completely different from those of 6-ring and 5-ring compounds studied heretofore.

Spectral Types for Convex Compounds

The transitions from high filled to low empty $t=1$ shells in the larger 6-ring convex hydrocarbons are formally identical with those in the catacondensed

systems such as naphthalene. They should therefore give rise to similar $^{1,3}L_b$, $^{1,3}L_a$, $^{1,3}B_b$, $^{1,3}B_a$ transitions[13,14] at the longest wavelengths, and these types of singlets are in fact clear in the pyrene and coronene spectra.[15] The lowest transitions between the $t=1$ and $t=2$ orbitals are forbidden by symmetry. Low transitions between the $t=2$ orbitals are allowed, but it is not certain how to identify them and they probably lie at shorter wavelengths than the $t=1$ group. (The Coulson-Rushbrooke theorem would put the first unfilled $t=2$ orbital above the first unfilled $t=1$ orbital in a real periodic network.)

The ^1L transitions are not so weak in pyrene as in the catacondensed hydrocarbons. This means the configurational interaction, or mixing of pairs of one-electron-excited states of the same symmetry, is not as strong here[13] as it is in benzene and the catacondensed rings. The latter molecules, with much of this type of configurational interaction (called by Moffitt first-order configurational interaction[14]), are called "round-field" molecules—meaning that angular momentum is a good quantum number—in a paper describing the effect of these interactions on general spectral type.[16] Pyrene, styrene, and other molecules which have less mixing are called "long-field" molecules—meaning that linear momentum is beginning to be a better quantum number than angular momentum. The nonconvex molecules[15] seem to have even more long-field character than the pyrenes; their ^1L and ^1B transitions are of about equal intensity, and a distinction between their angular momenta seems no longer meaningful.

Other Convex Molecules

By altering Fig. 7, we may apply it qualitatively to other convex molecules not quite so round as those we have been considering.

First, we recall that the polyene orbitals (A) correspond to the orbitals of type $t=1$ in Fig. 7 but without the double degeneracy. The catacondensed orbitals (B) correspond to the $t=1$ orbitals with the double degeneracy. The pyrene-coronene-ovalene series orbitals (D) correspond to the $t=1$ and $t=2$ orbitals with the double degeneracy. It seems a reasonable interpolation to assume that the intermediate series of oblong molecules starting with the members (1) pyrene, (2) anthanthrene or 1,12-benzoperylene, (Fig. 6), etc., in which the inner perimeter is a polyene, will have orbitals (C) like the $t=1$ orbitals with degeneracy plus the $t=2$ orbitals without. This agrees with the method of bookkeeping of orbitals stated earlier.

We may now have other molecules intermediate in type between the members of these four series, such as benzopyrene or naphthopyrene (Fig. 6), with (C) orbitals plus extra (B) orbitals. The spectrum of pyrene changes in going to benzopyrene[15] in much the same way as the spectrum of phenanthrene changes in going to benzanthracene. This suggests that we can deal with the benzopyrene change in the same way: by adding an additional degenerate $t=1$ orbital to pyrene to take care of the four new perimeter pi electrons; compressing the other $t=1$ orbital energies closer together since the perimeter is longer; and leaving the number and position of the $t=2$ orbitals almost unchanged. The strict degeneracy of the round box orbitals was already removed in pyrene; the orbital energies will probably be split still further in benzopyrene; but, following the procedure used with the catacondensed rings, we can probably regard these effects as secondary. (We cannot deal with the change from naphthalene to fluoranthene or from benzofluoranthene to rubicene as easily as with the benzopyrene change, because the appearance of odd rings in the system changes the bookkeeping.)

We may deal with any other convex molecule in the same way: we derive its orbital types and energies from those of the largest skeleton of type (C) or (D), etc., which it contains, by adding enough $t=1$ orbitals to hold the additional perimeter electrons, compressing the original $t=1$ orbital energies, and so on. Changes in symmetry will of course change the selection rules, so that new transitions will become conspicuous[17] on going to a system of lower symmetry.

These qualitative arguments help to justify us in using the same general orbital scheme, the same addition of angular momenta, and the same letters for classification of states in all convex molecules. They account for some of the regular changes in the spectra with addition of rings to the molecule (annelation) which were found by Clar[15] for the pericondensed as well as for the catacondensed hydrocarbons.

ACKNOWLEDGMENT

I am indebted to Dr. Hans Kuhn for an interesting discussion which led to this study of densities in the box model. He has stressed elsewhere the analogy between the free-electron wave functions and those of a vibrating membrane satisfying a two-dimensional wave equation.[18] I wish to thank Mr. Theodore N. Sarachman for help in molding and casting the plaster models.

[15] E. Clar, *Aromatische Kohlenwasserstoffe* (Springer-Verlag, Berlin, 1952), second edition.
[16] J. R. Platt, J. Chem. Phys. **18**, 1168 (1950).
[17] J. R. Platt, J. Chem. Phys. **19**, 1415 (1951).
[18] H. Kuhn, Z. Elektrochem. **55**, 220 (1951).

Letters to the Editor

THIS section will accept reports of new work, provided these are terse and contain few figures, and especially few half-tone cuts. The Editorial Board will not hold itself responsible for opinions expressed by the correspondents. Contributions to this section should not exceed 600 words in length and must reach the office of the Editor not later than the 15th of the second month preceding that of the issue in which the Letter is to appear. No proof will be sent to the authors. A publication charge of $10.00 per Letter is made which, when honored, will entitle the Institution to 100 free reprints.

Microwave Investigation of Hindered Rotation and Inversion of Methylamine*

K. SHIMODA, T. NISHIKAWA, AND T. ITOH
Department of Physics, Faculty of Science, University of Tokyo, Tokyo, Japan
(Received May 14, 1954)

MICROWAVE spectrum of methylamine molecule has been studied in the frequency range between 7 and 30 kMc/sec. More than two hundred lines and their Stark effects have been measured.

The analysis and assignment of these lines are rather difficult, since the methylamine is an asymmetric top rotor, the amine group of which is rotatable with respect to the methyl group, and in addition it may invert itself about nitrogen. The rotational energy levels are described by the quantum numbers, J, K, τ, and n, according to the theory of Dennison and others[1] as in the methyl alcohol. J and K are usual rotational quantum numbers, n is the quantum number of torsional vibration, and τ $(=1,2,3)$ is the quantum number of hindered rotation. Besides, each rotational level is split into two levels, $+$ and $-$, by the inversion effect. Lines of the spectrum are divided into two kinds. The one is the lines of $\Delta J=0$ and the other is $\Delta J=\pm 1$. Most lines of the observed spectrum should be due to the transitions $\Delta K=\pm 1$, $\Delta(K+\tau)=0$, $\Delta n=0$, and $+\leftrightarrow-$, while some of the weaker lines may be due to the transitions $\Delta K=0$.

We have found seven series of lines denoted by p_1, p_2, q_1, q_2, r_1, r_2, and s_1 which correspond to the transitions $\Delta J=0$. In Fig. 1 frequencies of series members are plotted against estimated J values though accurate values of J have not yet been determined except for p_1 series. Recently Lide traced these series up to 34 kMc/sec and his results[2] are also quoted in Fig. 1.

Lines which belong to p series show the first-order Stark effects, resulting from the intrinsic degeneracy of the levels having $K+\tau-1$ not divisible by 3. On the other hand, Stark effects of q, r, and s series are those of the second order. Values of $K+\tau-1$ of these series, therefore, must be divisible by 3. Among them, q series show primarily the first order Stark effects in the lower field strength ($\lesssim$100 v/cm). This may be explained by the intermediate coupling of Stark effect and nuclear quadrupole effect of N^{14}.

TABLE I. Assignment of series.

Series	Assignment $K,\tau,n\rightarrow K',\tau',n'$	Frequency of the initial line: Observed (Mc/sec)	Frequency of the initial line: Calculated (Mc/sec)	Nuclear statistical weight[a]	Magnitude of inversion doubling: Observed (Mc/sec)	Magnitude of inversion doubling: Calculated (Mc/sec)
p_1	0,3,1→1,2,1	26 733.54	(26 700)	3	6903.3	(6900)
p_2	0,3,1→1,2,1	33 636.8	(33 600)	1		
q_1	0,1,0→1,3,0	···	79 000	3	~5000	10 000
q_2	0,1,0→1,3,0	···	89 000	1		
r_1	1,3,1→2,2,1	···	102 000	3	~10 000	20 000
r_2	1,3,1→2,2,1	···	122 000	1		
s_1	1,3,1→0,1,1	~0	0	3	≳30 000	35 000
s_2	1,3,1→0,1,1	···	35 000	1		

[a] The values 3 and 1 correspond to the triplet and singlet spin states of two protons in the amine group.

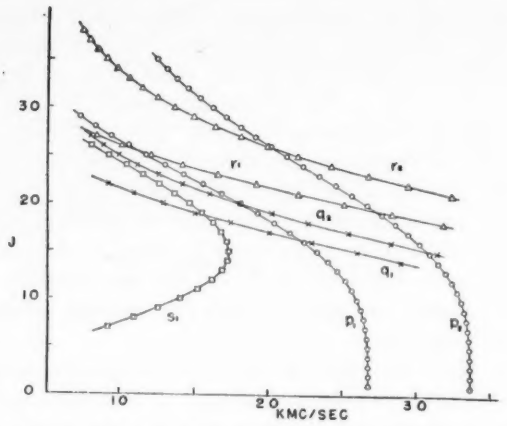

FIG. 1. Frequencies of the lines of series plotted against their rotational quantum number J. J values are only approximate except for p series.

p_1 series couples with p_2, q_1, with q_2, and r_1 with r_2, forming pairs of inversion doubling, while the partner of s_1 series would be out of the observed range. With the theoretical consideration, we have assigned K, τ, and n of these series as shown in Table I. The starting positions of the series and magnitudes of inversion doublings are also listed in Table I with calculated values based on the assumed values in parentheses. The magnitudes of inversion doublings depend considerably on the quantum numbers, K, τ, and n, through the coupling between inversion and hindered rotation. From these results, the height of potential barrier hindering internal rotation has been determined to be about 680 cm^{-1}.

As to the $\Delta J=\pm 1$ lines, Lide assigned three lines and calculated the rotational constants of this molecule assuming the rigid rotor model.[3] His results, however, must be somewhat modified by the effect of hindered rotation and inversion upon overall molecular rotation. We have also found some ten lines which belong to the transitions $\Delta J=\pm 1$, though the consistent assignment has not yet been made. Precise molecular constants cannot be obtained until the lines of $\Delta J=\pm 1$ are completely analysed.

Detailed results and discussions will be published in the J. Phys. Soc. Japan. We express our thanks to Dr. D. R. Lide for his kind information of his results.

* Preliminary results of this work have been reported at Symposium on Molecular Physics, Nikko, held on the occasion of the International Conference on Theoretical Physics, Kyoto-Tokyo, September, 1953. See also K. Shimoda and T. Nishikawa, J. Phys. Soc. Japan **8**, 133, 425 (1953).

[1] J. S. Koehler and D. M. Dennison, Phys. Rev. **57**, 1006 (1940); D. G. Burkhard and D. M. Dennison, Phys. Rev. **84**, 408 (1951); E. V. Ivash and D. M. Dennison, J. Chem. Phys. **21**, 1804 (1953).

[2] Private communication.

[3] D. R. Lide, J. Chem. Phys. **20**, 1812 (1952); **21**, 571 (1953).

Temperature Dependence of Microwave Absorption Coefficient

KRISHNAJI AND PREM SWARUP
Department of Physics, University of Allahabad, Allahabad, India
(Received January 18, 1954)

BIRNBAUM and Maryott[1] have recently reported the absorption in the low-frequency wing of the NH_3 inversion spectrum and have shown therein that α varies as T^{-3}. We feel that their data do not conclusively show that α varies as T^{-3}. We[2] have also collected sufficient data on the absorption coefficient of a few vapors and gases and have studied temperature dependence of microwave absorption coefficients at 3.33-cm wavelength. While

a detailed paper awaits publication,[3] it was felt necessary to write this note on Birnbaum and Maryott's work on temperature variation of the absorption coefficient of ammonia.

The quantum mechanical expression for the absorption coefficient of Van Vleck and Weisskopf[4] has been found to be applicable at low pressures only.[5] The fact led to the theoretical work of Anderson,[6] Margenau,[7] Leslie,[8] and Mizushima.[9] All of them on accounting for simple collision, dipole interaction, and perturbations, etc., by different approaches have given final expressions for $\langle\Delta\nu\rangle_{Av}$. Although none has treated temperature factor separately from the expressions of $\langle\Delta\nu\rangle_{Av}$ we find that $\langle\Delta\nu\rangle_{Av}$ should vary with temperature as T^{-1}. The "hard sphere" kinetic theory predicts that $\langle\Delta\nu\rangle_{Av}$ should vary with temperature as $T^{-\frac{1}{2}}$.

The Van Vleck-Weisskopf expression for absorption coefficient at a frequency (cm^{-1}) is:

$$\frac{\alpha}{\tilde{\nu}^2}=\frac{4\pi^2\Sigma N_{JK}|\mu_{JK}|^2}{3kT}\left[\frac{\langle\Delta\nu\rangle_{Av}}{\langle\Delta\nu\rangle_{Av}^2+(\tilde{\nu}-\tilde{\nu}_0)^2}+\frac{\langle\Delta\nu\rangle_{Av}}{\langle\Delta\nu\rangle_{Av}^2+(\tilde{\nu}+\nu_0)^2}\right].$$

If the frequency $\tilde{\nu}$ is far removed from the resonant frequency $\tilde{\nu}_0(cm^{-1})$ and the pressure is low, it can be simplified to:

$$\alpha=\frac{(\text{constant})}{T^2}\cdot\langle\Delta\nu\rangle_{Av}\text{ at constant pressure.}$$

From the above expression we find that the absorption coefficient will vary with temperature as T^{-3} in support of Anderson or Margenau theory and as $T^{-5/2}$ on kinetic theory.

Table I gives the results of Birnbaum and Maryott as well as the values of $\alpha T^{5/2}$ calculated by us from their own data.

TABLE I.

Temperature	αT^3		$\alpha T^{5/2}$	
−12°C	75.6		4.68	
25	78.3		4.53	
39	74.7	deviation	4.22	deviation
60	74.2	from mean	4.06	from mean
80	75		4.0	
100	78.3	5.5%	4.05	5.5%

Our calculation shows that the constancy of $\alpha T^{5/2}$ over a sufficiently large temperature range of 39° to 100°C is about the same as the constancy of αT^3 over the same range of temperature. It is thus seen that a clear conclusion regarding the temperature dependence of α for NH_3 is not possible from their data.

We have collected data on absorption coefficient of ammonia at 3.33-cm wavelength between −8° and 50°C at various pressures. Several sets were taken and graphs were plotted between $\log\alpha$ and $\log T$ at various pressures. The variation of the absorption coefficient can be put as: $\alpha_1=\alpha_2(T_2/T_1)^x$, we have calculated the value of x on both theories, i.e., $\langle\Delta\nu\rangle_{Av}$ varying as T^{-1} and $T^{-\frac{1}{2}}$ at various pressures, of course, giving due account to the shift of $\langle\nu_0\rangle_{Av}$ with pressure and nonlinear variation of $\langle\Delta\nu\rangle_{Av}$ with pressure. The experimental value of x is found out from the slope of the $\log\alpha$ *vs* $\log T$ graphs. The following is the illustrative data of observed and theoretical values of x. It is apparent from the Table II that experimental values of x are in better agreement with values calculated on assuming that $\langle\Delta\nu\rangle_{Av}\propto T^{-\frac{1}{2}}$ and as the pressure is decreased the experimental value of x is closer to 5/2 than 3 giving a conclusion that the line-width parameter varies as $T^{-\frac{1}{2}}$ and not T^{-1} in the case of NH_3. It may, however, be mentioned that our measurements in other gases have indicated T^{-3} law variation of the absorption coefficient at low pressures.

TABLE II.

Pressure cm	Exptl x	$T^{-\frac{1}{2}}$ Law x	T^{-1} Law x
15	2.40	2.43	2.84
30	2.28	2.28	2.35
50	1.50	2.00	2.05

[1] G. Birnbaum, and A. A. Maryott, J. Chem. Phys. **21**, 1775 (1953).
[2] Krishnaji and Prem Swarup, J. Sci. Ind. Research (India) **12B**, 1 (1953); J. Appl. Phys. **24**, 2527 (1953).
[3] Prem Swarup, J. Sci. Ind. Research (India) (to be published).
[4] J. H. Van Vleck, and V. F. Weisskopf, Revs. Mod. Phys. **17**, 225 (1945).
[5] W. Gordy, *et al.*, *Microwave Spectroscopy* (*W*), 1953; this book contains exhaustive bibliography on the subject.
[6] P. W. Anderson, Phys. Rev. **76**, 647 (1949).
[7] H. Margenau, Phys. Rev. **76**, 121 and 1423 (1949).
[8] D. C. M. Leslie, Phil. Mag. **42**, 37 (1951).
[9] M. Mizushima, Phys. Rev. **83**, 94 (1951).

Temperature Dependence of the Microwave Absorption of NH_3

G. BIRNBAUM AND A. A. MARYOTT
National Bureau of Standards, Washington, D. C.

(Received April 12, 1954)

IN the preceding letter Krishnaji and Prem Swarup, after arbitrarily disregarding data over about half of the temperature interval, maintain that our data[1] cannot distinguish between a T^{-3} and a $T^{-5/2}$ temperature dependence. A least-squares treatment of our data over the entire interval −12 to 100°C gives $\alpha\propto T^{-2.94}\pm0.09$ where ±0.09 is the standard deviation. When interpreted in terms of the Van Vleck-Weisskopf relation, this result, obtained at a wavelength of 10.6 cm and at pressures sufficiently low to make unnecessary corrections for the variations in resonant frequencies and collision diameters, leads directly to a variation of the line breadth parameter as T^{-1} rather than as $T^{-\frac{1}{2}}$.

[1] G. Birnbaum and A. A. Maryott, J. Chem. Phys. **21**, 1774 (1953).

Lattice Vibration Specific Heat of Graphite

TAKEO NAGAMIYA, *Osaka University, Osaka, Japan*
AND
KOZO KOMATSU, *Naniwa University, Osaka, Japan*

(Received January 12, 1954)

IN the 1953 issues of this Journal two papers appeared[1,2] which dealt with the lattice dynamics and specific heat of graphite. In both papers the vibration of each honeycomb net plane with atomic displacements perpendicular to the plane is treated using a potential energy of the form $(\frac{1}{2})\alpha\Sigma(z_i-z_{i-1})^2$ where z_i and z_{i-1} are the displacements of neighboring atoms in the plane and α is a positive constant. Evidently this assumption for the potential energy is inadequate, because this form of the potential energy follows only from a finite surface tension of the net plane. In 1951 we[3] made another kind of treatment of the same problem which consisted in assuming a set of continuous elastic plates loosely coupled with each other, but the following points of our paper have been critcized by one of the papers cited above, due to Krumhansl and Brooks: 1. The strain energy should be a quadratic function of the strain components if we regard graphite as a homogeneous anisotropic elastic solid, and it should follow that for long waves ω^2 (ω: circular characteristic frequency) is a quadratic function of the components of the wave vector, whereas our result is not so—our result is $\omega^2=A(\sigma_z^2+\sigma_y^2)^2+c\sigma_z^2$. 2. In our theory, the phase velocity for the z vibration vanishes for the infinitely long wave $\sigma=0$ which is physically absurd. 3. The thin plate treatment can only be applicable to a crystalline plate of many atomic thicknesses, in which case the specific heat should be sensitive to this thickness. So, we should like to make a short comment on this problem and further to report a result which we recently obtained.

The third point above cannot be justified. A hexagonal net plane when macroscopically seen should have a bending modulus as

well as a shear modulus and an extensional modulus. It is therefore quite legitimate to approximate it by a thin elastic plate, and indeed we have an atomistic foundation of this continuum model by an unpublished work by Kitano at Naniwa University (we hope to publish it before long). The first two points literally taken are absurd, but we think as follows. In our treatment we neglected the modulus for the slip between adjacent plates but this is surely an over-simplification for waves with small wave vectors. The neglect of this modulus makes it possible to separate the vibrations of graphite into those in which the atomic displacements are perpendicular to the plates and those in which they are parallel to the plates. Taking account of this modulus, we are no longer able to separate them, and it can be shown that the specific heat follows the T^3 law at low temperatures and approximately T^2 law at higher temperatures if the slip modulus is assumed small compared with other moduli. At the same time the points of difficulty above disappear. Krumhansl and Brooks apparently obtained a similar result of the transition from T^3 to T^2 law, but this was not due to a slip modulus but to their inadequate assumption of a surface tension, instead of a bending modulus. Our preliminary calculation shows that the slip modulus plays a role only below a few degrees absolute and that the temperature of transition from T^3 to T^2 law is approximately given by $kT\sim nh/4\pi\rho\kappa$ (n rigidity corresponding to the slip between adjacent hexagonal planes, h Planck's constant, ρ volume density, $\rho\kappa^2/c$ bending modulus of a single hexagonal plane, c interplanar distance). Details will be published elsewhere.

[1] J. Krumhansl and H. Brooks, J. Chem. Phys. 21, 1663 (1953).
[2] H. B. Rosenstock, J. Chem. Phys. 21, 2064 (1953).
[3] K. Komatsu and T. Nagamiya, J. Phys. Soc. (Japan) 6, 438 (1951).

Some Aspects of Pair Interactions for a Linear Array of Sites, as Applied to Adsorption Problems

ROBERT F. STEINER
Naval Medical Research Institute, National Naval Medical Center, Bethesda, Maryland
(Received December 2, 1953)

THERE exists a large class of adsorption processes for which the Ising one-dimensional model is valid and useful, such as the binding of ions or molecules by linear macromolecules.[1] In the following, we consider the effect of pair interactions between both first and second nearest neighbors upon adsorption by a linear array of sites.

By straightforward combinatorial methods we obtain for the configurational partition function for B sites, of which i are filled, containing k_1 first nearest neighbor pairs, k_2 second nearest neighbor pairs, and n_2 clusters of occupied sites with two or more members:

$$\Omega_{B,i}=\sum_{k_1=0}^{k_1=i-1}\ \sum_{n_2=1}^{n_2=\text{smaller of } k_1 \text{ and } i-k_1}\ \sum_{k_2=k_1-n_2}^{k_2=i-n_2-1} C_{n_2}^{i-k_1}\,C_{n_2-1}^{k_1-1}\,C_{k_2-k_1+n_2}^{i-k_1-1}\,C_{i-k_2-n_2}^{B-2i+k_1+2}\times\exp\left\{-\frac{1}{KT}(k_1\epsilon_1+k_2\epsilon_2)\right\} \quad (1)$$

where

$$C_m^n=\frac{n!}{m!\,(n-m)!},$$

ϵ_1, ϵ_2 = energy of interaction for first and second nearest neighbor pairs, respectively.

When B is small ($<\sim 15$) we have for the average value of i in terms of the free adsorbate concentration c and the intrinsic association constant for binding by a single site, K_0:

$$\bar{i}=\sum_{i=0}^{i=B} i(cK_0)^i\Omega_{B,i}\Big/\left(1+\sum_{i=0}^{i=B}(cK_0)^i\Omega_{B,i}\right). \quad (2)$$

When B is large, (1) is expressible in terms of λ_1, λ_2, and λ_3, the number of triplet clusters of types AAA, AAO (or OAA), and AOA, respectively. Noting that $K_1=\lambda_1+\lambda_2/2$, $K_2=\lambda_3+\lambda_1$, and $n_2=\lambda_2/2$, we maximize (1) by setting $\partial\ln\Omega_{B,i}/\partial\lambda_1$, $\partial\ln\Omega_{B,i}/\partial\lambda_2$, and $\partial\ln\Omega_{B,i}/\partial\lambda_3$ equal to zero. Introducing also $\lambda_4(=2i-2\lambda_3-2\lambda_1-\lambda_2)$, $\lambda_5(=i-\lambda_2-\lambda_1)$, and $\lambda_6(=B-3i+2\lambda_1+\lambda_2+\lambda_3)$ for the numbers of clusters of types OOA (or AOO), OAO, and OOO, respectively, we obtain the following quasi-chemical expressions:[2,3]

$$-a\frac{\bar{\lambda}_4^2}{\bar{\lambda}_3\bar{\lambda}_6}=4e^{\epsilon_2/KT}=4\eta_2^{-1},$$
$$-b\frac{\bar{\lambda}_5\bar{\lambda}_1}{\bar{\lambda}_2^2}=\tfrac{1}{4}\eta_2, \quad (3)$$
$$-c\frac{\bar{\lambda}_5^2\bar{\lambda}_4^2\bar{k}_1(B-2i+\bar{k}_1)}{\bar{\lambda}_2^2\bar{\lambda}_6^2(i-\bar{k}_1)^2}=e^{\epsilon_1/KT}=\eta_1^{-1}.$$

We have for the chemical potential μ_c of the complex species, and the absolute activity of free adsorbate σ:

$$-\frac{\mu_c}{KT}=-\ln\sigma=\ln f_A+\partial\frac{\ln\Omega_{B,i}}{\partial i};$$
$$f_A=\text{partition function for bound species.} \quad (4)$$

From (1), (3), and (4), we have the following isotherm, in terms of the reduced quantities θ, α_1, α_2, and α_3, which are equal to i/B, $\bar{\lambda}_1/B$, $\bar{\lambda}_2/B$, and $\bar{\lambda}_3/B$, respectively:

$$\sigma=f_A^{-1}\frac{(\theta-\alpha_1-\alpha_2)(1-2\theta+\alpha_1+\alpha_2/2)^2(\theta-\alpha_1-\alpha_2/2-\alpha_3)^2}{(\theta-\alpha_1-\alpha_2/2)^2(1-3\theta+2\alpha_1+\alpha_2+\alpha_3)^3}. \quad (5)$$

If ϵ_2 is not large in comparison with ϵ_1, so that the quasi-chemical approximation holds for groups of two sites we have

$$\frac{\bar{k}_1(B-2i+\bar{k}_1)}{(i-k_1)^2}=\eta_1. \quad (6)$$

From (3) and (6) we obtain

$$\alpha_2=\frac{2\alpha_1}{\eta_2}\left\{\left(1-\eta_2+\frac{\theta\eta_2}{\alpha_1}\right)^{\frac{1}{2}}-1\right\}, \quad (7a)$$

$$\alpha_3=\eta_1^{-1}\alpha_1(2\theta-2\alpha_1-\alpha_2)^2(1-3\theta+2\alpha_1+\alpha_2)/\{(\theta-\alpha_1-\alpha_2)(\alpha_1+\alpha_2/2)(1-2\theta+\alpha_1+\alpha_2/2)-\eta_1^{-1}\alpha_1(2\theta-2\alpha_1-\alpha_2)^2\}, \quad (7b)$$

$$\alpha_1+\alpha_1/\eta_2\left\{\left(1-\eta_2+\frac{\theta\eta_2}{\alpha_1}\right)^{\frac{1}{2}}-1\right\}=[\{4\theta(1-\theta)\times(\eta_1-1)+1\}^{\frac{1}{2}}/2(1-\eta_1)]-\tfrac{1}{2}(1-\eta_1)+\theta. \quad (7c)$$

Equation (7c) is readily solvable for α_1. α_2 and α_3 are then obtainable from (7a) and (7b). If ϵ_2 is sufficiently large so that (6) does not hold, we have in place of (7):

$$\left\{2\psi_1\psi_2^{\frac{1}{2}}(1-2\theta+\psi_2)^{\frac{1}{2}}-2\eta_1^{-\frac{1}{2}}\left[\frac{\alpha_1}{\eta_2}\left(\left(1-\eta_2+\frac{\theta\eta_2}{\alpha_1}\right)^{\frac{1}{2}}-1\right)\right]\times(1-3\theta+2\psi_2)\right\}\{\psi_1\psi_2(1-2\theta+\psi_2)-4\eta_1^{-1}\alpha_1(\theta-\psi_2)^2\}$$
$$-4\eta_1^{-1}\alpha_1(\theta-\psi_2)(1-3\theta+2\psi_2)\left\{2\psi_1\psi_2^{\frac{1}{2}}(1-2\theta+\psi_2)^{\frac{1}{2}}+\eta_1^{-\frac{1}{2}}\left[\frac{\alpha_1}{\eta_2}\left(\left(1-\eta_2+\frac{\theta\eta_2}{\alpha_1}\right)^{\frac{1}{2}}-1\right)\right]\left(\theta-\psi_2\right)\right\}=0, \quad (7d)$$

where

$$\psi_1=\theta-\alpha_1-\alpha_2$$
$$=\theta-\alpha_1-\frac{2\alpha_1}{\eta_2}\left\{\left(1-\eta_2+\frac{\theta\eta_2}{\alpha_1}\right)^{\frac{1}{2}}-1\right\},$$
$$\psi_2=\alpha_1+\alpha_2/2=\alpha_1\left\{1+\frac{2}{\eta_2}\left(\left(1-\eta_2+\frac{\theta\eta_2}{\alpha_1}\right)^{\frac{1}{2}}-1\right)\right\}.$$

Equation (7d) is numerically solvable for α_1. Equations (7) and (5) allow the computation of the complete adsorption isotherm for binding by a one-dimensional array of sites and should be

useful in interpreting experimental data upon the binding of ions by nuclei acid and other polyelectrolytes.

[1] Z. Ising, Physik **31**, 253 (1925).
[2] Rushbrook and Ursell, Proc. Cambridge Phil. Soc. **44**, 263 (1948).
[3] Temperly, Proc. Cambridge Phil. Soc. **40**, 239 (1944).

Microwave Spectrum of Ethyl Chloride

ROSELIN S. WAGNER AND B. P. DAILEY
Department of Chemistry, Columbia University, New York 27, New York
(Received June 11, 1954)

THIS is a preliminary report on the microwave spectrum of ethyl chloride. From the assumed parameters, C−C 1.54A, C−Cl 1.78A, C−H 1.103A, H−C−H angle 110° 20′ (in $-CH_2Cl$), H−C−H angle 109° 28′ (in $-CH_3$), and the C−C−Cl angle 111° 30′, calculation of the moments of inertia indicate that ethyl chloride is a nearly prolate rotor ($\chi=-0.95$) with the dipole moment having components along the A and B principal axes.

It has been possible to identify four transitions for $C_2H_5Cl^{35}$ and two transitions for $C_2H_5Cl^{37}$ on the basis of their Stark patterns and quadrupole hyperfine structure. These transitions involve the dipole component along the A axis. These transitions should be four times as strong as those involving the B component. From the frequencies of these transitions four rotational constants have been calculated (see Table I). Table II lists the undisplaced frequencies calculated from the quadrupole hyperfine pattern. As yet, no "B"-type transitions have been identified which would give a value for the largest rotational constant.

An investigation of two different deuterated species should yield eight more rotational constants. Thus sufficient information would be at hand to determine unambiguously the structure, including a more accurate value for the C−C distance than is now available.

Since our assumed model gives calculated values for B and C which are fairly close to the observed ones, it is probably not greatly different from the correct structure. This model indicates that the C−Cl bond is oriented at an angle of 26° 30′ from the A axis, which most nearly represents the axis of a symmetric top. From an analysis of the quadrupole hyperfine structure, eqQ along this axis is −48.44 Mc and $\eta=0.46$ for $C_2H_5Cl^{35}$, and eqQ is −36.9 Mc and $\eta=0.47$, for $C_2H_5Cl^{37}$. Thus, we estimate that eqQ along the C−Cl bond is −69.1 Mc for $C_2H_5Cl^{35}$ and −52.6 Mc and $C_2H_5Cl^{37}$.

The most accurately reported value for eqQ for CH_3Cl^{35} and CH_3Cl^{37} are −74.77 and −58.93, respectively.[1] The lower values for ethyl chloride are in agreement with the qualitative argument that replacing a hydrogen with a methyl group increases the ionic character of the C−Cl bond. This would lead to a reduced value for eqQ as is observed. Further, R. Livingston[2] has reported for solid ethyl chloride an eqQ of 65.95 Mc. Thus there is an apparent 4.6 percent increase in ionic character for the C−Cl bond in ethyl chloride in going from the gas to the solid state. In methyl chloride the solid state value for eqQ is 68.4,[3] indicating a change of 8.5 percent in ionic character.

TABLE I.

Calculated rotational constants	Observed rotational constants
A =30 124 Mc (a)	
B = 5501 Mc (a)	B =5493.76 Mc (a)
C = 4951 Mc (a)	C =4962.24 Mc (a)
A =33 328 Mc (b)	
B = 5351 Mc (b)	B =5397.29 Mc (b)
C = 4905 Mc (b)	C =4812.22 Mc (b)
(a) for $C_2H_5Cl^{35}$	(b) for $C_2H_5Cl^{37}$

TABLE II.

Transitions	Observed frequencies (in Mc)
$1_{11}\rightarrow 2_{12}$	20 380.39 (a)
$1_{10}\rightarrow 2_{11}$	21 443.42 (a)
$2_{21}\rightarrow 3_{22}$	31 368.07 (a)
$2_{20}\rightarrow 3_{21}$	31 400.29 (a)
$1_{11}\rightarrow 2_{12}$	19 980.38 (b)
$1_{10}\rightarrow 2_{11}$	21 004.09 (b)
(a) for $C_2H_5Cl^{35}$	(b) $C_2H_5Cl^{37}$

It was found possible to analyze the ground state transitions of ethyl chloride by assuming it to be a rigid rotor. However, vibrational satellites have been observed which can be attributed to rotational transitions of the molecule in the first excited state of torsional oscillation. From intensity ratio measurements, the torsional frequency is calculated to be 215 cm^{-1}. There is no previous assignment of a torsional frequency in the literature. For a reduced moment of 4.76×10^{-40} gcm^2, a sinusoidal barrier height of 3000 cal/mole is obtained. Barrier heights, calculated from the thermodynamic data, of 2700 cal/mole[4] and 4700 cal/mole[5] have been reported.

Further work on the deuterated samples should allow a more accurate determination of the molecular parameters, furnishing more accurate values for the quadrupole coupling constant and the barrier height.

[1] J. Kraitchman and B. P. Dailey, J. Chem. Phys. (to be published).
[2] R. Livingston, J. Chem. Phys. **20**, 7 (1952).
[3] R. Livingston, J. Chem. Phys. **19**, 1434 (1951).
[4] A. Eucken and E. U. Franck, Z. Electrochem. **52**, 195–204 (1948).
[5] J. Gordon and W. F. Giauque, J. Am. Chem. Soc. **70**, 1506 (1948).

Geometry of VIX_4 Molecules

FELIX LACHMAN
Commonwealth Forestry Bureau, Forest Products Research Laboratory, Princes Risborough, Bucks, England
(Received February 1, 1954)

EXPERIMENTAL data are available for the molecular structure of $TeCl_4$,[1] SeF_4,[2] and $TeBr_4$ and TeI_4,[3] also for $Se(C_6H_5)_2Br_2$,[4] $Se(C_6H_5)_2Cl_2$,[5] $IO_2F_2^-$,[6] and CrO_2Cl_2.[7]

For the coordination number four, Kimball[8] envisages the following arrangements: (a) regular tetrahedron (Td symmetry),

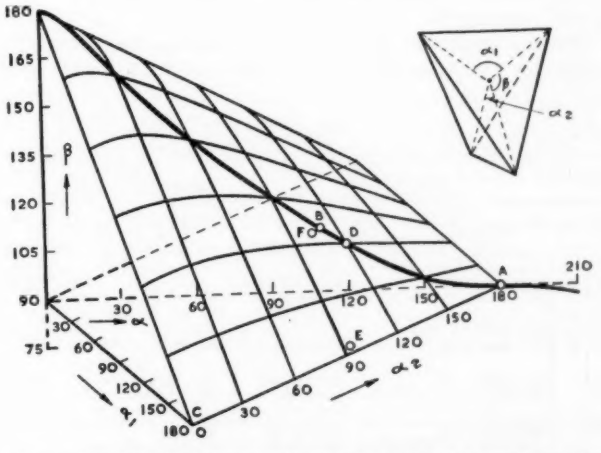

FIG. 1. Relationships between valency angles (α_1,α_2,β) in configurations of even-symmetry types: (a) surface bounded by 4 straight lines—orthorhombic sphenoid, (b) bold line (for $0°<\alpha<180°$)—tetragonal sphenoid, (c) bold line (for $180°<\alpha<360°$)—tetragonal pyramid, (d) A—tetragonal plane, (e) B—regular tetrahedron, (f) line AC, in particular section 90–120°, —"$TeCl_4$ structure" (4, 5, 6, 3), (g) D—SeF_4 (2) (h) E—$TeCl_4$ (1) (i) F—CrO_2Cl_2 (7).

bonds from sp^3 and sd^3; (b) tetragonal plane (D_{4h}), dsp^2, d^2p^2; (c) tetragonal pyramid (C_{4v}), p^3d, pd^3, d^4, and (d) irregular tetrahedron (C_{3v}; a trigonal pyramid with the central atom not necessarily inside the base triangle), dp^3, d^3p, d^2sp. Kimball fails to quote examples for (c) and (d) which seem to be unstable configurations. Dyatkina[9] says that experimental electron and x-ray diffraction data available are incompatible with the C_{3v} symmetry. She also affirms[10] that no hybridization with the unshared electron pair is required to explain results obtained for $TeCl_4$, the Se diphenyl dihalides and $IO_2F_2^-$, and using Kimball's group theory method, obtains a reduction table for the C_{2v} symmetry (probably related to spd^2, p^3d, pd^3, d^4). This fifth configuration is called the "$TeCl_4$ structure".[11] The formation of configuration with C_{2v} instead of C_{3v} can be due to the fact that, in the former case, a strong π bond is possible with a d electron, while with C_{3v} strong π bonds are impossible.

The regular tetrahedron displays the σ^4 valency state; Kimball's "irregular tetrahedron" $\sigma^3\pi$; the "$TeCl_4$ structure" $\sigma^2\pi^2$; the tetragonal plane π^4, and the tetragonal pyramid also π^4, but with nonequivalent bonds.

The experimentally found VIX_4 structures are of *even* symmetry types.* Assuming equivalent bonds, they can be summarized as follows. The lowest symmetry form is the orthorhombic sphenoid in which 2 opposite angles (α_1, α_2) are unequal and the remaining 4 angles (β) are equal. We obtain

$$\cos(\tfrac{1}{2}\alpha_1)\cos(\tfrac{1}{2}\alpha_2) = -\cos\beta. \qquad (1)$$

When $\alpha_1=\alpha_2$, a tetragonal sphenoid is obtained (see reference 2 where, for SeF_4, the angles are $\alpha_1=\alpha_2=120°$, $\beta=104.5°$), with a modified equation $\cos^2(\frac{1}{2}\alpha) = -\cos\beta$, or $\cos\alpha+2\cos\beta=-1$.[12]

A regular tetrahedron ($3\cos\alpha=-1$, or $\alpha=109°\,28'$) is obtained with $\alpha=\beta$, a tetragonal plane with $\alpha=180°$ ($\beta=90°$), and a tetragonal pyramid with $\alpha_2=360°-\alpha_1$, yielding the relationship $\cos^2(\frac{1}{2}\alpha)=\cos\beta$ or $\cos\alpha-2\cos\beta=-1$, where α is the angle between the opposite and β that between the adjacent apical edges.

Finally, $\alpha_1=180°$ and $\beta=90°$ in the orthorhombic sphenoid give the "$TeCl_4$ structure"[9,10] in which "two of the halogen atoms are on one line with the central atom and the other 2 are located in a plane perpendicular to this line." The majority of the ClTeCl angles have been found to be $93\pm3°$.[1] If the majority is $\frac{5}{6}$ (i.e., $\alpha_2=\beta=93\pm3°$), then $\alpha_1=ca\ 171\pm9°$. For $\alpha_1=180°$ and $\beta=90°$ we have $\alpha_2=0/0$. Values between 90° and 120° have been found for this angle in different molecules and ions with "$TeCl_4$ structure".[4-6] The reliability of (1) may be affected by a later finding;[13] however, provisional structures of $TeBr_4$ and TeI_4, determined in a recent unpublished research,[3] give again $\alpha_1=180°$, $\beta=90°$, and $\alpha_2=90-120°$.

Valency angles in the regular tetrahedron are $\cos^{-1}(-\frac{1}{3})$; those in "$TeCl_4$-structure" molecules, $\cos^{-1}(-1)$, and $\cos^{-1}(0\cdots-\frac{1}{2})$; those in the tetragonal plane, $\cos^{-1}(0)$ and $\cos^{-1}(-1)$. Bowen's[2] distorted tetrahedron has angles $\cos^{-1}(-\frac{1}{2})$ and $\cos^{-1}(-\frac{1}{4})$. It seems worth while to check whether this "rule of unit-fraction cosines" applies to other angles, e.g., whether α_2 in "$TeCl_4$" can only assume "permitted" values between 90° and 120°.

Heavy central atoms (and unequal peripheral atoms?) seem to produce the "$TeCl_4$ structure"; lighter central atoms appear to favor the tetragonal sphenoidal structure; it might be expected that SCl_4 and SF_4 would yield the regular tetrahedron. The CrO_2Cl_2 molecule is a tetrahedron distorted owing to the heterogeneity of bonds.

All models that can be derived from Eq. (1) (for $\alpha_1 \geqslant \alpha_2$) are shown in Table I.

Similarly, for the irregular tetrahedron (C_{3v}),

7	α,β	$\alpha=120-0°$; $\beta=90-180°$.	trigonal pyramid	d^3p, dp^3, d^2sp	C_{3v}	?

Models 3 and 7 are not borne out by experiments; 2, 5, and 6 are the fundamental forms, and so perhaps is, 4.

* For Kimball's "irregular tetrahedra" (with equivalent bonds) one obtains the relationship $\cos\alpha=\frac{1}{3}(3\cos^2\beta-1)=\frac{1}{3}(3\cos2\beta+1)$, where α is the valency angle between the 3 nonapical bonds and β that between the apical and nonapical bond.

[1] D. P. Stevenson and V. Schomaker, J. Am. Chem. Soc. **62**, 1267 (1940).
[2] H. J. M. Bowen, Nature **172**, 171 (1953).
[3] S. C. Abrahams (private communication).
[4] J. D. McCullough and G. Hamburger, J. Am. Chem. Soc. **63**, 803 (1941).
[5] J. D. McCullough and G. Hamburger, J. Am. Chem. Soc. **64**, 508 (1942).
[6] L. Helmholz and M. T. Rogers, J. Am. Chem. Soc. **62**, 1537 (1940).
[7] Smyth, Grossman, and Ginsburg, J. Am. Chem. Soc. **62**, 192 (1940).
[8] G. E. Kimball, J. Chem. Phys. **8**, 188 (1940).
[9] M. Diatkina, Acta physicochim. U.R.S.S. **20**, 407–10 (1945).
[10] M. Dyatkina, Zhur. fiz. khim. **20**, 363–4 (1946).
[11] Y. K. Syrkin and M. E. Dyatkina, *Structure of Molecules*, 1950, p. 348.
[12] F. Lachman, Nature **172**, 499 (1953).
[13] V. Schomaker and R. Glauber, Nature **170**, 290 (1952).

TABLE I.

		Valency angles	Model	Electrons participating in σ bonds	Symmetry	Example
1	α_1,α_2,β	general form	orthorhombic sphenoid		C_{2v}	$[CrO_2Cl_2]$
2	α_1,α_2,β	$\alpha_1=180°$; $\beta=90°$; $\alpha_2=90-120°$.	"$TeCl_4$ structure"	d^3p, dp^3, d^4, d^2sp		$TeCl_4$
3	α_1,α_2,β	$\alpha_2=360°-\alpha_1$; $\beta<90°$.	tetragonal pyramid	d^3p, dp^3, d^4	C_{4v}	?
4	α,β	general form [$\alpha=120°$; $\beta=104.5°$?]	tetragonal sphenoid	d^3p, dp^3, d^4, d^2sp	S_4	SeF_4
5	α,β	$\alpha=180°$; $\beta=90°$.	tetragonal plane	dsp^2, d^2p^2	D_{4h}	$[PtCl_4^{2-}]$
6	α	$\alpha=109°\,28'$	regular tetrahedron	sd^3, sp^3	T_d	$[CF_4]$

Bond Angle, Dipole Moment, and Base Strength

JULIAN H. GIBBS
General Electric Company, Research Laboratory, Schenectady, New York

(Received June 2, 1954)

THE purpose of this letter is to point out that orbital hybridization, as determined by bond angle, can account for the variations in electric dipole moment and base strength among the hydrogen and organic (methyl, phenyl) compounds of the elements of the Vth, VIth, and VIIth main groups of the periodic system.

As Table I shows, the moments of the hydrides decrease with increasing atomic number of the heavy element in a vertical series (e.g., $\mu H_2O > \mu H_2S$), whereas the carbon compounds exhibit a maximum (maximum in bold face type) at the second row element (e.g., $\mu(CH_3)_2O < \mu(CH_3)_2S$).[1]

This difference is difficult to explain with the usual electronegativity arguments. However, recent LCAO calculations[2] for the first-row hydrides suggest that the lone-pair electrons make the major contribution ot the molecular moment, since a large

TABLE I. Bond angles and dipole moments of compounds of the Vth, VIth, and VIIth columns of the periodic table.

	Column V Substituent			Column VI Substituent			Column VII Substituent		
	H_3	$(CH_3)_3$	ϕ_3	H_2	$(CH_3)_2$	ϕ_2	H	CH_3	ϕ
Row I	107° **1.47D**	108° 0.65D	... 0.26D	104° **1.85D**	110° 1.30D	... 1.33D	**1.91D**	1.81D	1.58D
Row II	93.5° 0.55D	100° ...	... **1.45D**	92.3° 0.92D	104° **1.40D**	... **1.52D**	1.08D	**1.87D**	**1.71D**
Row III	92° 0.22D	96° ...	... 1.07D	... ...	... ...	... 1.38D	0.80D	1.80D	1.70D

degree of hybridization of the heavy element orients its low-pair charge cloud outward on the "back" side of the molecule.

The lone-pair moments will be governed by (a) the size and (b) the degree of hybridization (asymmetry) of the relevant atomic orbitals. The usual assumption that the bonding orbital axes are coincident with the bond axes affords a measure of the hybridization factor. Thus the available bond-angle data (see Table I) indicate that the degree of hybridization of the heavy elements decreases with increasing atomic number, from nearly tetrahedral sp^3 toward 90° p bonding, rapidly in the case of the hydrides and slowly in the case of the carbon compounds.

This suggests the following explanation of the dipole moment variations. If there were no loss in hybridization, the lone-pair moment would increase with increasing atomic number because of the increase in the orbital size. In the case of the organic compounds, this effect is not overcome by the slow decrease in hybridization until the third-row element is reached. In the case of the hydrogen compounds, on the other hand, the loss in hybridization at the second-row element is already very great and the moment is already decreasing. This explanation has been fully supported by LCAO calculations similar to those of Pople[2] but too lengthy for this letter.

The same hybridization rule accounts for the major variations in the strength of the bases formed by the Vth group elements. The energy of an acid-base reaction involving one of them may be obtained from a two-step path: (1) the base first absorbs the energy required to promote it to the state of complete tetrahedral hybridization; (2) it offers its hybridized lone pair to the acid in the exothermic formation of a fourth bond. The energy associated with the second step will be approximately the same for the various compounds of a given Vth group element. Therefore, in the consideration of the large variation in base strength among the phosphines, for example, it is only necessary to consider the variation in the energy required for the first step.

According to the bond angles, trimethyl phosphine is much more highly hybridized than phosphine. Inasmuch as considerably less energy should therefore be required to promote trimethyl phosphine to the completely hybridized state, it should be a much stronger base than phosphine. The best estimates of the base constants are $10^{-5.33}$ for trimethyl phosphine[3] and 10^{-28} for phosphine.[4] Methyl phosphine and dimethyl phosphine exhibit intermediate base strengths[3] as expected.

The amines display a much smaller variation in base strength than the phosphines. This is in accordance with the approximate equality of the bond angles for these compounds.

It should be noted that the variations in base strength among the compounds of the VIth and VIIth group elements are analogous to those of the compounds of the fifth series. For example, dimethyl sulfide exhibits pronounced basic properties whereas H_2S does not.

[1] C. P. Smyth, J. Phys. Chem. **41**, 209 (1937).
[2] J. E. Lennard-Jones and J. A. Pople, Proc. Roy. Soc. (London) **A202**, 166 (1950); J. A. Pople, Proc. Roy. Soc. (London) **A202**, 323 (1950); A. B. F. Duncan and J. A. Pople, Trans. Faraday Soc. **49**, 3, 217 (1953).
[3] Sei Sujushi, dissertation, Purdue University (1949); H. C. Brown. J. Am. Chem. Soc. **67**, 503 (1945).
[4] R. E. Weston, Jr., and J. Bigeleisen, Paper at Chicago Meeting of Division of Physical and Inorganic Chemistry, American Chemical Society, Sept. 6–11, 1953.

A Method of Determining the Dissociation Energy of Nitrogen*

W. F. Sheehan, Jr.
Gates and Crellin Laboratories of Chemistry, California Institute of Technology, Pasadena 4, California
(Received May 24, 1954)

THERE has been much discussion[1] of the merits of three possible values of $D_0(N_2)$, 7.38 ev, 8.57 ev, and 9.76 ev. Although the intermediate value has been eliminated[2] as the true value, it may be possible by this method to establish not only which of these two but which of these three is correct.

A study of the approach to equilibrium of a nonequilibrium mixture of $N^{14}N^{14}$, $N^{14}N^{15}$, and $N^{15}N^{15}$ or the appearance of the rotational or mass spectrum of $N^{14}N^{15}$ in a mixture of $N^{14}N^{14}$ and $N^{15}N^{15}$ may fix $D_0(N_2)$ according to the probable mechanism:

$$M_1+h\nu\rightarrow M_1^*, \quad (1)$$

$$M_1^*+N^{14}N^{14}\rightarrow M_1+2N^{14}, \quad (2)$$

$$M_1^*+N^{15}N^{15}\rightarrow M_1+2N^{15}, \quad (3)$$

$$M_2+N^{14,15}+N^{14,15}\rightarrow M_2+N^{14,15}N^{14,15}, \quad (4)$$

where M_1 is Kr or Xe; where M_1^* is Kr* ($4s^24p^55s$), Xe*($5s^25p^56s$), or perhaps even $N^{14,15}$ after (2) or (3); and where M_2 is Kr, Xe, N_2, or the wall. For Kr*($4s^24p^55s$), produced in the mixture of N_2 and Kr by fluorescing Kr*, has an energy of 9.910 ev ($^3P_2$) and Xe*($5s^25p^56s$), similarly, has energies of 8.313 ev and 8.435 ev ($^3P_{2,1}$) relative to the $^1S_0$ ground states.

Since the most probable change is that in which a minimum of excitation energy is converted to kinetic energy, dissociation of N_2 by Kr* and not by Xe* would confirm the dissociation limit at 9.76 ev, and a choice could be made between the values 9.76 ev and 7.38 ev upon establishing whether or not some of the nitrogen atoms produced in (2) and (3) are in the ^2D state. On the other hand, dissociation by Xe* and not by Kr* would indicate that $D_0(N_2)$ has the unlikely value of 8.57 ev, thermal energy supplying the defect in energy, or that the suppositions about the simplicity of the mechanism which seems to flow from the use of pure reactants and about the transfer of energy in (2) and (3) must be qualified. No reaction according to (2), (3), and (4) would indicate that the third possible value, 7.38 ev, is correct provided there are for these reactions no impediments such as too short a lifetime of M_1^*, low efficiency for (2) and (3), or an activation energy for dissociation to unexcited atoms. Since dissociation by both Kr* and Xe* would require a study of the mechanism, the experiment with Xe* is of value in checking the various suppositions even if 8.57 ev is not considered a possible value.

Outlined some time ago,[3] these experiments have not been undertaken because of a lack of vacuum ultraviolet apparatus.

* Contribution No. 1902 from the Gates and Crellin Laboratories of Chemistry, California Institute of Technology, Pasadena 4, California.
[1] A. G. Gaydon, *Dissociation Energies* (Chapman and Hall, Ltd., London, 1947).
[2] A. E. Douglas and G. Herzberg, Can. J. Phys. **29**, 294 (1951).
[3] W. F. Sheehan, Jr., thesis, California Institute of Technology (1952), Proposition 7.

Thermodynamic Functions for Borine Carbonyl

H. J. Galbraith
Callery Chemical Company, Callery, Pennsylvania
(Received May 26, 1954)

GORDY and Ring have made microwave measurements[1] on the rotational transitions $J=1\rightarrow2$, $J=2\rightarrow3$ for borine carbonyl and deuteroborine carbonyl which completely determine the structure of the molecule. Cowan has made a normal coordinate analysis[2] for borine carbonyl, assigning fundamental frequencies which are in agreement with infrared experimental data. The thermodynamic functions for the molecule can, therefore, be calculated.

Shepp and Bauer have calculated the entropy[3] at 300°K. The author has calculated C_p^0, $(H^0-E_0^0/T)$, $(F^0-E_0^0/T)$, and S^0 for borine carbonyl from 100°K to 600°K at intervals of 20°. The results are presented in Table I.

A summary of the data used for the calculations follows:

The interatomic distances in Angstrom units are; $d_{BH}=1.194$, $d_{BC}=1.540$, $d_{CO}=1.131$. Angle $HBH=113°, 52'$.

The fundamental frequencies in reciprocal centimeters are: 2360, 2164, 1105, 692, 2440, 1392, 809, and 315. The first four frequencies are nondegenerate; the last four are doubly degenerate.

The molecule has type C_{3v} symmetry.

The constants used for the calculations are: $h=6.62377\times10^{-27}$

TABLE I. Thermodynamic functions for borine carbonyl.

T °K	C_p^0 cal/mole °K	$\frac{H^0-E_0^0}{T}$ cal/mole °K	$\frac{-F^0-E_0^0}{T}$ cal/mole °K	S^0 cal/mole °K
100	8.86	8.15	39.40	47.55
120	9.37	8.31	40.90	49.21
140	9.87	8.50	42.19	50.69
160	10.38	8.70	43.34	52.04
180	10.88	8.91	44.38	53.29
200	11.39	9.14	45.33	54.47
220	11.90	9.36	46.21	55.58
240	12.41	9.60	47.03	56.63
260	12.92	9.83	47.81	57.65
273.16	13.25	9.99	48.30	58.29
280	13.42	10.07	48.55	58.62
298.16	13.86	10.29	49.19	59.48
300	13.91	10.31	49.25	59.56
320	14.40	10.55	49.93	60.48
340	14.88	10.79	50.57	61.36
360	15.32	11.03	51.20	62.23
380	15.77	11.27	51.80	63.07
400	16.21	11.50	52.38	63.89
420	16.63	11.74	52.95	64.69
440	17.05	11.97	53.50	65.47
460	17.45	12.20	54.04	66.24
480	17.85	12.43	54.56	66.99
500	18.23	12.65	55.07	67.72
520	18.60	12.87	55.58	68.45
540	18.97	13.09	56.07	69.16
560	19.33	13.31	56.55	69.85
580	19.67	13.52	57.02	70.54
600	20.01	13.73	57.48	71.21

erg sec, $k=1.380257\times10^{-16}$ erg/deg, $No=6.02380\times10^{23}$, and $R=1.98719$ cal/mole deg. These are taken from the recent compilation by Rossini *et al.*[4]

The calculated moments of inertia in gram cm² are: $I_A=I_B=96.265\times10^{-40}$ $I_C=6.7016\times10^{-40}$.

Calculation of the vibrational contributions was facilitated by the Einstein tables of Johnston, Savedoff, and Belzer.[5]

[1] W. Gordy and H. Ring, Phys. Rev. **78**, 512 (1950).
[2] R. D. Cowan, J. Chem. Phys. **18**, 1101 (1950).
[3] A. Shepp and S. H. Bauer, J. Am. Chem. Soc. **76**, 265 (1954).
[4] Rossini, Gucker, Johnston, Pauling, and Vinal, J. Am. Chem. Soc. **74**, 2699 (1952).
[5] Johnston, Savedoff, and Belzer, Contributions to the Thermodynamic Functions of a Planck-Einstein Oscillator in One Degree of Freedom. ONR Report July, 1949.

Electronic Transitions in the Nitrite Ion

WILLIAM G. TRAWICK AND W. H. EBERHARDT
School of Chemistry, Georgia Institute of Technology, Atlanta, Georgia
(Received June 14, 1954)

A STUDY of the polarized ultraviolet absorption spectra of single crystals of sodium nitrite at liquid nitrogen temperature has yielded the following information:

1. The absorption band with maximum around 3500A appears to have an origin at 3851.4A and is polarized in the *a* direction of the crystal, i.e., perpendicular to the plane of the nitrite ion.[1] This absorption is believed to be due to a transition in which one of the unshared electrons on the nitrogen atom is raised to an antibonding π orbital of the ion ($n_N\rightarrow\pi^*$). This assignment is consistent with the fact that this band is absent in the nitroalkyls, nitryl chloride, and the nitrate ion where the corresponding electrons on the nitrogen are shared with other atoms and hence stabilized. We have also found the band to be absent in crystalline silver nitrite where the crystal structure is similar, but the internuclear distances[2] and chemical properties suggest a weak electron-pair bond between the silver ion and the nitrogen of the nitrite ion. However, absorption in this region is present in nitrous acid and the alkyl nitrites both in solution and in the gas.

2. On the basis of some incomplete measurements, the 2050A band appears to be polarized in the *c* direction, i.e., in the plane of the ion and perpendicular to the C_2 axis of the ion. It is assigned as a $\pi\rightarrow\pi^*$ transition and is comparable to the strong bands in the nitrate ion, NO_2, NO_2Cl, the nitroalkyls, and alkyl nitrites at approximately the same place in the spectrum.

3. The absorption band that is found about 3100A in the nitrate ion, NO_3Cl, nitric acid, and the nitroalkyls and which McConnell[3] believes to be an $n\rightarrow\pi^*$ transition appears in the alkaline nitrite ion solution also at about 3000A. In the crystal at liquid nitrogen temperature we find a weaker absorption in this region polarized in the *a* direction which at room temperature gives the effect of broadening the 3600A band. We ascribe this band to a transition in which one of the nonbonding oxygen electrons jumps to the antibonding π orbital of the ion, i.e., $n_0\rightarrow\pi^*$. This assignment is based on the difference in valence state ionization potentials[4] of oxygen and nitrogen which suggests a displacement of the order of one electron volt (or about 800A) to the blue from the $n_N\rightarrow\pi^*$ band. Such a calculation is only a crude estimate at best, but the direction and order of magnitude suggested seem significant. In addition an appreciable difference is found between neutral and acidified solutions of ethyl nitrite in water-ethanol mixtures in the vicinity of 3100–3400A where certain maxima in neutral solutions are greatly weakened in acidic solutions. Maxima above 3400A which are attributed to the $n_N\rightarrow\pi^*$ transitions are not as strongly affected by such a change in acidity.

A more detailed report of this study and its significance in the interpretation of the electronic spectra of other triatomic molecules will be presented in the near future.

[1] G. E. Ziegler, Phys. Rev. **38**, 1040 (1931); Gene B. Carpenter, Acta Cryst. **5**, 132 (1952); Mary R. Truter, Acta Cryst. **7**, 73 (1954).
[2] J. A. A. Ketelaar, Z. Krist. **95**, 383 (1936).
[3] Harden McConnell, J. Chem. Phys. **20**, 700 (1952).
[4] R. S. Mulliken, J. Chem. Phys. **2**, 792 (1934).

On the Stability of Metallo-Organic Compounds. II

H. H. JAFFÉ
Venereal Disease Experimental Laboratory, U. S. Public Health Service, School of Public Health, University of North Carolina, Chapel Hill, North Carolina
(Received May 24, 1954)

A ROUGH estimation of the major terms contributing to metal-carbon bond energies has recently been reported.[1] The calculations were made only for elements of the second and third periods, and only for bonds between metals and alkyl radicals. The calculations are now being refined, and extended to metals of other periods and to carbon atoms in other types of organic radicals. Some preliminary results of considerable interest which arose early in this work will be reported in this communication.

Calculation of the relevant overlap integrals (*OI*'s) showed that the bond energies generally decrease with increasing atomic weight within any group in the periodic system. This observation is in agreement with empirical evidence.[2] The appreciable difference in covalent bond energy (i.e., in the X_{ij} terms[1]) between transition metals and other elements persists in the fourth period. This observation agrees with the fact that the preparation of alkyl-derivatives of the transition metals of the higher periods has met with little more success than the preparation of alkyls of the transition metals of the third period.

In comparing carbon-metal bond energies involving different organic radicals, a number of factors need consideration. For this comparison it is important to realize that the quantity estimated is the *mean dissociation energy* of all the carbon metal bonds in a compound. The nature of the organic radical will affect this quantity through (1) the state of hybridization of the carbon atom, (2) the π-electron resonance energy, and (3) the rearrangement energy of the organic radical.

The effect of the state of hybridization of the carbon atom is most readily accessible to estimation, and can be divided into three factors: the effect of (*a*) the *OI*'s, (*b*) the ionization potential of the carbon atom, and (*c*) the ionic resonance energy. Calcula-

tions show that increasing s character [from $C(sp^3)$ to $C(sp)$] invariably increases the OI's. This effect is most pronounced in the elements of groups IA and IB of the periodic system, and decreases with increasing group number. The electronegativity of carbon atoms increases with the amount of s character, and so does the valence state ionization potential.[3] In going from aliphatic to unsaturated carbon atoms, the latter factor increases the X_{ij} terms, while the former raises the ionic resonance energy for all elements which are less electronegative than carbon.

All the elements under consideration, with the possible exception of the group IVB elements, possess either vacant, or singly or doubly occupied low-lying $p\pi$ or $d\pi$ orbitals. Hence, resonance of the type $Me-C=C \leftrightarrow {}^{+}Me=C-C^{-}$ must make some contribution to the ground state of compounds involving unsaturated radicals, and hence to the bond dissociation energies discussed here. The quantitative evaluation of this effect, even to the crudest approximation, depends on a rough knowledge of certain Coulomb and resonance integrals, the estimation of which is now under investigation.

The most difficult problem is that of evaluation of rearrangement energies of the organic radicals. It appears clear that this quantity is smallest for the phenyl radical, where little geometric rearrangement is possible; the values for the vinyl, ethynyl, and alkyl radicals should be larger, but their estimation poses a major difficulty.

Thus it is seen that all the quantities considered combine to make aromatic metallo-organic compounds more stable than their aliphatic analogs. With the possible exception of the rearrangement energies, all the factors discussed also make unsaturated (vinyl and ethynyl) derivatives of metals more stable than their aliphatic analogs. These findings are in agreement with general experimental observations.

The most striking differences in stability of the metallo-organic compounds of a single metal are encountered in the derivatives of copper and silver (e.g., copper alkyls decompose $<-40°$, copper phenyl $\sim 80°$, and copper acetylide explodes $\sim 120°$). It appears significant that the OI's calculated for carbon atoms in different states of hybridization vary most strongly for these elements.

Many refinements and better quantitative treatments of the concepts discussed here require certain parameters closely connected with valence state energies. A detailed report will be postponed until work on the parameters is complete.

[1] H. H. Jaffé and G. O. Doak, J. Chem. Phys. 21, 196, 1118 (1953).
[2] N. V. Sidgwick, *The Chemical Elements and their Compounds* (Clarenden Press, Oxford, 1950), Vol. I, pp. 298–301.
[3] R. S. Mulliken, J. Phys. Chem. 56, 295 (1952).

Kinetics of Oxidation of Ammonia by Nitric Oxide*

HENRY WISE AND MAURICE F. FRECH
Jet Propulsion Laboratory, California Institute of Technology, Pasadena, California
(Received May 17, 1954)

ALTHOUGH all the known gaseous reactions of third order involve nitric oxide as one of the reacting molecules,[1] those chemical transformations in which the bond between the nitrogen and oxygen atoms is broken have indicated more complicated reaction kinetics.[2–4] The reaction between NH_3 and NO is of special interest since each reactant exhibits a high degree of thermal stability in the absence of catalytic surfaces.

The experimental measurements to be described were carried out in a static system composed of a quartz reaction vessel (volume =1560 ml, surface-to-volume-ratio=1.12 cm^{-1}) contained in a furnace whose temperature could be accurately controlled.[5] The desired partial pressure of each reactant was introduced into the heated reactor where the mixture was allowed to react for a specified time interval. The progress of the reaction was determined indirectly by observing the change in the total pressure of the system on a differential manometer filled with "Fluorolube S."† The solubility of ammonia in the manometric fluid is small and saturation of the surface layer of the liquid quickly occurs. Nitric oxide on the other hand shows a much greater tendency to dissolve in the "Fluorolube S." However, at the beginning of each experiment by first introducing ammonia into the reactor and subsequently the nitric oxide, the manometer fluid was protected from interaction with NO by the "buffer" of ammonia present in both limbs of the differential manometer. By means of such procedure reproducible rate measurements were obtained. In order to prevent condensation of water vapor, the capillary tubing connecting the manometer and the reaction vessel was heated electrically to 120°C.

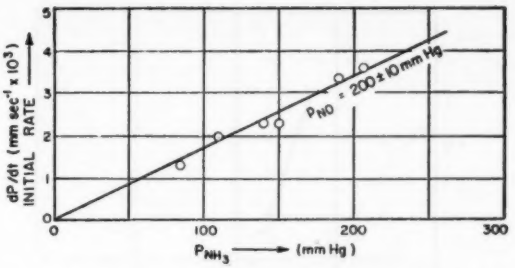

FIG. 1. Initial rate of pressure change as a function of ammonia concentration at 9940 K.

Anhydrous ammonia‡ (purity 99.9 percent) and purified[6] nitric oxide‡ (purity 99.9 percent) were used in these measurements.

The experimental measurements of the rate of reaction were carried out in a temperature range from 990°K to 1150°K. The order of the reaction with respect to each of the reactants was evaluated by the differential method of Van't Hoff.[7] As shown by the data in Fig. 1, the initial rate of pressure change is proportional to the first power of ammonia. However, the kinetics vary linearly with the square root of the partial pressure of nitric oxide (Fig. 2). The specific reaction rate constants calculated from the resulting rate equation $dP/dt = k \cdot p_{NH_3} \cdot p_{NO}^{\frac{1}{2}}$ are summarized in Fig. 3. Graphical analysis yields the following rate expression for the reaction between ammonia and nitric oxide:

$$k = 1.1 \times 10^{11} e^{-54\,700/RT} \text{ mm}^{-\frac{1}{2}} \text{ sec}^{-1}.$$

The experimental results do not lend themselves to a detailed analysis of the mechanism of reaction. Qualitatively the kinetics

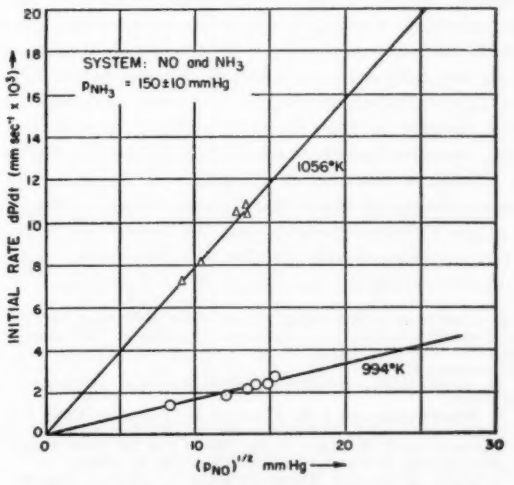

FIG. 2. Initial rate of pressure change as a function of nitric oxide concentration.

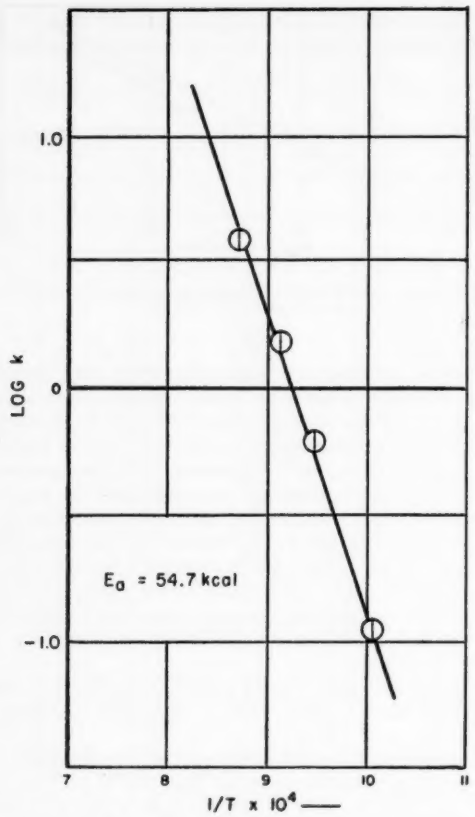

FIG. 3. Variation of specific reaction rate constant with temperature.

of this chemical transformation exhibit certain similarities with that observed in the interaction of ammonia and oxygen. In both systems the formation of hydrogen as an intermediate has been reported when the initial concentration of oxidizer is small.[8,9] The spectroscopic observation of strong NH bands emitted by ammonia flames burning with O_2 and NO, respectively,[10,11] further suggests that dehydrogenation of the ammonia molecule is inherent to the mechanism of oxidation. The source of the NH radicals may be sought in the reaction $NH_3+O\rightarrow NH+H_2O$ proposed in the mechanism of catalytic oxidation of ammonia.[12] Since in the temperature region of the experimental measurements the thermal decomposition of NO is predominantly a heterogeneous process[5] of relatively low activation energy, the degradation of the NO molecule may produce the oxygen atom necessary for such an initiating step. In marked contrast to the NH_3-O_2 flames, the combustion of ammonia with nitric oxide shows a very striking decrease in the intensity of NH_2-band emission.[10,13] It appears, therefore, that the reaction $NH_2+NO\rightarrow N_2+H_2O$ is very rapid relative to the rate of formation of the imine radical.[8] This fact also suggests that in this reacting system the dehydrogenation of the ammonia molecule does not proceed via $NH_3\rightarrow NH_2\rightarrow NH$ as postulated for the reaction of NH_3 with O_2,[11] but rather that the NH radical is a precursor to the NH_2 radical.

* This paper presents the results of one phase of research carried out at the Jet Propulsion Laboratory, California Institute of Technology, under Contract No. DA-04-495-Ord 18, sponsored by the Department of the Army, Ordnance Corps.

[1] C. N. Hinshelwood, *Kinetics of Chemical Change* (Clarendon Press, Oxford, 1940).
[2] C. N. Hinshelwood and J. W. Mitchell, J. Chem. Soc. **1936**, 378.
[3] C. P. Fenimore and J. R. Kelso, J. Am. Chem. Soc. **74**, 1593 (1952).
[4] F. Kaufman and J. R. Kelso, J. Am. Chem. Soc. **74**, 2694 (1952).
[5] H. Wise and M. F. Frech, J. Chem. Phys. **20**, 22 (1952).
† A product of Hooker Electrochemical Company, Niagara Falls, New York.
‡ Obtained from the Matheson Company, Joliet, Illinois.
[6] Johnston and Giauque, J. Am. Chem. Soc. **51**, 3194 (1928).
[7] J. H. Van't Hoff *Etudes de dynamique chimique* (R. Muller and Company, Amsterdam, 1884), p. 87.
[8] C. H. Bamford, Trans. Faraday Soc., **35**, 568 (1939).
[9] H. Wise and M. F. Frech, J. Chem. Phys. **21**, 948 (1953).
[10] B. B. Fogarty and H. G. Wolfhard, Nature **168**, 1122 (1951).
[11] H. G. Wolfhard and W. G. Parker, Proc. Phys. Soc. **62**, 722 (1949).
[12] M. Bodenstein, Z. Elektrochem. **41**, 466 (1935).
[13] M. Farber and A. J. Darnell, J. Chem. Phys. (to be published).

Ground and Excited Electronic States of Phosgene

JULES DUCHESNE
Institut d'Astrophysique, University of Liège, Cointe-Sclessin, Belgium
(Received May 18, 1954)

THE purpose of this note is to study the vibration potential functions of the ground and first excited states of $COCl_2$ with a view to getting information about their structure. The method followed is the same as that already used by the author in the similar case of $CSCl_2$.[1] We shall first consider the ground state of C_{2v} symmetry, the planar fundamental vibrations and molecular dimensions of which are as follows:[2]

$$a_1\begin{cases}\nu_1=1827\ \text{cm}^{-1}\\ \nu_2=575\ \text{cm}^{-1}\\ \nu_3=297\ \text{cm}^{-1},\end{cases}\qquad b_2\begin{cases}\nu_4=849\ \text{cm}^{-1}\\ \nu_5=240\ \text{cm}^{-1}.\end{cases}$$

$l_1(\text{CO})=1.166\text{A};\quad l_{2,3}(\text{CCl})=1.746\text{A};\quad \theta(\text{ClCCl})=111.3°.$

The most general form of potential energy function is[1]

$$2U=f_1\Delta l_1^2+f_2\sum_2^3\Delta l_i^2+f_\theta l_2^2\Delta\theta^2+f_\phi l_2^2\Delta\phi^2$$
$$+2f\Delta l_2\Delta l_3+2\gamma_c l_2\Delta l_1\Delta\theta+2f_c\sum_2^3\Delta l_1\Delta_i$$
$$+2g_c' l_2\sum_2^3\Delta l_i\Delta\phi+2g_c'' l_2\sum_2^3\Delta l_i\Delta\theta,$$

where ϕ is the ClCO bond angle at the equilibrium position. If we make the reasonable assumption that f_c is positive, whereas γ_c and g_1 are negative, and that $|\gamma_c|$ cannot be smaller than 0.12, then the most likely values deduced for the force constants, expressed in 10^5 dynes/cm units, are

$$a_1\begin{cases}f_1=14\\ f_2'(\equiv f_2+f)=4.074\\ \Gamma(\equiv 2f+f_\phi/2)=0.95,\end{cases}\qquad a_1\begin{cases}f_c=0.946\\ \gamma_c=-0.139\\ g_1(\equiv 2g_c'-4g_c'')=-1,\end{cases}$$

$$b_2\begin{cases}f_2''(\equiv f_2-f)=3.793\\ f_\phi=0.169,\end{cases}\qquad b_2\,|\,g_2(\equiv 2g_c')=0.6.$$

The values obtained for the CO valency bond f_1 and the internuclear distance, instead of being the same as for COH_2, where 12.3×10^5 dynes/cm^3 and 1.21A,[4] respectively, were found, are more closely related to those of CO_2, for which $f_1=15.5$[3] and $l_1(\text{CO})=1.158\text{A}$.[5] From Coulson's general formulas[6] giving the hybridization ratios of three plane hybrids at the carbon atom, it is deduced that, for $\theta=111.3°$, the σ bond in CO must be almost of the diagonal sp type as in CO_2. This is presumably on account of the strong electrostatic repulsions between the electrons in the lone-orbital of the oxygen atom and those in the CCl bond orbitals. However these bonds, which would therefore be expected to be of the sp^3 type, are shorter than the corresponding internuclear distance (1.781A) in CH_3Cl.[7] This contraction might be explained on assuming a rather considerable π bonding in the CCl bonds and this will be shown to be the case.

Let us now turn our attention to the first electronic upper level* which is known to result from an $n\rightarrow\pi^*$ excitation. The corresponding transition $A_1\rightarrow A_2^*$ lies in the ultraviolet region between 3050 and 2380A, the analysis of which has revealed two totally symmetrical vibrations,[8] i.e., $\nu_2^*=422\ \text{cm}^{-1}$ and $\nu_3^*=254\ \text{cm}^{-1}$. In order to be able to calculate the potential function of the excited

state, the C_{2v} symmetry has been kept, by analogy with what was proved for thiophosgene.[1] Furthermore, values of 1400 cm^{-1} and 125° were respectively adopted for ν_1^* and θ^*. An increase of about 14° for the ClCCl angle is not only suggested by the similar behavior of thiophosgene,[1] but is also supported by the long progressions, involving the ClCCl bending vibration, which appear in the band system with a maximum of intensity at the fourth band.[8] Then, assuming $f_c^*=0.6$, $\gamma_c^*=-0.1$, $g_1^*=-0.6$, according to a rule formulated earlier,[1] the values deduced for the valency force constants are

$$f_1^*=8.25;\quad f_2'^*=2.54;\quad \Gamma^*=0.60.$$

The CO and CCl bond distances of the upper state which may be derived from Badger's relation[9] are 1.26 and 1.86A, respectively. Any reasonable change in the value of ν_1^* would not modify significantly these results. As a matter of fact, the considerable decrease of the CO bond strength measures the antibonding power of the π^* electron. On the other hand, contrary to what occurs for $CSCl_2$, $f_2'^*$ is lowered as much as f_1^* and Γ^*. This shows that the π^* orbital in $COCl_2$ is strongly delocalized and that, in the ground state, the CO and CCl bonds are conjugated to a large extent. Thus, the contraction of the CCl bonds already discussed is now explained. The relative smallness of Γ^* confirms the important part played by the lone-pair electrons in the determination of the bond angles.[1]

Acknowledgment is made to Mr. I. Ottelet for help in the computational part of this work.

[1] J. Duchesne, J. Chem. Phys. **21**, 548 (1953); Bull. acad. roy. sci. Belg. **39**, 697 (1953); J. phys. radium **15**, 211, 1954; J. Duchesne and L. Burnelle, J. Chem. Phys. **21**, 2005 (1953).
[2] Nielsen, Burke, Woltz, and Jones, J. Chem. Phys. **20**, 596 (1952); G. W. Robinson, ibid. **21**, 1741 (1953).
[3] J. W. Linnett, Quart. Rev. Chem. Soc. **1**, 73 (1947).
[4] R. B. Lawrance and M. W. P. Strandberg, Phys. Rev. **83**, 363 (1951).
[5] D. M. Dennison, Revs. Mod. Phys. **12**, 175 (1940).
[6] C. A. Coulson, *V. Henri Mem. Vol.* (Desoer, Liège, 1947), p. 15.
[7] Dailey, Mays, and Townes, Phys. Rev. **76**, 136 (1949).
[8] In order to avoid confusion all the symbols concerned with the excited state are marked with an asterisk as suggested before (see reference 1).
[9] V. Henri and O. R. Howell, Proc. Roy. Soc. (London) **A128**, 178 (1930).
[9] R. M. Badger, J. Chem. Phys. **3**, 710 (1935).

Microwave Absorption in the Mixture (Phenyl Isothiocyanate + Diethylamine)

P. K. KADABA
Department of Physics, Michigan State College, East Lansing, Michigan
(Received June 4, 1954)

THE investigation on the dielectric relaxation of pure polar liquids as, for example, in the homologous series of straight chain alkylbromides[1] has led to the close parallelism of the relaxation process and that of viscous flow. It was interesting to investigate the extent of such similarity in certain dipolar mixtures which are conspicuous for their abnormal viscosity as the concentration of one of the components is varied continuously. A typical example is provided by the irreversible binary system (phenyl isothiocyanate+diethylamine) which has a very sharp maximum in the curve relating viscosity to concentration.[2] The maximum occurs for equimolecular proportions of the two components and is invariant with respect to temperature. The maximum is about 26 000 times greater than that calculated by the additive law of viscosity.[2] The fact that the mixing of the two liquids is accompanied by such a large evolution of heat and contraction of volume and that the mixture shows such marked deviation of viscosity from the additive law of mixtures, leads to the conclusion that a new compound is formed at all concentrations, and at the mole fraction of 0.5 corresponding to the maximum in the viscosity *vs* concentration curve, the two components are completely dissociated and the new compound which has the structure of a substituted thiourea is formed. The formation of such molecular complexes could be the result of the dipolar association and hydrogen bonding between the two species of molecules.

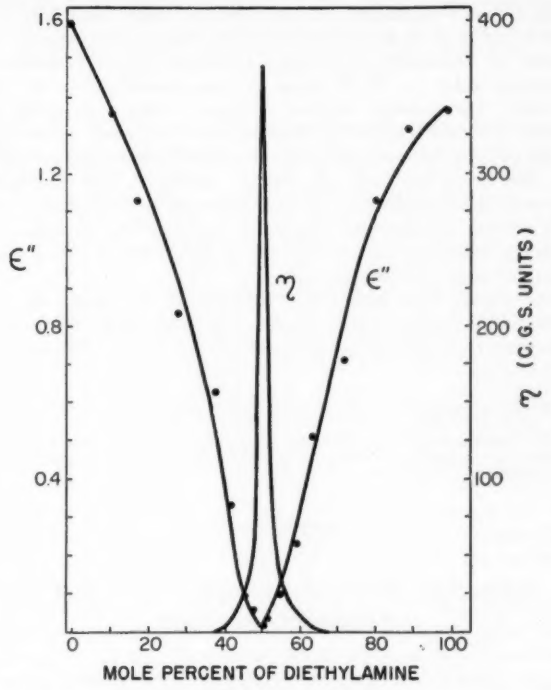

FIG. 1. Variation of dielectric loss (ϵ'') and viscosity (η) with concentration. (The data for viscosity is taken from reference 2.)

The loss factor ϵ'' of the microwave dielectric constant of the above mixture was measured at a single frequency of 14 200 Mc, and at a constant temperature of (25.1±0.05)°C over the concentration range 0 to 100 mole percent of diethylamine. Over the concentration range 0 to 40 percent and 60 to 100 percent of diethylamine a cross guide directional coupler was used to measure the reflection coefficient and hence the loss factor. Between the range 40 to 60 percent the high viscosity and the low loss of the mixture precluded the use of a movable plunger as well as the directional coupler, and the loss was computed by substituting a standing wave detector for the directional coupler. A plot of ϵ'' *vs* concentration (Fig. 1) has a minimum at the concentration of 50 mole percent but the rise of the curve on either side is not so steep as one would expect by assuming the close parallelism between the relaxation time τ and the viscosity η. The similarity between τ and η can be estimated in a qualitative way by computing the constant $(\tau/\eta=c)$ or better $c^{\frac{1}{3}}$ at the various concentrations

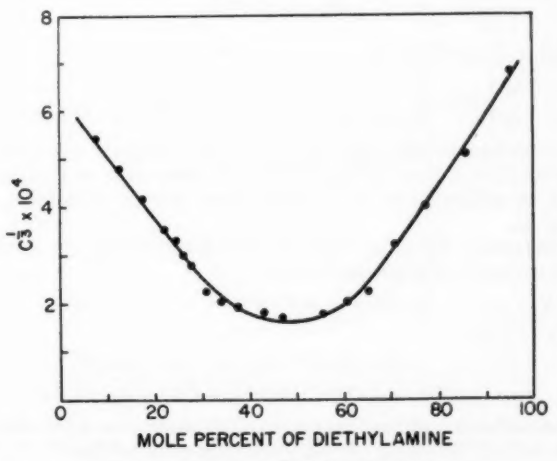

FIG. 2. Variation of $c^{\frac{1}{3}}$ with concentration.

using Debye's expression for the dielectric loss.[3] Such a plot is shown in Fig. 2. It is interesting to note that c^1 decreases as the degree of molecular complexity increases and approaches a minimum value at the 50 mole percent concentration. On the contrary, the familiar relation between τ and η as given by Debye,[3] *viz.* ($\tau=4\pi\eta a^3/kT$), would lead one to expect an increase in the value of the constant c^1 as the degree of molecular complexity, and hence the molecular radius, increases. The conclusion that one can possibly draw from the present investigation is the lack of any appropriate similarity between the processes of dielectric relaxation and viscous flow in liquid mixtures of a great degree of molecular complexity.

The author is indebted to Professor R. D. Spence for his guidance during the course of this work. The author also wishes to express his gratitude for the award of the Alumni Postdoctoral Fellowship.

[1] See for example the paper by C. P. Smyth and others in J. Am. Chem. Soc. **70**, 4102 (1948).
[2] N. Kurnakov and S. Zemchuzny, Z. physik. Chem. **83**, 481 (1913).
[3] See, for example, P. Debye, *Polar Molecules* (The Chemical Catalog Company, Inc., New York).

Ellipsoidal Molecular Shape and Dielectric Relaxation Analysis

J. Ph. Poley
Physical Laboratory, National Defense Research Council, The Hague, The Netherlands
(Received May 20, 1954)

THE main quantities governing the relaxation of simple polar molecules are the molecular relaxation time τ, the molecular shape, and the actual internal field. As was shown by Bolton[1] an analysis of dielectric data according to Onsager's field assumption[2] leads to a relaxation curve differing markedly from a semicircle, to be expected on basis of a Debye analysis,[3] following Cole and Cole.[4]

The Onsager model, however, assumed the molecule under consideration to be spherical.

The author investigated the influence of ellipsoidal molecular shape on the relaxation curve.

For ellipsoidal molecules (semiaxes a, b, and c), with dipole moment in the direction of the a axis, and depolarization factor A_a,[5] the general relation can be derived.[6]

$$\epsilon-1=4\pi N\cdot\frac{1}{3}\cdot\sum_a^c i\alpha_i\cdot E_{ri}+\frac{4\pi N}{3kT}\cdot\frac{E_{ra}}{1-\alpha_a f_a}\cdot\mu^2. \quad (1)$$

In (1) an approximation suggested by Scholte[6] can be inserted, writing

$$\frac{1}{3}\cdot\sum_a^c i\alpha_i\cdot E_{ri}=\alpha\cdot E_r. \quad (2)$$

This leads finally to the concise relation

$$\frac{4\pi N}{3kT}\cdot\mu^2=\frac{(2\epsilon+1)\cdot(\epsilon-\epsilon_\infty)\cdot\{\epsilon-(\epsilon-\epsilon_\infty)A_a\}^2}{(2\epsilon+\epsilon_\infty)\cdot\epsilon\cdot\{\epsilon-(\epsilon-1)A_a\}\cdot\{1+(\epsilon_\infty-1)A_a\}^2}. \quad (3)$$

Comparison of this new Eq. (3) with analogous relations of Abbott and Bolton[6] or Buckingham[7,8] shows that no preference can be attributed to one of them, using present data for ϵ, ϵ_∞, and A_a.

Extending (3) to the case of relaxation,[3] writing $\epsilon^*=\epsilon'-j\epsilon''$, the corresponding relation is found:

$$\frac{4\pi N}{3kT}\cdot\frac{\mu^2}{1+j\omega\tau}=\frac{(2\epsilon^*+1)\cdot(\epsilon^*-\epsilon_\infty)\cdot\{\epsilon^*-(\epsilon^*-\epsilon_\infty)A_a\}^2}{(2\epsilon^*+\epsilon_\infty)\cdot\epsilon^*\cdot\{\epsilon^*-(\epsilon^*-1)A_a\}\cdot\{1+(\epsilon_\infty-1)A_a\}^2}. \quad (4)$$

The author established the course of ϵ'' *versus* ϵ' as a function of $\omega\tau$ and A_a, by solving (4) using trial-and-error method.

The result is given in Fig. 1 for several values of A_a, with

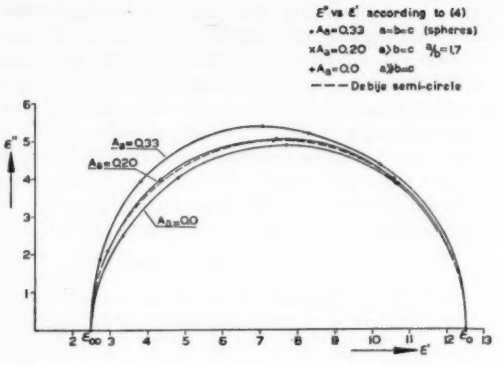

FIG. 1.

$\epsilon_0=12.5$ and $\epsilon_\infty=2.5$. The semicircle standing for a Debye analysis is inserted in dashed lines.

Since actual molecular shapes will often have values of A_a smaller than 0.20, our treatment shows that in practice a relaxation curve for a substance having one relaxation time will be hardly distinguishable from a Debye semicircle, owing to measuring inaccuracies.

As in practice a Debye semicircle analysis is applied to dielectric relaxation data,[4,9–11] without further comment or justification of the abandonment of the improvement obtained in dielectric theory by the introduction of the Onsager reaction field, the above discussion provides the theoretical justification of this proceeding.

A more extensive study of this subject, together with experimental verifications, will be published elsewhere.[12]

[1] H. C. Bolton, J. Chem. Phys. **16**, 486 (1948).
[2] L. Onsager, J. Am. Chem. Soc. **58**, 1486 (1936).
[3] P. Debye, *Polar Molecules* (Dover Publications, 1945), Chap. V.
[4] K. S. Cole and R. H. Cole, J. Chem. Phys. **9**, 341 (1941).
[5] Th. G. Scholte, thesis, Leyden, 1950; Physica, **15**, 437, 450 (1949).
[6] J. A. Abbott and H. C. Bolton, Trans. Faraday Soc. **48**, 422 (1952).
[7] A. D. Buckingham, Trans. Faraday Soc. **49**, 881 (1953).
[8] A. D. Buckingham, Australian J. Chem. **6**, 93 (1953).
[9] C. P. Smyth, J. Am. Chem. Soc. **70**, 4093, 4097, 4102 (1948).
[10] J. A. Saxton, *Meteorological Factors in Radio-Wave Propagation* (1946) 292.
[11] C. H. Collie, Proc. Phys. Soc. (London) **60**, 145 (1948).
[12] J. Ph. Poley, Appl. Sci. Research (to be published).

Continuous Radiation from the Rare Gases in the Vacuum Ultraviolet

Carl Kenty
Lamp Division, General Electric Company, Nela Park, Cleveland, Ohio
(Received June 14, 1954)

TANAKA and Zelikoff[1] have recently reported a continuum in the vacuum ultraviolet in Xe. Exciting Xe at 30-mm pressure with high frequency, they found the contiunum to extend from 1470 with diminishing intensity to about 2200 A.

The present experiments, done independently of the work of Tanaka and Zelikoff, show this continuum[2] in Xe and also reveal a strong continuum in Kr extending somewhat less far toward the red. Evidence was also obtained for corresponding continua in A and Ne, but much farther in the U.V.

A highly exhausted Nonex tube, Fig. 1(a), having a thin quartz window (thickness 3 mils) and filled with 60–120-mm Xe having impurities <1 in 10^7, is traversed by a diffuse discharge of 1–2 ma ac or dc filling the tube and having only a continuous visible spectrum and producing a blue fluorescence in the Nonex. A glass tube with Zn_2SiO_4: Mn phosphor on its end and through which a desired gas flows, extends into the side tube. With this "probe" at 5 mm from the window the phosphor brightness increases about 20-fold when laboratory air or O_2 is replaced by N_2. Absorption data[3] for O_2 places such radiation at about 1750 A.

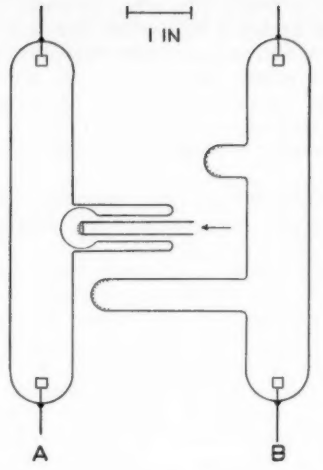

FIG. 1.

By varying the probe distance the observed absorption indicates a strong continuum of radiation extending considerably beyond 1750 in both directions.[4] The Zn_2SiO_4:Mn (and also the Nonex) fluorescence is relatively small at 10-mm pressure and absent at 1 mm. It is inferred that the continuum is absent at 1 mm and that Nonex does not fluoresce to Xe resonance lines.

Results for Kr are somewhat the same as for Xe. But the Zn_2SiO_4:Mn brightness is considerably less and decreases more sharply when N_2 is replaced by O_2. The Nonex also fluoresces less brightly. It is inferred that Kr has a continuum similar to Xe but further in the U.V. Its long wavelength limit is judged to extend to at least 1800 A. Following Tanaka and Zelikoff[1] for the case of Xe, this radiation in Kr is ascribed to transitions between Kr_2 molecules and the repulsive state of two normal atoms.

Colli and Facchini[5] have reported evidence for a vacuum ultraviolet continuum in A. In the present experiments, using A, no fluorescence of the phosphor or of the Nonex could be observed. To study A, Ne and He, tubes were constructed as in Fig. 1(b). Here, X is the thermoluminescent phosphor[6] $CaSO_4$:Mn, which responds to radiations shorter than 1300 A. The strength of the radiation exciting the $CaSO_4$:Mn was inferred from the discharge time necessary to produce substantial saturation. The thermoluminescence, obtained by subsequent heating to 180°C, was absent for Xe, rather weak for Kr, strong for A and Ne, and rather weak for He. Comparison of the strengths of the radiations reaching down the short and long side tubes indicated little if any absorption in the gas. It is inferred that continua exist in A somewhere between 1066 A and 1300 A, or beyond and in Ne between 746 and 1300 A or beyond.

If tubes are made of quartz, the walls fluoresce (and phosphoresce) a deep violet under the Xe continuum and much O_3 is produced. With Kr both effects are considerably weaker, and with A and Ne entirely absent. An Xe tube coated internally with Zn_2SiO_4:Mn had a luminous efficiency at 0.5 ma of 6 l.p.w.

As the current is increased in these tubes (any rare gas) the discharge suddenly constricts to a thread-like form characterized by the usual line spectrum and a considerably lower voltage. The behavior suggests that the diffuse form depends on ions produced from or through rare gas molecules; while the constricted form, ionized 10^3 or 10^4 times as high, operates by the usual 2-stage ionization of rare gas atoms.

[1] Yoshio Tanaka and Murray Zelikoff, J. Opt. Soc. Am. **44**, 254 (1954); Phys. Rev. **93**, 933 (1954).
[2] C. Kenty, Phys. Rev. **93**, 651 (1954).
[3] Wanatabe, Inn, and Zelikoff, J. Chem. Phys. **21**, 1026 (1953).
[4] J. R. Dacey and J. W. Hodgins, Can. J. Research **28**, 90 (1950); and M. H. J. Wijnen and H. A. Taylor, J. Chem. Phys. **21**, 233 (1953), report a small transmission of 1470 A through fused quartz 2 mils thick.
[5] L. Colli and U. Facchini, reported at the Washington Conference on Gaseous Electronics October 22–24, 1953.
[6] See, for example, K. Wanatabe, Phys. Rev. **83**, 785 (1951).

Lower Electronic States of the Free NH_2 Radical

JIRO HIGUCHI
Laboratory of Physical Chemistry, Tokyo Institute of Technology, Ookayama, Meguro-ku, Tokyo, Japan
(Received June 11, 1954)

RECENTLY the so-called α bands of ammonia, long known from emission spectra of oxy-ammonia flame and electric discharges, were shown to be due to the free NH_2 radical by Herzberg and Ramsay using a flash photolysis of ammonia.[1] Little has, however, been done on its theoretical interpretation. The electronic states and the structures of the free NH_2 radical are, therefore, investigated here. The method used is the LCAO SCF one developed by Roothaan[2] and the details are similar to those in the case of the CH radical,[3] which has recently been reported, except in the following points: the atomic integrals are obtained from the Hartree-Fock SCF AOs in the ^4S state of the nitrogen atom;[4] the many-center integrals are approximately obtained from the Slater AOs in which the $\delta(2s$ and $2p)$ and $\delta'(1s)$ for the nitrogen are taken as 1.90 and 6.757, respectively; the one-electron three-center integrals are calculated by following Oohata's method,[5] while the two-electron ones by modifying Mulliken's approximation.[6] The spatial configuration of the radical is assumed as an isosceles triangle, and the internuclear distance between the nitrogen and the hydrogen is taken as 1.01A as in the ammonia molecule.[7]

The LCAO SCF calculation is carried out for the ground state ($^2B_1$) only. By using the LCAO SCF MOs so obtained the lower electronic states are calculated without configuration interaction, and are shown in Fig. 1 (according to Mulliken's choice of axes). The electronic configurations of these states are as follows:

$$^2B_1 \quad K(1a_1)^2(1b_2)^2(2a_1)^2(1b_1)^1$$
$$^2A_1 \quad K(1a_1)^2(1b_2)^2(2a_1)^1(1b_1)^2$$
$$^4A_2 \quad K(1a_1)^2(1b_2)^2(2a_1)^1(1b_1)^1(2b_2)^1$$
$$^2B_2 \quad K(1a_1)^2(1b_2)^1(2a_1)^2(1b_1)^2.$$

The equilibrium valence angles of the $^2B_1$ and the $^2A_1$ state

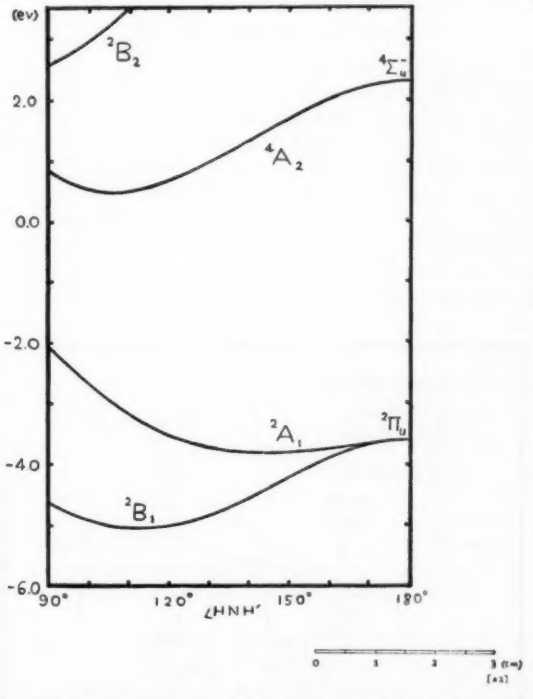

FIG. 1. The lower electronic states of the free NH_2 radical (without configuration interaction). The origin of energy is chosen to be $N(^4S)+2H(^2S)$.

obtained are very close to Luft's estimation (110° and 135–160°, respectively).[8] It is of interest to see that the tetrahedral structure of valence angle is almost preserved in the ground state of the radical as in the ammonia molecule. The calculated value of a $^2B_1 \rightarrow {}^2A_1$ transition (1.8 ev) is in fairly good agreement with the experimental data, in which the observed absorption spectrum is in the region of 4500–7400A.[1] The $^2B_2$ state is, however, calculated to locate higher than in Mulliken's prediction.[1] This is mainly due to the facts that the present calculation ignores configuration interaction and that the variational procedure is carried out for the $^2B_1$ state only. Especially, the second $^2B_2$ state $K(1a_1)^2(1b_2)^2(2a_1)^2(2b_2)^1$ is very close to the lowest $^2B_2$ state, and then the effect of configuration interaction may be probably large. The experimental results will be explained more clearly if configuration interaction is included.

The complete details of the calculation will be published later.

The author wishes to thank Dr. S. Shida and Dr. K. Niira for their helpful discussions and suggestions. He also expresses his thanks to Mr. K. Oohata and Mr. S. Maeda for their kind discussions and permission to use the unpublished data on the auxiliary function of the three-center integrals.

[1] G. Herzberg and D. A. Ramsay, Discussions Faraday Soc., No. 14, 11 (1952).
[2] C. C. J. Roothaan, Revs. Modern Phys. **23**, 69 (1951).
[3] J. Higuchi, J. Chem. Phys. (to be published).
[4] D. R. Hartree and W. Hartree, Proc. Roy. Soc. (London) **A193**, 299 (1948).
[5] K. Oohata, Busseiron Kenkyu **50**, 38 (1952).
[6] R. S. Mulliken, J. chim. phys. **46**, 500 and 521 (1949).
[7] H. Sponer, *Molekülspektren I. Tabellen* (Verlag Julius Springer, Berlin, 1935), p. 80.
[8] N. W. Luft, Discussions Faraday Soc. No. **14**, 114 (1952).

An Infrared Study of the BF_3-BCl_3 Reaction*

R. E. Nightingale and Bryce Crawford, Jr.
School of Chemistry, University of Minnesota, Minneapolis 14, Minnesota
(Received June 18, 1954)

A PRELIMINARY kinetic study has been made of the gas-phase reaction,

$$BF_3+BCl_3 \rightarrow BFCl_2+BF_2Cl.$$

A fast-scanning infrared spectrometer[1] was used to follow the changes in intensity of the appropriate absorption bands.

The reaction was carried out in apparatus similar to that used in previous studies of rapid gas-phase reactions.[2] An 11.4-cm absorption cell with rocksalt windows was employed. The reacting gases were admitted to the evacuated cell from storage bulbs through jet tips insuring rapid mixing of the reacting gases.

Matheson BF_3 was used without purification except that a quantity of the gas was condensed and redistilled into a storage bulb, the middle third of the distillate being taken. The BF_3 was pressurized with dry nitrogen. The other jet storage bulb was filled with Matheson Technical BCl_3 which had been redistilled in the same way as the BF_3 and was pressurized to the same total pressure. Halocarbon grease was used on the stopcocks and ground joints of the vacuum system since Apiezon stopcock grease was rapidly attacked by these gases. Pressures were read with a mercury manometer without any noticeable attack of the mercury.

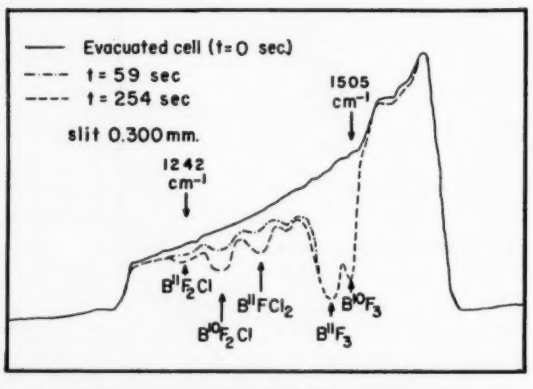

FIG. 1. Infrared spectra of the BF_3-BCl_3 reaction.

With the spectrometer running, the stopcocks leading to the absorption cell were opened simultaneously and absorption bands of BF_3, $BFCl_2$, and BF_2Cl were recorded. Figure 1 shows the results of a typical experiment in which the spectral region was scanned about 3 times a second. In this case the initial pressure of BF_3 and BCl_3 was 6.6 mm Hg and the total pressure was 342 mm Hg at 23°C.

This reaction does not go to completion and so the back reaction would have to be considered in a detailed kinetic study. However, from the data early in the reaction the half-life for the forward rate is estimated to be on the order of 10 minutes. This would call for a second-order rate constant of about 5×10^3 cc $(\text{mole})^{-1}$ $(\text{sec})^{-1}$. Garvin and Kistiakowsky[3] have studied the reaction of BF_3 with tri-, di-, and monomethyl amine and found these reactions to be extremely rapid. In this reaction a complex $R_3N{:}BF_3$ is formed with a very small energy of activation. One might expect the BF_3-BCl_3 reaction to be very rapid if it goes through a bridged intermediate similar to B_2H_6 or Al_2Cl_6. In view of the rather slow rate this does not seem to be the case; at least, the reaction must involve a significant activation energy.

We would like to thank Professor R. A. Ogg, Jr., of Stanford University for calling this interesting reaction to our attention. We are also very grateful to Professor M. K. Wilson of Harvard University for supplying us with spectra of the molecules, BF_3, BCl_3, $BFCl_2$, and BF_2Cl and their vibrational assignments.

* This work was supported by the U. S. Navy, Bureau of Ordnance through contract with the University of Minnesota.
[1] Wheatley, Vincent, Rotenberg, and Cowan, J. Opt. Soc. Am. **41**, 665 (1951).
[2] Cowan, Vincent, and Crawford, J. Opt. Soc. Am. **43**, 710 (1953); Nightingale, Cowan, and Crawford, J. Chem. Phys. **21**, 1398 (1953).
[3] D. Garvin and G. B. Kistiakowsky, J. Chem. Phys. **20**, 105 (1952).

Selection Rules and Frequencies of the Skeletal Vibrations of Long Chain Polymers in the Crystalline State

C. Y. Liang, G. B. B. M. Sutherland, and S. Krimm
The Harrison M. Randall Laboratory of Physics, University of Michigan, Ann Arbor, Michigan
(Received June 14, 1954)

IN the interpretation of the infrared spectra of long chain polymers attention has hitherto been concentrated almost exclusively on the identification of nonskeletal frequencies, such as those characteristic of CH, OH, NH, and carbon-halogen groups, and the majority of the bands occurring below 1300 cm^{-1} are either unassigned or vaguely referred to as skeletal vibrations. In the course of a systematic study of the spectra of a variety of polymers between 2.5μ and 100μ we have found that the following method of dealing with the skeletal frequencies offers considerable promise.

The skeletal frequencies of long chain paraffins have been discussed by Kirkwood,[1] Pitzer,[2] Mizushima and Simanouti,[3] and others.[4–6] Kirkwood and Pitzer used a modification of the Born-Karman treatment[7] of a one-dimensional lattice and arrived at equations of the form

$$\nu_{\pm}^2(k_1,k_2,\lambda)=0 \text{ (for in plane frequencies)} \quad (1)$$

and

$$\nu^2(k_3,\lambda)=0 \text{ (for out of plane frequencies)}, \quad (2)$$

where λ is the phase difference between successive carbon atoms in the chain, which is assumed to be a planar zig-zag, and the

k's are force constants. We have found this method very useful although we would suggest that the possible values of λ should be governed by the equation

$$\lambda=\pi 1/(N-1) \quad \text{with} \quad 1=0, 1, 2\cdots N-1, \tag{3}$$

instead of

$$\lambda=\pi 1/N \quad \text{with} \quad 1=1, 2\cdots N-1, \tag{4}$$

where N is the total number of atoms in the finite chain.

However, out of all of these $3N$ skeletal frequencies (which include the translation and rotation of the molecule as a whole), only a very small number can give rise to infrared absorption if the molecule is in the crystalline state. The fundamentals which can be strong in absorption are only those in which corresponding atoms in each unit cell move in phase. For a finite chain, the intensity of those vibrations in which unit cells do not move in phase can be shown to be very much weaker; for an infinite chain they will have zero intensity. Thus, if there are p atoms of a single chain within the unit cell then, according to the above criterion, only those modes for which

$$\lambda=2\pi r/p \text{ (where } r=0, 1, \cdots p-1) \tag{5}$$

can be potentially active in absorption. Whether even those will be active depends on the change of dipole moment associated with them. This gives a maximum of $3p$ potentially active skeletal vibrations, of which 4 are of zero frequency and correspond to 3 translational motions and the rotational motion of the molecule about the chain axis. The computation of these $3p-4$ fundamentals from Eqs. (1) and (2) is a relatively simple matter and the vibration patterns can also be derived so that the dichroism can be predicted.

For instance in polyethylene, where x-ray investigations indicate that $p=2$, there should therefore be two potentially active fundamentals. Taking $\lambda=0$ and $\lambda=\pi$ [the possible values from Eq. (5)], we calculate the respective frequencies of these potentially active fundamentals as $\nu_+(0)=1070$ cm^{-1} and $\nu_+(\pi)=1137$ cm^{-1}. The vibration patterns of these and the other four zero frequencies are shown in Fig. 1. Thus, the higher frequency should exhibit parallel dichroism with respect to the chain direction while the opposite should be true for the lower frequency. It should be noted that interactions between neighboring chains are neglected in this case.

For, $p=4$, six new frequencies are possible, corresponding to the additional values of λ, *viz.*, $\pi/2$ and $3\pi/2$. Their vibration patterns are also given in Fig. 1. It will be observed that they really consist of 3 doubly degenerate vibrations, which are computed to be $\nu_+(\pi/2)=\nu_+(3\pi/2)=980$ cm^{-1}, $\nu_-(\pi/2)=\nu_-(3\pi/2)=438$ cm^{-1}, and $\nu(\pi/2)=\nu(3\pi/2)=198$ cm^{-1}. Bands are observed near these positions for many vinyl polymers such as polyvinyl chloride.

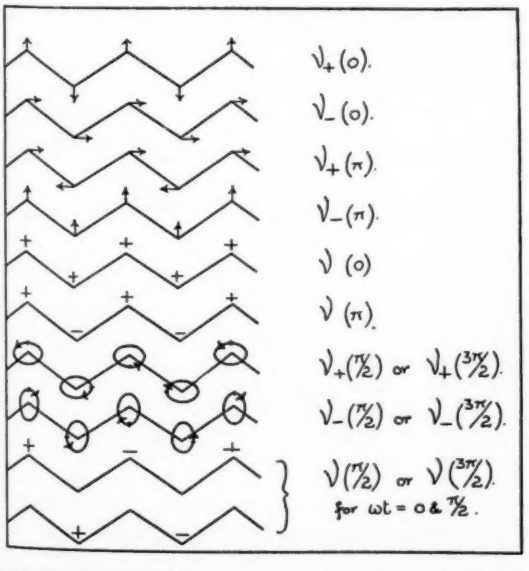

FIG. 1. Fundamental skeletal modes of long chain molecules. The modes for $p=2$ are $\nu_+(0)$, $\nu_-(0)$, $\nu_+(\pi)$, $\nu_-(\pi)$, $\nu(0)$, and $\nu(\pi)$. The remaining modes are the additional ones obtained for $p=4$.

A full discussion of this method and its applications will be given later in conjunction with the publication of our new experimental work on the spectra of high polymers.

One of us (C. Y. Liang) is grateful for financial support from the E. I. duPont de Nemours and Company, Inc.

[1] J. G. Kirkwood, J. Chem. Phys. **7**, 506 (1939).
[2] K. S. Pitzer, J. Chem. Phys. **8**, 711 (1940).
[3] S. Mizushima and T. Simanouti, J. Am. Chem. Soc. **71**, 1320 (1949).
[4] L. Kellner, Trans. Faraday Soc. **41**, 217 (1945).
[5] L. Kellner, Proc. Phys. Soc. (London) **A64**, 521 (1951).
[6] Whitcomb, Nielsen, and Thomas, J. Chem. Phys. **8**, 143 (1940).
[7] M. Born and T. v. Karman, Physik. Z. **13**, 297 (1912).

Conduction by Oxide Ion in the Solid State

J. L. WEININGER AND P. D. ZEMANY
General Electric Research Laboratory, Schenectady, New York
(Received June 14, 1954)

IN 1943 Wagner[1] postulated $O^=$ transport as the means of conduction in the Nernst glower. He pointed out that Nernst had observed qualitatively the evolution of oxygen at the anode. Evidence regarding the structure of this ceramic was obtained by Hund who studied the density and x-ray diffraction of mixed oxides.[2] He showed that in the composition region corresponding to the Nernst glower the lower valent cation substituted in the lattice which resulted in oxide ion ($O^=$) vacancies. These, in turn, provided a path for diffusing $O^=$ ions which, because of their size, would have had to be stationary in the absence of vacancies. These were permissive hypotheses but not positive experimental proof.

We have been able to demonstrate that the $0^=$ ion is a carrier by observing quantitatively the evolution of oxygen on passing current through a Nernst glower (obtained from the Stupakoff Company).

The glower was a cylindrical piece of ceramic (0.5 inch long, 0.05 inch diameter) of the type used as a light source on infrared spectrometers. This material has a normal composition of 85 mole percent ZrO_2 and 15 mole percent Y_2O_3. Our x-ray emission spectrography showed several percent hafnium and minor amounts of some rare earths. These glowers were suspended in a quartz tube by their own platinum leads. The tube was sealed to the sample inlet of a mass spectrometer and located in a furnace which could be heated to 1100°C. Only the ceramic, platinum leads, and quartz were located in the heated zone so that any gas evolved could not be readsorbed.

The rate of evolution of gases from the glower could be determined as a function of temperature and current flowing through the glower. These rates were found to be dependent on the history of the material. The rate of oxygen production was measured with the spectrometer and accounted for 7 to 80 percent of the current by Faraday's laws. The efficiency decreased with increasing temperature and age. Carbon dioxide was also evolved as a function of current. Other gases (CO, H_2S, SO_2, HCl) were desorbed on heating the glower initially but their rates were independent of the passage of current through the glower. We assume that CO_2 arose from the reaction of oxygen with residue of an organic binder used in the manufacture of the ceramic. Thus the oxide ion conductivity may be considerably larger than the values given.

For the purpose of illustration Fig. 1 presents the rate of evolution of oxygen as a function of current through the glower under different conditions. The equation of line 5 is $\Delta O_2/\Delta t=40\,000\ I$ where $\Delta O_2/\Delta t$ is the rate of oxygen evolution and I, the current in milliamperes. The value of the constant applies when the rate of

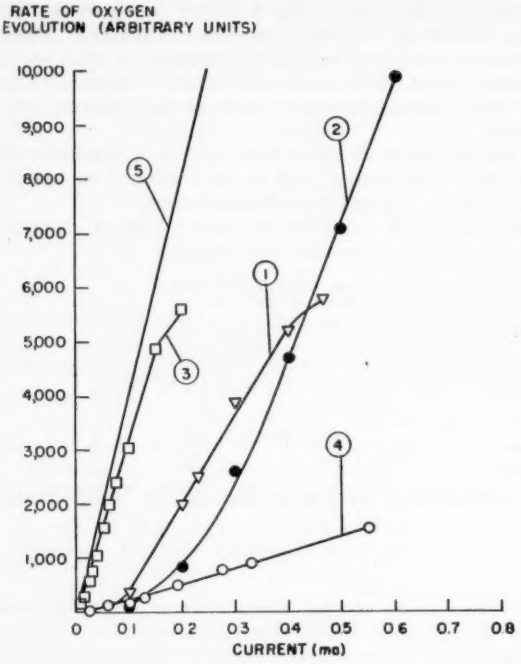

FIG. 1. Oxygen evolution *versus* current. (1) New glower (*A*) after degassing in vacuum (12 hours at 900°C) and 8 hours previous use, measurements at 620°C. (2) Same glower, after series 1, at 1017°C. (3) Glower *B*, previously used as infrared source in spectrometer (in air, *ca* 500 hours, 1800°C) degassed (at 900°C), measurements made at 595°C. (4) Glower *B*, after 3 days use at various temperatures, this measurement at 460°C. (5) Theoretical O_2 evolution on basis of 100 percent $O^=$ transport.

oxygen evolution is expressed in the arbitrary units of Fig. 1, i.e., 1 unit equals 3.9×10^{10} molecules/sec which is the calibration of our mass spectrometer.

Visual evidence of irreversible changes in the material was a blackening of the ceramic starting at the cathode and extending throughout its volume towards the anode with increasing time.

We suggest that oxide ions are responsible for an appreciable fraction of the current carried in a Nernst glower. We are now investigating the electrical properties of better defined mixed oxide systems.

We wish to acknowledge the suggestion of this problem by Dr. R. S. McDonald and Dr. H. G. Pfeiffer and helpful discussions with them and Dr. F. J. Norton.

[1] C. Wagner, Naturwiss. **31**, 265 (1943).
[2] F. Hund, Z. Elektrochem. **55**, 363 (1951); Z. anorg. Chem. **274**, 105 (1953).

Relation of Nuclear Quadrupole Couplings to the Chemical Bond*

WALTER GORDY
Department of Physics, Duke University, Durham, North Carolina
(Received May 11, 1954)

IN a previous communication[1] I have attempted to show that a consistent interpretation of the quadrupole couplings of halogen nuclei can be made without assumption of large *s* hybridization (18 to 20 percent) of the Cl bonding orbital as was done by Townes and Dailey[2] for ICl, provided that a suitable revision of the ionic character electronegativity relation is made. Solid state couplings in homo polar molecules such as Cl_2, Br_2, and I_2, where no appreciable ionic character effects exist, have been in conformity[3] with the interpretation that the *s* character in halogen bond orbitals is small. The difficulty of the large asymmetry parameters of I_2 mentioned in the previous note[1] has been cleared up[4] without the requirement of *s* hybridization. Furthermore, the ionic character electronegativity relation,

$$\text{ionic character} \approx \frac{|x_A - x_B|}{2}, \tag{1}$$

obtained from quadrupole coupling with the assumption of no *s* hybridization of the Hal orbitals seems to be borne out by later experience. (Fig. 1.) A plot of the extensive data available for polyatomic molecules including solids gives a wider scattering about the same curve. Whether $1-|\text{mole } eQq/2\times\text{atomic } eQq|$ is regarded as representing ionic character, it is evident that Fig. 1 demonstrates an orderly relation between electronegativity difference and quadrupole coupling.

Recently Schatz,[5] applying the Heitler-London theory, predicts from the Cl coupling that the bonding orbitals in Cl_2 have 17 percent *s* character, and further predicts with the same theory a possible Cl coupling in gaseous HCl which is twice that in solid HCl in magnitude or about −110 Mc. Figure 1 indicates a coupling of −61 Mc for gaseous HCl, a magnitude only 12 percent greater than the value for the solid state and in agreement with the expected increase of about 10 percent in the ionic character of the solid over the gas. Furthermore, the same relation predicts the Br and I coupling in the similar molecules HBr and HI to within 5 percent and 0.1 percent of their observed values. There is no apparent reason why HCl should be an exception. Its dipole moment is in complete accord with the amount of ionic character, 45 percent, predicted by Eq. (1) if no hybridization is assumed.[1]

If one applies the Heitler-London theory as did Schatz, with the customary normalization, one finds that the "overlap charge density" reduces the "atomic orbital density" by a factor of $1/(1+S^2)$, and thereby increases in magnitude the total coupling (assuming pure *p* orbitals) by a factor of $(1+S^2)$ when the small contribution of the overlap charge to the coupling is neglected. Here *S* is the overlap integral. When the molecular orbital theory is applied in a similar way, the predicted coupling is increased by a still greater factor, or by $(1+S)$. It is my belief that such an application of either theory to the calculation of quadrupole coupling is incorrect. It implies that in the formation of the covalent bond significant charge density is actually lifted from regions in near the nucleus to an approximate distance of the covalent radius from both nuclei. From energy considerations this seems highly improbable, as has been pointed out already[3]. The overlap charge concentration can be formed more cheaply, I would suppose, by a redistribution of charge density of the outer regions of the atoms. Because of the inverse cube variation of *q* with *r* these outer distortions have only slight influence on the nuclear coupling, and one is justified in setting $S=0$ for an evalua-

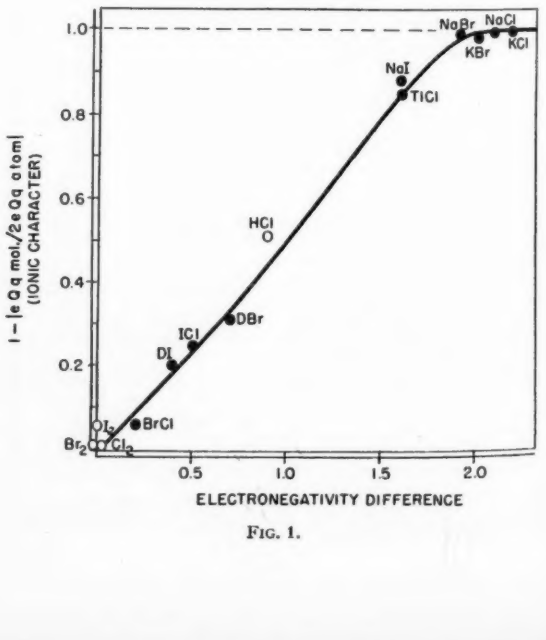

FIG. 1.

tion of the field gradient at the nucleus. The problem is thereby reduced to an atomic orbital one, with the filling of the atomic orbitals being influenced by bond properties such as ionic character and hybridization. This procedure was employed for derivation of the specialized formulas by Gordy *et al.*[3] It is unsatisfactory in that it does not account for the covalent bond energy, just as methods which have been used successfully to calculate the covalent bond energy do not give correctly the nuclear coupling. The more desirable comprehensive treatment requires a set of wave functions which give the correct charge distribution both near the nucleus and in the overlap region—but such a treatment has not yet been made.

* This research was supported by the United States Air Force through the Office of Scientific Research of the Air Research and Development Command.

[1] W. Gordy, J. Chem. Phys. **19**, 792 (1951).
[2] C. H. Townes and B. P. Dailey, J. Chem. Phys. **17**, 782 (1949).
[3] Gordy, Smith, and Trambarulo, *Microwave Spectroscopy* (John Wiley and Sons, Inc., New York, 1953), p. 272. See also Ch. VII.
[4] Robinson, Dehmelt, and Gordy, J. Chem. Phys. **22**, 511 (1954).
[5] P. N. Schatz, J. Chem. Phys. **22**, 695 (1954); **22**, 755 (1954).

Erratum: Concentration Dependence of Differential Capacity in Electrolytes at the Electrocapillarity Maximum

[J. Chem. Phys. **22**, 763–764 (1954)]

J. Ross Macdonald
Texas Instruments Incorporated, Dallas, Texas

J. Ross McDonald should read

J. Ross Macdonald.

Erratum: Relation between Vapor Pressure and Viscosity of Liquids

[J. Chem. Phys. **22**, 349 (1954)]

Shashanka Shekhar Mitra
Department of Physics, Allahabad University, Allahabad, India

EQUATION (1) should be read as

$$\log P+n\log\eta+n'(\log\eta)^2=C,$$

instead of

$$\log P+n\log\eta=n'(\log\eta)^2=C.$$

On the Transformation of Internal Coordinates

E. J. O'Reilly, Jr.
1425 *Kanawha Street, Hyattsville, Maryland*
(Received June 1, 1954)

IN constructing the elements of the secular equation according to the method of Wilson[1] it is necessary to determine the transformation properties of the internal coordinates under the operations of the symmetry group to which the molecule belongs. Tobin[2] has indicated in a general fashion these transformation properties. To minimize error, however, where complex internal coordinates are encountered it has been found convenient to first determine the transformation properties of the unit bond vectors which define the internal coordinate. Then explicit transformation of the internal coordinate q_i under the operation R yields q_i'. The transformed coordinate q_i' is readily associated with the untransformed coordinates q_j in terms of the $\mathbf{e}$ vectors by means of the relations of vector analysis.

Examples may be drawn from the case of a hexatomic planar system of V_h symmetry (Fig. 1). Torsion about the central bond may be defined after Günthard[3] by the coordinate $r\Delta\delta_1$, the change in the dihedral angle between planes (1, 3, 2) and (5, 4, 6). The transformation properties of the i-th internal coordinate under the symmetry group operation R_k may be characterized by the term $f_{ij}{}^k$. The operation R_k is mathematically equivalent to multiplication by an orthogonal rotation matrix whose determinant has the value $f=\pm1$. Further by definition,

$$r\Delta\delta_i=r(\delta_i-\delta_i{}^*),$$

where δ_i is the value of the coordinate in the equilibrium position, and $\delta_i{}^*$ is its corresponding value in the distorted position. Since

$$R_k[r\Delta\delta_i]=f_{ij}{}^k r\Delta\delta_j,$$

and

$$R_k[r(\delta_i-\delta_i{}^*)]=f_{ij}{}^k r(\delta_j-\delta_j{}^*),$$

it follows that the transformation properties $f_{ij}{}^k$ of $r\Delta\delta_i$ are identical to those of $r\delta_i$.

For this example, δ_1 may be defined[3] as

$$\delta_1=\cos^{-1}\{\mathbf{e}_4\times[\mathbf{e}_4\times(\mathbf{e}_1\times\mathbf{e}_2)]\cdot\mathbf{e}_4\times(\mathbf{e}_5\times\mathbf{e}_6)\}.$$

The operations C_x, i, and C_x, on δ_1 yield, respectively,

$$\delta_1'=\cos^{-1}\{-\mathbf{e}_4\times[-\mathbf{e}_4\times(\mathbf{e}_5\times\mathbf{e}_6)]\cdot-\mathbf{e}_4\times(\mathbf{e}_1\times\mathbf{e}_2)p^n\}$$
$$\delta_1''=\cos^{-1}\{-\mathbf{e}_4\times[-\mathbf{e}_4\times(\mathbf{e}_5\times\mathbf{e}_6)]\cdot-\mathbf{e}_4\times(\mathbf{e}_1\times\mathbf{e}_2)p^n\}$$
$$\delta_1'''=\cos^{-1}\{-\mathbf{e}_4\times[-\mathbf{e}_4\times(\mathbf{e}_6\times\mathbf{e}_5)]\cdot-\mathbf{e}_4\times(\mathbf{e}_2\times\mathbf{e}_1)p^n\}.$$

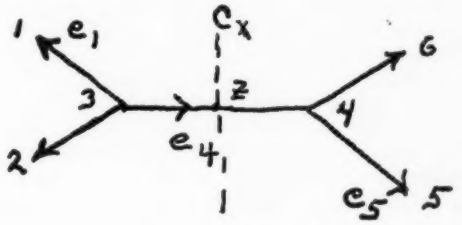

FIG. 1.

Here n is the number of cross products in the expression, and p is $+1$ or -1 for a proper or improper rotation, respectively. The factor p^n arises from the formal identity of the cross product as a pseudovector, where

$$\mathbf{c}=\mathbf{a}\times\mathbf{b};\quad c_k=\delta_{ijk}a_ib_j$$

and δ_{ijk} is the unit skew-symmetric tensor, which changes sign under an improper rotation.

Use of the various identity relations among the terms of a scalar triple product relate the transformed coordinates

$$\delta_1=\cos^{-1}(\mathbf{A}\times\mathbf{B}\cdot\mathbf{C})$$
$$\delta_1'=\cos^{-1}(-\mathbf{A}\times-\mathbf{C}\cdot-\mathbf{B})(1)=\delta_1$$
$$\delta_1''=\cos^{-1}(-\mathbf{A}\times-\mathbf{C}\cdot-\mathbf{B})(-1)=-\delta_1$$
$$\delta_1'''=\cos^{-1}(-\mathbf{A}\times\mathbf{C}\cdot\mathbf{B})(1)=\delta_1.$$

The wagging of the extreme atoms may be described by two coordinates $r\Delta\gamma_1$ and $r\Delta\gamma_2$ which designate the change in the angles formed between the central bond and the normals to planes (132) and (546), respectively. γ_i is defined as

$$\gamma_1=\cos^{-1}(\mathbf{e}_4\cdot\mathbf{e}_1\times\mathbf{e}_2)$$
$$\gamma_2=\cos^{-1}(-\mathbf{e}_4\cdot\mathbf{e}_5\times\mathbf{e}_6).$$

Under the operations C_x, i, and C_x, γ_1 transforms to

$$\gamma_1'=\cos^{-1}(-e_4\cdot e_5\times e_6)(1)=\gamma_2$$
$$\gamma_1''=\cos^{-1}(-e_4\cdot e_5\times e_6)(-1)=-\gamma_2$$
$$\gamma_1'''=\cos^{-1}(-e_4\cdot e_6\times e_5)(1)=-\gamma_2.$$

[1] E. B. Wilson, J. Chem. Phys. **7**, 1047 (1939); **9**, 76 (1941).
[2] M. C. Tobin, J. Chem. Phys. **20**, 1980 (1952).
[3] H. Günthard *et al.*, Helv. Chim. Acta, **32**, 1784 (1949).

Direct Determination of the Heat of Sublimation of Carbon

WILLIAM A. CHUPKA, *Harvard University, Cambridge, Massachusetts*
Argonne National Laboratory, Lemont, Illinois
AND
MARK G. INGHRAM, *University of Chicago, Chicago, Illinois*
Argonne National Laboratory, Lemont, Illinois
(Received May 24, 1954)

THE ideal experiment for determining the heat of sublimation of carbon would employ a Knudsen cell with interior of graphite, together with methods for determining the concentration of the molecular species in the effusing vapor. The ratio (σ) of aperture area to total interior surface area of the cell should be small enough to maintain equilibrium vapor pressure of all species inside the cell.

Two investigations[1,2] have employed Knudsen cells, but without analysis of the effusing vapor. The results of Brewer *et al.* were interpreted as supporting a value of $L_C=170$ kcal/mole, while those of Doehaerd *et al.* are convincing evidence for a low value of L_C if it is assumed that a large fraction of the effusing vapor consists of carbon atoms.

We have obtained results with a tantalum Knudsen cell with graphite liner of internal area $\sim$12 cm^2 mounted in a mass spectrometer to provide analysis of the vapor. The cell is heated by electron bombardment. Retarding and deflecting plates allow only electrically neutral vapor to enter the ionization chamber of the mass spectrometer source. A sylphon-operated shutter between the cell and the ionization chamber permits distinguishing between ions formed from the effusing vapor and those formed from residual gases. The method of analysis of the effusing vapor is that employed in investigating evaporation from graphite surfaces.[3] The absolute pressure of each component was determined by comparison of ion intensity with that from a standard. Our calibration was made by introducing a weighed amount of Ag into the oven, vaporizing the entire amount, and integrating the ion intensity over time. Using such a standard estimation of the relative ionization cross sections of the standard and the species under investigation provides the greatest error. This error should be less than a factor of two or three in pressure.

A preliminary experiment has been carried out using an effusion hole of 1.0 mm diameter (σ approximately 1/1500). With a Knudsen cell temperature of 2400°K, the relative intensities of C^+, C_2^+, and C_3^+ were found to be about equal. Comparison of C^+ ion intensity with the Ag^+ standard indicated the vapor pressure of C atoms was 2×10^{-8} atmos assuming the ratio of the ionization cross sections of Ag to that of C to be two. The vapor pressure of C atoms calculated from $L_C=170.4$ kcal is 6×10^{-8} atmos. Since this is within our experimental error, it can be concluded that $L_C=170.4$ kcal. A value of $L_C=140$ kcal would give a pressure well outside the experimental error.

In addition to the molecular species mentioned above, the C_5^+ is unexpectedly prominent, the C_5^+/C^+ ratio being about two at 2400°K. This may possibly provide the explanation of the results of Doehaerd *et al.*, which indicate the presence of some species with an extremely low evaporation coefficient of the order of 10^{-3} or less, which forms the major part of the effusing vapor when σ is very low. Using previously reported techniques,[3] both C_4 and C_5 have been detected in vaporization of carbon filaments, the ratios C^+/C_4^+ and C^+/C_5^+ being very roughly 50 and 10, respectively, at about 2700°K. Higher molecular weight species were less than C by two or more orders of magnitude. Accurate ratios and temperature dependence have not yet been measured.

It may be mentioned that if the C_5 molecule is a five-membered ring, as seems probable, it might be expected to have considerable activation energy of condensation (and consequently a low condensation coefficient) since this would involve breaking the ring. If the vapor measured by Doehaerd *et al.* consisted mostly of C_5, it would require that C_5 be an extremely stable molecule with carbon-carbon bond energies of about 135 kcal. Further speculation seems unwarranted until experiments covering a range of temperatures and of σ are completed.

[1] Brewer, Gilles, and Jenkins, J. Chem. Phys. **16**, 797 (1948).
[2] Doehaerd, Goldfinger, and Waelbroeck, Bull. Soc. Chim. Belg. **62**, 498 (1953).
[3] W. Chupka and M. Inghram, J. Chem. Phys. **21**, 371 (1953); **21**, 1313 (1953).